Int J Thermophys (2008) 29:2102–2115
DOI 10.1007/s10765-007-0261-4

Metrological Aspects of Auto-normalized Front Photopyroelectric Method to Measure Thermal Effusivity in Liquids

G. Gutiérrez-Juárez · R. Ivanov · J. P. Pichardo-Molina · M. Vargas-Luna · J. J. Alvarado-Gil · A. Camacho

Published online: 21 September 2007

Abstract The metrological aspects related to the sensitivity and signal-to-noise ratio of the auto-normalized front pyroelectric technique for the measurement of thermal effusivity in liquids are investigated. The effect of the thermally thick approximation in the theoretical expressions for the photopyroelectric signal and its effect on the sensitivity of the technique are discussed. It is shown that the sensitivity of the technique decreases with frequency. In contrast, the signal-to-noise ratio increases for higher frequencies.

Keywords Photopyroelectric technique · Sensitivity · Signal-to-noise ratio · Thermal effusivity

G. Gutiérrez-Juárez (✉) · M. Vargas-Luna
Instituto de Física de la Universidad de Guanajuato, Loma del bosque 103, Lomas del Campestre, Leon, Gto, C.P. 37150, México
e-mail: ggutj@fisica.ugto.mx

R. Ivanov
Facultad de Física, Universidad Autónoma de Zacatecas, Av. Preparatoria 301, Col. Progreso, Zacatecas, Zac., C.P. 98060, México

J. P. Pichardo-Molina
Centro de Investigaciones en Óptica, Loma del Bosque 115, Lomas del Campestre, Leon, Gto, C.P. 37150, México

J. J. Alvarado-Gil
Departamento de Física Aplicada, CINVESTAV- Mérida, Cordemex , Merida, Yuc, C.P. 97310, México

A. Camacho
Universidad Tecnológica de León, Blvd. Universidad Tecnológica 225, San Carlos, Leon, Gto, 37670, México

Molecular Physics
Vol. 106, No. 1, 10 January 2008, 113–126

Taylor & Francis
Taylor & Francis Group

RESEARCH ARTICLE

Thermodynamics of a long-range triangle-well fluid

F.F. Betancourt-Cárdenas[a], L.A. Galicia-Luna[a]*, A.L. Benavides[b], J.A. Ramírez[b] and E. Schöll-Paschinger[c]

[a]*Instituto Politécnico Nacional, ESIQIE, Laboratorio de Termodinámica, UPALM, Zacatenco 07738, Lindavista, México, D.F., México;* [b]*Instituto de Física, Universidad de Guanajuato, León 37150, México;* [c]*Fakultät für Physik, Universität Wien, A-1090 Wien, Austria*

(*Received 2 November 2007; final version received 27 November 2007*)

The long-range triangle-well fluid has been studied using three different approaches: firstly, by an analytical equation of state obtained by a perturbation theory, secondly via a self-consistent integral equation theory, the so-called self-consistent Ornstein–Zernike approach (SCOZA) which is presently one of the most accurate liquid-state theories, and finally by Monte Carlo simulations. We present vapour–liquid phase diagrams and thermodynamic properties such as the internal energy and the pressure as a function of the density at different temperatures and for several values of the potential range. We assess the accuracy of the theoretical approaches by comparison with Monte Carlo simulations: the SCOZA method accurately predicts the thermodynamics of these systems and the first-order perturbation theory reproduces the overall thermodynamic behaviour for ranges greater than two molecular diameters except that it overestimates the critical point. The simplicity of the equation of state and the fact that it is analytical in the potential range makes it a good candidate to be used for calculating other thermodynamic properties and as an ingredient in more complex theoretical approaches.

Keywords: thermodynamics; liquids; SCF

1. Introduction

The triangle-well potential (TW) is a very simple model potential that, like the square-well potential, is able to reproduce the thermodynamic properties and the vapour–liquid phase transition of simple real fluids. Due to its simple algebraic form the thermodynamic properties can be obtained rather easily from different statistical mechanics techniques such as perturbation theories, integral equation theories and molecular simulation [1–14]. This potential is given by

$$\phi(x) = \begin{cases} \infty, & x < 1, \\ \varepsilon(x-\lambda)/(\lambda-1), & 1 \le x \le \lambda, \\ 0, & \lambda < x, \end{cases} \qquad (1)$$

where $x = r/\sigma$ is the reduced distance, ε is the potential depth, σ is the diameter of the hard core, and λ is the range of the potential. The potential is graphically illustrated in Figure 1 together with the square-well potential. In contrast to the square-well potential this potential continuously goes to zero as the intermolecular distance increases. This behaviour is found for more complex interaction potentials such as the Sutherland, the Lennard–Jones and the hard-core Yukawa potentials. However, in contrast to these potentials the TW potential has a finite range, thus avoiding the problems occurring in long-range systems.

Although the simplicity of this potential is similar to that of the discontinuous square-well potential, the TW potential has not been as widely studied as the square-well potential in the context of fluids. There are only a few studies reported in the literature that we summarise in the following.

This model potential was first introduced by Nagamiya [1] (according to Feinberg and De Rocco [2]) to investigate one-dimensional fluids and he found that this potential exhibits a liquid–vapour transition. In 1964, Feinberg and De Rocco [2] presented the

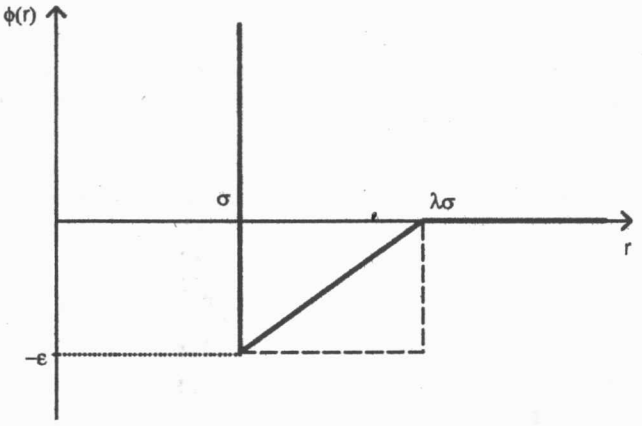

Figure 1. Triangle-well potential and square-well potential.

*Corresponding author. Email: lgalicial@ipn.mx

ISSN 0026–8976 print/ISSN 1362–3028 online

DOI: 10.1080/00268970701832397
http://www.informaworld.com

Photochemistry and Photobiology, 2008, 84: 627–631

Magnetic Properties of Synthetic Eumelanin—Preliminary Results†

M. E. Cano*[1], R. Castañeda-Priego[2], A. Gil-Villegas[2], M. A. Sosa[2], P. Schio[3], A. J. A. de Oliveira[3], F. Chen[4], O. Baffa[4] and C. F. O. Graeff[5]

[1]Centro Universitario de la Ciénega, Universidad de Guadalajara, Ocotlán, Jalisco, Mexico
[2]Instituto de Física, Universidad de Guanajuato, León, Guanajuato, Mexico
[3]Departamento de Física, Universidade Federal de São Carlos, São Carlos, Brazil
[4]Faculdade de Filosofia, Ciencias e Letras de Ribeirão Preto, Universidade de São Paulo, Ribeirão Preto, Brazil
[5]Departamento de Física, FC, Universidade Estadual Paulista, Bauru, Brazil

Received 1 September 2007, accepted 21 December 2007, DOI: 10.1111/j.1751-1097.2008.00302.x

ABSTRACT

We report an experimental and theoretical study of magnetic properties of synthetic eumelanin. The magnetization curves are determined by using both a vibrating sample magnetometer and a superconducting quantum interferometer device in an extended range of magnetic fields ranging from −10 kOe to 10 kOe at different temperatures. We find that the eumelanin magnetization can be qualitatively explained in terms of a simple model of dipolar spheres with an intrinsic magnetic moment. The latter one is experimentally measured by using X-band electron paramagnetic resonance. Our findings indicate that synthetic melanins are superparamagnetic.

INTRODUCTION

Melanin is a biologic pigment present in several human organs. In the eyes it is mainly concentrated in the iris, which takes a dark color depending on its amount. In skin and hair it can be classified into two groups—eumelanin (brown/black) and pheomelanin (red/yellow). In the skin it performs the essential function of preventing damage caused by solar ultraviolet radiation (1). In the brain, melanin is known as neuromelanin, a granular natural pigment of dark brown hue. Neuromelanin is very common in neurons of the substantia nigra, which is located in the human midbrain. This area of the human brain seems to suffer severe neuromelanin degradation during Parkinson's disease (2). Melanin is also present in some animals where it performs different physiologic functions (3). Melanin has the ability to capture and release metal ions without any apparent change in morphology; this has been interpreted as indicative of a structure which allows the efficient transport of metal ions without damage (4).

Recently, both X- and Q-band electron paramagnetic resonance (EPR) spectroscopies have been extensively used to investigate and understand the induced changes in the neuromelanin ferrodomains (5,6). On the other hand, preliminary results on mesencephalic neuromelanin to patients with Parkinson's disease showed a smaller total magnetization than the control group (7). Recent research into the electronic properties of eumelanin has indicated that it may consist of basic oligomers adhering to one another (4).

In this work, we are interested in the study of magnetic properties of synthetic eumelanin by combining experimental and computer simulations. Basically, the magnetic moment per particle is experimentally measured and it is used in a theoretical model which consists of magnetic dipolar spheres coupled to an external magnetic field. This model is used in a standard Monte Carlo (MC) simulation to numerically compute the magnetization curve. Our simulation data are compared with experimental results obtained by using a vibrating sample magnetometer (VSM) and a superconducting quantum interference device (SQUID) on synthetic eumelanins at different temperature conditions.

MATERIALS AND METHODS

Eumelanin is synthesized from a mixture of L-dopa with benzoyl peroxide in a dimethyl sulfoxide solvent. Complete details of the synthesis process can be found in Dezidério *et al.* (8). Three aliquots of 0.1 g of melanin are weighed using a Mettler Toledo analytic balance with 0.01 mg precision. The powder is placed in three small identical nonpermeable capsules made from gelatine normally used as a drug vial for oral medicine.

EPR measurements—eumelanin spin concentration and magnetic moment determination. For the determination of the effective eumelanin spin magnetic moment, the absolute spin concentration must be known. The spin concentration can be determined by comparing the EPR spectrum of the unknown sample (eumelanin) with that of a sample with known spin concentration (standard sample). In our case we have used an amorphous silicon sample as a standard with a calibrated spin concentration of 1.13×10^{15}. The number of spins for the unknown sample is then calculated with the equation proposed by Poole and Charles (9) and by Warren and Fitzgerald (10)

$$A = \frac{3.63y(\Delta H_{pp})^2}{GH_{mod}}, \quad (1)$$

where A represents the spin concentration, y is the peak-to-peak signal amplitude (for eumelanin or silicon), ΔH_{pp} is the signal line width (for eumelanin or silicon), H_{mod} is the modulation amplitude and G is the amplifier receiver gain. The shape factor 3.63 corresponds to a Lorentzian line shape, which reasonably describes the eumelanin spectrum (see Fig. 1). If a sample with known spin concentration, A_2, and line shape is used, the spin concentration can be calculated by the relation

†This invited paper is part of the Symposium-in-Print: Melanins.

*Corresponding author email: graeff@fc.unesp.br (C. F. O. Graeff)

Density Dependent Interactions and Structure of Charged Colloidal Dispersions in the Weak Screening Regime

L. F. Rojas-Ochoa,[1,2] R. Castañeda-Priego,[3] V. Lobaskin,[4,*] A. Stradner,[2] F. Scheffold,[2] and P. Schurtenberger[2]

[1]*Departamento de Física, Cinvestav-IPN, Av. Instituto Politécnico Nacional 2508, 07360 México D. F., Mexico*

[2]*Physics Department, University of Fribourg, Chemin de Musée 3, 1700 Fribourg, Switzerland*

[3]*Instituto de Física, Universidad de Guanajuato, Loma del Bosque 103, 37150 León, Mexico*

[4]*Physik-Department, Technische Universität München, James-Franck-Str., D-85747 Garching, Germany*

(Received 20 June 2007; published 2 May 2008)

We determine the structure of charge-stabilized colloidal suspensions at low ionic strength over an extended range of particle volume fractions using a combination of light and small angle neutron scattering experiments. The variation of the structure factor with concentration is analyzed within a one-component model of a colloidal suspension. We show that the observed structural behavior corresponds to a nonmonotonic density dependence of the colloid effective charge and the mean interparticle interaction energy. Our findings are corroborated by similar observations from primitive model computer simulations of salt-free colloidal suspensions.

DOI: 10.1103/PhysRevLett.100.178304 PACS numbers: 82.70.Dd, 61.05.fg, 61.20.Gy

Deionized colloidal dispersions have recently attracted much experimental [1–3] and theoretical attention [4–7] because of their unique role as simple model systems in the field of surface charge regulation. In addition to experimental challenges posed by these systems, such as the need of control over the ionic strength of the medium, a number of intriguing observations have been made that challenge classical theories of electrostatic screening and electrokinetics (e.g., see [1,8,9] and references therein). Some of the conceptual difficulties in the understanding of these systems stem from the counterion dominance in the ionic cloud of the colloid, which makes the screening ability of the medium dependent on the colloidal concentration. At the same time, the counterion condensation, which is controlled by the balance of the counterion chemical potential between the bulk suspension and the condensed layer, would depend on the concentration through the state-dependent screening parameters [4,10,11]. Therefore, modeling these systems within the usual one-component description can only be achieved using effective density-dependent interaction parameters, charge, and screening length [12]. The dependence of the colloid effective charge on the volume fraction [4,5,13] or background ionic strength [14] has been predicted in a few mean-field models and is expected to be nonmonotonic. However, this nonmonotonic behavior has never been validated experimentally.

In this Letter, we present a study of the density dependence of the colloidal structure and interactions at low ionic strength. Experiments have been carried out over a wider range of concentrations than in any previous work. We analyze the particle structure factor obtained from light and neutron scattering at different particle volume fractions and demonstrate that (i) the variation of colloidal structure in deionized suspensions can be interpreted in terms of a one-component model (OCM) that considers Yukawa-like pair interactions between colloids with state-dependent parameters, and (ii) the nonmonotonic concentration dependence of the interaction energy, as characterized by the colloid effective charge, is a general feature of deionized colloidal dispersions. Primitive model (PM) numerical simulations of salt-free suspensions corroborate our observations.

Stock suspensions of negatively charged particles (sulfonate polystyrene latex) were purchased from Interfacial Dynamics Corporation (Portland, USA) and master dispersions were prepared following the protocol described in Ref. [15,16]. The samples were prepared by diluting the master suspensions directly into quartz cells with water-ethanol mixtures, filtered several times (pore size 0.2 μm) to remove dust particles. These mixtures were chosen in order to avoid crystallization by modifying the solvent dielectric constant [17], thereby providing a well controlled model system of charged dispersions with volume fractions as high as $\sim$16%. Accurate values of particle radii and polydispersities, as obtained from DLS and SANS experiments, are given in Table I.

The effective interparticle interaction can be quantified through the analysis of the suspension static structure. This requires probing length scales comparable to the size of the particles. Usually, such information can be obtained from

TABLE I. Polystyrene latex spheres used in the experiments. Bjerrum length, $\lambda_B = e^2/(4\pi\epsilon\epsilon_0 k_B T)$, from the dielectric permittivity data in Ref. [17].

Sample #	Radius (nm)	Bjerrum length (nm)	Volume fraction (%)	Scattering Technique
*S*1	54.9 ± 6.4	1.296	0.035–01.15	3D-DLS
*S*2	58.7 ± 8.6	1.383	0.135–01.48	3D-DLS
*S*3	54.7 ± 5.3	1.482	2.500–15.50	SANS

Density Dependent Interactions and Structure of Charged Colloidal Dispersions in the Weak Screening Regime

L. F. Rojas-Ochoa,[1,2] R. Castañeda-Priego,[3] V. Lobaskin,[4,*] A. Stradner,[2] F. Scheffold,[2] and P. Schurtenberger[2]

[1]*Departamento de Física, Cinvestav-IPN, Av. Instituto Politécnico Nacional 2508, 07360 México D. F., Mexico*

[2]*Physics Department, University of Fribourg, Chemin de Musée 3, 1700 Fribourg, Switzerland*

[3]*Instituto de Física, Universidad de Guanajuato, Loma del Bosque 103, 37150 León, Mexico*

[4]*Physik-Department, Technische Universität München, James-Franck-Str., D-85747 Garching, Germany*

(Received 20 June 2007; published 2 May 2008)

We determine the structure of charge-stabilized colloidal suspensions at low ionic strength over an extended range of particle volume fractions using a combination of light and small angle neutron scattering experiments. The variation of the structure factor with concentration is analyzed within a one-component model of a colloidal suspension. We show that the observed structural behavior corresponds to a nonmonotonic density dependence of the colloid effective charge and the mean interparticle interaction energy. Our findings are corroborated by similar observations from primitive model computer simulations of salt-free colloidal suspensions.

DOI: 10.1103/PhysRevLett.100.178304 PACS numbers: 82.70.Dd, 61.05.fg, 61.20.Gy

Deionized colloidal dispersions have recently attracted much experimental [1–3] and theoretical attention [4–7] because of their unique role as simple model systems in the field of surface charge regulation. In addition to experimental challenges posed by these systems, such as the need of control over the ionic strength of the medium, a number of intriguing observations have been made that challenge classical theories of electrostatic screening and electrokinetics (e.g., see [1,8,9] and references therein). Some of the conceptual difficulties in the understanding of these systems stem from the counterion dominance in the ionic cloud of the colloid, which makes the screening ability of the medium dependent on the colloidal concentration. At the same time, the counterion condensation, which is controlled by the balance of the counterion chemical potential between the bulk suspension and the condensed layer, would depend on the concentration through the state-dependent screening parameters [4,10,11]. Therefore, modeling these systems within the usual one-component description can only be achieved using effective density-dependent interaction parameters, charge, and screening length [12]. The dependence of the colloid effective charge on the volume fraction [4,5,13] or background ionic strength [14] has been predicted in a few mean-field models and is expected to be nonmonotonic. However, this nonmonotonic behavior has never been validated experimentally.

In this Letter, we present a study of the density dependence of the colloidal structure and interactions at low ionic strength. Experiments have been carried out over a wider range of concentrations than in any previous work. We analyze the particle structure factor obtained from light and neutron scattering at different particle volume fractions and demonstrate that (i) the variation of colloidal structure in deionized suspensions can be interpreted in terms of a one-component model (OCM) that considers Yukawa-like pair interactions between colloids with state-dependent parameters, and (ii) the nonmonotonic concentration dependence of the interaction energy, as characterized by the colloid effective charge, is a general feature of deionized colloidal dispersions. Primitive model (PM) numerical simulations of salt-free suspensions corroborate our observations.

Stock suspensions of negatively charged particles (sulfonate polystyrene latex) were purchased from Interfacial Dynamics Corporation (Portland, USA) and master dispersions were prepared following the protocol described in Ref. [15,16]. The samples were prepared by diluting the master suspensions directly into quartz cells with water-ethanol mixtures, filtered several times (pore size 0.2 μm) to remove dust particles. These mixtures were chosen in order to avoid crystallization by modifying the solvent dielectric constant [17], thereby providing a well controlled model system of charged dispersions with volume fractions as high as $\sim$16%. Accurate values of particle radii and polydispersities, as obtained from DLS and SANS experiments, are given in Table I.

The effective interparticle interaction can be quantified through the analysis of the suspension static structure. This requires probing length scales comparable to the size of the particles. Usually, such information can be obtained from

TABLE I. Polystyrene latex spheres used in the experiments. Bjerrum length, $\lambda_B = e^2/(4\pi\epsilon\epsilon_0 k_B T)$, from the dielectric permittivity data in Ref. [17].

Sample #	Radius (nm)	Bjerrum length (nm)	Volume fraction (%)	Scattering Technique
*S*1	54.9 ± 6.4	1.296	0.035–01.15	3D-DLS
*S*2	58.7 ± 8.6	1.383	0.135–01.48	3D-DLS
*S*3	54.7 ± 5.3	1.482	2.500–15.50	SANS

PHYSICAL REVIEW E 77, 041407 (2008)

Superparamagnetic colloids confined in narrow corrugated substrates

S. Herrera-Velarde and R. Castañeda-Priego*

Instituto de Física, Universidad de Guanajuato, Loma del Bosque 103, Lomas del Campestre, 37150 León, Guanajuato, Mexico

(Received 5 November 2007; revised manuscript received 19 March 2008; published 22 April 2008)

We report a Brownian dynamics simulation study of the structure and dynamics of superparamagnetic colloids subject to external substrate potentials and confined in narrow channels. Our study is motivated by the importance of phenomena like commensurable-incommensurable phase transitions, anomalous diffusion, and stochastic activation processes that are closely related to the system under investigation. We focus mainly on the role of the substrate in the order-disorder mechanisms that lead to a rich variety of commensurate and incommensurate phases, as well as its effect on the single-file diffusion in interacting systems and the depinning transition in one dimension.

DOI: 10.1103/PhysRevE.77.041407 PACS number(s): 82.70.−y, 61.20.−p

I. INTRODUCTION

The study of static and dynamic properties of interacting colloidal particles in the presence of external fields is an interesting and complex subject that has grown in the last few years. This subject is increasingly important because a quantitative understanding of colloidal dispersions under external fields allows elucidation of the physical properties of other complex systems that are of industrial, chemical, and biological relevance. For example, colloidal particles under external laser fields have highlighted the importance of the ordering and dynamics of atomic systems on surfaces, such as atomic monolayers [1,2], and the relevance of stochastic resonance in nonlinear bistable systems [3]. For a review of colloids under external control see, for instance, Ref. [4].

During the last few decades, the study of dynamical properties in quasi-one dimensional (quasi-1D) channels has become a fascinating topic from both theoretical and experimental points of view. This is due to the fact that the dynamics of fluids in restricted geometries is very different from that in the bulk. For example, when the channel is so narrow that mutual passage is not possible, a correlation between subsequent displacements emerges, so that the motion of individual particles requires the collective motion of many other particles in the same direction; this leads to a subdiffusive process characterized by an anomalous mean-square displacement of the form $\lim_{t\gg\tau} W(t)=2F\sqrt{t}$ [6], where F is the so-called single-file diffusion (SFD) mobility factor. Particularly, interacting particles in narrow channels and subject to external fields represent an interesting model system to study several topics, such as the basis of commensurate-incommensurate transitions, the SFD in the inhomogeneous case, and the conditions for depinning in 1D, as well as the study of nonlinear dynamics in systems with anharmonic interactions [7].

In recent years, experimental corroboration of SFD has been performed successfully by several research groups [8–10]. In particular, Lutz *et al.* [11,12] created 1D circular channels by means of scanning optical tweezers in order to avoid the presence of lateral confinement walls. This experimental setup allows a reduction of the dissipative hydrodynamic interactions, thus leading to higher particle mobility. This technique has elucidated the typical diffusion of charged colloids in a free single file—i.e., in the absence of a substrate.

Nowadays, due to several experimental and theoretical studies, the diffusion on homogeneous substrates is now understood, but the dynamical properties on corrugated surfaces are still less known, although the latter case is more relevant for modeling atomic surfaces. Furthermore, there is no experimental evidence of the way in which a modulated substrate affects the physical properties of interacting particles along the channel. Nonetheless, from a simulation point of view, the mobility of noninteracting pointlike particles on periodic substrates [13] and the diffusion of charged colloids under modulated sinusoidal substrates [14] have shown that the presence of the substrate does not invalidate the diffusive behavior $W(t)\propto\sqrt{t}$.

Although most experimental results for SFD have been performed with charged colloids, the study of the same phenomenon in similar systems permits one to gain a better understanding of the relevant physical processes that can take place, such as anomalous diffusion, hopping rate of particles in periodic potentials, and depinning transition, among others. In the present work, motivated by whether the rich scenario of novel phases and dynamical processes are dependent of the kind of interaction potential, we extend our previous study for charged colloids [14] to the case of superparamagnetic colloids. We basically study the commensurate-incommensurate phases and the subdiffusive process of colloids with dipolelike interactions in narrow corrugated channels over an extended range of substrate strengths. We should mention that our results can be corroborated in experiments of colloidal particles confined in 1D optical channels and subject to periodic light-forces [11,12]. The latter ones are commonly used for modeling periodic substrates [2].

The paper is organized as follows. In Sec. II we describe the interaction potential between colloids, the Brownian simulation algorithm, and the main quantities to characterize the structure and dynamics of the system. In Sec. III, the substrate-free case is analyzed in terms of the potential strength. In Sec. IV, the pair distribution function and the

*ramoncp@fisica.ugto.mx

Eur. Phys. J. Special Topics **153**, 147–150 (2008)

DOI: 10.1140/epjst/e2008-00414-8

THE EUROPEAN PHYSICAL JOURNAL
SPECIAL TOPICS

Photothermal and micro-thermal characterization of metal coated diamond crystallites

I. Delgadillo-Holtfort[1,3], E. Neubauer[2], J.S. Antoniow[4], J. Gibkes[3], M. Chirtoc[4], B.K. Bein[3], and J. Pelzl[3,4]

[1] Instituto de Física de la Universidad de Guanajuato, IFUG, Apdo. E-143 León, Gto., Mexico
[2] ARC Seibersdorf Research, Dept. Materials Research, 2444 Seibersdorf, Austria
[3] Institut für Experimentalphysik, Ruhr-Universitat, 44801 Bochum, Germany
[4] LTP, UTAP, Université de Reims, BP. 1039, 51687 Reims Cedex 2, France

Abstract. Photoacoustic effect and scanning near field microscopy have been applied to characterise the thermal properties of diamond crystallites which were coated by a Cu film, a Cr-film and a Cr-Cu film. The Cu-coated diamond exhibits a considerable thermal barrier at the Cu-diamond interface which had disappeared for the crystallites with a thin bond Cr-layer between diamond and Cu. The local inspection of the thermal conductivity with a thermal nano-probe operated in the 3ω-mode reveals slight local variations of the thermal conductivity of the Cr-coated crystallite.

1 Introduction

CVD diamond coatings are now frequently used to protect the surface of the materials against abrasion or to enhance the thermal conductance of the surface areas [1]. Although diamond is the most rigid material with the highest thermal conductivity its electrical conductivity is rather poor at room temperature. A way to overcome this drawback could be the preparation of protecting films made of metal coated diamond particles. This work is devoted to the investigation of the influence of Cu coatings on the thermal transport properties of single coated diamond particles and on the effect of Cr bond layers between the diamond particle and the Cu coating. The size of the diamond particles was about 300 μm. The thickness of the coatings of elèctrolytically and CVD deposited Cu, Cr and Cu-Cr varied between 200 nm and 50 μm. Photoacoustic (PA) effect and photothermal infrared radiometry (PTR) have been applied to measure depth profiles of the thermal effusivity, photo-pyroelectric experiments were used to determine the thermal diffusivity governing the heat flow across the crystallites and the 3ω method was used to investigate the lateral variation of the thermal conductivity in near surface regions of the coated and non-coated diamond crystallites [2]. In this contribution we report on first results obtained with the PA effect and the 3ω method.

2 Experimental

The photoacoustic measurements were performed with a set-up based on modulated laser heating in the frequency interval between 100 Hz and 3.6 kHz below the first acoustic resonance of photoacoustic cell [3]. The crystallites were mounted on a thin glass plate in the middle of the cell without having contact to each other. The signals were calibrated with the signals of

Eur. Phys. J. Special Topics **153**, 259–262 (2008)

DOI: 10.1140/epjst/e2008-00440-6

THE EUROPEAN PHYSICAL JOURNAL
SPECIAL TOPICS

Photoacoustic and photothermal radiometry spectra of implanted Si wafers

D.M. Todorović[1], M. Pawlak[2], I. Delgadillo-Holtfort[3], and J. Pelzl[4]

[1] Center for multidisciplinary studies, University of Belgrade, Belgrade, Serbia
[2] Instytut Fizyki, Uniwersytet Mikołaja Kopernika, ul. Grudziadzka 5/7, 87-100 Torun, Poland
[3] Instituto de Fisica de la Universidad de Guanajuato, IFUG, Apdo. Postal E-143 Leon, Gto., Mexico
[4] Experimental Physik, Festkoerperspektroskopie, Ruhr-Universitaet, Bochum, Germany

Abstract. The effects of Ar^{+8} and O^{+6} ion implantation of Si were investigated by photoacoustic (PA) and photothermal radiometry (PTR) methods. The surface of Si sample was treated with Ar^{+8} or O^{+6} ions with various doses. Amplitude and phase PA spectra of Si with and without ion-implantation were measured and analyzed in the wavelength range from 800 to 1600 nm (the energy range from 0.75 to 1.55 eV) and frequency of modulation, from 1 Hz to 100 kHz.

1 Introduction

Ion implantation has several advantages over the conventional doping techniques such as precise control of the depth and concentration of dopant and it is not limited by solubility constraints. However, it introduces considerable amount of lattice defects, which will modify optical, thermal and electrical properties of the surface layer of material.

The photothermal and photoacoustic effects in semiconductor are based on the photogeneration of electron-hole pairs, i.e. plasma waves, generated by the absorbed intensity-modulated excitation. Depth-dependent plasma waves contribute to the generation of periodic heat and mechanical vibrations, i.e. thermal and elastic waves. These waves can be manifested in various ways: one is sound generation - the PA generation. There are three mechanisms of PA generation [1]. The propagation of thermal waves through the sample and through the surrounding gas, which. is in contact with the sample, produces acoustic waves in the gas – thermodiffusion (TD) mechanism of PA generation [2]. The thermal waves cause also surface sample vibrations, where they cause expansion of the surrounding gas – thermoelastic (TE) mechanism of PA generation [3]. The photoexcited carriers produce periodic elastic deformation in the sample – electronic deformation (ED) [4,5].

Plasma and thermal waves can cause the infrared radiation from sample – PTR signal. Investigation of the PTR signal dependence on the surface conditions for optical excitation will lead to knowledge for the various carrier transport parameters (carrier lifetime, surface recombination velocity, etc) [6].

In this work the effect of Ar^{+8} and O^{+6} ion implantation of Si was investigated by photoacoustic (PA) spectroscopy, PA frequency scans in transmission and photothermal radiometry (PTR) methods.

2 Experimental results and analyze

The surface of Si samples was implanted with: (1) Ar^{+8} ions with energy of 120 keV and implantation doses 5.0×10^{13}, 5.5×10^{14}, and 5.0×10^{15} ions/cm^2 (wafer was p-type, 5 k ohm cm,

Bioelectromagnetics (2008)

Brief Communication

Pulsed Electromagnetic Fields Induced Femoral Metaphyseal Bone Thickness Changes in the Rat

S. Márquez-Gamiño,[1]* F. Sotelo,[1] M. Sosa,[2] C. Caudillo,[1] G. Holguín,[2] M. Ramos,[2] F. Mesa,[2] J. Bernal,[2] and T. Córdova[2]

[1]*Instituto de Investigación Sobre el Trabajo, Universidad de Guanajuato, León, Gto., México*

[2]*Instituto de Física, Universidad de Guanajuato, León, Gto., México*

The effect of 1 Hz, 30 mT pulsed magnetic fields on young adult rat femoral metaphyseal bone thickness was assessed. Ten same litter, female Wistar rats were studied: five of them underwent 30 min magnetic stimulation sessions for 20 consecutive days. The anterior and posterior cortical, as well as trabecular bone transverse thicknesses were measured. The results obtained under clear field microscopy in stimulated and control histological cuts were (in μm) 398 ± 32 versus 260 ± 22 ($P = 0.002$), 380 ± 68 versus 252 ± 21 ($P = 0.03$), and 168 ± 11 versus 112 ± 11 ($P = 0.002$), respectively. The transcranial magnetic stimulation system, approved for human therapy, generates pulsed electromagnetic fields, which induce a significant thickness increase in cortical and trabecular in vivo stimulated bone tissues. This is the first time this effect in healthy animals is shown. Bioelectromagnetics, 2008. © 2008 Wiley-Liss, Inc.

Key words: pulsed magnetic stimulation; cortical bone; trabecular bone

There is a great interest in understanding the effects of the interaction between electromagnetic fields and biological systems, particularly human beings. In the last 30 years, the evolution of different degrees of osteoporosis has been studied using magnetic stimulation, both in experimental and clinical research. Most of the experimental outcomes suggest a positive effect on bone density [Basset, 1982; Chang and Chang, 2003]. Additionally, it is important to underline that pulsed electromagnetic fields (PEMF) are currently being used in the treatment of several diseases [Sadafi, 1998], particularly some affecting the nervous system [Fierro et al., 2006; Lee et al., 2006; Pape et al., 2006; Webster et al., 2006].

Basset et al. [1979] used Helmholtz coils to favour osteogenesis for the first time. Recently, Chang and Chang [2003] demonstrated that PEMF inhibits trabecular loss in ovariectomised rats, without any effects observed on bone cortical thickness. Nevertheless, bone loss prevention using different stimulation intensities, frequencies and exposition times, have been reported [Basset et al., 1979; Cruess et al., 1983; Mishima, 1988; Simske et al., 1991; Skerry et al., 1991; Takayama et al., 1990; Yan et al., 1998]. In recent studies concerning PEMF influence upon bone cell cultures, both osteoblasts [Diniz et al., 2002; Chang et al., 2004a] and osteoclasts [Shankar et al., 1998; Chang et al., 2003, 2004b] were affected.

Until now, the reported outcomes point out that the PEMF parameters, including wave shape, frequency, repetition index and intensity of the magnetic and electric induced fields, affect the stimulus efficacy [Pilla, 2002]. These studies are valuable contributions for understanding how the electromagnetic fields affect

Grant sponsor: CONACyT; Grant number: 38749-E.

G. Holguín's present address is Escuela de Física, Facultad de Ciencias, Universidad Autónoma de Santo Domingo, Sto. Domingo, Rep. Dominicana.

*Correspondence to: Dr. S. Márquez-Gamiño, Instituto de Investigación Sobre el Trabajo, Universidad de Guanajuato, A. Postal 607, León, Gto., 37000, México.
E-mail: smgamino@fisica.ugto.mx

Received for review 30 January 2007; Final revision received 15 October 2007

DOI 10.1002/bem.20396
Published online in Wiley InterScience (www.interscience.wiley.com).

IOP PUBLISHING EUROPEAN JOURNAL OF PHYSICS

Eur. J. Phys. **29** (2008) 345–354 doi:10.1088/0143-0807/29/2/015

Understanding the magnetic susceptibility measurements by using an analytical scale

M E Cano[1,2,3], T Cordova-Fraga[1], M Sosa[1], J Bernal-Alvarado[1] and O Baffa[2]

[1] Instituto de Física, Universidad de Guanajuato, Loma del Bosque 103, Lomas del Campestre, 37150 León, Gto., Mexico
[2] FFCLRP-Universidade de São Paulo, Av. Bandeirantes 3900, CEP 14040–901 Ribeirão Preto, S. P., Brazil
[3] Centro Universitario de la Ciénega, Universidad de Guadalajara, Av. Universidad 1115, Ocotlán, Jal., Mexico

E-mail: mecano@fisica.ugto.mx

Received 12 December 2007, in final form 16 January 2008
Published 20 February 2008
Online at stacks.iop.org/EJP/29/345

Abstract

A description of the measurement procedure, related theory and experimental data analysis of the magnetic susceptibility of materials is given. A short review of previous papers in the line of this subject is presented. This work covers the whole experimental process, in detail, and presents a pragmatic approach for pedagogical sake.

1. Introduction

The physical properties of matter are quantified by a set of numbers, the characteristic parameters of each substance. In the case of magnetic interactions, the materials have one of the three properties: diamagnetisms, paramagnetism or ferromagnetism. The specific presence in the matter of one of these characteristics depends on the number of paired electronic spins in the sample. In particular, the diamagnetism is originated by the magnetic orbital moment induced by the application of an external magnetic field with intensity $\vec{H}$. The paramagnetism and ferromagnetism have their origins in the averaged alignment of the spin magnetic moment in the direction of $\vec{H}$ [1–4]. The quantification of the response of the matter in terms of these three properties is named the magnetic susceptibility (χ), which is a dimensionless constant. Nevertheless, the experimental statement of the magnetic nature of a sample is not an easy task. In general, the measurement of this quantity implies the determination of the components of a second rank tensor [2, 3].

Gender difference in the gastric emptying measured by magnetogastrography using a semi-solid test meal

Teodoro Córdova-Fraga,[1] José María De la Roca-Chiapas,[1] Silvia Solís,[2] Modesto Sosa,[1] Jesús Bernal-Alvarado,[1] Enedino Hernández,[1] Martha Hernández-González[3]

[1] *Instituto de Física, Universidad de Guanajuato, León, Gto. México.*
[2] *Instituto de Investigaciones Médicas, Universidad de Guanajuato, León, Gto. México.*
[3] *Unidad de Investigación en Epidemiología Clínica, UMAE Nº.1 IMSS Bajío, León, Gto. México.*

Acta Gastroenterol Latinoam 2008;38:240-245

Summary

Background/aims: evidence of gender-related differences in gastric emptying have been reported in the literature. Usually, those researches have focusing only with solid or liquid meal and invasive techniques. The objective of this study was to know the differences in the half time of gastric emptying and frequency of peristaltic contractions measured with magnetogastrography (MGG) on healthy subjects, using a semi-solid test meal. **Methods:** *the study was carried out in 16 healthy subjects without gastrointestinal disease history, they were divided in two groups, 8 male and 8 female. A test meal composed by 250 ml of yogurt and 3 grs of magnetite (Fe_3O_4), was employed.* **Results:** *the gastric emptying half times were found to be 32.3±10.8 and 36.0±6.7 minutes, for men and women, respectively. Magnetogastrography modality presented in this study is a useful technique to measure the gastric emptying and the peristaltic contractions frequency. The studies were performed in healthy subjects without side effects. Using this technique a significant statistical difference ($p<0.05$) on gastric emptying from healthy volunteers was obtained between men and women.* **Conclusions:** *a contribution of this study was to demonstrate the feasibility of magnetogastrography to analyze gender differences in the gastric emptying half time using a semi-solid test meal.*

Key words: *magnetogastrography, gastric emptying, peristaltic contractions, gender differences.*

Correspondence: *José María De la Roca-Chiapas*
Loma del Bosque 103, Lomas del Campestre 37150, León, Gto. México
Tel: (52-477)7885100 Office 8475; Fax 8410.
E-mail: joseroca@fisica.ugto.mx

Diferencias de género en el vaciado gástrico medido por magnetogastrografía usando un alimento de prueba semisólido

Resumen

Introducción/objetivo: se ha reportado en la literatura evidencia de las diferencias relativas al género en el vaciado gástrico. Generalmente se ha enfocando la investigación sólo con alimento de prueba sólido o líquido y con técnicas invasivas. El objetivo de este estudio fue conocer las diferencias en el tiempo medio de vaciado gástrico y la frecuencia de las contracciones peristálticas medidas con magnetogastrografía (MGG) en sujetos sanos, usando un alimento de prueba semisólido. **Métodos:** *el estudio fue realizado en 16 sujetos sanos sin historia de enfermedades gastrointestinales. Fueron divididos en dos grupos: 8 mujeres y 8 hombres. Se empleó un alimento de prueba compuesto por 250 ml de yogurt y 3 grs de magnetita (Fe_3O_4).* **Resultados:** *los tiempos medios de vaciado gástrico encontrados fueron de 32.3±10.8 y 36.0±6.7 minutos, para los hombres y mujeres, respectivamente. La modalidad de magnetogastrografía presentada en este estudio es una técnica útil para medir el vaciado gástrico y la frecuencia de contracciones peristálticas. Los estudios fueron realizados en sujetos sanos sin efectos secundarios. Usando esta técnica se obtuvo una diferencia estadística significativa ($p<0.05$) en el vaciado gástrico entre hombres y mujeres sanos.* **Conclusiones:** *una contribución de este estudio fue demostrar la viabilidad de la magnetogastrografía para analizar las diferencias de género en el tiempo medio de vaciado gástrico usando un alimento de prueba semisólido.*

INVESTIGACIÓN REVISTA MEXICANA DE FÍSICA 54 (3) 180–187 JUNIO 2008

Optical spectroscopy and multivariate analysis of biomedical optics

J.L. Pichardo-Molina and C. Araujo-Andrade
Centro de Investigaciones en Óptica, A.C.,
Loma del Bosque No.115, Col. Lomas del Campestre, 37150, León, Gto. México.

G. Gutiérrez-Juárez
Instituto de Física de la Universidad de Guanajuato,
Apartado Postal E-143, 37150 León, Gto. México.

Recibido el 9 de mayo de 2007; aceptado el 5 de marzo de 2008

Although some optical spectroscopy methods were introduced more than ten decades ago, they are still finding new applications in many areas of science. Specifically, medicine and biology are two areas of research where optical methods may facilitate and improve the study and characterization of tissue and biological molecules in order to improve medical diagnosis. Optical spectroscopy can aid in the study and detection of some diseases faster than standard laboratory techniques. This work demonstrates applications of Micro-Raman spectroscopy and multivariate analysis to biomedical problems such as: breast cancer detection, toxoplasmosis study through indirect antibody detection, and discrimination between antibody isotypes (IgG and IgM).

Keywords: Colostrum; multivariate; NIR; Raman; serum.

Algunas espectroscopias ópticas existen desde hace más de diez décadas; sin embargo, en recientes años estas técnicas se han aplicado en distintas áreas del conocimiento. Por otro lado, la medicina y la biología son dos áreas de investigación donde la óptica puede facilitar el estudio y caracterización de tejidos y moléculas biológicas con el fin de mejorar el diagnóstico clínico. Las espectroscopias ópticas pueden ayudar en el estudio y detección de algunas enfermedades de manera mas rápida que las técnicas estándar de laboratorio. En este trabajo, mostramos algunas aplicaciones de la espectroscopia Raman y del análisis multivariante en algunos problemas específicos del área biomédica, por ejemplo: detección de cáncer de mama, diagnóstico de la toxoplasmosis e identificación de isotipos (IgG e IgM).

Descriptores: Calostro; multivariado; NIR; Raman; suero.

PACS: 87.64.Je; 89.20.-a; 87.14.-g

1. Introduction

Medicine and biotechnology are two areas where the constant development of new and more sophisticated techniques is required in order to make better and faster decisions related to clinical diagnosis. Physicians base their diagnoses principally on the use of three kinds of information: clinical, laboratory, and image analysis. Consequently, the new proposed techniques should improve upon the current procedures for early detection of disease.

The medical community is not only interested in techniques that improve the clinical diagnosis; they are also interested in noninvasive techniques that are less expensive, and especially in those techniques that do not require a sophisticated technician. In the last three decades, the most promising noninvasive techniques for characterization and analysis have been related to the use of visible or near infrared light. Light has been used to investigate materials and to obtain corresponding information due to the interaction of radiation with the material under study. Optical techniques are based primarily on the simple idea that light passes through the material in small quantities (transmission, diffusion, reflection, or dispersion) and emerges with information about the material through which it has passed (tissue, serum, etc.).

Following this direction, optical techniques such as absorption (UV-Vis, NIR, MIR), fluorescence, reflectance (UV-Vis, NIR, MIR), Raman, and Micro-Raman spectroscopies have shown great potential for biomedical applications, for example glucose determination [1–6], tissue and biological sample characterization [7-10], monitoring of cell proliferation [11], quantitative analysis of serum samples [12], measurement of carotenoids in the skin and retina [13, 14], measurements of brain activity [15], to assess neural activation during object processing in infants [16], studies on immunoassays [17], *in vivo* disease diagnosis [18], breast cancer detection in tissue or in serum blood [19–23], and also alcohol testing and beverage identification have all been studied using optical spectroscopies and multivariate techniques [24, 25].

Raman and Micro-Raman spectroscopy provide information on molecular structure by means of the normal vibrational modes of the molecule under study. The interaction of the light with the sample causes an energy exchange between photons and molecules, and this interaction causes the scattering of the photons, in which the majority change direction (Rayleigh scattering), but only a few (1 in 1×10^8 photons) change in frequency (Raman scattering) [26, 27]. In addition, infrared spectroscopy obeys Beer's law, by which light is absorbed through the sample and the transmitted or reflected light is detected at the same frequency as the incident light.

The principal objective of this paper is to show potential applications of optical spectroscopies, specifically Raman spectroscopy, to biomedical problems.

IOP PUBLISHING JOURNAL OF PHYSICS D: APPLIED PHYSICS

J. Phys. D: Appl. Phys. **41** (2008) 085106 (8pp) doi:10.1088/0022-3727/41/8/085106

Differential sensor in front photopyroelectric technique: I. Theory

R Ivanov[1], G Gutierrez-Juarez[2], J L Pichardo-Molina[3], I Moreno[1], A Cruz-Orea[4] and E Marín[5]

[1] Facultad de Física, Universidad Autónoma de Zacatecas, Calz. Solidaridad Esquina Paseo de la Bufa s/n, C.P. 98060, Zacatecas, Zac., México

[2] Instituto de Física, Universidad de Guanajuato, Loma del Bosque 103, Lomas del Campestre, C.P. 37150, León, Gto., México

[3] Centro de Investigaciones en Óptica, Loma del Bosque 115, Lomas del Campestre, C.P. 37150, León, Gto., México

[4] Departamento de Física, CINVESTAV-IPN, Av. IPN 2508, San Pedro Zacatenco, C.P. 07360, México D.F., México

[5] Centro de Investigación en Ciencia Aplicada y Tecnología Avanzada, Instituto Politécnico Nacional, Legaría 694, Colonia Irrigación, C.P. 11500, México D. F., México

E-mail: rumen@planck.reduaz.mx

Received 27 December 2007, in final form 16 February 2008
Published 14 March 2008
Online at stacks.iop.org/JPhysD/41/085106

Abstract

In this paper the theory of the differential front photopyroelectric technique is developed. The thermal effusivity measurements of a sample through photopyroelectric direct (no-differential) experiments do not have sufficient resolution and accuracy to detect small changes in the thermal effusivity. To assess minor variations in this thermal magnitude, differential methods should be used. These methods compare properties of a reference sample and another unknown sample, which are placed separately in both halves of the differential cell. It is shown that in order to achieve better metrological properties of the differential measurement and electromagnetic interference immunity, the signals of both halves must be subtracted directly at the output of the two parallel connected pyroelectric sensors. The thickness of the samples should have the maximum possible value, at least 10 times higher than the thermal diffusion length for minimum frequency. The results of numerical simulations for the amplitude, phase, real and imaginary parts with water as a reference sample and the other sample with a thermal effusivity very close to that of water (contaminated water) are presented. These results show that measurements should be made in the nearly ideal voltage mode, which ensures a better signal-to-noise ratio than the ideal current mode.

1. Introduction

Photoacoustic (PA) and photothermal techniques (PT) have been used for many years in non-destructive evaluation of different materials. Among the PT, the photopyroelectric (PPE) technique has proved to be a very useful tool for measuring the thermal properties of liquid samples, primarily the thermal effusivity (e) and diffusivity (α) [1, 2]. The PPE technique has two experimental configurations; the first one is the back photopyroelectric (BPPE) configuration [3–5], in which the sample is illuminated directly. The second is the front photopyroelectric (FPPE) configuration [6–9] in which the PPE detector is illuminated.

From the metrological point of view, each technique can be used in a direct or differential mode. In the direct mode, the physical parameter is measured in an absolute way. In the differential mode, two samples are used, one corresponding to the reference material with well-known parameters, and the other is a sample for which its parameters have been slightly modified. The idea of this mode is to obtain the difference between the parameters. Knowing this difference and the corresponding parameter value of a reference material, we can find the parameter value of the unknown sample with high accuracy. Both types of measurements are very useful; however, when the objective is to measure small variations

Int J Thermophys
DOI 10.1007/s10765-008-0411-3

Benefits of the Mycorrhizal Fungi in Tomato Leaves Measured by Open Photoacoustic Cell Technique: Interpretation of the Diffusion Parameters

S. Sánchez-Rocha · M. Vargas-Luna · G. Gutiérrez-Juárez · R. Huerta-Franco · V. Olalde-Portugal

Abstract The open photoacoustic cell technique was used to measure tomato leaves from plants with and without mycorrhizal fungi (*Glomus fasciculatum*). Based on measurement of the photobaric contribution of the photoacoustic signal, the exponential parameter of the diffusion behavior for this contribution was calculated. From this value, the oxygen diffusion coefficient was derived. The changes in the oxygen-diffusion-coefficient-dependent exponential parameter are statistically significant ($p < 0.05$) and are consistent with the expected benefits of mycorrhizal symbiosis. Potentially similar results obtained from the photothermal contribution are discussed.

Keywords Mycorrhiza · Oxygen diffusion coefficient · Photoacoustic · Thermal diffusivity · Tomato

1 Introduction

Mycorrhiza is a symbiotic association between plants and fungi, in which the fungi colonize the cortical tissue of roots [1]. This relationship benefits both organisms. In the case of the plant, it improves mineral uptake, particularly the uptake of phosphorous

S. Sánchez-Rocha · V. Olalde-Portugal
CINVESTAV Unidad Irapuato, Km 9.6, Libramiento Norte, Carretera Irapuato-León, 36500 Irapuato, GTO, México

M. Vargas-Luna (✉) · G. Gutiérrez-Juárez
Instituto de Física, Universidad de Guanajuato, Loma del Bosque 103, Lomas del Campestre, 37150 León, GTO, México
e-mail: mvargas@fisica.ugto.mx

R. Huerta-Franco
Instituto de Investigaciones sobre el Trabajo, Universidad de Guanajuato, Av. Eugenio Garza Sada 572, Lomas del Campestre, 37150 León, GTO, México

Int J Thermophys
DOI 10.1007/s10765-008-0540-8

Study of Skin Phantoms by Photothermal Radiometry in Frequency Domain and Multivariate Methods

J. L. Pichardo-Molina · G. Gutiérez-Juárez · A. Landa-Hernandez · O. Barbosa-Garcia · R. Ivanov · M. R. Huerta-Franco

Abstract In this paper the use of the photothermal radiometry technique in the frequency domain (PRTF) and the use of multivariate methods in the study of two types of skin phantoms: (a) one in which skin pigmentation was simulated dyeing the gel phantom and (b) the other consists of exposure of animal skin samples to different degrees of thermal damage. In experiment (a), gel phantoms were prepared with different concentrations of methylene blue (MB). The mean values of the radiometry signal (RS) show significant differences in only those cases in which changes in the concentration of MB were higher than 0.38 mM. This result was confirmed with a t test for independent samples of the data ($p < 0.05$). The mean values of the amplitude and phase signal do not permit discrimination between phantoms with changes in pigmentation equal to or lower than this value. However, principal component analysis (PCA) demonstrated that it is possible to discriminate between phantoms with changes in molar concentration equal to 0.38 mM (for the phase signal). In the case of experiment (b), the following four groups of pork skin samples were analyzed: one

J. L. Pichardo-Molina (✉) · O. Barbosa-Garcia
Centro de Investigaciones en Óptica A. C., Loma del Bosque 115,
Col. Lomas del Campestre, C.P. 37150 León, Gto, México
e-mail: jpichardo@cio.mx

G. Gutiérez-Juárez · A. Landa-Hernandez
Instituto de Física, Universidad de Guanajuato,
A. P. E-143, 37150 León, Gto, México

R. Ivanov
Facultad de Física, Universidad Autónoma de Zacatecas,
Calz. Solidaridad Esquina Paseo de la Bufa s/n,
C.P. 98060 Zacatecas, ZAC, México

M. R. Huerta-Franco
Instituto de Investigaciones Sobre el Trabajo,
Universidad de Guanajuato, E Garza Sada 220, Lomas del Campestre, 37150 León, Gto, México

Published online: 20 November 2008

DIF-08-A18

Anexo 135.2

Eur. Phys. J. Special Topics **153**, 171–173 (2008)

DOI: 10.1140/epjst/e2008-00420-x

THE EUROPEAN PHYSICAL JOURNAL
SPECIAL TOPICS

Metrological aspects of thermal relaxation technique by radiation loss for volumetric heat capacity measurements

G. Gutiérrez-Juárez[1], D. Acosta-Avalos[2], R. Medina[3], M. Vargas-Luna[1], and J.J. Alvarado-Gil[3]

[1] Instituto de Física de la Universidad de Guanajuato, A.P.E-143, CP 37150, León, Gto., México
[2] Centro Brasileiro de Pesquisas Físicas, Rió de Janeiro, Brasil
[3] CINVESTAV-Unidad Mérida, Antigua Carretera a Progreso Km. 6, CP 97310, Mérida, México

Abstract. One of the best-known methods to measure the heat capacity of solids consists in the illumination of the sample and the analysis of the thermal relaxation when the illumination is stopped. In this work, the energy balance equation with heat losses due to radiation is solved exactly. This is used to establish the limits of the usual approximations used to obtain the heat capacity from the experimental data. It is shown that large temperature changes, induced by the heat source during the experiment can generate errors in the calculation of heat capacity when the traditional approach is used.

1 Introduction

In the thermal relaxation method, a thin sample is attached to a holder and isolated from the surrounding environment inside a Dewar chamber in which a vacuum of around 1 mtorr is present. The sample previously blackened with a very thin layer of black paint, is illuminated by a continuous light source. The time that the sample takes to heat or to cool when the illumination is interrupted is used to determine the heat capacity [1–3]. In this configuration the losses due to convection and conduction can be minimized. The theoretical approach that is used is based on the energy balance equation with heat losses due only to radiation and it is considered that the changes of temperature are much lower than the bath temperature.

In this paper it is shown that, the energy balance equation with losses by radiation for plate shape solid, can be solved exactly. We get the temperature evolution as a function of time, and these results can be used to determine the heat capacity with higher accuracy than the traditional methods. It is also shown that the theoretical predictions of previous works can be obtained and that the limits and applicability of the usual approach can be explored.

2 Theory

Let the intensity of the heat flux be given by a continuous light beam of power P_0. When the light is turned on, the temperature of the sample is increased from the bath temperature to a maximum temperature. On the other hand, when the light is turned off, the temperature decreases, from the maximum temperature to the bath temperature. The energy balance equation can be written as

$$\frac{\partial Q}{\partial t} = P_0 - P_R, \tag{1}$$

DIF-08-A19 135.1

Density Dependent Interactions and Structure of Charged Colloidal Dispersions in the Weak Screening Regime

L. F. Rojas-Ochoa,[1,2] R. Castañeda-Priego,[3] V. Lobaskin,[4,*] A. Stradner,[2] F. Scheffold,[2] and P. Schurtenberger[2]

[1]*Departamento de Física, Cinvestav-IPN, Av. Instituto Politécnico Nacional 2508, 07360 México D. F., Mexico*

[2]*Physics Department, University of Fribourg, Chemin de Musée 3, 1700 Fribourg, Switzerland*

[3]*Instituto de Física, Universidad de Guanajuato, Loma del Bosque 103, 37150 León, Mexico*

[4]*Physik-Department, Technische Universität München, James-Franck-Str., D-85747 Garching, Germany*

(Received 20 June 2007; published 2 May 2008)

We determine the structure of charge-stabilized colloidal suspensions at low ionic strength over an extended range of particle volume fractions using a combination of light and small angle neutron scattering experiments. The variation of the structure factor with concentration is analyzed within a one-component model of a colloidal suspension. We show that the observed structural behavior corresponds to a nonmonotonic density dependence of the colloid effective charge and the mean interparticle interaction energy. Our findings are corroborated by similar observations from primitive model computer simulations of salt-free colloidal suspensions.

DOI: 10.1103/PhysRevLett.100.178304 PACS numbers: 82.70.Dd, 61.05.fg, 61.20.Gy

Deionized colloidal dispersions have recently attracted much experimental [1–3] and theoretical attention [4–7] because of their unique role as simple model systems in the field of surface charge regulation. In addition to experimental challenges posed by these systems, such as the need of control over the ionic strength of the medium, a number of intriguing observations have been made that challenge classical theories of electrostatic screening and electrokinetics (e.g., see [1,8,9] and references therein). Some of the conceptual difficulties in the understanding of these systems stem from the counterion dominance in the ionic cloud of the colloid, which makes the screening ability of the medium dependent on the colloidal concentration. At the same time, the counterion condensation, which is controlled by the balance of the counterion chemical potential between the bulk suspension and the condensed layer, would depend on the concentration through the state-dependent screening parameters [4,10,11]. Therefore, modeling these systems within the usual one-component description can only be achieved using effective density-dependent interaction parameters, charge, and screening length [12]. The dependence of the colloid effective charge on the volume fraction [4,5,13] or background ionic strength [14] has been predicted in a few mean-field models and is expected to be nonmonotonic. However, this nonmonotonic behavior has never been validated experimentally.

In this Letter, we present a study of the density dependence of the colloidal structure and interactions at low ionic strength. Experiments have been carried out over a wider range of concentrations than in any previous work. We analyze the particle structure factor obtained from light and neutron scattering at different particle volume fractions and demonstrate that (i) the variation of colloidal structure in deionized suspensions can be interpreted in terms of a one-component model (OCM) that considers Yukawa-like pair interactions between colloids with state-dependent parameters, and (ii) the nonmonotonic concentration dependence of the interaction energy, as characterized by the colloid effective charge, is a general feature of deionized colloidal dispersions. Primitive model (PM) numerical simulations of salt-free suspensions corroborate our observations.

Stock suspensions of negatively charged particles (sulfonate polystyrene latex) were purchased from Interfacial Dynamics Corporation (Portland, USA) and master dispersions were prepared following the protocol described in Ref. [15,16]. The samples were prepared by diluting the master suspensions directly into quartz cells with water-ethanol mixtures, filtered several times (pore size 0.2 μm) to remove dust particles. These mixtures were chosen in order to avoid crystallization by modifying the solvent dielectric constant [17], thereby providing a well controlled model system of charged dispersions with volume fractions as high as ~16%. Accurate values of particle radii and polydispersities, as obtained from DLS and SANS experiments, are given in Table I.

The effective interparticle interaction can be quantified through the analysis of the suspension static structure. This requires probing length scales comparable to the size of the particles. Usually, such information can be obtained from

TABLE I. Polystyrene latex spheres used in the experiments. Bjerrum length, $\lambda_B = e^2/(4\pi\epsilon\epsilon_0 k_B T)$, from the dielectric permittivity data in Ref. [17].

Sample #	Radius (nm)	Bjerrum length (nm)	Volume fraction (%)	Scattering Technique
*S*1	54.9 ± 6.4	1.296	0.035–01.15	3D-DLS
*S*2	58.7 ± 8.6	1.383	0.135–01.48	3D-DLS
*S*3	54.7 ± 5.3	1.482	2.500–15.50	SANS

DIF-08-A20

Online Submissions: wjg.wjgnet.com
wjg@wjgnet.com
doi:10.3748/wjg.14.5707

World J Gastroenterol 2008 October 7; 14(37): 5707-5711
World Journal of Gastroenterology ISSN 1007-9327

RAPID COMMUNICATION

Effects of anatomical position on esophageal transit time: A biomagnetic diagnostic technique

Teodoro Cordova-Fraga, Modesto Sosa, Carlos Wiechers, Jose Maria De la Roca-Chiapas, Alejandro Maldonado Moreles, Jesus Bernal-Alvarado, Raquel Huerta-Franco

Teodoro Cordova-Fraga, Modesto Sosa, Carlos Wiechers, Jose Maria De la Roca-Chiapas, Alejandro Maldonado Moreles, Jesus Bernal-Alvarado, Instituto de Física, Universidad de Guanajuato, León 37150, Gto., Mexico
Raquel Huerta-Franco, Instituto de Investigaciones sobre el Trabajo, Universidad de Guanajuato, León 37150, Gto., Mexico
Author contributions: Cordova-Fraga T and Sosa M designed the study; De la Roca-Chiapas JM and Huerta-Franco R wrote the manuscript; Wiechers C, Maldonado Moreles A and Bernal-Alvarado J contributed in data collection and conducted research; Huerta-Franco R and De la Roca-Chiapas JM contributed in analytic input and data analysis.
Supported by CONACYT grant, No. J51082
Correspondence to: Jose Maria De la Roca-Chiapas, Instituto de Física, Universidad de Guanajuato, Loma del Bosque 103, Lomas del Campestre, León 37150, Gto., Mexico. joseroca@fisica.ugto.mx
Telephone: +52-477-7885100 Fax: +52-477-7885100-8410
Received: May 10, 2008 Revised: August 11, 2008
Accepted: August 18, 2008
Published online: October 7, 2008

Abstract

AIM: To study the esophageal transit time (ETT) and compare its mean value among three anatomical inclinations of the body; and to analyze the correlation of ETT to body mass index (BMI).

METHODS: A biomagnetic technique was implemented to perform this study: (1) The transit time of a magnetic marker (MM) through the esophagus was measured using two fluxgate sensors placed over the chest of 14 healthy subjects; (2) the ETT was assessed in three anatomical positions (at upright, fowler, and supine positions; 90°, 45° and 0°, respectively).

RESULTS: ANOVA and Tuckey post-hoc tests demonstrated significant differences between ETT mean of the different positions. The ETT means were 5.2 ± 1.1 s, 6.1 ± 1.5 s, and 23.6 ± 9.2 s for 90°, 45° and 0°, respectively. Pearson correlation results were r = -0.716 and $P < 0.001$ by subjects' anatomical position, and r = -0.024 and $P > 0.05$ according the subject's BMI.

CONCLUSION: We demonstrated that using this biomagnetic technique, it is possible to measure the ETT and the effects of the anatomical position on the ETT.

Key words: Transit time; Magnetic marker; Esophagus; Anatomical position; Non-invasive

Peer reviewer: Michael F Vaezi, Department of Gastroenterology and Hepatology, Vanderbilt University Medical Center, 1501 TVC, Nashville, TN 37232-5280, United States

Cordova-Fraga T, Sosa M, Wiechers C, De la Roca-Chiapas JM, Maldonado Moreles A, Bernal-Alvarado J, Huerta-Franco R. Effects of anatomical position on esophageal transit time: A biomagnetic diagnostic technique. *World J Gastroenterol* 2008; 14(37): 5707-5711 Available from: URL: http://www.wjgnet.com/1007-9327/14/5707.asp DOI: http://dx.doi.org/10.3748/wjg.14.5707

INTRODUCTION

The esophageal phase is the last phase in the swallow process; it includes the propulsion of the meal through the esophagus toward the stomach. The esophageal transit time (ETT) reported for solid and semisolid meals is between 4 and 8 s, whereas liquid ETT lasts approximately 1 to 2 s in healthy people[1]. A diagnosis of gastroesophageal reflux disease should include the presence of a pathological reflux in patients lacking another motility disorder or damage in the esophagus[2,3]. If this condition can not be met, then the evaluation should include the assessment of disintegration time of oral tablets before they enter the stomach[4]. Currently, diagnosis of gastroesophageal reflux diseases is made with endoscopy[5,6], manometry[3], imaging methods[7], impedance[8], scintigraphy[9] and other techniques[2,10]. These assessments are useful to quantify the liquid and solid volumes retained in the esophagus. Currently, the scintigraphic technique is the gold standard test accepted to assess ETT and it is indicated in cases where the manometric and barometric studies do not give a differential diagnosis[11].

The ETT assessment is used to complete the diagnosis of diseases, such as gastroesophageal reflux[12-14], dysphagia[15,16], esophagitis[17,18], and achalasia[6,19,20]. The latter studies are commonly performed with scintigraphic and manometric techniques[21], in healthy[22], geriatric[23], and pediatric patients[24], despite the use of ionizing radiation and catheters in each test, respectively. Recently, several assessments were performed using the biomagnetic technique, including gastric emptying time[25] and colon

INVESTIGACIÓN REVISTA MEXICANA DE FÍSICA 54 (2) 135–140 ABRIL 2008

Numerical simulation of the dynamical properties of the human tympanum

E. Alvarado-Anell and M. Sosa*
Instituto de Física, Universidad de Guanajuato,
Apartado Postal E-143, 37000 León, Gto., México.

M.A. Moreles
Centro de Investigación en Matemáticas,
Apartado Postal 402, 36240 Guanajuato, Gto., México.

Recibido el 26 de octubre de 2007; aceptado el 12 de febrero de 2008

A numerical simulation of the dynamical properties of the tympanic membrane is presented. A simple and different simulation of the vibratory patterns of the coupled system of the tympanum-malleus have been assessed by proposing the modeling of the tympanum through the vibrations of a forced elastic membrane, whereas the effect of the manubrium is introduced through a forced semi-membrane. We propose the superposition of these waveforms as a model for describing the vibrations of the coupled system of the tympanum-malleus. Both waveforms have analytical representations leading to simple computations. The results of the simulation for the vibrational mode (1,1) show an amplitude for the membrane larger than those for the handle of the malleus. The maximum amplitude obtained was around 1 μm, at a test frequency of 2 kHz. Also, level curves corresponding to the simulated vibrational modes were obtained. The numerical model presented can be easily handled to change input parameters, such as sound pressure and frequency. Also, other situations such as the conical shape of the tympanum or some asymmetries could be considered.

Keywords: Tympanum-malleus system; membrane vibrations; forced semi-membrane.

Una simulación numérica de las propiedades dinámicas de la membrana timpánica es presentada. Un método simple y distinto de simulación de los patrones de vibración del sistema acoplado tímpano-martillo ha sido evaluado proponiendo la modelación del tímpano a través de las vibrâciones de una membrana elástica forzada, en tanto que el efecto del mango del martillo es introducido a través de una semi-membrana. Se propóne la superposición de estos dos estados como un modelo para describir las vibraciones del sistema acoplado tímpano-martillo. Ambas soluciones tienen representaciones analíticas que llevan a cálculos computacionales simples. Los resultados de la simulación para el modo vibracional (1,1) muestran una amplitud para la membrana mayor que aquella para el mango del martillo. La máxima amplitud obtenida fue de aproximadamente 1 μm, a una frecuencia de prueba de 2 kHz. Además, curvas de nivel correspondientes a los modos vibraciones simulados fueron obtenidos. El modelo numérico presentado puede ser fácilmente manipulado para cambiar los parámetros de entrada, tales como la presión y frecuencia del sonido. Así mismo, otras situaciones tales como la forma cónica del tímpano o algunas asimetrías pudieran ser consideradas.

Descriptores: Sistema tímpano-martillo; vibraciones de membrana; semi-membrana forzada.

PACS: 01.55; 02.70; 87.15.Aa

1. Introduction

The study of the dynamics of the human tympanic membrane (TM) is essential for a better understanding of the hearing mechanism of the middle ear (ME). Experimental methods for studying the TM vibrations and the sound transmission through the normal ME have been performed on temporal bones in human cadaveric and animals, by using different experimental procedures. Simultaneously, computerized theoretical modeling of the human ME have been extensively carried out. Several pathological conditions such as stiffness, fixation of the ossicular chain, chain disarticulation, etc., have been also analyzed.

In recent years, finite-element models (FEM) of the ME have become generally used, due in part to the modern computational power and the feasibility of this technique of modeling very complex systems such as the ME.

Three-dimensional FEMs of the ME including the TM, external auditory meatus, ossicular chain, ME cavity and ME ligaments and muscles, and also morphologic data and boundary conditions have been developed [1-5].

Several FEMs have particularly emphasized the role of both the geometric and mechanical properties of the TM and the coupling of the manubrium on the eardrum. Bornitz *et al.* [6] used a FEM of the human ME for parameter estimation of the TM, by comparison of the natural frequencies and mode shapes of the TM between the model and the specimens. Drescher *et al.* [7] studied the geometric properties of a human cadaver TM specimen and its coupling with the malleus by using a finite shell model. The mechanical coupling between the TM and the manubrium was also investigated by Funnell [8]. He demonstrated the critical role of curvature in the behavior of the eardrum. Mechanical properties of the manubrium were examined by Funnell *et al.* [9] by using a FEM of a cat eardrum. They found that a significant degree of manubrial bending occurs in the model. Lesser and Williams [10] applied FEMs in a two-dimensional cross-sectional model of the TM and the malleus. The shape of the displaced TM was found to be sensitive to several factors such as the elastic modulus of the membrane and the presence and position of the rotation of the malleus. Also, Decraemer

Vol. 114 (2008) *ACTA PHYSICA POLONICA A* No. 6–A

Optical and Acoustical Methods in Science and Technology

Characterization of Metal Coated Diamond Crystallites by Combined Photoacoustic Effect and Photothermal Radiometry

I. Delgadillo-Holtfort[a], J. Gibkes[b], M. Chirtoc[c], E. Neubauer[d], B.K. Bein[b] and J. Pelzl[b]

[a]Instituto de Física de la Universidad de Guanajuato, IFUG
Apdo. E-143 León, Gto., Mexico
[b]Institut für Experimentalphysik, Ruhr-Universität, D-44801 Bochum, Germany
[c]LTP, UTAP, Université de Reims, BP 1039, 51687 Reims Cedex 2, France
[d]ARC Seibersdorf Research, Dept. Materials Research
A-2444 Seibersdorf, Austria

Photoacoustic effect and photothermal radiometry were applied to characterise the thermal properties of diamond crystallites which were coated by a Cu film, a Cr film and a Cr–Cu film. The Cu-coated diamond exhibits a considerable thermal barrier at the Cu–diamond interface which had disappeared for the crystallites with a thin bond Cr layer between diamond and Cu. The comparison of the responses of both measurement techniques reveals the non-negligible influence of the optical absorption in the visible and IR on the deduced thermal parameters.

PACS numbers: 82.47.Pm, 43.35.Ud, 78.20.Nv, 65.40.–b, 66.70.+f

1. Introduction

Diamond is the most rigid material with the highest thermal conductivity but it is an electrical insulator. By bringing together a metal and diamond a material with both a high thermal and a high electrical conduction would be achievable [1]. However, when using metal coatings, a thermal contact resistance at the interface generally occurs. One way to reduce this thermal contact resistance is to modify the interface, e.g. by using appropriate coatings. We have set up a research project to investigate the influence of Cu coatings on the thermal transport properties and optical properties of single coated diamond particles and to study the

Pattern formation and Interactions of Like-Charged Colloidal Particles at the Air/Water Interface

J. Ruiz-Garcia[1,*], B. I. Ivlev[1] and A. Gil-Villegas[2]

[1]*Instituto de Física, Universidad Autónoma de San Luis Potosí, Alvaro Obregón 64, 78000 San Luis Potosí, S.L.P., México.*
[2]*Instituto de Física, Universidad de Guanajuato, León, Guanajuato 37150, México*

Abstract. In the last decade, there have been experimental reports on the formation of colloidal mesostructures at the air/water interface. These patterns, range from the formation of transient colloidal chains and soap-froth structures that evolve to more energetically stable colloidal clusters. If the surface colloidal density is high, a crystalline-like structure can also be formed. This kind of mesostructures has been observed in particles that range in size from a few nanometers to a few microns. In the case of micron-size charged colloidal particles, the charge asymmetries on the particle's surface at the air/water interface produce the formation of dipole-dipole interaction, which should be repulsive. The formation of these mesostructures, where the equilibrium distance among particles is in the micrometer range, has been interpreted as the result of a competition between long-range repulsive and attractive interactions. Measurements of the pair interaction potential in these systems show clear evidence of micron-range attractive interactions between the colloidal particles, whose pattern formation behavior has been reproduced by computer simulations that use such micrometer range attractive interaction. However, a good theoretical understanding on the origin of the attractive component is still missing. Here, we review our main findings on these systems and we discussed them in view of recent results obtained by other groups.

Keywords: Pattern formation, Colloidal interactions, air/water interface, like-charge attractions, computer simulations
PACS: 82.70.Dd, 83.80.Hj, 81.16.Dn, 68.90.+g, 68.37.-d, 68.03.-g
***Corresponding author. E-mail:** jaime@dec1.ifisica.uaslp.mx

1. INTRODUCTION

Colloidal solutions are normally made up by particles that range in size from a few nanometer to a few microns suspended in solvent medium; smaller particles can be considered of atomic size and bigger particles, c. a. >10 μm, will easily precipitate. Many biological, natural and industrial colloidal systems are known, for example human plasma, soluble proteins, clay microplates, mineral oxides particles, micelles, polymer lattices, paints, milk, etc. In many cases, aggregation of the particles is undesirable, for example in human plasma and paints. In other processes aggregation is highly desirable, and could be promoted to accelerate the aggregation of particles, for example, in the separation by aggregation or flocculation of minerals, ceramic powder, wastewater treatment and bimolecular recovery.[2]

CP979, *Recent Developments in Physical Chemistry, 3rd Mexican Meeting on Mathematical and Experimental Physics*, edited by E. Díaz-Herrera and E. Juaristi

In order to modify the characteristics of the colloidal solution, to improve the stability or to accelerate aggregation, a good understanding of the colloidal interactions is important. Although many external factors, such as the ionic strength of the medium and impurities, can affect the stability of colloidal suspensions, the presence of ions or impurities, put on purpose or released by the container, can screen the electrostatic interactions, leading to aggregation of the particles by van der Waals forces.

The theory of Derjaguin-Landau-Verwey-Overbeek (DLVO) has been very successful to understand the stability of charged colloidal systems in bulk.[3] The DLVO theory predicts that highly charged colloidal particles will be stabilized by Coulomb interactions; this is, the mutual electrostatic repulsion among the particles stabilizes the suspension against van der Waals attractive interactions, due to the formation of a potential barrier that prevents the particles to fall at the so-called primary minimum, where they can form colloidal aggregates. The primary minimum is the global minimum of the system and therefore particle aggregates are thermodynamically stable. However, for a clean system if the thermal energy is not sufficient to make the particles to overcome the electrostatic potential barrier, a colloidal suspension can be indefinitely metastable without particle aggregation.

On the other hand, studies on the behavior of micron-size colloidal particles on interfaces have attracted much interest in the last decade, mainly due to the potential applications of these two-dimensional systems. For example, the self-assembly of nanoparticles at fluid-fluid interfaces can be used to prepare highly organized two-dimensional crystal-like structures. In particular, Langmuir balance techniques has been used to change the surface density of particles at the air/water interface and, therefore, the interparticle distance; Then the particle's monolayer can be transfer onto a solid substrate at high surface density, where a monolayer crystal is well formed.[2] In principle, a three-dimensional multilayer can be built layer-by-layer in a controlled way. Particles adsorbed at interfaces can also play an important role in industrial processes, for example, the high stability of micron-size particles at interfaces can be used to improve the stability of emulsions and foams.[3,4]

It is the stability of two-dimensional colloidal systems that has attracted the attention of many groups, and much work is being done that includes experiments, theory and simulations. Fig. 1 shows schematically how charged colloidal particles lie and interact at the air water interface.[5] Only the part of the particles that is located in the water gets charged, and due to this charge asymmetry it was proposed that the interaction can be though off of a dipole-dipole type, i. e. the interaction potential is given by $V_0(r) = \frac{2Q^2\lambda_D^2}{\varepsilon r^3}$, where $V_0(r)$ is the dipole-dipole interaction potential, Q is the number of dissociated ions, λ_D is the Debye length, and r is the separation between the particles.

Biomedical Applications of Terahertz Spectroscopy: A Brief Review

M. Vargas-Luna[a] and R. Huerta-Franco[b]

[a]*Instituto de Física, Universidad de Guanajuato, Loma del Bosque 103, Lomas del Campestre CP 37150 León Gto. México..*
[b]*Instituto de Investigaciones sobre el Trabajo,Av. Eugenio Garza Sada 530, Lomas del Campestre, CP 37150, León Gto. México*

Abstract. The Terahertz (THz) window of the electromagnetic spectrum has been partially explored but almost unexploited commercially. In recent years there has been an increased interest and a technological boost in THz research for detection systems, material characterization and imaging. Among many hot topics the researchers are interested in medical applications, and protein characterization. We present a general overview of the field showing some of the handicaps and promises of this region of the electromagnetic spectrum.

Keywords: Terahertz, medicine, biology, proteins.
PACS: 87.50.U-, 13.40.-f, 61.80.Ba, 82.50.Bc.

INTRODUCTION

The electronic technology for generation of electromagnetic radiation has its upper threshold of energy in microwaves around 50 GHz[1], being possible to get higher frequencies harmonically [2]. On the other hand, the optical technology has a low energy frontier, most far infrared sources hardly goes beyond 10 THz.

At THz frequencies the photon energies lay below the thermal noise at room temperatures, so the common alternative is the cryogenic systems (bolometer detector) working at Helium liquid temperatures.

The wavelength range that lies in between these two thresholds is low covered by either of these technologies. This is the so called THz gap.

The interest in this frequency radiation range date the end of nineteenth century [3,4]. But the lack of useful technology for generation of electromagnetic pulses with picosecond time length made the topic not to reborn until the seventies [5] creating big expectations for useful applications. In the nineties the development of coherent radiation generators and detectors in THz materialized partially these expectations [6]. From this point, researchers started to look extensively for portable devices at room temperature with sources of non negligible intensities that up to now seems to be the main handicap of the proposed methodologies for this radiation.

CP1032, *Medical Physics - Tenth Symposium on Medical Physics, edited* by G. Herrera Corral and L. M. Montaño Zetina

Application of the Optoacoustic Technique to Obtain Depth Profiles of Phantoms of Soft Tissues

M.P. Reyes-Yépez, M.E. Cano, F.M., Vargas-Luna, I. Delgadillo-Holtfort

Instituto de Física, Universidad de Guanajuato, Loma del Bosque 103, Lomas del Campestre, C.P. 37150, León, Gto.

Abstract. In this work we implemented an optoacoustic system that uses home-made acoustic transducers having PVDF of 110 μm thickness as piezosensor. The excitation source consisted of a pulsed Nd:YAG at the wavelength of 1064 nm. Soft tissue phantoms of water, gelatin and low-fat milk were used to imitate the optical properties of mammalian tissue. These phantoms were constructed containing an object with enhanced absorption optical properties. These inclusions were used to simulate abnormal tissue within the phantom. With the constructed transducers we were able to detect the inclusions of 1.64 mm thickness using an intensity of about 100 mJ/cm^2. The signal coming from the object's edge starts to be detectable at distances that are dependent of both the object's depth and the scattering properties of the phantom.

Keywords: Optoacoustic, piezoelectric transducer.
PACS: 43.35.Sx, 43.38.Fx

INTRODUCTION

Breast cancer is the third cause of death for Mexican women [1], this because its detection is first detected at advanced stages of the disease. It is well know that detection of tumors at early stages allows application of moderate and effective treatment for the patients with minimal side effects. Therefore, early tumor detection can significantly increase survival rate and substantially decrease complications associated with this disease.

In this work we focused upon applied optoacoustic technique because it seems to be a promising tool for breast cancer detection. We present the results that we obtained when used a home-made piezoelectric transducer in order to detect optoacoustic signal of an object with enhanced optical absorption coefficient inside soft tissue phantom.

PRINCIPLES OF OPTOACOUSTIC TECHNIQUE

The basic principle of optoacoustic technique is generation of transient stress in tissue under laser irradiation conditions of temporal stress confinement in the volume of diagnostic interest [2]. This condition means that laser energy is deposited upon the irradiated volume much faster than the stress resulting from thermal expansion of the irradiated volume can propagate the distance equal to desirable spatial resolution.

CP1032, *Medical Physics - Tenth Symposium on Medical Physics, edited* by G. Herrera Corral and L. M. Montaño Zetina

The absorption of la
Subsequently, thermal e
irradiated volume. When
tissue, it carries out quant
can be detected by piezo
recorded by a digital oscill

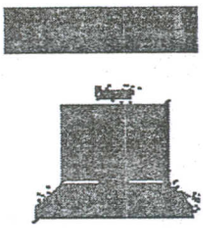

FIGURE 1. Schematic

M

A Q-switched Nd:YAG
near-infrared pulses of 1(
mJ/cm^2 approximately, w
(MPE) [3]. MPE levels ar
exposure time and pulse re

Laser-induced pressure
that use PVDF 110μm thic
signal was acquired by a d

To simulate optical pro
of water, gelatin and mill
gelatin and 100 ml of low-
attenuation coefficient, μ_{ef}
in vivo [4,5]. The phantor
moved at steps of 1 mm.

For the measurement,
aligned, whereas the phan
the phantom-transducer int

F

With the methodology
an object placed within sof

Magnetogastrography in patients with Functional Dyspepsia

De la Roca-Chiapas J M[1], Cordova-Fraga T[1], Zarate A[2], Solis Ortiz S[3] Bernal JJ[1], Vargas M[1] and Sosa M[1]

[1] Instituto de Física de la Universidad de Guanajuato,
Loma del Bosque 103, Lomas del campestre 37150, León, Guanajuato, México
[2]Unidad Médica de alta especialidad no.1 Bajío, Instituto Mexicano del Seguro Social
[3]Instituto de Investigaciones Médicas, Universidad de Guanajuato

Corresponding author: joseroca@fisica.ugto.mx

ABSTRACT

The Functional Dyspepsia is characterized by epigastric pain, postprandial inflammation, nausea and sensation of early satiety. As far as we know there are not studies to measure gastric emptying and peristaltic contractions by Magnetogastrography technique (MGG) in patients with Functional Dyspepsia. The assessment was performed in prone position, 10 minutes after the ingestion of an oral contrast, which consists of 4 g of magnetite (Fe_3O_4) diluted in a 250 g of yogurt. The patients with Functional Dyspepsia presented in average a larger gastric emptying time than those subjects without the disease ($p<0.01$).

Keyword: Magnetogastrography, gastric emptying, functional dyspepsia, peristaltic contractions.

INTRODUCTION

The activity of the stomach has been used as an important factor for clinical diagnosis in several pathologies. In particular the study of gastric emptying is used for diagnostic evaluation of gastrointestinal diseases, such as gastroparesis [1] and Functional Dyspepsia (FD) [2].

The FD is characterized by epigastric pain, postprandial inflammation, nausea and sensation of early satiety [3].

The magnetogastrography (MGG) is a non invasive and low cost method to assess gastric emptying time and the peristaltic contractions of the stomach by means of magnetic tracers. [4]

The gastric emptying time $t_{½}$ is defined as the time in which half of the gastric content is emptied. This parameter depends on the methodology and experimental conditions, for example it is reported that for liquid food (500 ml) with high caloric content, using ultrasonography in healthy subjects, this time is 67 ± 17 minutes [5] and in other work using yogurt was obtained a time of 31.3 ± 11 in healthy subjects [6].

The objective of the present study was to determine the half time of gastric emptying and the peristaltic contractions measured by MGG in people with FD compared with healthy subjects using a semisolid test meal.

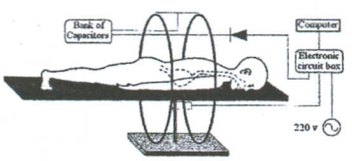

Figure1. Schematic view of the magnetogastrography technique

METHOD

The assessment was performed in a group of 10 patients diagnosed with FD with a mean age of 31.6±9.6 years and compared with a control group of 10 healthy subjects with a mean age of 25.1± 9 years. The subjects attended with overnight fasting. The assessment was performed in prone position, 10 minutes after the ingestion of an oral contrast, which consists of 4 g of magnetite (Fe_3O_4) diluted in a 250 g of yogurt. The subjects underwent a magnetic pulse of 32 mT to magnetize the magnetite and then the data collection was performed by 5 minutes to record the de-magnetization of the sample. The above procedure

DIF-08-05

Chemometric Techniques on the Analysis of Raman Spectra of Serum Blood Samples of Breast Cancer Patients

L N Rocha-Osornio[a], J. L Pichardo-Molina[a], O Barbosa-Garcia[a], C Frausto-Reyes[a] and C Araujo-Andrade[a], R Huerta-Franco, and G Gutiérrez-Juárez

[a]Centro de Investigaciones en Optica, A.P. 1-948, 3700 León Gto., Mexico.
[b]Instituto de Investigaciones Sobre el Trabajo, Universidad de Guanajuato, Lomas del Campestre, C.P. 37150 León, Gto, México

ABSTRACT

Raman spectroscopy and Multivariate methods were used to study serum blood samples of control and breast cancer patients. Blood samples were obtained from 11 patients and 12 controls from the central region of Mexico. Our results show that principal component analysis is able to discriminate serum sample of breast cancer patients from those of control group, also the loading vectors of PCA plotted as a function of Raman shift shown which bands permitted to make the maximum discrimination between both groups of samples.

Keywords: Blood, multivariate methods, principal component analysis, Raman, serum

1. INTRODUCTION

Breast cancer disease affects mainly to women population, in fact the International statistics reported from developed countries reveals that breast cancer disease has a high rate of incidence of deaths related with this disease [1]. An early detection of breast cancer can help to diminish the number of deaths related to this disease.

Currently, different imaging techniques permit to detect internal anomalies in the breast tissue; the more common techniques are X-ray imaging, ultrasound, magnetic resonance (MR), and positron emission tomography (PET) [2].

Digital mammography is the most used test for breast cancer detection; however, this technique only can offer information about the suspicious lesions in the breast, these lesions could be related or not with cancer. Therefore, the X-ray image information always is under the analysis, of the subjective interpretation of the specialist. In the case of an anomaly will be observed, a biopsy is recommended to corroborate, if it is cancer or not. The disadvantages of X-ray are: the technique not permit a permanent o continuously monitoring of patients, it can not detect small calcifications, and it is not recommended on those women who have implants. MR is a technique with high contrast and resolution, and can be used in women with implants. However, the cost of this test is very expensive for developing countries. PET is a technique with high contrast and resolution and also can be used to detect other kinds of cancers, however, PET still is an experimental technique, and few hospitals around the world have access to this equipment. On the other hand, the use of the radioactive contrast causes a constant controversy among the medical community.

As regards of it, the scientific medical community has a strong interest in developing new, more sophisticated and non-invasive techniques for detecting diseases. In the last three decades, different studies have been demonstrated that optical techniques can be a helpful on cancer detection, some of the most used are: optical coherent tomography, pulse photoacoustic, and also Fluorescence, Raman and IR spectroscopes [3]. The great advantage of the optical techniques is that they do not require the removal of tissue from the body. By illuminating a tissue sample, it is possible to get biochemical information by the interaction of the light with the tissue, light absorption, emission or scattering.

Biomedical Applications of Light Scattering II, edited by Adam Wax, Vadim Backman
Proc. of SPIE Vol. 6864, 686416, (2008) · 1605-7422/08/$18 · doi: 10.1117/12.765184

Solid Test Meal to Measure the Gastric Emptying with Magnetogastrography

MG Reynaga-Ornelas [1] , JM De la Roca-Chiapas [2]. T Cordova-Fraga [2], JJ Bernal [2], M Sosa [2].

1Facultad de Medicina, Universidad de Guanajuato, 20 de enero 929, Col Obregón, León. Gto., México

2Instituto de Física, Universidad de Guanajuato, Loma del Bosque 103, Lomas del Campestre,37150 León, Gto., México

Abstract. The gastric emptying is the time of evacuating the food ingested from the stomach to the duodenum in a controlled rate. Diverse studies express the results of the gastric emptying in form of half -time ($t_{1/2}$). The Magnetogastrography (MGG) is a biomagnetic technique that has the advantage of not being invasive, radiation free and does not interfere with the privacy of the subject. The objective was to analyze the magnetic signal of magnetic tracers mixed in a solid food to measure gastric emptying using Magnetogastrography. The ingested test meal displayed a magnetic signal, which served to obtain the signal registered by the fluxgate and the peristaltic contractions could be calculated while the stomach was emptying. The solid food product developed results to work satisfactorily in magnetogastrography.

Keywords: solid test meal, gastric emptying, magnetogastrography.
PACS: 85.70.-w, 87.61.Ff

INTRODUCTION

The gastric emptying is the time of evacuating the food ingested from the stomach to the duodenum in a controlled rate. The gastric emptying is caused by peristaltic contractions. The peristaltic waves begin in the middle of stomach in the so called pacemaker zone, transporting the mixed content to luminal and impelling the antral content towards pylorus[1]. The half time of gastric emptying is used in order to diagnose gastrointestinal disorders or to evaluate the pharmacokinetics of drugs.

Diverse studies express the results of the gastric emptying in form of half – time or average time ($t_{1/2}$) [2]. There are a great variety of methods to measure the gastric emptying like Scintigraphy in which a standardized food is administered with a isotopic marker for solids has been gotten up (usually is technetium$_{99}$) at the moment is considered as the referenced diagnostic technique in the study of the gastric emptying.

It is important to choose a defined and precise technique for the gastric emptying measurement since all known methods present advantages and disadvantages. The Magnetogastrography (MGG) is a biomagnetic technique that has the advantage of not being invasive, radiation free and does not interfere with the subject´s privacy [3].

There are multiple applications reported such as the detection of the gastrointestinal motor activity [4,5]. The gastric emptying has been reported through magnetic tracers in form of average time of gastric emptying ($t_{1/2}$), calculated by means of linear regression, as well as the results of the value of the peristaltic contractions measured with MGG in healthy voluntary men [3]. Nevertheless, diverse magnetogastrography studies used only a semisolid test meal as a vehicle to transport the magnetic tracers.

CP1032, *Medical Physics - Tenth Symposium on Medical Physics, edited* by G. Herrera Corral and L. M. Montaño Zetina

Propulsion Velocity and ETT on Biomagnetic Assessment of the Human Esophagus

T Cordova-Fraga[a], E Cano[a], C Bravo-Miranda[a], R Huerta[b], JM De la Roca-Chiapas[a], JJ Bernal[a], M Sosa[a]

[a] *Instituto de Física, Universidad de Guanajuato, Loma del Bosque 103, 37150 León, Gto., México*
[b] *Instituto de Investigaciones sobre el Trabajo*, Universidad de Guanajuato, León, Gto., México.

Abstract. Esophagus transit time measurement is a common clinical practical. Biomagnetic techniques and modern instrumentation can perform non invasive and functional assessments of the gastrointestinal tract. This study presents the evaluation of the esophagus transit time and propulsion velocity of a magnetic marker from the mouth to stomach using water vs. a swallow easy substance recently patented. A group of ten healthy subjects from 45 to 55 years, were evaluated in identical conditions for two times, they ingested randomly a magnetic marker in an anatomical body position of 45°, one times with water and the other one with a patented substance developed in order to help the subjects to swallow pills. The esophagus transit time was shorter when the subjects ingested the magnetic marker with the swallow easy substance than they ingested the magnetic marker with same quantity of water

Keywords: Esophagus transit time, biomagnetism, propulsion velocity.
PACS: 75.20.-g, 07.55.Jg, 28.41.Rc, 47.80.Cb, 96.15.Gh

INTRODUCTION

The esophagic phase is the last one in the deglution process. It includes the motion of the meal through the esophagus toward the stomach.

The clinic use of the Esophagus Transit Time (ETT) assessment helps to perform a differential diagnosis of diseases like gastroesophagic reflux [1]. Such studies are commonly performed with scintigraphy and manometry [2], despite the disadvantages of the last ones, like the use of ionizing radiation and catheters, respectively.

Besides a large number of different techniques available for ETT measurement, biomagnetism is a relative new one, which has advantages over those techniques. It lacks of ionization radiation, it is comfortable, reliable and does not invade the privacy of the patient.

There are reported multiple applications of biomagnetism for the detection of the gastrointestinal motor activity [3]. In the case of the ETT assessment, the use of a bio-susceptometer had been reported, using 5 gr of a mixture of Mn powder and ferrite ($MnFe_2O_4$), as magnetic tracer (MT) [4]. A value of 3.8 ± 0.8 s has been reported for ETT with scintigraphy, while with a biomagnetic technique, based on the use of magnetic susceptometers, has been reported 4.6 ± 0.9 s [4].

Biomagnetic techniques and modern instrumentation can perform non invasive and functional assessments of the gastrointestinal (GI) tract [4]. This study presents the evaluation of the ETT and propulsion velocity of a magnetic marker from the mouth to stomach using water vs. a swallow easy substance recently patented.

CP1032, *Medical Physics - Tenth Symposium on Medical Physics, edited* by G. Herrera Corral and L. M. Montaño Zetina

REINTEGRACION DE LA CIENCIA A LA CULTURA: TEATRO INTERACTIVO COMO MODALIDAD PARA DIVULGACION

Gustavo Jaime-Muñoz[1], Isabel Delgadillo-Holtfort[2]
Instituto de Física de la Universidad de Guanajuato
Loma del Bosque No. 103, Lomas del Campestre, C.P. 37150, León, Guanajuato, México.
[1]gustavojaimem@gmail.com, [2]delgadillo_holtfort@yahoo.de

RESUMEN:

En este trabajo se detallan en general algunas características de la propuesta de teatro interactivo con fines de divulgación, y se expone la manera en la que el grupo de divulgación al que los autores pertenecen lo ha venido llevando a cabo hasta el momento.

1. INTRODUCCIÓN:

En tiempos recientes existe la tendencia de manejar los conceptos de ciencia y cultura como cosas separadas y fundamentalmente diferentes, entendiendo como manifestaciones culturales únicamente aquellas relacionadas con las llamadas artes y humanidades. Sin embargo, tal y como el premio Nobel de Física Rudolf L. Mößbauer lo expresa al referirse de manera particular a la Física: "La Física fue, es y seguirá siendo, una parte fundamental de las ciencias naturales, una parte integral de nuestra cultura y la fundamentacion de nuestra tecnología." [1]. Para darse cuenta de lo erróneo de desvincular a la ciencia de la cultura, obsérvese simplemente la influencia que los avances tecnológicos, basados desde luego en los logros científicos, tienen en la sociedad moderna. Labor de la divulgación científica es procurar devolver a las ciencias naturales la parte que les corresponde dentro del contexto cultural.

La propuesta de mezclar el teatro con la divulgación no es algo reciente. Existe una trayectoria del teatro para la divulgación desde el siglo XXI. Sin embargo, el carácter de estas propuestas se limita a una divulgación de carácter biográfico que no se ocupa de manera central ni con los fenómenos ni con sus explicaciones.

En México, la perspectiva no es muy diferente a lo realizado a nivel mundial. Es por esto que surge la necesidad de crear, mantener mas propuestas de este tipo. De estas bases surge la idea de crear un espectáculo mágico-teatral-interactivo, con un fondo científico en donde los "trucos" presentados tienen una explicación científica, expuesta al publico *in situ* en un lenguaje accesible al tipo de auditorio presente. Es importante hacer énfasis en la importancia de no alimentar la falsa idea de que la ciencia es magia, y mucho menos que los científicos son

DIF-08-M9

Application of the Pulsed Photoacoustic Spectroscopy in Biomedicine

G. Gutiérrez-Juárez [a, b], M. J. Sims, S. K. Gupta, and J. A. Viator [b]

Department of Biological Engineering and Department of Dermatology
University of Missouri, Columbia, Missouri 65211, USA

Abstract. The use of optical spectroscopy as a diagnostic tool in biomedical applications and research has grown considerably in the last two decades. One of them is the pulsed photoacoustic or optoacoustic, which promises to be one of the most important tools for disease diagnostic studies, because while most spectroscopies exploit the optical nature of the light-tissue interaction, this field of photoacoustics uses optical energy to generate an acoustic wave which propagates in the tissue environment. The acoustic wave propagation is fundamentally related to various tissue properties and an analysis of the wave dynamics can provide insights into these properties. This work presents a review on pulsed photoacoustic spectroscopy of several photoacoustic methods to derive information about tissue and tissue phantoms.

Keywords: Photoacoustic effect, optoacoustics, biomedical instrumentation, spectroscopies.
PACS: 78.20.Hp, 43.35.Sx, 87.85.Ox, 87.80.Dj.

INTRODUCTION

The photoacoustic (PA) effect is the generation of ultrasound waves by the absorption of electromagnetic energy. All energy beams, such as those comprised of visible and infrared radiation, X rays, electrons, protons, ions and other particles, are capable of generating the PA effect when they interact with matter, however in biomedical applications the most popular method of producing PA waves is pulsed light energy. Light consists of non-ionizing radiation, which is not harmful to the human body. The advantage of photoacoustics over purely optical diagnostic methods is primarily one of the signal propagation distance and hence, the size and depth of the region under investigation. In the biological media, light propagation is dominated by scattering. The difficulty of modeling light scattering in complicated media limits the utility of optical diagnostics. A scattering coefficient in human tissue may be about 200 cm^{-1}, giving a mean free path due to scattering of a few tens of microns. For example, human skin has a scattering coefficient of about 200 cm^{-1} in the red wavelengths, while human aortic tissue has a scattering coefficient of about 300 cm^{-1} [1]. Light propagation distances greater than a few millimeters result in loss of coherence and polarization and hence the imaging ability. Acoustic wave

[a] Permanent address: Instituto de Física de la Universidad de Guanajuato, Lòma del Bosque 103, Lomas del Campestre, 37150, León, Gto. México.
[b] Authors whom correspondence should be addressed: gutierrezjuareag@missouri.edu and viatorj@missouri.edu

CP1032, *Medical Physics - Tenth Symposium on Medical Physics, edited* by G. Herrera Corral and L. M. Montaño Zetina

82.1

propagation is not affected by optically turbid media in this way. The effe acoustic wave by the turbid media is only in its generation, which is depende optical absorption. Acoustic propagation in tissue can be characterized by reflections and viscoelastic attenuation.

There are several mechanisms to generate the PA waves, however in soft t generation is the result of two different mechanisms: optical absorption fol thermal de-excitation, more precisely by thermal expansion [2]. The ther expansion mechanism is used for biomedical diagnosis for a variety of Firstly, it does not break or change the properties of the object under study. S it has a linear or a definite relationship with many of the physical parar diverse materials. And finally it is non-destructive or non-invasive in applica as materials test and medial diagnosis. Figure 1 provides a summary of th ways capable of generating PA waves, with the thermoelastic mechanism mar

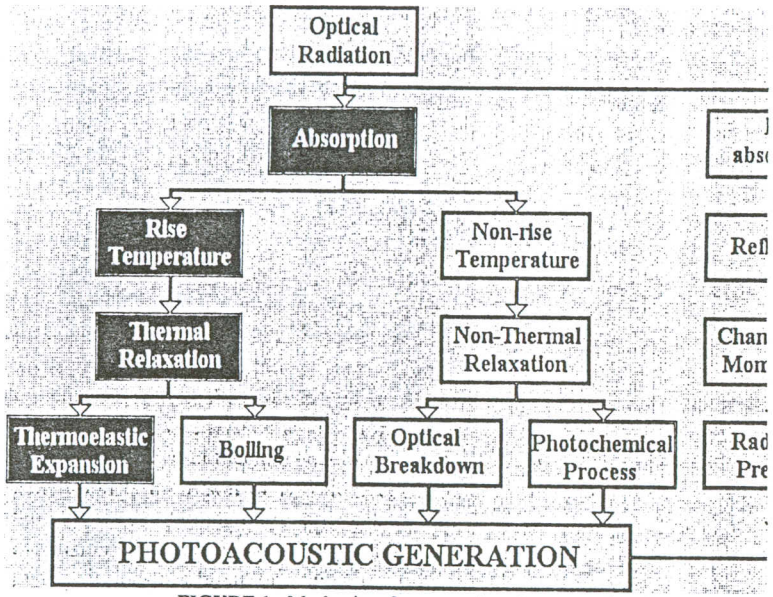

FIGURE 1: Mechanism for generating photoacoustic effect.

In order to get an efficient thermoelastic expansion two conditions must namely stress and thermal confinement. The stress and thermal confinemer that the optical pulse duration is shorter than the time required for the d energy to propagate away acoustically and thermally, respectively.

USE OF PULSED PHOTOACOUSTIC SPECTROSCOPY BIOMEDICINE

After the 19th century investigations by Bell and others, photoacoustic remained essentially dormant until the 1930's, with trace gas analysis by Vi Pfund, Luft, and others [3]. These early studies were conducted with C

83

Modeling soft matter with colloids

S. Herrera-Velarde, F. Córdoba-Valdés, J. C. Mixteco-Sánchez and R. Castañeda-Priego

Instituto de Física, Universidad de Guanajuato, Loma del Bosque 103, Loma del Campestre, 37150, León, Mexico

Abstract. Colloids are present in a large variety of biological, chemical and physical systems. In the last few years, they have been used as model systems which allow understanding fundamental processes in atomic systems or elucidating problems in soft condensed matter. The success of colloids to be used as well-controlled model systems resides in the fact that the relevant interactions between colloids are easily and independently tuneable and the colloid position is accessible by means of optical techniques, thus allowing a direct comparison with simulations and theoretical calculations. In this contribution, we briefly show the versatility of colloids as model systems to, on one hand, understand the effective interactions that emerge in soft matter physics when unobservable components of the system are integrated out or contracted of the description and, on the other hand, to quantify the effects of soft and periodic external fields on the structural and dynamics properties of many-body systems.

Keywords: Colloids, effective interactions, external fields
PACS: 82.70.Dd, 47.57.J-

INTRODUCTION

Colloids are mesoscopic objects with a size between $10nm$ to a few μm which possess, either natural or artificial, different shapes (spherical and non-spherical) and typically are dispersed in an aqueous environment [1]. Besides their industrial, chemical and biological relevance, colloids permit to highlight the basic principles and mechanisms in many-body systems, i.e., complex fluids, with competing attractive and repulsive interactions. By adjusting the type of interaction between colloids, a rich variety of ergodic and non-ergodic transitions can be observed. Moreover, colloidal dispersions under external fields (or substrates) have illustrated the importance of the ordering and dynamics of atomic systems on surfaces such as atomic monolayers [2]. From experimental point of view, particle-particle and particle-substrate can be both realized in a large variety and modified continuously [3]. These extraordinary experimental features together with the striking advantage that inherent properties can be studied simultaneously with complementary methods, such as theory and computer simulations, make to colloids to be considered as excellent model systems for soft condensed matter.

In this paper, we briefly discuss the effective interactions that emerge in soft matter physics when unobservable components of the system are integrated out or contracted of the description. Also, we study the effects of soft and periodic external fields on the structure and dynamics of many-body systems. In particular, in section II we investigate the depletion forces between two large hard-colloids immersed in a bath of small hard-colloids [4]; we basically emphasize the role of bridge functions on the depletion

CP979, *Recent Developments in Physical Chemistry, 3rd Mexican Meeting on Mathematical and Experimental Physics*, edited by E. Díaz-Herrera and E. Juaristi

REFERENCES

1. R. J. Nordstrom, L. Burke, J. M. Niloff, and J. F. Myrtle, *Lasers Surg. Med.* **29**, 118-127 (2001).
2. M. G. Muller, T. A. Valdez, I. Georgakoudi, V. Backman, et al,, *Cancer* **97**, 1681-1692 (2003).
3. B. C. Wilson, ', Optical-Thermal Response of Laser-Irradiated Tissue, A. J. Welch and M. J. C. van Gemert, Eds., Plenum Press, New York (1995).
4. T. Joshua Pfefer, L. Stephanie Matchette, Carrie L. Bennett et al. *J. Biomed. Opt.* **8**, 206-215 (2003)
5. Q. Liu and N. Ramanujam, *J. Opt. Soc. Am. A* **24**, 4, (2007).
6. M. C. Skala, G. M. Palmer, K. M. Vrotsos, A. Gendron-Fitzpatrick, and N. Ramanujam, *Opt. Express* **15**, 7863-7875 (2007.)
   and applications (Wiley, New York, 1984).
7. G. M. Palmer, C. Zhu, T. M. Breslin, F. Xu, K. W. Gilchrist, and N. Ramanujam, *IEEE Trans. Biomed. Eng.* **50** (11), 1233Ũ1242 (2003).
8. W. M. Lin, X. Yuan, P. Yuen, W. I. Wei, et al., *J. Biomed. Opt.* **9**(1),180-186 (2004).
9. T. J. Farrel, B. C. Wilson, M. S Patterson. *Phys. Med. Biol.***12**(37), 2281-2286 (1992)
10. K. Hoffman, T. Gambichler, A. Rick, M. Kreutz, M. Anscheutz, et al., *Br. J. Dermatol.* **149**, 801-809 (2003).

82.2

DIF-08-411

Photoacoustic Characterization of Human Skin Phantom with Superficial Anomalies: Preliminary Results

R. Pérez-Solano [a], F. J. Cervantes-Lozano [a], R. Chiu-Zarate [b], R. Huerta-Franco [c], and G. Gutiérrez-Juárez [a, 1]

[a] *Instituto de Física de la Universidad de Guanajuato, Lomas del Bosque, 103, Lomas del Campestre, 37150, León, Gto., México.*
[b] *Centro Universitario de los Lagos, Universidad de Guadalajara, Enrique Díaz de León s/n. Paseos de la Montaña. Lagos de Moreno, Jalisco*
[c] *Instituto de Investigaciones sobre el Trabajo, Universidad de Guanajuato, Eugenio Garza Sada 572, Lomas del Campestre, 37150, León Gto. México*

Abstract. Pulsed photoacoustic characterization of a human skin phantom with superficial anomalies has been done with a homemade sensor. The sensor was done with a PVDF film and was used in the backward detection mode. The phantoms were agar gelatin slabs with the thickness of 100 mm and superficial anomalies were simulated by plastic spheres immersed in the slabs. The sensitivity and resolution of the sensor to measure buried anomalies it is reported.

Keywords: Photoacoustic effect, optoacoustics, biomedical instrumentation.
PACS: 78.20.Hp, 43.35.Sx, 87.85.Ox.

INTRODUCTION

The availability of lasers suitable for inducing acoustic waves in tissue and the need for new diagnostic methods has made photoacoustics a field rich in innovation in the use of laser induced acoustic waves, mainly in PA imaging [1]. In the field of biomedical imaging, this is dominated by radiographic methods, which utilizes ionizing radiation as the probing means. Other imaging methods include magnetic resonance imaging, nuclear medicine imaging, and ultrasound imaging [2]. While these modalities are successful, mature technologies, there exist short comings in each area. Some of these short comings may be appropriately addressed by photoacoustic (PA) imaging, particularly in applications that target specific regions on the centimeter scale, while requiring spatial resolution on the order of tens of microns. There are two ways for the detection of the PA effect, directly by using piezoelectric transducers or indirectly by optical methods [1, 3]. In this report we present a characterization of a skin phantom with superficial anomalies, which was done with a homemade PA probe based in PVDF piezoeletric transducer.

[1] Authors whom correspondence should be addressed: perez200787@yahoo.com.mx, ggul@fisica.ugto.mx

CP1032, *Medical Physics - Tenth Symposium on Medical Physics, edited* by G. Herrera Corral and L. M. Montaño Zetina

Registration of Intravascular Pressure Curves: Magneto-Mechanical Evaluation

Maldonado-Moreles, Martín A.; Córdova-Fraga, T.; Cano, M. E.; Solorio-Meza, Sergio E.; Sosa, M. A.

MEDICAL PHYSICS: Tenth Mexican Symposium on Medical Physics. AIP Conference Proceedings, Volume 1032, pp. 302-305 (2008).

In this work, graphs of the intravascular blood pressures at both the left primitive carotid artery and the left jugular vein are presented, by using a ``magneto-mechanical'' technique with pulse-pressure gauge, a device designed especially to register the magnetic flux variability of a magnetic marker placed superficially on the skin over a blood vessel. It is presented the implementation of a device used for registration of the magnetic induction generated by the periodical movements of a magnetic marker (MM) by using a magnetoresistive transductor, which is placed superficially on the skin (non-invasive) over a blood vessel, at the cervical level in the path of the left carotid, identified by the amplitude of the arterial pulse.

Keywords: Blood flow in cardiovascular system, Blood-brain barrier, General theory and mathematical aspects, Therapeutic applications, Medical imaging: general
DOI: 10.1063/1.2979298

Biomagnetic Signals of the Large Intestine

Cordova, T.; Bradshaw, L. A.; Adilton, A.; Sosa, M.

MEDICAL PHYSICS: Tenth Mexican Symposium on Medical Physics. AIP Conference Proceedings, Volume 1032, pp. 37-44 (2008).

Large intestine is part of the gastrointestinal tract with an average length, in adults, of 1.5 m. The gold standard technique in clinical medicine is the colonoscopy. Nevertheless, other techniques are capable of presenting information on physiological processes which take place in this part of the gastrointestinal system. Three recent studies are discussed in this paper in order to make this information more widely available. The authors consider that the biomagnetic technique could be easily implemented in hospitals around the world. Options will be available for research and clinical medicine.

Keywords: Superconducting quantum interference devices, Magnetic resonance imaging, Ionizing-radiation therapy physics, Radiation treatment, Magnetometers for magnetic field measurements
DOI: 10.1063/1.2979301

Revista Mexicana de Cardiología

Volumen 20, Número 1
Enero - Marzo 2009
pp 29 - 34

Anexo 134.2

DIF-09-A0

Investigación experimental

Instrumentación y uso de un dispositivo para medir actividad eléctrica de corazón y estómago

Hernández-Ledezma FU,* Córdova-Fraga T,* Hernández-González MA,** Vargas-Luna M,* Cano ME,*** De la Roca-Chiapas JM,* Solorio S**

RESUMEN

Introducción: Al igual que el corazón, el estómago posee su propio marcapasos en donde se genera un pulso eléctrico regular y recurrente llamado ritmo eléctrico basal (REB) de alrededor de 3 ciclos por minuto (cpm). **Objetivo:** Presentar una modalidad de medición simultánea o por separado de electrocardiografía y electrogastrografía en un solo dispositivo portátil, inalámbrico y de bajo costo. **Material y métodos:** Medición simultánea de actividad eléctrica gástrica (AEG) y la actividad eléctrica de corazón en estado pre y postprandial en sujetos jóvenes y sanos. **Resultados:** Con el dispositivo que se presenta se han realizado estudios para la obtención, en el caso del corazón, del complejo P-QRS-T y se ha obtenido actividad eléctrica de la región gástrica; los resultados obtenidos en sujetos jóvenes y sanos en estado pre y postprandial, midiendo simultáneamente con dicho dispositivo han sido equivalentes a dispositivos comerciales para el mismo fin. **Discusión:** El dispositivo presentado por ser portátil, de bajo costo y con capacidad de ser inalámbrico, se plantea como posible aplicación en clínica y en hospitales. Las aplicaciones son diversas, como el monitoreo de pacientes diabéticos con neuropatía. La opción de tener en forma simultánea ambas mediciones hace más atractivo el dispositivo para uso extensivo.

Palabras clave: Electrocardiografía, electrogastrografía, dispositivo portátil.

ABSTRACT

Introduction: *Similar than what happens in the heart, the stomach has its own pacemaker in which a electrical signal called basal electrical rhythm, is generated at a rate of 3 cpm.* ***Objective:*** *To have in a single, low cost, portable and wireless device, the capability of evaluating electrogastrography and electrocardiography either simultaneously or separately.* ***Materials and methods:*** *Simultaneous evaluation of electrical activity of the heart and stomach in a pre and post-prandial state protocol.* ***Results:*** *With the device presented in this work we have evaluated heart activity obtaining P-QRS-T complex. Also the same apparatus has the capability of evaluating electrical activity of the gastric region in a pre and post-prandial conditions protocol.* ***Discussion:*** *We suggest the clinical application of this device in clinics and hospitals for monitoring diabetic patients with neuropathy. The device is portable with the option if wireless data transmission of heart or/and stomach electrical activity.*

Key words: *Electrocardiography, electrogastrography, portable device.*

Acrónimos

ECG = Electrocàrdiograma.
REB = Ritmo eléctrico basal.
cpm = Ciclos por minuto.
AEG = Actividad eléctrica gástrica.
ECGf = Electrocardiógrafo.
EGGf = Electrogastrógrafo.

Trabajo ganador del 2° lugar Premio Dr. Mariano Ledesma al Investigador Joven. XIII Congreso Nacional, Asociación Nacional de Cardiólogos, Guadalajara, Jal., octubre 2008.

* Instituto de Física, Universidad de Guanajuato.
** Instituto Mexicano del Seguro Social, Hospital UMAE No. 1 Bajío.
*** Centro Universitario de la Ciénega, Universidad de Guadalajara.

INTRODUCCIÓN

Las contracciones rítmicas del corazón están controladas por una serie ordenada de descargas eléctricas que en sujetos sanos poseen aproximadamente la misma forma, dándole el nombre de complejo P-QRS-T. Al registro en el tiempo del complejo P-QRS-T se le llama electrocardiograma (ECG). Como el corazón, el estómago posee su propio marcapasos generador de un ritmo eléctrico regular y recurrente llamado ritmo eléctrico basal (REB) u onda lenta de 3 ciclos por minuto (cpm), lo cual produce las contracciones peristálticas gástricas. Aquí se identifican tres estados particulares, ayuno, postprandial y neuro-hormonal.[1,2] Mediante

Medical Engineering & Physics 31 (2009) 770–774

Contents lists available at ScienceDirect

Medical Engineering & Physics

journal homepage: www.elsevier.com/locate/medengphy

Use of short-term bio-impedance for gastric motility assessment

R. Huerta-Franco [a,*], M. Vargas-Luna [b], E. Hernandez [b], K. Capaccione [c], T. Cordova [b]

[a] Department of Labor Research and Applied Science, DCS, Campus-León, The University of Guanajuato, Av Eugenio Garza Sada 572, Lomas del Campestre, 37150 Leon Gto, Mexico
[b] Department of Engineering Physics, DCI, Campus-León, The University of Guanajuato, Loma del Bosque 103, Lomas del Campestre, 37150 Leon Gto, Mexico
[c] College of Arts and Science, New York University, 100 Wasington Square East, New York, NY 10003, USA

ARTICLE INFO

Article history:
Received 24 June 2008
Received in revised form 13 February 2009
Accepted 16 February 2009

PACS:
87.00.00
87.61.Tg
87.19.xu
87.19.rf

Keywords:
Gastric
Motility
Emptying
Bio-impedance
Time domain

ABSTRACT

Gastric motility (GM) has been assessed using bio-impedance (BI) techniques in the time domain using short term recordings and analyzing mainly the median of the area under the fast Fourier transform (FFT) spectra. The BI technique has been applied to the gastric system mainly for gastric emptying (GE) studies. However, gastric motility evaluation using BI has not been fully implemented. In this study, we propose the use of the BI technique for the evaluation of gastric motility considering global features of the fast FFT spectra. The study was performed in eleven healthy subjects who were evaluated in fasting and postprandial conditions. The results indicate that the use of the median of the area under the FFT spectra is equivalent to the use of the main peak of the spectra to determine the changes in gastric motility from the fasting to the postprandial state. This demonstrates that BI is a valid technique for gastric motility evaluation in short time recordings.

1. Introduction

The mechanical movement of the stomach or gastric motility (GM) consists of peristaltic waves caused by ring contractions through the distal gastric wall due to mioelectrical activity. The gastric mioelectrical activity has an average frequency of three cycles per minute (cpm), 2.5–3.75 cpm in normal conditions [1]; GM has similar frequency due to such stimulation [2]. Frequencies of GM higher than 3.75 cpm are considered as a tachygastric condition. Similarly, lower frequencies for GM are known as bradygastria (<2.5 cpm). The purpose of these gastric movements is to facilitate food processing and gastric emptying (GE). Both phenomena, GM and GE, have been monitored in clinical settings, using a great variety of methods. For example, in the assessment of the GE, one of the most common methods used is scintigraphy. This method has become the gold standard for GE assessment, and in this way could be considered an indirect method of measuring GM [3]. Among the direct techniques, antro duodenal manometry uses a catheter with pressure sensors to measure the intensity and frequency of motility in a specific region of the gastrointestinal (GI) tract. Electrogastrography records myoelectrical impulses through cutaneous or internal sensors on either side of the gastric wall. Manometry and electrogastrography have been compared [4] and show poor correlation over time due to the fact that the electrical impulses do not always result in movement. Ultrasonography is another technique used for the measurement of GM and GE. It works best when used to assess the passage of liquids, but has the advantage of being non-invasive [3]. In both GM and GE assessments, the balance between invasiveness and sensitivity is not always easy to maintain. Currently, the techniques to evaluate GE and GM are active areas of research [5,6].

In the evaluation of GM and GE, the bio-impedance (BI) technique may be a useful method for clinical assessment because it is non-invasive, easy to administer, and straightforward to interpret. Both epigastric impedance and electrogastrography generate a data set consisting of information from the whole GI sensitive region. In the BI technique, the conductivity and resistivity are used as the principal variables. This technique has been reported [7] for GE assessments since 1985. These GE evaluations using the BI technique are performed during long and continuous periods of time, recording the amplitude of the impedance or conductance of the gastric region by assessing its general behavior over time. Although

* Corresponding author at: Instituto de Investigaciones Sobre el Trabajo, Universidad de Guanajuato, Av Eugenio Garza Sada 572, Lomas del Campestre, 37150 León Gto, Mexico. Tel.: +52 477 718 4721; fax: +52 477 773 7037.
E-mail address: huertafranco@hotmail.com (R. Huerta-Franco).

1350-4533/$ – see front matter © 2009 IPEM. Published by Elsevier Ltd. All rights reserved.
doi:10.1016/j.medengphy.2009.02.008

Dynamic Arrest in Charged Colloidal Systems Exhibiting Large-Scale Structural Heterogeneities

C. Haro-Pérez,[1,*] L. F. Rojas-Ochoa,[2] R. Castañeda-Priego,[3] M. Quesada-Pérez,[4] J. Callejas-Fernández,[1] R. Hidalgo-Álvarez,[1] and V. Trappe[5,†]

[1]*Grupo de Física de Fluidos y Biocoloides, Departamento de Física Aplicada, Universidad de Granada, 18071 Granada, Spain*
[2]*Departamento de Física, Cinvestav-IPN, 07360 México Distrito Federal, Mexico*
[3]*Instituto de Física, Universidad de Guanajuato, 37150 León, Mexico*
[4]*Departamento de Física, Escuela Politécnica Superior de Linares, Universidad de Jaén, 23700 Linares, Spain*
[5]*Département de Physique, Université de Fribourg, 1700 Fribourg, Switzerland*

(Received 8 March 2008; revised manuscript received 9 September 2008; published 5 January 2009)

Suspensions of charged liposomes are found to exhibit typical features of strongly repulsive fluid systems at short length scales, while exhibiting structural heterogeneities at larger length scales that are characteristic of attractive systems. We model the static structure factor of these systems using effective pair interaction potentials composed of a long-range attraction and a shorter range repulsion. Our modeling of the static structure yields conditions for dynamically arrested states at larger volume fractions, which we find to agree with the experimentally observed dynamics.

DOI: 10.1103/PhysRevLett.102.018301 PACS numbers: 82.70.Dd, 81.05.Kf

Charged colloids have been extensively used as model systems to study the static and dynamic properties of strongly interacting particles in both in- and out-of-equilibrium states [1]. In many cases their phase behavior could be described by the well established Derjaguin-Landau-Verwey-Overbeek theory [2]; a theory that considers the interactions between charged colloids to be determined by repulsive screened Coulomb interactions. More recently, however, experimental and theoretical investigations of highly charged colloidal suspensions showed evidence for the existence of effective long-range attractions between like-charged particles (for a review see [3]). In particular, structural investigations reporting gas-crystal and gas-liquid coexistence associated to the formation of voids [4] led to controversial discussions on the limitation of the Derjaguin-Landau-Verwey-Overbeek theory. Despite the enhanced efforts in understanding the origin of these phenomena, our comprehension of the phase behavior of highly charged colloidal systems remains far from complete. In particular, implications of effective attractions on the dynamical properties of charged colloids remain to be addressed.

In this Letter we report on an experimental investigation of the volume fraction dependent structural and dynamic properties of charged liposome suspensions at quasideionized conditions. For all volume fractions investigated, the suspensions are characterized by structural heterogeneities at large length scales, while exhibiting typical features of strongly repulsive, disordered fluid systems at shorter length scales. We successfully model the static structure factor by effective pair interaction potentials that comprise a long-range attraction and a shorter range repulsion. This modeling reveals an unusual development of the effective particle-particle interactions with volume fraction. In particular, the position of the repulsive barrier ceases to decrease at large volume fractions, which causes a dynamic arrest of the system. Our findings indicate that in highly charged colloidal systems the formation of structural heterogeneities and the dynamic arrest have a common origin.

Our liposomes are composed of phosphatidylserine (PS) and egg phosphatidylcholine (PC) at a ratio of PS/PC ~ 1. They are prepared by using the technique described in Ref. [5], yielding unilamellar vesicles with a mean diameter of $d = 120 \pm 12$ nm as determined by static and dynamic light scattering. For the pH conditions used in this study (pH ~ 7) the zwitterionic phospholipid PC is uncharged, such that the total surface charge of the liposome is determined by the monovalent ionic phospholipid PS. We estimate the number of dissociated charges to be $\sim$2000 electrons per particle. Because of the small size and high surface charge, shape fluctuations are insignificant, such that our vesicles can be considered as charged spherical colloids. We prepare suspensions with volume fractions ranging from $\phi = 0.009$ to $\phi = 0.12$. To ensure the lowest possible ionic strength, we seal the suspensions in contact with a mixed bed of ion exchanger resin in cylindrical quartz cells 5 days prior to our light scattering experiments. Such treatment with an ionic exchange resin results for pure water in a reduction of the ionic strength from 10^{-5} to $10^{-6}M$. None of our samples exhibit the typical iridescence, which is usually observed when charged colloids organize into crystals at low ionic strength. Instead, for ϕ up to 0.06 we observe that the viscosity gradually increases during a few hours after the liposome dispersion has been put into contact with the resin. For the two largest ϕ investigated, $\phi = 0.09$ and $\phi = 0.12$, we find a strikingly different behavior. Shaking up the just prepared mixture of dispersion and resin transforms the sample into an elastic solid that withstands even rigorous shaking. Upon addition of a small quantity of a

Anexo 135.3

DIF-09-A05

International Journal of Bioelectromagnetism
Vol. 11, No. 1, pp. 54 - 58, 2009

www.ijbem.org

Arterial tension throughout the cardiac cycle: Bioelectromagnetic Assessment

T Cordova[a], M A Maldonado[a], J Castro[a], M E Cano[b], S Solorio[c], M A Hernandez[c], M Sosa[a], J J Bernal[a], R Huerta-Franco[d], Gavin O'Mahony[e] and M Vargas[a]

[a]Dept. Ingeniería Física DCI-Leon, Universidad de Guanajuato, Leon, Gto., Mexico.
[b]Centro Universitario de la Ciénega, Universidad de Guadalajara campus-Ocotlan, Jal. Mexico
[c]Unidad Medica de Alta Especialidad-IMSS-T1 Leon, Gto., Mexico.
[d]Dept. de Ciencias Aplicadas al Trabajo DCI-Leon, Universidad de Guanajuato, Leon, Gto., Mexico.
[e]Lenox Hill Hospital, New York City, NY, USA

Corresponding author: theo@fisica.ugto.mx, phone 52+477 788-5100, exts: Office 8454, fax 8410, Lab 8475

Abstract. Presented here is a method for using magnetism to record the cardiac cycle in humans. The study was performed in a shielded room using a magnetometer magnetoresistor and a magnetic marker. A group of fifteen subjects were simultaneously evaluated using this biomagnetic modality and also a standard electrocardiogram. The morphology of the curves obtained were analysed and the cardiac cycle was identified. This biomagnetic modality is capable of recording a graphic representation of arterial pressure in humans. It, therefore, could be implemented in the hospital setting for non-invasive real time continuous monitoring of blood pressure over protracted periods.

Keywords: magnetioresistor, magnetic marker, arterial pressure, electrocardigram, catheterism.

1. Background

Blood pressure (BP) is defined as the force exerted by circulating blood on the walls of the body's arteries and constitutes one of the principal clinical vital signs. Arterial pressure is most commonly measured via a sphygmomanometer device [Pannier et al., 2002]. For each heartbeat, BP varies between systolic and diastolic pressures. The systolic pressure is the peak pressure in the arteries, which occurs early in the cardiac cycle when the ventricles are contracting. Diastolic BP is the minimum pressure in the arteries, and occurs late in the cardiac cycle when the ventricles are filled with blood, see Fig 1. An invasive technique for assessment the BP, consists of a procedure in which the BP is measured inside the blood vessel using an intra-arterial catheter connected to a sensitive pressure transducer. Although invasive, this procedure is considered the gold standard technique for measuring arterial pressure because it is more accurate than sphygomanometry [Kurtz et al., 2005] and can be used to detect rapid variations in BP.

Recently, a new method using a magnetic device for recording arterial pressure has been implemented in our laboratory. This is being tested and correlated with several devices used in clinical medicine, in particular with electrocardiography. A graphical analysis of both bio-magnetically recorded carotid arterial waveform and standard electrocardiogram is presented in this study.

2. Material and Methods

Biomagnetism has different sources, natural and artificial. The latter is used when a biomagnetic signal is too weak to be recorded using a magnetic sensor that operates at room temperature. The specific modality used in this study was the use of a magnetic marker attached to the skin of a volunteer's neck.

Throughout the procedure all subjects were in the supine position, see Fig. 1, as previously reported [Maldonado-Moreles *et al.*, 2008]. Assuming magnetic dipole behavior, equation (1); the signal from the magnetic marker was recorded with a magnetoresistor magnetometer in an unshielded room, equipped with an electronic circuit and a LabVIEW platform.

DIF-09-A06

International Journal of Bioelectromagnetism www.ijbem.org
Vol. 11, No. 1, pp. 54 - 58, 2009

Arterial tension throughout the cardiac cycle: Bioelectromagnetic Assessment

T Cordova[a], M A Maldonado[a], J Castro[a], M E Cano[b], S Solorio[c], M A Hernandez[c], M Sosa[a], J J Bernal[a], R Huerta-Franco[d], Gavin O'Mahony[e] and M Vargas[a]

[a]*Dept. Ingeniería Física DCI-Leon, Universidad de Guanajuato, Leon, Gto., Mexico.*
[b]*Centro Universitario de la Ciénega, Universidad de Guadalajara campus-Ocotlan, Jal. Mexico*
[c]*Unidad Medica de Alta Especialidad-IMSS-T1 Leon, Gto., Mexico.*
[d]*Dept. de Ciencias Aplicadas al Trabajo DCI-Leon, Universidad de Guanajuato, Leon, Gto., Mexico.*
[e]*Lenox Hill Hospital, New York City, NY, USA*

Corresponding author: theo@fisica.ugto.mx, phone 52+477 788-5100, exts: Office 8454, fax 8410, Lab 8475

Abstract. Presented here is a method for using magnetism to record the cardiac cycle in humans. The study was performed in a shielded room using a magnetometer magnetoresistor and a magnetic marker. A group of fifteen subjects were simultaneously evaluated using this biomagnetic modality and also a standard electrocardiogram. The morphology of the curves obtained were analysed and the cardiac cycle was identified. This biomagnetic modality is capable of recording a graphic representation of arterial pressure in humans. It, therefore, could be implemented in the hospital setting for non-invasive real time continuous monitoring of blood pressure over protracted periods.

Keywords: magnetioresistor, magnetic marker, arterial pressure, electrocardigram, catheterism.

1. Background

Blood pressure (BP) is defined as the force exerted by circulating blood on the walls of the body's arteries and constitutes one of the principal clinical vital signs. Arterial pressure is most commonly measured via a sphygmomanometer device [Pannier et al., 2002]. For each heartbeat, BP varies between systolic and diastolic pressures. The systolic pressure is the peak pressure in the arteries, which occurs early in the cardiac cycle when the ventricles are contracting. Diastolic BP is the minimum pressure in the arteries, and occurs late in the cardiac cycle when the ventricles are filled with blood, see Fig 1. An invasive technique for assessment the BP, consists of a procedure in which the BP is measured inside the blood vessel using an intra-arterial catheter connected to a sensitive pressure transducer. Although invasive, this procedure is considered the gold standard technique for measuring arterial pressure because it is more accurate than sphygomanometry [Kurtz et al., 2005] and can be used to detect rapid variations in BP.

Recently, a new method using a magnetic device for recording arterial pressure has been implemented in our laboratory. This is being tested and correlated with several devices used in clinical medicine, in particular with electrocardiography. A graphical analysis of both bio-magnetically recorded carotid arterial waveform and standard electrocardiogram is presented in this study.

2. Material and Methods

Biomagnetism has different sources, natural and artificial. The latter is used when a biomagnetic signal is too weak to be recorded using a magnetic sensor that operates at room temperature. The specific modality used in this study was the use of a magnetic marker attached to the skin of a volunteer's neck.

Throughout the procedure all subjects were in the supine position, see Fig. 1, as previously reported [Maldonado-Moreles *et al.*, 2008]. Assuming magnetic dipole behavior, equation (1); the signal from the magnetic marker was recorded with a magnetoresistor magnetometer in an unshielded room, equipped with an electronic circuit and a LabVIEW platform.

Diffusion in two-dimensional colloidal systems on periodic substrates

Salvador Herrera-Velarde and Ramón Castañeda-Priego*

Instituto de Física, Universidad de Guanajuato, Loma del Bosque 103, Col. Lomas del Campestre, 37150 León, Guanajuato, Mexico

(Received 8 August 2008; revised manuscript received 9 March 2009; published 27 April 2009)

We study the diffusive behavior of two-dimensional charged colloidal suspensions subjected to a sinusoidal substrate by means of Brownian dynamics simulations. We mainly focus on the dependence of the mean-square displacement on the substrate strength. Our findings show a variation in the particle diffusion due to a substrate-induced distortion of the dynamic cage of nearest-neighbor colloids. This mechanism leads to a transition from normal diffusion at short times to subdiffusion on intermediate time scales. However, at long times normal diffusion is recovered. We also show that the variation in the long-time self-diffusion coefficient may be associated with the freezing and re-entrant melting transitions.

DOI: 10.1103/PhysRevE.79.041407 PACS number(s): 82.70.−y, 61.20.−p

I. INTRODUCTION

The study of transport properties in restricted dimensions is crucial to understand dynamical processes that occur in confinement conditions. For example, studies of Brownian particles in narrow channels, where no mutual passage is possible, have elucidated the activation of dynamic modes responsible for a subdiffusive process known as single-file diffusion [1–4]. Also, the study of the dynamical properties of noninteracting particles on solid surfaces has explained the anomalous diffusion in crystalline substrates [5,6]. Furthermore, the dynamics of biological motors and macromolecules occurs usually under confinement, i.e., heterogeneous substrates or cell membranes [7,8].

Generally speaking, the dynamics in confinement depends on the substrate-particle interaction, i.e., the topology of the substrate, the particle-particle interaction, temperature, and particle density. Basically, both interactions define the energetic landscape where particles diffuse. In atomic systems, it is difficult to quantify such energetic landscape. However, micron-sized particles, i.e., colloids, are ideal candidates for studying diffusion of interacting particles in external potentials since the energetic landscape can be easily controlled [9]. In particular, in the last few years two-dimensional (2D) colloidal systems created artificially by confining the colloids between two glass plates or two media (e.g., air-water interface) [10,11] have served as fascinating and well-controlled model systems to study phenomena such as freezing [12], the controversial chargelike attraction [13], and many-body effective interactions [14], among others.

From both theoretical and experimental points of view, the 2D colloidal systems exposed to periodic laser fields have been the focus of extensive investigations. Since the pioneering work of Chowdhury *et al.* [15], such systems have been found to exhibit a rich phase behavior with a solidlike order that depends on both the suspension properties and the substrate parameters, e.g., strength and periodicity [16,17]. Related research also deals with topics such as strain-induced domain formation [18], laser-induced freezing (LIF), and melting [19–23].

Although the phase behavior of 2D colloids exposed to light forces is well understood, less is known about the corresponding dynamical properties. A few works reported in such direction show a rich variety of pinned and dynamic states including pinned smectic, pinned buckled, two-phase flow, and moving partially ordered structures [24,25]. Nonetheless, the dependence of the mean-square displacement (MSD) on the substrate strength has not been analyzed in detail. The MSD is a suitable quantity for studying the dynamical behavior at different time scales. Recently, the MSD of a single Brownian particle in random and quasicrystalline potentials has been investigated [26]. Interestingly, Schmiedeberg *et al.* [26] demonstrated that although quasicrystalline potentials exhibit long-range positional order the nonequilibrium Brownian motion is very similar to the motion in a random substrate.

In this work, the MSD $[W(t)]$ of charged colloids in monolayers subjected to sinusoidal-like substrates with a commensurability ratio $p=1$ is measured by means of Brownian dynamics (BD) simulations. With the increasing of the substrate strength, we observe a transition from normal diffusion, $W(t) \propto t$, at short times to subdiffusion at intermediate times, $W(t) \propto t^{\alpha}$, described by a variable exponent α. Such transition is explained in terms of a substrate-induced distortion of the dynamic cage of nearest-neighbor colloids. At long times normal diffusion is recovered, i.e., $\alpha=1$, with a self-diffusion coefficient that varies with the substrate strength and becomes smaller than that of the free-particle diffusion coefficient. We particularly show that the variation in the MSD at long times may be associated with the freezing and the re-entrant melting transitions [15,20,22].

The paper is organized as follows. In Sec. II, we describe the two-dimensional colloidal model system and the Brownian dynamics simulation technique. We also review the structural and dynamic properties in the substrate-free case. In Sec. III, the MSD and the average energy per particle as function of the substrate strength are discussed. Finally, the paper ends with concluding remarks.

II. MODEL SYSTEM, BROWNIAN DYNAMICS SIMULATION, AND SUBSTRATE-FREE CASE

A. Model system and Brownian dynamics simulation

Let us consider a two-dimensional system consisting of N particles and a particle number density $\rho=N/A$, with A being

*ramoncp@fisica.ugto.mx

DIF-09-A08

Anexo 134.1

INSTRUMENTACION REVISTA MEXICANA DE FÍSICA 55 (2) 145–148 ABRIL 2009

A methodology to measure the volume of spheroid and oblong solid bodies based on artificial vision technique

T. Cordova-Fraga[a], J. Bernal-Alvarado[a], J.C. Martinez[a,b], M. Sosa[a], M. Vargas[a], E. Hernandez[a], and R. Huerta[c]

[a] *Physics Institute, University of Guanajuato, Loma del Bosque 103, Leon, Gto., 37150, México, e-mail: bernal@fisica.ugto.mx*

[b] *Centro de Bachillerato Tecnológico Industrial y de Servicios, No. 225, Prolongación Avellano s/n, 37140 Leon Gto., México.*

[c] *Work Research Institute, University of Guanajuato, Av. Eugenio Garza Sada 572, Leon, Gto., 37157, México.*

Recibido el 16 de mayo de 2008; aceptado el 02 de marzo de 2009

A methodology for assessing the volume of spheroid and oblong solid bodies is presented. Samples were mounted on a revolving platform that was driven by a computer-controlled stepping motor. Four hundred views (photographs) of each sample were acquired as they were uniformly rotated in the azimuth direction. The image processing was based on the artificial vision technique called *segmentation*. Using the information of the instantaneous radius and the small angle of rotation in each step, the numerical integration of the volume was performed. Images were captured using a CCD camera and the entire system was controlled by a routine developed in LabVIEW™ 6.1. Two sets of geometrical bodies (polystyrene cylinders and spheres) and three kinds of biological samples were measured. For the sake of comparison, each body was also measured by means of both a micrometric caliper and the displaced volume of water inside a vessel. The ANOVA correlation parameters between the proposed methodology and the hydrostatic procedure were found to be: $r = 0.9924$ and $p = 0.0001$, with $\alpha = 0.05$. The coincidence between the results obtained with artificial vision and the hydrostatic technique was greater than 98% for spheres and cylinders. On the other hand, it was only up to 95% for the samples with non-regular shaped bodies (chicken hearts, kidneys and carrots). The purpose of the paper is to discuss in detail a simple technique which could be of interest to students of science and engineering.

Keywords: Artificial vision; volume assessment; image processing.

Una metodología para evaluar el volumen de cuerpos sólidos esferoidales y oblongos es presentada. Las muestras fueron montadas en una plataforma giratoria, manejada por un motor de paso controlado por una computadora. 400 vistas (fotografías) de cada muestra fueron adquiridas a medida que ellas fueron uniformemente rotadas en la dirección azimutal. El procesamiento de imagen estuvo basado en la técnica de visión artificial llamada *segmentación*. Usando la información del radio instantáneo y el pequeño ángulo de rotación en cada etapa, la integración numérica del volumen fue desarrollada. Las imágenes fueron capturadas usando una cámara CCD y el sistema completo fue controlado por una rutina desarrollada en LabVIEW™ 6.1. Dos conjuntos de cuerpos geométricos (cilindros y esferas de poliestireno) y tres clases de muestras biológicas fueron medidos. Para fines de comparación, cada cuerpo fue también medido por medio de un pie de rey micrométrico, así como el volumen de agua desplazada dentro de un envase. Los siguientes parámetros de correlación ANOVA entre la metodología propuesta y el procedimiento hidrostático fueron encontrados: $r = 0.9924$ y $p = 0.0001$, con $\alpha = 0.05$. La coincidencia entre los resultados obtenidos con vision artificial y la técnica hidrostática fue mayor a 98% para esferas y cilindros. Por otro lado, fue de alrededor de 95% para las muestras con cuerpos de forma irregular (corazones de pollo, riñones y zanahorias). El propósito del artículo es discutir con detalle una técnica simple la cual pudiera ser de interés para estudiantes de ciencias e ingeniería.

Descriptores: Visión artificial; evaluación de volumen; procesamiento de imagen.

PACS: 01.50.hv; 01.50.Lc; 07.05.Rm

1. Introduction

The assessment of body volumes is a routine procedure of interest in a variety of applications. In particular, the determination of the volume of some organs or parts of the body by using images obtained with different techniques such as magnetic resonance imaging [1], X-ray absorptiometry [2], computed tomography [3,4], etc, is a common practice in medicine. Also, a procedure to measure solid body volumes directly, in several fields of science, is the hydrostatic weighing (HW) technique [5], currently considered a *gold standard*. On the other hand, the artificial vision (AV) technique is an important research field in the recognizing of geometrical patterns and shapes to reconstruct volumes [6-8]. In this paper, a methodology to measure volumes of solid bodies with spheroid and oblong shapes is implemented. It is based on the automatic acquisition of images by means of AV techniques, using a personal computer (PC), a charge coupled device camera (CCDc) and a LabView™ 6.1 (LV) programming environment.

2. Material and methods

2.1. Mathematical algorithm

An algorithm for numerical integration was implemented in a program written on LV platform. Also, a system of AV was

DIF-09-A09

Anexo 135.1

Online Submissions: wjg.wjgnet.com
wjg@wjgnet.com
doi:10.3748/wjg.15.4763

World J Gastroenterol 2009 October 14; 15(38): 4763-4769
World Journal of Gastroenterology ISSN 1007-9327

BRIEF ARTICLES

Effects of metoclopramide on gastric motility measured by short-term bio-impedance

María-Raquel Huerta-Franco, Miguel Vargas-Luna, Kathleen M Capaccione, Etna Yañez-Roldán, Ulises Hernández-Ledezma, Ismael Morales-Mata, Teodoro Córdova-Fraga

María-Raquel Huerta-Franco, Ismael Morales-Mata, Department of Applied Science and Labor Research, DCS-Campus León, University of Guanajuato, Av. Eugenio Garza Sada 572, Colonia Lomas del Campestre, 37150 León Gto, México

Miguel Vargas-Luna, Etna Yañez-Roldán, Ulises Hernández-Ledezma, Teodoro Córdova-Fraga, Department of Physical Engineering, DCI-Campus León, University of Guanajuato, Lomas del Bosque 103, Lomas del Campestre, 37150 León Gto, México

Kathleen M Capaccione, Robert Wood Johnson Medical School, The University of Medicine and Dentistry of New Jersey, 675 Hoes Lane, Piscataway, NJ 08854-5635, United States

Author contributions: Huerta-Franco MR and Vargas-Luna M designed the study, carried out measurements, data analysis, interpretation and drafting of the manuscript; Capaccione KM performed measurements and drafting of the manuscript; Yañez-Roldán E performed measurements and data analysis; Hernández-Ledezma U contributed to software design; Morales-Mata I contributed to hardware design; Córdova-Fraga T contributed to data analysis and interpretation.

Supported by A grant from CONACYT (J50182), The University of Guanajuato (DINPO 00098-08) and the Dean's Undergraduate Research Fund from The College of Arts and Science, New York University

Correspondence to: María-Raquel Huerta-Franco, MD, PhD, Department of Applied Science and Labor Research, DCS-Campus León, University of Guanajuato, Av. Eugenio Garza Sada 572, Colonia Lomas del Campestre, 37150 León Gto, México. huertafranco@hotmail.com
Telephone: +52-477-7184721 Fax: +52-477-7184721
Received: June 6, 2009 Revised: August 26, 2009
Accepted: September 1, 2009
Published online: October 14, 2009

Abstract

AIM: To analyze the accuracy of short-term bio-impedance as a means of measuring gastric motility.

METHODS: We evaluated differences in the short-term electrical bio-impedance signal from the gastric region in the following conditions: (1) fasting state, (2) after the administration of metoclopramide (a drug that induces an increase in gastric motility) and (3) after food ingestion in 23 healthy volunteers. We recorded the real component of the electrical impedance signal from the gastric region for 1000 s. We performed a Fast Fourier Transform (FFT) on this data and then compared the signal among the fasting, medicated, and postprandial conditions using the median of the area under the curve, the relative area under the curve and the main peak activity.

RESULTS: The median of the area under the curve of the frequency range in the region between 2-8 cycles per minute (cpm) decreased from 4.7 cpm in the fasting condition to 4.0 cpm in the medicated state (t = 3.32, P = 0.004). This concurred with the decrease seen in the relative area under the FFT curve in the region from 4 to 8 cpm from 38.3% to 26.6% (t = 2.81, P = 0.012) and the increase in area in the region from 2 to 4 cpm from 22.4% to 27.7%, respectively (t = -2.5, P = 0.022). Finally the main peak position also decreased in the region from 2 to 8 cpm. Main peak activity in the fasting state was 4.72 cpm and declined to 3.45 cpm in the medicated state (t = 2.47, P = 0.025). There was a decrease from the fasting state to the postprandial state at 3.02 cpm (t = 4.0, P = 0.0013).

CONCLUSION: Short-term electrical bio-impedance can assess gastric motility changes in individuals experiencing gastric stress by analyzing the area medians and relative areas under the FFT curve.

Key words: Bio-impedance; Fast Fourier Transform; Gastric motility; Metoclopramide; Postprandial

Peer reviewer: Atsushi Nakajima, Professor, Division of Gastroenterology, Yokohama City University Graduate School of Medicine, 3-9 Fuku-ura, Kanazawa-ku, Yokohama 236-0004, Japan

Huerta-Franco MR, Vargas-Luna M, Capaccione KM, Yañez-Roldán E, Hernández-Ledezma U, Morales-Mata I, Córdova-Fraga T. Effects of metoclopramide on gastric motility measured by short-term bio-impedance. *World J Gastroenterol* 2009; 15(38): 4763-4769 Available from: URL: http://www.wjgnet.com/1007-9327/15/4763.asp DOI: http://dx.doi.org/10.3748/wjg.15.4763

Fluid Phase Equilibria 286 (2009) 113–119

Contents lists available at ScienceDirect

Fluid Phase Equilibria

journal homepage: www.elsevier.com/locate/fluid

Predicting adsorption isotherms of asphaltenes in porous materials

Martín Castro[a], José L. Mendoza de la Cruz[a], Eduardo Buenrostro-Gonzalez[a], Simón López-Ramírez[a], Alejandro Gil-Villegas[b,*]

[a] Instituto Mexicano del Petróleo, Eje Central Lázaro Cárdenas Norte 152, Col. San Bartolo Atepehuacán, C.P. 07730 México, D.F., Mexico
[b] Departamento de Ingeniería Física, DCI Campus León de la Universidad de Guanajuato, Lomas del Bosque 103, Colonia Lomas del Campestre, León, Guanajuato, C.P. 37150 México, Mexico

ARTICLE INFO

Article history:
Received 26 February 2009
Received in revised form 17 July 2009
Accepted 13 August 2009
Available online 22 August 2009

Keywords:
SAFT-VR
Adsorption isotherms
Porous materials
Asphaltenes

ABSTRACT

In this paper we present a molecular thermodynamics approach for the modeling of adsorption isotherms of asphaltenes adsorbed on Berea sandstone, Bedford limestone and dolomite rock, using a model for bulk asphaltenes precipitation and a quasi-two-dimensional approach for confined fluids [E. Buenrostro-González, C. Lira-Galeana, A. Gil-Villegas, J. Wu, AIChE J., 50 (2004) 2552–2570; A. Martínez, M. Castro, C. McCabe A. Gil-Villegas, J. Chem. Phys. 126 (2007) 074707, respectively], both based on the Statistical Associating Fluid Theory for Potentials of Variable Range [A. Gil-Villegas, A. Galindo, P.J. Whitehead, S.J. Mills, G. Jackson, A.N. Burgess, J. Chem. Phys. 106 (1997) 4168–4186]. The theory is applied to model adsorption isotherms from experimental data of asphaltenes extracted from a dead sample of heavy crude oil from a Mexican reservoir. The theoretical results give the right Langmuir Type II adsorption isotherms observed experimentally. The model requires the determination of ten molecular parameters related to the size of the particles and the square-well potentials used to describe the particle–surface and particle–particle interactions at the bulk and adsorbed phases. Nine parameters are taken from previous published results about the behavior of asphaltenes in bulk phases and the adsorption of several molecular fluids onto activated carbon and graphite surfaces. The remaining parameter, the energy strength of the particle–surface interaction, is adjusted to reproduce the experimental data, obtaining values that are consistent with Molecular Mechanics calculations for asphaltenes adsorbed on different surfaces and solutions. Although the agreement between theory and experiments shows some deviations at low bulk concentrations, the model reproduces adsorption data at high concentrations where other semi-empirical approaches fail.

1. Introduction

Asphaltenes adsorption on reservoir rocks modifies the relative proportions of the total pores surface area which are in contact with the formation fluids [1,2], and reservoir wettability is a major factor controlling the location, fluid distribution, and flow properties of the system [3,4]. The subject of surfactant adsorption on polar surfaces from non-polar and weakly polar non-aqueous solutions is largely unexplored [5], and in the case of adsorption of asphaltenes, the nature of those processes is still not understood [1,6–9].

The liquid phase adsorption is a very complex phenomenon due to the presence of solvent molecules, formation of molecular aggregates, irregular packing and multilayer coverage [8,10]. In the case of asphaltenes, the extent of their adsorption on mineral surfaces relies on an important way on their tendency to aggregate and separate from the crude oil in response to changes in oil solvency.

Asphaltenes are the most heavy and polar fraction in the crude oil. The asphaltene fraction is formed by many series of relatively large molecules containing aromatic rings, several heteroaromatic and napthenic ring plus relatively short paraffinic branches [11,12]. The adsorption of asphaltenes on solids is the result of favorable interactions of the asphaltene species or its aggregates with chemical species on or near the mineral surface. Different interparticle forces are responsible of this effect, individually or due to the interplay between them. The major forces that can contribute to the adsorption process are electrostatic, charge transfer, van der Waals, hydrogen-bonding and steric interactions [4,13,14].

Adsorption of asphaltenes on various dry mineral surfaces has been the subject of many investigations [15]. As a result of these studies, both monolayer [1–4,16–18] and multilayer [4,5,7,8] adsorption behavior have been reported, depending on the solvent and source of asphaltenes used in experiments. For studies

* Corresponding author. Tel.: +52 4777885100x8415; fax: +52 4777885100x8410.
E-mail addresses: mgcastro13@gmail.com (M. Castro), jlmendoz@imp.mx (J.L.M. de la Cruz), ebuenro@imp.mx (E. Buenrostro-Gonzalez), slopezr@imp.mx (S. López-Ramírez), gil@fisica.ugto.mx (A. Gil-Villegas).

0378-3812/$ – see front matter © 2009 Elsevier B.V. All rights reserved.
doi:10.1016/j.fluid.2009.08.009

High Resolution Electronic Spectroscopy of *o*- and *m*-Toluidine in the Gas Phase. Barrier Height Determinations for the Methyl Group Torsional Motions†

Philip J. Morgan, Leonardo Alvarez-Valtierra,‡ and David W. Pratt*

Department of Chemistry, University of Pittsburgh, Pittsburgh, Pennsylvania 15260

Received: April 30, 2009; Revised Manuscript Received: June 4, 2009

High resolution electronic spectra of *o*- and *m*-toluidine have each been recorded for the $S_1 \leftarrow S_0$ origin band transitions of the isolated molecules. Each spectrum is split into two sub-bands owing to tunneling motions along the methyl group torsional coordinate. Analyses of these data provide information about the preferred configurations of the methyl groups and the barriers opposing their motions in both the ground and excited electronic states. Despite their apparent similarities, the experiments reveal that these properties are quite different in the two molecules. Possible reasons for this behavior are discussed.

I. Introduction

The subject of internal rotation has been studied extensively for many years, especially concerning molecules containing an attached methyl group.[1−8] Of particular interest is the effect that different neighboring groups have on the potential barrier heights of a methyl group attached to a benzene ring. In toluene itself, internal rotation of the methyl group is relatively free in both the ground electronic state (S_0) and the lowest excited electronic state (S_1). The measured barriers are ∼5 and ∼25 cm^{-1}, respectively.[6] However, substitution of a second ring hydrogen atom with a methoxy group changes this situation dramatically. A recent study of 2- and 3-methylanisole[7] showed that the methyl group internal motions are significantly more rigid in one of the electronic states and less rigid in the other, with the corresponding barriers depending on the positions of the two groups relative to one another.

In this contribution, we report on a similar study of 2- and 3-methylaniline (*o*- and *m*-toluidine) in which an amino group replaces the methoxy group in the methylanisoles. This problem has been addressed before by Ito and co-workers[2] using low resolution fluorescence excitation spectroscopy (FES). These studies showed that the potential barrier of the methyl rotor in *o*-toluidine is very large in the ground state but very small in the first excited electronic state. The opposite behavior was observed for *m*-toluidine with nearly free internal rotation in the ground state and much more rigid internal rotation in the excited state. Okuyama et al.[2] found no change in conformation of the methyl group upon excitation in either *o*- or *m*-toluidine. It is the goal of the present work to determine if these conclusions are correct and to explore in greater detail the factors that might be responsible for these remarkable effects. Our tool is high resolution FES, as in the case of the methylanisoles.[7]

II. Experimental Section

Both *o*-toluidine and *m*-toluidine were purchased from Sigma Aldrich and used as received. Rotationally resolved $S_1 \leftarrow S_0$ excitation spectra were recorded using the molecular beam laser spectrometer described elsewhere.[9] Briefly, samples were heated to ∼45 °C in a quartz source, seeded in dry argon gas (>90% purity), and then expanded through a 240 μm tip nozzle. The expansion was skimmed ∼2 cm downstream with a 1 mm diameter skimmer to form a molecular beam and then crossed 15 cm downstream of the nozzle with a laser beam operating in the UV. The laser radiation was generated by a ring dye laser operating in the visible (Rhodamine 590 dye) whose output was externally doubled using a Wavetrain frequency doubler (572 and 600 BBO nm crystals) to produce ∼2 mW of UV radiation with a line width of ∼1 MHz. Fluorescence was collected with spatially selective optics and detected by a photon counting system and a PMT. All spectra were recorded using the jba95 data acquisition software.[10] Typical scan lengths were 4 cm^{-1} over 1000 s. The I_2 absorption spectrum was used to determine the absolute transition frequencies of the excitation spectrum to an accuracy of ±30 MHz. A stabilized etalon was used to produce relative frequency markers having a mode-matched free spectral range of 599.5040 ± 0.0010 MHz in the UV, corresponding to a free spectral range of 299.7520 ± 0.0005 MHz in the visible. The resulting spectra were fit using the jb95 least-squares fitting program.[11]

Theoretical calculations were performed using the Gaussian 03 suite of programs[12] to supplement the experiments. Geometry optimizations of both *o*-toluidine and *m*-toluidine in the ground state were performed at the MP2 level of theory with a 6-31G** basis set. Configuration interaction singles (CIS) calculations with a 6-31G** basis set were performed on the excited state.

III. Results

Figure 1 shows the vibrationally resolved fluorescence excitation spectra of *o*-toluidine and *m*-toluidine obtained by Ito and co-workers.[5] In this figure, a labeling scheme of the vibrational bands $0a_1$, 1e, 2e, and so forth is used where a number indexes the upper state torsional levels and a letter designates their symmetries. In the infinite barrier limit, the levels $0a_1$ and 1e, 2e and $3a_1$, and so forth are degenerate. Reduction of this barrier leads to a methyl group tunneling motion that lifts the degeneracy of the $0a_1$, 1e; 2e, $3a_1$; and so forth levels in both electronic states. The origin band of *o*-toluidine appears at 34316.9 cm^{-1}, red shifted with respect to toluene by more than 3000 cm^{-1}. The origin band of *m*-toluidine is red shifted by an even larger amount, appearing at 33820.2 cm^{-1}. As assigned by Okuyama et al.,[4] the 1e band

† Part of the "Robert W. Field Festschrift".

* To whom correspondence should be addressed. E-mail: pratt@pitt.edu.

‡ Present address: División de Ciencias e Ingenierías, Universidad de Guanajuato, Campus León. León, Gto. 37150, México.

10.1021/jp904023x CCC: $40.75
Published on Web 07/01/2009

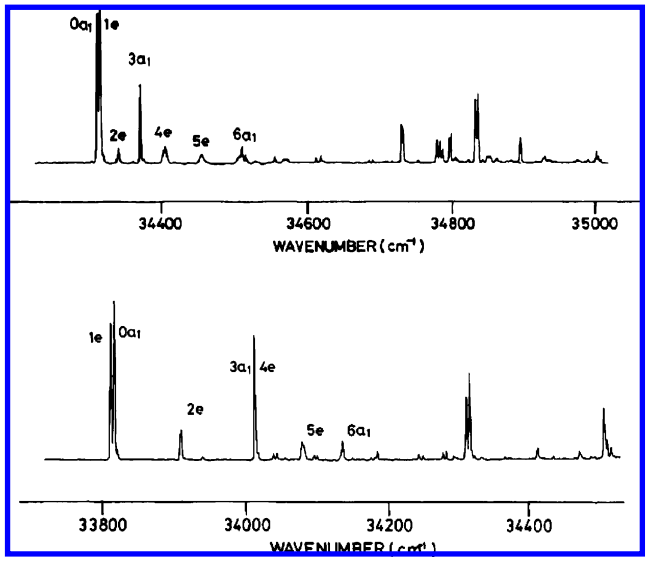

Figure 1. Vibrationally resolved fluorescence excitation spectra of *o*-toluidine (top) and *m*-toluidine (bottom) (ref 2).

is blue shifted with respect to the $0a_1$ band for *o*-toluidine but is red-shifted with respect to the $0a_1$ band for *m*-toluidine. These assignments suggest that the potential barriers for the methyl group torsional motion in both electronic states are significantly influenced by the relative positions of the methyl and amino groups on the benzene ring.

High resolution experiments have been performed to validate these conclusions. Figure 2 shows the rotationally resolved $S_1 \leftarrow S_0$ fluorescence excitation spectrum of band $0a_1$ in *o*-toluidine. The spectrum spans approximately 2.9 cm^{-1} and exhibits both *a*- and *b*-type transitions. The spectrum was fit using rigid-rotor Hamiltonians[13] for both electronic states, confirming its identity as the $0a_1$ vibronic band. First, a simulated spectrum was generated using estimated rotational constants from the ab initio calculations. Single transitions from the simulated spectrum were then assigned to corresponding transitions in the experimental spectrum, using the fitting program jb95.[11] A linear least-squares fitting procedure was finally used to optimize the rotational constants from a comparison of the observed and calculated transitions. The bottom of Figure 2 shows a portion of the fit spectrum, where a standard deviation of 1.40 MHz was obtained by fitting 135 lines. The band was found to be a hybrid band, having 59% *a*-type and 41% *b*-type transition character. The spectrum was fit using a Voigt line shape profile for individual transitions with Gaussian widths of 20 MHz and Lorentzian widths of 38 MHz, corresponding to a fluorescence lifetime of $\tau = 4.2$ ns. Table 1 lists all of the inertial parameters obtained from the fit of the spectrum.

TABLE 1: Rotational Constants of *o*-Toluidine in Its Ground and Excited Electronic States[a]

parameter	*o*-toluidine $0a_1$	*o*-toluidine 1e[b]	theoretical[c]
A'' (MHz)	3230.9 (1)	3228.5 (1)	3243.6
B'' (MHz)	2189.0 (1)	2189.1 (1)	2185.9
C'' (MHz)	1316.8 (1)	1316.9 (1)	1318.7
ΔA (MHz)	−74.3 (1)	−113.4 (1)	−91.5
ΔB (MHz)	−1.8 (1)	−8.3 (1)	21.1
ΔC (MHz)	−20.8 (1)	−20.5 (1)	−9.8
$\Delta I''$ (amu Å^2)	−3.51	−3.65	−3.77
$\Delta I'$ (amu Å^2)	−1.21	−4.15	−3.21
TM angle to *a*-inertial axis	±40(2)°	±40(2)°	+42°

[a] Numbers in parentheses are the standard deviations of the last significant figure. [b] See Table 3 for additional information about the first-order torsion-rotation perturbation coefficients that were used in the fit of this spectrum. [c] Geometry optimization calculations done at the MP2/6-31G** and CIS/6-31G** levels of theory.

Band 1e of *o*-toluidine located at 34320.2 cm^{-1} is shown in Figure 3 and spans approximately 2.8 cm^{-1}. Unlike the $0a_1$ band in this molecule, the high resolution spectrum of the 1e band in *o*-toluidine exhibits further splittings of the individual rovibronic transitions into two components. This confirms its identity as the 1e band. The normally degenerate rovibronic transitions in this band are coupled by the torsion-rotation interaction, leading to a K-dependent splitting in the high resolution spectrum.[14] These splittings are described by the

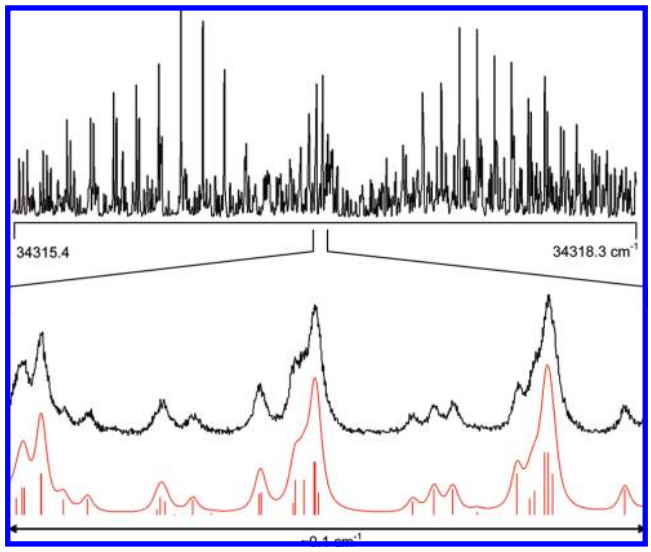

Figure 2. Rotationally resolved fluorescence excitation spectrum of the $0a_1$ band of *o*-toluidine with origin at 34316.9 cm^{-1}. The lower part of the figure shows an expanded view of the Q-branch region. In this view, the upper trace is the experimental spectrum, and the lower trace is the simulated spectrum. Individual lines represent the transitions responsible for the spectrum. The band was fit using a Voigt line shape profile.

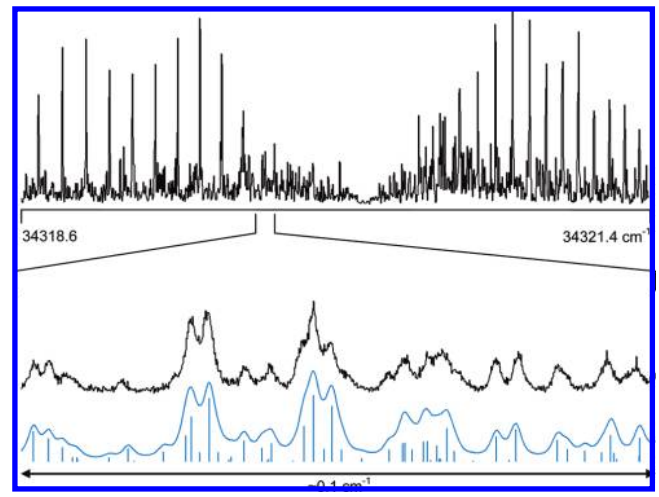

Figure 3. Rotationally resolved fluorescence excitation spectrum of the 1e band of *o*-toluidine with origin at 34320.2 cm^{-1}. The lower part of the figure shows an expanded view of the P-branch region. In this view, the upper trace is the experimental spectrum, and the lower trace is the simulated spectrum. Individual lines represent the transitions responsible for the spectrum. The band was fit using a Voigt line shape profile.

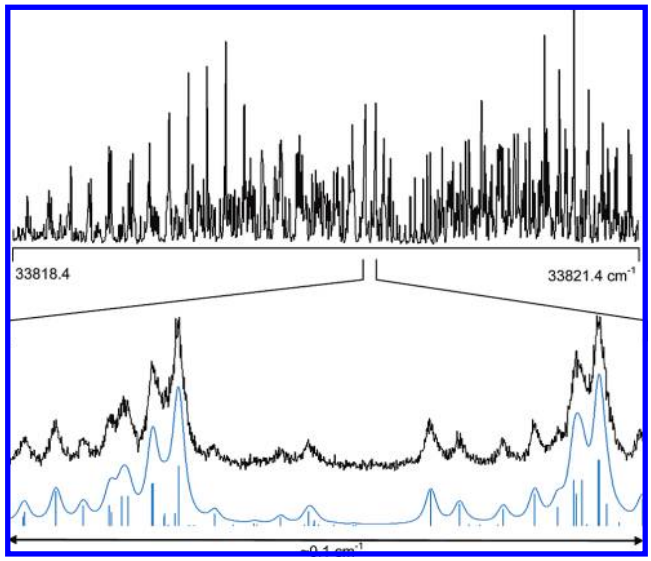

Figure 4. Rotationally resolved fluorescence excitation spectrum of the $0a_1$ band of *m*-toluidine with origin at 33820.2 cm^{-1}. The lower part of the figure shows an expanded view of the Q-branch region. In this view, the upper trace is the experimental spectrum, and the lower trace is the simulated spectrum. Individual lines represent the transitions responsible for the spectrum. The band was fit using a Voigt line shape profile.

following "non-rigid" rotor Hamiltonian for both electronic states:[3,13]

$$H_{\mathrm{eff}}^{\mathrm{E}} = A_{\mathrm{E}}P_a^2 + B_{\mathrm{E}}P_b^2 + CP_c^2 + FW_{\mathrm{E}}^{(1)}(\rho_a P_a + \rho_b P_b) \quad (1)$$

Here, A_{E} and B_{E} are the effective rotational constants given by

$$A_{\mathrm{E}} = A + FW_{\mathrm{E}}^{(2)}\rho_a^2, \qquad B_{\mathrm{E}} = B + FW_{\mathrm{E}}^{(2)}\rho_b^2 \quad (2)$$

F is the internal rotor constant, $W_{\mathrm{E}}^{(1)}$and $W_{\mathrm{E}}^{(2)}$ are the first- and second-order perturbation terms, first written down by Herschbach,[15] and ρ_a and ρ_b are weighted direction cosines of the angle between the axis of internal rotation and the *a*- and *b*-inertial axes of the molecule, where $\rho_a = \lambda_a(I_\alpha/I_a)$. I_α is the moment of inertia of the methyl group, and r is a reduction factor

$$r = 1 - \sum(\lambda_g^2 I_\alpha/I_g), \quad g = a, b, c \quad (3)$$

A portion of the fit spectrum of the 1e band of *o*-toluidine is shown at the bottom of Figure 3; a standard deviation of 7.82 MHz was obtained from a fit of 100 lines. The inertial parameters obtained from the fit of the spectrum are also listed in Table 1. The inertial parameters obtained for the 1e band of *o*-toluidine are consistent with those obtained by Kalkman and Meerts.[16]

The rotationally resolved spectrum of the $0a_1$ band of *m*-toluidine spans approximately 3.0 cm^{-1} and is shown in Figure 4. No additional splittings appear in this spectrum. Hence, it was fit using rigid-rotor Hamiltonians for both electronic states, confirming its identity as an a_1 vibronic band. The bottom of Figure 4 shows a portion of the fit at full experimental resolution; 153 lines were assigned and a standard deviation of 1.73 MHz was obtained. The spectrum was again fit with a Voigt line shape profile with Gaussian widths of 20 MHz and

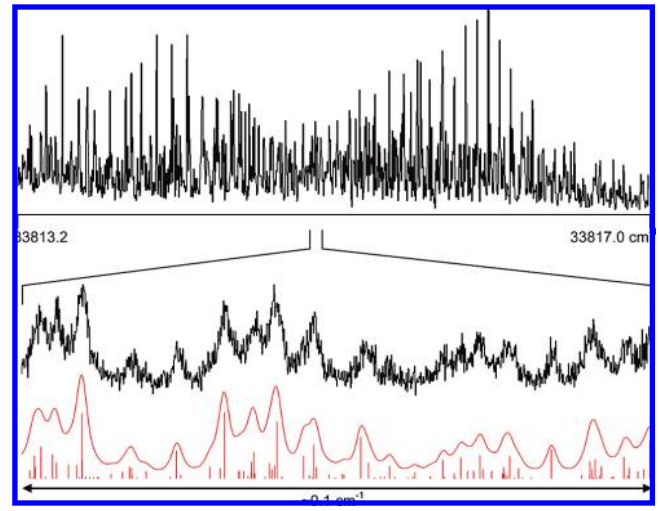

Figure 5. Rotationally resolved fluorescence excitation spectrum of the 1e band of *m*-toluidine with origin at 33814.9 cm^{-1}. The lower part of the figure shows an expanded view of the Q-branch region. In this view, the upper trace is the experimental spectrum, and the lower trace is the simulated spectrum. Individual lines represent the transitions responsible for the spectrum. The band was fit using a Voigt line shape profile.

Lorentzian widths of 38 MHz, corresponding to a lifetime of $\tau = 4.2$ ns. The origin band of *m*-toluidine was also found to be as hybrid band with 48% *a*-type and 52% *b*-type transition character. The inertial parameters obtained from the fit of the spectrum are listed in Table 2.

Figure 5 shows the rotationally resolved spectrum of the 1e band of *m*-toluidine located at 33814.9 cm^{-1}. As in the case of the 1e band for *o*-toluidine, this band could not be fit using a rigid-rotor Hamiltonian and required the addition of perturbation terms. This is again a result of the torsion-rotation interaction lifting the degeneracies of certain rovibronic transitions, confirming the identity of this vibronic band as the 1e band. The Hamiltonian in eq 1 was again used to obtain a fit with a standard deviation of 3.24 MHz for the 115 assigned lines. A comparison of the simulated spectrum to the experimental shows excellent agreement and can be seen in the bottom of Figure 5. The inertial parameters obtained from the fit are also listed in Table 2. Neither 1e band required the use of Watson distortion terms in the fit.[17]

IV. Discussion

4.1. Ground and Excited State Conformers. Tables 1 and 2 list the ground and excited state rotational constants for both

TABLE 2: Rotational Constants of *m*-Toluidine in Its Ground and Excited Electronic States[a]

parameter	*m*-toluidine $0a_1$	*m*-toluidine 1e[b]	theoretical[c]
A'' (MHz)	3701.3 (1)	3700.2 (1)	3637.7
B'' (MHz)	1795.9 (1)	1795.4 (1)	1796.3
C'' (MHz)	1210.4 (1)	1210.3 (1)	1211.5
ΔA (MHz)	−164.7 (1)	−164.9 (1)	−46.5
ΔB (MHz)	−7.1 (1)	−7.0 (1)	9.0
ΔC (MHz)	−12.9 (1)	−12.9 (1)	−1.3
$\Delta I''$ (amu Å^2)	−0.414	−0.508	−3.12
$\Delta I'$ (amu Å^2)	−3.40	−3.50	−3.06
TM angle to *a*-inertial axis	±46(2)°	±46(2)°	+45°

[a] Numbers in parentheses are the standard deviations of the last significant figure. [b] See Table 3 for additional information about the first-order torsion-rotation perturbation coefficients that were used in the fit of this spectrum. [c] Geometry optimization calculation done at the MP2/6-31G** and CIS/6-31G** levels of theory.

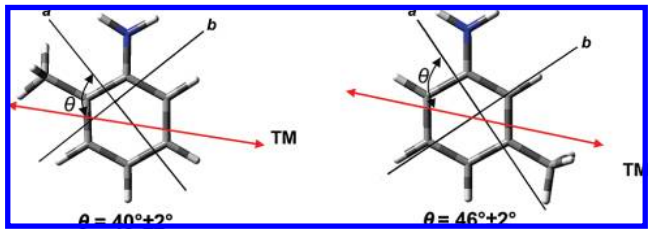

Figure 6. Ground-state structures and $S_1 \leftarrow S_0$ TM orientation vectors in the *o*- and *m*-toluidines.

origin bands of *o*-toluidine and *m*-toluidine, respectively, along with the corresponding theoretical values. Comparisons between the theoretical and experimental rotational constants of both molecules confirm their respective identities. It can be seen that the set of rotational constants obtained for both *o*- and *m*-toluidine are very different from one another.

These differences in the values of the ground and excited rotational constants can be easily understood from Figure 6, which depicts the ground state molecular structures of *o*- and *m*-toluidine in their *ab* inertial planes. The *a* and *b* axes are rotated with respect to their "canonical" positions owing to the simultaneous presence of the $-NH_2$ and $-CH_3$ groups. In *o*-toluidine, the *a* axis lies between the two substituents, passing through the connecting ring C−C bond, whereas in *m*-toluidine, the *b* axis lies between them, passing through the adjacent C−H bond. As a result, the $-NH_2$ group in *m*-toluidine lies closer to the *a* inertial axis, giving it the larger *A* value. Correspondingly, the $-NH_2$ group in *o*-toluidine lies closer to the *b* axis, giving it the larger *B* value. The *C* value of *o*-toluidine is larger than that of *m*-toluidine owing to the displacement of its COM relative to the center of the ring.

The ground state inertial defect values of the $0a_1$ and 1e methyl torsional bands in *o*-toluidine are close to the value expected for an attached methyl group (−3.30 amu Å^2), −3.51 and −3.65 amu Å^2, respectively. (The slightly more negative values of ΔI can be attributed to some nonplanar character of the attached $-NH_2$ group.) However, the inertial defect values of the $0a_1$ and 1e methyl torsional bands in *m*-toluidine are significantly less in magnitude, −0.414 and −0.508 amu Å^2, respectively. Moreover, the ΔI value of the $0a_1$ level in *o*-toluidine decreases in magnitude to −1.21 amu Å^2, the ΔI value of the 1e level in *o*-toluidine increases in magnitude to −4.15 amu Å^2, and the ΔI values of the $0a_1$ and 1e level in *m*-toluidine increase in magnitude to −3.40 and −3.50 amu Å^2, respectively, when the molecules are excited to their S_1 states.

Figure 6 also shows the $S_1 \leftarrow S_0$ transition moment (TM) orientations in the inertial frames of both molecules. Two orientations are possible, making angles of approximately $\theta = \pm 45°$ with respect to *a* in both *o*- and *m*-toluidine. Taking θ to be negative orients the TM vector approximately parallel to the C−N bond in both molecules, whereas taking θ to be positive orients the TM vector approximately perpendicular to the C−N bond in both molecules. If the S_1 states of *o*- and *m*-toluidine are both L_b states, then the perpendicular orientation is expected if the $-NH_2$ group is the "dominant" substituent.

The molecular orbitals (MOs) that participate in the $S_1 \leftarrow S_0$ transitions of the two molecules are shown in Figure 7, together with the corresponding MOs of toluene and aniline. Each transition is predicted by theory to be primarily highest occupied molecular orbital (HOMO)−lowest unoccupied molecular orbital (LUMO) in nature. But the relevant MOs in *o*- and *m*-toluidine are clearly much more similar to those of aniline than to those of toluene. The TM orientations are also similar,

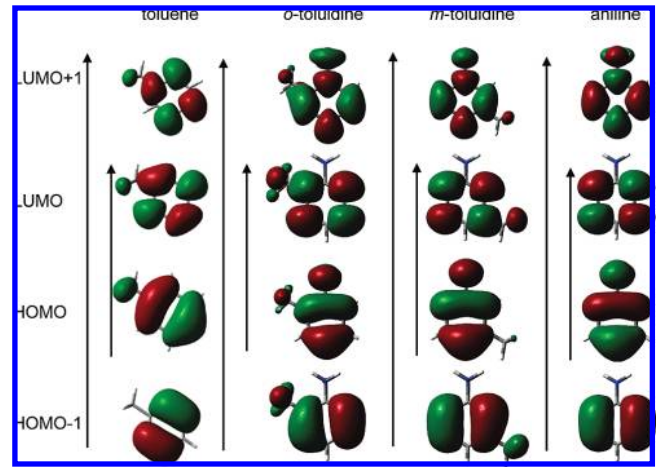

Figure 7. Frontier molecular orbitals calculated at the CIS/6-31G(d,p) level of toluene, *o*-toluidine, *m*-toluidine, and aniline. All transitions are primarily HOMO→LUMO.

as is clear from Figure 7. Thus, we conclude that the amino group is the dominant substituent in the two molecules, and that the $S_1 \leftarrow S_0$ TM vector is oriented approximately perpendicular to the C−N bond in both species.

Experimental confirmation of this conclusion can be done using an analysis first carried out by Plusquellic and Pratt.[18] If we take the inertial axis frames to be those shown in Figure 6, we know that the torsion-rotation parameters D_a and D_b, and ρ_a and ρ_b must have the same signs in this configuration (cf. Table 3). Therefore, either $\rho_a > 0$ and $\rho_b > 0$ or $\rho_a < 0$ and $\rho_b < 0$, depending on the sense of rotation of the methyl rotor relative to its own C_3 axis. It has been found in the previous study that the line positions in the computed E↔E torsional bands are insensitive to the choice of signs, but that the calculated line intensities are sensitive to choice of signs. Therefore, the correct relative intensities of the *a*- and *b*-type lines would be given by either $\rho_a > 0$ and $\rho_b > 0$ or $\rho_a < 0$ and $\rho_b < 0$ if $\theta_{TM} > 0$, and $\rho_a < 0$ and $\rho_b > 0$ or $\rho_a > 0$ and $\rho_b < 0$ if $\theta_{TM} < 0$. Since we know that ρ_a and ρ_b must have the same signs, we can deduce that the θ_{TM} must be positive, which is also the sign choice that gives the correct relative intensities. Theory agrees with these determinations (Tables 1 and 2).

Upon excitation, both molecules exhibit a large decrease in the *A* rotational constant and much smaller decreases in *B* (and *C*); $\Delta A \sim -100$ and $\Delta B \sim -10$ MHz in *o*-toluidine and $\Delta A \sim -150$ and $\Delta B \sim -10$ MHz in *m*-toluidine. Aniline, by contrast,

TABLE 3: First-Order Torsion-Rotation Perturbation Coefficients in the Hamiltonian and Deduced Barrier Heights for *e*-Symmetry Torsional Bands in *o*- and *m*-Toluidine[a]

parameter	*o*-toluidine 1e band	*m*-toluidine 1e band
D_a'' (MHz)	0.23[b]	6406.1 (1)
D_b'' (MHz)	0.069[b]	1719.7 (1)
$W^{(1)''}$	7.64×10^{-5}	1.911
s''	59.202	0.769
V_3'' (cm^{-1})	703[b]	9.45
D_a' (MHz)	2628.4 (1)	21.5 (1)
D_b' (MHz)	1004.7 (1)	26.4 (30)
$W^{(1)'}$	0.873	0.006
s'	3.702	27.269
V_3' (cm^{-1})	44.9	322

[a] Numbers in parentheses are the standard deviations of the last significant figure. [b] Torsion-rotation terms derived from an assumed barrier height of 703 cm^{-1} (ref 2).

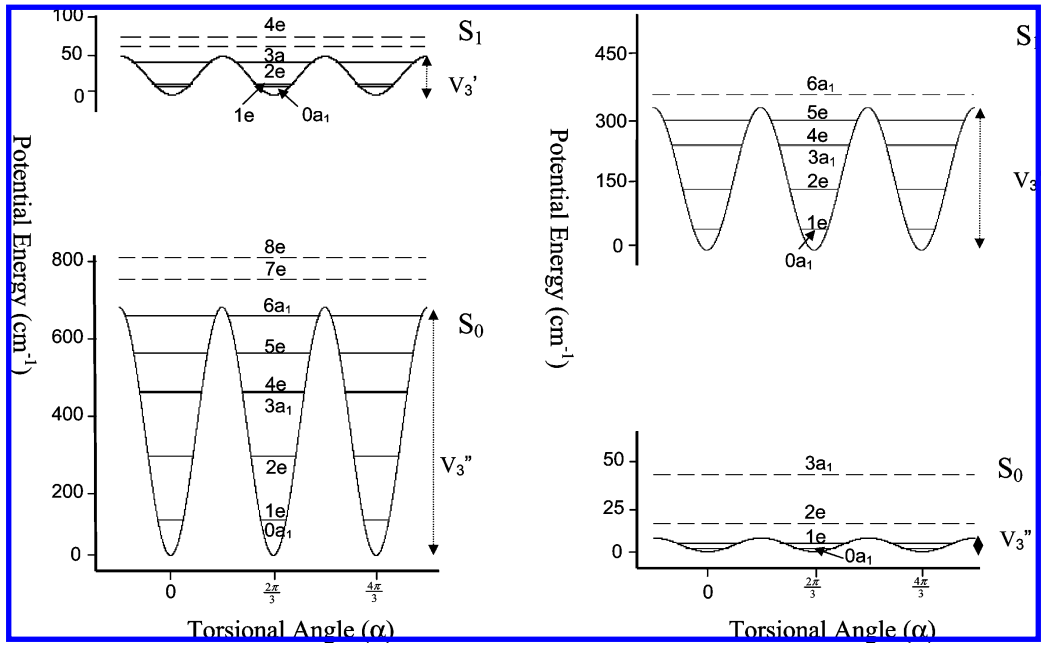

Figure 8. Torsional energy curves of *o*-toluidine (left) and *m*-toluidine (right).

has $\Delta A \sim -300$ and $\Delta B \sim +40$ MHz.[19] The changes in aniline have their origin in a quinoidal distortion of the S_1 state; the "perpendicular" C−C ring bonds are longer than the "parallel" ones. The smaller (in-magnitude) values ΔA and ΔB in the toluidines, in which similar distortions are occurring, may be attributed to the tilts of their inertial axes with respect to those of aniline. Curiously, the values of ΔA and ΔB are significantly different in the $0a_1$ and 1e torsional levels of the S_1 state of *o*-toluidine.

4.2. Methyl Torsional Barriers. The torsional parameters $D_g(= FW_E^{(1)}\rho_g,\ g = a, b, c)$ obtained from the fits of the 1e bands of *o*- and *m*-toluidine are listed in Table 3. Using Herschbach's tables, both the reduced barrier heights (s) and the corresponding 3-fold barriers $V_3(= (9/4)F \cdot s)$ could be calculated. Because of the very large barrier in the ground electronic state, values of the torsion-rotation terms for *o*-toluidine in the S_0 state were not experimentally measured. Instead, they were calculated from the barrier height of $V_3'' = 703$ cm^{-1} obtained by Okuyama et al.[2] (Barrier heights much larger than 500 cm^{-1} do not produce measurable perturbations at our experimental resolution.) A reduced barrier height of 59.202 was calculated and the first-order perturbation coefficient ($W_E^{(1)} = 7.64 \times 10^{-5}$) was obtained through interpolation, yielding torsion-rotation terms of $D_a = 0.23$ and $D_b = 0.069$ MHz. In the S_1 state, the torsion-rotation terms were found to be much larger and could be determined by experiment ($D_a = 2628.4$ and $D_b = 1004.7$ MHz). The reduced barrier height was obtained through interpolation of the first-order perturbation coefficient ($W_E^{(1)} = 0.873$) and a value of 3.702 ($V_3' = 44.89$ cm^{-1}) was calculated.

Interestingly, the opposite behavior was observed in *m*-toluidine, where the torsion-rotation terms in the S_0 state are quite large ($D_a = 6406.1$ and $D_b = 1719.7$ MHz) but much smaller in the S_1 state ($D_a = 21.5$ and $D_b = 26.4$ MHz). This resulted in calculated reduced barrier heights of 0.769 ($V_3 = 9.45$ cm^{-1}) in the ground state and 27.269 ($V_3' = 322.23$ cm^{-1}) in the excited state. These results are consistent with the finding that the 1e band is blue shifted with respect to the $0a_1$ origin band in *o*-toluidine and red shifted in *m*-toluidine. The corresponding potential energy curves for both *o*- and *m*-toluidine are shown in Figure 8.

As mentioned earlier, the observed inertial defect values of *o*-toluidine in the excited state (∼−1.2 amu Å^2) and *m*-toluidine in the ground state (∼−0.5 amu Å^2) are much smaller than the expected value for a methyl group attached to an aromatic plane (−3.3 amu Å^2). It can be seen that the small inertial defect values occur whenever the 3-fold potential barrier heights are small, while the expected and larger values occur when the barrier heights are much larger. This general trend has been observed before, most notably in 2- and 3-methylanisole.[3] Because of the planarity of the ring to which the methyl group is attached, the inertial defect is zero in the free rotor limit for an internal rotor that is collinear with an inertial axis of the molecule. This also holds to a good approximation for an arbitrary orientation of the symmetry axis of the methyl group in the symmetry plane of the molecule.[20] The smaller the barrier height, the more the inertial defect value approaches zero, as observed in both molecules.

The barrier heights obtained for the ground and excited states of both molecules are consistent with those measured by Okuyama et al.[2]

4.3. Origins of the Torsional Barriers. As has been previously shown in the methylpyrimidines[2] and the methylanisoles,[3] the preferred configuration (staggered or eclipsed) and the potential energy curve along the torsional coordinate have their origins in two factors, the position of the methyl group relative to other ring substituents and differences in the π-bond orders of the adjacent C−C bonds. (The staggered and eclipsed configurations are shown below in Scheme 1, where S denotes the attached substituent in the plane of the benzene ring.) According to theory, the methyl group in *o*-toluidine is staggered, whereas the methyl group in *m*-toluidine is eclipsed, in the electronic ground states of the two molecules. The

SCHEME 1

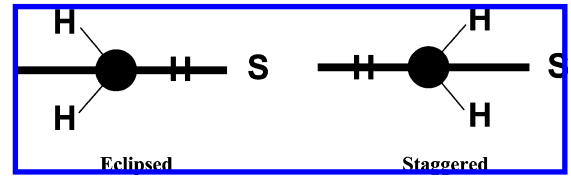

staggered configuration of the methyl group in *o*-toluidine can be attributed to both factors. There is a repulsive steric interaction of the in-plane hydrogen atom with the amino group, and the C_2-C_3 bond has a higher π-bond order than the C_1-C_2 bond. (The C_1-C_2 bond is 1.18 pm longer than the C_2-C_3 bond.) The repulsive steric interaction is absent in *m*-toluidine, so the small preference for the eclipsed conformation of the methyl group in this molecule can be traced to the slightly higher π-bond order of the C_2-C_3 bond. (The C_3-C_4 bond is 0.02 pm longer than the C_2-C_3 bond.)

Excitation of the two molecules to their S_1 states has a significant impact on the methyl rotor potentials, owing to a quinoidal distortion of the aromatic ring. Thus, in *m*-toluidine, this results in a larger difference of the S_1 π-bond orders of the adjacent C−C bonds. The difference between the C_2-C_3 and C_3-C_4 bond lengths is now about 0.14 pm, an increase of 0.12 pm. This further stabilizes the eclipsed form and produces a significant increase in the magnitude of the barrier height, $V_3(S_0) = 9.45 \rightarrow V_3(S_1) = 322$ cm^{-1}. In *o*-toluidine, the difference between the C_1-C_2 and C_2-C_3 bond lengths is now 0.86 pm on excitation of the S_1 state, a decrease of about 0.3 pm. Therefore, the staggered form is still favored in the S_1 state but there is a significant decrease in the magnitude of the barrier height, $V_3(S_0) = 703 \rightarrow V_3(S_1) = 44.9$ cm^{-1}. Some reduction in the magnitude of the repulsive term also would be expected, since all C−C bonds in the S_1 state are longer than in the S_0 state. Thus, light-induced changes in the π-electron distributions of the aromatic rings have a major impact on the preferred geometries and dynamic behaviors of the attached methyl groups.

5. Conclusions

Rotationally resolved $S_1 \leftarrow S_0$ fluorescence excitation studies of *o*- and *m*-toluidine have been performed. Analysis of the results reveals that the amino group is the dominant substituent in the electronic transition; the $S_1 \leftarrow S_0$ transition moment is essentially perpendicular to the position of attachment of this group in both molecules. The resulting S_1 states have significantly different π-electron distributions in the aromatic ring, compared to the ground states. As a consequence, the preferred configurations and potential barriers that govern the motion of the attached methyl groups in the two molecules are quite different.

Acknowledgment. We thank David F. Plusquellic (NIST) for the JB95 fitting program used for the data analysis and Jens-Uwe Grabow (U. Hannover) for helpful discussions. This work has been supported by NSF (CHE-0615755).

References and Notes

(1) Spangler, L. H.; Pratt, D. W. In *Jet Spectroscopy and Molecular Dynamics*; Hollas, J. M., Phillips, D., Eds.; Chapman & Hall: London, 1995; p 366−398 and references therein.

(2) Okuyama, K.; Yoshihara, K.; Ito, M. *Laser Chem.* **1987**, *7*, 197–212.

(3) Tan, X. Q.; Majewski, W. A.; Plusquellic, D. F.; Pratt, D. W. *J. Chem. Phys.* **1991**, *94*, 7721–33.

(4) Tan, X. Q.; Clouthier, D. J.; Judge, R. H.; Plusquellic, D. F.; Tomer, J. L.; Pratt, D. W. *J. Chem. Phys.* **1991**, *95*, 7862–71.

(5) Tan, X. Q.; Pratt, D. W. *J. Chem. Phys.* **1994**, *100*, 7061–7.

(6) Borst, D. R.; Pratt, D. W. *J. Chem. Phys.* **2000**, *113*, 3658–3669.

(7) Alvarez-Valtierra, L.; Yi, J. T.; Pratt, D. W. *J. Phys. Chem.* **2006**, *110B*, 19914–19922.

(8) Alvarez-Valtierra, L.; Tan, X.-Q.; Pratt, D. W. *J. Phys. Chem.* **2007**, *111A*, 12802–12809.

(9) Majewski, W. A.; Pfanstiel, J. F.; Plusquellic, D. F.; Pratt, D. W. In *Techniques of Chemistry*; Rizzo, T. R., Myers, A. B., Eds.; Wiley & Sons: New York, 1995; Vol. 23, pp 101−48.

(10) Plusquellic, D. F. Ph.D. Thesis, University of Pittsburgh, Pittsburgh, PA, 1992.

(11) Plusquellic, D. F.; Suenram, R. D.; Mate, B.; Jensen, J. O.; Samuels, A. C. *J. Chem. Phys.* **2001**, *115*, 3057–3067.

(12) Frisch, M. J.; Trucks, G. W.; Schlegel, H. B.; Scuseria, G. E.; Robb, M. A.; Cheeseman, J. R.; Montgomery, J. A. J.; Vreven, T.; Kudin, K. N.; Burant, J. C.; Millam, J. M.; Iyengar, S. S.; Tomasi, J.; Barone, V.; Mennucci, B.; Cossi, M.; Scalmani, G.; Rega, N.; Petersson, G. A.; Nakatsuji, H.; Hada, M.; Ehara, M.; Toyota, K.; Fukuda, R.; Hasegawa, J.; Ishida, M.; Nakajima, T.; Honda, Y.; Kitao, O.; Nakai, H.; Klene, M.; Li, X.; Knox, J. E.; Hratchian, H. P.; Cross, J. B.; Bakken, V.; Adamo, C.; Jaramillo, J.; Gomperts, R.; Stratmann, R. E.; Yazyev, O.; Austin, A. J.; Cammi, R.; Pomelli, C.; Ochterski, J. W.; Ayala, P. Y.; Morokuma, K.; Voth, G. A.; Salvador, P.; Dannenberg, J. J.; Zakrzewski, V. G.; Dapprich, S.; Daniels, A. D.; Strain, M. C.; Farkas, O.; Malick, D. K.; Rabuck, A. D.; Raghavachari, K.; Foresman, J. B.; Ortiz, J. V.; Cui, Q.; Baboul, A. G.; Clifford, S.; Cioslowski, J.; Stefanov, B. B.; Liu, G.; Liashenko, A.; Piskorz, P.; Komaromi, I.; Martin, R. L.; Fox, D. J.; Keith, T.; Al-Laham, M. A.; Peng, C. Y.; Nanayakkara, A.; Challacombe, M.; Gill, P. M. W.; Johnson, B.; Chen, W.; Wong, M. W.; Gonzalez, C.; Pople, J. A. *Gaussian 03*, rev. 6.0; Gaussian, Inc.: Wallingford CT, 2004.

(13) Gordy, W.; Cook, R. L. *Microwave Molecular Spectra*, 3rd ed.; John Wiley & Sons: New York, 1984.

(14) Tan, X. Q.; Majewski, W. A.; Plusquellic, D. F.; Pratt, D. W.; Meerts, W. L. *J. Chem. Phys.* **1989**, *90*, 2521–2.

(15) Herschbach, D. R. *J. Chem. Phys.* **1959**, *31*, 91–108.

(16) Kalkman, I. V. Ph.D. Thesis, Radboud University, Nijmegen, The Netherlands, 2008.

(17) Watson, J. K. G. In *Vibrational Spectra and Structure*; Durig, J. R., Ed.; Elsevier: Amsterdam, The Netherlands, 1977; Vol. 6, pp 1−89.

(18) Plusquellic, D. F.; Pratt, D. W. *J. Chem. Phys.* **1992**, *97*, 8970–8976.

(19) Sinclair, W. E.; Pratt, D. W. *J. Chem. Phys.* **1996**, *105*, 7942–7956.

(20) Trinkaus, A. Diplom Thesis, University of Freiburg, 1967.

JP904023X

Applied Clay Science 43 (2009) 243–247

Contents lists available at ScienceDirect

Applied Clay Science

journal homepage: www.elsevier.com/locate/clay

Thermally treated soil clays as ceramic raw materials: Characterization by X-ray diffraction, photoacoustic spectroscopy and electron spin resonance

L. Mota [a], R. Toledo [a], R.T. Faria Jr. [a], E.C. da Silva [a,*], H. Vargas [a], I. Delgadillo-Holtfort [b]

[a] Laboratório de Ciências Físicas (LCFIS), Centro de Ciência e Tecnologia (CCT), Universidade Estadual do Norte Fluminense Darcy Ribeiro (UENF), Avenida Alberto Lamego, 2000, 28013-602, Campos dos Goytacazes, RJ, Brazil

[b] Instituto de Física, Universidad de Guanajuato, Lomas del Bosque 103, Lomas del Campestre, León Gto., 37150 Mexico

ARTICLE INFO

Article history:
Received 25 April 2008
Received in revised form 26 July 2008
Accepted 29 July 2008
Available online 5 August 2008

Keywords:
Red ceramic
XRD
PAS
ESR

ABSTRACT

Soil clay used as ceramic raw material under heat treatment was investigated using X-ray diffraction, X-ray fluorescence, photoacoustic spectroscopy — PAS and electron spin resonance — ESR. The results indicated the presence of at least three different sites for the Fe^{3+} ions, one of them representative of a set of distorted cubic sites. The optical absorption spectra obtained with the photoacoustic technique showed bands associated with d–d transitions of Fe^{3+} ions. Mullite and hematite were detected in the 1100 °C heated samples. Crystalline–amorphous–crystalline transformations were detected between 110 °C and 1100 °C. The conclusion drawn from photoacoustic and magnetic resonance measurements agreed very well with that obtained by X-ray diffraction.

1. Introduction

In a tropical country, walls, red bricks, tiles and other building pieces are often exposed to enhanced temperature and therefore, thermal properties of the raw material just as the final products play an important role in the indoor climate of the houses (Alexandre et al., 1999). In a previous work, photoacoustic spectroscopy (PAS), X-ray diffraction and electron spin resonance (ESR) were applied to characterize the soil of the quaternary sedimentary basin of Campos dos Goytacazes, RJ, Brazil, which has a high content of clay minerals (Manhães et al., 2002). More recently, the photoacoustic technique (PA) has been applied to determine some important properties, such as thermal diffusivity, heat capacity, thermal conductivity and thermal effusivity of the soil clay fraction (Mota et al., in press). Thermal properties were very sensitive to amorphous–crystalline phase transitions of clays heated above 900 °C, typical temperatures applied in the manufacturing process of ceramic materials.

The economic value of the ceramic product is affected by its red pigmentation, which is mainly due to the presence of hydr(oxides) of Fe(III). These iron oxides occur in soil either as coatings on individual clay particles, or as discrete, fine particles in the clay mass. A small fraction of iron ions can also be present as substitutional cations in the tetrahedral or octahedral sheets (Moore and Reynolds, 1997; Manhães et al., 2002). Depending on its content and location, Fe(III) may substantially affect the suitability of natural clays for industrial applications, such as paper coating or ceramics.

A systematic study on selected raw materials used by ceramic industries is presented. The X-ray fluorescence was used to determine Fe concentration. Quantitative phase analysis was performed using the Rietveld method (Young et al., 1995). Photoacoustic spectroscopy — PAS was applied to study the optical absorption spectra, also related to the Fe content and its valence state. Electron Spin resonance — ESR measurements were performed to study the average crystalline symmetry around Fe ions.

2. Materials and methods

2.1. Sample preparation

The samples originate from a site of the quaternary sedimentary basin of Campos dos Goytacazes, RJ, Brazil. It is a low altitude plain which extends 50 km away from the Atlantic Ocean. Soil from this region has a high content of clay minerals. The sediments of this basin were deposited by the Paraíba do Sul River meandering over its flood plain. Samples were collected from stratified layers localized between 1.2 m and 2.7 m above the free ground water, which is about 3 m below ground. The green samples were dried at 110 °C for 24 h to eliminate water. They were ground and passed through a sieve with nominal aperture of 75 μm (mesh size 200, ASTM). The obtained powdered material, comprising about 95% (in mass) of the original sample, was representative of the soil studied. The powdered samples were used for the X-ray diffraction, Photoacoustic spectroscopy and Electron Spin Resonance experiments. For X-ray fluorescence measurements, 4 g of powdered material was pressed (at 226 MPa, press CHARLOTT) into disks (32 mm diameter and thickness 3 mm). The

* Corresponding author. Tel.: +55 22 2726 1574; fax: +55 22 2726 1532.
E-mail address: ecorrea@uenf.br (E.C. da Silva).

0169-1317/$ – see front matter © 2008 Elsevier B.V. All rights reserved.
doi:10.1016/j.clay.2008.07.025

De la Roca-Chiapas, José María; Cordova-Fraga, Teodoro; Barbosa Sabanero, Gloria; Macías de la Cruz, J. Humberto; Cano, M.E.; Pacheco Hain, Aleph; Rivera Cisneros, Antonio; Solís, Silvia; Sosa, Modesto

Aplicaciones Interdisciplinarias entre Física, Medicina y Psicología
Acta Universitaria, Vol. 19, Núm. 2, septiembre, 2009, pp. 71-75
Universidad de Guanajuato
México

Disponible en: http://redalyc.uaemex.mx/src/inicio/ArtPdfRed.jsp?iCve=41612893011

Acta Universitaria
ISSN (Versión impresa): 0188-6266
vargase@quijote.ugto.mx
Universidad de Guanajuato
México

Aplicaciones Interdisciplinarias entre Física, Medicina y Psicología

José María De la Roca-Chiapas.*****, Teodoro Cordova-Fraga**, Gloria Barbosa Sabanero***, J. Humberto Macías de la Cruz****, M.E. Cano******, Aleph Pacheco Hain**, Antonio Rivera Cisneros*, Silvia Solís*** y Modesto Sosa**.*

RESUMEN

El presente trabajo muestra dos líneas de investigación que vinculan a la física, la medicina y la psicología. La primera consiste en la Mecano-magnetogastrografía que sirve para medir el vaciamiento gástrico así como las contracciones peristálticas las cuales se evaluaron junto con estados emocionales para conocer la influencia del estrés, ansiedad y depresión en las respuestas fisiológicas. La segunda consiste en la psicomagnetobiología como un modelo de inducción de cáncer y de estrés que permiten comparar marcadores bioquímicos, caracterización espectroscópica y obtener imágenes a través de un escáner magnético, la cual podría utilizarse en el diagnóstico y el uso de la hipertermia como tratamiento del cáncer. La Mecano-magnetogastrografía es una técnica útil para medir el vaciado gástrico, que no es invasiva, no usa radiación ionizante y demuestra que a través de la lectura de los campos magnéticos del trazador magnético ingerido se puede obtener información sobre el vaciado gástrico y contracciones peristálticas presentando resultados reproducibles. En cuanto a la línea de investigación que llamamos psicomagnetobiología, se ha usado la inducción de cáncer con *N-metil-N-nitrosourea*, resultando con cáncer mamario el 58% de las ratas.

ABSTRACT

This paper presents two lines of research linking physics, medicine and psychology. The first is the mechanical magnetogastrography used to measure gastric emptying and peristaltic contractions and its relationship to evaluate the physiological behavior related to emotional states. The second is the psicomagnetobiology as a model of induction of cancer stress and biochemical markers that enable the comparison, spectroscopic characterization and imaging using a magnetic scanner, which could be used in the diagnosis and the use of hyperthermia as a treatment for cancer. The Mecano-magnetogastrography is a useful technique for measuring gastric emptying, which is not invasive, does not use ionizing radiation and demonstrates that through the reading of the magnetic fields of magnetic tracer ingested can obtain information on gastric emptying and peristaltic contraction, presented reproducible results. In terms of research we call psicomagnetobiology has been used for induction of cancer with N-methyl-N-nitrosourea, resulting in breast cancer 58% of rats.

Recibido: 15 de Junio de 2009
Aceptado: 4 de Septiembre de 2009

INTRODUCCIÓN

El presente trabajo muestra de manera sucinta la importancia de las relaciones interdisciplinarias, así como los métodos por los cuales se ha llegado a resultados de investigación. El abordaje de problemas de salud se ha podido realizar con la participación de diferentes ciencias como la medicina, psicología y física médica.

Palabras clave:
Estudios interdisciplinarios; Psicomagnetobiología; Mecano-magnetogastrografía.

Keywords:
Interdisciplinary studies; Psicomagnetobiology; Mecano-magnetogastrography.

Desde el enfoque interdisciplinario presentamos dos casos exitosos y los métodos o formas en como se han llegado a los resultados. El primero consiste en el desarrollo tecnológico de la Mecano–Magnetogastrografía (MMGG) el cual sirve para medir el vaciado gástrico y las contracciones peristálticas, lo cual se ha vinculado a la psicología al estudiar la influencia de los estados emocionales como la ansiedad, depresión y estrés en pacientes con Dispepsia Funcional y en personas sanas. La MMGG se usa también como método para evaluar trastornos gastrointestinales como la Gastroparesía.

* Departamento de Psicología, División de Ciencias de la Salud del Campus León. Universidad de Guanajuato, 37150 León, Gto., México. Correo electrónico: joseroca@fisica.ugto.mx.
** Departamento de Ingeniería Física, División de Ciencias e Ingenierías del Campus León. Universidad de Guanajuato, 37150, León, Gto., México.
*** Departamento de Ciencias Médicas, División de Ciencias de la Salud del Campus León. Universidad de Guanajuato, 37150 León, Gto., México.
**** Departamento de Medicina, División de Ciencias de la Salud del Campus León. Universidad de Guanajuato, 37150 León, Gto., México.
***** Asociación Cultural Nueva Acrópolis México, 37480 León, Gto., México.
****** Centro Universitario de la Ciénaga. Universidad de Guadalajara, Ocotlán, Jal., México.

Universidad de Guanajuato

Detección fotoacústica de objetos enterrados y cáncer de mama

Jesús Alberto Mendoza-Torres y Gerardo Gutiérrez-Juárez
Departamento de Ingeniería Física,
División de Ciencias e Ingenierías-Campus León (DCI-CL),

Palabras clave: Transductor Piezoeléctrico, Espectroscopia Fotoacústica, Cáncer, Efecto Fotoacústico

Utilizando la espectroscopia fotoacústica pulsada, se realizo una imagen bidimensional de un objeto ópticamente opaco (1 cm^2 x 5 mm), enterrado en un gel de agar (3 cm de diámetro y altura de 9 cm) con esparcimiento óptico. El objeto fue detectado por un transductor de ultrasonido comercial utilizando un láser de Nd: YAG con pulsos de 10 ns. La profundidad máxima a la que se pudo detectar el objeto fue 6 cm, medida desde el detector acústico. Se discute la aplicación de la espectroscopia fotoacústica como una técnica de diagnostico en la detección del cáncer de mama.

Introducción

En las últimas dos décadas las ***espectroscopias ópticas*** han estado ganando terreno como herramienta de diagnóstico en investigaciones biomédicas. Estas tecnologías surgen como apoyo a las actuales, es decir, no vienen a sustituir los métodos actuales, ni mucho menos a resolver por si solas los problemas biomédicos, solo son un complemento para llegar a rincones donde están limitados los métodos convencionales. Una de estas espectroscopias es la ***Espectroscopia Fotoacústica***, la cual promete ser una de las herramientas con mayor futuro para el diagnostico de enfermedades.

Lo anterior se debe a que la mayoría de las espectroscopias usan la naturaleza óptica de la luz tanto para estimular a los tejidos como para detectar los efectos que causa en ellos y, debido al alto esparcimiento de la luz en los tejidos, la capacidad de detección se ve reducida considerablemente. En cambio, en la fotoacústica la luz se utiliza únicamente para generar ondas acústicas en los tejidos, y dado que el coeficiente de esparcimiento de estas ondas es un orden de magnitud menor que para las ondas de luz,a la capacidad de resolución se incrementa considerablemente [1].

El ***efecto fotoacústico*** (PA), es base física de la optoacústica y consiste en la generación de una onda acústica después de que un objeto absorbió radiación electromagnética del laser.

En la biomedicina, la ventaja que tiene la optoacústica sobre las espectroscopias puramente ópticas, es principalmente una, y tiene que ver con la distancia de propagación de la señal, y por lo tanto del tamaño y profundidad del tejido que se desea investigar [3].

El coeficiente de esparcimiento en tejidos humanos es aproximadamente de 200 cm^{-1}, dando un camino libre medio debido a la dispersión de unas pocas decenas de micras [1, 2]. Por ejemplo, el coeficiente de esparcimiento de la piel humana es de aproximadamente 200 cm^{-1} a longitudes de onda en el rango del rojo, mientras que en tejido aórtico humano tiene un coeficiente de dispersión de 300 cm^{-1} [2].

Si la luz se propaga una distancia mayor a unos cuantos milímetros, pierde coherencia y por tanto, la capacidad de hacer una imagen. Sin embargo, la propagación de ondas acústicas no se ve afectada por los medios ópticamente turbios.

El efecto que ocasionan los medios turbios en la onda acústica solo aparece en su generación, ya que ésta depende de la absorción óptica del tejido, se trata de una

DIF-09-M2

Anexo 81.1

EFECTO DE LA ESTIMULACION ÓPTICA DEL PBA PC6 SOBRE LA VARIABILIDAD CARDIACA EN SUJETOS SOMETIDOS A ESTRÉS.

Meave Sánchez NM, División de Ciencias de la Salud, Universidad de Guanajuato; Vargas Luna FM, Departamento de Ciencias exactas e Ingenierías, Universidad de Guanajuato; Huerta Franco R, López Aguilera BA, Pérez Cárdenas P, Sánchez Vázquez, M.

RESUMEN

El presente trabajo es parte de un estudio multidisciplinario en el que participaron médicos y físicos en la evaluación de la función cardiaca, gástrica y de la piel ante estímulos de estrés. En particular se presenta un análisis de la variabilidad cardiaca de un grupo de sujetos sometidos a estrés acústico con estimulación del PBA PC6 con estimulación óptica (láser).

INTRODUCCIÓN

La acupuntura es una parte de la "Medicina tradicional China" originada hace aproximadamente 5000 años. Los puntos de acupuntura también conocidos como Puntos Biológicamente Activos (PBA) son áreas de menor resistencia al paso de corriente eléctrica. No obstante actualmente dichos puntos son estimulados igualmente con luz laser (acupuntura laser).

Las razones del uso de la acupuntura para modificar la respuesta asociada al estrés se basa en el supuesto de que la estimulación de algunos PBA reduce la actividad simpática del SNA bajo condiciones de estrés. La base teórica de la interacción láser-PBA no está entendida. Algunos estudios en animales demuestran que la estimulación somática aferente puede disminuir la actividad simpática. En un estudio realizado por Zengyong y colaboradores [1] en 3 grupos de personas sometidos a estrés, observaron que la frecuencia cardiaca disminuía al estimular PC6 y LI4 en el periodo postestimulación mientras que la misma maniobra realizada superficialmente (sin la inserción de agujas) no producía ningún efecto en el grupo control.

El PBA Neiguan PC6, es el sexto punto del meridiano pericardium que se encuentra en el antebrazo, los puntos de este meridiano modulan la actividad de la frecuencia cardiaca, ya que ante un estímulo de estrés, el SNA actúa aumentándola mientras que el uso de la acupuntura tiende a disminuirla en estos puntos.

En el estudio de la respuesta al estrés es importante la evaluación de la variabilidad cardiaca, ésta se determina en algunos estudios con las diferencias de duración de los intervalos R-R', lo que se traduce en cambios en el ritmo cardiaco. Estas fluctuaciones del ritmo cardiaco o variabilidad cardiaca se mide en tres regiones del espectro en frecuencias (figura 1). LF (frecuencia baja) que corresponde a las fluctuaciones lentas de la frecuencia cardiaca, reflejado en la modulación simpática del nodo sinusal; HF (frecuencia alta) es una medida de las arritmias sinusales debido a la respiración y puede ser considerada como un índice de la respuesta parasimpática. La razón LF/HF es considerada como el balance simpatovagal[1,2].

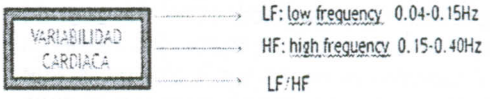

Figura.1 Regiones consideradas en el espectro de frecuencias de la variabilidad cardiaca

OBJETIVO

Por los antecedentes citados, en este trabajo nos planteamos la pregunta de que si la estimulación de PC6 con aculaser modifica la variabilidad cardiaca de sujetos sometidos a diversas pruebas de estrés.

Molecular Modeling Coupled To Reactive Separation Systems Design

F.A.Perdomo, A. Gil-Villegas, A. Martínez, P.Coutiño
Department of Physical Engineering, Sciences and Engineering Division,
University of Guanajuato,
León 37150, México.

Process design in chemical engineering is based on kinetics models and thermophysical properties strongly dependent on experimental measurements which are generally expensive and very time consuming, or under specific conditions could be unfeasible. Computer simulations can be implemented to overcome some of these limitations. An important problem in chemical engineering is the accurate prediction of reaction and phase equilibrium for complex chemical systems in reaction-separation (or hybrid) process design, like reactive distillation, extraction or adsorption. There are two general approaches to solve this problem: 1) the standard one based on the equality of chemical potentials derived from cubic and empirical equations of state, as well as group contribution methods and 2) systems modeled by computer simulations, using specific intermolecular interactions between the constituent molecules. In this work we present results using molecular modeling coupled to a mass exchanger process design, where the reaction can take place into or between phases. The Reactive Monte Carlo method (Smith and Triska, 1994), (Johnson, et al, 1994). and the Statistical Associating Fluid Theory for Potentials of Variable Range (Gil-Villegas, et al, 1997) are applied to model phase equilibrium when chemical reactions are present in mixtures of industrial interest, such as a mixture of water, alcohols and organic acid mixtures.

1. Introduction

The reactive mass-exchange process is a process where the chemical reaction and separation of the reaction mixture occur simultaneously and combined (in one apparatus) with predominant removing of target reaction products. Process design in chemical engineering has been based on kinetics models and properties strongly dependents on experimental measurement whose determination generally is expensive, very time consuming, or under specific conditions are unfeasible. On the other hand, computer simulation can be implemented to overcome some of these problems, using molecular models. A particular case and important problem in chemical engineering is the accurate prediction of reaction and phase equilibrium for complex chemical systems for reaction-separation process (or hybrid process) design like reactive distillation,

IMPLEMENTACIÓN DE UN SISTEMA OPTOACÚSTICO PARA ENCONTRAR OBJETOS DENTRO DE FANTASMAS DE TEJIDO BLANDO REALIZANDO UN BARRIDO LATERAL EN LA SUPERFICIE DEL FANTASMA

M.P. Reyes-Yépez, M.E. Cano-González, F.M., Vargas-Luna, I. Delgadillo-Holtfort

Instituto de Física, Universidad de Guanajuato, Loma del Bosque 103, Lomas del Campestre, C.P. 37150, León, Gto.

RESUMEN

El principio de la técnica optoacústica es la generación de una onda de ultrasonido inducida en el medio de interés por la excitación con energía láser pulsada. El contraste empleado en ésta técnica, está basado en la diferencia de coeficientes de absorción óptica entre el objeto que se quiere observar y el medio en que esta inmerso, lo que hace que esta técnica en comparación al ultrasonido y rayos-X, sea una herramienta prometedora para detección de anormalidades dentro de la mama en etapas tempranas.

En el presente trabajo, mostramos los resultados que obtuvimos al implementar la técnica optoacústica en un fantasma de tejido blando con un objeto de mayor coeficiente de absorción óptica dentro. Para la detección de la señal optoacústica construimos transductores que tienen como elemento activo PVDF de 110 μm de espesor. La fuente de excitación fue un láser pulsado de Nd:YAG (λ=1064 nm). Los fantasmas de tejido blando fueron elaborados con agua, leche baja en grasa y grenetina mezclados en diferentes concentraciones, estos fantasmas fueron empleados para simular las propiedades de absorción óptica de la mama, durante su elaboración se introdujeron objetos con mayor absorción óptica, los cuales simularon tejido anormal. Con los transductores que construimos logramos detectar objetos de 1.64 mm. de espesor. Las señales provenientes de los bordes del objeto empiezan a ser detectadas a distancias que dependen de la profundidad del objeto y las propiedades de dispersión del fantasma

INTRODUCCIÓN

El cáncer de mama es la tercer causa de mortalidad en las mujeres mexicanas [1], esto se debe, en la mayoría de los casos, a que su detección se realiza en etapas avanzadas. Se sabe que la detección de tumores en etapas tempranas, permite la aplicación de un tratamiento moderado, efectivo y con mínimos efectos colaterales para los pacientes. Además, la detección temprana de cáncer aumenta significativamente la esperanza de vida y sustancialmente decrece las complicaciones asociadas a esta enfermedad.

La mamografía y el ultrasonido son dos de las principales técnicas que actualmente son empleadas para diagnosticar cáncer de mama. Dichas técnicas no están libres de limitaciones: la mamografía falla en la detección de tumores en tejidos radiológicamente densos, por otro lado, el ultrasonido no es capaz de detectar tumores con propiedades mecánicas similares, debido a que el tejido normal y anómalo en la mama son similares mecánicamente hablando, esta técnica ofrece un pobre contraste[2].

En este trabajo implementamos un sistema para aplicar la técnica optoacústica, nos enfocamos en esta técnica ya que en posteriores investigaciones se ha demostrado que es una herramienta prometedora en la detección temprana de cáncer de mama, debido a que el contraste que podemos obtener, esta basado en las diferencias de las propiedades de absorción óptica entre los tejidos. Además, presentamos los resultados que obtuvimos usando un sensor piezoeléctrico casero para detectar la señal optoacústica que genera un objeto con coeficiente de absorción óptica mayor que el del medio en el que esta inmerso.

THE JOURNAL OF PHYSICAL CHEMISTRY Letters

pubs.acs.org/JPCL

Stark-Effect Studies of 1-Phenylpyrrole in the Gas Phase. Dipole Reversal upon Electronic Excitation

J. A. Thomas, J. W. Young, A. J. Fleisher, L. Alvarez-Valtierra,† and D. W. Pratt*

Department of Chemistry, University of Pittsburgh, Pittsburgh, Pennsylvania 15260

ABSTRACT High-resolution fluorescence excitation experiments on 1-phenylpyrrole in a molecular beam, both in the absence and presence of an applied electric field, show that the electronic state responsible for the strong features in the gas-phase UV absorption spectrum is the ^1L_b state, that this state is significantly more planar than the ground state, and that the direction of the permanent electric dipole moment in the ^1L_b state is reversed relative to that of the ground state. Implications of these findings for intramolecular charge transfer in the isolated molecule are discussed.

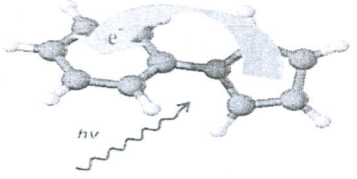

SECTION Dynamics, Clusters, Excited States

The molecule 1-phenylpyrrole (1PP) has attracted much attention since it was discovered in 1983 that it exhibits a long wavelength shoulder in its fluorescence spectrum in acetonitrile.[1] Originally, it was thought that electronic excitation led to the formation of a twisted intramolecular charge-transfer (TICT) state which might be stabilized in a polar solvent.[2] Later, it was shown in a supersonic jet study of 1PP[3] that the electronically excited S_1 state, though twisted, is more planar than the ground electronic state. However, Proppe et al.[4] have argued on the basis of a theoretical study of TICT in 1PP that the transition studied by Okuyama et al.[3] may not correspond "to the electronic transition responsible for the spectroscopic feature with maximum intensity in the lowest-energy region of the absorption spectrum", thereby creating some doubt about the relevance of the gas-phase results.

Photoinduced ICT states of organic compounds play a fundamental role in many processes of current interest.[5] For this reason, we report here the results of a high-resolution laser study of 1PP in a molecular beam, both in the absence and presence of a static electric field. These results show that the state responsible for the strong feature in the absorption spectrum is the ^1L_b state, that this state is significantly more planar than the ground electronic state, and that the direction of the permanent electric dipole moment in this state is reversed relative to that in the ground electronic state. Reversal of the dipole direction may play a previously unappreciated role in the CT process in many molecules.

Detailed descriptions of our experimental methods are given in the Supporting Information. There, we also present the results of both vibrationally and rotationally resolved experiments on 1PP in the absence of an electric field. The vibrationally resolved fluorescence excitation spectrum is virtually identical to that presented by Okuyama et al.;[3] the first 1000 cm^{-1} are dominated by a long progression of bands spaced by intervals of ~50 cm^{-1}. Rotationally resolved spectra of three of these bands at +269.0, +316.9, and +364.5 cm^{-1} with respect to the weak origin band (originally assigned as T_0^8, T_1^9, and T_0^{10}, where T represents a ring-torsional mode[3]) show that all transitions originate in the same ground-state vibrational level, that the upper-state vibrational levels reached in the three transitions all have inertial defects that are substantially lower (in magnitude) than those of the ground state, and that the PES along the torsional coordinate in the excited state most likely has a greatly reduced barrier to planarity and a greatly increased barrier to perpendicularity compared to the ground state.

Also relevant to the issue of CT in the electronically excited state of 1PP is the behavior of the electronic spectrum in the presence of an electric field. Figure 1 shows an example, the high-resolution spectrum of the 0_0^0 + 269 cm^{-1} band at zero field, and selected portions of this spectrum at Stark fields of 211, 423, and 846 V/cm. Like the other bands examined at high resolution, this band is a hybrid band consisting of 87.5% b-type character and 12.5% c-type character. No a-type character is observed. This shows that the state accessed in these experiments is a ^1L_b state (in the language of Proppe et al.[4], the 1^1B state, comprised principally of two one-electron excitations, 42.6% HOMO−1 to LUMO+1 and 26.7% HOMO−2 to LUMO). Excitation of this state utilizes a transition moment that is perpendicular to the long axis of the molecule, lying in the plane of the benzene ring, and rotated by 21° around the *a*-axis of 1PP (see I).

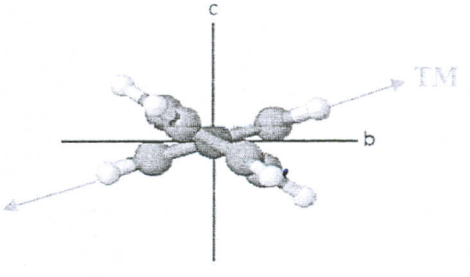

I

The electric field tuning behavior of a specific transition in an electronic spectrum depends on the values of all three

Received Date: May 18, 2010
Accepted Date: June 9, 2010
Published on Web Date: June 14, 2010

DOI: 10.1021/jz100653j | J. Phys. Chem. Lett. 2010, 1, 2017–2019

High resolution electronic spectroscopy of 4-methylanisole in the gas phase. Barrier height determinations for the methyl group torsional motion

Philip J. Morgan, Leonardo Alvarez-Valtierra† and David W. Pratt*

Received 12th January 2010, Accepted 10th May 2010
First published as an Advance Article on the web 25th May 2010
DOI: 10.1039/c000757a

Rotationally resolved fluorescence excitation spectra of the $S_1 \leftarrow S_0$ origin band transition of 4-methylanisole have been recorded in the gas phase. The origin band spectrum is split into two subbands owing to tunneling motions along the methyl group torsional coordinate. An analysis of this data provides information about the preferred configuration of the methyl group and the barrier opposing its motion in both the ground and excited electronic states. The results show that electronic excitation has a significant impact on the torsional dynamics of the isolated molecule.

1. Introduction

Rotationally resolved electronic spectroscopy is an extremely sensitive probe of the motions of atoms (or small groups of atoms) in large molecules. In past reports, we have described applications of this technique to proton transfer dynamics in base-pair dimers linked by hydrogen bonds,[1] to the internal rotation dynamics of water molecules in weakly bound complexes of aromatic molecules,[2] and to large amplitude vibrations in "floppy" molecules,[3] in both their ground and excited electronic states. Recently, it has even proved possible to identify using high resolution methods the specific vibrational pathways that lead to conical intersections of two electronically excited states in the biologically relevant indole molecule.[4]

In this report, we focus on the hindered internal rotation of a methyl group attached to an aromatic frame. Previous investigations of 2-methylanisole (2MA) and 3-methylanisole (3MA) have revealed that the barriers opposing the methyl group torsional motion depend on the relative positions of the substituent groups, in both electronic states.[5,6] These studies have shown that 2MA possesses a relatively large ground state barrier and a small excited state barrier, while 3MA possesses a small ground state barrier and a much larger excited state barrier. The methylanilines *o*- and *m*-toluidine also exhibit this behavior.[7]

On the other hand, if the two substituent groups are in the *para* position with respect to each other, it also has been shown that the methyl group torsional motion is relatively free in both the ground and excited states, as in the case of *p*-toluidine.[8] The present study focuses on another molecule of this type, 4-methylanisole (4MA). Our objective is to determine the methyl group torsional barriers in 4MA and compare them to those for 2MA and 3MA, to explore further the dramatic sensitivity of methyl rotor barrier heights to the position of substitution in an aromatic molecule.

Department of Chemistry, University of Pittsburgh, Pittsburgh, PA 15260, USA. E-mail: pratt@pitt.edu
† Present address: División de Ciencias e Ingenierías, Universidad de Guanajuato, Campus León. León, Gto. 37150, México.

2. Experimental

4MA was purchased from Sigma-Aldrich and used as received. Vibrationally resolved $S_1 \leftarrow S_0$ excitation spectra were recorded in the following manner. The second harmonic of a Quanta Ray Nd^{3+}:YAG (Model DCR-1A) laser was used to pump a dye laser (Model PDL-1) containing Rhodamine 575 dye in order to achieve the desired frequency. The visible light output was externally frequency doubled using a potassium dihydrogen phosphate (KDP) crystal. The visible light was then filtered out and the ultraviolet (UV) light with a spectral resolution of ~ 1 cm^{-1} was then passed into the vacuum chamber containing the sample source. 4MA was heated to ~ 45 °C and seeded into ~ 780 Torr of dry argon gas (> 90% purity). The sample mixture was then expanded through a 1 mm diameter orifice pulsed valve, a General Valve Series 9 operating at 10 Hz, into the vacuum chamber (10^{-5} Torr). The sample was crossed 2 cm downstream with the UV light. The fluorescence was collected using a photomultiplier tube (PMT) which is positioned at right angles to both the molecular and laser beams. The data were processed using a boxcar integrator (Stanford Research Systems), interfaced with Quick Data Acquisition software (Version 1.0.5) to record the data.

Rotationally resolved $S_1 \leftarrow S_0$ excitation spectra were recorded using a molecular beam laser spectrometer, described elsewhere.[9] Briefly, samples were heated to ~ 45° C in a quartz source, seeded in dry argon gas (> 90% purity), and expanded through a 240 μm tip nozzle. The expansion was skimmed $\sim$ 2 cm downstream with a 1 mm diameter skimmer to form a molecular beam and then crossed 15 cm downstream of the nozzle with a laser beam operating in the UV. The laser radiation was generated by a modified continuous ring dye laser operating in the visible (Rhodamine 590 dye) along with

JOURNAL OF AGRICULTURAL AND FOOD CHEMISTRY
ARTICLE

J. Agric. Food Chem. 2010, 58, 3689–3693 3689
DOI:10.1021/jf904472e

X-ray Absorption Spectroscopy (XAS) Corroboration of the Uptake and Storage of CeO_2 Nanoparticles and Assessment of Their Differential Toxicity in Four Edible Plant Species

MARTHA L. LÓPEZ-MORENO,[†,||] GUADALUPE DE LA ROSA,[†,§] JOSÉ A. HERNÁNDEZ-VIEZCAS,[†] JOSÉ R. PERALTA-VIDEA,[†] AND JORGE L. GARDEA-TORRESDEY*[,†,‡]

[†]Department of Chemistry, University of Texas at El Paso, and [‡]Environmental Sciences and Engineering Ph.D. Program, University of Texas at El Paso, 500 West University Avenue, El Paso, Texas 79968, [§]Departamento de Ingeniería Química, Universidad de Guanajuato, Col. N. Alta s/n, Guanajuato, Guanajuato 36050, Mexico, and [||]Department of Chemistry, University of Puerto Rico at Mayaguez, Mayaguez, PR 00681

Fate, transport, and possible toxicity of cerium oxide nanoparticles (nanoceria, CeO_2) are still unknown. In this study, seeds of alfalfa (*Medicago sativa*), corn (*Zea mays*), cucumber (*Cucumis sativus*), and tomato (*Lycopersicon esculentum*) were treated with nanoceria at 0–4000 mg L^{-1}. The cerium uptake and oxidation state within tissues were determined using inductively coupled plasma–optical emission spectroscopy (ICP–OES) and X-ray absorption spectroscopy (XAS), respectively. The germination rate and root elongation were also determined. Results showed that nanoceria significantly reduced corn germination (about 30% at 2000 mg L^{-1}; $p < 0.05$), and at 2000 mg L^{-1}, the germination of tomato and cucumber was reduced by 30 and 20%, respectively ($p < 0.05$). The root growth was significantly promoted ($p < 0.05$) by nanoceria in cucumber and corn but reduced ($p < 0.05$) in alfalfa and tomato. At almost all concentrations, nanoceria promoted shoot elongation in the four plant species. XAS data clearly showed the nanoceria within tissues of the four plant species. To the authors' knowledge, this is the first report on the presence nanoceria within plants.

KEYWORDS: Nanoceria; toxicity; cerium speciation; cerium absorption; edible plants

INTRODUCTION

Nanosized materials include particles of 100 nm or less. Currently, engineered nanomaterials (NMs), widely known as nanoparticles (NPs), are been used in medicine, electronics, catalysis, cosmetics, and pharmaceuticals (*1*). Dissimilar to bulk materials, NPs have individual physical and chemical properties pertaining to their morphology and composition. Size, shape, purity, and catalytic activity of NPs determine their interaction with the environment and living organisms (*2*). Nanoceria (CeO_2 NPs) are synthesized for application in engineering processes involving catalysts, polishing agents, fuel additives, and microelectronics (*3*). Release of this NM and its impact on living organisms, including humans, are practically unknown and, in fact, a subject of interest among scientists, governments, industries, and ordinary people (*4*).

Rare earth elements (REEs), such as Ce, La, Pr, and Nd, have been used to improve growth and yield of several crops (*5*), which in some ways has increased their deposition in localized environments (*6*). Reports indicate that bulk REEs, especially Ce^{3+} compounds, accumulated in plants (*7*–*10*); however, to the authors' knowledge, few reports exist on the uptake, accumulation, and biotransformation of nanoceria in living organisms. For instance, Thill and collaborators (*11*) investigated the toxicity of CeO_2 NPs in *Escherichia coli*. They found that nanoceria can be absorbed by the outer membrane of *E. coli*, inducing toxicity through reduction on the surface of bacteria. Auffan et al. (*12*) affirmed that nanoceria are reduced in biological media because Ce^{4+} absorb UV light and nanoceria are able to store oxygen because of their antioxidant properties. Despite the physicochemical properties, NP reactivity is size-dependent because of the surface/volume ratio or surface area (*13*). These researchers found that different sizes of nanoceria can provoke diverse toxicity reactions in aquatic organisms, such as the green algae *Pseudokirchneriella subcapitata* and crustaceans *Daphnia magna* and *Thamnocephalus platyurus*. To the authors' knowledge, there are no reports on the uptake of nanoceria by terrestrial plants.

In the present study, seeds of the edible plants, cucumber (*Cucumis sativus*), tomato (*Lycopersicum esculentum*), alfalfa (*Medicago sativa*), and corn (*Zea mays*), were selected to determine the phytotoxicity and uptake of commercial CeO_2 NPs. These species were selected because of their worldwide importance as crop plants (*14*) and were treated following the United States Environmental Protection Agency (U.S. EPA) guidelines for seed germination and root elongation toxicity tests (*15*). Alfalfa was included in this study because it is a very important forage in the southwestern U.S. and has been extensively studied by several research groups.

In this study, suspensions of 7 nm cubic CeO_2 NPs were prepared at 0, 500, 1000, 2000, and 4000 mg L^{-1}. NP phytotoxicity on seed germination was determined through the percentage

*To whom correspondence should be addressed. Telephone: (915) 747-5359. Fax: (915) 747-5748. E-mail: jgardea@utep.edu.

Published on Web 02/26/2010

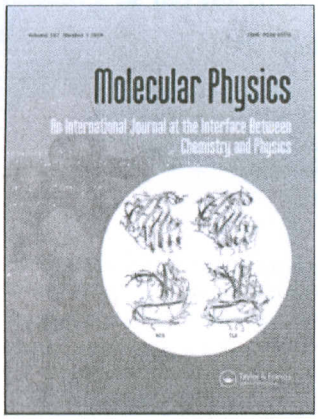

Molecular Physics
Publication details, including instructions for authors and subscription information:
http://www.informaworld.com/smpp/title~content=t713395160

A parametrisation of the direct correlation function for the square-shoulder fluid

I. Guillén-Escamilla [a]; E. Schöll-Paschinger [b]; R. Castañeda-Priego [c]
[a] Departamento de Ciencias Naturales y Exactas, CU-Valles, Universidad de Guadalajara, Ameca, Mexico [b] Department für Materialwissenschaften und Prozesstechnik, Universität für Bodenkultu, A-1190 Vienna, Austria [c] División de Ciencias e Ingenierías, Campus León, Universidad de Guanajuato, 37150 León, Guanajuato, Mexico

Online publication date: 16 February 2010

To cite this Article Guillén-Escamilla, I., Schöll-Paschinger, E. and Castañeda-Priego, R.(2010) 'A parametrisation of the direct correlation function for the square-shoulder fluid', Molecular Physics, 108: 2, 141 — 150
To link to this Article: DOI: 10.1080/00268970903539592
URL: http://dx.doi.org/10.1080/00268970903539592

Structure and effective interactions in parallel monolayers of charged spherical colloids

C. Contreras-Aburto,[1,a] J. M. Méndez-Alcaraz,[1,b] and R. Castañeda-Priego[2,c]
[1]*Departamento de Física, Cinvestav, Av. IPN 2508, Col. San Pedro Zacatenco, 07360 México, D. F., Mexico*
[2]*División de Ciencias e Ingenierías, Campus León de la Universidad de Guanajuato, Loma del Bosque 103, Col. Lomas del Campestre, 37150 León, Guanajuato, Mexico*

(Received 11 December 2009; accepted 29 March 2010; published online 7 May 2010)

We study the microstructure and the effective interactions of model suspensions consisting of Yukawa-like colloidal particles homogeneously distributed in equally spaced parallel planar monolayers. All the particles interact with each other, but particle transfer between monolayers is not allowed. The spacing between the layers defines the effective system dimensionality. When the layer spacing is comparable to the particle size, the system shows quasi-three-dimensional behavior, whereas for large distances the layers behave as effective two-dimensional systems. We find that effective attractions between like-charged particles can be triggered by adjusting the interlayer spacing, showing that the distance between adjacent layers is an excellent control parameter for the effective interparticle interactions. Our study is based on Brownian dynamics simulations and the integral equations theory of liquids. The effective potentials are accounted for by exploiting the invariance of the Ornstein–Zernike matrix equation under contractions of the description, and on assuming that the difference between bare and effective bridge functions can be neglected. We find that the hypernetted chain approximation does not account properly for the effective interactions in layered systems. © *2010 American Institute of Physics*. [doi:10.1063/1.3407454]

I. INTRODUCTION

The study of confinement effects on the statics and dynamics of colloidal dispersions is a very interesting and challenging subject of current colloid science. It is relevant to multidisciplinary sciences[1] such as physics, chemistry, and biology, which in turn are key to technological applications such as nanotechnology and drug targeting. For example, the blood in microvessels and organelles inside the cells can be modeled as a confined colloidal system.[2]

One of the paradigm models in the study of confinement effects is the system of colloids confined between two parallel plates. It has been shown that the phase behavior and the structural properties of the confined colloids depend strongly on the distance between the two plates.[3–13] One of the salient phenomena of this model system is the appearance of colloidal monolayers that are parallel to the confining walls.[7] This self-organization phenomenon occurs also in molecular systems.[4,14]

Another realization of colloidal monolayers is the confinement of colloidal particles at fluid interfaces.[15,16] In these systems, the effective interactions between the trapped particles can be modified, for example, by bringing the supporting substrate closer to the interface.[17] Another example is the well-known liposome-DNA complex, which can be described as a set of rodlike colloids forming parallel monolayer assemblies.[18–20]

Besides the examples of layered systems mentioned above, there exists in the literature a number of studies on the phase behavior of charged particles in layered configurations. For example, Peeters and co-workers[21–23] studied the stability and the different lattice geometries in electronic crystalline bilayers at the ground state, as well as the corresponding melting criteria. Interestingly, they found that the bilayer systems exhibit a much richer variety of crystalline structures with respect to variations in layer density and interlayer separation, while the classical single layer crystallizes only in a hexagonal lattices. An extension of these studies at finite temperatures was performed by Weis *et al.*[24] Additionally, studies on the phase behavior of layered colloidal or dusty plasma have been performed by several groups.[25–31] For instance, Löwen and co-workers have studied sheared colloidal layers as well as the effects that emerge when increasing the number of layers.[30,31]

Thus, it is very important to study the static and dynamic properties of parallel colloidal monolayers. To do this study, one can start by specifying the physical mechanism responsible for the layer formation. However, as a first approximation, in this work, we consider sets of parallel monolayers that where created by some mechanism and focus only on the properties of the layers without consider the mechanism responsible for their formation. The explicit consideration of a substrate, as well as effects arising from external fields, are considered elsewhere.[32]

In this work, we study the microstructure and effective

[a]Present address: Institut für Festkörperforschung, Teilinstitut Weiche Materie, Forschungszentrum Jülich, D-52425 Jülich, Germany. Electronic mail: c.contreras-aburto@fz-juelich.de.
[b]Electronic mail: jmendez@fis.cinvestav.mx.
[c]Electronic mail: ramoncp@fisica.ugto.mx.

Ordering and single-file diffusion in colloidal systems

Salvador Herrera-Velarde,[1] Adalberto Zamudio-Ojeda,[2] and Ramón Castañeda-Priego[3,a)]
[1]*Instituto de Física, Benemérita Universidad Autónoma de Puebla, Apartado Postal J-48, Puebla 72570, Mexico and Department of Applied Mathematics, The University of Western Ontario, London, Ontario N6A 5B7, Canada*
[2]*Departamento de Ciencias Naturales y Exactas, CUV, Universidad de Guadalajara, Carretera Guadalajara-Ameca Km 45.5, Ameca, Jalisco 46600, Mexico*
[3]*División de Ciencias e Ingenierías, Campus León, Universidad de Guanajuato, Loma del Bosque 103, Lomas del Campestre, León 37150, Guanajuato, Mexico and Department of Chemical Engineering, University of Delaware, 150 Academy Street, Newark, Delaware 19716, USA*

(Received 13 June 2010; accepted 23 July 2010; published online 16 September 2010)

The structural properties and the single-file diffusion in one-dimensional interacting colloidal systems are studied by means of Brownian dynamics simulations. We consider three types of particle interactions, namely, Weeks–Chandler–Andersen, screened Coulomb, and superparamagnetic potentials. We find that, regardless of the interaction potential, at low densities particles are distributed in a typical fluidlike structure and at higher densities or potential strengths become spatially correlated at long-distances. Particularly, our findings demonstrate that one-dimensional systems, with particles interacting repulsively, show common structural and dynamical behaviors at the boundary in which the degree of ordering changes dramatically; the main peak of the static structure factor becomes highly narrow with a height of $S_c \approx 7$, whereas the reduced mobility factor F, which is associated with the single-file diffusion at long-times or long wavelengths, reaches values $F^* \approx 0.1$. These features are analyzed and discussed in the context of a local order-disorder transition. © *2010 American Institute of Physics*. [doi:10.1063/1.3479003]

I. INTRODUCTION

The existence of a true thermodynamic phase transition or long-range structural order in one-dimensional (1D) systems with interactions of either short or intermediate range would be very surprising but fascinating. The physical boundaries where such transition might occur is still a controversial topic which remains in debate.[1,2] For example, van Hove's theorem is one of the most known rigorous proofs about the absence of 1D phase transitions.[1] In his seminal work, van Hove proved that a thermodynamic phase transition, defined as singularities in the free energy, cannot occur for short-range interacting 1D systems. In spite of the fact that van Hove's theorem applies only under these specific conditions, sometimes it is employed as a general statement to rule out the existence of 1D phase transitions. Nowadays there is the common belief that 1D systems cannot exhibit phase transitions unless particles interact through long-range interactions.[2–4] The absence of a thermodynamic phase transition for 1D systems has been discussed recently by Cuesta and Sánchez,[1] who examined critically such issue. The authors presented 1D examples which seem to exhibit a true thermodynamic phase transition in spite of both the dimension and the range of the interactions. At the same time, they also extended the validity of van Hove's theorem to include systems of pointlike particles as well as specific systems in the presence of external fields. Nevertheless, as the authors in Refs. 1 and 4 remarked, at this point a general theorem that remains valid for any kind of 1D system does not exist.

In the context of soft matter, 1D system research was practically unnoticed during the last century. This can be understood because the experimental conditions to have a true 1D channel was not an easy task;[5,6] experimental studies were lacking for a long time. Wei *et al.*[7] introduced a new experimental setup consisting of mesoscopic superparamagnetic colloidal particles confined in 1D topographical channels. For the first time, they were able to perform systematic studies of the dynamic process known as single-file diffusion. Later on, a renewed interest in 1D colloidal systems is clearly evident.[7–14]

Single-file diffusion is the process concerned about diffusion of particles in quasi-1D geometries where the particles exhibit random-walk movements in channels so narrow that no mutual passage is possible.[15] Rigorous theoretical results for single-file diffusion have been derived in detail for the simple case of hard rod systems,[16–19] where it is predicted that the mean-square displacement (MSD), $W(t)$, for times much longer that the direct interaction time τ, i.e., the time that a particle needs to move a significant fraction of the mean particle distance, is given by the relation[6]

$$\lim_{t \gg \tau} W(t) = 2F\sqrt{t}, \tag{1}$$

where F is the so-called single-file diffusion mobility factor. Recently, from theoretical point of view, Kollmann[20] demonstrated that relation (1) remains valid for overdamped systems as long as the correlation between particles is of finite range, the particles interact identically and either in absence of hydrodynamic interactions or treated on a pairwise addi-

a)Electronic mail: ramoncp@fisica.ugto.mx.

DIF-10-A08

Thermodynamics of Binary and Ternary Solutions of Multivalent Electrolytes with Formation of 1:1 and 1:2 Complexes, within the Mean Spherical Approximation

José Torres-Arenas,*,†,‡ Jean-Pierre Simonin,*,† Olivier Bernard,† Alexandre Ruas,§ and Philippe Moisy§

Physicochimie des Electrolytes, Colloïdes et Sciences Analytiques (PECSA), CNRS-UMR 7195, UPMC Université Paris 06, Boite 51, 4 Place Jussieu, 75252 Paris, France, División de Ciencias e Ingenierías, Campus León, Universidad de Guanajuato, Loma del Bosque 103, Colonia Loma del Campestre, León, Guanajuato, 37150, México., Commissariat á l'Énergie Atomique/Marcoule/DEN/DRCP, BP 17171, 30207 Bagnols-sur-Ceze Cedex, France

The mean activity ($\gamma_\pm$) and osmotic (Φ) coefficients for binary and ternary aqueous solutions of trivalent electrolytes (mainly made up of lanthanide salts) are described in the framework of the primitive model of ionic solutions, using the binding mean spherical approximation (BiMSA). This model, based on the Wertheim formalism, accounts for (chemical or electrostatic) association of ions. In this work, the multivalent cation and the anion are allowed to form 1:1 (pairs) and 1:2 (trimers) complexes. Expressions for $\gamma_\pm$ and Φ are given which satisfy the Gibbs−Duhem relation. The model involves concentration-dependent cation size and effective relative permittivity, variations that can be interpreted in terms of solvent effects. The theory is applied to aqueous solutions of binary and ternary mixtures at 25 °C with common anion.

Introduction

Lanthanides and actinides compose about one-third of the periodic table and are of particular importance from both theoretical and practical points of view.[1−3]

It is well-known that lanthanides(III) and actinides(III) exhibit several similar properties along their series because of their similarity in external electron configuration and size. The effective radii of the lanthanide and actinide cations decrease across the series (the so-called lanthanide/actinide contraction), reaching ca. 20 and 15% in the case of lanthanide and actinide ions, respectively.[4] This phenomenon causes an increase in the strength of cation−anion and cation−dipole interactions (with the dipole of water). Increased strength of ion−dipole interactions, in turn, implies that the heavy members of both series bind water more closely than the light members. Besides, the coordination numbers (CNs) of lanthanides(III) and actinides(III) in aqueous solutions decrease from 9 to 8 from the beginning to the end of both series,[4] varying with the crystallographic radius as an S-shaped curve with a discontinuity around the europium−gadolinium and berkelium−californium cations, respectively.

Lanthanide and actinide salts are generally well-soluble in aqueous solutions, the high dielectric constant of water allowing dissociation of ionic species and the water producing an efficient solvation of cations. However, in the case of actinides, an acid is generally added to the solution in order to avoid hydrolysis of the metal cation. So, in the industry of reprocessing of nuclear wastes, nitric acid is used at concentrations in the range of 1−7 mol L^{-1}.

In these operations, the trivalent rare earth ions are difficult to separate from each other, but their highly unsymmetrical mixing and complex formation with 1−1 salting-out agents in concentrated solutions can improve their separation. In addition, because of the strong similarity of the various lanthanide(III) and actinide(III) cations, any theory describing the properties of lanthanide(III) solutions may also be suitable for those containing trivalent actinide electrolytes.

In the past, we have applied the mean spherical approximation[5−8] (MSA) to describe the thermodynamics of real ionic solutions.[9−13] Aqueous solutions of pure salts and mixtures, possibly associating, were considered up to very high concentrations, generally to saturation at 25 °C. The model was developed at the McMillan−Mayer level of solutions in which the solvent is regarded as a continuum that manifests itself through its dielectric permittivity. In these studies, the formation of 1:1 complexes was taken into account within the binding MSA (BiMSA)[14] also known as associative MSA (AMSA)[15] or polymer MSA.[16]

In the BiMSA, the strong short-range attractive interaction is modeled by an orientationally averaged sticky interaction potential (sticky-electrolyte model) and the electrostatic interaction is described in the primitive MSA. The MSA is an analytic theory applicable to the primitive model of ionic solutions in which the solvent is regarded as a continuum, as well as to models with molecular solvent. One of the remarkable properties of the MSA for electrolytes is that its mathematical solution can be expressed in terms of a single screening parameter Γ, which plays a role similar to that of the Debye−Hückel screening parameter κ. In these solutions, ionic association may occur in two different ways: through ion pairing in which the clustering process is due to strong Coulomb interactions or via chemical association with the formation of a true chemical bond. The BiMSA theory can accommodate both of these mechanisms. Notice that the BiMSA naturally contains a mass action law for the ion association equilibrium.

Besides solutions of monovalent and divalent electrolytes, we have used the BiMSA in the case of trivalent lanthanide salt solutions up to high concentrations.[17] The predictive capability of this approach was assessed in the case of aqueous

* To whom correspondence should be addressed. E-mail: jtorres@fisica.ugto.mx (J.T.-A.); jpsimonin@gmail.com (J.-P.S.).
† UPMC Université Paris 06.
‡ Universidad de Guanajuato.
§ Commissariat á l'Énergie Atomique/Marcoule/DEN/DRCP.

10.1021/ie901323x
Published on Web 01/07/2010

DIF-10-A08

Thermodynamics of Binary and Ternary Solutions of Multivalent Electrolytes with Formation of 1:1 and 1:2 Complexes, within the Mean Spherical Approximation

José Torres-Arenas,*,†,‡ Jean-Pierre Simonin,*,† Olivier Bernard,† Alexandre Ruas,§ and Philippe Moisy§

Physicochimie des Electrolytes, Colloïdes et Sciences Analytiques (PECSA), CNRS-UMR 7195, UPMC Université Paris 06, Boite 51, 4 Place Jussieu, 75252 Paris, France, División de Ciencias e Ingenierías, Campus León, Universidad de Guanajuato, Loma del Bosque 103, Colonia Loma del Campestre, León, Guanajuato, 37150, México., Commissariat á l'Énergie Atomique/Marcoule/DEN/DRCP, BP 17171, 30207 Bagnols-sur-Ceze Cedex, France

The mean activity ($\gamma_{\pm}$) and osmotic (Φ) coefficients for binary and ternary aqueous solutions of trivalent electrolytes (mainly made up of lanthanide salts) are described in the framework of the primitive model of ionic solutions, using the binding mean spherical approximation (BiMSA). This model, based on the Wertheim formalism, accounts for (chemical or electrostatic) association of ions. In this work, the multivalent cation and the anion are allowed to form 1:1 (pairs) and 1:2 (trimers) complexes. Expressions for $\gamma_{\pm}$ and Φ are given which satisfy the Gibbs−Duhem relation. The model involves concentration-dependent cation size and effective relative permittivity, variations that can be interpreted in terms of solvent effects. The theory is applied to aqueous solutions of binary and ternary mixtures at 25 °C with common anion.

Introduction

Lanthanides and actinides compose about one-third of the periodic table and are of particular importance from both theoretical and practical points of view.[1−3]

It is well-known that lanthanides(III) and actinides(III) exhibit several similar properties along their series because of their similarity in external electron configuration and size. The effective radii of the lanthanide and actinide cations decrease across the series (the so-called lanthanide/actinide contraction), reaching ca. 20 and 15% in the case of lanthanide and actinide ions, respectively.[4] This phenomenon causes an increase in the strength of cation−anion and cation−dipole interactions (with the dipole of water). Increased strength of ion−dipole interactions, in turn, implies that the heavy members of both series bind water more closely than the light members. Besides, the coordination numbers (CNs) of lanthanides(III) and actinides(III) in aqueous solutions decrease from 9 to 8 from the beginning to the end of both series,[4] varying with the crystallographic radius as an S-shaped curve with a discontinuity around the europium−gadolinium and berkelium−californium cations, respectively.

Lanthanide and actinide salts are generally well-soluble in aqueous solutions, the high dielectric constant of water allowing dissociation of ionic species and the water producing an efficient solvation of cations. However, in the case of actinides, an acid is generally added to the solution in order to avoid hydrolysis of the metal cation. So, in the industry of reprocessing of nuclear wastes, nitric acid is used at concentrations in the range of 1−7 mol L^{-1}.

In these operations, the trivalent rare earth ions are difficult to separate from each other, but their highly unsymmetrical mixing and complex formation with 1−1 salting-out agents in concentrated solutions can improve their separation. In addition, because of the strong similarity of the various lanthanide(III) and actinide(III) cations, any theory describing the properties of lanthanide(III) solutions may also be suitable for those containing trivalent actinide electrolytes.

In the past, we have applied the mean spherical approximation[5−8] (MSA) to describe the thermodynamics of real ionic solutions.[9−13] Aqueous solutions of pure salts and mixtures, possibly associating, were considered up to very high concentrations, generally to saturation at 25 °C. The model was developed at the McMillan−Mayer level of solutions in which the solvent is regarded as a continuum that manifests itself through its dielectric permittivity. In these studies, the formation of 1:1 complexes was taken into account within the binding MSA (BiMSA)[14] also known as associative MSA (AMSA)[15] or polymer MSA.[16]

In the BiMSA, the strong short-range attractive interaction is modeled by an orientationally averaged sticky interaction potential (sticky-electrolyte model) and the electrostatic interaction is described in the primitive MSA. The MSA is an analytic theory applicable to the primitive model of ionic solutions in which the solvent is regarded as a continuum, as well as to models with molecular solvent. One of the remarkable properties of the MSA for electrolytes is that its mathematical solution can be expressed in terms of a single screening parameter Γ, which plays a role similar to that of the Debye−Hückel screening parameter κ. In these solutions, ionic association may occur in two different ways: through ion pairing in which the clustering process is due to strong Coulomb interactions or via chemical association with the formation of a true chemical bond. The BiMSA theory can accommodate both of these mechanisms. Notice that the BiMSA naturally contains a mass action law for the ion association equilibrium.

Besides solutions of monovalent and divalent electrolytes, we have used the BiMSA in the case of trivalent lanthanide salt solutions up to high concentrations.[17] The predictive capability of this approach was assessed in the case of aqueous

* To whom correspondence should be addressed. E-mail: jtorres@fisica.ugto.mx (J.T.-A.); jpsimonin@gmail.com (J.-P.S.).
† UPMC Université Paris 06.
‡ Universidad de Guanajuato.
§ Commissariat á l'Énergie Atomique/Marcoule/DEN/DRCP.

10.1021/ie901323x
Published on Web 01/07/2010

Discrete perturbation theory for the hard-core attractive and repulsive Yukawa potentials

J. Torres-Arenas,[1,a] L. A. Cervantes,[2] A. L. Benavides,[1] G. A. Chapela,[3] and F. del Río[3]
[1]*División de Ciencias e Ingenierías, Universidad de Guanajuato, Loma del Bosque 103, Colonia Lomas del Campestre, León, Guanajuato CP 37150, Mexico*
[2]*Dirección de Planeación, Universidad de Guanajuato, Lascuráin de Retana 5, Guanajuato Centro, Guanajuato CP 36000, Mexico*
[3]*Departamento de Física, Universidad Autónoma Metropolitana-Iztapalapa, Distrito Federal, México 09340, Mexico*

(Received 7 August 2009; accepted 10 December 2009; published online 15 January 2010)

In this work we apply the discrete perturbation theory [A. L. Benavides and A. Gil-Villegas, Mol. Phys. **97**, 1225 (1999)] to obtain an equation of state for the case of two continuous potentials: the hard-core attractive Yukawa potential and the hard-core repulsive Yukawa potential. The main advantage of the presented equation of state is that it is an explicit analytical expression in the parameters that characterize the intermolecular interactions. With a suitable choice of their inverse screening length parameter one can model the behavior of different systems. This feature allows us to make a systematic study of the effect of the variation in the parameters on the thermodynamic properties of this system. We analyze single phase properties at different conditions of density and temperature, and vapor-liquid phase diagrams for several values of the reduced inverse screening length parameter within the interval $\kappa^*=0.1-5.0$. The theoretical predictions are compared with available and new Monte Carlo simulation data. Good agreement is found for most of the cases and better predictions are found for the long-range ones. The Yukawa potential is an example of a family of hard-core plus a tail (attractive or repulsive) function that asymptotically goes to zero as the separations between particles increase. We would expect that similar results could be found for other potentials with these characteristics. © *2010 American Institute of Physics*.
[doi:10.1063/1.3281416]

I. INTRODUCTION

The discrete perturbation theory (DPT) is a theory for discrete-potentials fluids that are a sequence of steps [square-well (SW) and square-shoulder (SS)], based only on the knowledge of accurate SW free-energy perturbation terms. Although originally designed for discontinuous potentials, it is more suitable for continuous ones for which a fine discretization can be done.[1]

The DPT has been applied to different intermolecular potentials. With the purpose to mimic the behavior of single-component fluids that exhibit multiple fluid-fluid transitions, the SS+SW potential was studied and it was observed that the DPT reproduced qualitatively well the phase diagram of these systems.[2,3] It seems that the DPT predictions improve as the difference between consecutive steps diminishes, as for the Lennard-Jonesium case.[4,5] Another application of this theory was for the Jagla ramp potential, a potential with two characteristic lengths, suitable to predict some of the water-type anomalies.[6] Besides, this theory has been used to describe binary mixtures[7] and the adsorption of fluids onto solid surfaces.[8]

In all the previous studies, the DPT used the SW terms from the equations of state of Gil-Villegas *et al.*[9] and Benavides and del Río[10] for SW intermediate and long ranges, respectively. Nevertheless, the DPT can be improved if better expressions for the SW perturbation terms are available for *all* the SW ranges. Recently, Espíndola *et al.*[11] have obtained an improved fourth-order perturbation equation of state for the SW fluid, including better expressions for the first-order and second-order free-energy terms.

In this work, these improved first-order and second-order SW terms were used in the DPT to emphasize that this technique can be used for hard-core continuous potentials. In order to illustrate the good DPT performance we have selected the hard-core attractive Yukawa (HCAY) potential and the hard-core repulsive Yukawa (HCRY) potential

$$u(r)=\begin{cases}\infty, & r<\sigma\\ \pm\epsilon\dfrac{\exp[-\kappa(r-\sigma)]}{r/\sigma}, & r\geq\sigma\end{cases}, \tag{1}$$

where σ is the hard-core diameter, ϵ is the energy contact value, and κ is the inverse screening length. The minus sign corresponds to the HCAY potential and the positive sign to the HCRY potential. These potentials have been extensively studied by the statistical mechanics techniques, and have been used in different important physics contexts as effective potentials. For instance, it is well known that the effective potential between charged particles immersed in a neutralizing medium is shorter ranged than the bare Cou-

[a]Author to whom correspondence should be addressed. Electronic mail: jtorres@fisica.ugto.mx. FAX: (52 477) 7885100 ext. 8410.

Thermodynamics of Binary and Ternary Solutions of Multivalent Electrolytes with Formation of 1:1 and 1:2 Complexes, within the Mean Spherical Approximation

José Torres-Arenas,*,†,‡ Jean-Pierre Simonin,*,† Olivier Bernard,† Alexandre Ruas,§ and Philippe Moisy§

Physicochimie des Electrolytes, Colloïdes et Sciences Analytiques (PECSA), CNRS-UMR 7195, UPMC Université Paris 06, Boite 51, 4 Place Jussieu, 75252 Paris, France, División de Ciencias e Ingenierías, Campus León, Universidad de Guanajuato, Loma del Bosque 103, Colonia Loma del Campestre, León, Guanajuato, 37150, México., Commissariat á l'Énergie Atomique/Marcoule/DEN/DRCP, BP 17171, 30207 Bagnols-sur-Ceze Cedex, France

The mean activity ($\gamma_{\pm}$) and osmotic (Φ) coefficients for binary and ternary aqueous solutions of trivalent electrolytes (mainly made up of lanthanide salts) are described in the framework of the primitive model of ionic solutions, using the binding mean spherical approximation (BiMSA). This model, based on the Wertheim formalism, accounts for (chemical or electrostatic) association of ions. In this work, the multivalent cation and the anion are allowed to form 1:1 (pairs) and 1:2 (trimers) complexes. Expressions for $\gamma_{\pm}$ and Φ are given which satisfy the Gibbs–Duhem relation. The model involves concentration-dependent cation size and effective relative permittivity, variations that can be interpreted in terms of solvent effects. The theory is applied to aqueous solutions of binary and ternary mixtures at 25 °C with common anion.

Introduction

Lanthanides and actinides compose about one-third of the periodic table and are of particular importance from both theoretical and practical points of view.[1−3]

It is well-known that lanthanides(III) and actinides(III) exhibit several similar properties along their series because of their similarity in external electron configuration and size. The effective radii of the lanthanide and actinide cations decrease across the series (the so-called lanthanide/actinide contraction), reaching ca. 20 and 15% in the case of lanthanide and actinide ions, respectively.[4] This phenomenon causes an increase in the strength of cation−anion and cation−dipole interactions (with the dipole of water). Increased strength of ion−dipole interactions, in turn, implies that the heavy members of both series bind water more closely than the light members. Besides, the coordination numbers (CNs) of lanthanides(III) and actinides(III) in aqueous solutions decrease from 9 to 8 from the beginning to the end of both series,[4] varying with the crystallographic radius as an S-shaped curve with a discontinuity around the europium−gadolinium and berkelium−californium cations, respectively.

Lanthanide and actinide salts are generally well-soluble in aqueous solutions, the high dielectric constant of water allowing dissociation of ionic species and the water producing an efficient solvation of cations. However, in the case of actinides, an acid is generally added to the solution in order to avoid hydrolysis of the metal cation. So, in the industry of reprocessing of nuclear wastes, nitric acid is used at concentrations in the range of 1−7 mol L^{-1}.

In these operations, the trivalent rare earth ions are difficult to separate from each other, but their highly unsymmetrical mixing and complex formation with 1−1 salting-out agents in concentrated solutions can improve their separation. In addition, because of the strong similarity of the various lanthanide(III) and actinide(III) cations, any theory describing the properties of lanthanide(III) solutions may also be suitable for those containing trivalent actinide electrolytes.

In the past, we have applied the mean spherical approximation[5−8] (MSA) to describe the thermodynamics of real ionic solutions.[9−13] Aqueous solutions of pure salts and mixtures, possibly associating, were considered up to very high concentrations, generally to saturation at 25 °C. The model was developed at the McMillan−Mayer level of solutions in which the solvent is regarded as a continuum that manifests itself through its dielectric permittivity. In these studies, the formation of 1:1 complexes was taken into account within the binding MSA (BiMSA)[14] also known as associative MSA (AMSA)[15] or polymer MSA.[16]

In the BiMSA, the strong short-range attractive interaction is modeled by an orientationally averaged sticky interaction potential (sticky-electrolyte model) and the electrostatic interaction is described in the primitive MSA. The MSA is an analytic theory applicable to the primitive model of ionic solutions in which the solvent is regarded as a continuum, as well as to models with molecular solvent. One of the remarkable properties of the MSA for electrolytes is that its mathematical solution can be expressed in terms of a single screening parameter Γ, which plays a role similar to that of the Debye−Hückel screening parameter κ. In these solutions, ionic association may occur in two different ways: through ion pairing in which the clustering process is due to strong Coulomb interactions or via chemical association with the formation of a true chemical bond. The BiMSA theory can accommodate both of these mechanisms. Notice that the BiMSA naturally contains a mass action law for the ion association equilibrium.

Besides solutions of monovalent and divalent electrolytes, we have used the BiMSA in the case of trivalent lanthanide salt solutions up to high concentrations.[17] The predictive capability of this approach was assessed in the case of aqueous

* To whom correspondence should be addressed. E-mail: jtorres@fisica.ugto.mx (J.T.-A.); jpsimonin@gmail.com (J.-P.S.).
† UPMC Université Paris 06.
‡ Universidad de Guanajuato.
§ Commissariat á l'Énergie Atomique/Marcoule/DEN/DRCP.

10.1021/ie901323x
Published on Web 01/07/2010

International Journal of Bioelectromagnetism
Vol. 12, No. 2, pp. 76 - 80, 2010
www.ijbem.org

Electric Characterization of Skin Near Biological Active Points and Meridians

F.M. Vargas-Luna[a], E.A. Perez-Alday[a], M.R. Huerta-Franco[b] and I. Delgadillo-Holtfort[a]

[a] *Departamento de Ingeniería Fisica, DCI-Campus Leon, Universidad de Guanajuato, León, México*
[b] *Departamento de Ciencias Aplicadas al Trabajo, DCS-Campus Leon, Universidad de Guanajuato, León, México.*

Correspondence: F.M. Vargas-Luna, Departamento de Ingeniería Fisica, DCI-Campus Leon, Universidad de Guanajuato. Loma del Bosque 103, Lomas del Campestre, 37150, León Gto. México. E-mail: mvargas@fisica.ugto.mx, phone +52 477 788 5100 Ext 8472, fax +52 477 788 51 00 Ext 8410

Abstract. Electric properties of the skin of eighteen young and healthy volunteers were evaluated around four of the so called Biological Active Points or acupoints (PC6, PC4, Li4, St36) and around a section of the pericarium (PC) meridian. These acupoints show significant lower resistance than the corresponding adjacent points. Additionally, acupoints show lower variability of this parameter than control points. PC meridian was evaluated along 10 cm from the wrist in points separated 0.5 cm. The mean value of the resistance was lower in meridian points than the corresponding resistance of non meridian line points. Nevertheless, comparing the resistance values of only meridian points, only one meridian point (from four PC points covered by the measurements) could be associated with acupoint according to its electrical characteristics that have significant lower resistance compared to neighbor points on the meridian line. Resistance variability was statistically similar in both meridian and non meridian points so this parameter could be valuable only using a non meridian control point for comparison.

Keywords: Acupuncture Points; Meridians; Bioimpedance; Electrical Variability; Skin Resistance

1. Introduction

In 1997 The National Institute of Health from the USA and in 2003 the World Health Organization declared that there is enough evidence to recognize the Acupuncture as an alternative treatment to prevent and cure diverse pathologies [NIH Consensus Statement 1997, WHO; 2003].

The stimulation of Biological Active Points (BAP)'s or acupoints is performed introducing the needles into the skin by internal mechanical stimulation (according to the traditional acupuncture methodology) consisting in the rotation of the inserted needle. Nowadays the BAP are stimulated with many techniques: 1) with electrical stimulation yielding to the so called electro-acupuncture, 2) with thermal stimulation by moxibustion, 3) by optical stimulation as in laser-acupuncture and 4) the external mechanical stimulation known as acu-pressure besides of the magnetic stimulation used in other alternative therapies.

Although acupuncture is "accepted" like an alternative therapy, still non conclusive investigation related to its physical principle of action exists. However, many results have been published in topics related to clinical trials and experiments made by physicians, testing the efficacy of the acupuncture. The scientific conclusions are controversial mainly among the occidental researchers [Ernst 2006]. At the same time, the research on physical properties of these acupoints and their meridians is scarce and again controversial [Ahn 2008].

Among the physical properties of BAP, the electrical properties, mainly electrical resistance or conductance have a relevant role in the characterization of these skin points. The most accepted result about that is the lower electrical resistance of BAP compared with surrounded points. This of course is still under strong controversy as it was mentioned above [Ahn 2008]. Nevertheless the usual BAP technique to localize acupoints uses the high conductance property by surface measurements.

In the surface evaluation of BAP there exists a set of factors that influence the measurement [Ahn 2007]: 1) the stratum corneum, 2) the electrode pressure, 3) the skin hydration, 4) the electrode polarizability, and 5) subcutaneous fat tissue, among others.

Med Biol Eng Comput (2010) 48:727–729
DOI 10.1007/s11517-010-0625-y

LETTER

Scintigraphy vs. mechanical magnetogastrography: gastric emptying analysis

J. M. De la Roca-Chiapas · T. Córdova-Fraga · G. Reynaga · S. Solorio · M. Sosa · A. E. Rivera-Cisneros · J. J. Bernal · M. Vargas-Luna

Received: 28 December 2009 / Accepted: 21 April 2010 / Published online: 21 May 2010

Abstract Scintigraphy technique is considered the gold standard for gastric emptying evaluations. Lately mechanical magnetogastrography (MMG) technique has emerged as an alternative for these assessments. This study presents the determination of reference values for MMG in order to validate this novel technique in gastric emptying measurements. Both methodologies were used in young and healthy subjects provided with a solid test meal. The measurements were performed with 2 days of difference. Bland–Altman analysis of the data was performed to conclude about the feasibility of MMG as a good alternative test for gastric emptying assessments. Using MMG, an average of the gastric emptying half-time of 57.6 ± 25.8 min was obtained, whereas the same parameter obtained by scintigraphy was 52.2 ± 12.9 min. In conclusion, the use of MMG technique is in concordance with the results using the gold standard technique for gastric emptying measurements.

Keywords Mechanical magnetogastrography · Scintigraphy · Gastric emptying

J. M. De la Roca-Chiapas (✉) · A. E. Rivera-Cisneros
Psychology Department, University of Guanajuato, Campus Leon, Av. De la Rosas 501, Jardines de Jerez, 37530 Leon, Gto., Mexico
e-mail: joseroca@fisica.ugto.mx

T. Córdova-Fraga · M. Sosa · J. J. Bernal · M. Vargas-Luna
Physical Engineering Department, University of Guanajuato, Campus Leon, 37150 Leon, Gto., Mexico

G. Reynaga
Medicine & Nutrition Department, University of Guanajuato, Campus Leon, 37000 Leon, Gto., Mexico

S. Solorio
Clinical Epidemiology Research Unit, UMAE No. 1, IMSS, 37000 Leon, Gto., Mexico

J. M. De la Roca-Chiapas
International Organization New Acropolis Mexico, Leon, Gto., Mexico

1 Introduction

Gastric emptying rate is used as an indicator for several gastrointestinal disorder diagnosis, such as diabetic gastroparesis [14], functional dyspepsia [12], among others. It is expressed as the emptying half-time, $\tau_{1/2}$ [18], indicating the time required to evacuate half of the luminal content. This parameter is evaluated using different methods; however, it is recommended the use of scintigraphy technique by the anterior/posterior method and 90 min of evaluation time [19], although there are protocols using different times for emptying liquid and/or solid material [8].

Several studies reported different emptying half-time values with their corresponding confidence interval. Of course these variations come from particular measurement conditions, sample size, and the characteristics of the population under study. As an example of natural difference of gastric emptying rates between two populations it can be mentioned the men versus women difference [10], probably related to hormone influence. Therefore, for women it is recommended to perform the evaluations during the first 10 days of the menstrual cycle [9].

Many methods exist for gastric emptying evaluation such as electrogastrography [4] which records gastric electrical activity through internal or cutaneous electrodes. The ultrasonography technique images the luminal content volume inside the stomach [15]. The 13C-octanoic acid

Int J Thermophys (2010) 31:784–792
DOI 10.1007/s10765-010-0770-4

Optical Photoacoustic Detection of Circulating Melanoma Cells *In Vitro*

G. Gutiérrez-Juárez · S. K. Gupta · Ryan M. Weight · L. Polo-Parada · C. Papagiorgio · J. D. Bunch · J. A. Viator

Received: 26 June 2009 / Accepted: 27 May 2010 / Published online: 22 June 2010

Abstract The purpose of this research was to investigate the sensitivity of a system for the detection of circulating melanoma cells based on the thermoelastic properties of melanoma. The method employs photoacoustic (PA) excitation coupled with an optical transducer capable of determining the presence of cells within the circulating system in vitro. The transducer is based on stress wave-induced changes of the optical reflectance of a glass–water interface, probed with a continuous laser beam that is incident at an angle close to the critical angle of total internal reflection. A frequency tripled Nd:YAG laser pumping an optical parametric oscillator was employed to provide 532 nm and 620 nm laser light with a pulse duration of 10 ns. A custom-made flow chamber was used as an excitation and acoustic wave collection device. The targets were a human melanoma cell line HS 936 with an average diameter of about 15 μm. Melanoma cells were suspended in 10 mL of two types of media. The first

G. Gutiérrez-Juárez
Division de Ciencias e Ingenierias Campus Leon, Universidad de Guanajuato, Leon, Guanajuato 37150, Mexico

G. Gutiérrez-Juárez · S. K. Gupta · J. A. Viator (✉)
Department of Biological Engineering, University of Missouri, Columbia, MO 65211, USA
e-mail: viatorj@missouri.edu

J. A. Viator
Department of Dermatology, University of Missouri, Columbia, MO 65211, USA

L. Polo-Parada
Department of Medical Pharmacology and Physiology, University of Missouri, Columbia, MO 65211, USA

L. Polo-Parada · C. Papagiorgio · J. D. Bunch
Dalton Cardiovascular Research Center, University of Missouri, Columbia, MO 65211, USA

R. M. Weight
Kansas City University of Medicine and Biosciences, Kansas City, MO, USA

A XY magnetic scanning device for magnetic tracers: Preliminary results

Pacheco AH[a], Cano ME[b], Córdova-Fraga T[a], De la Roca JM[c], Hernández-Sámano A[a].

[a]*Divisón de Ciencias e Ingenierias de la Universidad de Guanajuato. Loma del Bosque 103, Lomas del Campestre, 37150 León, Gto., México.*

[b]*Centro Universitario de la Ciénega de la Universidad de Guadalajara, Av. Universidad, 1115, col Florida, Ocotlán, Jal., México*

[c]*Asociación Cultural Nueva Acropolis México, León, Guanajuato, México Blvd. González Boca Negra 1207, col León Moderno León, Guanajuato, México*

Correspondence: Cano ME, Centro Universitario de la Cienega, Ocotlán, Jalisco, México. E-mail: mecano@cuci.udg.mx

Abstract. In this paper it is presented the maps of magnetic field obtained in phantoms magnetically marked, wich were produced in the laboratory. Using a mobile device automatic two-way, developed to detect changes in magnetic flux, which is based on an array of magnetoresistive sensors designed to detect magnetic fields of 100mT to 10 nT. There are also stages in the development of experimental and discusses the prospects for using this device.

Keywords: Magnetic; Magnetorresistive; Scanning; Tissue

1. Introduction

There are currently several devices for obtain images inside the human body, that have resulted in techniques of imaging, commonly used in laboratories of hospitals, with the aim of helping doctors to deliver clinical diagnostics, for example: Radiographs whose physical principle is based on the emission of x rays through a material, or well, obtaining images using a Nuclear Magnetic Resonance (NMR), where the physical principle used is funded on quantum mechanics and is based on the detection by means of antennas the radio waves emitted by atomic nucleus. They previously suffered an alignment by using an intense uniform magnetic field and small localized field gradients subsequently the nucleus are perturbed using radiofrequency waves. Ultrasound images, whose reconstruction was based on the detection of acoustic waves using small arrangements of piezoelectric transducers, which recorded the sound wave that bounces in the material medium (echo). There are also other types of images based on the detection of X-ray, known as Computed Axial Tomography (CT scan), which is based on the detection of radiation absorbed by a material medium, similar to the radiograph, with the difference that a CT scan, the detector makes a sweep around a circle in the axial plane to the sample under study, while recording images.

Some of the above techniques can be supplemented by substances that improve the quality of an image called contrast media, these substances can be radio-opaque elements such as barium or highly paramagnetic heavy elements such as gadolinium, however, there are other techniques for obtaining medical images such as the Nuclear Medicine (NM) and Positron Emission Tomography (PET) using cameras for detection and short-lived radioactive isotopes.

The aim of this work is to demonstrate a novel device based on magnetoresistive sensors designed to obtain two-dimensional maps of the magnetic flux in phantoms prepared in the laboratory using a mixture of Vaseline and magnetite (Fe_3O_2) as a magnetic tracer. This kind of magnetic tracer has been used in some biomagnetic studies developed in humans. [Córdova] and [Carneiro] carried out studies of gastric motility, for which it was necessary that the tracer was ingested by the volunteers, they underscore the fact that this substance is not absorbed by the body, and this same type of iron oxide were also used for studies of hyperthermia induced cell magnetically as tracer tumour tissue, see for examples [Bahadur, Hergt].

On the other hand, have developed some similar measurement devices that use transducers of the same nature as our own, like the [Cano *et. al.*], who developed a magnetic 16-channel scanner for imaging magnetic surfaces, either developed by [Leyva *et. al.*], which was used to determine images of ferromagnetic tracers. In these devices (unlike ours) the array of sensors remains static while the sample moves in a plane above them.

Lasers in Surgery and Medicine 42:274–281 (2010)

Detection of Melanoma Cells In Vitro Using an Optical Detector of Photoacoustic Waves

Gerardo Gutierrez-Juarez,[1,2] Sagar K. Gupta,[2] Mays Al-Shaer, MD,[2] Luis Polo-Parada, PhD,[2] Paul S. Dale, MD,[2] Chris Papageorgio, MD,[2] and John A. Viator, PhD[2]*

[1]*University of Guanajuato, Leon, Mexico*

[2]*University of Missouri, Columbia, Missouri 65211*

Background and Objective: Circulating tumor cells have been shown to correlate positively with metastatic disease state in patients with advanced cancer. We have demonstrated the ability to detect melanoma cells in a flow system by generating and detecting photoacoustic waves in melanoma cells. This method is similar to flow cytometry, although using photoacoustics rather than fluorescence. Previously, we used piezoelectric films as our acoustic sensors. However, such films have indicated false-positive signals due to unwanted direct interactions between photons from the high laser fluence in the flow system and the film itself. We have adapted an optical detection scheme that obviates the need for piezoelectric films.

Study Design/Materials and Methods: Our photoacoustic system comprised a tunable laser system with an output of 410–710 nm with a pulse duration of 5 nanoseconds. The light was delivered by optical fiber to a glass microcuvette that contained saline buffer suspensions of melanoma and white blood cells. We used a continuous HeNe laser to provide a probe beam that reflected off of a glass and water interface in close proximity to the microcuvette. The beam was detected by a high-speed photodiode. When a photoacoustic wave was generated in the microcuvette, the wave propagated and changed the reflectance of the beam due to index of refraction change in the water. This perturbation was used to detect the presence of melanoma cells.

Results: We determined a detection threshold of about one individual melanoma cell with no pyroelectric noise indicated in the signals.

Conclusions: The optical reflectance method provides sensitivity to detect small numbers of melanoma cells without created false-positive signals from pyroelectric interference, showing promise as a means to perform tests for circulating melanoma cells in blood samples. Lasers Surg. Med. 42:274–281, 2010. © 2010 Wiley-Liss, Inc.

Key words: cancer; metastasis; optical reflectance; optoacoustic; Q-switched

INTRODUCTION

Circulating tumor cells (CTCs) are those cells that detach from a primary or secondary tumor and spread to distant organs via the blood or lymph systems [1–5]. CTCs have been shown to correlate with metastatic disease state and their detection and quantification may be used by clinicians to optimize the therapy of cancer patients. CTCs may occur as one cell among millions of normal blood cells and may originate from solid tumors or hematological malignancies such as leukemia. Many methods have been proposed to find CTCs, but due to their rare occurrence no accepted method has been implemented in clinical practice.

RT-PCR, immunomagnetic separation, micro-fluidics, and automated digital microscopy have all been investigated as means for CTC detection [6–8]. All of these methods suffer from a combination of sensitivity problem, the need for specialists for sample analysis, and slow processing time. RT-PCR in particular has been hampered by high cost and difficult preparation. While it has successfully been used to detect CTCs in a research setting, its peculiar absence in clinical diagnosis is due to these short comings.

Automated digital microscopy has been used along with fiber-optic array scanning, although the need for single cell passes requires several hours for testing a single sample. Immunomagnetic separation has been used widely in research and has even manifested as a commercial device, the CellSearch system. However, this system requires manual imaging of suspect cells and takes hours to process a single sample.

Flow cytometry, however, is used routinely to count leukemia cells using fluorescence detection [9]. This method uses high flow rates of single cells through a detection volume within which cells pass. This method is effective for finding large numbers of CTCs, although rare CTCs from solid tumors would probably pass unnoticed. For leukemia, CTCs are not rare events, as the disease itself is characterized by a proliferation of malignant cells in the blood stream.

We have developed a system for detecting circulating melanoma cells (CMCs) exploiting the natural chromophore,

Contract grant sponsor: ASLMS, Missouri Life Sciences Research Board; Contract grant sponsor: Wallace H. Coulter Foundation.

*Correspondence to: John A. Viator, PhD, 240C Life Sciences Center, 1201 E Rollins Road, Columbia, MO 65211-7310.
E-mail: viatorj@missouri.edu

Accepted 28 December 2009
Published online 23 March 2010 in Wiley InterScience (www.interscience.wiley.com).
DOI 10.1002/lsm.20894

Fluid Phase Equilibria 293 (2010) 182–189

Contents lists available at ScienceDirect

Fluid Phase Equilibria

journal homepage: www.elsevier.com/locate/fluid

Molecular thermodynamics of biodiesel fuel compounds

Felipe A. Perdomo, Alejandro Gil-Villegas*

Department of Physical Engineering, Sciences and Engineering Division, University of Guanajuato Campus León. Lomas del Bosque 103, Fracc. Lomas del Campestre, León 37150, Guanajuato, Mexico

ARTICLE INFO

Article history:
Received 11 December 2009
Received in revised form 3 March 2010
Accepted 6 March 2010
Available online 16 March 2010

Keywords:
Biodiesel fuel
SAFT
Phase diagrams
Molecular thermodynamics

ABSTRACT

Biodiesel fuel is a biodegradable clean energetic resource comprised by a mixture of monoalkyl esters of long chain fatty acids that can be obtained from a wide variety of raw materials. In terms of sulfur content, flash point, aromatic content, biodegradability and low emission of greenhouse-gases effect, biodiesel fuel is better than diesel fuel. In this paper we present a molecular-thermodynamic modeling of the phase equilibria of three very common long-chain alkylesters biodiesel compounds: methyl cis-9-octadecenoate (methyl oleate), methyl hexadecanoate (methyl palmitate) and methyl cis,cis,cis-9,12,15-octadecatrienoate (methyl linolenate). For all the cases, molecules are represented as chains of spherical segments that can associate due to the presence of short-ranged attractive sites. These attractive sites as well as the intermolecular interaction between monomer segments are modeled via square-well potentials of variable range (SW), following the Statistical Associating Fluid Theory for Potentials of Variable Range (SAFT-VR; A. Gil-Villegas, A. Galindo, P.J. Whitehead, S.J. Mills, G. Jackson, A.N. Burgess, J. Chem. Phys. 106(1997)4168–4186). The optimized values of the parameters for each pure component are obtained by fitting to vapor pressure and saturated liquid densities data, derived from the empirical Helmholtz free-energy reported recently by Huber et al. (M.L. Huber, E.W. Lemmon, A. Kazakov, L.S. Ott, T.J. Bruno, Energy Fuels 23(2009)3790–3797). Predictions are improved by the use of a discrete potential, instead of a SW potential, to represent segment–segment interactions, that can be tuned to give an optimized description of the liquid–vapor coexistence properties. The results obtained can be used to model reacting systems to produce biodiesel, based on esterification of fatty acids in presence of acid catalyst or on the transesterification with basic catalyst.

1. Introduction

Biodiesel fuel is a renewable fuel comprised by a mixture of monoalkyl esters of long chain fatty acids. It can be obtained from a wide variety of raw material like vegetable oils or animal fat of any type. Biodiesel could be used as an alternative clean energetic resource, which is biodegradable, renewable and non-toxic. Its properties and compounds depend on raw implemented material and alcohol used in its manufacturing. As an example, the most common compounds present in soy-based biodiesel are the fatty acid methyl esters: methyl palmitate, methyl stereate, methyl oleate, methyl linoleate and methyl linolenate [1]. Due to the strong molecular similarities between biodiesel and parafinic diesel derived from petroleum, this alternative fuel can help to solve the demand for fuel for diesel engines, since no engine modifications are required to maintain the engine performance when diesel is substituted by biodiesel. Additionally, biodiesel is better than diesel fuel in terms of sulfur content, flash point, aromatic content, biodegradability and low emission of greenhouse-gases effect [2].

These facts have led to a worldwide increased interest in the production and application of biodiesel fuels. Methylesters of fatty acids commonly have been produced by the transesterification reaction of triglycerides of vegetables oils with methanol using a basic catalyst [3]. However, another alternative paths for optimal biodiesel production have been investigated, for example, from direct esterification of fatty acid in presence of acid catalyst [4], or from rapeseed oils as prepared in supercritical methanol [5]. Whatever the process-production path considered, the knowledge of thermophysical properties of the biodiesel fuel produced is required, and is not possible to measure such properties for all types of biodiesel fuels blends. Therefore, the development of a molecular thermodynamic model is needed to provide such properties and predict the phase equilibria between compounds.

The modeling of thermodynamic properties of species in a biodiesel fuel blend is demanding, since these compounds have a big molecular size, strong intermolecular interactions, and hydrogen-bonded complex structures, like clusters and rings. However, robust equations of state (EoS) for associating fluids have been derived along the last two decades, based on Wertheim's pertur-

* Corresponding author.
E-mail address: gil@fisica.ugto.mx (A. Gil-Villegas).

0378-3812/$ – see front matter © 2010 Elsevier B.V. All rights reserved.
doi:10.1016/j.fluid.2010.03.011

Estimation of phase behavior and thermophysical properties of Biodiesel blends using SAFT-VR

Felipe A.Perdomo, Alejandro Gil-Villegas
Departmen of Physical Engineering,Science and Engineering Division, University of Guanajuato León,Guanajuato; México

September 27, 2010

Abstract

We present an efficient approach based in the statistical associating fluid theory for chain molecules with attractive potentials of variable range(SAFT-VR; A.Gil-Villegas, A.Galindo, P.J. Whitehead, S.J. Mills, G.Jackson, A.N. Burgess, *J.Chem.Phys.* 106 (1997) 4168) to modeling the thermodynamic properties, chemical and phase equilibria of long-chain alkylesters mixtures (Biodesel Blends).The Molecules presents in the systems(reacting or non-reacting) are represented as chains of spheical segments that can associate due to the presence of short-ranged attractive sites. These attractive sites as well as the intermolecular interaction between monomers segments are modeled via square-well potentials of Variable Range.The pure fatty acid methyl esters component parameters are taken of our earlier work, where we develop a molecular thermodyanmic model for biodiesel fuel compounds. For the thermodynamics of mixtures we implemented a standard combining and mixing rule for mixtures of non-conformal molecules.(A.Galindo, L.A.Davies, A.Gil-Villegas, G.Jackson, *Mol.Phys.* 93 (1998) 241).The selecction of corresponding mixing rule was made whith the purpose of observing the behavior of the biodiesel blend under and below of vapor-liquid critical point of mixture. The phase equilibria of the mixtures was described implementing a global stability analysis due to formation of several phases at specific composition and temperature conditions as well as the construction of binary and thernary phase diagrams. Due to the complex nature of involved species, the simultaneous equilibria (chemical and phase equilibria) was calculed implementing an efficient and robust algorithm based in the Helmhotz free energy mixture minimization as well as a stability criterion for multiphase reacting system.For comparing theorical results against experimental data points, we designed a experimental set-up for mesuring chemical and phase equilibria of the esterification of lauric acid (dodecanoic acid) with methanol to produce methyl laureate, with this system we can obseved a vapor-liquid-iquid phase separation.The simultaneous equilibrium was described very accurately.

1 Molecular model for Thermodynamic of mixtures in Biodiesel Blends

Chemically, Biodiesel is formed by several fatty acid alkylesters , which depending of its composition in each compound form a specific Biodiesel Blend. In this work the systems that we consider are conformed specially by long-chain alkylesters multicomponet mixtures. This systems will be represented by mean a mixture of homonuclear chains molecules formed from tangentially bondend monomers (spherical segments) , this chain molecules can associate due

Molecular Thermodynamic Model for predicting Chemical Equilibria of FAMES Biodiesel compounds Using SAFT-VR

Felipe A.Perdomo, Alejandro Gil-Villegas, Beatriz M. Millán , Guillermo Mendoza
Departmen of Physical Engineering,Science and Engineering Division, University of Guanajuato León,Guanajuato; México

September 27, 2010

Abstract

We present an efficient approach based in the statistical associating fluid theory for chain molecules with attractive potentials of variable range(SAFT-VR; A.Gil-Villegas, A.Galindo, P.J. Whitehead, S.J. Mills, G.Jackson, A.N. Burgess, *J.Chem.Phys.* 106 (1997) 4168) to modeling the chemical equilibria of long-chain fatty acid monohydric alcohol esters (Biodesel compounds). The Molecules presents in the reactive system are represented as chains of spherical segments that can associate due to the presence of short-ranged attractive sites. These attractive sites as well as the intermolecular interaction between monomers segments are modeled via square-well potentials of Variable Range.For the thermodynamics of mixtures we implemented a standard combining and mixing rule for mixtures of non-conformal molecules.(A.Galindo, L.A.Davies, A.Gil-Villegas, G.Jackson, *Mol.Phys.* 93 (1998) 241). We designed a experimental set-up for mesuring chemical and phase equilibria of the esterification of lauric acid (dodecanoic acid) with methanol to produce methyl laureate, with this system we can obseved liquid-iquid phase separation.The simultaneous equilibrium was described very accurately.

1 Introduction

Biodiesel is defined as a liquid hydrocarbon fuel commonly composed of fatty acid methyl esters (FAMES) whose molecular composition may change according to the feed-stock used for the fuel synthesis. The transesterificattion of vegetable oils and animal fats is the most used method to produce biodiesel, generating a by product with comercial value, glycerol [1].An attractive ecological alternative is to convert hazardous waste for enviroment like yellow greases an used vegetable oils to biodiesel. The problem with these source of low cost , oils and fats, is that they contain large amount of free fatty acids that can not be converted to biodiesel using an alkaline catalyst (transesterification) due to presence of unwanted secondary reactions like saponification (soap formation)that dificult the biodiesel separation after reaction and reduce drastically the process efficiency. An alternative to avoid these unwanted effects is to carry on a direct esterification of fatty acids in presence of acids catalyst before transesterifyning the triglycerides with an alkaline catalyst. Esterification of fatty acids is a common practice in the chemical industtry becouse, additionally, fatty esters are also important fine chemicals used in the manufacturing of cosmetics, detergents and surfactants, and therefore in the open literature exists several works where investigate the synthesis of a wide range of fatty acid esters [2] , [3].In a previous work [4] we have propoused a molecular model fatty acid methyl esters Biodiesel compounds ,

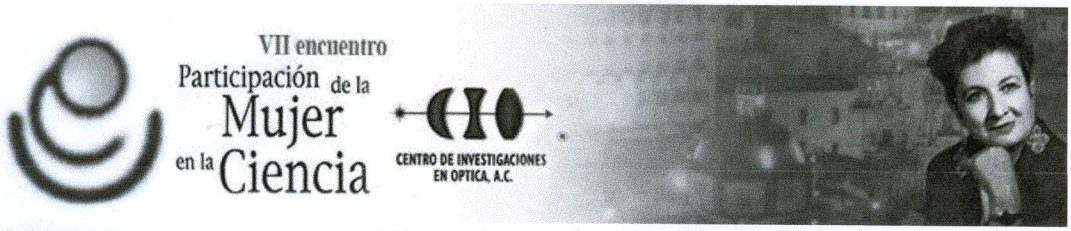

RESPUESTA CEREBRAL INDUCIDA POR DOLOR TERMICO Y ELECTROACUPUNTURA

María-Raquel, Huerta-Franco[a], Miguel Vargas L[b], Ismael Morales M[a], Corina Flores H[a], Ana Lilia González Y[a], Elba Huerta Fc, Isabel Delgadillo[b]

[a]Departamento de Ciencias Aplicadas al Trabajo, DCS-CL, Universidad de Guanajuato, Avenida Eugenio Garza Sada No. 572, Colonia Lomas del Campestre, Segunda Sección, León Guanajuato, México, huertafranco@hotmail.com
[b]Departamento de Ingeniería Física, DCI-CL, Universidad de Guanajuato.Loma del Bosque No. 103, Colonia Lomas del Campestre, León, Guanajuato, México, email. mvargas@fisica.ugto.mx.
[c]Departamento de Clínicas Odontológicas, Universidad de Guadalajara.
e_verushka@yahoo.com.mx

RESUMEN

El objetivo de este estudio, fue evaluar la respuesta cerebral al dolor térmico con resonancia magnética funcional (RMF), y evaluar el efecto analgésico de electro-acupuntura (EA). **Métodos:** A 13 sujetos sanos se les aplico dolor térmico (DT) en una sesión, una semana después recibieron DT más estimulación con EA. El estimulo con EA, se les aplico durante 80 segundos en los puntos (Hegu, LI-4 y Zusanli, ST-36) o dos puntos control (no acupuntura). Las imágenes cerebrales con RMF se tomaron en forma continua durante el estudio. Los datos se procesaron usando SPM99. Con las imágenes cerebrales de cada sujeto se construyó un mapa cerebral grupal utilizando el procedimiento aleatorio ($p<0.001$) tanto para las condiciones: dolor (D), dolor más EA (D+EA) y dolor más Sham (D+S). **Resultados:** El estimulo doloroso produjo una respuesta significativa o respuesta BOLD (Blood Oxigenated Level Dependent) en las siguientes áreas cerebrales: ínsula y claustro/ínsula en forma bilateral, corteza cingulada derecha y corteza sensorial. En general, después de aplicar EA se redujo en un 70% la señal cerebral BOLD producida por dolor. Después de aplicar electro acupuntura en puntos sham o control, esta disminución fue de solo 27% ($p <0.001$). **Conclusiones:** el dolor térmico activa áreas cerebrales relacionadas con la neuro-matriz del dolor. La estimulación de los acupuntos produce cambios mayores, comparado con el efecto de los puntos que no corresponden a acupuntura.

INTRODUCCION

Los efectos analgésicos de electro-acupuntura, ya se habían probado en otros modelos de dolor provocado en animales y humanos (1-3). Sin embargo, la evidencia de los efectos benéficos de acupuntura en estudios clínicos es controversial. Por ejemplo, en pacientes con problemas de migraña se ha probado que la acupuntura fue superior al placebo (sham acupuntura), aunque ambos tratamientos fueron más efectivos que él no aplicar ninguna intervención (4,5). Recientemente se ha probado que la electroacupuntura es superior que la estimulación sham en el tratamiento de pacientes con dolor crónico (3,6). Aunque diversos estudios prueban los efectos analgésicos con acupuntura, queda la interrogante de cuál es el mecanismo por el cual electro-acupuntura produce su efecto analgésico. Y si este efecto analgésico se produce a través de activar diversas vías de señalización a nivel endógenos como el sistema inmune, endocrino, o genético, o si los efectos analgésicos se producen a través de la activación de la inhibición de vías neuronales relacionadas con híper-algesia (1,2). En relación a la primer pregunta, se ha demostrado que la EAC a bajas frecuencias (2 Hz, 0.07 mA) alivia el dolor provocado por inflamación en artritis inducida por colágeno. El mecanismo por el que se cree produce analgesia es por la activación de receptores muscarínicos

Veranos de la INVESTIGACIÓN CIENTÍFICA 2010

ISBN: 978-607-441-085-3

Instrumentación para el Monitoreo de Estrés en Señales Fisiológicas.

De Anda Villa Manuel[1]: manuelde@licifug.ugto.mx, Vargas Luna Francisco Miguel[1]: mvargas@fisica.ugto.mx
Huerta-Franco Raquel[2], Morales-Mata Ismael[2], Sánchez Ramos Alonso[1], Ramírez Miranda Emanuel[3], Moreno Zegbe Estephania[3], Armendáriz Sáenz Claudia[4],

[1]Departamento de Ingeniería Física, DCI- CL Universidad de Guanajuato.
[2]Departamento de Ciencias Aplicadas al Trabajo, DCS-CL U. de Guanajuato
[3]Centro de Ciencias biomédicas, Universidad Autónoma de Aguascalientes
[4]Facultad de ingeniería mecánica y eléctrica, Universidad Autónoma de Coahuila.

Resumen: Se presentan resultados experimentales del monitoreo de estrés a través de señales electrocardiográficas (ECG) obtenidas mediante un electrocardiógrafo profesional marca Biopac. A su vez, se presenta la comparación de estas señales con las señales obtenidas mediante un electrocardiógrafo construido en el laboratorio de Física Médica. Las señales fueron tomadas de sujetos sanos antes, durante y después de ser sometidos a la prueba de estrés sicológica de Stroop. A partir de los picos R de la señal electrocardiográica, se obtuvo la variabilidad de la frecuencia cardiaca (VFC). El análisis de la VFC se realizó comparando áreas bajo el espectro de la transformada de Fourier a baja y alta frecuencias. Se compararon estos parámetros en el total de los sujetos, antes, durante y después de la prueba de Stroop. La razón de las áreas baja/alta frecuencia fue significativamente mayor después de la prueba de Stroop comparada con la etapa antes de dicha prueba. La señal ECG obtenida con el Biopac correlaciona altamente con la obtenida con el dispositivo construido en laboratorio.

Palabras clave: Estrés, Variabilidad Cardiaca, Stroop, Intervalos RR.

Introducción

Los intervalos RR de una señal electrocardiográfica (ECG) definen la frecuencia cardiaca (FC). En un mismo individuo existe una variación natural de este intervalo, es decir, existen fluctuaciones de dichos valores respecto a un valor promedio o característico, esto se conoce como variabilidad cardiaca (VC). En estas fluctuaciones se identifica la influencia del Sistema Nervioso Autónomo (SNA). Las fluctuaciones de baja frecuencia (LF por sus siglas en inglés): 0.04 – 0.15 Hz (Fig. 1), son mediadas por el sistema simpático mientras que las de alta frecuencia (HF por sus siglas en inglés): 0.15 – 0.4 Hz (Fig. 1), son influenciadas por el sistema nervioso simpático y parasimpático [1]. El sistema nervioso simpático tiene mayor influencia al estar el sujeto sometido a estrés, mientras que el sistema nervioso parasimpático tiene menos influencia en la misma situación.

Las metodologías para analizar la VC son diversas, pero una de las más aceptadas es la comparación de las áreas bajo el espectro en frecuencia de estos datos, en el rango de baja y alta frecuencia. La razón entre estas áreas da un índice

Veranos de la INVESTIGACIÓN CIENTÍFICA 2010

ISBN: 978-607-441-085-3

Variación de señales fisiológicas en pruebas de estrés con estimulación de acupuntos

Sánchez Ramos Alonso[1]: aloncete@licifug.ugto.mx,
Morales-Mata Ismael[2]: i_morales_mata@hotmail.com,
Huerta-Franco Raquel[2], De Anda Villa Manuel[1], Vargas Luna Miguel[1], Ramírez Miranda Emanuel[3], Moreno Zegbe Estephania[3], Armendáriz Sáenz Claudia[4],

[1]Departamento de Ingeniería Física, DCI- CL Universidad de Guanajuato.
[2]Departamento de Ciencias Aplicadas al Trabajo, DCS-CL U. de Guanajuato
[3]Centro de Ciencias biomédicas, Universidad Autónoma de Aguascalientes
[4]Facultad de ingeniería mecánica y eléctrica, Universidad Autónoma de Coahuila.

Resumen

Objetivo: Medir el efecto de la estimulación óptica del punto de acupuntura PC6 en pruebas de estrés.
Se analizaron los cambios mediante una Transformada Rápida de Fourier en la señal gástrica y cardiaca evaluada a través de registros de electrocardiograma (ECG) y electrogastrografía (EGG) como resultado del estrés psicológico aplicado a través de la prueba de Stroop. Se registraron los cambios en estas respuestas al aplicar aleatoriamente a los voluntarios un estímulo superficial en el punto PC6 de acupuntura mediante aculaser. Se estudiaron 15 voluntarios con edades de 17 a 24 años de los cuales diez eran varones y cinco mujeres. El paradigma de estudio fue el siguiente: a) registro basal antes de la prueba de señales gástricas y electrocardiográficas (10 minutos); b) registro de las mismas señales fisiológicas durante la prueba de Stroop (alrededor de 2 minutos y medio); y c) registro después de la prueba (3 minutos).
De los 15 voluntarios se estimuló ópticamente a 8 sujetos unilateralmente durante los últimos 5 minutos del registro basal y durante la prueba de Stroop en el punto de acupuntura PC6 con un aculaser.
Los resultados indican que existe un aumento significativo en la frecuencia cardiaca durante la prueba de estrés. La mediana del área bajo el espectro en frecuencias entre 2 y 8 cpm muestra un aumento después de la prueba lo que indica una disminución de la motilidad gástrica (2-4 cpm) lo que está de acuerdo con el efecto fisiológico del estrés. Al comparar los datos de los voluntarios estimulados con aculaser con los no estimulados durante la prueba de Stroop vemos una mediana mayor en sujetos estimulados. Este resultado indica un efecto contrario al reportado en trabajos de acupuntura, dando un aparente mayor estrés en sujetos estimulados.

Palabras clave: Estrés, motilidad gástrica, electrocardiograma, electrogastrografía, acupuntura.

Fluid Phase Equilibria 306 (2011) 124–128

Contents lists available at ScienceDirect

Fluid Phase Equilibria

journal homepage: www.elsevier.com/locate/fluid

Predicting thermophysical properties of biodiesel fuel blends using the SAFT-VR approach

Felipe A. Perdomo, Alejandro Gil-Villegas*

Department of Physical Engineering, Sciences and Engineering Division, University of Guanajuato Campus Leïon, Lomas del Bosque 103, Fracc, Lomas del Campestre, Leïon 37150, Guanajuato, Mexico

ARTICLE INFO

Article history:
Received 2 November 2010
Received in revised form 22 February 2011
Accepted 24 February 2011
Available online 5 March 2011

Keywords:
Statistical associating fluid theory (SAFT)
Biodiesel blends
Speed of sound
Heat capacity

ABSTRACT

Modeling of thermophysical properties and phase equilibria of long-chain methylesters mixtures are presented, using the SAFT-VR approach for mixtures. Molecules are represented as chains of spherical segments that can associate due to the presence of short-ranged attractive sites, using previous molecular parameters obtained for pure fatty acid methyl esters. These attractive sites as well as the intermolecular interactions between monomers segments are modeled via variable-ranged square-well potentials. The cross-energy binary-interaction parameter of the extended Berthelot combining rule was fitted to liquid densities and speed of sound. Very good predictions are obtained for isochoric heat capacities and for binary and ternary phase diagrams.

1. Introduction

Biofuels are now seen as promising and sustainable alternative fuels due to depletion in fossil energies and the enviromental impact generated by petroleum-based fuels. The world production of liquid biofuels in 2008 was approximately 87 Gl of liquid biofuels, which is close to the volume of liquid fossile-fuel consumption of Germany in the same year [1]. The combustion of biomass-derived liquid fuels such as biodiesels has gained significant importance in practical combustion systems such as diesel engines, requiring a better chemical–physics analysis of these systems. Although various biodiesel blends are currently accepted in the market, the availability of information about thermophysical properties for these systems will become more critical in the near future. Additionaly, depending on the kind of feed-stock used for fuel synthesis, its molecular composition as well as its physical and chemical properties varies [2], resulting impractical and expensive to rely only on the measurement of such properties for all biodiesel fuel possibilities. Previous work dealing with this issue has been done by Olivera et al. [3] and Huber et al. [4]. The first authors have evaluated the capability of the Cubic-Plus-Association Equation of State (CPA EoS) [5] to model systems that contain glycerol like byproduct in alkylesters synthesis. On the other hand, the second authors developed an equation of state based on experimental data of thermodynamic properties of a soy based biodiesel fuel.

In our previous article [6], the SAFT-VR approach [7,8] was used to model the vapor–liquid equilibria of three fatty acid methyl esters (FAME) biodiesel compounds. Each FAME was modeled as a chain of spherical segments that can associate due to presence of short-ranged attractive sites. These attractive sites as well as the intermolecular interaction between monomers segments were modeled by square-well potentials of variable range.

In this work we continue the study of the application of SAFT-VR to model biodiesel blends, by determining isochoric heat capacities, speed of sound as well as the phase diagram of binary and ternary FAME mixtures, considering that a biodiesel that is energetically equivalent to a fosil diesel must work in a combustion chamber with typical values of pressures of the order of 45 Mpa and temperatures within the range of 473 K–1073 K [2].

Results obtained are good enough in order to determine the specific influence of each one of the mixture components in the biodiesel blends thermophysical properties, specifically, the residue curve map, that is a very important engineering tool to study complex fluids mixtures in the context of petrochemical, petroleum refining and process engineering for mixtures separation applications.

2. Thermodynamics of biodiesel blends

Biodiesel is formed by several fatty acid alkylesters, and their composition form a specific biodiesel blend. The three FAME considered in this study are methyl linolenate, methyl palmitate and methyl oleate, that can be represented by homonuclear chains molecules formed from tangentially bonded spherical segments that associate due to the presence of short-ranged attractive sites

* Corresponding author. Tel.: +52 4777 885 100.
E-mail addresses: gil@fisica.ugto.mx, agilvm@gmail.com, agilvm@yahoo.com (A. Gil-Villegas).

0378-3812/$ – see front matter © 2011 Elsevier B.V. All rights reserved.
doi:10.1016/j.fluid.2011.02.021

Modelling Adsorption Isotherms of Binary Mixtures of Carbon Dioxide, Methane and Nitrogen

Martín Castro[1], Alejandro Martínez[2] and Alejandro Gil-Villegas[2*] *(1) IPICyT, Instituto Potosino de Investigación Científica y Tecnologíca, Apartado Postal 3-74, Tamgamanga, San Luis Potosí, 78216, S.L.P., México. (2) Department of Physical Engineering, Sciences and Engineering Division, University of Guanajauto Campus León, Lomas del Bosque 103, Fracc. Lomas del Campestre, León 37150, Guanajuato, México.*

(Received 9 December 2010; accepted 8 February 2011)

ABSTRACT: A molecular-based approach for modelling mixtures adsorbed onto solid surfaces using the Statistical Associating Fluid Theory for Potentials of Variable Range (SAFT-VR) for three- and two-dimensional systems is presented in this work. The theory is used to describe the adsorption of binary mixtures of carbon dioxide, methane and nitrogen onto dry activated carbon, describing the overall adsorption phase diagram reported for these systems even at high pressures.

INTRODUCTION

The processes of adsorption and diffusion of fluids in porous media is of great interest in the chemical industry, with applications on environmental remediation being of specific concern (Patel *et al.* 1972; Ruthven 1984; Yang 1987). The design of the optimized process requires a good understanding of the adsorption equilibrium of mixtures. Theories of adsorption where systems are composed of several compounds have been developed on the basis of classical thermodynamics and statistical mechanics. At low pressures, theories for ideal adsorption solutions (Myers and Prausnitz 1965) or simplified statistical thermodynamic models (Ruthven and Wong 1985) can reproduce experimental systems. However, more robust equations of state are required at high pressures.

Recently, adsorption isotherms for simple single-component fluids have been studied using the Statistical Associating Fluid Theory for Potentials of Variable Range (SAFT-VR) (Gil-Villegas *et al.* 1997) adapted for two-dimensional (2D) fluids interacting with discrete potentials (Martínez *et al.* 2007; Jiménez *et al.* 2008). This approach has been applied to model adsorption isotherms for pure molecular fluids, such as methane, nitrogen, carbon dioxide, ethane, ethylene and propane, adsorbed onto activated carbon and silica gel (Martínez *et al.* 2007; Jiménez *et al.* 2008; Castro *et al.* 2010), as well as asphaltenes adsorbed onto Berea sandstone, Bedford limestone and dolomite rock (Castro *et al.* 2009). In all cases, very good agreement was found.

In the present work, we present an extension of this approach in order to model mixtures within a one-fluid van der Waals approximation (Lee 1988; Galindo *et al.* 1998) that has been used previously for 3D mixtures modelled by SAFT-VR (Galindo *et al.* 1998; McCabe *et al.* 1999). This theory is applied to describe adsorption isotherms of methane/nitrogen, methane/carbon

*Author to whom all correspondence should be addressed. E-mail: agilvm@gmail.com.

On the importance of thermodynamic self-consistency for calculating clusterlike pair correlations in hard-core double Yukawa fluids

Jung Min Kim,[1] Ramón Castañeda-Priego,[1,2,a)] Yun Liu,[1,3] and Norman J. Wagner[1]
[1]*Center for Neutron Science, Department of Chemical Engineering, University of Delaware, Newark, Delaware 19716, USA*
[2]*División de Ciencias e Ingenierías, Universidad de Guanajuato, Loma del Bosque 103, 37150 León, Mexico*
[3]*The NIST Center for Neutron Research, National Institute of Standards and Technology, Gaithersburg, Maryland 20899-6100, USA*

(Received 20 September 2010; accepted 4 December 2010; published online 11 February 2011)

Understanding the mechanisms of clustering in colloids, nanoparticles, and proteins is of significant interest in material science and both chemical and pharmaceutical industries. Recently, using an integral equation theory formalism, Bomont *et al.* [J. Chem. Phys. **132**, 184508 (2010)] studied theoretically the temperature dependence, at a fixed density, of the cluster formation in systems where particles interact with a hard-core double Yukawa potential composed of a short-range attraction and a long-range repulsion. In this paper, we provide evidence that the low-q peak in the static structure factor, frequently associated with the formation of clusters, is a common behavior in systems with competing interactions. In particular, we demonstrate that, based on a thermodynamic self-consistency criterion, accurate structural functions are obtained for different choices of closure relations. Moreover, we explore the dependence of the low-q peak on the particle number density, temperature, and potential parameters. Our findings indicate that enforcing thermodynamic self-consistency is the key factor to calculate both thermodynamic properties and static structure factors, including the low-q behavior, for colloidal dispersions with both attractive and repulsive interactions. Additionally, a simple analysis of the mean number of neighboring particles provides a qualitative description of some of the cluster features. © *2011 American Institute of Physics.* [doi:10.1063/1.3530785]

I. INTRODUCTION

In a recent work, the equilibrium microstructure of clusterlike fluids, where particles interact through a hard-core double Yukawa (HCDY) potential with a short-range attraction and a long-range repulsion, was accurately predicted by enforcing thermodynamic self-consistency and using a mixed closure that interpolates between the hypernetted chain (HNC) and Martynov–Sarkisov closure relations.[1] The study of such a fluid draws interest because it leads to a more in-depth understanding of globular protein solutions,[2,3] colloidal dispersions,[4,5] and food science.[6]

Cluster fluids are typically found in systems with competing interactions.[2,3] The cluster formation results from the competition of the length scales associated with the attractive and repulsive contributions of the interaction potential. However, the full physical comprehension of the clustering mechanism is not yet understood. Therefore, the use of simplified models together with complementary methods, namely, experiments, computer simulations, and theoretical formulations, is needed to explore in detail the mechanisms that lead to the formation of particle agglomeration. Hence, the development of accurate theoretical frameworks opens up the possibility of exploring some features of the clustered systems.

As previously noted in the study of the square well (SW) potential, the range of parameters over which one can successfully achieve thermodynamic self-consistency within the integral equation formalism depends strongly on the choice of the closure relation.[7] However, in their original work, Bergenholtz *et al.*[7] reversed the hybridized mean spherical approximation (HMSA) closure[8] to verify that enforcing the thermodynamic self-consistency is a key factor to obtain accurate static structure factors rather than attempting to improve the closure relations, i.e., the resulting structures are equivalent irrespective of the closure selected.

In this paper, we demonstrate that the reversed HMSA (rHMSA) closure provides an equally accurate route to predicting the microstructure and thermodynamics of equilibrium clustered fluids. We apply the same procedure by self-consistently solving the rHMSA closure for the HCDY fluids; our results are corroborated with Monte Carlo (MC) computer simulations.

After the present introduction, Sec. II describes both the theoretical and MC computer simulation methods to calculate the static properties of HCDY fluids. In Sec. III we show that our results indicate that decreasing temperature gives rise, in addition to the typical particle–particle correlation, to a low-q peak in the structure factor, which indicates the presence of liquidlike clusters. In particular, the resulting (partial) clustering is related to the appearance of a kind of particle agglomeration, where particles are able to rearrange their configuration in the whole available volume due to the competition between

a)Author to whom correspondence should be addressed. Electronic mail: ramoncp@fisica.ugto.mx. Tel.: +52-477-7885100. Fax: +52-477-7885100.

Dynamical Arrest Transition in Nanoparticle Dispersions with Short-Range Interactions

Aaron P. R. Eberle,[1] Norman J. Wagner,[1] and Ramón Castañeda-Priego[1,2]

[1]*Center for Neutron Science and Department of Chemical Engineering, University of Delaware, Newark, Delaware 19716, USA*
[2]*División de Ciencias e Ingenierías, Universidad de Guanajuato, 37150 León, Mexico*

(Received 6 January 2011; revised manuscript received 10 February 2011; published 11 March 2011)

We measure the dynamical arrest transition in a model, thermoreversible, adhesive hard sphere dispersion. At low volume fractions ϕ, below the critical point, gelation occurs within the gas-liquid phase boundary. For ϕ slightly below and above the critical concentration, the phase boundary follows the predicted percolation transition. At high ϕ, it melds into the predicted attractive-driven glass transition. Our results demonstrate that for ϕ above ~20% physical gelation is an extension of the attractive-driven glass line and occurs without competition for macroscopic phase separation.

DOI: 10.1103/PhysRevLett.106.105704 PACS numbers: 64.70.pv, 64.75.Xc, 82.70.Dd

Colloidal glasses are characterized by a dynamical arrest of the disperse phase and transition out of equilibrium resulting in a loss of ergodicity [1]. For hard spheres, the repulsive-driven glass (RDG) transition is well known to occur at volume fraction $\phi \sim 0.58$ [2]. The addition of a short-range attraction, as in the case of adhesive hard spheres (AHSs), can induce an additional glassy state, an attractive-driven glass (ADG) [3]. While dynamical arrest at high concentrations can be well described with simulation techniques and the mode-coupling theory (MCT), the transition at intermediate ϕ, often termed gelation, is less clear [4]. In the recent literature there has been significant debate on the location of the gel line in relation to the ADG transition and the gas-liquid coexistence region. Recent experiments and simulations have shown that for depletion aggregation gelation is a result of spinodal decomposition such that the gel line intersects the gas-liquid coexistence region to the right of the critical point [5]. Yet it has been shown in model systems, such as the thermoreversible octadecyl silica, that stable gels can form around or below the critical ϕ [6–11]. In support of this, the percolation theory [12] and simulations [13] predict the formation of clusters large enough to span the system without competition for phase separation at low ϕ. Early studies by MCT and Monte Carlo (MC) simulations suggest that gelation is an extension to lower concentrations of the ADG line in a similar manner to percolation [3,14]. However, numerical simulations have shown that previous MCT results overestimate the location of the gel line, suggesting the phase boundary is buried within the coexistence region [4,15]. While the fluid-to-gel phase transition for depletion-driven aggregation has become clearer, it is debatable whether the location of the phase transition is universal to all AHS systems. In this Letter, we directly address this debate by experimentally studying the dynamical arrest transition of a model AHS nanoparticle system ($\Delta = 0.01$, where Δ is the square-well width and in units of σ, the particle diameter). Our results show a continuous boundary that intersects the gas-liquid coexistence region below the critical concentration without competition for phase separation and suggests that gelation is dependent on the physical mechanism of attraction.

In this work, we use the widely studied octadecyl-coated silica particles, synthesized by using the method of van Helden, Jansen, and Vrij [16] and suspended in *n*-tetradecane. The specific details of our particles and their extensive characterization can be found elsewhere [17]. The particle core has a diameter $\sigma = 28.0 \pm 0.1$ nm and polydispersity PD $= 0.10 \pm 0.005$. The dispersion ϕ was calculated based on a combined fractional density of the core and shell and verified by small-angle neutron scattering (SANS). The interparticle potential, and resultant aggregation, is controlled via temperature as a direct manifestation of a fluid-to-solid phase transition of the brush [17]. The brush molecular chain freezing induces a reversible molecular attraction that manifests as short-range attraction between particles.

Measurements were performed for a wide range of dispersion concentrations: $\phi = 0.09 \pm 0.01$ to 0.52 ± 0.01. We define gelation and determine the gel temperature (T_{gel}) to within ± 0.1 °C by using a combination of the classic Winter-Chambon [18] rheological criterion further corroborated with fiber-optic quasielastic light scattering. At T_{gel} we observe a single phase that is stable for weeks. Although the highest ϕ approach the ADG line, we refer to the dynamical arrest transition for all the dispersions as the gel transition within this Letter. SANS is used to probe the nanostructure of the dispersion at and around T_{gel}. Quantitative modeling of the SANS scattering profiles yields the strength of attraction.

Small-amplitude oscillatory shear rheological measurements used to identify the transition from the fluid state to dynamical arrest [18] are shown in Fig. 1. The small-amplitude oscillatory shear results for a temperature ramp experiment for one dispersion, $\phi = 0.12$, can be seen in Fig. 1(a). At high temperatures ($T > \sim 31$ °C), in the fluid state, the suspension exhibits a negligible G', but as the system is quenched the suspension transitions to a

Renormalized jellium mean-field approximation for binary mixtures of charged colloids

José Marcos Falcón-González[1] and Ramón Castañeda-Priego[1,2,*]

[1]*División de Ciencias e Ingenierías, Campus León, Universidad de Guanajuato, Loma del Bosque 103, Lomas del Campestre, 37150 León, Guanajuato, Mexico*

[2]*Center for Neutron Science, Chemical Engineering Department, University of Delaware, 150 Academy Street, Newark, Delaware 19716, USA*

(Received 3 November 2010; revised manuscript received 10 February 2011; published 4 April 2011)

In this work the renormalized jellium model of colloidal suspensions, originally proposed by Trizac and Levin [Phys. Rev. E **69**, 031403 (2004)], is extended to study mechanisms of charge renormalization in binary mixtures of charged colloids. We here apply our recent reformulation that introduces the requirement of self-consistency directly into the Poisson-Boltzmann equation, i.e., the background charge is explicitly replaced by the effective one, thus facilitating the whole charge renormalization scheme. We briefly discuss the reformulated model for monodisperse charged suspensions composed of either spheres or rods. In particular, we put emphasis on the effects of the surface charge variation, mixture composition, and particle size on the charge regulation of charge-stabilized colloidal suspensions.

DOI: 10.1103/PhysRevE.83.041401 PACS number(s): 82.70.Dd, 61.72.Lk

I. INTRODUCTION

During the past few decades charged colloidal suspensions have been the subject of intense research. The origin of such interest resides in the fact that charged colloids are important for either industrial or medical applications and, from a statistical mechanics point of view, represent a unique model system to understand both the phase behavior and the effective interaction potentials in many-body systems [1,2].

Effective interactions appear naturally in the description of colloidal systems because, on the one hand, most of the experimental techniques [3,4] are not able to probe all the components in the system, i.e., solvent molecules and microions, and, on the other hand, the incorporation of all the degrees of freedom in any theoretical framework is an impossible task. Hence, one has to deal with different levels of description that permit us to explain and understand, for instance, the suspension thermodynamics or both static and dynamic correlations between charged colloids, see, e.g., Refs. [1,2] and references therein.

In the simplest level of description, one usually considers the solvent as a dielectric continuum of permittivity ε. This description is known as the primitive model and cannot be applied directly to study a real colloidal suspension due to the large difference in size and charge between the colloids and microions. However, it is common to map a charged colloidal suspension onto an asymmetric electrolyte [1,5–12]. This mapping is restricted to moderate charge asymmetries due to the treatment of long-range interactions becoming a time-consuming problem. One way to overcome this situation is to implement many-colloid mean-field computations [13,14]. At this level, the microions are integrated out of the description and the force on any colloid depends on the positions of all other colloids in the system. Technically, this is done by solving the nonlinear Poisson-Boltzmann (PB) equation for each colloidal configuration; the so-called multicentered PB solver is described in detail in Ref. [14]. Unfortunately, this procedure also becomes very demanding, in particular, at moderate and high particle concentrations. Then, one has to resort to arguments of isotropy and homogeneity of the whole suspension to assume that the microion distribution is symmetric around each charged colloid. Thus, the resulting PB equation is now tractable and provides a good estimation of the system osmotic pressure within the weak coupling regime [15].

Poisson-Boltzmann–based approximations are useful not only to evaluate thermodynamic properties of charged colloidal suspensions but also to account for condensation of counterions onto charged polyelectrolytes [1,2,16–21] or to explain complex transport phenomena in biological systems, such as the nonmonotonic density dependence of the diffusion of DNA fragments [22]. However, alternative frameworks that also describe the condensation effect or charge renormalization have been proposed in recent years. For example, approximations based on integral equations theory that incorporate explicitly solvent details allow us to understand the charge renormalization in nanoparticle dispersions [23–26]. Nevertheless, such approximations cannot be straightforwardly applied to situations in which particles are highly charged or in concentrated suspensions. Therefore, one has to deal with mean-field approaches that are able to explain some of the physical properties in such cases. However, mean-field models also need further approximations at different levels, for instance, in the Hamiltonian [19–21] or directly into the PB equation [27,28], for their solution. Interestingly, even the simplest degree of approximation leads to results that usually agree nicely with either primitive model simulations or experiments [21].

Within the PB mean-field description, the ion-ion correlation is completely neglected and in some models (cell- and jellium-like) the colloid-colloid correlation is introduced *a priori* by assuming a given form for the radial distribution function between colloids. Additionally, the PB description allows us to compute the effective (charge and screening) parameters when a Yukawa-like potential among colloids is explicitly assumed. It is known that this particular potential accurately reproduces the long-distance interaction of two colloids immersed in a salt sea but it should be kept in mind that it usually fails at short distances [29]. Moreover, it has been demonstrated that the force that a colloid feels due to the

*ramoncp@fisica.ugto.mx

Physica A 390 (2011) 3637–3644

Contents lists available at SciVerse ScienceDirect

Physica A

journal homepage: www.elsevier.com/locate/physa

A modified soft-core fluid model for the direct correlation function of the square-shoulder and square-well fluids

I. Guillén-Escamilla [a], E. Schöll-Paschinger [b], R. Castañeda-Priego [c,*]

[a] CU-Valles, Universidad de Guadalajara, Carretera Guadalajara-Ameca km. 45.5, 46600, Ameca, Jalisco, Mexico

[b] Department für Materialwissenschaften und Prozesstechnik, Universität für Bodenkultu, Muthgase 107, A-1190 Vienna, Austria

[c] Departamento de Ingeniería Física, División de Ciencias e Ingenierías, Campus León, Universidad de Guanajuato, Loma del Bosque 103, Col. Lomas del Campestre, 37150 León, Guanajuato, Mexico

ARTICLE INFO

Article history:
Received 21 June 2009
Received in revised form 31 March 2011
Available online 12 June 2011

Keywords:
Square-shoulder fluid
Square-well fluid
Direct correlation function
Ornstein–Zernike equation
MC simulations

ABSTRACT

We propose a simple analytical expression of the direct correlation function for the square-shoulder and square-well fluids. Our approximation is based on an ansatz for the direct correlation function of a modified soft-core fluid, whose parameters are adjusted by fitting the data obtained from Monte Carlo computer simulations. Moreover, it is complemented with a Wertheim-like parametrization to reproduce correctly the direct correlation inside the hard-core. We demonstrate that this approach is in quantitative agreement with the numerical solution of the Ornstein–Zernike equation within the Percus–Yevick approximation. We also show that our results are accurate in a large regime of densities for different interaction ranges and potential strengths. Therefore, this opens up the possibility of introducing the square-shoulder or the square-well potentials as new reference systems in advanced theoretical approximations.

1. Introduction

During the past few years, physicists have dealt with the nature of the (effective) interactions between particles in either simple or complex fluids [1–3]. Usually, the resulting interaction is not given in analytic form. However, a simplified version of such interaction potential can provide a realistic description of the system properties. For example, the so-called discrete potential fluids have provided a useful description to study the thermodynamic properties of a large variety of fluids. One can find in the literature that systems like water [4], methanol [5], polymers [6], electrolytes [7], among others, can be successfully modeled by using the well-known square-shoulder (SS) or square-well (SW) (or a combination of them) fluids. An advantage of both SS and SW fluids is that they can be used to discretize continuous potentials thus facilitating their incorporation in elaborated theoretical frameworks [8,9]; this discretization procedure allows to capture, in a simple way, the structural and thermodynamic properties of continuous potentials [10–12].

In fact, due to the potential application of the SS fluid in different approaches, a renewed interest on its structural and thermodynamic properties has been recently reported [13–15]. Particularly, we have introduced a simple soft-core fluid model to include a parametrization of the direct correlation function of the SS fluid. Moreover, Yuste et al. [14] have developed an analytic approximation based on the rational function approximation method to obtain a simple expression for its radial distribution function. Noteworthy, in our recent work [13] we only focused on the SS fluid while here both SS and SW fluids are explicitly considered.

* Corresponding author. Tel.: +52 477 7885100; fax: +52 477 7885100.
E-mail address: ramoncp@fisica.ugto.mx (R. Castañeda-Priego).

0378-4371/$ – see front matter © 2011 Elsevier B.V. All rights reserved.
doi:10.1016/j.physa.2011.05.031

ARTÍCULO DE INVESTIGACIÓN ORIGINAL

REVISTA MEXICANA DE INGENIERÍA BIOMÉDICA
SOMIB
Vol. XXXII, Núm. 1
Julio 2011
pp 20 - 24

Magnetic characterization of solid food to gastric emptying studies by mechanical-magnetogastrography assessment

Córdova-Fraga T*
Rodríguez D*
De la Roca-Chiapas JM*
Sosa M*
Hernández MA**
Vargas M*
Solorio SE**
Bernal JJ*

* Departamento de Ingeniería Física-DCI, Universidad de Guanajuato Campus León.
** Unidad Médica de Alta Especialidad IMSS, Clínica T-1 León, Guanajuato.

Correspondence:
Teodoro Córdova-Fraga,
E-mail: theo@fisica.ugto.mx.
Tel. 52 (477) 7885100

Received article: 26/may/2010
Accepted article: 14/february/2011

ABSTRACT

Mechanical-Magnetogastrography (M-MGG) is a technique that has been used to measure gastric emptying in healthy subjects and patients with gastrointestinal pathologies. This has allowed implementing a non-invasive technology, free of ionizing-radiation and it may be used in diagnostic tests in clinical medicine. The characterization of a phantom which has a magnetic behavior similar to that observed in gastric emptying studies carried out in persons is presented. A fluxgate magnetometer was used to record the signal in a magnetic unshielded room. Phantom included nine identical deposits prepared with magnetite, Fe_3O_4 and flour. The behavior of the experiment is identical to studies previously reported in evaluations of healthy people and patients.

Key Words: Mechanical-magnetogastrography, gastric emptying, magnetic stimulator.

RESUMEN

La magnetogastrografía mecánica (M-MGG) es una técnica que ha sido usada para medir el vaciado gástrico en pacientes sanos y pacientes con patologías gastrointestinales. Esto ha permitido la implementación de una tecnología no invasiva, libre de radiación ionizante que puede ser utilizada para pruebas clínicas en medicina. En este artículo, la caracterización de un «phantom» que tiene un comportamiento magnético similar a los estudios realizados para el proceso de vaciado gástrico es presentada. Un magnetómetro de flujo magnético fue utilizado para registrar la señal en un cuarto sin aislamiento magnético. El «phantom» incluyó depósitos idénticos preparados con magnetita, Fe_3O_4 y flúor. El comportamiento de los experimentos obtenidos es idéntico a estudios previamente reportados en las evaluaciones de personas sanas y pacientes con alguna patología.

Palabras clave: Magnetogastrografía mecánica, vaciado gástrico, estimulador magnético.

INTRODUCTION

Biomagnetic gastrointestinal (GI) system assessment began in the late fifties and early sixties[1,2]. However, these biomagnetic devices and techniques began to expand their applications until the early seventies of the past century. Cohen in 1969 used the magnetometer to measure the direct current fields of many parts of the body, and established the first orders of magnitude depending on the biomagnetic source registered[3-5]. In the seventies, further studies of the GI system were published[6-8]. This technique, applied

International Journal of Bioelectromagnetism
Vol. 13, No. 4, pp. 245-248, 2011

Measuring Gastroesophageal Region Frequencies for Long time: Preliminary Results

E Hernández-Torres[a], T Cordova[a], Huetzin Pérez[a], M Sosa[a], O Reynoso-Orozco[c], ME Cano[c] and A Mendosa[c]

[a]*Dept. Physics & Engineering, University of Guanajuato campus León, GTO, MEXICO.*
[b] *Centro Universitario de la Ciénega, Universidad de Guadalajara, México.*
[c]*UMAE, Clínica T1-León, Instituto Mexicano del Seguro Social, GTO, México.*

E-mail: theo@fisica.ugto.mx, phone 52 (477) 788-5100, ext: office 8475, fax 8410, Lab 8475

Abstract Measurements registered in the gastro-esophageal section with a implemented biomagnetic modality is presented, this procedure is based on magnetic markers and magnetometers system. It is shown that with this biomgneti modality of evaluation, the gastric-esophageal activity can be monitored per prolonged times and in well defined regions. Registered frequencies in specific zones agree with the values traditionally reported in literature and it is also shown that with this biomagnetic modality it is possible to measure the speed of transit of the alimentary bolus in the esophagus.

Keywords: gastroesophagica motility, esofágical activity, magnetic markers, magnetometers.

1. Introduction

The main aim in this work is to show a new biomagnetic modality in order to measure gastro-esophageal motility. Several studies have been performed with this purpose, evaluating the contractions through the gastrointestinal (GI), as well as studies of gastric emptying carried out in our Lab [Cordova *et al.,* 2004, Cordova-Fraga *et al.*, 2005, De la Roca *et al.*, 2007, and Cordova-Fraga *et al.*, 2008]. In these studies were used ferromagnetic particles as magnetic tracers, they have shown a great utility to describe the gastric emptying and gastric contractions. Unfortunately, this is the only segment of the GI tract where motor function information is measured, this can be because of magnetic particles are not concentrated in a small space, so the magnetic intensity signal is not enough to be recorded by a magnetometer who works at room temperature. Nevertheless, some advantages in using magnetic techniques are ability to assess gastric activity as gastric peristalsis, half time of gastric emptying, influence of stress in the gastric emptying and colon transit time in different stages of the menstrual cycle, as well as the gastric transit that can be evaluated with other techniques like MRI technique. (NMR). [Di Pace *et al.*, 2011]. Although is possible to monitor the esophageal activity taking place, in the same way that in manometry, placing two sensors, in different positions from the esophagus.

In this study is presented an implementation of a magnetic marker and a fluxgate sensor, the first one was fixed through esophagus and gastric segments while the magnetic signal was recorded outside of the human body.

2. Material and Methods

In this study 6 healthy subjects without GI diseases were evaluated, they gave their written consent prior to participation in this study, which was performed according to the Treaty of Helsinki. The measurement procedures begin with the positioning of two magnetic particles in bottom of the stomach helped with an endoscope, so the starting point of magnets was well defined. Magnets were united to a

World Journal of Gastrointestinal Pathophysiology

Online Submissions: http://www.wjgnet.com/2150-5330office
wjgp@wjgnet.com
doi:10.4291/wjgp.v2.i5.65

World J Gastrointest Pathophysiol 2011 October 15; 2(5): 65-71
ISSN 2150-5330 (online)

EDITORIAL

Biomagnetic techniques for evaluating gastric emptying, peristaltic contraction and transit time

Jose María De la Roca-Chiapas, Teodoro Cordova-Fraga

Jose María De la Roca-Chiapas, Division of Health Sciences, Department of Psychology, University of Guanajuato, Campus Leon, C.P. 37670, Leon, Guanajuato, Mexico
Teodoro Cordova-Fraga, Department of Physical Engineering, University of Guanajuato, Campus Leon, 37150 Leon, Guanajuato, Mexico
Author contributions: De la Roca-Chiapas JM and Cordova-Fraga T designed the study, wrote the manuscript, conducted research and assisted with data analysis.
Supported by PROMEP Grant Ugto-PTC-183 and Ugto-CA-37
Correspondence to: Jose María De la Roca-Chiapas, PhD, Division of Health Sciences, Department of Psychology, University of Guanajuato, Blvd. Puente Milenio 1001, Fraccion del Predio San Carlos, C.P. 37670, Leon, Guanajuato, Mexico. josema_delaroca@yahoo.com.mx
Telephone: +52-477-2674900-3664 Fax: +52-477-2674900-3664
Received: March 3, 2011 Revised: August 31, 2011
Accepted: September 7, 2011
Published online: October 15, 2011

Abstract

Biomagnetic techniques were used to measure motility in various parts of the gastrointestinal (GI) tract, particularly a new technique for detecting magnetic markers and tracers. A coil was used to enhance the signal from a magnetic tracer in the GI tract and the signal was detected using a fluxgate magnetometer or a magnetoresistor in an unshielded room. Estimates of esophageal transit time were affected by the position of the subject. The reproducibility of estimates derived using the new biomagnetic technique was greater than 85% and it yielded estimates similar to those obtained using scintigraphy. This technique is suitable for studying the effect of emotional state on GI physiology and for measuring GI transit time. The biomagnetic technique can be used to evaluate digesta transit time in the esophagus, stomach and colon, peristaltic frequency and gastric emptying and is easy to use in the hospital setting.

Key words: Biomagnetic techniques; Magnetogastrography; Gastric emptying; Scintigraphy; Peristaltic contractions

Peer reviewers: Daniel Keszthelyi, Dr., Institute of Maastricht, PO Box 5800, Maastricht 6202 AZ, The Netherlands; Stelios F Assimakopoulos, Dr., Department of Internal Medicine, University Hospital of Patras, Patras 26504, Greece; Angelo Izzo, Professor, Department of Experimental Pharmacology, University of Naples Federico II, via D Montesano 49, 80131 Naples, Italy

De la Roca-Chiapas JM, Cordova-Fraga T. Biomagnetic techniques for evaluating gastric emptying, peristaltic contraction and transit time. *World J Gastrointest Pathophysiol* 2011; 2(5): 65-71
Available from: URL: http://www.wjgnet.com/2150-5330/full/v2/i5/65.htm DOI: http://dx.doi.org/10.4291/wjgp.v2.i5.65

INTRODUCTION

Gastrointestinal (GI) diseases include gastritis[1], gastroesophageal reflux[2,3], dyspepsia[4-6], irritable bowel syndrome[4,7-9] and gastritis associated with cancer[10], inflammation[11], emotional state[12], obstruction[13], *Helicobacter pylori* infection[14,15] and gastroenteritis[1,16]. If people are susceptible to these diseases and dysfunctions[17], there is a high probability that they will undergo clinical diagnosis for GI disease at least once during their lifetime.

The search for ways to diagnose GI diseases and define normal gastric activity has generated a variety of techniques, some of which are invasive or expose the patient to a high dose of ionizing radiation. Nevertheless, it is important to point out that they have been used to monitor diseases such as diabetic gastroparesis. One of these traditional techniques, scintigraphy, is considered the gold standard for GI tract disease diagnosis[6,18]. However, alternative noninvasive techniques such as the 13C octanoic acid[19,20], superficial electrogastrography[21], ultrasound[22] and biomagnetism are available[12,23-28].

ARTÍCULO DE INVESTIGACIÓN ORIGINAL

REVISTA MEXICANA DE INGENIERÍA BIOMÉDICA
SOMIB
Vol. XXXII, Núm. 2
Diciembre 2011
pp 93 - 99

Frequency response of an electric equivalent circuit for a skin type system

F. Gómez-Aguilar,*
J. Bernal-Alvarado,*
J. Rosales-García,**
M. Guía-Calderón,**
T. Córdova-Fraga,*
M. Sosa-Aquino*

* Departamento de Ingeniería Física, DCI, campus León, Universidad de Guanajuato.
** Departamento de Ingeniería Eléctrica, DICIS, campus Irapuato-Salamanca, Universidad de Guanajuato.

Correspondence:
F. Gómez-Aguilar
Loma del Bosque Núm. 103 Col. Lomas del Campestre, 37150. León, Guanajuato.
E-mail: jfga@fisica.ugto.mx

Received article: 10/abril/2011
Accepted article: 19/noviembre/2011

Este artículo puede ser consultado en versión completa en: http://www.medigraphic.com/ingenieriabiomedica

ABSTRACT

In the present work we consider a theoretical representation of an electrical circuit equivalent to a multilayer biological system. The proposed system is of the skin type, containing epidermis, dermis and the subcutaneous tissue. Electrical circuit theory is used, and the behavior of the system is shown in the form of Nyquist and Bode plots. The proposed theoretical approach is a general treatment to describe the bioelectrical transport in a three-layered system, especially in the electrical impedance spectroscopy studies.

Key words: Circuit theory, bioelectric transport, frequency response.

RESUMEN

En el presente trabajo se considera una representación teórica de un circuito eléctrico equivalente a un sistema biológico de múltiples capas. El sistema propuesto es del tipo piel, que contiene la epidermis, la dermis y el tejido subcutáneo. Esto se realiza mediante la teoría de circuitos eléctricos, y el comportamiento del sistema se muestra en forma de diagramas de Nyquist y Bode. El enfoque teórico propuesto es un tratamiento general para describir el transporte bioeléctrico en un sistema de tres capas, especialmente en los estudios de espectroscopia de impedancia eléctrica.

Palabras clave: Teoría de circuitos, transporte bioeléctrico, respuesta en frecuencia.

INTRODUCTION

According to Rigaud[1] who at the beginning of the 20th century began to study the structure of biological tissues based on their electrical properties, biological tissues are conductors and their resistance varies with frequency. The electrical property of any biological tissue depends on its intrinsic structure. In the case of human skin, the impedance can vary with the thickness and moisture content of the organ, the concentration and activity of sweat glands, injuries, age of subject and environmental factors such as temperature and humidity. Electrical impedance studies in biological systems, including human skin, generally, relate to direct measurements of impedance and phase angle as functions of frequency, voltage or current applied[2-6]. In 1974, Burton[7] applied the Bode analysis to measurements of impedance and phase angle of the skin. Through this method, a passive equivalent circuit can be using and considered as a «black box» to plot its impedance and phase angle *versus* frequency. The only necessary assumption is that the system consists only of linear passive elements[7-8]. Although the resulting model is not necessarily unique[7], it describes the system with great precision in the range of frequencies studied. The electrical impedance spectroscopy (EIA) has proven useful in the characterization of biomaterials, recording the behavior of their intrinsic properties by applying a sinusoidal excitation signal. The application of this technique evaluates the bio-

AIP Review of Scientific Instruments

An induction heater device for studies of magnetic hyperthermia and specific absorption ratio measurements

M. E. Cano, A. Barrera, J. C. Estrada, A. Hernandez, and T. Cordova

Citation: Rev. Sci. Instrum. **82**, 114904 (2011); doi: 10.1063/1.3658818
View online: http://dx.doi.org/10.1063/1.3658818
View Table of Contents: http://rsi.aip.org/resource/1/RSINAK/v82/i11
Published by the American Institute of Physics.

Revista Brasileira de Física Médica. 2011;5(2):161-4.

Gastric assessment by images processing of ultrasound in LabVIEW platform: preliminary results

Avaliação gástrica pelo processamento de imagens de ultrassom na plataforma LabVIEW: resultados preliminares

T. Córdova[1,2], M. Sosa[1], J. J. Bernal[1], A. Hernandez[1], G. D. Gutiérrez[1], D. Rodriguez[1], S. Solorio[3], M. A. Hernandez[3], M. Vargas[1], I. Delgadillo[1], G. Moreno[1], J. G. Villalpando[2] and C. R. Contreras[2]

[1]Departamento de Ingeniería Física, Universidad de Guanajuato, Campus León – México.
[2]Facultad de Ingeniería en Computación y Electrónica, Universidad De La Salle Bajío – México.
[3]Unidad Médica de Alta Especialidad, Clínica T1-León, Instituto Mexicano del Seguro Social – México.

Abstract

Nowadays, the gold technique in gastric evaluations still is scintigraphy in spite of ionization radiation dose per patient undergoing this procedure. Gastro images with ultrasound technique are controversial, because the stomach is a hollow cavity filled with gas in basal conditions or in fast state. Fortunately, a stomach with food is recommended in gastric motility and gastric emptying assessment. So, a lack of air in stomach contributes in this kind of study and in recordings of excellent images by ultrasound. In this study, a digital image processing of gastric ultrasound is presented. Whole automated routine and implemented filters are described in order to use this procedure in gastric peristalsis and gastric emptying evaluations. Ten volunteers were recruited and required to attend the measurements about dominant frequency, with values of at least 3 cpm. Although the behavior stomach activity is observed in dynamic graph, an analysis in frequency space is performed.

Keywords: gastric, peristalsis, ultrasound, emptying, LabVIEW.

Resumo

Hoje em dia, a técnica de ouro nas avaliações gástricas ainda é a cintilografia apesar da dose de radiação de ionização por paciente submetido a esse procedimento. As imagens gástricas com a técnica do ultrassom são controversas, pois o estômago é uma cavidade oca preenchida com gás em condições basais ou em estado rápido. Felizmente, um estômago com comida é recomendado em motilidade gástrica, como também na avaliação do esvaziamento gástrico. Portanto, falta de ar no estômago contribui para este tipo de estudo e para gravações de excelentes imagens por ultrassom. Neste estudo, o processamento da imagem digital do ultrassom gástrico é apresentado. Uma rotina totalmente automatizada e filtros implementados estão descritos para usar este procedimento no peristaltismo gástrico e nas avaliações de esvaziamento gástrico. Dez voluntários foram avaliados em relação à frequência dominante, com valores de no mínimo 3 cpm. Embora a atividade estomacal comportamental seja observada em gráfico de dinâmica, uma análise de frequência espacial é realizada.

Palavras-chave: gástrico, peristaltismo, ultrassonografia, esvaziamento, LabVIEW.

Introduction

The gastrointestinal system evaluation is, currently, as important as other clinical procedures, like heart monitoring. If patients are not adequately treated, they may die. This is especially important for some kinds of patients, for instance, diabetes patients with problems of gastroparesis. The scintigraphy technique is now the gold standard in this evaluation, despite ionizing radiations that undergo the persons[1]. There are other imaging techniques for this study, like the ultrasound, that has been an alternative for assessment and monitoring of the gastric activity in the last years[2-6], although it has still not taken off, which could be due to a lack of conclusive results and proper procedure, leading to results highly correlated with the gold standard technique, scintigraphy.

A routine for processing ultrasound images of stomach, implemented in LabVIEW platform, is presented. This has been used to perform evaluations of

Corresponding author: Teodoro Córdova – Departamento de Ingeniería Física – DCI, Universidad de Guanajuato, campus León – Loma del Bosque, 103 – Lomas del Campestre – León, GTO, Mexico – E-mail: theo@fisica.ugto.mx

68.2

Molecular Physics
Vol. 109, No. 11, 10 June 2011, 1467–1476

Taylor & Francis
Taylor & Francis Group

RESEARCH ARTICLE

Properties of a hard-core Yukawa fluid in a uniform gravitational field obtained by a hybrid DFT-Monte Carlo method

José Torres-Arenas[a], Carlos Avendaño[b], Libertad Morales-Anda[a] and Alejandro Gil-Villegas[a]*

[a]*Departmento de Ingeniería Física, División de Ciencias e Ingenierías Campus León, Universidad de Guanajuato, Colonia Lomas del Campestre, León, 37150, México;* [b]*Department of Chemical Engineering, Imperial College London, South Kensington Campus, London, SW7 2AZ, UK*

(Received 24 November 2010; final version received 16 February 2011)

A hybrid self-consistent method using a Density Functional Theory (DFT) and Monte Carlo (MC) simulations has been applied to obtain the density profiles of a hard-core monocomponent Yukawa fluid under the action of a gravitational field. In this method the properties of a N-particles fluid are obtained from a one-particle MC simulation in the presence of a $N-1$ particles effective field, which is calculated by DFT within a local density approximation. The combined DFT/MC calculation is repeated in a self-consistent way until a desirable degree of accuracy is obtained. Two different approximations are used to feed the DFT approach, the mean spherical approximation (MSA) and the statistical associating fluid theory of variable range (SAFT-VR). Results compare very well with direct N-particles MC simulations in the NVT ensemble, for 3000 particles, with a significant reduction in the computing time.

Keywords: Monte Carlo simulations; density functional theory; Yukawa fluid

1. Introduction

Colloidal suspensions are particles in the mesoscopic scale dispersed in a continuous matrix of another material, which are commonly found in nature and every day life. Colloidal suspensions are important in different research areas for their broad number of applications ranging from material science to drug-delivery processes [1]. Although time and length-scale of colloids are completely different compared to the scales of atoms and molecules, some of their processes are very similar. This analogy between atoms and colloids has improved the comprehension of many interesting phenomenon like crystal nucleation and growth, glass transition, and interparticle interactions, with the advantage that colloids can be observed directly in real space [2–4]. Thus the knowledge of their thermodynamic and structural properties are undoubtedly necessary not only as a test of theoretical approaches but also for technological applications.

One of the main subjects in colloidal science is the control of the assembly of the particles to form ordered structures. In this context, the use of external fields (EF) to control colloidal assembly has become an important topic in the last decades [5,6]. EF may included electric and magnetic fields, temperature gradients, gravity and even confining walls to manipulate the ordered structures. For example, under suitable conditions of temperature, concentration and ionic-strength, charged-stabilized colloidal particles exhibit spatial inhomogeneities by the presence of gravity, forming ordered structures at the bottom of the sample [7–11]. This phenonemon is explained as a competition between three main factors, namely interparticle interaction, entropy, and gravitational field. The sedimentation phenomenon has been studied extensively by experiments of regular shape colloidal particles having as a starting point the pioneering work of Jean Perrin [12]. Remarkable experiments in sedimentation of spherical particles with very low polydispersity were reported by Takano and Hachisu [13], by Pusey and co-workers [14,15], and by Piazza *et al.* [16], where a test of the hard-sphere (HS) equation of state (EOS) [17–19] was achieved using the equilibrium sedimentation profiles of charged-stabilized colloids, establishing formally the use of HS as a simple and suitable model to study structural properties of sterically-stabilized spherical colloidal particles. Similar results were reported by Biben *et al.* [20] and by Marechal and Dijkstra [11] using Monte Carlo simulation of HS in a gravitational field. An entropic

*Corresponding author. Email: gil@fisica.ugto.mx

ISSN 0026-8976 print/ISSN 1362-3028 online

DOI: 10.1080/00268976.2011.565287
http://www.informaworld.com

THE JOURNAL OF CHEMICAL PHYSICS 134, 234507 (2011)

Statistical thermodynamics of fluids with both dipole and quadrupole moments

Ana L. Benavides,[1,a)] Francisco J. García Delgado,[1] Francisco Gámez,[2] Santiago Lago,[2] and Benito Garzón[3]
[1]*Departamento Ingeniería Física, División de Ciencias e Ingenierías, Campus León, Universidad de Guanajuato, Apdo. E-413, León, Guanajuato 37150, México*
[2] *Departamento Sistemas Físicos, Químicos y Naturales, Universidad Pablo de Olavide, Ctra. de Utrera Km. 1, Seville 41013, Spain*
[3]*Facultad de Farmacia, Universidad San Pablo CEU, Madrid, Spain*

(Received 2 March 2011; accepted 22 May 2011; published online 17 June 2011)

New Gibbs ensemble simulation data for a polar fluid modeled by a square-well potential plus dipole-dipole, dipole-quadrupole, and quadrupole-quadrupole interactions are presented. This simulation data is used in order to assess the applicability of the multipolar square-well perturbation theory [A. L. Benavides, Y. Guevara, and F. del Río, Physica A **202**, 420 (1994)] to systems where more than one term in the multipole expansion is relevant. It is found that this theory is able to reproduce qualitatively well the vapor-liquid phase diagram for different multipolar moment strengths, corresponding to typical values of real molecules, except in the critical region. Hence, this theory is used to model the behavior of substances with multiple chemical bonds such as carbon monoxide and nitrous oxide and we found that with a suitable choice of the values of the intermolecular parameters, the vapor-liquid equilibrium of these species is adequately estimated. © *2011 American Institute of Physics*. [doi:10.1063/1.3599465]

I. INTRODUCTION

One of the more fruitful approaches within the statistical mechanics of fluids has been to model thermodynamic properties with the simplest intermolecular potential functions able to reproduce the features of interest. Given the importance of polar fluids in process engineering and other branches of applied science,[1,2] various interaction models have been developed in the last few decades.[3–22] Most of these models include overlap and/or dispersion forces through hard-sphere (HS), Lennard-Jones, or Yukawa (Y) potentials besides the electrostatic interactions. Perhaps the most commonly used is the Stockmayer potential[3] which consists in a Lennard-Jones potential plus dipolar interactions. The multipolar square-well model is one of the simplest model manifest overlap and dispersion forces through a square-well (SW) potential together with dipole-dipole, quadrupole-quadrupole, dipole-quadrupole, octopole-octopole, or hexadecapole-hexadecapole interactions. The multipolar square-well perturbation theory provides an analytic equation of state for polar fluids (MSWEOS) based on the statistical-mechanics perturbation theory that has been developed and used to analyze on a consistent basis, the effects of the range of the SW potential as well as the strength of polar moments.[9,10] This MSWEOS has the advantage that several analytic equations of state for SW potentials are available in the literature which is an important ingredient in this theory. This advantage can also be found in the polar fluids works of Alavi and Feyzi,[19] and of Henderson *et al.*,[12] that considered for the overlap and dispersion terms the SW and the Y potential, respectively.

More recently and taking a step further, the MSWEOS has been successfully applied to model thermodynamic properties of real single component polar substances which first nonzero multipole moments were: the dipole moment (water and ammonia), the quadrupole moment (carbon dioxide and nitrogen), the octopole moment (methane and carbon tetrafluoride), and the hexadecapole moment (sulphur hexafluoride).[23–27] Thus, this theory can be applied to model the behavior of single component real substances of quasi-spherical shape. Besides, this MSWEOS could be used as an important ingredient to study more complex fluids, in more elaborated theories such as the Statistical Associating Fluid Theories, as for example: SAFT-VR-D (Ref. 15) or SAFT-VR-Q (Ref. 18) to model the polar monomer interactions, or in coarse-graining modeling theories.[28]

Briefly, the MSWEOS is made up of separate terms representing the effects of overlap and dispersion forces on one hand,modeled by a SW term, and of point multipolar interactions on the other. In spite of its success, the MSWEOS has been rigorously tested against simulation results either for SW + dipole-dipole and for SW + quadrupole-quadrupole potentials.[29] In this work, we present the results of Gibbs ensemble Monte Carlo (GEMC) simulations for SW + dipole-dipole + dipole-quadrupole + quadrupole-quadrupole interactions. We included the crossed dipole-quadrupole interaction in order to assess the applicability of the MSWEOS to systems where more than one term in the multipole expansion is relevant. Although the importance of crossed interactions have been suggested,[11,13,20] this work presents together with the work of Vrabec and Gross,[20] one

[a)]Author to whom correspondence should be addressed. Electronic mail: alb@fisica.ugto.mx. Tel.: +55 477 7885100 ext 8422. Fax: +55 477 7885100 ext 8410.

Perturbation theory for multipolar discrete fluids

Ana L. Benavides[1,a] and Francisco Gámez[2]
[1]*Dpto. Ingeniería Física, División de Ciencias e Ingenierías, Campus León, Universidad de Guanajuato, Apdo. E-413, León, Guanajuato, 37150, México*
[2]*Dpto. Sistemas Físicos, Químicos y Naturales, Universidad Pablo de Olavide, Ctra. de Utrera Km. 1, Seville 41013, Spain*

(Received 10 July 2011; accepted 16 September 2011; published online 7 October 2011)

An analytical expression for the Helmholtz free energy of discrete multipolar potentials as a function of density, temperature, and intermolecular parameters is obtained as an extension of the multipolar square-well perturbation theory [A. L. Benavides, Y. Guevara, and F. del Río, Physica A **202**, 420 (1994)]. The presented procedure is suitable for the description of a more general intermolecular potential model taking into account the overlap and dispersion forces through a discrete potential represented by a sequence of square-shoulders and wells, as well as electrostatic interactions. The main advantage of this approach is that since the Helmholtz free energy is given as an explicit expression in terms of the intermolecular parameters characterizing the interaction, the properties of interest can be easily obtained through usual thermodynamic relations. Besides, since a great variety of discretized potentials can be used with this equation of state, its applicability is very vast. By varying the intermolecular parameters, some illustrative cases are considered, and their phase diagrams are tested against available simulation data. It is found that this theoretical approach is able to reproduce qualitatively and quantitatively well the vapor-liquid equilibrium of the chosen potentials with different multipole moment of varied strengths, except in the critical region. © *2011 American Institute of Physics*. [doi:10.1063/1.3646733]

I. INTRODUCTION

The use of simple molecular models is very important to understand processes in related but more complex systems. From the statistical mechanics perspective, discrete potentials, mainly hard sphere (HS) or square well (SW), are the reference systems for elaborated theories trying to give an in-depth description of the complex phenomenon from an atomistic point of view. The conclusions extracted within this simple approximation serve as a foundation to extrapolate to the more complicated model that is unfeasible to study without an unaffordable computational cost. One example of these methodologies is the perturbation theories (see, for example, a recent review on this approach by Zhou and Solana[1]). Particularly, HS model is the most common reference potential to build these theories since an accurate analytical equation of state (EOS) was derived by Carnahan and Starling[2] in 1969. However, by itself the HS model is not able to account for phenomena provoked by attractive interactions, such as vapor-liquid equilibrium. Hence, in perturbation theories in order to describe this type of transitions the attractive interactions are included as a modulation of the pure repulsive reference system that is considered to dominate the structure of the fluid. First works of this kind applied to discrete potentials were restricted to the SW.[3–6] In the nineties, Benavides and Gil-Villegas[7] afforded this field of research with a general Barker-Henderson-type perturbation-based equation of state[3] in the framework of the high temperature expansion. It was called the discrete perturbation theory (DPT) and it is supported on a potential that consisted of a hard core plus a piecewise function constructed as a sequence of attractive and repulsive steps. The main advantage of this approach is that the thermodynamics properties of several intermolecular potentials can be studied with only the knowledge of suitable expressions for the first- and second-order Helmholtz free energy perturbation terms of a SW fluid of variable range λ. Although originally considered for hard-core discontinuous potentials and successfully applied to a square-shoulder-square-well (SS+SW) potential,[8] it also accurately describes the thermodynamics of other interesting hard-core potentials, such as Jagla ramp-type,[9] Yukawa potentials,[10] and soft continuous potentials, such as Lennard-Jones.[11] However, non-polar fluids are nearly the exception in nature, and the effect of multipolar moments is relevant in the thermodynamics of real fluids. For example, for water, Abascal and Vega[12,13] have found by using simulation studies with different intermolecular models that even though the dipolar interaction is the leading-order contribution to the free energy in the fluid and solid phases, the quadrupolar interaction stabilizes some of the solid phases and hence an accurate description of the phase diagram of dense phases should consider this contribution. Besides, the description of the vapor-liquid equilibrium of simple polar molecules is not good enough if these interactions are not considered (see Ref. 14 and references therein). So, polar fluids represent an important field of research from both theoretical and application points of view.[15,16] Nevertheless, the use of reliable distribution of charge is usually restricted to molecular simulation using force fields that

[a]Author to whom correspondence should be addressed. Electronic mail: analaura.benavides@gmail.com. Tel.: +55 477 7885100 ext. 8422. Fax: +55 477 7885100 ext. 8410.

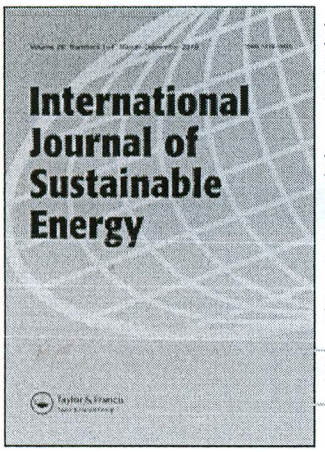

International Journal of Sustainable Energy
Publication details, including instructions for authors and subscription information:
http://www.informaworld.com/smpp/title~content=t713651728

Detailed calculations of the solar irradiance and optimized set-ups of Sun collectors, by the example of central Mexico

Carsten Holtfort[a]; Isabel Delgadillo-Holtfort[a]; Klaus-Peter Schröder[b]
[a] Departamento de Ingeniería Física, División de Ciencias e Ingenierías, Universidad de Guanajuato, León Gto., México [b] Departamento de Astronomía, División de Ciencias Naturales y Exactas, Universidad de Guanajuato, Guanajuato Gto., México

First published on: 04 January 2011

To cite this Article Holtfort, Carsten , Delgadillo-Holtfort, Isabel and Schröder, Klaus-Peter(2011) 'Detailed calculations of the solar irradiance and optimized set-ups of Sun collectors, by the example of central Mexico', International Journal of Sustainable Energy,, First published on: 04 January 2011 (iFirst)
To link to this Article: DOI: 10.1080/1478646X.2010.539299
URL: http://dx.doi.org/10.1080/1478646X.2010.539299

Modelo esféricamente simétrico de la señal fotoacústica en el dominio temporal producida por objetos micrométricos: el caso de células de melanoma *in vitro*

Rafael Pérez Solano[1], Luis Polo-Parada[2*], y Gerardo Gutiérrez Juárez[1*]

[1] División de Ciencias e Ingenierías, Campus León, Universidad de Guanajuato. Loma del Bosque 103, Col. Lomas del Campestre, C. P. 37150, León, Gto.

[2] University of Missouri. Columbia, MO 65211

* Correspondencia: ggutj@fisica.ugto.mx, poloparadl@missouri.edu

En este trabajo, una expresión analítica de la presión fotoacústica (PA) generada por objetos esféricamente simétricos con una densidad de energía por unidad de tiempo efectiva, se obtuvo utilizando la fórmula de Kirchhoff, como solución de la ecuación de onda PA. Suponiendo que el mecanismo dominante en tejidos biológicos es el de expansión termolelástica y, que las células de melanoma poseen una simetría esférica, se utilizó la expresión analítica encontrada para estudiar el comportamiento de la presión PA generada por células de melanoma *in vitro* en el régimen diluido. Se estudiaron los casos de una, dos y una monocapa de células. Finalmente se compararon los resultados analíticos con resultados experimentales previamente obtenidos, [1, 2]. Se encuentra que existe una buena concordancia cualitativa entre teoría y experimento.

I. INTRODUCCIÓN

La técnica fotoacústica (PA, de PhotoAcoustic) tiene como fundamento físico al efecto PA. Éste se refiere a la generación de una onda acústica debido a la absorción de fotones. La generación de una señal PA es el resultado de los efectos causados por el incremento de temperatura, que se siguen después de iluminar un objeto. En el dominio temporal se han reportado al menos seis mecanismos de generación del efecto PA, [3]. Dependiendo de las características de absorción óptica de las muestras y de la potencia del láser, la onda PA es generada por medio de uno, o una combinación de estos mecanismos.

Int. J. Pure Appl. Sci. Technol., 2(2) (2011), pp. 26-45

International Journal of Pure and Applied Sciences and Technology

ISSN 2229 - 6107

Available online at ***www.ijopaasat.in***

Research Paper

Characterization of Simulated Mechanical – Electrical Properties of PVDF and PZT Piezoelectric Material for Use in the Pulsed Optoacoustic Spectroscopy

Raúl A. Reyes-Villagrana[1,*], Gerardo Gutiérrez-Juárez[1] and Rumen Ivanov Tsonchev[2]

[1] Departamento de Ingeniería Física, División de Ciencias e Ingeniería Física, Universidad de Guanajuato Campus León, Lomas del Bosque #103, Lomas del Campestre, C.P. 37150, León, Guanajuato, México.

[2] Unidad Académica de Física, Universidad Autónoma de Zacatecas, Calzada Solidaridad, esq. Paseo a la Bufa s/n, Fracc. Progreso, C.P. 98068, Zacatecas, Zacatecas, México.

* Corresponding author, e-mail: rreyes@fisica.ugto.mx,

(Received: 21-02-2011; Accepted: 10-03-2011)

Abstract: *During the last decade there has been increased research on breast cancer detection using the pulsed optoacoustic spectroscopy technique (POS), where mostly commercial ultrasonic sensors are used to detect the received signal. However, it has been continually difficult to obtain the correct signal because adequate detectors for this technique have not been developed. This paper presents a model to compare and determine the output signal of the piezoelectric active element for the design of an acoustic wave detector to apply to the POS without a signal conditioning stage. We compared two types of piezoelectric materials: piezoceramic PZT-5A and piezopolymer PVDF with different thickness widths. We adopted the Leach model to analyze the thickness-mode system. We applied the pulse – echo which is similar in the detection of the POS, to model the system using the properties of a commercial sensor considered as a source of excitation and taking water as a means of propagation. We used the Morris and Hutchens model with electronic simulation software OrCAD. The results are presented and discussed.*

Keywords: Characterization, OrCAD, Piezoelectric, PVDF, PZT-5A, Simulation.

OPEN ACCESS Freely available online

PLoS one

Hysteresis in Pressure-Driven DNA Denaturation

Enrique Hernández-Lemus[1,2]*, Luz Adriana Nicasio-Collazo[3], Ramón Castañeda-Priego[3]*

1 Computational Genomics Department, National Institute of Genomic Medicine, México, D.F., México, **2** Center for Complexity Sciences, National Autonomous University of México, México, D.F., México, **3** Division of Sciences and Engineering, University of Guanajuato, León, Guanajuato, México

Abstract

In the past, a great deal of attention has been drawn to thermal driven denaturation processes. In recent years, however, the discovery of stress-induced denaturation, observed at the one-molecule level, has revealed new insights into the complex phenomena involved in the thermo-mechanics of DNA function. Understanding the effect of local pressure variations in DNA stability is thus an appealing topic. Such processes as cellular stress, dehydration, and changes in the ionic strength of the medium could explain local pressure changes that will affect the molecular mechanics of DNA and hence its stability. In this work, a theory that accounts for hysteresis in pressure-driven DNA denaturation is proposed. We here combine an irreversible thermodynamic approach with an equation of state based on the Poisson-Boltzmann cell model. The latter one provides a good description of the osmotic pressure over a wide range of DNA concentrations. The resulting theoretical framework predicts, in general, the process of denaturation and, in particular, hysteresis curves for a DNA sequence in terms of system parameters such as salt concentration, density of DNA molecules and temperature in addition to structural and configurational states of DNA. Furthermore, this formalism can be naturally extended to more complex situations, for example, in cases where the host medium is made up of asymmetric salts or in the description of the (helical-like) charge distribution along the DNA molecule. Moreover, since this study incorporates the effect of pressure through a thermodynamic analysis, much of what is known from temperature-driven experiments will shed light on the pressure-induced melting issue.

Citation: Hernández-Lemus E, Nicasio-Collazo LA, Castañeda-Priego R (2012) Hysteresis in Pressure-Driven DNA Denaturation. PLoS ONE 7(4): e33789. doi:10.1371/journal.pone.0033789

Editor: Alejandro Raul Hernandez Montoya, Universidad Veracruzana, Mexico

Received September 7, 2011; **Accepted** February 17, 2012; **Published** April 9, 2012

Funding: Financial support from the Integral Program for Institutional Strengthening (PIFI for its Spanish acronym) of the Secretaria de Educacion Publica (Mexico's Ministry of Education) 3.4, and Mexico's National Council of Science and Technology (CONACyT for its Spanish acronym) (grant nos. 61418/2007 and.102339/2008), as well as federal funding from the National Institute of Genomic Medicine (Mexico) is acknowledged. The funders had no role in study design, data collection and analysis, decision to publish, or preparation of the manuscript.

Competing Interests: The authors have declared that no competing interests exist.

* E-mail: ehernandez@inmegen.gob.mx (EH-L); ramoncp@fisica.ugto.mx (RC-P)

Introduction

The molecule of Deoxyribonucleic acid (DNA) is a very complex one, both from the physicochemical point of view, as well as its obvious biological function. In recent times many of its dynamic and structural features have re-attracted the attention of the scientific community. Clearly, the number of sophisticated experiments (spectroscopical, biochemical, mechanical tests, among others), many of them at the one-molecule level, has increased [1–3] whereas deep theoretical studies ranging from continuous mechanics to quantum chemistry and statistical physics abound [4–7]. The variety of available experimental and theoretical findings is thus almost endless see, e.g., [8–10] and references therein. Nevertheless, there is a lack of a conceptual framework to categorize and analyze this enormous bunch of information. A thermodynamic theory seems to be the ideal candidate for doing such a task. Since many of the interesting features of the behavior of DNA are dynamic in nature and due to the fact that many of them occur in a mesoscopic scale, a non-equilibrium thermodynamic treatment is therefore appropriate. Of course, such a general theory does not seem to be at hand at the moment. Nonetheless, in this work we will try to establish some grounds of it, specifically with respect to the problem of DNA melting, since it is one of the most important features which is closely related with the biological function of genetic transcription [11,12].

Nowadays, it is well understood that the static structure of complex biological molecules is not sufficient to explain their functions. A well-established fact is that such biomolecules, specifically proteins and nucleic acid heteropolymers reveal, apart from the usual molecular vibrations, purely stochastic transitions between a multitude of conformational substates [13]. This fact is particularly true for the DNA molecule which undergoes large conformational changes during transcription or replication. Several physiological reasons are behind such a large number of conformational states. On one hand, such a large number of conformational states is needed for the selective catalysis mechanisms involved in the highly accurate mechanisms of genomic expression. On the other hand, at a fundamental physical level, it has been possible to show experimentally that a single chromosome is made up of one DNA molecule that is some 4 to 10 cm long (see [4] and references 4 and 5 therein). So that the entire genome contained on a human cell is about 2 m long. For this reason the genome is highly compacted in a variety of complex arrays within each cell [11,12]. The ternary structure of DNA has been proved to be helicoidal (the double helix); the length of the molecule is much larger than its diameter, so it is common to describe it as a one dimensional deformable string [5,14,15] or, sometimes, like a highly charged rod [16]. Such an oversimplification is useful only when one is not interested in phenomena related to its internal structure [17]. Additionally, the fundamental biological features of the DNA function are replication and transcription; both phenomena are so complex that a fundamental (physical) description of them is unavailable at the moment.

Langmuir

Article

pubs.acs.org/Langmuir

Dynamical Arrest, Percolation, Gelation, and Glass Formation in Model Nanoparticle Dispersions with Thermoreversible Adhesive Interactions

Aaron P. R. Eberle,[‡,†] Ramón Castañeda-Priego,[‡,§] Jung M. Kim,[‡] and Norman J. Wagner*[,‡]

[‡]Center for Neutron Science, Department of Chemical Engineering, University of Delaware, Newark, Delaware 19716, United States
[†]NIST Center for Neutron Research, National Institute of Standards and Technology, Gaithersburg, Maryland 20899, United States
[§]División de Ciencias e Ingenierías, Universidad de Guanajuato, Loma del Bosque 103 37150 León, Mexico

ABSTRACT: We report an experimental study of the dynamical arrest transition for a model system consisting of octadecyl coated silica suspended in *n*-tetradecane from dilute to concentrated conditions spanning the state diagram. The dispersion's interparticle potential is tuned by temperature affecting the brush conformation leading to a thermoreversible model system. The critical temperature for dynamical arrest, T^*, is determined as a function of dispersion volume fraction by small-amplitude dynamic oscillatory shear rheology. We corroborate this transition temperature by measuring a power-law decay of the autocorrelation function and a loss of ergodicity via fiber-optic quasi-elastic light scattering. The structure at T^* is measured using small-angle neutron scattering. The scattering intensity is fit to extract the interparticle pair-potential using the Ornstein−Zernike equation with the Percus−Yevick closure approximation, assuming a square-well interaction potential with a short-range interaction (1% of particle diameter).[1] The strength of attraction is characterized using the Baxter temperature[2] and mapped onto the adhesive hard sphere state diagram. The experiments show a continuous dynamical arrest transition line that follows the predicted dynamical percolation line until $\phi \approx 0.41$ where it subtends the predictions toward the mode coupling theory attractive-driven glass line. An alternative analysis of the phase transition through the reduced second virial coefficient B_2^* shows a change in the functional dependence of B_2^* on particle concentration around $\phi \approx 0.36$. We propose this signifies the location of a gel-to-glass transition. The results presented herein differ from those observed for depletion flocculated dispersion of micrometer-sized particles in polymer solutions, where dynamical arrest is a consequence of multicomponent phase separation, suggesting dynamical arrest is sensitive to the physical mechanism of attraction.

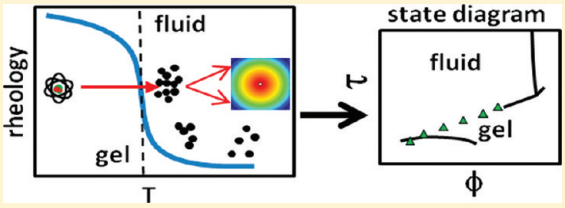

1. INTRODUCTION

The macroscopic behavior of colloidal dispersions can change from a fluid to solid-like state as a result of a nonequilibrium dynamical arrest transition of the disperse phase when either the volume fraction, ϕ, or the interparticle potential, $\Phi(r)$, is varied.[3,4] For hard spheres (HS), at $\phi \approx 0.58$ dynamical arrest occurs through the "caging" of particles by their nearest neighbors forming a repulsive driven glass (RDG).[3] The addition of a short-ranged attraction can relax this constraint and fluidize the dispersion at constant ϕ, while attractions will ultimately lead to a glass and possible multiple glassy states for one dispersion.[5] In addition, dynamical arrest driven by attraction can occur at much lower ϕ,[6−12] although the particle density defining the transition between glass and a gel is ill defined.[13] Generally speaking, dynamical arrest leading to a macroscopically homogeneous sample in moderately high to low concentrated dispersions $\phi < \sim 0.40$ is often termed "gelation" and is characterized by a network of particles that displays large scale fractal properties without any significant order. Similarly, colloidal glasses are disordered solids.

A short-ranged attraction in a colloidal system will cause structural reordering of the disperse phase. For strengths of attraction larger than the thermal energy (k_BT) larger bodies composed of individual particles form, such as fractal aggregates or cluster.[14−16] Above a threshold ϕ, these structures will percolate through the system resulting in an infinitely large cluster leading to bulk dynamical arrest.[6,17,18] It is well established that dynamical arrest can occur in very dilute colloidal systems ($\phi \approx 10^{-4}$) that interact with a relatively large attractive strength and form irreversible bonds.[6]

Three general classes of model systems have been used to study fractal aggregation, flocculation, gelation, and glass formation. One example is charge stabilized colloidal latex with added electrolyte,[19] but other examples exist such as colloidal gold and silica, as well as carbon black.[7] Typically, the attraction is due to London-van der Waals dispersion forces and flocculation is induced by screening the stabilizing electrostatic repulsive forces from surface charges by the addition of an electrolyte.[20] For sufficient electrolyte addition such that repulsive interactions are negligible and in the absence of

Received: September 6, 2011
Revised: December 5, 2011
Published: December 9, 2011

IOP PUBLISHING JOURNAL OF PHYSICS: CONDENSED MATTER
J. Phys.: Condens. Matter **24** (2012) 065102 (7pp) doi:10.1088/0953-8984/24/6/065102

On the calculation of the structure of charge-stabilized colloidal dispersions using density-dependent potentials

R Castañeda-Priego[1], V Lobaskin[2], J C Mixteco-Sánchez[3], L F Rojas-Ochoa[4] and P Linse[5]

[1] División de Ciencias e Ingenierías, Campus León, de la Universidad de Guanajuato, Loma del Bosque 103, 37150 León, Guanajuato, Mexico
[2] School of Physics and Complex and Adaptive Systems Laboratory, University College Dublin, Belfield, Dublin 4, Ireland
[3] UPIIG-IPN, Mineral de Valenciana 200, 36275 Silao de la Victoria, Guanajuato, Mexico
[4] Departamento de Física, Cinvestav-IPN, Avenida Instituto Politécnico Nacional 2508, 07360 México DF, Mexico
[5] Physical Chemistry, Lund University, PO Box 124, SE-221 00 Lund, Sweden

E-mail: ramoncp@fisica.ugto.mx

Received 27 September 2011, in final form 18 November 2011
Published 10 January 2012
Online at stacks.iop.org/JPhysCM/24/065102

Abstract
The structure of charge-stabilized colloidal dispersions has been studied through a one-component model using a Yukawa potential with density-dependent parameters examined with integral equation theory and Monte Carlo simulations. Partial thermodynamic consistency was guaranteed by considering the osmotic pressure of the dispersion from the approximate mean-field renormalized jellium and Poisson–Boltzmann cell models. The colloidal structures could be accurately described by the Ornstein–Zernike equation with the Rogers–Young closure by using the osmotic pressure from the renormalized jellium model. Although we explicitly show that the correct effective pair-potential obtained from the inverse Monte Carlo method deviates from the Yukawa shape, the osmotic pressure constraint allows us to have a good description of the colloidal structure without losing information on the system thermodynamics. Our findings are corroborated by primitive model simulations of salt-free colloidal dispersions.

(Some figures may appear in colour only in the online journal)

1. Introduction

From a composition point of view, charged colloidal dispersions are complex fluids made up of a large number of particles of different types. The charged colloids are accompanied by an equivalent amount of small and oppositely charged microions. In addition, at least two different species of salt ions are often present. Although the microions are not directly detectable by most experimental techniques, they strongly modify the electrostatic interaction between the colloids and therefore cannot be simply neglected in theoretical models. The larger number of microions, as compared to colloids, implies their significant contribution to the osmotic pressure, thus playing an important role in the thermodynamics of the dispersion [1–3]. The large size and charge asymmetries between the colloids and microions make it difficult to treat both of them explicitly in many theoretical frameworks. It is therefore a common practice to map multi-component models of charged colloidal dispersion onto a one-component model (OCM), in which the microions are integrated out and the colloidal particles interact via effective pair potentials [1, 4]. For weakly charged species, where the colloid–microion interaction is small as compared to the thermal energy, the corresponding

WJGP World Journal of Gastrointestinal Pathophysiology

Online Submissions: http://www.wjgnet.com/2150-5330office
wjgp@wjgnet.com
doi:10.4291/wjgp.v3.i1.10

World J Gastrointest Pathophysiol 2012 February 15; 3(1): 10-18
ISSN 2150-5330 (online)

Electrical bioimpedance and other techniques for gastric emptying and motility evaluation

María Raquel Huerta-Franco, Miguel Vargas-Luna, Juana Berenice Montes-Frausto, Corina Flores-Hernández, Ismael Morales-Mata

María Raquel Huerta-Franco, Corina Flores-Hernández, Ismael Morales-Mata, Health Science Division, Department of Applied Sciences to Work, University of Guanajuato, Av Eugenio Garza Sada 572, Lomas del Campestre, 37150 León, Guanajuato, México

Miguel Vargas-Luna, Juana Berenice Montes-Frausto, Science and Engineering Division, Department of Physical Engineering, University of Guanajuato, Loma del Bosque 103, Lomas del Campestre, 37150 León, Guanajuato, México

Author contributions: Huerta-Franco MR, Vargas-Luna M designed and conducted the study and wrote the manuscript; Morales-Mata I performed the data acquisition and instrumentation review; Montes-Frausto JB and Flores-Hernández C contributed to the data collection, reviewed the literature and provided analytical input.

Supported by Dirección de Apoyo a la Investigación y Posgrado, 2009-2010, University of Guanajuato

Correspondence to: María Raquel Huerta-Franco, PhD, Health Science Division, Department of Applied Sciences to Work, University of Guanajuato, Av Eugenio Garza Sada 572, Lomas del Campestre, 37150 León, Guanajuato, México. mrhuertafranco@ugto.mx
Telephone: +52-477-2569688 Fax: +52- 477-7885100

Received: August 27, 2011 Revised: December 6, 2011
Accepted: February 8, 2012
Published online: February 15, 2012

Abstract

The aim of this article is to identify non-invasive, inexpensive, highly sensitive and accurate techniques for evaluating and diagnosing gastric diseases. In the case of the stomach, there are highly sensitive and specific methods for assessing gastric motility and emptying (GME). However, these methods are invasive, expensive and/or not technically feasible for all clinicians and patients. We present a summary of the most relevant international information on non-invasive methods and techniques for clinically evaluating GME. We particularly emphasize the potential of gastric electrical bioimpedance (EBI). EBI was initially used mainly in gastric emptying studies and was essentially abandoned in favor of techniques such as electrogastrography and the gold standard, scintigraphy. The current research evaluating the utility of gastric EBI either combines this technique with other frequently used techniques or uses new methods for gastric EBI signal analysis. In this context, we discuss our results and those of other researchers who have worked with gastric EBI. In this review article, we present the following topics: (1) a description of the oldest methods and procedures for evaluating GME; (2) an explanation of the methods currently used to evaluate gastric activity; and (3) a perspective on the newest trends and techniques in clinical and research GME methods. We conclude that gastric EBI is a highly effective non-invasive, easy to use and inexpensive technique for assessing GME.

Key words: Gastrointestinal motility; Gastric emptying; Bioimpedance technique; Diagnostic techniques; Digestive system

Peer reviewer: Shi Liu, Professor, Department of Gastroenterology, Union Hospital of Tongji Medical College, Huazhong University of Science and Technology, 1277 Jiefang Road, Wuhan 430022, Hubei Province, China

Huerta-Franco MR, Vargas-Luna M, Montes-Frausto JB, Flores-Hernández C, Morales-Mata I. Electrical bioimpedance and other techniques for gastric emptying and motility evaluation. *World J Gastrointest Pathophysiol* 2012; 3(1): 10-18 Available from: URL: http://www.wjgnet.com/2150-5330/full/v3/i1/10.htm DOI: http://dx.doi.org/10.4291/wjgp.v3.i1.10

A HISTORICAL PERSPECTIVE ON ASSESSING GASTRIC FUNCTION

The study of gastric anatomy, physiology and pathol-

Journal of Bioelectromagnetism
Vol. 14, No.1, pp.22-26, 2012

DIF-12-A08

Magnetic *vs.* Sphygmomanometry Cardiac Pressure

T Cordova[a,c,*], F Gomez[a], L Romero[b], MA Hernadez[b], CR Contreras[c], S Solorio[b], M Sosa[a] and J. Bernal[b]

[a]Dept. Ingeniería Física-DCI, Universidad de Guanajuato campus Leon, GTO, Mexico.
[b]UMAE, Clínica T1-León, Instituto Mexicano del Seguro Social, GTO, México.
[c]F. de Ingenieria en Computacion y Electronica, Universidad De La Salle Bajio, Leon GTO, México

*Correspondence: Cordova T, Dept. Ingeniería Física-DCI, Universidad de Guanajuato campus Leon, GTO, Mexico.
E-mail: theo@fisica.ugto.mx, phone 52(477) 788-5100, exts: Fax 8410, Of. 8454, Lab. 8475.

Abstract. A comparative study carried out in humans with a digital manual sphygmomanometer *vs.* magneto mechanical cardiac pressure device is presented. In this study 38 healthy subject were enrolled. This device includes a small magnet and a magnetometer and it is able to record graphic behavior identical to cardiac catheter technique, with the versatility to perform signal acquisition at skin level. The study was performed in IMSS hospital, where 38 patients were enrolled in order to be evaluated with both techniques. A high correlations was found between these techniques, where Systolic blood pressure, sleeping was around $r = 0.91$ with p – values of 0.0001, and Lying systolic blood pressure around $r = 0.14$ with p – values of 0.3381. Such, this new methodology may be an alternative to have this device in ER-hospital, Intensive therapy rooms and it could prevent catheterize surgical intervention. This is a cardiac signal modality at skin level, with a portable device.

Keywords: blood vessel, biomagnetic signal, magnetic marker.

1. Introduction

One of the principal clinical vital signs is the evaluation a monitoring of blood pressure (BP), which ones is defined as the force exerted by circulating blood on the walls of the body's arteries and constitutes. Arterial pressure is most commonly measured via a sphygmomanometer device [Pannier *et al.*, 2002]. For each heartbeat, BP varies between systolic and diastolic pressures. The systolic pressure is the peak pressure in the arteries, which occurs early in the cardiac cycle when the ventricles are contracting. Diastolic BP is the minimum pressure in the arteries, and occurs late in the cardiac cycle when the ventricles are filled with blood.

An invasive technique for assessment the BP consists of a procedure in which it is measured inside the blood vessel using an intra-arterial catheter connected to a sensitive pressure transducer. Although invasive, this procedure is considered the gold standard technique for measuring arterial pressure because it is more accurate than Sphygmomanometry [Kurtz *et al.*, 2005] and can be used to detect rapid variations in BP.

Recently, a patenting register was requested of a magnetometer device development in our laboratory, this is a magnetomechanical cardiac pressure associated with heart activity. This single device is noninvasive, capable of recording arterial and vein behavior.

In this paper the validation of a device for magnetomechanical cardiac pressure (MMCP) is presented, this evaluation was performed in terms of repeatability and reproducibility, considering the sphygmomanometer as a reference method on the analysis of correlation between the MMCP and the conventional methods.

2. Methods

The arterial blood pressure measurements were performed with the patient at rest in a quiet area without the presence of magnetic stimuli that could alter SNR reason. With a sphygmomanometer appropriate to the patient's condition (covering 80% of the circumference of the patient's arm, bringing the manometer to 30 mmHg than expected, based on noise and fluctuations Korotcoff gauge for determining systolic pressure and verify using the index and middle fingers of the patient's pulse as the pulse of the digital arteries can cause substantial errors in the sampling [Vazquez *et al.*, 20009]. Each measurement was performed at the patient sitting and recumbent; see Fig 1, [Maldonado-Morel *et al.*, 2008].

Appl Magn Reson (2012) 42:161–167
DOI 10.1007/s00723-011-0267-8

Applied
Magnetic Resonance

Medlar (*Achras Sapota* L.) as Oral Contrast Agent for MRI of the Gastrointestinal Tract

Teodoro Cordova-Fraga · Modesto Sosa · Martha Alicia Hernandez-Gonzalez · Jose Antonio Reyes-Aguilera · Sergio Solorio · Chystian Ramirez · Evelia Bautista-Flores · Guadalupe Reynaga · Mario Avila-Rodriguez · Jose Maria De la Roca-Chiapas

Received: 3 June 2011 / Published online: 2 October 2011

Abstract Magnetic resonance imaging (MRI) of the gastrointestinal (GI) tract is still limited due to the lack of widely available oral contrast agents (OCA). The availability of OCA for MRI of the GI tract is a necessity; different fruits might be implemented as OCA in order to solve this need throughout the year. The objective of this study is to present an alternative fruit as a clinical OCA for MRI of the GI

T. Cordova-Fraga (✉) · M. Sosa
Departamento de Ingeniería Física–DCI, Universidad de Guanajuato campus León, León, GTO, Mexico
e-mail: theo@fisica.ugto.mx

M. A. Hernandez-Gonzalez
Internal Medicine Department, HGZ 21, IMSS, León, GTO, Mexico

J. A. Reyes-Aguilera
Departamento de Ingenierías Química, Electrónica y Biomédica-DCI, Universidad de Guanajuato campus León, León, GTO, Mexico

S. Solorio · C. Ramirez
Unit of Medical Research, UMAE 1 Bajío, IMSS, León, GTO, Mexico

E. Bautista-Flores
Radiology and Imaging Department, UMAE 1 Bajío, IMSS, León, GTO, Mexico

G. Reynaga
Departamento de Medicina y Nutrición–DCS, Universidad de Guanajuato campus León, León, GTO, Mexico

M. Avila-Rodriguez
Departamento de Química–CNE, Universidad de Guanajuato campus Guanajuato, Guanajuato, GTO, Mexico

J. M. De la Roca-Chiapas
Departamento de Psicología–DCS, Universidad de Guanajuato campus León, León, GTO, Mexico

DIF-12-A10

Superficial magnetic imaging by an xy-scanner of three magnetoresistive channels

M. E. Cano,[1,a)] A. H. Pacheco,[2] T. Cordova,[3] E. E. Mazon,[1] and A. Barrera[1]
[1]*Centro Universitario de la Ciénega, Universidad de Guadalajara. Av. Universidad, 47020 Ocotlán, JAL, Mexico*
[2]*Centro Nacional de Metrología. Carretera a los Cues km 45, El Marqués, 76246 Querétaro, QRO. Mexico*
[3]*Departamento de Ingeniería Física, Universidad de Guanajuato campus León. Loma del Bosque 103, Lomas del Campestre, 37150 León, GTO, Mexico*

(Received 9 November 2011; accepted 26 February 2012; published online 15 March 2012)

A scanning system developed for planar magnetic surfaces composed of a moving line of three magnetoresistive ultrasensitive transducers, complemented by a signal conditioning circuit is presented. After the calibration of the sensors, it was used to determine magnetized surface images with different shapes to evaluate the sensitivity of the device, and the images are represented in gray levels on a scale from 0 to 255 intensities, to get a visual representation of the magnetic field strength. The device is shown to be sensitive enough to detect gradients homogeneities and discontinuities in the magnetic field maps and images of magnetic susceptibility. © *2012 American Institute of Physics*. [http://dx.doi.org/10.1063/1.3694002]

I. INTRODUCTION

Several techniques for magnetic imaging are available currently and generally they are based on using highly sensitive transducers that can detect magnetic field variations in some orders of magnitude smaller than the magnetic field of the earth.[1] The register of static or variable magnetic fields from 1 T to 1 nT is possible by using arrangements of coils connected to magnetic flux integrators,[2] Hall effect transducers,[3] and magnetoresistive sensors, this last translating a magnetic field to differential voltage.[4] Nevertheless, the SQUID (superconducting quantum interference device) magnetometer has the best sensibility for magnetic flux variations from 1 nT to 1 fT.[5]

A wide range of applications have a need to use superficial magnetic images since they provide useful information about the physical system under study, particularly in geophysics, where the magnetic images reveal information about minerals prior to geological interpretation.[6–9] Also, in the medical area, MRI (magnetic resonance imaging) is one of the most powerful techniques for performing millimetric evaluations inside of human bodies.

The magnetic image's reconstruction process involves using mathematical tools in order to solve the biomagnetic inverse problem.[10,11] The concept is, starting from the magnetic map (including the noise) measured for our detection system, it is possible to obtain the initial distribution of sources. This is opposite from the forward problem, where initially we know the source and it is possible to predict the magnetic flux density.[12] Indeed, there are several models for resolution of the inverse problem of magnetic sources: the Bayesian probabilistic,[13] the spatial filtering of Fourier,[14] and the Wiener filtering parameters.[15] This last one has been used, first in reconstruction of magnetic images generated by mapping the response of the ac biosusceptometer at short distances due to the presence of a ferrite powder dispersed in a planar gel matrix with different shapes, Moreira *et al.*,[16] and in an image's reconstruction from records with a multichannel line of magnetoresistive transducers Leyva *et al.*,[17]. Finally, a similar device was developed using a system with less sensitive transducers, increasing to 16 channels focusing mainly in the determination of magnetic maps and employing the method of Spatial Fourier Filtering in reconstruction of some images,[18] but was not performed an analysis of the magnetic susceptibility and neither comparison with any reference on the magnetized samples, in order to have quantitative information about the distribution of magnetic sources.

In this work, is shown a simple device for magnetic imaging using ultra-sensitive magnetoresistive elements, in a compact arrangement of three sensors that move in a rectangular plane. This magnetic probe can determine contours of magnetized areas with possible applications in the centimeter scale. In contrast to the devices reported in Ref. 18, replacing the kind of magnetic transducer and coupled to a simple RC filtering stage, we have improved the sensitivity in the magnetic field detection and with the sensors arranged in a new design, they are suitable to be displaced under the sample during the measurements process, making possible to obtain the magnetic images with the same resolution employing fewer electronic components; therefore, in experiments of magnetic imaging where the sample must to be static, this technique is a better alternative. Additionally, in order to test the capability of imaging we also presented magnetic field maps of various quasi bidimensional phantoms prepared in the laboratory, in which you can see the borders and internal details. The main aim of this paper is to demonstrate the viability to obtain maps of magnetic field and magnetic susceptibility images using this new and simple scanning system.

a)Author to whom correspondence should be addressed. Electronic mail: eduardo.cano@cuci.udg.mx.

INVESTIGACIÓN Revista Mexicana de Física **58** (2012) 348–352 AGOSTO 2012

Fractional mechanical oscillators

J.F. Gómez-Aguilar[a,*], J.J. Rosales-García[b], J.J. Bernal-Alvarado[a], T. Córdova-Fraga[a], and R. Guzmán-Cabrera[b]

[a] *Departamento de Física, División de Ciencias e Ingenierías Campus León, Universidad de Guanajuato, Lomas del Bosque s/n, Lomas del Campestre, León Guanajuato, México, e-mail: (jfga, bernal, teo)@fisica.ugto.mx*

[b] *Departamento de Ingeniería Eléctrica, División de Ingenierías Campus Irapuato-Salamanca, Universidad de Guanajuato, Carretera Salamanca-Valle de Santiago, km. 3.5 + 1.8 km, Comunidad de Palo Blanco, Salamanca Guanajuato México, e-mail: (rosales, guzmanc)@ugto.mx*

**Tel: +52 (477) 788-5100 ext. 8449.*

Recibido el 15 de febrero de 2012; aceptado el 21 de mayo de 2012

In this contribution we propose a new fractional differential equation to describe the mechanical oscillations of a simple system. In particular, we analyze the systems mass-spring and spring-damper. The order of the derivatives is $0 < \gamma \leq 1$. In order to be consistent with the physical equation a new parameter σ is introduced. This parameter characterizes the existence of fractional structures in the system. A relation between the fractional order time derivative γ and the new parameter σ is found. Due to this relation the solutions of the corresponding fractional differential equations are given in terms of the Mittag-Leffler function depending only on the parameter γ. The classical cases are recovered by taking the limit when $\gamma = 1$.

Keywords: Fractional calculus; mechanical oscillators; caputo derivative; fractional structures.

En esta contribución se propone una nueva ecuación diferencial fraccionaria que describe las oscilaciones mecánicas de un sistema simple. En particular, se analizan los sistemas masa-resorte y resorte-amortiguador. El orden de las derivadas es $0 < \gamma \leq 1$. Para mantener la consistencia con la ecuación física se introduce un nuevo parámetro σ. Este parámetro caracteriza la existencia de estructuras fraccionarias en el sistema. Se muestra que existe una relación entre el orden de la derivada fraccionaria γ y el nuevo parámetro σ. Debido a esta relación las soluciones de las correspondientes ecuaciones diferenciales fraccionarias estan dadas en terminos de la función de Mittag-Leffler, cuyas soluciones dependen solo del orden fraccionario γ. Los casos clásicos son recuperados en el límite cuando $\gamma = 1$.

Descriptores: Calculo fraccionario; oscilaciones mecanicas; derivada de caputo; estructuras fraccionarias.

PACS: 45.10.Hj; 46.40.Ff; 45.20.D-

1. Introduction

Although the application of Fractional Calculus (FC) has attracted interest of researches in recent decades, it has a long history when the derivative of order 0.5 has been described by Leibniz in a letter to L'Hospital in 1695. A reviewing paper on applications and the formalism can be found in [1]. FC, involving derivatives and integrals of non-integer order, is historically the first generalization of the classical calculus [2-5]. Many physical phenomena have "intrinsic" fractional order description, hence, FC is necessary in order to explain them. In many applications FC provides a more accurate model of physical systems thàn ordinary calculus do. Since its success in the description of anomalous diffusion [6], non-integer order calculus, both in one dimension and in multidimensional space, has become an important tool in many areas of physics, mechanics, chemistry, engineering, finances and bioengineering [7-10]. Fundamental physical considerations in favor of the use of models based on derivatives of non-integer order are given in [11-13]. Another large field which requires the use of FC is the theory of fractals [14]. Fractional derivatives provide an excellent instrument for the description of memory and hereditary properties of various materials and processes [15]. This is the main advantage of FC in comparison with the classical integer-order models, in which such effects are in fact neglected.

In a paper of Ryabov it is discussed the fractional oscillator equation involving fractional time derivatives of the Riemann-Liouville type [16]. Naber in [17], studied the linearly damped oscillator equation, written as a fractional derivative in the Caputo representation. The solution is found analytically and a comparison with the ordinary linearly damped oscillator is made. In [18] was considered the fractional oscillator, being a generalization of the conventional linear oscillator, in the framework of fractional calculus. It is interpreted as an ensemble of ordinary harmonic oscillators governed by a stochastic time arrow. Despite introducing the fractional time derivatives the cases mentioned above seem to be justified, there is no clear understanding of the basic reason for fractional derivation in physics. Therefore, it is interesting to analyze a simple physical system and try to understand their fully behavior given by a fractional differential equation.

The aim of this work is to give a simple alternative to construct fractional differential equations for physical systems. In particular, we analyze the systems mass-spring and

DIF-12-012

Article

Application of the Numerical Laplace Transform on the Simulation of Fractional Differential Equations

José F. Gómez*, J. J. Rosales, J. J. Bernal & T. Cordova

*Department Physics Engineering, DCI, Campus León, University of Gto. León Gto., México

Abstract

This work presents an overview of a methodology based on the Numerical Laplace Transform (NLT) and applied to analysis of a three physical system from the point of view of FC. The basic development of the method is described, with its main qualitative advantages as compared to conventional time domain methods. The errors due to truncation and sampling when converting a frequency domain signal to the time domain are analyzed. Finally, results obtained with this tool are shown. Comparisons with time domain methods reveal a high accuracy of the NLT in several studies.

Keywords: Fractional Calculus, Mittag-Leffler type Functions, Numerical Laplace Transforms, Fractional Differential Equation.

1. Introduction

HISTORY OF THE TNL

The Fourier and Laplace transforms are very powerful analysis tools for the solution of differential and integral equations. However, their application to practical problems is limited, given that the transformation from time to frequency domain and viceversa can be very difficult or even impossible. Besides, the time domain function may not be defined analytically, but rather through graphics, experimental measurements, sections or in discrete form. To overcome these situations, numerical transformations have been used instead of the analytical expressions.

The numerical inversion of the Laplace transform was introduced in the 60s by Bellman, approximating the Laplace integral by a Gauss-Legendre polynomial [1]. From 1965 to 1973, a group lead by Mullineux applied discrete Fourier transforms in analyzing transients in power systems [2-3], naming their technique Modified Fourier Transform (MFT), since the algorithm was adapted to reducing truncation and discretization errors. In 1973, Ametani introduced the use of the Fast Fourier Transform algorithm (FFT) to obtain computer time savings, and the MFT became a much more attractive analysis method [4]. The term Numerical Laplace Transform was introduced in 1978 by Wilcox, who formulated the MFT in terms of the Laplace

* Correspondence: José F. Gómez, E-mail: jfga@fisica.ugto.mx

Photoacoustic Tomography System

J. D. Martínez-Ramírez[1] ,R. Quispe-Siccha[2], C. García-Segundo[3], F. J. González[4], R. Espinosa-Luna[5], G. Gutiérrez-Juárez*[6]

[1,4] Instituto de Investigación en Comunicación Óptica, UASLP.
Av. Karakorum, 1470 Lomas 4a. 78210 San Luis Potosí, SLP México.
[2,3] Centro de Ciencias Aplicadas y Desarrollo Tecnológico de la UNAM.
Circuito Exterior S/N C.P. 04510 Cd. Universitaria,
México, D. F. A. P. 70-186
[5] Centro de Investigaciones en Óptica.
Loma del Bosque 115, Lomas del Campestre,
C. P.: 37150, León, Gto., México. A. P. 1-948.
[6] División de Ciencias e Ingenierías,
Universidad de Guanajuato-Campus León.
Loma del Bosque 103, Lomas del Campestre,
C. P.: 37150, León, Gto., México. A. P.: E-143.
*ggutj@fisica.ugto.mx

1ST INTERNATIONAL CONGRESS ON INSTRUMENTATION AND APPLIED SCIENCES

ABSTRACT
Based on the pulsed photoacoustic effect, we set up an experimental system to obtain bi-dimensional images of optically-opaque samples embedded within the bulk of turbid medium. The turbid medium was made of agar gel mixed with single-sized nanoparticles; with these materials we induce an optical absorption and an optical scattering like that appearing in human tissues. The PA signals are generated from the absorption processes in the buried target, and then traveling through the bulk of scatter medium. The optical absorption properties and the shape of target, defines the amplitude and shape of the PA signals. This time the laser pulses are set from a pulsed Nd: YAG laser, with pulse width of 10 ns, at rate repetition of 10 Hz and wavelength set at 1064 nm. The signals generated in this way are registered by means of an ultrasonic transducer with resonance cut at 10 MHz. The sample was rotated to obtain as many as 36 projections which are used to feed an image reconstruction forward-projection algorithm based on the Radon Transform. As result we obtain 2D tomographic slices of three different samples.

Keywords: Photoacoustic imaging, radon transform, tomography.

RESUMEN
Basados en el efecto fotoacústico pulsado, se desarrolló un dispositivo experimental para generar imágenes bidimensionales de muestras ópticamente opacas ocultas en un medio turbio. El medio turbio se hizo de agar y nanopartículas monodispersas, con estos materiales indujimos una absorción y esparcimiento óptico semejante al de los tejidos humanos. La señal PA se genera por la absorción óptica del la muestra; una vez producida viaja a través del medio esparsor. Las propiedades de ópticas de la muestra así como la forma de éste definen la amplitud y forma de la señal PA. En el sistema fotoacústico se utilizaron pulsos láser de Nd: YAG de 10 ns, con frecuencia de repetición de 10Hz, y longitud de onda de 1064 nm. Las señales generadas fueron registradas por un transductor ultrasónico con frecuencia de corte de 10 MHz. Tanto la muestra como el medio esparsor se rotaron para obtener 36 proyecciones, las cuales fueron utilizadas para alimentar un algoritmo de reconstrucción de imágenes basado en la transformada de Radon. Como resultado se obtuvieron imágenes tomográficas 2D de tres muestras distintas.

1. Introduction

Because of its non-invasive properties, in last decades, optical tomographies have been accepted as a diagnostic tool in biomedical imaging researches. The basis of the technique is to exploit the light-tissue interaction and its optical contrast in terms of optical absorption, from where one can obtain images. Notice that, since the tissue presents large amounts of light scattering, the option of optically reconstructing a tomographic image is not good enough. However, the photoacoustic tomography (PAT) [1-7] is a novel imaging technique that combines the high optical contrast of the optical tomographies with the high resolution of the ultrasound imaging. The PAT is

Climacteric Cardiovascular Changes Evaluated by Heart Rate Variability and Detrended Fluctuation Analysis

M.R. Huerta-Franco[1], M. Vargas-Luna[2], and J.B. Montes[2]

[1]University of Guanajuato, Department Labor Science Research, DCI-CL, León Gto., México
[2]University of Guanajuato, Department of Physical Engineering, DCS-CL, León Gto., México

***Abstract*— During climacteric, women experience physical and psychological changes due to declining ovarian estrogen. The cardiovascular system is one of those affected. However, there are not sufficient studies of the effects of the climacteric on heart function. The fluctuations of the heart rate are the most common way to analyze the changes in heart function. In this work, ten minutes of ECG signal at rest were recorded for a group of 57 healthy climacteric females. In this study, two methodologies were used to analyze the ECG signal: Heart Rate Variability (HRV) and Detrended Fluctuation Analysis (DFA). The results show that there are significant differences in the heart rate fluctuation among pre-, peri-, and post-menopausal females.**

Keywords— **Climacteric, Heart Rate Variability, Detrended Fluctuation Analysis.**

I. Introduction

Climacteric is a period of life characterized by physical and physiological changes that marks the end of the reproductive capacity of women and terminates with the completion of menopause [1-5]. This period is characterized by a decrease in estrogen serum levels being more marked in postmenopausal than in pre- or peri-menopausal females [3-5]. In particular, postmenopausal females have an increased risk of stroke and cardiovascular events and also an increased risk of morbid-mortality [6]. It is only recently when published studies on cardiac variability in post-menopausal women during treatment with estrogens have appeared [6]. However, there are not sufficient studies that compare the heart rate variability during climacteric period in females with different concentrations of estrogen serum levels (pre-, peri-, and post-menopausal females).

The Heart Rate Variability (HRV), obtained from RR intervals from an ECG recording, is influenced by the Autonomous Nervous System [7]. Low frequency (LF) fluctuations, identified in the range from 0.04 to 0.15 Hz, are associated with the sympathetic system, whereas the high frequency (HF) fluctuations, belonging to the range from 0.15 to 0.4 Hz, are influenced by parasympathetic systems [8]. The changes of the frequency spectrum are due to several causes [9-14]. Balance index is the most common parameter to be considered in cardiovascular evaluation. This quantity is calculated by the ratio of the LF over HF contribution to the frequency spectrum. We observed that relative changes, of low frequency contribution, show the same significance, but in the other direction, that high frequency region does. Therefore, in this work only the LF area of the spectrum was considered for the evaluation of the HRV.

Detrended Fluctuation Analysis (DFA) is used to analyze noisy signals using a scaling analysis, giving long range power law correlation exponents. DFA has been used already to analyze HR fluctuations [15]. DFA is calculated as follows: The time series is zero averaged by subtracting its mean value. Then, a new series is obtained by partial integration of the zero averaged series. This new series is divided into K boxes equally sized (N points) and each data box is lineally fitted. This linear fit is subtracted in each box to have the detrended fluctuation function. For each box the mean square root fluctuation of this function F(N) is calculated. F(N) and n can have a power law relation, this is $F(N) \sim N^{\alpha}$, where α is the scaling or correlation exponent. Alpha should be different of 0.5 to talk about a correlated signal [16].

II. Methodology

A group of 57 women, aged 40-60 (mean ± SD: ± years) was recruited. Written informed consent was obtained from all participating subjects, and the study was conducted according to the Declaration of Helsinki. Subjects were divided into three groups; 1) 18 premenopausal female (Pre-) with estrogen serum levels of X±SD; 2) 18 perimenopausal female with estrogen serum levels of X±SD and 3) 20 postmenopausal female with estrogen serum levels of X±SD.

R-R intervals from ECG were recorded during 10 minutes at rest, using a BIOPAC 150.

Analysis of the HR fluctuations was performed using Malt Lab to obtain areas under LF and HF regions from frequency spectrum of the HRV. For DFA, alpha scaling parameters were obtained for boxes having from 4 data points to more than 40 data points, divided in three regions: 1) from 4 to 10 data points boxes, b) from 11 to 40 data points boxes and c) more than 40 data points boxes. Statis-

NIST CENTER for NEUTRON RESEARCH

accomplishments & opportunities

2011

NIST
National Institute of
Standards and Technology
U.S. Department of Commerce

NIST SP 1127

Neutron scattering techniques shed new light on gel formation

A.P.R. Eberle[1,2], N.J. Wagner[2] and R. Castañeda-Priego[2,3]

Colloidal dispersions are used in many household products ranging from paints to shaving cream to gelatin and even to foods such as salad dressings or mayonnaise. The stability and processing of these and similar products highly depend on the state of the material. Of particular interest is the phase transition from fluid to a solid, called a gel at low particle volume fractions, $\phi < \approx 0.40$, and a glass at higher volume fractions. While the phase behavior for such systems has been studied for decades, the boundary separating a fluid from a gel is still debated.

In this work we study gelation using a model nanoparticle system with thermoreversible interactions. The system consists of nanometer spheres of silica dioxide (≈ 30 nm) coated with a short carbon chain (C_{14}), and suspended in tetradecane. At high temperatures $T > \approx 32$ °C the particles are stable and the system behaves like a simple hard sphere fluid. Upon quenching the system, particles aggregate in connection with a phase transition of the molecular brush [1]. This in-turn causes a short-range attraction between particles, and if the particle volume fraction is sufficient, $\phi \geq 0.05$, the system will form a stress-supporting gel. We define gelation and determine the gel temperature (T_{gel}) to within ± 0.1 °C using a combination of rheological experiments and an experimental study of the dynamics using fiber-optic quasi-elastic light scattering (FOQELS). Finally, we study the structure of the dispersion at and around the gel transition using small-angle neutron scattering (SANS).

Small-amplitude oscillatory shear (SAOS) rheological measurements are used to identify the transition from the fluid state to the gel state employing a well-defined criterion established for cross linking polymer resins [2]. The SAOS results for a temperature ramp experiment for one dispersion, $\phi = 0.12$, can be seen in Fig. 1. At high temperatures ($T > \approx 31$ °C), in the fluid state, the suspension exhibits a negligible storage modulus G', which defines the amount of elastic energy the fluid can store.

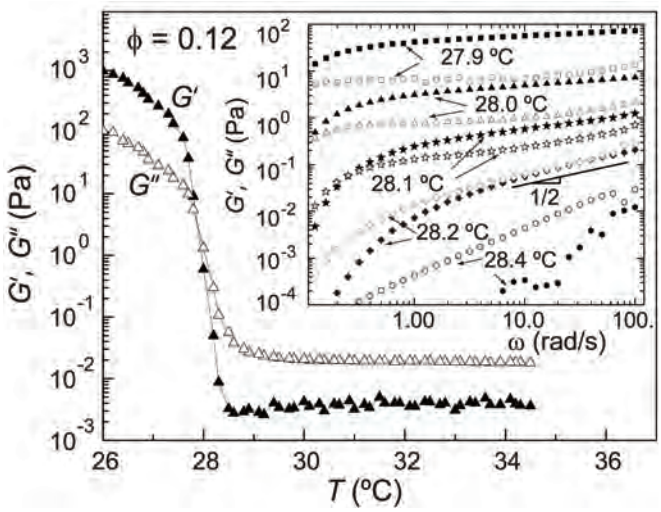

FIGURE 1: Storage, G′ (closed symbols), and loss, G″ (open symbols), moduli vs. temperature in a small-amplitude oscillatory (stress amplitude, σ_0 = 17.68 mPa, frequency, $\omega = 2\pi$ rad/s) temperature ramp experiment (ramp rate 0.2 °C/min). Inset: G′ and G″ from frequency sweep measurements at temperatures around the gel-point. Data are offset vertically for clarity by factors 0.03, 0.05, 0.08, and 0.2 for temperatures (28.4, 28.2, 28.1, and 28) °C, respectively.

As the system is quenched to lower temperatures from the fluid state, the elastic modulus increases over five orders of magnitude in the narrow temperature range of 29 °C to 27 °C. This shows the suspension undergoes a transition to a strong viscoelastic solid similar to cooled Jello. Frequency sweep measurements provide a determination of the strength of the gel. Frequency sweep experiments on the same sample can be seen in the inset to Fig. 1 as a function of temperature near the gel point. At the highest temperature shown, 28.4 °C, G″ (the loss modulus) is larger than G′ over the whole frequency range tested. As the temperature is decreased to 28.2 °C, G′ and G″ become comparable at high frequencies. At lower temperatures the sample has a greater elastic modulus, characteristic of solid-like behavior. At 28.2 °C, G′ and G″ are nearly equal with power law slopes of ½, over more than a decade of frequency, which is a characteristic feature of gelation [2]. The gel temperature is confirmed using FOQELS (not shown) which provides a measure of the particles' dynamics. From FOQELS measurements it can be shown that the dynamics decrease and exhibit an entire relaxation spectrum at the gel temperature determined from rheology.

[1]NIST Center for Neutron Research, National Institute of Standards and Technology, Gaithersburg, MD 20899
[2]University of Delaware, Newark, DE 19716, USA
[3]Universidad de Guanajuato, 37150 León, Mexico

Evaluation of the Cardiac Response to Psychological Stress by Short-Term ECG Recordings: Heart Rate Variability and Detrended Fluctuation Analysis

M. Vargas-Luna[1], M.R. Huerta-Franco[2] and J.B. Montes[1]

[1]University of Guanajuato, Department Physical Engineering, DCI-CL, León Gto., México
[2]University of Guanajuato, Department of Labor Science Research, DCS-CL, León Gto., México

Abstract— **Cardiovascular response to acute stress is a widely addressed topic because there is a clinical association of psychological and physical stress with high risk for stroke and cardiovascular events and also with the increase of morbid-mortality of the population. The Heart Rate Variability (HRV) is one of the most common methods of evaluation although some other alternatives have been emerged to complement the information about this response. One of these alternatives is the Detrended Fluctuation Analysis (DFA). Here we present a comparison between the results from HRV via the area under low frequency spectrum versus those from DFA via the scaling parameter alpha. Fifty seven healthy women, aging between 40 and 60 years old, were evaluated according to the following paradigm: 1) ECG in basal state (ten min); 2) ECG during psychological stress test (Stroop test, 3 min); and 3) ECG in basal state (three min). DFA shows comparable results with HRV, using few data points boxes and having the main effect after Stroop Test, contrary to the HRV where the main change is observed when Stroop test was applied.**

Keywords— **Heart Rate Variability, Detrended Fluctuation Analysis, Stress, Stroop.**

I. Introduction

The Heart Rate Variability (HRV) is obtained from RR intervals of an ECG signal. These variations of the heart rate are influenced by the Autonomous Nervous System [1]. Low frequency (LF) fluctuations are identified in the range from 0.04 to 0.15 Hz, and they are influenced mainly by the sympathetic system whereas the high frequency (HF) fluctuations, belonging to the range from 0.15 to 0.4 Hz, are influenced by parasympathetic systems [2]. These contributions to the HRV spectrum can change due to several causes [3-5], including stress states [1,6-8]. Usually, a balance index is calculated by the ratio of the LF over HF contribution to the frequency spectrum. In this work, we used LF area as an alternative to LF/HF index. This alternative was used because very low frequencies are not well defined due to the short term recordings of the ECG during Stroop psychological stress test.

Detrended Fluctuation Analysis (DFA) has been used to analyze noisy signals by a scaling analysis giving long range power law correlation exponents. Some studies have been done for analyzing HR fluctuations by DFA [9]. In summary DFA is calculated as follows: The time series is zero averaged by subtracting its mean value. After this, a new series is built by partial integration of the zero averaged series. This new series is divided into K boxes equally sized (N points) and each box is linearly fitted. This linear fit is subtracted in each box to have the detrended fluctuation function. For each box, of size N, the mean square root fluctuation F(N) is calculated. F(N) and N can have a power law relation, this is $F(N) \sim N^{\alpha}$, where α is the scaling or correlation exponent. Alpha should be different of 0.5 to talk about a correlated signal [10].

Psychological stress is widely investigated all over the world; however, the possibility of permanent monitoring of the physiological factors that yield information about the stress degree is not yet established. Moreover, the possibility of low cost permanent monitoring is the basis of a feedback program that may be used in treatments of stress control. Short term ECG recordings analysis is very important when stress tests, like Stroop test, are applied, this test cannot last for a long time.

II. Methodology

We analyze RR intervals from ECG recorded by a BIOPAC 150. A group of 57 healthy women, aging between 40 and 60 years, was evaluated before, during and after Stroop psychological stress tests. The Stroop test consists in a 3 min session during which words in color are projected upon a screen at the rate of one word per second [11]. The subject is asked to speak up the color of the word. During the first 40 s, words of several objects are shown, followed by one minute of words that name colors [11]. The written color sometimes corresponds to the color of the word and sometimes does not. Finally, again words of several objects, excluding names of colors, are shown [11]. The paradigm of study was as follows: a) ten minutes of ECG

PHYSICAL REVIEW D **75,** 076001 (2007)

Is there a paradox in CP asymmetries of $\tau^{\pm} \to K_{L,S}\pi^{\pm}\nu$ decays?

G. Calderón[*]
Instituto de Física de la Universidad de Guanajuato, C.P. 37150, León, Guanajuato, México

D. Delepine[†]
Instituto de Física de la Universidad de Guanajuato, C.P. 37150, León, Guanajuato, México

G. López Castro
Departamento de Física, Cinvestav, A.P. 14-740, 07000 México D.F, México
(Received 7 March 2007; published 20 April 2007)

Based on the description of unstable $K_{L,S}$ particles in quantum field theory (QFT), we compute the time-dependent probabilities for transitions between asymptotic states in $\tau^{\pm} \to [\pi^+\pi^-]_K\pi^{\pm}\nu$ decays, where the pair $[\pi^+\pi^-]_K$ is the product of (intermediate state) neutral kaon decays. Then we propose a definition of τ decays into K_L and K_S states, which reflects into the cancellation between their CP rate asymmetries, thus solving in a natural way the paradox pointed out in [I. I. Bigi and A. I. Sanda, Phys. Lett. B 625, 47 (2005).]. Since our definition of $K_{L,S}$ final states in τ decays is motivated on experimental grounds, our predictions for the integrated CP rate asymmetries can be tested in a dedicated experiment.

DOI: 10.1103/PhysRevD.75.076001 PACS numbers: 11.10.St, 11.30.Er, 13.35.Dx

I. INTRODUCTION

In a recent paper, Bigi and Sanda [1] have pointed out that $\tau^{\pm} \to K_{L,S}\pi^{\pm}\nu_\tau$ decays exhibit a CP asymmetry of the same size as the one measured in the charge asymmetry of semileptonic K_L decays. The "known" CP rate asymmetries for K_S and K_L final states [1]

$$\frac{\Gamma(\tau^+ \to K_S\pi^+\bar{\nu}) - \Gamma(\tau^- \to K_S\pi^-\nu)}{\Gamma(\tau^+ \to K_S\pi^+\bar{\nu}) + \Gamma(\tau^- \to K_S\pi^-\nu)} = |p|^2 - |q|^2, \tag{1}$$

$$\frac{\Gamma(\tau^+ \to K_L\pi^+\bar{\nu}) - \Gamma(\tau^- \to K_L\pi^-\nu)}{\Gamma(\tau^+ \to K_L\pi^+\bar{\nu}) + \Gamma(\tau^- \to K_L\pi^-\nu)} = |p|^2 - |q|^2, \tag{2}$$

turn out to be identical. If true, this would indicate a paradox because the total rates of τ^+ and τ^- would be different, in contradiction with the CPT theorem.

Bigi and Sanda [1] proposed a solution to this contradiction by looking at the time evolution of the K^0 ($\bar{K}^0$) state produced in τ^+ (τ^-) decays at $t = 0$. They concluded that the sum of time integrated rates (from $t = 0$ to ∞) over all the final states that can be reached by neutral kaon decays is free from such CP asymmetries, restoring the equality of the $\tau^{\pm}$ lifetimes. In their discussion of the problem [1], the interference of the $K_{S,L}$ states in the time-dependent rates plays an essential role in the cancellation of the contributions of pure K_L and K_S exponential decays.

In this paper we approach this problem from a different point of view. Based on the description of unstable $K_{L,S}$ particles in quantum field theory (QFT), we compute the time evolution of transition amplitudes between physical (*in* and *out*) states. Let us point out that, in the evaluation of the matrix elements giving rise to the rates that enter Eqs. (1) and (2), neutral kaons ($K_{L,S}$) are assumed to be *asymptotic* physical states (defined as *outgoing* states at $t \to +\infty$). Since unstable particles in QFT enter as intermediate states of the physical amplitudes, the paradox contained in Eqs. (1) and (2) does not appear. We compute the time-dependent probabilities for transitions between asymptotic states in $\tau^{\pm} \to [\pi^+\pi^-]_K\pi^{\pm}\nu$, where $[\pi^+\pi^-]_K$ is the pair produced from neutral kaon decays. Then we propose a definition of τ decays into $K_{L,S}$ states, which reflects into a natural cancellation between the CP rate asymmetries defined in Eqs. (1) and (2).

Searches for CP violation effects in a double kinematical distribution of $\tau^{\pm} \to K_S\pi^{\pm}\nu_\tau$ decays have been pursued recently by the CLEO Collaboration [2]. Prospects for improved experimental searches are interesting in the light of the larger data samples of τ pairs accumulated at B-factories [3]. These exclusive decays can be used to provide further tests on the violation of the CP symmetry [1,2,4,5]. On the other hand, within the standard model, the CP rate asymmetry turns out to be negligibly small (of order 10^{-12}) in $\tau^{\pm} \to K^{\pm}\pi^0\nu_\tau$ decays [5], opening a large window to consider the effects of New Physics contributions. Indeed, virtual effects of supersymmetric particles may enhance this CP rate asymmetry to the level of $10^{-7} \sim 10^{-6}$ [6].

II. TIME-DEPENDENT AMPLITUDES IN τ LEPTON DECAYS

In this section we focus on calculation of the time evolution amplitudes of τ lepton decays into asymptotic

[*]Electronic address: gecalde@gmail.com
[†]Electronic address: delepine@fisica.ugto.mx
[‡]Electronic address: glopez@fis.cinvestav.mx

Gen Relativ Gravit (2007) 39:1279–1286
DOI 10.1007/s10714-007-0470-y

RESEARCH ARTICLE

Flat rotation curves in scalar field galaxy halos

Tonatiuh Matos · L. Arturo Ureña–López

Received: 15 April 2006 / Accepted: 1 June 2007 / Published online: 11 July 2007

Abstract We start with a model where the dark matter is of scalar field nature, which condensates and form the dark halos of galaxies. In this work we study Bose–Einstein condensates (BEC) where the scalar field particles are in many different states, and not only in the ground state, as in a realistic BEC. We find that this model is in better agreement with the rotation curves of galaxies than previous models with scalar field dark matter.

1 Introduction

If one accepts Einstein's General Relativity as the correct description of the gravity force in galaxies, one is led to conclude that the so-called *flat* rotation curves are gravitationally sustained by the existence of some type of non-baryonic matter. As observations seem to suggest, this *dark matter* makes up to 90% of the total material content in most galaxies [1,2]. Experiments aimed to detect dark matter particles have been unsuccessful in having any positive signal for their existence [3], and then flat rotation curves still stand as one of the most striking observation for the presence of dark matter in galaxies. More recently, new micro-lensing observations also support the separate existence of dark matter [4,5].

The common wisdom assumes that baryonic matter dominates the central region of galaxies, whereas dark matter takes control of the outer parts. A simple exercise using

T. Matos
Departamento de Física, Centro de Investigación y de Estudios Avanzados del IPN,
A.P. 14-740, 07000 México D.F., Mexico

L. A. Ureña-López (✉)
Instituto de Física de la Universidad de Guanajuato,
A.P. E-143, C.P. 37150, León, Guanajuato, Mexico
e-mail: lurena@fisica.ugto.mx

PHYSICAL REVIEW D **76,** 074012 (2007)

Electron-positron annihilation into $\phi f_0(980)$ and clues for a new 1^{--} resonance

M. Napsuciale,[1,2] E. Oset,[1] K. Sasaki,[1] and C. A. Vaquera-Araujo[1,2]

[1]*Departamento de Física Teórica and Instituto de Física Corpuscular, Centro Mixto Universidad de Valencia–CSIC, 46000 Burjassot, Valencia, Spain*

[2]*Instituto de Física, Universidad de Guanajuato, Lomas del Bosque 103, Fraccionamiento Lomas del Campestre, 37150, León, Guanajuato, México*

(Received 26 June 2007; published 15 October 2007)

We study the $e^+e^- \to \phi\pi\pi$ reaction for pions in an isoscalar s wave which is dominated by loop mechanisms. For kaon loops we start from the conventional $R\chi PT$, but use the unitarized amplitude for $K\bar{K} - \pi\pi$ scattering and the full kaon form factor instead of the lowest order terms. We study also effects of vector mesons using $R\chi PT$ supplemented with the conventional anomalous term for VVP interactions and taking into account the effects of heavy vector mesons in the K^*K transition form factor. We find a peak in $m_{\pi\pi}$ around the $f_0(980)$ as in the experiment. Selecting the $\phi f_0(980)$ contribution as a function of the e^+e^- energy we also reproduce the experimental data except for a narrow peak, yielding support to the existence of a 1^{--} resonance above the $\phi f_0(980)$ threshold, coupling strongly to this state.

DOI: 10.1103/PhysRevD.76.074012 PACS numbers: 13.66.Bc, 12.39.Fe, 13.75.Lb

I. INTRODUCTION

The initial state radiation $e^+e^- \to \gamma_{\rm ISR} + \gamma^* \to \gamma_{\rm ISR} + X$ in electron-positron machines is being used to study electron-positron annihilation into hadronic states X, scanning energies below the original design in the so-called radiative return method. This method has proved to be useful both in the study of the properties of low-lying resonances in ϕ factories [1] as well as in the measurement of the cross section for electron-positron annihilation into different hadronic final states in B factories [2]. In the latter case it is possible to study electron-positron annihilation into hadronic states over the range from 1 up to 5 GeV with a clean identification of the desired final states over the hadronic background. Detailed analysis of some of these processes shows enhancements of the corresponding cross sections whose proper description seems to require the existence of new resonances. Indeed, a broad structure was found in the $e^+e^- \to \gamma_{\rm ISR} J/\psi\pi^+\pi^-$ cross section showing the existence of a resonance with a mass of about 4.26 GeV [3]. More recently, in studying the cross section as a function of the center of mass for $e^+e^- \to \gamma_{\rm ISR}\phi\pi\pi$ with the dipion mass close to the $f_0(980)$, another structure was found around 2.2 GeV indicating the existence of a new resonance with a mass of about 2.175 GeV and a width of 58 MeV [4].

For final pions in a C even state, the leading electromagnetic contributions to the $e^+e^- \to \phi\pi\pi$ process come from the exchange of a virtual photon. The quark lines of the ϕ and $\pi\pi$ final states are disconnected thus at tree level the $\gamma^* \to \phi\pi\pi$ can only be induced by sequential decays like $\gamma^* \to \omega\pi\pi \to \phi\pi\pi$ which are suppressed by the small $\omega - \phi$ mixing. We explored this possibility finding this contribution rather small. The natural mechanisms appear at one loop level. In particular for a dipion mass close to the $f_0(980)$ this process involves the $\gamma^*\phi f_0$ vertex function with a photon with a virtuality above 2 GeV. The very same vertex function appears also in one of the mechanisms (dominant in the case of neutral pions) for the radiative decay $\phi \to \pi\pi\gamma$ recently measured in electron-positron ϕ factories [5] but there photons are on-shell. The vertex function at $k^2 = 0$, the $\phi f_0\gamma$ coupling, appearing in these decays is an important piece in the elucidation of the structure of the lowest lying scalar nonet.

The $\phi \to \pi\pi\gamma$ decays have been studied in effective models for nonperturbative QCD [6] incorporating scalar degrees of freedom and in unitarized chiral perturbation theory [7] (see also applications to $\phi \to K^0\bar{K}^0\gamma$ in [8]). In both formalisms, the dynamics is dominated by the chain $\phi \to S\gamma \to \pi\pi\gamma$ where the $\phi \to S\gamma$ decay is induced at one loop level through charged kaon loops which couple to the explicit scalar fields in the former case or generate them dynamically through $K\bar{K} - \pi\pi$ rescattering in the latter case. The very same dynamics must be at work in the case of virtual photons and should be the dominant one for low photon virtualities. The calculation of such effects is the subject of this paper.

Unlike the case of the $\phi \to S\gamma$ decay where the real photon tests only the electric charge, here we have a highly virtual photon which couples to higher multipoles and the way to incorporate systematically the effects of kaon loops is to consider the full kaon form factor $F_{K^+}(k^2)$ in the γK^+K^- interaction. Furthermore, although the contribution of neutral kaons vanishes for real photons, in the case of virtual photons the $\gamma^*K^0\bar{K}^0$ coupling is not null and we must consider also neutral kaon loops with the corresponding form factor. The challenge here is the proper characterization of the kaon form factor at the energy of the reaction. Fortunately we have at our disposal both a theoretical calculation of the neutral and charged kaon form factors in $U\chi PT$ [9] and direct measurements [10] in the energy region of interest. In the former case, the kaon form factor is matched with the perturbative QCD predictions at

PHYSICAL REVIEW D **76,** 087302 (2007)

Noncommutativity and scalar field cosmology

W. Guzmán,[1,*] M. Sabido,[1,†] and J. Socorro[1,2,‡]

[1]*Instituto de Física de la Universidad de Guanajuato, A.P. E-143, C.P. 37150, León, Guanajuato, México*
[2]*Facultad de Ciencias de la Universidad Autónoma del Estado de México, Instituto Literario No. 100, Toluca, C.P. 50000, Edo Mex, México.*

(Received 18 June 2007; published 25 October 2007)

In this work we extend and apply a previous proposal to study noncommutative cosmology to the Friedmann-Robertson-Walker cosmological background coupled to a scalar field. This is done in classical and quantum scenarios. In both cases noncommutativity is introduced in the gravitational field as well as in the scalar field through a deformation of minisuperspace, and we are able to find exact solutions. Finally, the effects of noncommutativity on the classical evolution are analyzed.

DOI: 10.1103/PhysRevD.76.087302 PACS numbers: 98.80.Jk, 02.40.Gh, 04.60.Kz, 98.80.Qc

It is a common issue in cosmology to make use of scalar fields ϕ as the responsible agents of some of the most intriguing aspects of our Universe (see [1] and references therein). Just to mention a few, we find that scalar fields are used as the inflaton which seeds the primordial perturbations for structure formation during an early inflationary epoch, as the cold dark matter candidate responsible for the formation of the actual cosmological structure, and as the dark energy component which seems to be driving the current accelerated expansion of the Universe. The key feature for such flexibility of scalar fields (spin-0 bosons) is the freedom one has to propose a *scalar potential* $V(\phi)$, which encodes in itself the (non-gravitational) self-interactions among the scalar particles.

To study the very early Universe one of the simplest approaches is quantum cosmology. In this framework gravitational and matter variables have been reduced to a finite number of degrees of freedom. For homogenous cosmological models the metric depends only on time and gives a model with a finite dimensional configuration space, *minisuperspace* [2]. This simplification is used because a full quantum theory of gravity does not exist (although two main candidates have been constructed: string theory and loop quantum gravity), and these approximate models can be canonically quantized.

Since the end of the 20th century the old idea of noncommutative space-time [3] has been rekindled; the renewed interest is a consequence of the developments in M-theory and string theory [4]. Although most of the work of noncommutative field theory has been done in connection with Yang-Mills theory [5], several noncommutative models of gravity have been constructed [6]. All of these formulations of gravity in noncommutative space-time share a common issue; they are highly nonlinear and solutions to the noncommutative equations of motion are incredibly difficult. One may expect that at very early times nontrivial effects of noncommutativity could affect the evolution of the Universe, making the study of noncommutative cosmological models an interesting testing ground for noncommutativity. Unfortunately, as was already mentioned, the complexity of the field equations for noncommutative gravity makes a direct calculation of cosmological models a very complex task. On this line of reasoning, in the last few years there have been several attempts to study the possible effects of noncommutativity in the cosmological and inflationary scenario [7–9]. In [7] the authors in a cunning way avoid the difficult technicalities of analyzing noncommutative cosmological models when these are derived from the full noncommutative theory of gravity. They achieved this by introducing the effects of noncommutativity in quantum cosmology by deforming the minisuperspace variables and introducing the Moyal product of functions in the Wheeler-DeWitt equation (WDW), similar to noncommutative quantum mechanics [10]. Other authors have analyzed some phenomenological effects of noncommutativity in cosmology [9], but in their analysis they neglect the noncommutative effects on the gravitational sector. The aim of this paper is to construct a noncommutative formulation of a simple scalar field cosmological model in which the matter and gravitational sector are affected by the noncommutative deformation.

Let us start with the line element for a homogeneous, flat, and isotropic universe, the Friedmann-Robertson-Walker (FRW) metric

$$ds^2 = -N^2(t)dt^2 + e^{2\alpha(t)}[dr^2 + r^2 d\Omega^2], \qquad (1)$$

where $a(t) = e^{\alpha(t)}$ is the scale factor and $N(t)$ is the lapse function. The classical evolution is obtained by solving Einstein's field equations. Using the energy momentum tensor of a scalar field we get the Einsten-Klein-Gordon equations

$$H^2 = \frac{8\pi G}{3}\left(\frac{1}{2}\dot{\phi}^2 + V(\phi)\right), \qquad \ddot{\phi} + 3H\dot{\phi} = -\frac{\partial V(\phi)}{\partial \phi}, \qquad (2)$$

*wguzman@fisica.ugto.mx
†msabido@fisica.ugto.mx
‡socorro@fisica.ugto.mx

Int J Theor Phys (2007) 46: 2928–2934
DOI 10.1007/s10773-007-9405-3

Noncommutative Bianchi Type II Quantum Cosmology

M. Aguero · J.A.S. Aguilar · C. Ortiz · M. Sabido · J. Socorro

Published online: 30 May 2007

Abstract In this paper we present the noncommutative Bianchi Class A cosmological models coupled to barotropic perfect fluid. The commutative and noncommutative quantum solution to the Wheeler–DeWitt equation for any factor ordering, to the anisotropic Bianchi type II cosmological model are found, using a stiff fluid ($\gamma = 1$). In our toy model, we introduce noncommutative scale factors, is say, we consider that all minisuperspace variables q^i does not commute, so the simplectic structure was modified.

1 Introduction

In the last few years there has been several attempts to study the possible effects of noncommutativity in the cosmological scenario. In particular, Compean et al. [1–3] avoid the difficult technicalities of analyzing noncommutative cosmological models, when these are derived from the full noncommutative theory of gravity, see by example [4–11], their proposal is to introduce the effects of noncommutativity in quantum cosmology including one

M. Aguero (✉) · J.A.S. Aguilar · J. Socorro
Facultad de Ciencias de la Universidad Autónoma del Estado de México, Instituto Literario No. 100, C.P. 50000, Toluca, Edo de Mex, Mexico
e-mail: magxim@gmail.com

J.A.S. Aguilar
e-mail: polarequis@yahoo.com.mx

C. Ortiz · M. Sabido · J. Socorro
Instituto de Física de la Universidad de Guanajuato, A.P. E-143, C.P. 37150, León, Guanajuato, Mexico

C. Ortiz
e-mail: ortizca@fisica.ugto.mx

M. Sabido
e-mail: msabido@fisica.ugto.mx

J. Socorro
e-mail: socorro@fisica.ugto.mx

International Journal of Theoretical Physics, Vol. 46, No. 3, March 2007 (© 2007)
DOI: 10.1007/s10773-006-9143-y

Mass Parameter Quantization in the FRW Cosmological Model

J. Torres,[1,2] C. Ortiz,[1] J. Socorro,[1] and V. I. Tkach[1]

Received October 17, 2005; accepted March 13, 2006
Published Online: February 21, 2007

Using the canonical quantum theory apply to spherically symmetric pure gravitational systems, we present the study of the closed Friedmann-Robertson-Walker (FRW) cosmological model filled with pressureless matter (dust) content as a toy model. The Wheeler-DeWitt equation is view as the Schrödinger equation for the linear harmonic oscillator with energy E. We show that such type of universe has a quantized masses of the order of the Planck mass and harmonic oscillator wave functions, where a dual symmetry emerge among the quantum parameters.

KEY WORDS: quantum gravity; quantum cosmology; dual simmetry.

PACS Numbers: 04.20.Fy; 04.60.Ds; 04.70.-s; 04.70.Dy; 98.80.Hw.

1. INTRODUCTION

The absence of a fundamental understanding of physics at very high energies and, in particular, in the absence of a consistent quantum theory of gravity, there is no hope, at present, to meet an understanding of the quantum origin of the Universe in a definitive way. However, it appears desirable to develop highly and simplified, but consistent toy models, which contain as many as possible of those features which are believed will be present in a future complete quantum theory of gravity.

In order to give one possible mechanism for to find certain quantization rules for the parameters that describes our universe, we present the simpler approach, where we view the Wheeler-DeWitt equation at energy zero, obtained with the canonical procedure quantization for a closed FRW cosmological model filled with pressureless matter (dust) content, like the Schrödinger equation for a linear harmonic oscillator at energy E. This energy is associated with the mass parameter quantization, and such type of universe has a quantized masses of the order of

[1] Instituto de Física de la Universidad de Guanajuato, A.P. E-143, C.P. 37150, León, Guanajuato, México.
[2] To whom correspondence should be addressed; e-mail: jtorres_arenas@yahoo.com.mx.

PHYSICAL REVIEW D **78,** 114016 (2008)

Consistent scenario for $B \to PS$ decays

D. Delepine* and J. L. Lucio M.†

Instituto de Física, Universidad de Guanajuato Loma del Bosque # 103, Lomas del Campestre, 37150 León, Guanajuato, México

J. A. Mendoza S.‡

Depto. de Física-Matemáticas, Universidad de Pamplona Pamplona, Norte de Santander, Colombia

Carlos A. Ramírez§

Escuela de Física, Universidad Industrial de Santander, A.A. 678, Bucaramanga, Colombia

(Received 24 August 2008; published 11 December 2008)

We consider $B \to PS$ decays where P stands for pseudoscalar and S for a heavy (1500 MeV) scalar meson. We achieve agreement with available experimental data, which includes two orders of magnitude hierarchy, assuming the scalars mesons are two quark states. The contribution of the dipolar penguin operator $\mathcal{O}_{11}$ is quantified.

DOI: 10.1103/PhysRevD.78.114016 PACS numbers: 13.25.Hw, 12.39.Mk, 14.40.Cs

I. INTRODUCTION

The scalar sector below 2 GeV is poorly understood, nevertheless several features—like the presence of two multiplets and several of their properties—naturally arise in the analysis of a number of authors. A first set of scalars with masses around 1.5 GeV [1] is grouped in a heavy multiplet, including the $K_0^*(1430)$, $a_0(1450)$, $f_0(1500)$ for the octet, $f_0(1370)$ which is identified with the singlet and the $f_0(1710)$ which seems to be mainly glueball. The octet is nearly degenerate, like similar pseudoscalar, vector, axial vector and tensor multiplets, their widths are small (≤ 100 MeV). The mixing angles seems to be small except by the singlet-glueball which is around $-20°$, according to H. Y. Cheng in Ref. [2]. It has been more difficult to establish the lighter multiplet, even the existence and nature of some of their members is in doubt. The light multiplet should include the $a_0(980)$, $f_0(980)$ and the $\kappa = K_0^*(800)$ in the octet; while the singlet could be identified with the $\sigma = f_0(600)$. The mixing is not clear and their widths are very large. Ideally, the former multiplet can be identified as the ground state of quark-antiquark bound states with angular momenta one while the latter with the ground state of four quarks systems with zero angular momenta. In the real world an undetermined mixing between the two multiplets is expected. Alternatively both multiplets could be identified as quark-antiquark states with angular momenta one, the lighter being the ground state while the heavier the first excited state.

A full understanding of the scalar multiplets previously described remains a challenge, both from the experimental perspective as well as from the theoretical point of view [1]. To start with, there is not enough conclusive experimental information regarding the existence and properties of the scalars. Notice that the information is poor not because of the lack of sources of scalar mesons, for example, many of the decays of particles containing c or b quarks involve the production of scalar mesons. The information on the scalars is scarce because of the large width they have since that produces a large overlap with nearby resonances and with the background. In spite of those problems, precise experimental results are available [1,3,4] for the mass and width of the f_0 and K_0^*, for the β angle [5] of the Cabibbo-Kobayashi-Maskawa (CKM) matrix and for several partial widths. It has been speculated that the α angle can be extracted in processes involving scalars [6] and new projects like the LHCB [7] will improve the old measurements and obtain new results. Relevant to our work are the branching ratios for the $B \to PS$ decays measured by different groups, which show a nontrivial hierarchy. The experimental data collected in Table I suggest that, for $B \to PS$ decays including members of the heavy scalar multiplet, the order of magnitude of the branching ratios involving the $K_0^*(1430)$, the $f_0(1370)$, $f_0(1500)$ and the $a_0(1450)$ are different.

On the theoretical side the situation is not better. The origin of the difficulties are the nonperturbative regime of QCD and the limited computer capacity for the lattice approach. The nature of the observed scalars has been discussed at length, and proposals exist to identify them as 2 or 4 quark states, glueballs, molecules, etc., and several theoretical formalisms have been developed to calculate nonleptonic decays. The simplest one is the so-called "Naive Factorization Approach" (NFA) [9], which in general produces the correct order of magnitude and its predictions are in rough agreement with the experimental results. Discrepancies are known to occur in two cases, for "color suppressed" processes and when important rescattering effects are involved, for example, processes where direct CP violation is relevant [10,11]. The advantage of

*delepine@fisica.ugto.mx
†lucio@fisica.ugto.mx
‡jairoam@unipamplona.edu.co
§jpjramirez@yahoo.com

Supersymmetric *R* parity violation and *CP* asymmetry in semileptonic τ decays

D. Delepine*
Instituto de Física de la Universidad de Guanajuato, C.P. 37150, León, Guanajuato, México

G. Faisel† and S. Khalil‡
Ain Shams University, Faculty of Science, Cairo 11566, Egypt
and Center for Theoretical Physics, British University in Egypt, Shorouk City, Cairo, 11837, Egypt
(Received 15 October 2007; published 16 January 2008)

We analyze the *CP* violation in the semileptonic $|\Delta S| = 1$ τ decays in supersymmetric extensions of the standard model with *R* parity violating term. We show that the *CP* asymmetry of τ decay is enhanced significantly and the current experimental limits obtained by CLEO collaborations can be easily accommodated. We argue that observing *CP* violation in semileptonic τ decay would be a clear evidence for *R* parity violating supersymmetry extension of the standard model.

DOI: 10.1103/PhysRevD.77.016003 PACS numbers: 11.10.St, 11.30.Er, 13.35.Dx

I. INTRODUCTION

CP violation is one of the main open questions in high energy physics. In the standard model (SM), all *CP* violating observables should be explained by one complex phase δ_{CKM} in the Cabibbo-Kobayashi-Maskawa (CKM)quark mixing matrix. The effect of this phase was first observed in the kaon system and recently confirmed in *B* decays. The quark-lepton symmetry suggests that the lepton mixing matrix should also violate *CP* invariance. However, the situation in the lepton sector is very different. The only evidence for flavor violation in this sector comes from the neutrino oscillations and there is, so far, no confirmation for *CP* violation in leptonic decays. Hence, measuring *CP* asymmetry in τ decays will open a new window for studying *CP* violation.

In recent papers [1,2], it has been pointed out that $\tau^{\pm} \to K_{L,S}\pi^{\pm}\nu$ decays exhibit a *CP* asymmetry of the same size as the one measured in the charge asymmetry of semileptonic K_L decays. This large *CP* asymmetry is induced by the *CP* violation in $K^0 - \bar{K}_0$ mixing. But within the SM, the direct *CP* asymmetry rate of $\tau^{\pm} \to K^{\pm}\pi^0\nu$ is of order $O(10^{-12})$ [3]. This nearly vanishing asymmetry implies that the observation of any *CP* asymmetry in this τ decay channel would be a clear signal for the presence of *CP* violation beyond the SM.

Supersymmetry (SUSY) is one of the most interesting candidates for physics beyond the SM. Supersymmetry provides a new source of *CP* violation through complex couplings in the soft SUSY breaking terms. The *CP* asymmetry in the decay mode $\tau^{\pm} \to K^{\pm}\pi^0\nu$, in minimal supersymmetric extension of the SM with *R* parity conservation, has been computed in Ref. [4]. It was shown that the SUSY contributions can enhance the *CP* asymmetry rate in τ decay by many orders of magnitude. However, the typical value is of order $O(10^{-7})$ which is still much smaller than the current experimental bound.

The aim of this paper is to show that a significant enhancement for the *CP* asymmetry of $\tau^{\pm} \to K^{\pm}\pi^0\nu$ can be obtained in SUSY models with *R* parity violating terms. It turns out that the *R* parity violating terms (in particular, the Lepton number violating ones) induce a tree-level contribution to τ decay. This contribution is proportional to the *R* parity couplings λ and λ', which in general are complex. We find that this new source of *CP* violation enhances the asymmetry of τ decay. We impose new constraints on the couplings λ and λ' from the experimental limits, obtained by CLEO collaborations [5–8].

The paper is organized as follows. In Sec. II, some general features on τ semileptonic decays are recalled. Section III is devoted for analyzing the *CP* asymmetry of $\tau^{\pm} \to K^{\pm}\pi^0\nu$ in SUSY models with *R* parity violation. We derive the corresponding effective Hamiltonian and show the terms that violate *R* parity may give significant contribution to the *CP* asymmetry in τ decay. Finally, we give our conclusions in Sec. IV.

II. *CP* ASYMMETRY OF τ SEMILEPTONIC DECAY IN MSSM

In this section we analyze the *CP* asymmetry of τ semileptonic decay modes within the minimal supersymmetric standard model (MSSM); we will focus on the decay mode $\tau^{\pm} \to K^{\pm}\pi^0\nu$. The general amplitude for $\tau^-(p) \to K^-(k)\pi^0(k')\nu_\tau(p')$ is given by

$$\mathcal{M} = \frac{G_F V_{us}}{\sqrt{2}}\Big\{\bar{u}(p')\gamma^\mu(1-\gamma_5)u(p)F_V(t)\Big[(k-k')_\mu - \frac{\Delta^2}{t}q_\mu\Big] + \bar{u}(p')(1+\gamma_5)u(p)m_\tau\Lambda F_S(t)\frac{\Delta^2}{t} + F_T\langle K\pi|\bar{s}\sigma_{\mu\nu}u|0\rangle\bar{u}(p')\sigma^{\mu\nu}(1+\gamma_5)u(p)\Big\},$$

where $q = k + k'$ $(t = q^2)$ is the momentum transfer to the hadronic system, and $\Delta^2 \equiv m_K^2 - m_\pi^2$ and $F_{V,S,T}(t)$ are the

*delepine@fisica.ugto.mx
†gfaisel@bue.edu.eg
‡skhalil@bue.edu.eg

Mass gap for gravity localized on Weyl thick branes

N. Barbosa-Cendejas,[1,*] A. Herrera-Aguilar,[2,+] M. A. Reyes Santos,[1,‡] and C. Schubert[2,§]

[1]*Instituto de Física, Universidad de Guanajuato, Loma del Bosque 103, Frac. Lomas del Campestre, C.P. 37150 León, Guanajuato, México*

[2]*Instituto de Física y Matemáticas, Universidad Michoacana de San Nicolás de Hidalgo, Edificio C-3, Ciudad Universitaria, C.P. 58040, Morelia, Michoacán, México*

(Received 16 September 2007; revised manuscript received 25 April 2008; published 18 June 2008)

We consider thick brane configurations in a pure geometric Weyl integrable 5D space-time, a non-Riemannian generalization of Kaluza-Klein (KK) theory involving a geometric scalar field. Thus, the 5D theory describes gravity coupled to a self-interacting scalar field which gives rise to the structure of the thick branes. We continue the study of the properties of a previously found family of solutions which is smooth at the position of the brane but involves naked singularities in the fifth dimension. Analyzing their graviton spectrum, we find that a particularly interesting situation arises for a special case in which the 4D graviton is separated from the KK gravitons by a mass gap. The corresponding effective Schrödinger equation has a modified Pöschl-Teller potential and can be solved exactly. Apart from the massless 4D graviton, it contains one massive KK bound state, and the continuum spectrum of delocalized KK modes. We also discuss the mass hierarchy problem, and explicitly compute the corrections to Newton's law in the thin brane limit.

DOI: 10.1103/PhysRevD.77.126013 PACS numbers: 11.25.Mj, 04.50.−h, 11.10.Kk, 11.27.+d

I. INTRODUCTION

The success of brane world scenarios to address a number of high energy physics problems [1] and the expectation of possible experimental evidence for extra dimensions [2–7] have given rise to various modifications and generalizations of the initial thin brane models [4–7]. Among them we find several types of thick brane configurations: scalar smooth branes [8–10], tachyonic branes [11], branes on black holes [12,13], branes with nonminimally coupled scalar fields [14,15]; within this framework several physical aspects have been studied like localization of gravity [16–22] and matter fields [23], brane stability [24,25], critical phenomena [26], etc.

The model to be considered here is of the class introduced by [8]. It describes Weyl gravity coupled to a geometrical scalar field and constitutes a noncompact generalization of the Randall-Sundrum (RS) model [5,6] with the advantage that the 5D manifold is no longer restricted to be an orbifold and the branes in the action need not be introduced by hand.

In this paper, we briefly review localization of 4D gravity on previously constructed thick branes in a Weyl integrable manifold [21]. In Weyl geometry, a scalar field enters in the definition of the affine connection of the manifold, revealing its geometrical nature. Weyl integrable manifolds are invariant under Weyl rescalings (see, e.g., [20] for details); when this invariance is broken, via a self-interacting potential, for instance, the scalar field transforms into an observable degree of freedom.

Various classes of thick brane solutions have been discussed in the literature. In particular, in [8,9,11,15,16,18,26], it was proposed to smooth out the results obtained in the RS model with the aid of a scalar field. Moreover, the stability of these thick objects was considered in [24]. All these models have a continuous Kaluza-Klein (KK) graviton spectrum starting at zero mass, causing a need for explaining why such arbitrarily light extra gravitons have not led to detectable deviations from standard gravity. Although a number of mechanisms have been proposed how such light extra gravitons could go unobserved (see, e.g., [7]), it is obviously an interesting question whether thick brane solutions exist which have a mass gap and thereby avoid this problem altogether. Reconsidering some of the previously found families of solutions we have found one such case, and the main purpose of this paper is a detailed study of its properties.

The solution family in question involves a simple trigonometric warp factor [8,9,19–23]. Following [5,8,16], we study linear fluctuations of the classical metric and cast the wave equation for the transverse traceless modes in the form of a Schrödinger equation. Contrary to previous studies of this type of solutions, where the potential in this equation usually went to zero far from the brane, we fix the free parameter of the model in such a way that it asymptotes to a positive constant. The corresponding Schrödinger equation turns out to be exactly solvable, being of Pöschl-Teller type. Apart from the massless 4D graviton, it has one more bound state, describing a massive localized graviton, as well as a continuum tower of delocalized massive modes. Thus, it indeed leads to a mass gap for the graviton

*nandinii@ifm.umich.mx
+herrera@ifm.umich.mx
‡marco@fisica.ugto.mx
§schubert@ifm.umich.mx

Available online at www.sciencedirect.com
ScienceDirect
Physics Letters B 660 (2008) 147–153
PHYSICS LETTERS B
www.elsevier.com/locate/physletb

Study of Cabibbo suppressed decays of the D_s^+ charmed-strange meson involving a K_S^0

FOCUS Collaboration [1]

J.M. Link [a], P.M. Yager [a], J.C. Anjos [b], I. Bediaga [b], C. Castromonte [b], A.A. Machado [b], J. Magnin [b], A. Massafferri [b], J.M. de Miranda [b], I.M. Pepe [b], E. Polycarpo [b], A.C. dos Reis [b], S. Carrillo [c], E. Casimiro [c], E. Cuautle [c], A. Sánchez-Hernández [c], C. Uribe [c], F. Vázquez [c], L. Agostino [d], L. Cinquini [d], J.P. Cumalat [d,*], V. Frisullo [d], B. O'Reilly [d], I. Segoni [d], K. Stenson [d], R.S. Tucker [d], J.N. Butler [e], H.W.K. Cheung [e], G. Chiodini [e], I. Gaines [e], P.H. Garbincius [e], L.A. Garren [e], E. Gottschalk [e], P.H. Kasper [e], A.E. Kreymer [e], R. Kutschke [e], M. Wang [e], L. Benussi [f], S. Bianco [f], F.L. Fabbri [f], A. Zallo [f], M. Reyes [g], C. Cawlfield [h], D.Y. Kim [h], A. Rahimi [h], J. Wiss [h], R. Gardner [i], A. Kryemadhi [i], Y.S. Chung [j], J.S. Kang [j], B.R. Ko [j], J.W. Kwak [j], K.B. Lee [j], K. Cho [k], H. Park [k], G. Alimonti [l], S. Barberis [l], M. Boschini [l], A. Cerutti [l], P. D'Angelo [l], M. DiCorato [l], P. Dini [l], L. Edera [l], S. Erba [l], P. Inzani [l], F. Leveraro [l], S. Malvezzi [l], D. Menasce [l], M. Mezzadri [l], L. Moroni [l], D. Pedrini [l], C. Pontoglio [l], F. Prelz [l], M. Rovere [l], S. Sala [l], T.F. Davenport III [m], V. Arena [n], G. Boca [n], G. Bonomi [n], G. Gianini [n], G. Liguori [n], D. Lopes Pegna [n], M.M. Merlo [n], D. Pantea [n], S.P. Ratti [n], C. Riccardi [n], P. Vitulo [n], C. Göbel [o], J. Otalora [o], H. Hernandez [p], A.M. Lopez [p], H. Mendez [p], A. Paris [p], J. Quinones [p], J.E. Ramirez [p], Y. Zhang [p], J.R. Wilson [q], T. Handler [r], R. Mitchell [r], D. Engh [s], M. Hosack [s], W.E. Johns [s], E. Luiggi [s], M. Nehring [s], P.D. Sheldon [s], E.W. Vaandering [s], M. Webster [s], M. Sheaff [t]

[a] *University of California, Davis, CA 95616, USA*
[b] *Centro Brasileiro de Pesquisas Físicas, Rio de Janeiro, RJ, Brazil*
[c] *CINVESTAV, 07000 México City, DF, Mexico*
[d] *University of Colorado, Boulder, CO 80309, USA*
[e] *Fermi National Accelerator Laboratory, Batavia, IL 60510, USA*
[f] *Laboratori Nazionali di Frascati dell'INFN, Frascati I-00044, Italy*
[g] *University of Guanajuato, 37150 Leon, Guanajuato, Mexico*
[h] *University of Illinois, Urbana-Champaign, IL 61801, USA*
[i] *Indiana University, Bloomington, IN 47405, USA*
[j] *Korea University, Seoul 136-701, South Korea*
[k] *Kyungpook National University, Taegu 702-701, South Korea*
[l] *INFN and University of Milano, Milano, Italy*
[m] *University of North Carolina, Asheville, NC 28804, USA*
[n] *Dipartimento di Fisica Nucleare e Teorica and INFN, Pavia, Italy*
[o] *Pontifícia Universidade Católica, Rio de Janeiro, RJ, Brazil*
[p] *University of Puerto Rico, Mayaguez, PR 00681, USA*
[q] *University of South Carolina, Columbia, SC 29208, USA*

[*] Corresponding author.
E-mail address: john.p.cumalat@colorado.edu (J.P. Cumalat).
[1] See http://www-focus.fnal.gov/authors.html for additional author information.

0370-2693/$ – see front matter
doi:10.1016/j.physletb.2007.12.050

Available online at www.sciencedirect.com
ScienceDirect
Physics Letters B 661 (2008) 14–21
PHYSICS LETTERS B
www.elsevier.com/locate/physletb

Search for a pentaquark decaying to $\Xi^-\pi^-$

FOCUS Collaboration [1]

J.M. Link [a], P.M. Yager [a], J.C. Anjos [b], I. Bediaga [b], C. Castromonte [b], A.A. Machado [b], J. Magnin [b], A. Massafferri [b], J.M. de Miranda [b], I.M. Pepe [b], E. Polycarpo [b], A.C. dos Reis [b], S. Carrillo [c], E. Casimiro [c], E. Cuautle [c], A. Sánchez-Hernández [c], C. Uribe [c], F. Vázquez [c], L. Agostino [d], L. Cinquini [d], J.P. Cumalat [d], V. Frisullo [d], B. O'Reilly [d], I. Segoni [d], K. Stenson [d], J.N. Butler [e], H.W.K. Cheung [e], G. Chiodini [e], I. Gaines [e], P.H. Garbincius [e], L.A. Garren [e], E. Gottschalk [e], P.H. Kasper [e], A.E. Kreymer [e], R. Kutschke [e], M. Wang [e], L. Benussi [f], S. Bianco [f], F.L. Fabbri [f], A. Zallo [f], M. Reyes [g], C. Cawlfield [h], D.Y. Kim [h], A. Rahimi [h], J. Wiss [h], R. Gardner [i], A. Kryemadhi [i], Y.S. Chung [j], J.S. Kang [j], B.R. Ko [j], J.W. Kwak [j], K.B. Lee [j], K. Cho [k], H. Park [k], G. Alimonti [l], S. Barberis [l], M. Boschini [l], A. Cerutti [l], P. D'Angelo [l], M. DiCorato [l], P. Dini [l], L. Edera [l], S. Erba [l], P. Inzani [l], F. Leveraro [l], S. Malvezzi [l], D. Menasce [l], M. Mezzadri [l], L. Moroni [l], D. Pedrini [l], C. Pontoglio [l], F. Prelz [l], M. Rovere [l], S. Sala [l], T.F. Davenport III [m], V. Arena [n], G. Boca [n], G. Bonomi [n], G. Gianini [n], G. Liguori [n], D. Lopes Pegna [n], M.M. Merlo [n], D. Pantea [n], S.P. Ratti [n], C. Riccardi [n], P. Vitulo [n], C. Göbel [o], J. Otalora [o], H. Hernandez [p], A.M. Lopez [p], H. Mendez [p], A. Paris [p], J. Quinones [p], J.E. Ramirez [p,*], Y. Zhang [p], J.R. Wilson [q], T. Handler [r], R. Mitchell [r], D. Engh [s], M. Hosack [s], W.E. Johns [s], E. Luiggi [s], M. Nehring [s], P.D. Sheldon [s], E.W. Vaandering [s], M. Webster [s], M. Sheaff [t]

[a] *University of California, Davis, CA 95616, USA*
[b] *Centro Brasileiro de Pesquisas Físicas, Rio de Janeiro, RJ, Brazil*
[c] *CINVESTAV, 07000 México City, DF, Mexico*
[d] *University of Colorado, Boulder, CO 80309, USA*
[e] *Fermi National Accelerator Laboratory, Batavia, IL 60510, USA*
[f] *Laboratori Nazionali di Frascati dell'INFN, Frascati I-00044, Italy*
[g] *University of Guanajuato, 37150 Leon, Guanajuato, Mexico*
[h] *University of Illinois, Urbana-Champaign, IL 61801, USA*
[i] *Indiana University, Bloomington, IN 47405, USA*
[j] *Korea University, Seoul 136-701, South Korea*
[k] *Kyungpook National University, Taegu 702-701, South Korea*
[l] *INFN and University of Milano, Milano, Italy*
[m] *University of North Carolina, Asheville, NC 28804, USA*
[n] *Dipartimento di Fisica Nucleare e Teorica and INFN, Pavia, Italy*
[o] *Pontifícia Universidade Católica, Rio de Janeiro, RJ, Brazil*
[p] *University of Puerto Rico, Mayaguez, PR 00681, USA*
[q] *University of South Carolina, Columbia, SC 29208, USA*
[r] *University of Tennessee, Knoxville, TN 37996, USA*

[*] Corresponding author.
E-mail address: eduardo@charma.uprm.edu (J.E. Ramirez).
[1] See http://www-focus.fnal.gov/authors.html for additional author information.

0370-2693/$ – see front matter
doi:10.1016/j.physletb.2008.01.063

PHYSICAL REVIEW D **77,** 121301(R) (2008)

Triple unification of inflation, dark matter, and dark energy using a single field

Andrew R. Liddle,[1] Cédric Pahud,[1,2] and L. Arturo Ureña-López[3]

[1]*Astronomy Centre, University of Sussex, Brighton BN1 9QH, United Kingdom*

[2]*Institut d'Astrophysique de Paris, UMR 7095-CNRS, Université Pierre et Marie Curie, 98bis boulevard Arago, 75014 Paris, France*

[3]*Instituto de Física de la Universidad de Guanajuato, C.P. 37150, León, Guanajuato, México*

(Received 8 April 2008; published 19 June 2008)

We construct an explicit scenario whereby the same material driving inflation in the early universe can comprise dark matter in the present universe, using a simple quadratic potential. Following inflation and preheating, the density of inflaton/dark matter particles is reduced to the observed level by a period of thermal inflation, of a duration already invoked in the literature for other reasons. Within the context of the string landscape, one can further argue for a nonzero vacuum energy of this field, thus unifying inflation, dark matter, and dark energy into a single fundamental field.

DOI: 10.1103/PhysRevD.77.121301 PACS numbers: 98.80.Cq, 95.35.+d, 95.36.+x

I. INTRODUCTION

In a recent paper [1], two of us proposed a general scenario for unification of dark matter and inflation into a single field. The key ingredient is the survival of a residual amount of the inflaton field's energy density, which undergoes coherent oscillations and can serve as a cold dark matter candidate. In the context of the string landscape, one can further argue for a nonzero vacuum energy of this field on anthropic grounds, thus providing a single description of the three key unknowns of modern cosmology, namely, dark energy, dark matter, and the material responsible for early universe inflation.

In practice, however, realizing this scenario is nontrivial, due to the need for a long radiation-dominated era of the Universe encompassing the nucleosynthesis period. This requires that the amplitude of scalar field oscillations be extremely small after the energy trapped in the inflaton is released into normal particles. Preheating scenarios can provide part of the required reduction of the oscillation amplitude, but still leave it too high and in conflict with the observed dark matter to radiation density ratio.[1]

In this paper, we explore a modification to the original scenario of Ref. [1]. As we shall discuss below, after preheating the Universe undergoes a short period of radiation quickly followed by a period of matter domination driven by the relic energy density of the inflaton field itself. This early matter domination period is interrupted by a short second period of inflation, known as thermal inflation, driven by a separate field and perhaps associated with the supersymmetry breaking transition. We find that thermal inflation can reduce the oscillation amplitude of the scalar field to the desired level, and then provide a proper reheating of the Universe.

II. COSMOLOGICAL EVOLUTION

For definiteness, we consider throughout the model of Ref. [1] where the inflaton ϕ has potential $V_0 + \frac{1}{2}m^2\phi^2$. Here V_0 has the small value needed to explain the observed dark energy density, and otherwise does not play a significant role. For sufficiently large $|\phi| \gtrsim m_{\rm Pl}$, this potential drives inflation and produces density perturbations in agreement with observations provided $m \simeq 10^{-6} m_{\rm Pl}$. Subsequently $H \ll m$ at all times, where H is the Hubble parameter, and the ϕ field oscillates rapidly on the Hubble time scale. Such an oscillating field behaves as cold dark matter, both in the redshifting of the mean density $\rho_\phi \propto a^{-3}$ and in the evolution of perturbations.

Unless some mechanism exists to reduce the energy density of the oscillating field, and indeed to transform some of it into conventional material, it is not possible to recover a satisfactory big bang cosmology. The original resolution was reheating—the complete transfer of energy from the inflaton via single-particle decays. Later coherent decays, known as preheating [2–4,6], were invoked as well. Such decays may be extremely efficient when the inflaton oscillations are large, but if the only interactions present are annihilations, the process will necessarily shut off once the density reduces. This led Kofman, Linde, and Starobinsky [2,4] to propose that the residual field could act as dark matter, but in fact detailed calculations [1] show the relic abundance is far too high under standard assumptions. It has usually thus been considered that preheating is followed by a period of reheating leading to complete decay of the inflaton field.

Having recognized that an inefficient reheating is a main concern in our unification scenario, the authors in Refs. [7,8][2] suggest that plasma mass effects [10] could

[1]This holds for the original four-legs interaction studied in the preheating literature [2–4], though a complete decay of the inflaton can be obtained from the introduction of other couplings [5].

[2]There exists an sneutrino (which is a scalar field) unification model for inflation and dark matter [8,9], with similar properties to our phenomenological model; under certain conditions, our approach also applies to it.

International Journal of Modern Physics D
Vol. 18, No. 1 (2009) 95–106

World Scientific
www.worldscientific.com

WKB-TYPE APPROXIMATION TO NONCOMMUTATIVE QUANTUM COSMOLOGY

E. MENA

Centro Universitario de la Cienega,
Ave. Universidad 1115 Edif. B,
C.P. 47820 Ocotlán, Jalisco, México
emena@cuci.udg.mx

O. OBREGÓN* and M. SABIDO†

Instituto de Física de la Universidad de Guanajuato,
A.P. E-143, C.P. 37150, León, Guanajuato, México
**octavio@fisica.ugto.mx*
†*msabido@fisica.ugto.mx*

Received 28 February 2008
Communicated by A. A. Starobinsky

In this paper, we develop and apply the WKB-type approximation to several examples of noncommutative quantum cosmology, obtaining the time evolution of the noncommutative universe. This is accomplished by starting from a noncommutative quantum formulation of cosmology, where the noncommutativity is introduced by a deformation on the minisuperspace variables. This procedure gives a straightforward algorithm to incorporate noncommutativity into cosmology and inflation.

Keywords: Noncommutativity; cosmology.

1. Introduction

There has been a lot of interest in the old idea of noncommutative space–time,[1] and an immense amount of work has been done on this subject. This renewed interest is a consequence of the developments in M-theory and string theory, where in the description of the low-energy excitations of open strings, in the presence of a Neveu–Schwarz (NS) constant background B-field, a noncommutative effective low-energy gauge theory action[2,3] occurs in a natural way. Along the lines of noncommutative gauge theory, noncommutative theories of gravity have been constructed.[4–16] All of these formulations of gravity on noncommutative space–time are highly nonlinear and a direct calculation of cosmological models is incredibly difficult. One may naively expect noncommutative effects to be present at the Planck scale, so it is almost impossible to detect them, but due to the UV/IR mixing,[17,18] the effects of noncommutativity might be important at the cosmological scale.

Crossing the phantom divide in an interacting generalized Chaplygin gas

2008 J. Cosmol. Astropart. Phys. 2008 016

(http://iopscience.iop.org/1475-7516/2008/07/016)

Journal of Cosmology and Astroparticle Physics
An IOP and SISSA journal

Crossing the phantom divide in an interacting generalized Chaplygin gas

H García-Compeán[1,4], G García-Jiménez[2], O Obregón[3] and C Ramírez[2]

[1] Centro de Investigación y de Estudios Avanzados del IPN, Unidad Monterrey, Autopista al Aeropuerto km 9.5, CP 66600, Apodaca, NL, Mexico
[2] Facultad de Ciencias Físico Matemáticas, Universidad Autónoma de Puebla, PO Box 1364, 72000 Puebla, Mexico
[3] Instituto de Física de la Universidad de Guanajuato, PO Box E-143, 37150 León Gto., Mexico
E-mail: compean@fis.cinvestav.mx, ggarcia@fcfm.buap.mx, ggarcia@fisica.ugto.mx, octavio@fisica.ugto.mx and cramirez@fcfm.buap.mx

Received 12 April 2008
Accepted 3 July 2008
Published 23 July 2008

Online at stacks.iop.org/JCAP/2008/i=07/a=016
doi:10.1088/1475-7516/2008/07/016

Abstract. Unified generalized Chaplygin gas models assuming an interaction between dark energy and dark matter fluids have been previously proposed. Following these ideas, we consider a particular relation between dark densities, which allows the possibility of a time varying equation of state for dark energy that crosses the phantom divide at a recent epoch. Moreover, these densities decay throughout the evolution of the Universe, avoiding a big rip. We find also a scaling solution, i.e. these densities are asymptotically proportional in the future, which contributes to the solution of the coincidence problem.

Keywords: dark matter, dark energy theory, classical tests of cosmology

ArXiv ePrint: 0710.4283

[4] On leave from: Departamento de Física, Centro de Investigación y de Estudios Avanzados del IPN, México, AP 14-740, 07000, México DF, Mexico.

1475-7516/08/07016+11$30.00

JCAP07(2008)016

PHYSICAL REVIEW D **78,** 124008 (2008)

Twisted covariant noncommutative self-dual gravity

S. Estrada-Jiménez[*]
Centro de Estudios en Física y Matemáticas Básicas y Aplicadas, Universidad Autónoma de Chiapas, Calle 4 Oriente Norte 1428, Tuxtla Gutiérrez, Chiapas, México

H. García-Compeán[†]
Departamento de Física, Centro de Investigación y de Estudios Avanzados del IPN, P.O. Box 14-740, 07000 México D.F., México, and Centro de Investigación y de Estudios Avanzados del IPN, Unidad Monterrey, PIIT, Vía del Conocimiento 201, Autopista nueva al Aeropuerto km 9.5, 66600, Apodaca Nuevo León, México

O. Obregón[‡]
Instituto de Física de la Universidad de Guanajuato, P.O. Box E-143, 37150, León Gto., México

C. Ramírez[§]
Facultad de Ciencias Físico Matemáticas, Universidad Autónoma de Puebla, P.O. Box 1364, 72000, Puebla, México
(Received 19 September 2008; published 10 December 2008)

A twisted covariant formulation of noncommutative self-dual gravity is presented. The formulation for constructing twisted noncommutative Yang-Mills theories is used. It is shown that the noncommutative torsion is solved at any order of the θ expansion in terms of the tetrad and some extra fields of the theory. In the process the first order expansion in θ for the Plebański action is explicitly obtained.

DOI: 10.1103/PhysRevD.78.124008 PACS numbers: 04.70.Dy, 04.30.Nk, 04.62.+v, 11.10.Nx

I. INTRODUCTION

Noncommutative structures in field theory have been studied over the years and the subject has been introduced in several forms. The idea of noncommutative space-time seems to be first proposed by Heisenberg [1], as a possible cutoff to cure UV divergences in quantum field theory (for some historical remarks, see [2]). This idea was further developed by H. S. Snyder and applied to find an implementation of the Lorentz symmetry on a space-time with noncommuting coordinates [3]. Snyder's construction was realized in $(4 + 1)$-dimensional space-time, however it allows coordinate transformations which break down the Lorentz symmetry in a $(3 + 1)$ space-time subspace. The extension to include the gauge symmetry of the electromagnetic field was pursued in a second paper [4] (for a recent review, see [5]).

Deformation quantization and Connes's approach are two of the most used formulations of noncommutative spaces. On one hand, deformation quantization was first introduced in the context of phase-space quantization [6], some years before Snyder's paper and finally formulated as an alternative quantization method in Ref. [7] (for a review, see [8]). On the other hand, Connes's noncommutative geometry [9] is a rigorous mathematical setting containing nontrivial structures originated from von Neumann [10] and Gelfand-Naimark's results [11].

An important step done recently, was the discovery that noncommutative gauge theory is obtained naturally from nonperturbative string theory (D-brane physics) via the Seiberg-Witten map [12]. Furthermore, M-theory, in its M(atrix) theory approach, was also shown to be compatible with these noncommutative structures [13]. This relation to string theory has been one of the main motivations to further explore the physics of noncommutative theories.

Noncommutative field theory can incorporate nonlocal effects in field theory at the classical and quantum levels in an interesting and subtle way. For instance it gives rise to surprising effects like the IR/UV mixing [14] (for some reviews, see [15,16]). Recently nonperturbative studies (via Monte Carlo simulations) seem to support the existence of this mixing [17].

Noncommutative field theories can be carried over to $SU(N)$ gauge theories through the implementation of the universal enveloping algebra associated to the Lie algebra of the gauge group (of the limiting commutative field theory). Consequently, the standard model or grand unified theory's models [18] can be constructed in this way by using the Seiberg-Witten map. Similarly, noncommutative versions of topological and self-dual gravity [19] can be constructed by using the same methods.

In fact, there are numerous proposals of noncommutative gravity theories in four dimensions [20]. However, they do not have a clear relation to string theory as the gauge theory counterpart does [21]. Moreover, the diffeomorphism invariance turns out to be broken even at the classical level. This is the problem of covariance and there is evidence that noncommutative field theories also could be nonunitary and violate causality (see for instance, [22]).

[*]sendic@fis.cinvestav.mx
[†]compean@fis.cinvestav.mx
[‡]octavio@fisica.ugto.mx
[§]cramirez@fcfm.buap.mx

PHYSICAL REVIEW D **78,** 074031 (2008)

$X(2175)$ as a resonant state of the $\phi K\bar{K}$ system

A. Martínez Torres,[1] K. P. Khemchandani,[1,*] L. S. Geng,[1] M. Napsuciale,[1,2] and E. Oset[1]

[1]*Departamento de Física Teórica and IFIC, Centro Mixto Universidad de Valencia-CSIC, Institutos de Investigación de Paterna, Apartado 22085, 46071 Valencia, Spain*

[2]*Instituto de Física, Universidad de Guanajuato, Lomas del Bosque 103, Fraccionamiento Lomas del Campestre, 37150, León, Guanajuato, México*

(Received 29 January 2008; revised manuscript received 15 July 2008; published 30 October 2008)

We perform a Faddeev calculation for the three-meson system $\phi K\bar{K}$, taking the interaction between two pseudoscalar mesons and between a vector and a pseudoscalar meson from the chiral unitary approach. We obtain a neat resonance peak around a total mass of 2150 MeV and an invariant mass for the $K\bar{K}$ system around 970 MeV, very close to the $f_0(980)$ mass. The state appears in $I = 0$ and qualifies as a $\phi f_0(980)$ resonance. We enlarge the space of states including $\phi\pi\pi$, since $\pi\pi$ and $K\bar{K}$ build up the $f_0(980)$, and find moderate changes that serve to quantify theoretical uncertainties. No state is seen in $I = 1$. This finding provides a natural explanation for the recent state found at *BABAR* and BES, the $X(2175)$, which decays into $\phi f_0(980)$.

DOI: 10.1103/PhysRevD.78.074031 PACS numbers: 14.40.Cs, 21.45.−v, 25.75.Dw

I. INTRODUCTION

The discovery of the $X(2175)$ 1^{--} resonance in $e^+e^- \to \phi f_0(980)$ with initial state radiation at *BABAR* [1,2], also confirmed at BES in $J/\Psi \to \eta\phi f_0(980)$ [3], has stimulated research around its nontrivial nature in terms of quark components. The possibility of it being a tetraquark $s\bar{s}s\bar{s}$ is investigated within QCD sum rules in [4], and as a gluon hybrid $s\bar{s}g$ state has been discussed in [5,6]. A recent review on this issue can be seen in [7], where the basic problem of the expected large decay widths into two mesons of the states of these models, contrary to what is experimentally observed, is discussed. The basic data on this resonance from [1,2] are $M_X = 2175 \pm 10$ MeV and $\Gamma = 58 \pm 16 \pm 20$ MeV, which are consistent with the numbers quoted from BES $M_X = 2186 \pm 10 \pm 6$ MeV and $\Gamma = 65 \pm 25 \pm 17$ MeV. In Ref. [2] an indication of this resonance is seen as an increase of the $K^+K^-K^+K^-$ cross section around 2150 MeV. A detailed theoretical study of the $e^+e^- \to \phi f_0(980)$ reaction was done in Ref. [8] by means of loop diagrams involving kaons and K^*, using chiral amplitudes for the $K\bar{K} \to \pi\pi$ channel which contains the $f_0(980)$ pole generated dynamically by the theory. The study revealed that the loop mechanisms reproduced the background but failed to produce the peak around 2175 MeV, thus reinforcing the claims for a new resonance around this mass.

In the present paper, we advocate a very different picture for the $X(2175)$ resonance which allows for a reliable calculation and leads naturally to a very narrow width and no coupling to two pseudoscalar mesons. The picture is that the $X(2175)$ is an ordinary resonant state of $\phi f_0(980)$ due to the interaction of these components. The $f_0(980)$ resonance is dynamically generated from the interaction of $\pi\pi$ and $K\bar{K}$ treated as coupled channels within the chiral unitary approach of [9–11], qualifying as a kind of molecule with $\pi\pi$ and $K\bar{K}$ as its components, with a large coupling to $K\bar{K}$ and a weaker one to $\pi\pi$ [hence, the small width compared to that of the $\sigma(600)$]. Similar studies for the vector-pseudoscalar interaction have also been carried out using chiral dynamics in [12,13], which lead to the dynamical generation of the low-lying axial vectors. We shall follow the approach of Ref. [13] to deal with this part of the problem and will use the ϕK and $\phi\pi$ amplitudes obtained in that approach.

To study the $\phi f_0(980)$ interaction, we are thus forced to investigate the three-body system $\phi K\bar{K}$ considering the interaction of the three components among themselves and keeping in mind the expected strong correlations of the $K\bar{K}$ system to make the $f_0(980)$ resonance. For this purpose we have solved the Faddeev equations with coupled channels ϕK^+K^- and $\phi K^0\bar{K}^0$. The picture is later complemented with the addition of the $\phi\pi\pi$ state as a coupled channel. The study benefits from previous ones on the $\pi\bar{K}N$ and $\pi\pi N$ along with their coupled channels done in [14,15], where many $1/2^+$, strange, and nonstrange low-lying baryon resonances of the Particle Data Group [16] were reproduced. This success encourages us to extend the model of Refs. [14,15] to study the three-meson system, i.e., $\phi K\bar{K}$. One of the interesting findings of Refs. [14,15] was a cancellation of the off-shell part of the amplitudes with the genuine three-body forces that one obtains from the same chiral Lagrangians. This simplified technically the approach, and we shall stick to this formalism also here.

*Present address: Centro de Física Computacional, Departamento de Física, Universidade de Coimbra, P-3004-516 Coimbra, Portugal.

Electromagnetic couplings of elementary vector particles

M. Napsuciale,[1,2] S. Rodríguez,[3] E. G. Delgado-Acosta,[1] and M. Kirchbach[4]

[1]*Instituto de Física, Universidad de Guanajuato, Lomas del Bosque 103, Fraccionamiento Lomas del Campestre, 37150, León, Guanajuato, México*

[2]*Departamento de Física Teórica and Instituto de Física Corpuscular, Centro Mixto Universidad de Valencia-CSIC, 46000 Burjassot, Valencia, Spain*

[3]*Facultad de Ciencias Físico Matemáticas, Universidad Autònoma de Coahuila, Edificio "D", Unidad Camporredondo, CP 25280, Saltillo, Coahuila, México*

[4]*Instituto de Física, Universidad Autónoma de San Luis Potosí, Av. Manuel Nava 6, San Luis Potosí, 78290, S.L.P., México*

(Received 10 September 2007; published 9 January 2008)

On the basis of the three fundamental principles of (i) Poincaré symmetry of space-time, (ii) electromagnetic gauge symmetry, and (iii) unitarity, we construct an universal Lagrangian for the electromagnetic interactions of elementary vector particles, i.e., massive spin-1 particles transforming in the $(\frac{1}{2},\frac{1}{2})$ representation space of the homogeneous Lorentz group. We make the point that the first two symmetries alone do not fix the electromagnetic couplings uniquely but solely prescribe a general Lagrangian depending on two free parameters, here denoted by ξ and g. The first one defines the electric-dipole and the magnetic-quadrupole moments of the vector particle, while the second determines its magnetic-dipole and electric-quadrupole moments. In order to fix the parameters one needs an additional physical input suited for the implementation of the third principle. As such, one chooses Compton scattering off a vector target and requires the cross section to respect the unitarity bounds in the high-energy limit. As a result, we obtain the universal $g = 2$ and $\xi = 0$ values which completely characterize the electromagnetic couplings of the considered elementary vector field at tree level. The nature of this vector particle, Abelian versus non-Abelian, does not affect this structure. Merely, a partition of the $g = 2$ value into non-Abelian, g_{na}, and Abelian, $g_a = 2 - g_{na}$, contributions occurs for non-Abelian fields with the size of g_{na} being determined by the specific non-Abelian group appearing in the theory of interest, be it the standard model or any other theory.

DOI: 10.1103/PhysRevD.77.014009 PACS numbers: 13.60.Fz, 13.40.Em, 13.40.−f

I. INTRODUCTION

In the forthcoming years, energies ranging from several hundred GeV to a few TeVs are expected to become accessible at the particle accelerators, a progress which will facilitate testing various fundamental theoretical concepts. In particular, it is quite possible that some of the elementary high-spin particles predicted by supersymmetric- or excited-lepton theories could be observed either as gauge fields to some still unknown non-Abelian groups or as matter fields. Additional effects may or may not come from the more recently developed respective theories of large extra dimensions, noncommutative space-time, etc. In view of the theoretical uncertainties it appears quite important indeed to single out the impact of the first principles underlying the space-time on the properties of the elementary high-spin fields and in first place on their electromagnetic properties. As an example one may think of the value of the gyromagnetic factor, g. In recent time, voicing universality of the $g = 2$ value for particles of any spin becomes stronger (see Ref. [1] and references therein for a recent review). An indirect indication in favor of $g = 2$ is provided already by the Drell-Hearn-Gerasimov sum rule [2] (generalized by Weinberg [3] to any spin) which assigns to strong interactions the anomalous magnetic moment of the nucleon in terms of the $(g-2)e/2m$ difference. Ferrara, Porrati, and Telegdi made the point [4] that unitarity of the amplitude of Compton scattering off a target of *any spin s* demands for the universal value of $g = 2$. Specifically for spin-3/2, they showed that $g = 2$ also allows to avoid the pathology of acausal propagation [5] of such particles within an electromagnetic environment as suffered by the Rarita-Schwinger formalism. However, the resolution of this so-called Velo-Zwanziger problem was obtained at the cost of the introduction of *nonminimal* electromagnetic couplings. In contrast to the Ferrara, Porrati, and Telegdi approach, in the recently proposed covariant projector formalism of Ref. [6], spin-3/2 causal propagation and $g = 2$ were achieved by means of a Lagrangian containing *only minimal* couplings but of *second order* in the momenta. The latter formalism treats high-spins as appropriate sectors of finite-dimensional multispin valued homogeneous Lorentz group (HLG) representations that behave as invariant eigensubspaces of the two Casimir operators of the Poincaré group, the squared four-momentum, p^2, and the squared Pauli-Lubanski vector, $\mathcal{W}^2$. It is the goal of the present study to apply the covariant projector formalism to fields residing in the $(\frac{1}{2},\frac{1}{2})$ irreducible representation of the HLG, the massive vector fields, and explore consequences on their electromagnetic couplings.

PHYSICAL REVIEW D **79,** 034018 (2009)

ϕK^+K^- production in electron-positron annihilation

S. Gómez-Avila,[1] M. Napsuciale,[1] and E. Oset[2]

[1]*Instituto de Física, Universidad de Guanajuato, Lomas del Bosque 103, Fraccionamiento Lomas del Campestre, 37150, León, Guanajuato, México*

[2]*Departamento de Física Teórica and Instituto de Física Corpuscular, Centro Mixto Universidad de Valencia-CSIC, 46000 Burjassot, Valencia, Spain*

(Received 28 November 2007; published 18 February 2009)

In this work we study the $e^+e^- \to \phi K^+K^-$ reaction. The leading order electromagnetic contributions to this process involve the $\gamma^*\phi K^+K^-$ vertex function with a highly virtual photon. We calculate this function at low energies using $R\chi PT$ supplemented with the anomalous term for the $VV'P$ interactions. Tree-level contributions involve the kaon form factors and the K^*K transition form factors. We improve this result, valid for low photon virtualities, replacing the lowest order terms in the kaon form factors and K^*K transition form factors by the form factors as obtained in $U\chi PT$ in the former case and the ones extracted from recent data on $e^+e^- \to KK^*$ in the latter case. We calculate rescattering effects which involve meson-meson amplitudes. The corresponding result is improved using the unitarized meson-meson amplitudes containing the scalar poles instead of the lowest order terms. Using the *BABAR* value for $\mathrm{BR}(X \to \phi f_0)\Gamma(X \to e^+e^-)$, we calculate the contribution from intermediate $X(2175)$. A good description of data is obtained in the case of destructive interference between this contribution and the previous ones, but more accurate data on the isovector K^*K transition form factor is required in order to exclude contributions from an intermediate isovector resonance to $e^+e^- \to \phi K^+K^-$ around 2.2 GeV.

DOI: 10.1103/PhysRevD.79.034018 PACS numbers: 13.66.Bc, 12.39.Fe, 13.60.Le, 13.75.Lb

I. INTRODUCTION

Recently, using the radiative return method [1–3], a new state, the $X(2175)$ (also named $Y(2175)$ in the literature), was observed in $e^+e^- \to \phi\pi\pi$ with the dipion invariant mass close to the $f_0(980)$ region, explicitly, for $m_{\pi\pi} =$ 850–1100 MeV [2]. Later on this state was also detected at BES in the $J/\Psi \to \eta\phi f_0(980)$ reaction [4] and BELLE in $e^+e^- \to \phi\pi^+\pi^-$ [5]. In an update of the analysis of Ref. [2], results on the channel $e^+e^- \to \phi K^+K^-$ were presented in the form of the number of events as a function of the dikaon invariant mass [3]. Indeed, in this work, the cross section for $e^+e^- \to K^+K^-K^+K^-$ was measured as a function of the center of mass energy up to $\sqrt{s} =$ 4.54 MeV and it is shown there that this reaction is dominated by events where one kaon pair comes from the decay of a ϕ. Selecting events with a kaon pair within 10 MeV of the ϕ mass, an enhancement in the invariant mass of the other kaon pair close to threshold is observed and suggested to be due to the $f_0(980)$ tail, but the low statistics and uncertainties in the $f_0(980) \to K^+K^-$ line shape prevent the authors from presenting a cross section for $e^+e^- \to \phi f_0(980)$ using the ϕK^+K^- final state.

Inspired in the physics behind the radiative $\phi \to \pi\pi\gamma$ decay [6–8], a detailed theoretical study of $e^+e^- \to \phi\pi\pi$ for pions in the s wave was performed in [9]. The process $e^+e^- \to \phi f_0$ has been also studied in the context of Nambu-Jona-Lasinio models [10]. In Ref. [9], it was shown that the tree-level contributions through the $\omega - \phi$ mixing are negligible and $e^+e^- \to \phi\pi\pi$ proceeds through the production of off-shell $K\bar{K}$ and K^*K pairs, the successive decay of the off-shell kaon or K^* into an on-shell ϕ and an off-shell K, and the subsequent $K\bar{K} \to \pi\pi$ scattering. The starting point was the $R\chi PT$ Lagrangian [11] supplemented with the anomalous term for the $V'VP$ interactions. The corresponding predictions, valid for low virtualities of the exchanged photon and low dipion invariant mass were improved in two respects. First, the s-wave $K\bar{K} \to \pi\pi$ amplitudes entering the loop calculations were replaced by the full $K\bar{K} \to \pi\pi$ isoscalar amplitudes as calculated in $U\chi PT$, which contain the scalar poles [12,13]. Second, the lowest order terms of the kaon form factor were replaced by the full kaon form factor as calculated in $U\chi PT$ [14] which describes satisfactorily the scarce data for energies around 2 GeV [15,16]. Likewise, the K^*K isoscalar transition form factor arising from $R\chi PT$ and the anomalous term, was replaced by the transition form factors as extracted from data on $e^+e^- \to K^0K^\pm\pi^\mp$ [17].

The $f_0(980)$ couples strongly to the $K\bar{K}$ system and it should contribute to the mechanisms studied in [9] in the case of $\phi K\bar{K}$ production. Therefore it is worthy to study this channel also. As discussed above, some experimental data has been released for $e^+e^- \to \phi K^+K^-$. We devote this work to the study of this reaction in the framework developed in Ref. [9]. In contrast to the $\phi\pi\pi$ final state, the ϕK^+K^- final state is induced at tree level in this framework. Furthermore, as noticed in [3], the $f_0(980)$ pole is close to the threshold for the production of the dikaon system and the loop contributions can be enhanced by this pole thus a complete analysis requires to calculate rescattering contributions. In this concern, we know that the $a_0(980)$ meson couples strongly to the K^+K^- system

Available online at www.sciencedirect.com
ScienceDirect
Progress in Particle and Nuclear Physics 61 (2008) 260–275
Progress in Particle and Nuclear Physics
www.elsevier.com/locate/ppnp

Review

Photo- and electro-production of mesons on nucleons and nuclei

E. Oset[a,*], M. Döring[a], D. Strottman[a], D. Jido[b], M. Napsuciale[a], K. Sasaki[a], C.A. Vaquera-Araujo[a], M. Kaskulov[c], E. Hernandez[d], H. Nagahiro[e], S. Hirenzaki[f]

[a] *Dep. de Fisica Teorica and IFIC, Centro Mixto Universidad de Valencia, CSIC, Institutos de Investigación de Paterna, Aptd. 22085, 46071 Valencia, Spain*
[b] *Yukawa Institute for Theoretical Physics, Kyoto University, Kyoto, 606-8502, Japan*
[c] *Institut für Theoretische Physik, Universität Giessen, Germany*
[d] *Facultad de Ciencias, Universidad de Salamanca, E-37008 Salamanca, Spain*
[e] *Research Center for Nuclear Physics, Osaka University, Ibaraki, Osaka 567-0047, Japan*
[f] *Department of Physics, Nara Women's University, Nara 630-8506, Japan*

Abstract

In these lectures I will show some results obtained with the chiral unitary approach applied to the photo- and electro-production of mesons. The results for the photo-production of $\eta\pi^0 p$ and $K^0\pi^0\Sigma^+$, together with related reactions will be shown, having with common denominator the excitation of the $\Delta(1700)$ resonance which is one of those dynamically generated in the chiral unitary approach. Then I will show the results obtained for the $e^+e^- \to \phi f_0(980)$ reaction which reproduce the bulk of the data except for a pronounced peak, giving support to a new mesonic resonance, X(2175). Results will also be shown for the electromagnetic form factors of the $N^*(1535)$ resonance, also dynamically generated in this approach. Finally, I will show some results on the photo-production of the ω in the nuclei, showing that present experimental results claiming a shift of the ω mass in the medium are tied to a particular choice of background and are not conclusive. On the other hand, the same experimental results show unambiguously a huge increase of the ω width in the nuclear medium.

Keywords: Photo-production of mesons; Electro-production of mesons; Meson medium effects

1. Introduction

Nowadays it is commonly accepted that QCD is the theory of the strong interactions, with the quarks as building blocks for baryons and mesons, and the gluons as the mediators of the interaction. However, at low energies typical of the nuclear phenomena, perturbative calculations with the QCD Lagrangian are not possible and one has to resort to other techniques to use the information of the QCD Lagrangian. One of the most fruitful approaches has been the use of chiral perturbation theory, χPT [1–3]. The theory introduces effective Lagrangians which involve only observable particles, mesons and baryons, respects the basic symmetries of the original QCD Lagrangian, particularly chiral symmetry, and organizes these effective Lagrangians according to the number of derivatives of the meson and baryon fields.

* Corresponding author. Tel.: +34 96 354 35 25; fax: +34 96 354 34 88.
E-mail address: oset@ific.uv.es (E. Oset).

0146-6410/$ - see front matter © 2007 Elsevier B.V. All rights reserved.
doi:10.1016/j.ppnp.2007.12.024

Stationary oscillations in a damped wave equation from isospectral Bessel functions

N. Barbosa-Cendejas and M.A. Reyes
Instituto de Física, Universidad de Guanajuato,
Apartado Postal E143, 37150 León,Gto., México

Recibido el 2 de junio de 2008; aceptado el 29 de julio de 2008

Using the isospectral partners of the Bessel functions derived by Reyes *et al.* [1], we find, on one hand, that these functions show non-typical supersymmetric (SUSY) behavior and, on the other, that the isospectral partner of the classical wave equation is equivalent to that of a damped system whose oscillations do not vanish in time, but show a non-harmonic shape.

Keywords: Supersymmetry; Bessel functions.

Usando las compañeras isoespectrales de las funciones de Bessel obtenidas por Reyes *et al.* [1], encontramos, por un lado, que estas funciones muestran un comportamiento atípico de SUSY, mientras que, por otro lado, la compañera isoespectral de la ecuación de onda clásica es equivalente a la de un sistema amortiguado cuyas oscilaciones no desvanecen con el tiempo, sino que obtienen una forma que no es armónica.

Descriptores: Supersimetría; ecuación de Bessel.

PACS: 02.30.Hq; 03.65.-w; 11.30.Pb

1. Introduction

In quantum mechanics (QM), the number of problems that can be exactly solved is very limited, and one can only hope to get the approximate solution using a variety of methods, or turn to a modified problem which can be described in terms of the known exact problems. In fact, one of the main virtues of supersymmetric (SUSY) quantum mechanics is that there one can find an infinite number of one-parameter problems which possesses the same spectra as the known exact ones. If SUSY cannot be applied, one can still find isospectral solutions by using the classical factorization method, or the interwinning method, to look for new equations with the old spectra.

In classical mechanics, the only problem that can be directly compared to quantum mechanics is that described by the classical wave equation

$$\left(\nabla^2 - \frac{1}{v^2}\right)\psi(x,y;t) = 0, \tag{1}$$

but it has been stated before that there is no SUSY partner for this equation [2]. In fact, a factorization of the Bessel equation *a la* Infeld and Hull cannot be found [3]. However, the Bessel equation,

$$\frac{d^2J_n(r)}{dr^2} + \frac{1}{r}\frac{dJ_n(r)}{dr} + \left(1 - \frac{n^2}{r^2}\right)J_n(r) = 0\,, \tag{2}$$

with $n \geq 0$, which arises from the wave equation after separation of variables, still possesses a factorization in terms of raising and lowering operators defined by the equations [4]

$$A_n^+ J_n(r) = \left(\frac{d}{dr} - \frac{n}{r}\right)J_n(r) = -J_{n+1}(r)\,, \tag{3}$$

$$A_{n+1}^- J_{n+1}(r) = \left(\frac{d}{dr} + \frac{n+1}{r}\right)J_{n+1}(r) = J_n(r)\,, \tag{4}$$

respectively.

Following the work of Mielnik [5], who finds a family of potentials that posses the same spectrum as that of the one-dimensional harmonic oscillator, and the work of Piña [6] on the factorization of some special functions found in mathematical physics, Reyes *et al.* [1] are able to derive second-order differential equations that are 'isospectral' to the equations described in the Sturm-Liouville theory. Note that since the 'spectral' parameter n appears in A_n^+ and A_n^-, contrary to SUSYQM [5], it shows up in the partner equation in a more complicated fashion than the original equation.

As one can see, obtaining the isospectral partner of the Bessel equation is the first step toward an isospectral classical wave equation, this being the main purpose of this letter. But, before proceeding in this direction, we first show that the partner functions of the Bessel functions show a unique and unusual SUSY behavior. Then, we show that the isospectral classical wave equation that comes from the isospectral partner of the Bessel equation resembles the problem of damped waves, which nevertheless do not vanish in time, but show non-harmonic shapes due to this damping term.

PHYSICAL REVIEW D **79,** 093003 (2009)

Quantum field theory results for neutrino oscillations and new physics

D. Delepine[*] and Vannia Gonzalez Macias[†]

Physics department, Division de Ciencias e Ingenieras, Universidad de Guanajuato, Campus Leon, C.P. 37150, León, Guanajuato, México

Shaaban Khalil[‡]

Centre for Theoretical Physics, The British University in Egypt, El Sherouk City, Postal No, 11837, P.O. Box 43, Egypt

G. Lopez Castro[§]

Departamento de Fisica, Cinvestav, Apartado Postal 14-740, 07000 Mexico D.F., Mexico

(Received 19 January 2009; revised manuscript received 27 March 2009; published 14 May 2009)

The *CP* asymmetry in neutrino oscillations, assuming new physics at production and/or detection processes, is analyzed. We compute this *CP* asymmetry using the standard quantum field theory within a general new physics scenario that may generate new sources of *CP* and flavor violation. Well-known results for the *CP* asymmetry are reproduced in the case of $V-A$ operators, and additional contributions from new physics operators are derived. We apply this formalism to SUSY extensions of the standard model where the contributions from new operators could produce a *CP* asymmetry observable in the next generation of neutrino experiments.

DOI: 10.1103/PhysRevD.79.093003 PACS numbers: 14.60.Pq, 11.30.Er, 11.30.Hv, 13.15.+g

I. INTRODUCTION

Since the experimental results implying that the neutrinos are massive [1], it is expected to have *CP* violation phases in the leptonic sector. However, the situation in the leptonic sector is very different from the quark sector where the *CP* violation is clearly established in K and B mesons physics. The only evidence for flavor violation in the leptonic sector comes from neutrino oscillations and there is, so far, no confirmation for *CP* violation in leptonic decays. Hence, measuring any *CP* asymmetry in neutrino oscillation will open a new window to study *CP* violation and related problems as leptogenesis or *CP* violation in τ decays. New physics beyond the standard model (SM), like low energy supersymmetry, may be probed at the LHC and consequently new sources of *CP* and flavor violation can be expected. These new sources of *CP* and lepton flavor violation, also classified as nonstandard interactions (NSI), could give important contributions to the *CP* asymmetry in neutrino oscillation (see Refs. [2–5]).

In addition, a proper procedure to take into account these nonstandard interactions is important as neutrino experiments are reaching a high level of accuracy. Even if neutrino masses and lepton mixing matrices solve the solar and atmospheric neutrinos anomalies, it is clear that NSI could affect the oscillations parameters as determined by the next generation of neutrino experiments. Effects of NSI have been widely studied, considering their contributions to solar and atmospheric neutrino problems, in neutrinos factories, in conventional and upgraded neutrino beta beams, e^+e^- colliders, neutrino-electron and neutrino-nucleus scattering and in many other aspects of neutrino physics [5–13].

The interpretation of a possible *CP* asymmetry in neutrino oscillation due to the SM or NSI is still an open question. The following two hypothesis are usually considered in the analysis of *CP* asymmetry in neutrino oscillations: (i) The probability of a process associated to neutrino oscillation can be factorized into three independent parts: the production process, the oscillation probability and the detection cross section. (ii) The *CP* asymmetry in this process is due to the *CP* violating phase in the lepton mixing matrix. In a pioneering work, the authors of Ref. [2] have studied *CP* violating effects due to contributions from new neutrino interactions in the production and/or detection processes in neutrino oscillation experiments. However, only corrections to the $V-A$ SM charged current interactions were considered [2]. In Ref. [3], the $(V-A)(V-A)$ and $(V-A)(V+A)$ operators associated to muon decays, but not to the pion decay, have been considered. In muon decays, the interference between SM and new physics of $(V-A)(V+A)$ operators is suppressed by m_e/m_μ [14]. In Ref. [15], the quantum field theory formalism has been used to describe neutrino oscillations but new flavor interactions were not taken into account.

The goal of this paper is to go beyond this approximation and to propose a generic framework based on quantum field theory to get a simple expression for the *CP* asymmetry without imposing any assumptions on the operators generated by new physics. We shall show that in such a case, new contributions to the *CP* asymmetry appear and it could be important to take them into account once we want

[*]delepine@fisica.ugto.mx
[†]vanniagm@yahoo.com
[‡]Shaaban.Khalil@bue.edu.eg
[§]glopez@fis.cinvestav.mx

International Journal of Modern Physics D
Vol. 18, No. 4 (2009) 621–634

World Scientific
www.worldscientific.com

ON THE DYNAMICS OF A QUADRATIC SCALAR FIELD POTENTIAL

L. ARTURO UREÑA-LÓPEZ* and MAYRA J. REYES-IBARRA†
Departamento de Física, DCI, Campus León, Universidad de Guanajuato
C.P. 37150, León, Guanajuato, México
**lurena@fisica.ugto.mx*
†*mreyes@fisica.ugto.mx*

Received 18 June 2008
Revised 30 July 2008
Communicated by A. A. Starobinsky

We review the attractor properties of the simplest chaotic model of inflation, in which a minimally coupled scalar field is endowed with a quadratic scalar potential. The equations of motion in a flat Friedmann–Robertson–Walker universe are written as an autonomous system of equations, and the solutions of physical interest appear as critical points. This new formalism is then applied to the study of inflation dynamics, in which we can go beyond the known slow-roll approximation.

Keywords: Cosmology; scalar fields; inflation.

1. Introduction

One of the most-studied issues in cosmology is the dynamics of cosmological scalar fields, mostly because of their usefulness in providing models for different needed processes in the evolution of the universe. It is not an easy task at all to present a full bibliography on scalar fields, but a nice and comprehensive review was recently given by Copeland, Sami and Tsujikawa.[1]

A plethora of methods exist in the specialized literature for studying the dynamics of cosmological scalar fields, but only a few can be said to be extreme useful and of general applicability, in a field where exact solutions are rarely found.

One of these methods is the writing of the scalar and gravitational evolution equations in the form of a *dynamical system*. This is an idea that has pervaded the specialized literature on cosmological scalar fields.[2–4] The reason is that the theory of dynamical systems can show the existence of (fixed) stationary points that may represent important cosmological solutions; often these solutions are attractors which the system evolves to independently of the initial conditions. This is of wide interest in the case of inflationary and dark energy models.[1] However, the dynamical system approach is not always completely suitable for the study of scalar field dynamics.

A typical example is a scalar field model endowed with a quadratic potential. The first attempt for this case was made by Belinsky *et al.*[2] (see also Ref. 5), in

Bose-Einstein condensation of relativistic Scalar Field Dark Matter

2009 J. Cosmol. Astropart. Phys. 2009 014

(http://iopscience.iop.org/1475-7516/2009/01/014)

Journal of Cosmology and Astroparticle Physics
An IOP and SISSA journal

Bose-Einstein condensation of relativistic Scalar Field Dark Matter

L. Arturo Ureña-López

Instituto de Física de la Universidad de Guanajuato,
C.P. 37150, León, Guanajuato, México

E-mail: lurena@fisica.ugto.mx

Received September 11, 2008
Accepted December 4, 2008
Published January 9, 2009

Abstract. Standard thermodynamical results of ideal Bose gases are used to study the possible formation of a cosmological Bose-Einstein condensate in Scalar Field Dark Matter models; the main hypothesis is that the boson particles were in thermal equilibrium in the early Universe. It is then shown that the only relevant case needs the presence of both particles and anti-particles, and that it corresponds to models in which the bosonic particle is very light. Contrary to common wisdom, the condensate should be a relativistic phenomenon. Some cosmological implications are discussed in turn.

Keywords: dark matter; cosmological phase transitions; physics of the early universe

ArXiv ePrint: 0806.3093

JCAP01(2009)014

doi:10.1088/1475-7516/2009/01/014

PHYSICAL REVIEW D **80,** 123521 (2009)

Dynamics of scalar field dark matter with a cosh-like potential

Tonatiuh Matos,[1,*] José-Rubén Luévano,[2,†] Israel Quiros,[3,‡] L. Arturo Ureña-López,[4,§] and José Alberto Vázquez[1,‖]

[1]*Departamento de Física, Centro de Investigación y de Estudios Avanzados del IPN, Apartado Postal 14-740, 07000 México, Distrito Federal, Mexico*

[2]*Departamento de Ciencias Básicas, UAM-A, CP 02200, México, Distrito Federal, Mexico*

[3]*Universidad Central de Las Villas, Santa Clara, CP 54830, Cuba*

[4]*Departamento de Física, DCI, Campus León, Universidad de Guanajuato, CP 37150, León, Guanajuato, Mexico*

(Received 10 June 2009; published 17 December 2009)

The dynamics of a cosmological model of dark matter and dark energy represented by a scalar field endowed with a cosh-like potential plus a cosmological constant is investigated in detail. By studying the appropriate phase space of the equations of motion, it is shown that a standard evolution of the Universe is recovered for appropriate values of the free parameters, and that the only late-time attractor is always the de Sitter solution. We also discuss the appearance of scalar field oscillations corresponding to dark matter behavior.

DOI: 10.1103/PhysRevD.80.123521 PACS numbers: 98.80.−k, 95.35.+d, 95.36.+x, 98.80.Jk

I. INTRODUCTION

One of the greatest mysteries of modern cosmology doubtless is the nature of dark matter (DM) [1,2]; around 23% of the matter of the Universe is attractive, but of unknown nature. The most accepted DM candidates are particles from the minimal supersymmetric standard model [3,4]. The paradigm arising from this is the cold dark matter (CDM) model that has been proved at the cosmological level with great success. For example, it predicts very well the formation and clustering of galaxies [5].

Nevertheless, some inconsistencies of the model appear when compared with observations at the galactic level in the last decade. Among other problems, the predicted number of satellite galaxies around large galaxies is much bigger than the observed one [6], and the DM density profile at the center of galaxies seems to be less steep than predicted [7].

Even though there have been several attempts to deal with these inconsistencies [8], one compelling possibility is that the DM particle is a scalar field [9]. The idea is rooted in the fact that, for the sake of mathematical and physical consistency, almost all the unified theories of physics contain scalar fields as the simplest geometrical objects; these appear with a plethora of names: Higgs, inflatons, dilatons, scalerons, radions, etc. Moreover, the discovery of the dark energy (DE) renewed the interest of cosmologists in scalar fields (see [10] for a comprehensive review).

In Ref. [9,11] some of us proposed that a scalar field rolling down a convex self-interaction potential can be a reasonable candidate for DM, calling this paradigm scalar field dark matter (SFDM). This hypothesis has some nice features. For instance, SFDM does not need extra assumptions to explain the flat DM profile in the centers of galaxies [12], or the number of satellite galaxies around the Milky Way [13].

The SFDM hypothesis has been investigated for a number of self-interaction potentials like the cosh-like [11,14,15], and the quadratic ones [15,16], with the consequent discovery of several exact solutions of cosmological interest. However, within the cosmological context, a full and detailed study of the dynamics of SFDM models, to uncover their relevant asymptotic properties, is still desirable.

The main goal of the present paper is, precisely, to study, within the cosmological context and by means of the dynamical systems tools, the asymptotic properties of the SFDM model driven by a cosh-like potential. Several relevant cosmological solutions will be correlated with concepts like past and future attractors, signaling the way the cosmic dynamics transits from early-time to intermediate, and then to late-time asymptotic states.

It is shown that the SFDM model driven by a cosh-like potential with a cosmological constant term added can also describe the cosmic dynamics of the standard model ΛCDM. Due attention will be paid to the late-time oscillatory solution that can be associated with CDM behavior in the model.

The paper has been organized as follows. The relevant physical features of the model are discussed in Sec. II, and then, in Sec. III, its mathematical features are specified. The details of the dynamical systems study of the SFDM model with a cosh-like potential are given in Sec. IV.

*tmatos@fis.cinvestav.mx
†jrle@azc.uam.mx
‡iquiros@fisica.ugto.mx
§lurena@fisica.ugto.mx
‖jvazquez@fis.cinvestav.mx

PHYSICAL REVIEW D **79,** 063518 (2009)

Dynamics of interacting dark energy

Gabriela Caldera-Cabral[*] and Roy Maartens[†]
Insitute of Cosmology & Gravitation, University of Portsmouth, Portsmouth PO1 2EG, United Kingdom

L. Arturo Ureña-López[‡]
Departamento de Física, DCI, Campus León, Universidad de Guanajuato, C.P. 37150, León, Guanajuato, México
(Received 13 December 2008; published 18 March 2009)

Dark energy and dark matter are only indirectly measured via their gravitational effects. It is possible that there is an exchange of energy within the dark sector, and this offers an interesting alternative approach to the coincidence problem. We consider two broad classes of interacting models where the energy exchange is a linear combination of the dark sector densities. The first class has been previously investigated, but we define new variables and find a new exact solution, which allows for a more direct, transparent, and comprehensive analysis. The second class has not been investigated in general form before. We give general conditions on the parameters in both classes to avoid unphysical behavior (such as negative energy densities).

DOI: 10.1103/PhysRevD.79.063518 PACS numbers: 98.80.−k, 95.35.+d, 95.36.+x, 98.80.Jk

I. INTRODUCTION

Cosmological observations point to the existence of nonbaryonic cold matter and of a late-time acceleration of the Universe (see, e.g., [1–3]). If gravity is modeled on cosmological scales by general relativity, and if we assume that the Universe is homogeneous and isotropic on these scales, then the late-time acceleration is sourced by a dark energy component, and the Universe is dominated by the ''dark sector.'' The quest to uncover the true nature of dark matter (DM) and dark energy (DE) is one of the most pressing topics of modern cosmology.

One of the fundamental puzzles within this quest is the ''coincidence problem'': how is it that we seem to live in a time when the densities of DM and DE are of the same order of magnitude, given that they evolve very differently with redshift? An interesting proposal is that interaction between the dark fields could perhaps alleviate the coincidence problem. Various interaction models have been put forward and studied (see, e.g., [4–24]).

For a flat Friedmann-Robertson-Walker universe, the background dynamics after recombination are governed by the equations of energy balance and the Raychaudhuri field equation:

$$\dot{\rho}_b = -3H\rho_b, \tag{1a}$$

$$\dot{\rho}_c = -3H\rho_c + Q, \tag{1b}$$

$$\dot{\rho}_x = -3(1+w_x)H\rho_x - Q, \tag{1c}$$

$$\dot{H} = -4\pi G[\rho_b + \rho_c + (1+w_x)\rho_x], \tag{1d}$$

where $H = \dot{a}/a$ is the Hubble parameter, ρ_c is the cold DM density, ρ_b is the baryonic density, ρ_x is the density of DE, and $w_x < 0$ is its constant equation of state. The baryons only interact gravitationally with the dark sector, and Q is the rate of energy transfer in the dark sector. The Friedmann constraint equation is

$$H^2 = \frac{8\pi G}{3}(\rho_b + \rho_c + \rho_x). \tag{2}$$

Note that the field equations (1d) and (2) are independent of Q, because of total energy conservation. A positive $Q > 0$ represents transfer of energy from DE to DM; a negative $Q < 0$ represents transfer of energy from DM to DE.

In this paper, we consider interactions that are linear combinations of the dark sector densities:

$$Q = A_c\rho_c + A_x\rho_x. \tag{3}$$

Here the rate factors A_I are either proportional to H or constants, leading to two classes of interaction model:

$$\text{model I } A_I = 3\alpha_I H, \tag{4}$$

$$\text{model II } A_I = 3\Gamma_I, \tag{5}$$

where α_I are dimensionless constants and Γ_I are constant transfer rates. Observations impose the general constraint that the interaction should be subdominant today, so that

$$|\alpha_I| \ll 1, \qquad |\Gamma_I| \ll H_0. \tag{6}$$

Model I has been recently analyzed by [4] (and earlier work considered the special cases $\alpha_c = \alpha_x$ [5] and $\alpha_x = 0$ [6]). We use an alternative approach, defining new variables to simplify the parameter space and finding the general exact solution. We are able to recover previous results more directly and simply and to provide some new insights into the model.

The H in the Q-term for model I is motivated purely by mathematical simplicity. By contrast, the energy exchange in model II is motivated by similar models that have been

[*]Gaby.Calderacabral@port.ac.uk
[†]Roy.Maartens@port.ac.uk
[‡]lurena@fisica.ugto.mx

PHYSICAL REVIEW D **80,** 104020 (2009)

Towards a supersymmetric generalization of the Schwarzschild black hole

J. C. López-Domínguez,* O. Obregón,† and S. Zacarías‡

Departamento de Física, División de Ciencias e Ingenierías, Campus León, Universidad de Guanajuato, P.O. Box E-143, León, Guanajuato, México

(Received 23 June 2009; published 16 November 2009)

The Wheeler-DeWitt (WDW) equation for the Kantowski-Sachs model can also be understood as the WDW equation corresponding to the Schwarzschild black hole due to the well known diffeomorphism between these two metrics. The WDW equation and its solutions are ignorant of the coordinate patch one is using, only by imposing coordinate conditions we can differentiate between cosmological and black hole models. At that point, the foliation parameter t or r will appear in the solution of interest. In this work we supersymmetrize this WDW equation obtaining an extra term in the potential with two possible signs. The WKB method is then applied, giving rise to two classical equations. It is shown that the event horizon can never be reached because very near to it, the extra term in the potential, for each one of the equations, is more relevant than the one that corresponds to Schwarzschild. One can then study the asymptotic cases in which one of the two terms in the Hamiltonian dominates the behavior. One of them corresponds to the usual Schwarzschild black hole. We will study here the other two asymptotic regions; they provide three solutions. All of them have a singularity in $r = 0$ and depending on an integration constant C they can also present a singularity in $r = C^2$. Neither of these solutions have a Newtonian limit. The black hole solution we study is analyzed between the singularity $r = C^2$ and a maximum radius r_m. We find an associated mass, considering the related cosmological solution inside $r = C^2$, and based on the holographic principle an entropy can be assigned to this asymptotic solution.

DOI: 10.1103/PhysRevD.80.104020 PACS numbers: 04.70.Bw, 04.60.Ds, 04.65.+e, 12.60.Jv

I. INTRODUCTION

Black hole physics has been extensively studied in the literature. It is useless to try to address the many interesting aspects, even those related with a single topic. A very rich discussion exists in the literature in one of these topics, namely, that concerning black holes (event) horizons. One can begin by mentioning the fact that in general relativity [1], for stationary vacuum, solutions to the Einstein field equations event horizons arise. Moreover, classical collapse of astrophysical objects results in (future) event horizons [2]. The existence of an event horizon means that one has an inaccessible region, and therefore an external observer must then consider hidden states; pure states become density matrices. So that, seen from outside, the evolution results nonunitary, there is information loss. This is one of those things one has to live with, if one accepts the usual Carter-Penrose diagram. Modifications to this diagram have been proposed based on different theoretical frameworks and models all hinting to a more subtle history for collapse [3]. In classical numerical relativity calculations, event horizons are almost impossible to find with any certainty. Other definitions of horizons like local or quasilocal are used to be able to perform calculations that make sense [4]. It has also been claimed by several authors (see [5] and works cited therein) that there is a variety of physically realistic stellar collapse scenarios in which an event horizon does not in fact forms, so that the singularity remains exposed. Moreover, even though astronomers will recognize that what they have observed so far is compatible with the Schwarzschild or Kerr metrics [6], they will also argue that one cannot unambiguously conclude that the dark objects they observe are black holes in the sense of general relativity. There is an increasing consensus, or at least suspicion, within the general relativity community that event horizons are simply the wrong thing to be looking at. Other possible definitions of horizons have then been proposed; apparent [7], dynamical [8], trapping [9] horizons that make more physical sense. Very powerful and sophisticated methods have been developed since the birth of general relativity searching for solutions to its field equations. For a long time it has been known that changing the structure of spacetime (i.e. interchanging the coordinates $t \leftrightarrow r$), changes a static solution for a cosmological one and vice versa. The best known case is the Schwarzschild metric that under this particular diffeomorphism transforms into the Kantowski-Sachs metric [10]. This interchange of variables has been recently proposed as a method to generate new cosmological models from stationary axisymmetric solutions [11]. In string theory, it has been suggested that by interchanging $r \leftrightarrow it$ we can get time-dependent solutions also from static and stationary solutions. In this way we may relate Dp-branes solutions to S-brane solutions, i.e. time-dependent backgrounds of the theory [12]. On the other hand, there are proposals to obtain directly S-brane solutions [13]; thus, if cosmologi-

*jlopez@fisica.ugto.mx
†octavio@fisica.ugto.mx
‡szacarias@fisica.ugto.mx

Modern Physics Letters A
Vol. 24, No. 24 (2009) 1907–1914

World Scientific
www.worldscientific.com

ON NONCOMMUTATIVE MINISUPERSPACE, COSMOLOGY AND Λ

O. OBREGÓN* and M. SABIDO†

Instituto de Física de la Universidad de Guanajuato,
A.P. E-143, C.P. 37150, León, Guanajuato, México
**octavio@fisica.ugto.mx*
†*msabido@fisica.ugto.mx*

E. MENA

Centro Universitario de la Cienega, Ave. Universidad 1115 Edif. B,
C.P. 47820 Ocotlán, Jalisco, México
emena@cuci.udg.mx

Received 29 October 2008
Revised 5 February 2009

In this letter we study the effects of a noncommutative minisuperspace, including matter degrees of freedom on a toy model for FRW universe with cosmological constant. In this simple model the vacuum energy density is modified by the presence of the noncommutative minisuperspace parameter, from which we conjecture on the discrepancy between the calculated and observed vacuum energy density associated to Λ.

Keywords: Noncommutativity; cosmology.

PACS Nos.: 02.40.Gh, 95.36+x, 98.80.Qc

The cosmological constant problem has been addressed by means of different approaches for several years and still remains as one of the central issues of not only modern day cosmology but also particle physics.[1] The remarkable discovery and confirmation of the acceleration of the universe is usually attributed to a small, nonvanishing Λ. Unfortunately there is no known mechanism that guarantees a zero or nearly zero value for Λ in a stable or metastable vacuum. This has been complicated by the fact that its associated energy density has a similar value as that of the energy of present-day matter. These and other questions connected to the cosmological constant can be casted as three fundamental problems: why is the cosmological constant so small? why it is not zero? and why is it comparable to the matter energy-density (cosmic coincidence)? The apparent impossibility of addressing these questions has lead to speculate on the necessity of an anthropic

Behavioral and Brain Functions

BioMed Central

Coincident frequencies and relative phases among brain activity and hormonal signals

Behavioral and Brain Functions 2009, **5**:18 doi:10.1186/1744-9081-5-18

Silvia Solis-Ortiz (silviasolis17@prodigy.net.mx)
Rafael G Campos (rcampos@umich.mx)
Julian Felix (felix@fisica.ugto.mx)
Octavio Obregon (octavio@fisica.ugto.mx)

ISSN 1744-9081

Article type Methodology

Submission date 13 October 2008

Acceptance date 14 March 2009

Publication date 14 March 2009

Article URL http://www.behavioralandbrainfunctions.com/content/5/1/18

PHYSICAL REVIEW D **80,** 054002 (2009)

Compton scattering off elementary spin $\frac{3}{2}$ particles

E. G. Delgado-Acosta and M. Napsuciale

Departamento de Física, División de Ciencias e Ingenierías, Universidad de Guanajuato, Campus León, Lomas del Bosque 103, Fraccionamiento Lomas del Campestre, 37150, León, Guanajuato, México.

(Received 14 July 2009; published 1 September 2009)

We calculate Compton scattering off an elementary spin $\frac{3}{2}$ particle in a recently proposed framework for the description of high spin fields based on the projection onto eigensubspaces of the Casimir operators of the Poincaré group. We also calculate this process in the conventional Rarita-Schwinger formalism. Both formalisms yield the correct Thomson limit but the predictions for the angular distribution and total cross section differ beyond this point. We point out that the average squared amplitudes in the forward direction for Compton scattering off targets with spin $s = 0, \frac{1}{2}, 1$ are energy independent and have the common value $4e^4$. As a consequence, in the rest frame of the particle the differential cross section for Compton scattering in the forward direction is energy independent and coincides with the classical squared radius. We show that these properties are also satisfied by a spin $\frac{3}{2}$ target in the Poincaré projector formalism but not by the Rarita-Schwinger spin $\frac{3}{2}$ particle.

DOI: 10.1103/PhysRevD.80.054002 PACS numbers: 13.60.Fz, 13.40.Em, 13.40.−f

I. INTRODUCTION

A long standing problem in particle physics is the proper description of high spin fields. The widely used Rarita-Schwinger (RS) formalism [1] was shown to be inconsistent for interacting particles long ago [2], and lead to superluminical propagation of spin $\frac{3}{2}$ waves in the presence of an external electromagnetic field [3]. Similar and related problems have been found in the presence of other interactions [4].

Recently, a new formalism for the description of high spin fields was put forward by Napsuciale Kirchbach and Rodríguez [5] (NKR in the following), based on the projection onto eigensubspaces of the Casimir operators of the Poincaré group. In that work, it is shown that, under minimal coupling, the (parity-conserving) electromagnetic structure of a spin $\frac{3}{2}$ particle transforming in the $(1/2, 1/2) \otimes [(1/2, 0) \oplus (0, 1/2)]$ representation of the homogeneous Lorentz group (HLG) depend on two free parameters denoted by g and f. The propagation of spin $\frac{3}{2}$ waves was studied for the case $f = 0$ and it is shown there that the value of the gyromagnetic factor g is related to the causality of the propagation of spin $\frac{3}{2}$ waves and causal propagation is obtained for $g = 2$. This result relates the ''natural'' value of the gyromagnetic factor [6] to causality for spin $\frac{3}{2}$.

The case of spin 1 particles in the $(\frac{1}{2}, \frac{1}{2})$ representation space of the HLG was addressed in [7]. In this case, the most general electromagnetic interaction of a spin 1 vector particle was also shown to depend on two parameters (denoted by g and ξ) which cannot be fixed from the Poincaré projection alone. These parameters determine the electromagnetic structure of the particle and were fixed imposing unitarity at high energies for Compton scattering. This procedure fixes the parameters to $g = 2$ and $\xi = 0$ predicting a gyromagnetic factor $g = 2$, a related quadrupole electric moment $Q = -e(g - 1)/m^2$ and vanishing odd-parity couplings as a consequence of $\xi = 0$. The obtained couplings coincide with the ones predicted for the W boson in the standard model [8].

These results make it worthy to study the analogous problems for spin $\frac{3}{2}$ particles and this work is devoted to this purpose. The electromagnetic properties of spin $\frac{3}{2}$ particles have been addressed in a number of previous papers aiming to understand either the electromagnetic structure of hypothetical elementary particles or the electromagnetic properties of hadrons [6,9].

In this work, we study the electromagnetic structure of a spin $\frac{3}{2}$ particle in the NKR formalism and calculate Compton scattering both in the NKR and RS formalisms. We compare the predictions of these formalisms for the angular distribution and total cross section and notice that the average squared amplitude for Compton scattering of spin 0, $\frac{1}{2}$, and 1 particles in the forward direction is energy independent. This property is satisfied by spin $\frac{3}{2}$ particles in the NKR formalism but not in the Rarita-Schwinger one. This paper is organized as follows: in the next section we revisit the electromagnetic structure of a spin $\frac{3}{2}$ particle under $U(1)_{\rm em}$ gauge principle in the NKR formalism, extract the corresponding Feynman rules and prove that Ward identities are satisfied. In Sec. III, we calculate the amplitude for Compton scattering, show that it is gauge invariant, and work out the predictions for the differential and total cross sections. In Sec. IV, we calculate this process in the conventional Rarita-Schwinger formalism. We discuss our results in Sec. V and give a summary in Sec. VI.

II. ELECTROMAGNETIC INTERACTIONS OF SPIN $\frac{3}{2}$ PARTICLES IN THE NKR FORMALISM

The NKR Lagrangian for spin $\frac{3}{2}$ interacting particles with charge $-e$ has been discussed in [5] and we refer

Int J Theor Phys (2009) 48: 3567–3585
DOI 10.1007/s10773-009-0164-1

Scalar Field in the Bianchi I: Noncommutative Classical and Quantum Cosmology

J. Socorro · Luis O. Pimentel · C. Ortiz · M. Aguero

Received: 20 April 2009 / Accepted: 6 October 2009 / Published online: 20 October 2009

Abstract Using the ADM formalism in the minisuperspace, we obtain the commutative and noncommutative exact classical solutions and exact wave function to the Wheeler-DeWitt equation with an arbitrary factor ordering, for the anisotropic Bianchi type I cosmological model, coupled to a scalar field, cosmological term and barotropic perfect fluid. We introduce noncommutative scale factors, considering that all minisuperspace variables q^i do not commute, so the symplectic structure was modified. In the classical regime, it is shown that the anisotropic parameter $\beta_{\pm nc}$ and the field ϕ, for some value in the λ_{eff} cosmological term and noncommutative θ parameter, present a dynamical isotropization up to a critical cosmic time t_c; after this time, the effects of isotropization in the noncommutative minisuperspace seems to disappear. In the quantum regimen, the probability density presents a new structure that corresponds to the value of the noncommutativity parameter.

Keywords Noncommutative · Classical and quantum cosmology · Exact solutions

J. Socorro (✉) · C. Ortiz
Departamento de Física, DCI-Campus León, Universidad de Guanajuato, A.P. E-143, C.P. 37150 León, Guanajuato, México
e-mail: socorro@fisica.ugto.mx

C. Ortiz
e-mail: ortizgca@fisica.ugto.mx

J. Socorro · M. Aguero
Facultad de Ciencias de la Universidad Autónoma del Estado de México, Instituto Literario No. 100, Toluca, C.P. 50000 Edo de Mex, México

M. Aguero
e-mail: makxim@gmail.com

L.O. Pimentel
Departamento de Física, Universidad Autónoma Metropolitana, Apartado Postal 55-534, C.P. 09340 México, DF, México
e-mail: lopr@xanum.uam.mx

A new strategy for probing the Majorana neutrino CP violating phases and masses1

David Delepine, Vannia González Macias, Shaaban Khalil, and Gabriel López Castro

Citation: AIP Conf. Proc. **1361**, 395 (2011); doi: 10.1063/1.3622737
View online: http://dx.doi.org/10.1063/1.3622737
View Table of Contents: http://proceedings.aip.org/dbt/dbt.jsp?KEY=APCPCS&Volume=1361&Issue=1
Published by the American Institute of Physics.

A new strategy for probing the Majorana neutrino CP violating phases and masses[1]

David Delepine*, Vannia González Macias*, Shaaban Khalil† and Gabriel López Castro**

*Departamento de Fisica, División de Ciencias e Ingenierías de la Universidad de Guanajuato, C.P. 37150, León, Guanajuato, México.
†Centre for Theoretical Physics, The British University in Egypt, El Sherouk City, Postal No, 11837, P.O. Box 43, Egypt
**Departamento de Fisica, Cinvestav, Apartado Postal 14-740, 07000 Mexico D.F., Mexico

Abstract. We propose a new strategy for detecting the CP-violating phases and the effective mass of muon Majorana neutrinos by measuring observables associated with neutrino-antineutrino oscillations in $\pi^{\pm}$ decays. Within the generic framework of quantum field theory, we compute the non-factorizable probability for producing a pair of same-charged muons in $\pi^{\pm}$ decays as a distinctive signature of $\nu_\mu - \bar{\nu}_\mu$ oscillations. Using the neutrino-antineutrino oscillation probability reported by MINOS collaboration, a new stringent bound on the effective muon-neutrino mass is derived.

Keywords: lepton number violation, majorana phases, neutrino antineutrino oscillations
PACS: 11.30.Er, 14.60Pq, 14.60.St

INTRODUCTION

The measurement of the effective electron-neutrino mass in the neutrinoless double beta decay ($0\nu\beta\beta$) experiments can not restrict the two Majorana CP violating phases present in the PMNS mixing matrix [1, 2, 3]. This may be expected since in the ($0\nu\beta\beta$) one measures the lifetime of the decay of two neutrons in a nucleus into two protons and two electrons, which is a CP conserving quantity. Direct bounds on other effective neutrino mass parameters $\langle m_{ll} \rangle \equiv \sum_i U_{li}^2 m_{\nu_i}$ from present experimental data are very poor, which lead to negligible constraints on the neutrino masses and CP violating phases.

Here we propose a mechanism, based on neutrino-antineutrino oscillation [4, 5, 6, 7], to derive a strong bound on the effective mass of the muon-neutrino, using the results reported by the MINOS collaboration [8]. In addition, it provides a method for detecting the Majorana neutrino CP violating phases through measuring the CP asymmetry of the $\pi^{\pm}$ decay. It is worth noting that the probability of a process associated to neutrino oscillation is usually assumed to be factorized into three independent parts: the production process, the oscillation probability and the detection cross section. Here, we adopt the S-matrix amplitude method described in [9], in order to avoid the usual factorization scheme.

[1] work presented by Vannia Gonzalez Macias

XII Mexican Workshop on Particles and Fields
AIP Conf. Proc. 1361, 395-397 (2011); doi: 10.1063/1.3622737

PHYSICAL REVIEW D **81,** 036001 (2010)

Leptogenesis and reheating in complex hybrid inflation

Carlos Martínez-Prieto,[1,*] David Delepine,[2,†] and L. Arturo Ureña-López[2,‡]

[1]*Instituto de Física y Matemáticas de la Universidad Michoacana de San Nicolás de Hidalgo, Edificio C-3, Ciudad Universitaria, Apartado Postal 2-82, 58040, Morelia, Michoacán, Mexico*

[2]*Departamento de Física, DCI, Campus León, Universidad de Guanajuato, Codigo Postal 37150, León, Guanajuato, Mexico*

(Received 22 August 2009; published 3 February 2010)

We study the transformation into a baryon asymmetry of a charge initially stored in a complex (waterfall) scalar field at the end of a hybrid inflation phase as described by Delepine, Martinez, and Urena-Lopez [Phys. Rev. Lett. **98**, 161302 (2007)]. The waterfall field is coupled to right-handed neutrinos, and is also responsible for their Majorana masses. The charge is finally transferred to the leptons of the standard model through the decay of the right-handed neutrinos without introducing new *CP* violating interactions. Other needed processes, like the decay of the inflaton field and the reheating of the Universe, are also discussed in detail.

DOI: 10.1103/PhysRevD.81.036001 PACS numbers: 98.80.Cq, 11.30.Er, 11.30.Fs

I. INTRODUCTION

We have shown in a recent paper [1] that a complex hybrid inflation model can generate a charge asymmetry that may be further transferred into a baryon charge, then providing a possible solution to the baryogenesis problem of cosmology [2].

The scalar field potential associated with the complex hybrid inflation model is

$$V(\phi, a) = \frac{1}{4\lambda^2}(M^2 - \lambda^2|a|^2)^2 + \frac{1}{2}(m^2 + g^2|a|^2)\phi^2 + \frac{\delta}{4}a^2\phi^2 + \text{c.c.}, \quad (1)$$

where ϕ is the inflaton field and a is the (complex) waterfall field. Notice that there is an explicit term that violates the $U(1)$ global symmetry. The needed charge is generated at the end of inflation and is associated with the charge of the waterfall field a.

The aim of this paper is to discuss the transfer of the a charge to fermionic matter after the end of inflation. The task is not a simple one, there may be some transfer processes during the reheating phase of the Universe that can wash out the generated charge.

To fix ideas, we shall work on a leptogenesis model in which the a charge is transferred to standard model particles through interactions between the waterfall field a and a right-handed neutrino N_R. We assume that the a field has a leptonic number of 2, and that initially our Lagrangian conserves the leptonic number. The interaction Lagrangian reads

$$\mathcal{L}_{\text{int}} = h_Y \bar{\ell}_L \Phi N_R + h_2 \bar{N}_R^c N_R a + \text{H.c.}, \quad (2)$$

where Φ is the Higgs doublet, ℓ_L is the leptonic doublet, and h_Y is the usual Yukawa coupling.

The interaction Lagrangian (2) is inspired in the Majoron model and in the standard leptogenesis scenario [3–6]. Our model is then composed of just one family of leptons that contains one leptonic doublet and one right-handed neutrino.

A summary of the paper is as follows. In Sec. II we briefly review the inflationary dynamics of the complex hybrid inflation model as presented in Ref. [1]. In Sec. III we study the post-inflationary dynamics of the different fields involved in the model, and focus our attention in the stages of preheating and reheating. Section IV is entirely devoted to the study of the Boltzmann equations in order to estimate the amount of the a charge that is finally converted into a useful baryon charge. Finally, conclusions are presented in Sec. V.

II. INFLATIONARY DYNAMICS

The model is given by the potential (1), where g and λ are real constants, and δ is a complex parameter; for $\delta = 0$ we recover the standard hybrid inflation model [7]. The δ term violates the $U(1)$ symmetry associated with the complex field a. However, the potential (1) is *CP* conserving as the phase of complex parameter δ can be removed through a phase redefinition of the a field.

The scalar potential has a local maximum at $\phi = |a| = 0$ with a height given by $V(0, 0) = M^4/(4\lambda^2)$ that corresponds to a false vacuum. The true vacuum of the system corresponds to the global minimum located at $\phi = 0$ and $\lambda|a|/M = 1$; this true vacuum is degenerate. The $U(1)$ charge density at any time is given by $n_a = a_r\dot{a}_i - a_i\dot{a}_r$, where r and i refer to the real and imaginary components of the a field.

The constant term in the potential (1) is initially the dominant one, which is usually dubbed as false vacuum inflation [8]. In the regime of slow roll, the scale factor

*carlosr@ifm.umich.mx
†delepine@fisica.ugto.mx
‡lurena@fisica.ugto.mx

Physics Letters B 693 (2010) 467–476

Contents lists available at ScienceDirect

Physics Letters B

www.elsevier.com/locate/physletb

Charge asymmetries in $e^+e^- \to \pi^+\pi^-\gamma$ at the ϕ resonance

A. Gallegos [a], J.L. Lucio [b], G. Moreno [b], M. Napsuciale [b,*]

[a] Departamento de Ciencias Exactas y Tecnología, Centro Universitario de los Lagos, Universidad de Guadalajara, Enrique Díaz de León 1144, Colonia Paseos de la Montaña, 47460, Lagos de Moreno, Jalisco, Mexico

[b] Departamento de Física, División de Ciencias e Ingenierías, Universidad de Guanajuato, Campus León, Lomas del Bosque 103, Fraccionamiento Lomas del Campestre, 37150, León, Guanajuato, Mexico

ARTICLE INFO

Article history:
Received 23 September 2009
Received in revised form 25 July 2010
Accepted 1 September 2010
Available online 6 September 2010
Editor: W. Haxton

Keywords:
Charge asymmetry
Chiral Lagrangians

ABSTRACT

We consider the forward–backward pion charge asymmetry for the $e^+e^- \to \pi^+\pi^-\gamma$ process. At tree level we consider bremsstrahlung and double resonance contributions. Although the latter contribution is formally sub-leading, it is enhanced at low dipion invariant mass due to ρ resonant effects. We consider also four alternative models to describe the final state radiation at the loop level: Resonance Chiral Perturbation Theory, Unitarized Chiral Perturbation Theory, Kaon Loop Model and Linear Sigma Model. The last three models yield results compatible with experimental data. The Kaon Loop Model requires an energy dependent phase to achieve the agreement.

1. Introduction

The nature of low mass scalar mesons nonet is a long-standing puzzle. The ϕ radiative decays are expected to provide information about the $f_0(980)$ and $a_0(980)$ scalar mesons. Unfortunately data reported by the KLOE Collaboration on the ϕ decays to $f_0\gamma$ [1] and $a_0\gamma$ [2] — with $\pi^0\pi^0\gamma$ and $\pi^0\eta\gamma$ final states respectively — together with results for the $\phi \to \pi^+\pi^-\gamma$ process, including the $f_0\gamma$ as intermediate state [3], are not conclusive. In the latter work, results on the forward–backward asymmetry as a function of the $\pi^+\pi^-$ invariant mass are presented. The asymmetry is sensitive to the mechanisms involved in the final state radiation [4] and it provides information on the pion form factor [5]. Related work on the reaction $e^+e^- \to \pi^+\pi^-\gamma$ has been done aiming to elucidate the partonic structure of pions [6]. The asymmetry requires a non-vanishing interference between initial (ISR) and final (FSR) state radiation, the latter being strongly model dependent [7]. The invariant amplitude for the $e^+e^- \to \pi^+\pi^-\gamma$ process can be parameterized in terms of three independent Lorentz structures and thus the model dependence in FSR can be included in three scalar functions f_i [8]. The final state radiation has been calculated in different models. The simplest approximation has been named scalar QED [7,9] and it actually includes the ρ contributions to the pion form factor. The contribution of scalars ($f_0(980)$ and σ) have been also considered using a point-like $\phi f_0\gamma$ interaction, in the so-called "no-structure" model [7,9]. Later on, the tree level bremsstrahlung of final pions was calculated [5,8,10] within Resonance Chiral Perturbation Theory ($R\chi PT$) [11]. In particular, in [10] sub-leading intermediate vector mesons contributions like $e^+e^- \to \phi \to \rho^\pm\pi^\mp \to \pi^+\pi^-\gamma$, named double resonance contributions, were incorporated.

The aim of this Letter is to work out the one loop predictions for $e^+e^- \to \pi^+\pi^-\gamma$ at the ϕ resonance using four alternative models, namely $R\chi PT$, Unitarized Chiral Perturbation Theory ($U\chi PT$) [12] (containing actually a resummation of loops), Linear Sigma Model (LSM) [13,14] and the so-called "kaon-loop" model (KLM) [15]. In each case we add the tree level contributions from bremsstrahlung of pions and the intermediate double resonance, both proposed in [10]. We report the forward–backward pion charge asymmetry and compare our results with KLOE data.

The Letter is organized as follows: Section 2 includes the general formalism to describe the $e^+e^- \to \pi^+\pi^-\gamma$ process. In Section 3 we derive the scalar functions f_i that characterize the $R\chi PT$, LSM, $U\chi PT$ and KLM contributions, including the tree level bremsstrahlung and double resonance exchange. In Section 4 we present the numerical results and compare them with data. Finally, conclusions are given in Section 5.

* Corresponding author.
E-mail address: mauro@fisica.ugto.mx (M. Napsuciale).

0370-2693/$ – see front matter
doi:10.1016/j.physletb.2010.09.006

Supersymmetric classical cosmology

JCAP12(2010)011

(http://iopscience.iop.org/1475-7516/2010/12/011)

Journal of Cosmology and Astroparticle Physics
An IOP and SISSA journal

Supersymmetric classical cosmology

Celia Escamilla-Rivera,[a,b] **Octavio Obregón**[a] **and L. Arturo Ureña-López**[a]

[a]Departamento de Física, División de Ciencias e Ingenierías, Campus León, Universidad de Guanajuato, C.P. 37150, León, Gto., Mexico
[b]Fisika Teorikoaren eta Zientziaren Historia Saila, Zientzia eta Teknologia Fakultatea, Euskal Herriko Unibertsitatea, 644 Posta Kutxatila, 48080, Bilbao, Spain

E-mail: celia_escamilla@ehu.es, octavio@fisica.ugto.mx, lurena@fisica.ugto.mx

Received October 4, 2010
Revised November 19, 2010
Accepted November 26, 2010
Published December 10, 2010

Abstract. In this work a supersymmetric cosmological model is analyzed in which we consider a general superfield action of a homogeneous scalar field supermultiplet interacting with the scale factor in a supersymmetric FRW model. There appear fermionic superpartners associated with both the scale factor and the scalar field, and classical equations of motion are obtained from the super-Wheeler-DeWitt equation through the usual WKB method. The resulting supersymmetric Einstein-Klein-Gordon equations contain extra radiation and stiff matter terms, and we study their solutions in flat space for different scalar field potentials. The solutions are compared to the standard case, in particular those corresponding to the exponential potential, and their implications for the dynamics of the early Universe are discussed in turn.

Keywords: supersymmetry and cosmology, quantum cosmology, physics of the early universe

ArXiv ePrint: 1009.4233

doi:10.1088/1475-7516/2010/12/011

JCAP12(2010)011

PHYSICAL REVIEW D **82,** 044002 (2010)

Does Dirac-Born-Infeld modification of quadratic theories really matter?

Israel Quiros* and L. Arturo Ureña-López†

Departamento de Física, División de Ciencias e Ingenierías, Campus León, Universidad de Guanajuato, Código Postal 37150, León, Guanajuato, México

(Received 16 April 2010; published 4 August 2010)

We study the consequences of further modification of $f(R, R_{\mu\nu}R^{\mu\nu}, R_{\mu\nu\sigma\rho}R^{\mu\nu\sigma\rho})/f(R)$ theories by means of the Dirac-Born-Infeld procedure, which is the replacement of f by $\lambda(\sqrt{1+2f/\lambda}-1)$ (the free parameter λ fixes an additional energy scale). We pay special attention to the definition of masses of the linearized propagating degrees of freedom because they are important to judge the stability of the linearization around vacuum background spaces. In this context we discuss the subtleties associated with expanding $f(R, R_{\mu\nu}R^{\mu\nu}, R_{\mu\nu\sigma\rho}R^{\mu\nu\sigma\rho})$ Lagrangians around maximally symmetric spaces of constant curvature, as well as with equivalence of the linearized Lagrangian to a scalar-tensor theory. Investigation of the consequences of applying the Dirac-Born-Infeld (DBI) strategy to further modify quadratic theories on the stability of de Sitter vacuum, as well as its impact on the cosmological dynamics, are the main concern of this paper. We show that (i) although the DBI deformation does not affect the Ostrogradski stability, other important instabilities such as the Ricci and scalar-tachyon ones, may be indeed surmounted (sometimes at the cost of renouncing to the original motivation of the DBI strategy, to avoid singularities), and (ii) DBI transforming the original theory broadens its possibilities to do cosmology since the asymptotic structure of the DBI-dual theory is richer than in the standard case. In particular, either the dimension of the phase space is increased, or there appear bifurcations in the control-parameter space.

DOI: 10.1103/PhysRevD.82.044002 PACS numbers: 04.20.−q, 04.50.Kd, 95.36.+x, 98.80.−k

I. INTRODUCTION

Attempts to modify the Einstein-Hilbert (EH) action of general relativity (GR)

$$S_{\rm EH} = \frac{1}{2\kappa^2}\int d^4x\sqrt{|g|}(R-2\Lambda), \tag{1}$$

where $R = g^{\mu\nu}R_{\mu\nu}$ is the Ricci curvature scalar and Λ- the cosmological constant ($\kappa^2 = m_{\rm Pl}^{-2} = 8\pi G$), have been motivated by a number of reasons. In particular, renormalization at one loop demands that the Einstein-Hilbert action be supplemented by higher-order curvature terms [1].[1] Besides, when quantum or string theory corrections are taken into account, the effective low energy action for pure gravity admits higher-order curvature invariants [3].

More recently it has been suggested that the present cosmic speed-up could have its origin in—among other possibilities—corrections to the GR equations of motion generated by nonlinear contributions of the scalar curvature R in the pure gravity Lagrangian of $f(R)$ theories [4–7].

Solar System constraints on $f(R)$ theories that are able to accommodate present accelerated expansion of the Universe have been one of the most discussed subjects lately [8–13]. Comparison of these theories with Solar System measurements, relies on the weak-field limit expansion of the $f(R)$ Lagrangian and the consequent calculation of post-Newtonian contributions to the metric coefficients [8,9,11]. Nonetheless, even if $f(R)$ theories were not a viable alternative to explain current acceleration of the expansion, their relevance to study early-time inflation [14] might fuel further interest in these alternatives to general relativity.

Next in the degree of complexity are the so-called $f(R, R_{\mu\nu}R^{\mu\nu}, R_{\mu\nu\sigma\rho}R^{\mu\nu\sigma\rho})$—$f(R,\ldots)$ for short—theories [7,15–19]. The gravitational spectrum of the linearization of these theories consists of a massless spin-2 graviton plus two additional gravitational propagating degrees of freedom: a massive spin-0 excitation and a massive spin-2 propagating mode. The latter appears to be a ghost mode associated with the Weyl curvature invariant $C^2 \equiv C_{\mu\nu\sigma\lambda}C^{\mu\nu\sigma\lambda}$ [15–17]. Notwithstanding, there are ways to overcome (or at least to smooth out) the consequences of the would be massive spin-2 ghost mode [18].

There are additional ways to modify the EH GR action. For instance, the one based on the DBI procedure for smoothing out singularities [7,20,21].[2] According to this procedure the original Lagrangian density $\mathcal{L} = \sqrt{|g|}L$—whose singularities are to be cured—is replaced by one of the DBI form

*iquiros@fisica.ugto.mx
†lurena@fisica.ugto.mx

[1]Higher-order actions are indeed renormalizable but not unitary [2]).

[2]The proposal to remove initial as well as final singularities in modified gravity has been given in Ref. [22]. It was shown there that the addition of a R^2 term to otherwise divergent modified gravity makes it regular.

PHYSICAL REVIEW D **82,** 123535 (2010)

Bosonic gas as a galactic dark matter halo

L. Arturo Ureña-López[1,*] and Argelia Bernal[2,†]

[1]*Departamento de Física, División de Ciencias e Ingenierías, Campus León, Universidad de Guanajuato, C.P. 37150, León, Guanajuato, México*

[2]*Max-Planck-Institut für Gravitationsphysik (Albert-Einstein-Institut), Am Mühlenberg 1, 14476 Potsdam, Germany*

(Received 12 August 2010; published 30 December 2010)

We study in detail the properties of gravitationally bounded multistate configurations, made of spin-zero bosons, in the Newtonian regime. We show that the properties of such configurations, in particular, their stability, depend upon how the particles are distributed in the different states they are composed of. Numerical techniques are used to distinguish between stable and unstable solutions, and to determine the final configurations they evolve towards. Multistate equilibrium configurations could be used as models of galactic halos made of scalar field dark matter, whose rotation curves appear more realistic than in the case of single-state configurations.

DOI: 10.1103/PhysRevD.82.123535 PACS numbers: 95.35.+d, 04.40.−b, 04.62.+v, 98.62.Gq

I. INTRODUCTION

It has been known for a long time that, within the context of Einstein's General Relativity, the luminous matter content of galaxies cannot explain the so-called rotational curves (RC) [1–3], which are still considered one of the cornerstone evidences for the existence of nonbaryonic dark matter. There are many candidates for dark matter particles; the most popular ones are known as weak interactive massive particles (WIMPS) [4–6]. The accepted paradigm that describes the way in which those particles form structures is the so-called Lambda cold dark matter (ΛCDM) model [7–9].

An interesting alternative some of us have been working on is to consider a (real) scalar field as a dark matter candidate, a hypothesis that has been widely explored in the specialized literature by many other authors [10–25]; see also for a comprehensive review. In most scalar field models, the dark matter particle is an ultralight massive boson, with a Compton wavelength of astrophysical proportions and a very large mean number density, so that their collective behavior is well described by a classical scalar field. The scalar field dark matter (SFDM) model, as we shall call it in general, offers the same results as the ΛCDM model at large scales, up to linear order perturbations [14,16,23,25,27,28].

The RC problem has also been addressed using scalar fields; see for instance [10–12,17,29]. These works considered the dark matter halo as a Newtonian Bose-Einstein condensate (BEC), in which the scalar field dynamics is driven by the so-called Schroedinger-Poisson system of equations. However, none of the studies carried on so far have shown, undeniably, that these scalar field models can account for all features of realistic galactic halo.

The modeling of scalar field halos was based on the (nodeless) ground-state solutions of the SP system, which is the only stable solution, and the predicted rotation curves are marginally in agreement with the observed ones [11–13,30–32]. In all cases above, the only stable scalar field configuration is that in which boson particles are all in the ground state. The ground state is the only stable solution of the SP system against gravitational perturbations; other excited configurations are intrinsically unstable [18,32] (see also [33,34] and references therein).

The main purpose in this work is to further explore the proposal that was first put forward by Matos and Ureña-López in Ref. [35]: that realistic scalar field galaxy halos must be comprised of *multistate configurations*. As we shall show, equilibrium configurations of the SP system can be constructed in which many-particle states coexist simultaneously, so that the whole system is *stable* under small (radial) perturbations.[1] Probably not surprisingly, we have found that RC could be better fitted by these many-particle systems.

Although the inclusion of baryonic matter is indeed needed for fitting realistic RC, our stability study of configurations made only of SFDM is a first step towards such objective. Actually, *stable* dark matter halos are expected to be the sites of galaxy formation, see [8]. As we shall see too, a dark matter halo made of a multistate configuration clearly shows an improvement in the expected profile of RC at large radii, which is a promising motivation.

The plan of the paper is as follows. In Sec. II, we present the mathematical theory behind multiparticle states. In Sec. III, we show that their general properties depend upon the distribution of the particles in the different excited states. In Sec. IV, we give numerical evidence that there are stable configurations under small radial

*lurena@fisica.ugto.mx
†abernal@aei.mpg.de

[1]The relativistic version of the multistate hypothesis was studied recently in [36,37], in which stability was also confirmed.

Entropy **2010**, *12*, 2067-2076; doi:10.3390/e12092067

OPEN ACCESS

entropy

ISSN 1099-4300

www.mdpi.com/journal/entropy

Article

Superstatistics and Gravitation

Octavio Obregón

Departamento de Física, División de Ciencias e Ingenierías, Campus León, Universidad de Guanajuato, Loma del Bosque No. 103, Fracc. Lomas del Campestre, León, Guanajuato, Mexico;
E-Mail: octavio@fisica.ugto.mx; Tel.: +52-477-788-5109; Fax +52-477-788-5100 ext. 8440

Received: 31 Aug 2010 / Accepted: 8 September 2010 / Published: 27 September 2010

Abstract: We suggest to consider the spacetime as a non-equilibrium system with a long-term stationary state that possess as a spatio-temporally fluctuating quantity β. These systems can be described by a superposition of several statistics, "superstatistics". We propose a Gamma distribution for $f(\beta)$ that depends on a parameter p_l. By means of it the corresponding entropy is calculated, p_l is identified with the probability corresponding to this model. A generalized Newton's law of gravitation is then obtained following the entropic force formulation. We discuss some of the difficulties to try to get an associated theory of gravity.

Keywords: superstatistics; entropy; modified gravity

Classification: PACS 04.50.Kd, 04.70.Dy, 05.40.-a, 05.70.Ln, 89.70.Cf

1. Introduction

Several years ago Beck and Cohen [1,2] considered nonequilibrium systems with a long-term stationary state that possess a spatio-temporally fluctuating intensive quantity. They have shown that after averaging over the fluctuations one can obtain not only non-extensive statistical mechanics [3,4] but an infinite set of more general statistics that they called "superstatistics". In their work they selected the temperature as fluctuating quantity among various possible intensive quantities (e.g., chemical potential or energy dissipation) and showed for general distributions $f(\beta)$, how to get a kind of effective Boltzmann factor

$$B(E) = \int_0^\infty d\beta \; f(\beta) e^{-\beta E} \tag{1}$$

Unveiling the tachyon dynamics in the Carrollian limit

C. Escamilla-Rivera
Departamento de Física Teórica de la Universidad del País Vasco,
Bilbao, España, 48080,
e-mail: celrivera@fisica.ugto.mx

G. Garcia-Jimenez
Facultad de Ciencia Físico Matemáticas de la Universidad Autónoma de Puebla,
Puebla, México, 72000,
e-mail: ggarcia@fisica.ugto.mx

O. Obregon
Departamento de Física de la Universidad de Guanajuato,
Leon, Guanajuato, 37150, Mexico,
e-mail: obregon@fisica.ugto.mx

Recibido el 26 de marzo de 2010; aceptado el 16 de junio de 2010

We briefly study the dynamics at classical level of the Carrollian limit, with vanishing speed of light and no possible propagation of signals, for a simply effective action in a flat space with an open string tachyon as a scalar field. The canonical analysis of the theory indicates that the equation of motion is of Dirac type contrary to the non-relativistic case where the equation is of Schrodinger type. The ultimate intention is to analize the latter case with electromagnetic fluxes to find that in this case the open string tachyon cannot be interpreted as time.

Keywords: String theory; tachyon.

Estudiaremos brevemente la dinámica del Límite de Carroll a nivel clásico de una acción efectiva en un espacio plano y con un campo escalar del tipo taquión de cuerda abierta. El análisis canónico de la teoría indica que la ecuación de movimiento es del tipo Dirac, contrario al caso no relativista donde la ecuación es del tipo Schrödinger. Finalmente, analizaremos el caso con flujos electromagnéticos y encontraremos que el taquión de cuerda abierta no puede ser interpretado como el tiempo.

Descriptores: Teoría de cuerdas; taquión.

PACS: 11.25.Sq; 04.20.Fy; 02.30.Mv

1. Introduction

In past years the role of the tachyon in certain string theories has been explored and this has resulted in a better understanding of the D-brane decaying process [1,2]. The basic idea is that the usual open string vacuum is unstable, but there exists a stable vacuum with zero energy density which is stable, which a tachyon field $T(x)$ naturally moves to. Nevertheless, it seems that aspects of this process can be compared with some simple effective field theory models. In this case, maybe the simplest model was proposed by Sen [1]. This success of effective action methods, together with the difficulties of other approaches described encourages one to pursue this further and to attempt an exact description of the cosmology of tachyon rolling [3].

Moreover, in the case where there are electromagnetic fluxes, the tachyon field is on the same footing as a transverse scalar in the Dirac-Born-Infeld action for a brane [4]. In this case we look for a solution with a constant electromagnetic field and find that the condensed state at $V(T) \to 0$ is given by $\dot{T}^2+E^2 = 1$, where $\dot{T}$ means derivative with respect to the dimensionless time of tachyon field and $E = |\vec{E}|$. To understand the dynamics it is convenient to follow the Hamiltonian formulation of the theory.

The present manuscript is organized as follows. In Sec. 2 we review the role of the open string tachyon in field theory and how this scalar field takes place in the decaying process.

In Sec. 3 we describe what we have called the Carrollian limit mechanism for open string states. Since this entails familiarity with Carroll group, I planned to include also the Galilean group and the differences between them.

In Sec. 4 we discuss some aspects of this theory when is coupled to gravity.

In Sec. 5 we use the low energy effective action of the open string tachyon and take the two possible limits: first the Galileo limit (when $c \to \infty$), *i.e.,* the contravariant metric $\eta^{\mu\nu} = (-c^{-2}, 1, 1, 1)$ is well defined, contrary to the Carrollian limit (when $c \to 0$). For this case we obtain, in the Hamiltonian formulation, a Dirac type equation.

In Sec. 6 we use again the effective action and consider the case in which $F_{\mu\nu} \neq 0$ to find that the tachyon is accelerated and emits radiation in the direction of the electromagnetic field.

2. Open string tachyon in field theory

To understand clearly the tachyon dynamics we take into consideration a real scalar field ϕ in a flat space-time. The Lagrangian of this theory is given by

nature photonics

LETTERS

PUBLISHED ONLINE: 29 AUGUST 2010 | DOI: 10.1038/NPHOTON.2010.214

Hacking commercial quantum cryptography systems by tailored bright illumination

Lars Lydersen[1,2]*, Carlos Wiechers[3,4,5], Christoffer Wittmann[3,4], Dominique Elser[3,4], Johannes Skaar[1,2] and Vadim Makarov[1]

The peculiar properties of quantum mechanics allow two remote parties to communicate a private, secret key, which is protected from eavesdropping by the laws of physics[1–4]. So-called quantum key distribution (QKD) implementations always rely on detectors to measure the relevant quantum property of single photons[5]. Here we demonstrate experimentally that the detectors in two commercially available QKD systems can be fully remote-controlled using specially tailored bright illumination. This makes it possible to tracelessly acquire the full secret key; we propose an eavesdropping apparatus built from off-the-shelf components. The loophole is likely to be present in most QKD systems using avalanche photodiodes to detect single photons. We believe that our findings are crucial for strengthening the security of practical QKD, by identifying and patching technological deficiencies.

The field of quantum key distribution has evolved rapidly in recent decades. Today, quantum key distribution (QKD) implementations in laboratories can generate key over fibre channels with lengths up to 250 km (ref. 6), and a few QKD systems are even commercially available, promising enhanced security for data communication.

In all proofs for the security of QKD, assumptions are made for the devices involved. However, the components used for experimental realizations of QKD deviate from the models in the security proofs. This has led to iterations in which security threats caused by deviations have been discovered, and the loopholes have been closed either by modification of the implementation, or more general security proofs[7–9]. In other cases, information leaking to the eavesdropper has been quantified[10,11].

Attacks exploiting the most severe loopholes are usually experimentally unfeasible with current technology. A prominent example is the photon number splitting attack[12], which requires the eavesdropper Eve to perform a quantum non-demolition measurement of the photon number sent by Alice. The attack is still unfeasible, and has been nullified by improved QKD protocols[13,14]. In contrast, a more implementation-friendly attack is the time-shift attack[15] based on detector efficiency mismatch[16]. Experimentally however, this attack only gave a small information-theoretical advantage for Eve when applied to a modified version of a commercial QKD system[17]. In the attack, Eve captured partial information about the key in 4% of her attempts, such that she could improve her random (brute-force) search over all possible keys.

In this Letter, we demonstrate how two commercial QKD systems id3110 Clavis2 and QPN 5505, from the commercial vendors ID Quantique and MagiQ Technologies, can be fully cracked. We show experimentally that Eve can blind the gated detectors in the QKD systems using bright illumination, thereby converting them into classical, linear detectors. The detectors are then fully controlled by classical laser pulses superimposed over the bright continuous-wave (c.w.) illumination. Remarkably, the detectors exactly measure what is dictated by Eve; with matching measurement bases Bob detects exactly the bit value sent by Eve, whereas

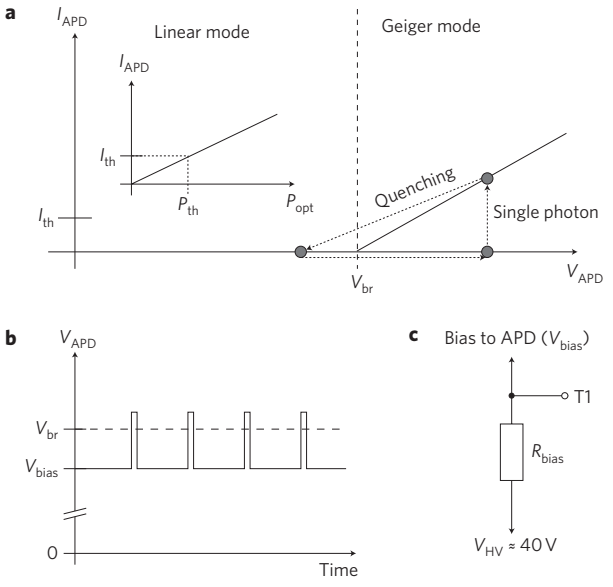

Figure 1 | APD as a single-photon detector. a, In Geiger mode, where the APD is reverse-biased above the breakdown voltage V_{br}, an absorbed single photon causes a large current I_{APD} through the APD. A detection signal called a 'click' occurs when I_{APD} crosses the threshold I_{th}. Afterwards, V_{APD} is lowered below V_{br} to quench the avalanche, before returning to Geiger mode. Below V_{br}, in the linear mode, the current I_{APD} is proportional to the incident optical power P_{opt}. Then I_{th} becomes an optical power threshold P_{th}. **b**, Commercial systems use gated detectors, with the APDs in Geiger mode only when a photon is expected, to reduce false detections called 'dark counts'. In practice, the APD is biased just below V_{br}, and periodical ~3 V voltage pulses create Geiger mode time regions, so-called 'gates'. **c**, In both systems, the bias high-voltage supply V_{HV} has impedance R_{bias} ($R_{bias} = 1\,k\Omega$ in Clavis2 and 20 kΩ in QPN 5505) before V_{bias} is applied to the APD at the point T1. Therefore, any current through R_{bias} reduces V_{bias} (see Supplementary Section I for more details).

[1]Department of Electronics and Telecommunications, Norwegian University of Science and Technology, NO-7491 Trondheim, Norway, [2]University Graduate Center, NO-2027 Kjeller, Norway, [3]Max Planck Institute for the Science of Light, Günther-Scharowsky-Strasse 1/Bau 24, 91058 Erlangen, Germany, [4]Institut für Optik, Information und Photonik, University of Erlangen-Nuremberg, Staudtstraße 7/B2, 91058 Erlangen, Germany, [5]Departamento de Física, Universidad de Guanajuato, Lomas del Bosque 103, Fraccionamiento Lomas del Campestre, 37150, León, Guanajuato, México.
*e-mail: lars.lydersen@iet.ntnu.no

Thermal blinding of gated detectors in quantum cryptography

Lars Lydersen,[1,2,*] **Carlos Wiechers,**[3,4,5] **Christoffer Wittmann,**[3,4] **Dominique Elser,**[3,4] **Johannes Skaar,**[1,2] **and Vadim Makarov**[1]

[1]*Department of Electronics and Telecommunications, Norwegian University of Science and Technology, NO-7491 Trondheim, Norway*
[2]*University Graduate Center, NO-2027 Kjeller, Norway*
[3]*Max Planck Institute for the Science of Light, Günther-Scharowsky-Str. 1/Bau 24, 91058 Erlangen, Germany*
[4]*Institut für Optik, Information und Photonik, University of Erlangen-Nuremberg, Staudtstraße 7/B2, 91058 Erlangen, Germany*
[5]*Departamento de Física, Universidad de Guanajuato, Lomas del Bosque 103, Fraccionamiento Lomas del Campestre, 37150, León, Guanajuato, México*
[*]*lars.lydersen@iet.ntnu.no*

Abstract: It has previously been shown that the gated detectors of two commercially available quantum key distribution (QKD) systems are blindable and controllable by an eavesdropper using continuous-wave illumination and short bright trigger pulses, manipulating voltages in the circuit [Nat. Photonics **4**, 686 (2010)]. This allows for an attack eavesdropping the full raw and secret key without increasing the quantum bit error rate (QBER). Here we show how thermal effects in detectors under bright illumination can lead to the same outcome. We demonstrate that the detectors in a commercial QKD system Clavis2 can be blinded by heating the avalanche photo diodes (APDs) using bright illumination, so-called *thermal blinding*. Further, the detectors can be triggered using short bright pulses once they are blind. For systems with pauses between packet transmission such as the plug-and-play systems, thermal inertia enables Eve to apply the bright blinding illumination *before* eavesdropping, making her more difficult to catch.

OCIS codes: (040.1345) Avalanche photodiodes (APDs); (040.5570) Quantum detectors; (270.5568) Quantum cryptography; (270.5570) Quantum detectors.

References and links

1. C. H. Bennett and G. Brassard, "Quantum cryptography: Public key distribution and coin tossing," in "Proceedings of IEEE International Conference on Computers, Systems, and Signal Processing," (IEEE Press, New York, Bangalore, India, 1984), pp. 175–179.
2. A. K. Ekert, "Quantum cryptography based on bell theorem," Phys. Rev. Lett. **67**, 661–663 (1991).
3. H.-K. Lo and H. F. Chau, "Unconditional security of quantum key distribution over arbitrarily long distances," Science **283**, 2050–2056 (1999).
4. P. W. Shor and J. Preskill, "Simple proof of security of the BB84 quantum key distribution protocol," Phys. Rev. Lett. **85**, 441–444 (2000).
5. D. Stucki, N. Walenta, F. Vannel, R. T. Thew, N. Gisin, H. Zbinden, S. Gray, C. R. Towery, and S. Ten, "High rate, long-distance quantum key distribution over 250 km of ultra low loss fibres," N. J. Phys. **11**, 075003 (2009).
6. Commercial QKD systems are available from at least two companies: ID Quantique (Switzerland), `http://www.idquantique.com`; MagiQ Technologies (USA), `http://www.magiqtech.com`.

#135153 - $15.00 USD Received 14 Sep 2010; revised 17 Nov 2010; accepted 13 Dec 2010; published 17 Dec 2010

Witnessing effective entanglement over a 2 km fiber channel

Christoffer Wittmann[1,2,†], Josef Fürst[1,2,†], Carlos Wiechers[1,2,3], Dominique Elser[1,2], Hauke Häseler[2,4], Norbert Lütkenhaus[1,2,4], and Gerd Leuchs[1,2]

[1]*Max Planck Institute for the Science of Light, Günther-Scharowsky-Str. 1 / Bau 24, 91058 Erlangen, Germany*
[2]*Institute of Optics, Information and Photonics, University Erlangen-Nuremberg, Staudtstraße 7/B2, 91058 Erlangen, Germany*
[3] *Departamento de Física, Universidad de Guanajuato, Lomas del Bosque 103, Fraccionamiento Lomas del Campestre, 37150, León, Guanajuato, México*
[4]*Institute for Quantum Computing, University of Waterloo, 200 University Avenue W., Waterloo, Ontario, Canada N2L 3G1*
† *Authors contributed equally to this work.*
Christoffer.Wittmann@mpl.mpg.de

Abstract: We present a fiber-based continuous-variable quantum key distribution system. In the scheme, a quantum signal of two non-orthogonal weak optical coherent states is sent through a fiber-based quantum channel. The receiver simultaneously measures conjugate quadratures of the light using two homodyne detectors. From the measured Q-function of the transmitted signal, we estimate the attenuation and the excess noise caused by the channel. The estimated excess noise originating from the channel and the channel attenuation including the quantum efficiency of the detection setup is investigated with respect to the detection of effective entanglement. The local oscillator is considered in the verification. We witness effective entanglement with a channel length of up to 2 km.

OCIS codes: (270.0270) Quantum optics; (270.5568) Quantum cryptography; (270.5570) Quantum detectors; (270.5585) Quantum information and processing.

References and links

1. A. Kerckhoffs, *La cryptographie militaire* (Journal des sciences militaires, Vol. IX, pp. 5-38, 1883).
2. C. Shannon, "Communication theory of secrecy systems," The Bell system Tech. J. **28**, 656–715 (1949).
3. G. Vernam, "Cipher printing telegraph systems for secret wire and radio telegraphic communications," J. Amer. Inst. Elect. Eng. p. 109 (1926).
4. C. Bennett and G. Brassard, "Quantum cryptography: Public key distribution and coin tossing," Proceedings of IEEE International Conference on Computers Systems and Signal Processing, Bangarore India pp. 175–179 (1984).
5. C. Bennett, F. Bessette, G. Brassard, L. Salvail, and J. Smolin, "Experimental quantum cryptography," J. Cryptology **5**, 3–28 (1992).
6. A. Ekert, J. Rarity, P. Tapster, and G. Palma, "Practical quantum cryptography based on 2-photon interferometry," Phys. Rev. Lett. **69**, 1293–1295 (1992).
7. A. Muller, J. Breguet, and N. Gisin, "Experimental demonstration of quantum cryptography using polarized photons in optical-fiber over more than 1 km," Europhys. Lett. **23**, 383–388 (1993).
8. D. Stucki, N. Gisin, O. Guinnard, G. Ribordy, and H. Zbinden, "Quantum key distribution over 67 km with a plug&play system," New J. Phys. **4**, 41 (2002).
9. D. Rosenberg, J. W. Harrington, P. R. Rice, P. A. Hiskett, C. G. Peterson, R. J. Hughes, A. E. Lita, S. W. Nam, and J. E. Nordholt, "Long-distance decoy-state quantum key distribution in optical fiber," Phys. Rev. Lett. **98**, 10503 (2007).

#120058 - $15.00 USD Received 16 Nov 2009; revised 1 Feb 2010; accepted 2 Feb 2010; published 19 Feb 2010

10. R. Ursin, F. Tiefenbacher, T. Schmitt-Manderbach, H. Weier, T. Scheidl, M. Lindenthal, B. Blauensteiner, T. Jennewein, J. Perdigues, P. Trojek, B. Ömer, M. Fürst, M. Meyenburg, J. Rarity, Z. Sodnik, C. Barbieri, H. Weinfurter, and A. Zeilinger, "Entanglement-based quantum communication over 144km," Nat. Phys. **3**, 481–486 (2007).
11. T. Schmitt-Manderbach, H. Weier, M. Fürst, R. Ursin, F. Tiefenbacher, T. Scheidl, J. Perdigues, Z. Sodnik, C. Kurtsiefer, J. G. Rarity, A. Zeilinger, and H. Weinfurter, "Experimental demonstration of free-space decoy-state quantum key distribution over 144 km," Phys. Rev. Lett. **98**, 010504 (2007).
12. T. C. Ralph, "Continuous variable quantum cryptography," Phys. Rev. A **61**, 010303 (1999).
13. C. Silberhorn, T. C. Ralph, N. Lütkenhaus, and G. Leuchs, "Continuous variable quantum cryptography: Beating the 3 dB loss limit," Phys. Rev. Lett. **89**, 167901 (2002).
14. F. Grosshans, G. V. Assche, J. Wenger, R. Brouri, N. J. Cerf, and P. Grangier, "Quantum key distribution using gaussian-modulated coherent states," Nature **421**, 238–241 (2003).
15. J. Lodewyck, M. Bloch, R. Garcia-Patron, S. Fossier, E. Karpov, E. Diamanti, T. Debuisschert, N. J. Cerf, R. Tualle-Brouri, S. W. McLaughlin, and P. Grangier, "Quantum key distribution over 25 km with an all-fiber continuous-variable system," Phys. Rev. A **76**, 042305–10 (2007).
16. B. Qi, L. Huang, L. Qian, and H. Lo, "Experimental study on the gaussian-modulated coherent-state quantum key distribution over standard telecommunication fibers," Phys. Rev. A **76**, 052323–9 (2007).
17. S. Lorenz, N. Korolkova, and G. Leuchs, "Continuous-variable quantum key distribution using polarization encoding and post selection," Appl. Phys. B **79**, 273–277 (2004).
18. A. M. Lance, T. Symul, V. Sharma, C. Weedbrook, T. C. Ralph, and P. K. Lam, "No-switching quantum key distribution using broadband modulated coherent light," Phys. Rev. Lett. **95**, 180503–4 (2005).
19. N. Gisin, S. Fasel, B. Kraus, H. Zbinden, and G. Ribordy, "Trojan-horse attacks on quantum-key-distribution systems," Phys. Rev. A **73**, 022320–6 (2006).
20. S. Pirandola, S. Mancini, S. Lloyd, and S. L. Braunstein, "Continuous-variable quantum cryptography using two-way quantum communication," Nat. Phys. **4**, 726–730 (2008).
21. C. Weedbrook, A. M. Lance, W. P. Bowen, T. Symul, T. C. Ralph, and P. K. Lam, "Coherent-state quantum key distribution without random basis switching," Phys. Rev. A **73**, 022316–9 (2006).
22. J. Lodewyck and P. Grangier, "Tight bound on the coherent-state quantum key distribution with heterodyne detection," Phys. Rev. A **76**, 022332–8 (2007).
23. D. Elser, T. Bartley, B. Heim, C. Wittmann, D. Sych, and G. Leuchs, "Feasibility of free space quantum key distribution with coherent polarization states," New J. Phys. **11**, 045014 (2009).
24. D. Elser, C. Wittmann, U. L. Andersen, O. Glöckl, S. Lorenz, C. Marquardt, and G. Leuchs, "Guided acoustic wave brillouin scattering in photonic crystal fibers," J. Phys. Conf. Ser. **92**, 012108 (2007).
25. N. Korolkova, G. Leuchs, R. Loudon, T. C. Ralph, and C. Silberhorn, "Polarization squeezing and continuous-variable polarization entanglement," Phys. Rev. A **65**, 052306 (2002).
26. H. Häseler, T. Moroder, and N. Lütkenhaus, "Testing quantum devices: Practical entanglement verification in bipartite optical systems," Phys. Rev. A **77**, 032303–11 (2008).
27. C. Dorrer, D. Kilper, H. Stuart, G. Raybon, and M. Raymer, "Linear optical sampling," IEEE Photonics Technol. Lett. **15**, 1746–1748 (2003).
28. C. H. Bennett, "Quantum cryptography using any two nonorthogonal states," Phys. Rev. Lett. **68**, 3121 (1992).
29. Y. Zhao, M. Heid, J. Rigas, and N. Lütkenhaus, "Asymptotic security of binary modulated continuous-variable quantum key distribution under collective attacks," Phys. Rev. A **79**, 012307–14 (2009).
30. M. Curty, M. Lewenstein, and N. Lütkenhaus, "Entanglement as a precondition for secure quantum key distribution," Phys. Rev. Lett. **92**, 217903 (2004).
31. C. H. Bennett, G. Brassard, and N. D. Mermin, "Quantum cryptography without bell's theorem," Phys. Rev. Lett. **68**, 557 (1992).
32. J. Rigas, O. Gühne, and N. Lütkenhaus, "Entanglement verification for quantum-key-distribution systems with an underlying bipartite qubit-mode structure," Phys. Rev. A **73**, 012341–6 (2006).
33. U. Leonhardt, *Measuring the Quantum State of Light* (Cambridge University Press, 1997).
34. M. Legré, H. Zbinden, and N. Gisin, "Implementation of continuous variable quantum cryptography in optical fibres using a go-&-return configuration," Quantum Inf. Comput. **6**, 326–335 (2006).
35. J. A. Nelder and R. Mead, "A simplex method for function minimization," The Computer Journal **7**, 308–313 (1965).
36. J. Shapiro and S. Wagner, "Phase and amplitude uncertainties in heterodyne detection," IEEE J. Quantum Electron. **20**, 803–813 (1984).
37. S. Stenholm, "Simultaneous measurement of conjugate variables," Ann. Phys. **218**, 233–254 (1992).
38. U. Leonhardt and H. Paul, "Realistic optical homodyne measurements and quasi-probability distributions," Phys. Rev. A **48**, 4598–4604 (1993).
39. H. Hansen, T. Aichele, C. Hettich, P. Lodahl, A. Lvovsky, J. Mlynek, and S. Schiller, "Ultrasensitive pulsed, balanced homodyne detector: application to time-domain quantum measurements," Opt. Lett. **26**, 1714–1716 (2001).
40. U. Leonhardt, J. A. Vaccaro, B. Böhmer, and H. Paul, "Canonical and measured phase distributions," Phys. Rev.

#120058 - $15.00 USD Received 16 Nov 2009; revised 1 Feb 2010; accepted 2 Feb 2010; published 19 Feb 2010

A **51**, 84 (1995).
41. H. Bachor and T. Ralph, *A guide to experiments in quantum optics* (Wiley-VCH Verlag, 2004).

1. Introduction

"Kerckhoffs' principle" [1] and Shannon's assumption "The enemy knows the system" [2] established the basis for modern cryptography and enhanced secure communication between two parties. With the proposal of the "one time pad" [3], the security aspect shifted from secure communication to secure key distribution between these two parties. Quantum key distribution (QKD), first proposed 1984 [4], offers a way to exchange a secret key using the quantum mechanical properties of light as the carrier of information. The security is thereby based on fundamental physical concepts.

First proof of principle experiments for QKD [5, 6, 7] were followed by practical implementations over long and extremely long distances [8, 9, 10, 11]. In parallel to these discrete-variable QKD systems, continuous-variable QKD using homodyne detection was proposed [12]. It was shown, that the limit of 3 dB channel attenuation can be overcome by the concept of postselection [13] and the postprocessing method reverse reconciliation [14]. Continuous-variable QKD has been tested on quantum channels of up to 25km length [15, 16] using homodyne detection and basis switching. Besides using a single homodyne detection, also simultaneous detection of both conjugate quadratures of the signal was demonstrated [17, 18]. Homodyne detection of conjugate quadratures referred to as heterodyne detection is particularly interesting for three reasons:

- Random numbers are not needed in the receiver's setup.
- The Trojan-horse attack [19], where Eve gains information by reading the basis choice in Bob's setup, is not possible.
- The heterodyne detection strategy achieves higher secure bit rates than schemes with homodyne detection in some QKD protocols [20, 21, 22].

Experiments using heterodyne detection on a long fiber channel, however, had not yet been demonstrated.

In this paper, we present a fiber-based QKD-system using a double-homodyne detection setup. As in previous experiments [17, 23], we use binary encoded continuous-variable quantum states consisting of a signal mode and a local oscillator mode. We adapt our previous polarization-based experiments to a fiber channel. To this end, our two mode states are sent through the quantum channel using a combination of time [15] and polarization multiplexing [16] of signal and local oscillator (LO). Therefore, detrimental effects from photon-phonon interactions (GAWBS) are avoided [24]. By describing the sent quantum information in the Stokes space [25], it is possible to verify effective entanglement in the measurement data according to the method in [26]. In contrast to all previous experiments, not only the signal but also the strong reference beam (LO) is considered in this security analysis. We show how to measure conjugate Stokes parameters with a freely drifting interferometric phase. The phase drift is monitored by additional classical calibration pulses on the quantum channel. Subsequently, Bob remaps his measurement data, similar to [16]. Finally, monitoring the intensity of the local oscillator at the detection stage allows us to unambiguously demonstrate the generation of quantum-correlated data.

The paper is organized as follows. In Section 2, we introduce our protocol and the Stokes formalism. In Section 3, we describe the setup focusing on the implementation of the detection part. In Section 4, noise characteristics of the system and the transmitted signal states are presented. Finally, the entanglement criterion is applied.

#120058 - $15.00 USD Received 16 Nov 2009; revised 1 Feb 2010; accepted 2 Feb 2010; published 19 Feb 2010

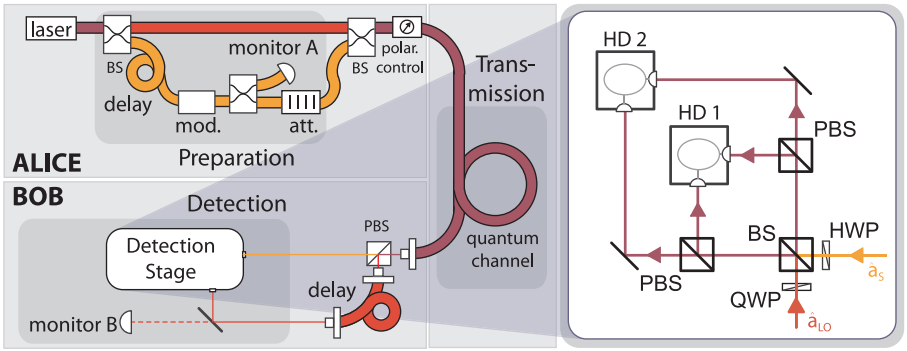

Fig. 1. (left) Schematics of the QKD setup, (right) the detection part is a random phase heterodyne detection using the polarization degree of freedom. Our scheme is similar to a technique called linear optical sampling [27]. In contrast to their system, we have a shot noise limited detection and a SNR improvement of about 40 dB.

2. The protocol

Our protocol is a continuous-variable adaptation of the two-state protocol proposed by Bennett [28]. Alice wishes to share a random bit string with Bob and starts by encoding binary information in the phase of coherent states. These two signal states $|\alpha\rangle$ and $|-\alpha\rangle$ are transmitted through a quantum channel and evolve to the output states ρ_0 and ρ_1, which are detected by Bob in a heterodyne setup. Bob records the expectation values and variances of two orthogonal quadratures, which allows him to reconstruct a bit value from each signal and to estimate the information potentially extracted by an eavesdropper. A detailed account of the classical data processing necessary to distill a secret key from the raw measurement outcomes is presented in Ref. [29].

This two-state protocol is attractive from an experimental point of view, since the signal preparation is the simplest possible. Theoretically, lower bounds on the achievable secret key rate have been evaluated in Ref. [29]. Unfortunately, those results are not applicable to practical scenarios, since the key rate drops too quickly with increasing excess noise. The theory needs further development to make the protocol more robust against noise.

Here, we show that our experiment can establish quantum correlations in the classical data held by Alice and Bob, which is a necessary precondition for the distillation of a secret key [30]. The existence of quantum correlations is proven through the verification of so-called *effective entanglement* [31], a theoretically constructed, alternative description of the signal source. In this description, Alice prepares bipartite states

$$|\Psi\rangle_{\mathrm{AB}} = \frac{1}{\sqrt{2}}(|0\rangle_{\mathrm{A}}|\alpha\rangle_{\mathrm{B}} + |1\rangle_{\mathrm{A}}|-\alpha\rangle_{\mathrm{B}}). \tag{1}$$

Her subsequent orthogonal projective measurements $\{|0\rangle_A\langle 0|, |1\rangle_A\langle 1|\}$ effectively prepare the signal states $|\pm\alpha\rangle_B$, with equal probability. The action of the quantum channel on the state $|\Psi\rangle_{AB}$ leads to an effective bipartite quantum state ρ_{AB} shared by Alice and Bob. It is their task to prove that the classical measurement data must come exclusively from entangled ρ_{AB}, i.e., their data is quantum correlated.

Due to the discrete-continuous structure of the setup, we use the Expectation Value Matrix method [26, 32] to verify the existence of quantum correlations. In this method, all measured expectation values are stored in a matrix, and the separability of this matrix is linked to the separability of the possible underlying quantum states. For a detailed description, the reader is

#120058 - $15.00 USD Received 16 Nov 2009; revised 1 Feb 2010; accepted 2 Feb 2010; published 19 Feb 2010

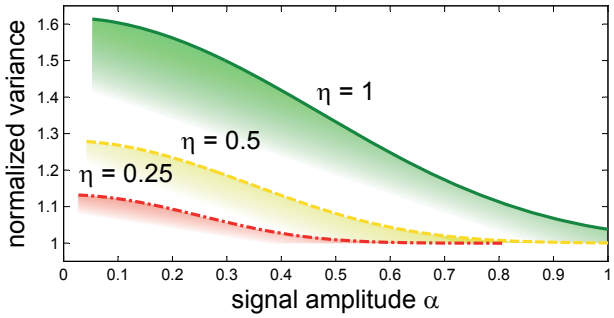

Fig. 2. Curves show lower bounds for quantum correlations. The variance of the Stokes operators is normalized by the local oscillator intensity resulting in the normalized variance $\mathrm{Var}(\hat{S}_{2,3})/\langle\hat{n}_{\mathrm{LO}}\rangle$. The different curves correspond to different channel transmissions η. Effective entanglement is verified in the shaded areas.

referred to Ref. [26]. Reference [26] also reveals a vulnerability of the protocol arising from an attack on the local oscillator mode. In a homodyne setup, the assumption that the local oscillator is a strong coherent state allows us to regard the measurement as the single-mode detection of the signal's quadrature [33]. Precisely this assumption allows Eve to perform an intercept-resend attack which modifies the intensities of signal and local oscillator modes. Such an attack will not show in Bob's quadrature detection, but could lead to data which is, at best, classically correlated and therefore not suitable for key generation.

To take this into account, we consider the binary signals as true two-mode states $|\pm\alpha\rangle\otimes|\alpha_{LO}\rangle$ and we regard the homodyne detection as a measurement of the quantum Stokes operators

$$\begin{aligned}\hat{S}_1 &= \hat{a}^\dagger_{LO}\hat{a}_{LO}-\hat{a}^\dagger_S\hat{a}_S=\hat{n}_{LO}-\hat{n}_s \\ \hat{S}_2 &= \hat{a}^\dagger_{LO}\hat{a}_S+\hat{a}^\dagger_S\hat{a}_{LO} \\ \hat{S}_3 &= i(\hat{a}^\dagger_S\hat{a}_{LO}-\hat{a}^\dagger_{LO}\hat{a}_S).\end{aligned} \tag{2}$$

The protocol gives access to the expectation values and variances of two of the Stokes operators, say $\hat{S}_2$ and $\hat{S}_3$. Then, a suitable Expectation Value Matrix is constructed as follows [26]:

$$\chi(\rho_{AB})=\begin{bmatrix}\left\langle|0\rangle\langle 0|\otimes B\right\rangle_{\rho_{AB}} & \left\langle|0\rangle\langle 1|\otimes B\right\rangle_{\rho_{AB}} \\ \left\langle|1\rangle\langle 0|\otimes B\right\rangle_{\rho_{AB}} & \left\langle|1\rangle\langle 1|\otimes B\right\rangle_{\rho_{AB}}\end{bmatrix} \tag{3}$$

with

$$B=\begin{bmatrix}\hat{1}_B & \hat{S}_2 & \hat{S}_3 \\ \hat{S}_2 & \hat{S}_2^2 & \hat{S}_2\hat{S}_3 \\ \hat{S}_3 & \hat{S}_3\hat{S}_2 & \hat{S}_3^2\end{bmatrix}. \tag{4}$$

Separability of the underlying state is then tested through the condition

$$\chi(\rho_{AB})^{T_A}\geq 0, \tag{5}$$

and violation of this certifies effective entanglement. The remaining Stokes operator $\hat{S}_1$ enters the Expectation Value Matrix through the symmetrizing step $\hat{S}_2\hat{S}_3=(\hat{S}_2\hat{S}_3+\hat{S}_3\hat{S}_2)/2+(\hat{S}_2\hat{S}_3-\hat{S}_3\hat{S}_2)/2=\{\hat{S}_2,\hat{S}_3\}/2+i\hat{S}_1$, which is instrumental to the verification process. However, due to practical reasons, the expectation value $\langle\hat{S}_1\rangle$ is not directly measured in our experiment, and

#120058 - $15.00 USD Received 16 Nov 2009; revised 1 Feb 2010; accepted 2 Feb 2010; published 19 Feb 2010

instead, we measure the photon number in the local oscillator mode (monitor B in Fig. 1(left)). We now show how this detour can provide a lower bound on $\langle \hat{S}_1 \rangle$:

Direct calculation leads to the relation

$$\hat{S}_2^2 + \hat{S}_3^2 = 2(\hat{S}_0 + 2\hat{n}_{LO}\hat{n}_s), \tag{6}$$

where $\hat{S}_0$ is defined as the total intensity $\hat{n}_s + \hat{n}_{LO}$. Equation (6) contains two quantities which are not directly accessible in our experiment, namely $\hat{S}_0$ and $\hat{n}_s$. The latter is easily replaced by the relation

$$\hat{n}_s = \frac{1}{2}(\hat{S}_0 - \hat{S}_1), \tag{7}$$

leading to

$$\hat{S}_1 = \hat{S}_0(1 + \frac{1}{\hat{n}_{LO}}) - \frac{\hat{S}_2^2 + \hat{S}_3^2}{2\hat{n}_{LO}}. \tag{8}$$

Finally, we use the relation $\langle \hat{S}_0 \rangle \geq \langle \hat{n}_{LO} \rangle$ to arrive at the desired bound

$$\langle \hat{S}_1 \rangle \geq 1 + \langle \hat{n}_{LO} \rangle - \frac{\langle \hat{S}_2^2 + \hat{S}_3^2 \rangle}{2\langle \hat{n}_{LO} \rangle}. \tag{9}$$

At this point, we can directly apply the Expectation Value Matrix method to verify the existence of quantum correlations, using the approximation (9) instead of the actual value of $\langle \hat{S}_1 \rangle$. Figure 2 shows the noise levels for different choices of input intensities, under the assumption that the noise is equal for both quadratures and both signal states. The variances are normalized by $\langle \hat{n}_{LO} \rangle$ to make the results independent of the local oscillator intensity. We observe that more noise can be tolerated when smaller signal amplitudes are chosen. Channel losses decrease the tolerable excess noise for quantum-correlated data.

3. Experimental setup

In this section, we first describe Alice's and Bob's optical hardware. We then separately discuss the detection scheme and finally explain the control software.

3.1. Optical setup

The optical setup of our QKD-system is shown in Fig. 1. The Alice module consists of a diode laser (*SLT5411* from *Sumitomo Electronic Industries* as used in [34]) pulsed by a self-made pulsed current supply. The laser pulses are approximately 100 ns long and have a wavelength of 1549.3 nm. The line width is 6.6 GHz at -10 dB of optical power and the coherence time is estimated with self-homodyning to be 0.2 ns. The laser pulses are split asymmetrically in the LO and the signal arm. The smaller fraction is used for the signal preparation. The signal arm consists of a delay fiber, a Mach-Zehnder modulator for amplitude modulation, a monitor detector, and an optical attenuator. This results in a shot noise limited weak signal at the single photon level. In the second fiber beamsplitter (BS) the LO pulses and the signal pulses are spatially combined with a 500 ns time shift. Additionally, the polarization of the pulses is chosen orthogonal. The last component in the Alice setup is a computer controlled polarization controller pre-compensating the slow polarization drift in the fiber channel.

In the Bob module the signal is demultiplexed with a polarizing beamsplitter (PBS). We control the second port of the PBS with a physical block to ensure the second input mode is in a vacuum state. The LO passes a delay fiber, while the signal is directly sent to the free-space detection setup. A monitor diode behind a highly reflective mirror measures the LO energy pulse by pulse. The polarization control is set such that the power on the monitor diode is maximized. Finally the signal is measured with our detection scheme shown in (Fig. 1 (right)).

#120058 - $15.00 USD Received 16 Nov 2009; revised 1 Feb 2010; accepted 2 Feb 2010; published 19 Feb 2010

3.2. Detection system

The detection system in Fig. 1 (right) consists of two homodyne detectors detecting two conjugate quadratures of the signal mode simultaneously. This was first investigated in [36, 37, 38]. Our scheme consists of free-space optics and therefore allows for easy and lossless manipulations of the polarization. The LO's polarization is then chosen to be circular. The signal's polarization is tilted by 45° with respect to H and V polarization. Both beams interfere on a polarization independent 50:50 beam splitter with acute angle of incidence.

For the H-polarized component, we label the relative phase between the signal and the bright LO $\phi_H = \phi_I$, where ϕ_I originates from interferometer drifts in sender and receiver modules. The phase shift of $\pi/2$ between two orthogonally polarized LO components results in a relative phase for the V-components of $\phi_V = \phi_I + \pi/2$. Both beams propagate to a PBS, which separates the H- and V-polarization. The reflected V-components impinge on the first homodyne detector (HD1), while the transmitted H-components impinge on the second homodyne detector (HD2). The difference of the photo currents is recorded.

Commonly, homodyne detectors are treated as quadrature detectors. We calculate the photon number difference $\hat{n}_-^{\mathrm{HD1}}$ detected by HD1 using the linearized field operators $\hat{a}_S = \alpha \cdot \hat{1} + \delta\hat{a}_S$ and $\hat{a}_{LO} = \alpha_{LO} \cdot \hat{1} + \delta\hat{a}_{LO}$. We assume that α_{LO} and α are real and $\alpha_{LO} \gg \alpha$. Additionally, the modes $S_\perp$ and $LO_\perp$, the modes orthogonally polarized to signal and LO, are in a vacuum state, i.e. $\hat{a}_{S_\perp} = \delta\hat{a}_{S_\perp}$ and $\hat{a}_{LO_\perp} = \delta\hat{a}_{LO_\perp}$. The last assumption is justified, since the other input port of the PBS is under Bob's control. The detected signal is found after a straightforward calculation to be

$$\begin{aligned} \hat{n}_-^{\mathrm{HD1}} &= \frac{1}{2}\left((\hat{a}_{LO}e^{i\phi_I} + \hat{a}_{LO_\perp}e^{i\phi_I})^\dagger(\hat{a}_S + \hat{a}_{S_\perp})\right. \\ &\quad \left. +(\hat{a}_S + \hat{a}_{S_\perp})^\dagger(\hat{a}_{LO}e^{i\phi_I} + \hat{a}_{LO_\perp}e^{i\phi_I})\right) \\ &= \alpha_{LO}\left(\cos(\phi_I)\cdot\alpha + \delta\hat{X}_{S,\phi_I} + \delta\hat{X}_{S_\perp}\right), \end{aligned} \tag{10}$$

where $\hat{X}_{M,\phi} = \frac{1}{2}(\hat{a}_M^\dagger e^{i\phi} + \hat{a}_M e^{-i\phi})$ is a quadrature operator for mode M with a phase ϕ. This quadrature measurement is derived analogously for HD2. It reads

$$\begin{aligned} \hat{n}_-^{\mathrm{HD2}} &= \frac{1}{2}\left((\hat{a}_{LO}e^{i\phi_I+\pi/2} - \hat{a}_{LO_\perp}e^{i\phi_I+\pi/2})^\dagger(\hat{a}_S - \hat{a}_{S_\perp})\right. \\ &\quad \left. +(\hat{a}_S - \hat{a}_{S_\perp})^\dagger(\hat{a}_{LO}e^{i\phi_I+\pi/2} - \hat{a}_{LO_\perp}e^{i\phi_I+\pi/2})\right) \\ &= \alpha_{LO}\left(\cos(\phi_I+\pi/2)\cdot\alpha + \delta\hat{X}_{S,\phi_I+\pi/2} + \delta\hat{X}_{S_\perp}\right). \end{aligned} \tag{11}$$

The vacuum input $S_\perp$ at the PBS adds additional 3 dB noise to the variance of the measurement. Therefore our setup is equivalent to a standard heterodyne detection. We do not stabilize the interferometric phase ϕ_I but let it drift freely. However, we have an inherent stabilization of the relative phase of $\phi_H - \phi_V = \pi/2$. Therefore two random but conjugate quadratures are measured with HD1 and HD2.

The simultaneous measurement of two conjugate quadratures depends strongly on the proper choice of the polarization of signal and LO in the detection setup. For balancing, a linearly polarized LO is equally split to both homodyne detectors. A weak signal beam is then sent into the detection scheme. The quadrature measurements of 4000 signals are averaged and the mean values are plotted in the two-dimensional measurement space of Fig. 3(a). Phase drifts of the interferometric phase will result in elliptical or circular graphs, depending on the angle of the quarter wave plate (QWP) in the LO path, corresponding to largely correlated measurements (elliptical) and uncorrelated measurements (circular). It is easy to show, that by turning the QWP, two quadratures with arbitrary relative angle can be measured. We desire uncorrelated measurements (orange trace in Fig. 3(a)).

#120058 - $15.00 USD Received 16 Nov 2009; revised 1 Feb 2010; accepted 2 Feb 2010; published 19 Feb 2010

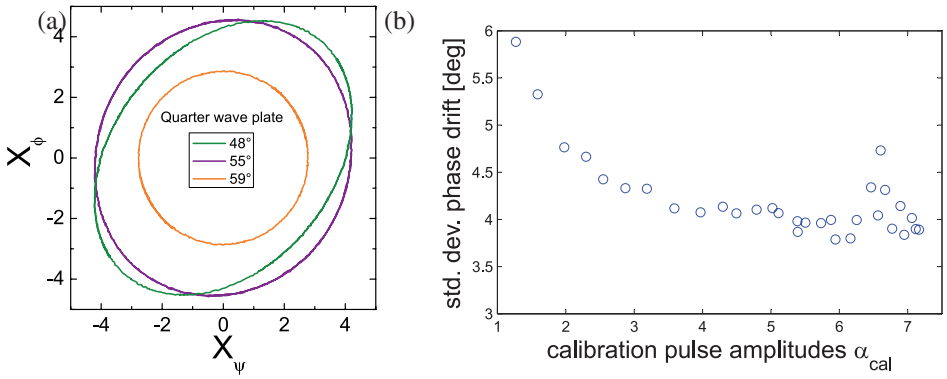

Fig. 3. (a) Lissajous figure of a phase randomized signal is measured for different settings of the QWP in the setup. If the measured quadratures X_ψ and X_ϕ are not orthogonal, the shape of the graph will be elliptical. We demonstrate that orthogonal quadratures are measured for the correct QWP angle (orange trace). (b) The phase is estimated from blocks of calibration pulses. The figure shows the standard deviation of the phase drift between different calibration blocks.

3.3. Electronics and automatization

In the following, we describe the electronic hardware, the control software and the steps in the postprocessing. The Alice electronics is essentially a 14-bit-D/A-converter to prepare the signal with a sampling rate of 20 MS/s. One port drives the laser with a pulse rate of 1 MHz. Another port produces rectangular pulses for the amplitude modulator. A third port synchronizes Bob's experiment with an electronic clock signal at approximately 1 kHz. The clock could be substituted for a synchronization using the LO monitor diode and calibration pulses as time stamp in future experiments.

A quaternary modulation is applied to the amplitude modulator to create the states $|\alpha\rangle$, $|-\alpha\rangle$, $|\alpha_{cal}\rangle$ and $|-\alpha_{cal}\rangle$, where α is the signal amplitude and α_{cal} is the amplitude of brighter "classical" calibration pulses sent along with the signal. The pulse pattern consists of four calibration pulses followed by 28 signal pulses.

To pre-compensate the polarization drift, we inserted the polarization control in Alice's setup. An optimal separation of signal and LO is obtained by maximizing the LO power on the monitor diode. The power is maximized either manually or with Bob's PC using a simplex method [35]. This demultiplexing method is very stable. It is furthermore lossless as opposed to a coupler with fixed splitting ratio [15].

In the following, we describe the electronic circuits. The difference signal in the homodyne detectors is amplified by charge sensitive amplifiers as in the design by [39]. The electrical pulse duration produced by the detectors is set to 400 ns (foot), which allows for repetition rates up to 2 MHz while maintaining linear amplification. The linearity was confirmed for all four photodiodes independently. Due to limitations of computing power, and an electronic signal due to LO light leaking into the signal arm, we run the experiment at 1 MHz. When varying the LO power for balanced homodyne detection of vacuum, we find a linear behavior of the signal variance versus the LO intensity. For typical LO power of 10^8 photons/pulse, the electronic noise is 20 dB below the signals variance. The common mode rejection ratio is always better that 40 dB. The detection efficiency of the homodyne detectors was 70%, including the quantum efficiency of the diodes (86%), the mode matching efficiency (95.4%) and the loss in optical components (10%).

Bob's 12-bit-A/D-converter digitizes the signal and the LO monitor detectors with 16 MS/s.

#120058 - $15.00 USD Received 16 Nov 2009; revised 1 Feb 2010; accepted 2 Feb 2010; published 19 Feb 2010

We reduce the number of samples by neglecting samples in between the pulses [1] and averaging 8 samples (approximately the electronic pulse length). These mean values are used to estimate the shot noise level, as shown in Eqn. (9). In the postprocessing, we estimate the mean value of the Stokes operators $\hat{S}_2$ and $\hat{S}_3$ for 1024 signal states. The displacement with respect to this mean value is considered as quantum signal. Long term fluctuations of the detector are thereby compensated.

The interferometric phase ϕ_I is estimated with the four bright calibration pulses in each 32-pulse-frame. To measure the phase noise, we calculate the phase drift between two calibration steps. We show the standard deviation of the phase drift in Fig. 3(b). We find that for weak calibration pulses the standard deviation depends on the calibration pulse amplitude. This stems from the limit for the phase estimation of weak coherent states [40]. For stronger amplitudes, the standard deviation of the phase drift is measured to be 4 degree for calibration times of $32\,\mu$s. With the estimated phase, we remap the coordinate system of the measured frame to the phase space of Alice's signal states. Subsequently, the data can be analyzed as described in the next section. The computational power needed for the complete postprocessing is high, but at 1MHz repetition rate the system runs continuously in realtime, as required for practical use in a QKD system.

4. Verification of effective entanglement

Reformulating the measurement in the Stokes representation (see Eqns. (2)) is of great importance for the security analysis of the system. We find that Eqns. (10) and (11) have the form of a simultaneous Stokes measurement of the $\hat{S}_\phi$- and the $\hat{S}_{\phi+\pi/2}$-operator, respectively, where $\hat{S}_\theta = \hat{S}_2\cos\theta + \hat{S}_3\sin\theta$. The Stokes operator $\hat{S}_1$ is estimated by the monitor diode, as shown in Eqn. (9).

To verify the effective entanglement in our experiment, we compare the measured excess noise to the theoretical upper noise bounds (see Fig. 2). The excess noise estimation demands a calibration step. The standard procedure to calibrate the shotnoise level is to probe vacuum. Therefore, we physically block the signal arm of the detection stage and monitor the noise power of the Stokes measurements, as well as the signal of the LO monitor diode. The shot-noise estimation thus corresponds to a measurement of the electronic gains in the detection system using a well known and low noise light beam[2]. In standard homodyne detection, the variance of the shot noise will then scale with the power of the LO in following measurements. However, a new aspect is introduced in Eqn. (9): If there is significant noise power in the $\hat{S}_2$- or $\hat{S}_3$-component of the signal states, the bound on $\langle\hat{S}_1\rangle$ will deteriorate, and with it the ability to detect quantum correlations. We estimate the contribution of the last term in Eqn. (9). We consider the worst case, i.e. the maximal reduction of the expectation value in each measurement run for a single amplitude (5 million signal pulses).

$$\frac{\langle\hat{S}_2^2\rangle}{\langle\hat{n}_{LO}\rangle} + \frac{\langle\hat{S}_3^2\rangle}{\langle\hat{n}_{LO}\rangle} \leq \frac{\gamma_{\mathrm{LO}}}{\gamma_{S_2}^2}\max\left(\frac{\langle\hat{u}_{S_2}^2\rangle}{\langle\hat{u}_{LO}\rangle}\right) + \frac{\gamma_{\mathrm{LO}}}{\gamma_{S_3}^2}\max\left(\frac{\langle\hat{u}_{S_3}^2\rangle}{\langle\hat{u}_{LO}\rangle}\right), \tag{12}$$

where γ_{S_i}, $\hat{u}_{S_i}$, γ_{LO} and $\hat{u}_{\mathrm{LO}}$ are gains and output voltages of the detectors for the $\hat{S}_i$-components ($i = 2,3$) and the LO power, respectively. The calibration measurement is used to measure the gain ratio. For an approximately shot noise limited beam we find

[1] In a QKD system the removed samples should be checked for manipulation attacks.

[2] If the LO has traveled through the eavesdropper's regime, it is mandatory to verify that the beam exhibits small excess noise compared to the detector's common mode rejection ratio, e.g. with an attenuation measurement [41].

#120058 - $15.00 USD Received 16 Nov 2009; revised 1 Feb 2010; accepted 2 Feb 2010; published 19 Feb 2010

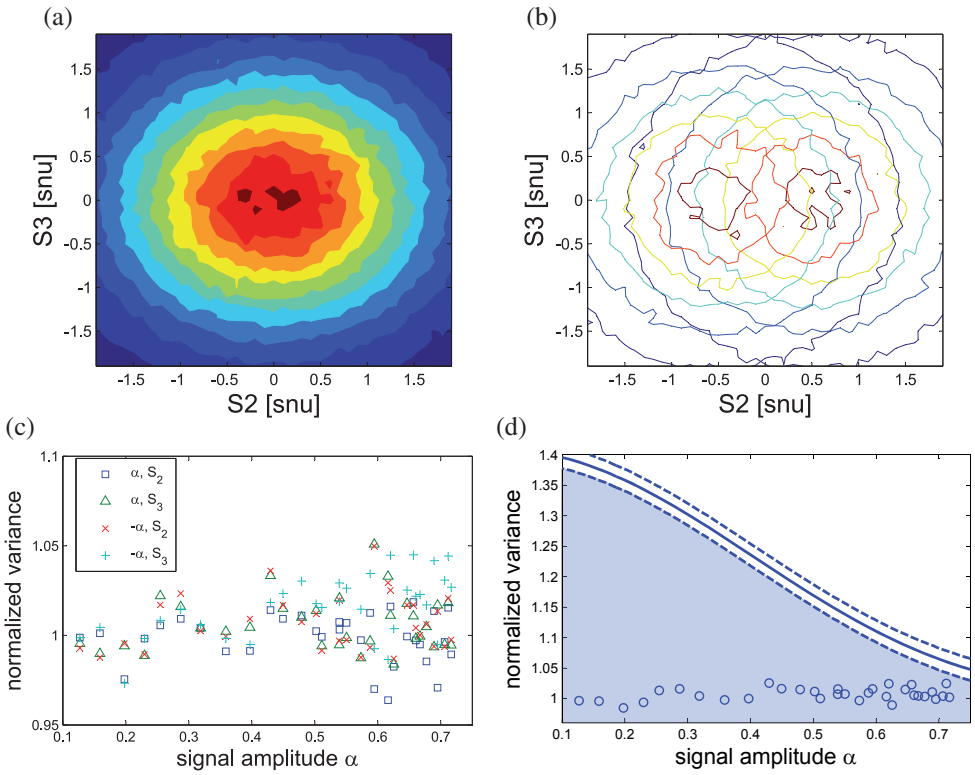

Fig. 4. Alice and Bob are connected back to back. (a) Combined Q-function generated from 5 million pulses with amplitudes $\alpha_S = 0.5$ (b) Q-functions for each signal state. (c) Excess noise estimated from Q-function for varying signal amplitudes. (d) Average excess noise (circles) compared to the bounds given by the entanglement criterion (solid line), shown with the 3-sigma confidentiality interval (dashed lines).

$$\frac{\gamma_{\mathrm{LO}}}{\gamma_{S_i}^2}\frac{\Delta^2\hat{u}_{S_i,\mathrm{snl}}}{\langle\hat{u}_{LO,\mathrm{snl}}\rangle} = \frac{\Delta^2\hat{S}_{i,\mathrm{snl}}}{\langle\hat{n}_{LO,\mathrm{snl}}\rangle} = 1. \tag{13}$$

The reduction of the normalized expectation value is fluctuating during the measurements. However, using Eqns. (12) and (13), we calculated that it never surpasses 10^{-3}. This factor is considered by shifting the bound for the entanglement verification. Another uncertainty in the level of shotnoise is the estimation error of the LO power. The LO power is measured for every signal pulse separately and therefore has a rather large standard deviation of $6 \cdot 10^{-3}$. We consider the deviation by plotting the three sigma confidence interval around the upper noise bound.

In our first measurement, we connected both modules back to back. The effective detection efficiency is therefore merely the 70% efficiency of the receiver module. The Q-functions are measured for the two signal states combined or separately as shown in Fig. 4(a) and (b), respectively. From the Q-functions, we estimate the mean value and the variance for both Stokes opertors of both signal states as shown in Fig. 4(c). We find that the variances are approximately equal. Their average variance is therefore compared to the upper bound of the variance given by the Expectation Value Matrix method. The comparison of upper bound and average variance is shown in 4(d). We find, that for all tested signal amplitudes the measured noise is below the

#120058 - $15.00 USD Received 16 Nov 2009; revised 1 Feb 2010; accepted 2 Feb 2010; published 19 Feb 2010

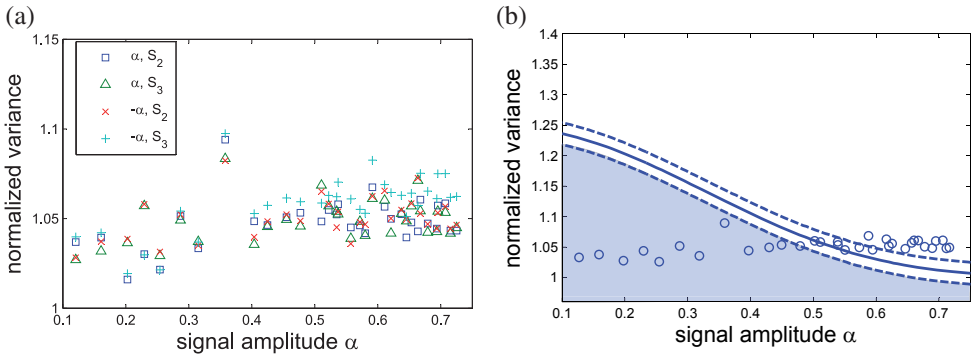

Fig. 5. Alice and Bob are connected with a 2 km optical fiber. (a) Excess noise estimated from Q-function measurement for varying signal amplitudes. (b) Average excess noise (circles) compared to the bounds given by the entanglement criterion (solid line), shown with the 3-sigma confidentiality interval (dashed lines).

3-sigma confidentiality interval. Therefore the effective entanglement is verified.

We then substitute the 2 m quantum channel with a 2 km standard optical fiber. The effective detection efficiency was 44.8%. The transmission of the channel decreases to 64% also due to additional splices. In an optimized setting, this attenuation corresponds to at least 10 km of fiber. Again, we estimate the mean values and the variance for both Stokes opertors of both signal states as shown in Fig. 5(a). Finally, we compare the average values to the upper bound of the variance given by the Expectation Value Matrix method (Fig. 5(b)). We find that for signal amplitudes below 0.45, effective entanglement is verified in our system.

5. Conclusion

In conclusion, we present a fiber-based continuous-variable quantum key distribution system. We demonstrate a receiver module, which simultaneously measures conjugate Stokes operators of light. This is the first simultaneous detection of conjugate Stokes operator of a quantum signal after a fiber channel. From the measured Q-function of the transmitted signal, we estimate the attenuation and the excess noise caused by the channel. For the measured amount of excess noise, the theory has not progressed far enough to generate an unconditionally secure and secret key. Nevertheless, we successfully witness effective entanglement with a channel length of up to 2 km considering both parts of the quantum signal, the signal and the LO mode.

Acknowledgement

The authors would like to thank Georgy Onishchukov for fruitful discussions and complementary hardware.

#120058 - $15.00 USD Received 16 Nov 2009; revised 1 Feb 2010; accepted 2 Feb 2010; published 19 Feb 2010

PHYSICAL REVIEW D **81,** 046002 (2010)

Minkowski vacuum transitions in (nongeometric) flux compactifications

Wilberth Herrera-Suárez[1,*] and Oscar Loaiza-Brito[2,†]

[1]*Centro de Investigación y de Estudios Avanzados del I.P.N., Unidad Monterrey Autopista Monterrey-Aeropuerto Km 10, 66600 Apodaca, Nuevo León, México*

[2]*Departamento de Física, División de Ciencias e Ingenierías, Campus León, Universidad de Guanajuato, P.O. Box E-143, León, Guanajuato, México*

(Received 24 August 2009; published 4 February 2010)

In this work we study the generalization of twisted homology to geometric and nongeometric backgrounds. In the process, we describe the necessary conditions to wrap a network of D-branes on twisted cycles. If the cycle is localized in time, we show how by an instantonic brane mediation, some D-branes transform into fluxes on different backgrounds, including nongeometric fluxes. As a consequence, we show that in the case of a IIB six-dimensional torus compactification on a simple orientifold, the flux superpotential is not invariant by this brane-flux transition, allowing the connection among different Minkowski vacuum solutions. For the case in which nongeometric fluxes are turned on, we also discuss some topological restrictions for the transition to occur. In this context, we show that there are some vacuum solutions protected to change by a brane-flux transition.

DOI: 10.1103/PhysRevD.81.046002 PACS numbers: 11.25.Mj, 04.20.Gz

I. INTRODUCTION

Incorporation of fluxes in string theory compactification has been a rich and fertile topic over the last decade [1,2]. Besides the important possibility to stabilize (perturbatively) all moduli at the minimum of a scalar potential generated by the fluxes, the presence of new kinds of fluxes has enriched our comprehension about geometry and topology on the internal spaces on which string theory is compactified.

The traditional way to realize the existence of these new fluxes, comes from performing T duality on a type IIB compactification threaded with Neveu-Schwarz-Neveu-Schwarz (NS-NS) flux. In this way, it is necessary to introduce fluxes referred to as *metric and nongeometric*. In [3] (see also [4] for a review) it was shown that the inclusion of nongeometric fluxes[1] in a tori compactification leads to two important facts. First, that the metric of a torus threaded with nongeometric fluxes (Q space) is not globally defined, and second, that the corresponding IIB superpotential does not preserve S duality.

The first statement means that it is impossible to consistently define one-cycles on the six-dimensional corresponding torus on which some nongeometric flux is supported. The reason for this comes from the application of Buscher rules to the flat torus metric, from which one gets that the metric is not invariant after performing a translation along one coordinate. Hence, the corresponding one-cycle is also ill-defined.

However, if one T dualizes back to the H space, the problem translates into a configuration involving NS-NS flux H_3. Specifically, it is inconsistent to define three-cycles on which the NS-NS-form is supported. This is the classical version of Freed-Witten anomaly [8]. Traditionally, in the literature the anomaly is cancelled by enforcing the pull back of fluxes to the D-branes to vanish. An alternative way to cancel it is to add extra D-branes.

In this context, a NS-NS flux pullbacks on the worldvolume of a D3-brane inducing the term $H_3 \wedge A_1$ over the four-dimensional worldvolume. The equations of motion for the gauge field A_1 are fulfilled once we add magnetic sources, otherwise the system suffers of an anomaly. By adding extra D1-branes ending at the former, the anomaly is cured. T dualizing forward in the appropriate coordinates, leads us to a configuration involving a net of D-branes in which is possible to wrap D1-branes in any one-cycle of the Q space as far as we consider D3-branes with one leg along a noncompact direction, and the other two wrapping internal coordinates, implying that we also require to twist the notion of a form. Notice that in the H space, we can safely take zero-, one- and two-cycles globally, but bigger ones require extra branes if NS-NS flux is present. The same applies for the Q space, but in this case we can only safely consider zero-cycles.

Yet, there are some D-branes that despite of being non-anomalous, could be unstable to decay into fluxes. In this paper, we shall concentrate in the above way to cancel the anomaly which does not require the fluxes to vanish at the D-branes. In terms of forms, the Freed-Witten anomaly implies the existence of an obstruction to define a 3-form supported on the same coordinates as H_3. This makes sense as soon as we think on a cycle as the locus on which we can safely wrap a D-brane [9].

Hence, by considering an adequate set of submanifolds (chains), we can wrap D-branes on generalized cycles

*wherrs@fis.cinvestav.mx

†oloaiza@fisica.ugto.mx

[1]For recent advances in nongeometric flux compactifications, see [5–7].

PHYSICAL REVIEW D **82,** 044008 (2010)

Inflation from supersymmetric quantum cosmology

J. Socorro[1,*] and Marco D'Oleire[2,†]

[1]*Departamento de Física, DCeI, Universidad de Guanajuato-Campus León, A.P. E-143, C.P. 37150, León, Guanajuato, México*
[2]*Facultad de Ciencias de la Universidad Autónoma del Estado de México, Instituto Literario No. 100, Toluca, C.P. 50000, Edo de Mex, México*

(Received 26 March 2010; published 5 August 2010)

We derive a special scalar field potential using the anisotropic Bianchi type I cosmological model from canonical quantum cosmology under determined conditions in the evolution to anisotropic variables $\beta_{\pm}$. In the process, we obtain a family of potentials that has been introduced by hand in the literature to explain cosmological data. Considering supersymmetric quantum cosmology, this family is scanned, fixing the exponential potential as more viable in the inflation scenario $V(\phi) = V_0 e^{-\sqrt{3}\phi}$.

DOI: 10.1103/PhysRevD.82.044008 PACS numbers: 04.60.Kz, 12.60.Jv, 98.80.Jk, 98.80.Qc

I. INTRODUCTION

One of the main problems of inflationary cosmology is to find a mechanism to derive in a natural way the appropriate scalar field potential in order to develop enough e-foldings of inflation. By natural, we understand a mechanism from which some theory provides a scalar field potential that offers the convenient features of inflation. In this work, we derive a scalar field potential from supersymmetric quantum cosmology that gives these conditions.

In a previous work, we determined scalar potentials from an exact solution to the Wheeler-DeWitt (WDW) equation in the quantum cosmology scenario [1], using as a toy model a homogenous and isotropic cosmological model. There we focus on solutions that may be relevant for the early universe constructed within the WKB approximation. Recently, these scalars potentials were obtained using a local supersymmetric scheme [2]. Nowadays it is a common issue in cosmology to make use of scalar fields ϕ as the responsible agents of some of the most intriguing aspects of our universe [3–11], such as inflation [12,13], dark matter, and dark energy [14]. The natural derivation of a scalar potential is a challenge, posing the following question: What physical processes provide the adequate scalar field potentials that govern the universe in determined epoch? To answer this question, we use the ideas of quantum cosmology to solve the Wheeler-DeWitt equation with a particular ansatz for the Bianchi type I universe wave function. In this scheme, we obtain two possible scenarios, the first one with a scalar exponential potential $V(\phi) = V_0 e^{\lambda\phi}$, and the second one giving a family of potentials, similar to those obtained in our previous work [1]. It is interesting that in the first scenario the λ parameter is not fixed by the quantum scheme, remaining as a free parameter of the theory. To fix it, we invoke a supersymmetric scale, using the tools of supersymmetric quantum cosmology in order to find the most viable scalar potential for the inflationary epoch, in this scale. To do this, we applied supersymmetry as a square root of general relativity [15–18], in which the Grassmann variables are only auxiliary and cannot be identified as the supersymmetric partners of the cosmological bosonic variables. Therefore, we construct a family of scalar potentials treating the quantum solutions to anisotropic Bianchi type I cosmological model in the anisotropic variables β_+ and β_-. The conditions we use give us a special structure for the scalar potential; by simplifying the Wheeler-DeWitt equation we obtain two cases: one in which both parameters $\beta_{\pm}$ have hyperbolic trigonometric functions as solutions, and another where β_- (β_+) have a trigonometric (hyperbolic trigonometric) behavior. This potential is also a good candidate, depending on the parameter value, in order to study inflation, dark matter, dark energy, or tachyon models [19]. The transform Wheeler-DeWitt equation can be solved using a particular ansatz in the WKB approximation (Bohmian representation [20]). This method has been used in the literature [21] to solve the cosmological Bianchi class A models, and in a particular, our result in the second case is similar to the one found in Ref. [1] for the isotropic Friedmann-Robertson-Walker (FRW) cosmological model. On the other hand, the best candidates for quantum solutions become those that have a damping behavior with respect to the scale factor, in the sense that we obtain a good classical solution using the WKB approximation in any scenario in the evolution of our universe [22,23]. The supersymmetric scheme has the particularity that is very restrictive because there are more constraints equations applied to the wave function. So, in this work we found that there exists a tendency for supersymmetric vacua to remain close to their semiclassical limits, because the exact solutions found are also the lowest-order WKB approximation, and do not correspond to the full quantum solutions found previously.

*socorro@fisica.ugto.mx
†marcodoleire@gmail.com

Anisotropic cosmology in Sáez-Ballester theory: classical and quantum solutions

J. Socorro* and M. Sabido**
Departamento de Física, DCeI, Universidad de Guanajuato-Campus León, Apartado Postal E-143, 37150, Guanajuato, México.

M.A. Sánchez and M.G. Frías Palos
Facultad de Ciencias de la Universidad Autónoma del Estado de México, Instituto Literario No. 100, Toluca, 50000, Edo de Mex, México.

Recibido el 25 de noviembre de 2009; aceptado el 16 de marzo de 2010

We use the Sáez-Ballester theory on anisotropic Bianchi I cosmological model, with barotropic flui and cosmological constant. We obtain the classical solution by using the Hamilton-Jacobi approach. Also the quantum regime is constructed and exact solutions to the Wheeler-DeWitt equation are found.

Keywords: Classical and quantum exact solutions; cosmology.

Usamos la teoría de Sáez-Ballester en el modelo anisotrópico Bianchi I con un fluid barotrópico y constante cosmológica. Obtenemos las soluciones clásicas usando el enfoque de Hamilton-Jacobi. El regimen cuántico también es construido y soluciones exactas a la ecuación de Wheeler-DeWitt son encontradas.

Descriptores: Soluciones clásicas y cuánticas exactas; cosmología.

PACS: 02.30.Jr; 04.60.Kz; 12.60.Jv; 98.80.Qc.

1. Introduction

In the 80's Saez and Ballester [1] formulated a scalar-tensor theory of gravity in which the metric is coupled to a dimensionless scalar field several papers in the classical regime have been written [2-5], yet a study of anisotropic models, where the anisotropy is introduced in the line element, has been connected. In this theory of gravity the strength of the coupling between gravity and the scalar fiel is determined by an arbitrary coupling function ω; one particularly interesting result is the appearance of an antigravity regime, which suggests a possible connection to the missing matter problem in non-fla FRW cosmologies. In particular, Armendariz-Picon, *et al.*, related this scenario to *K-essence* [6], which is characterized by a scalar fiel with a non-canonical kinetic energy. Usually K-essence models are restricted to lagrangian densities of the form

$$\mathrm{S} = \int \mathrm{d}^4\mathrm{x}\,\sqrt{-\mathrm{g}}\,\mathrm{f}(\phi)\,(\nabla\phi)^2\,; \tag{1}$$

one of the motivations for considering this type of lagrangian originates from string theory [7] and is relation to the Dark energy problem (for more details for K-essence applied to dark energy, see Ref. 8 and reference therein).

Furthermore, the quantization program of the theory is an open problem; this is related to the difficultie of building the ADM formalism. In order to proceed with the quantization program, we transform this theory to a conventional one, by interpreting the dimensionless scalar fiel as part of the energy-momentum tensor as an exotic matter component; this is achieved by an appropriate transformation of the coupling function ω, so that we can use this modifie theory where the ADM formalism is well known [9].

In this paper we use this formulation to obtain classical and quantum solutions for the anisotropic Bianchi type I cosmological model with cosmological constant Λ. The firs step is to write Sáez-Ballester formalism in the usual manner, that is, we calculate the corresponding energy-momentum tensor to the scalar fiel and give the equivalent lagrangian density. Next, we proceed to obtain the corresponding canonical lagrangian for the Bianchi type I metric and calculate the classical hamiltonian constraint $\mathcal{H}$, and finall fin the Wheeler-DeWitt (WDW) equation for the model.

The simplest generalization of the lagrangian density for the Sáez-Ballester theory [1] with cosmological constant, is

$$\mathcal{L}_{\mathrm{geo}} = (\mathrm{R} - 2\Lambda - \mathrm{F}(\phi)\phi_{,\gamma}\phi^{,\gamma})\,, \tag{2}$$

where $\phi^{,\gamma} = g^{\gamma\alpha}\phi_{,\alpha}$, R is the scalar curvature, and $F(\phi)$ a dimensionless functional of the scalar field In classical fiel theory, this formalism corresponds to null potential for ϕ, but with an exotic kinetic term due to the presence of $F(\phi)$.

From the lagrangian (2) we can build the complete action

$$\mathrm{I} = \int\limits_{\Sigma} \sqrt{-\mathrm{g}}(\mathcal{L}_{\mathrm{geo}} + \mathcal{L}_{\mathrm{mat}})\mathrm{d}^4\mathrm{x}, \tag{3}$$

where $\mathcal{L}_{mat}$ is the matter lagrangian, and g is the determinant of metric tensor. The fiel equations for this theory are

$$\mathrm{G}_{\alpha\beta}+\mathrm{g}_{\alpha\beta}\Lambda-\mathrm{F}(\phi)\left(\phi_{,\alpha}\phi_{,\beta}-\frac{1}{2}\mathrm{g}_{\alpha\beta}\phi_{,\gamma}\phi^{,\gamma}\right)=8\pi\mathcal{G}\mathrm{T}_{\alpha\beta},$$

$$2\mathrm{F}(\phi)\phi^{;\alpha}_{;\alpha}+\frac{\mathrm{dF}}{\mathrm{d}\phi}\phi_{,\gamma}\phi^{,\gamma}=0, \tag{4}$$

where $\mathcal{G}$ is the gravitational constant and as usual the semicolon means a covariant derivative.

PHYSICAL REVIEW D **84,** 096011 (2011)

Lepton number violation in top quark and neutral *B* meson decays

David Delepine,[1,*] G. López Castro,[2,†] and N. Quintero[2,‡]

[1]*Division de Ciencias e Ingenierías, Universidad de Guanajuato, Campus Leon, C.P. 37150, León, Guanajuato, México*

[2]*Departamento de Física, Centro de Investigación y de Estudios Avanzados, Apartado Postal 14-740, 07000 México D.F., México*

(Received 31 August 2011; published 17 November 2011)

Lepton number violation can be induced by Majorana neutrinos in four-body decays of the neutral B meson and the top quark. We study the effects of Majorana neutrinos in these $|\Delta L| = 2$ decays in a scenario where a single heavy neutrino can enhance the amplitude via the resonant mechanism. Using current bounds on heavy neutrino mixings, the most optimistic branching ratios turn out to be at the level of 10^{-6} for $\bar{B}^0 \to D^+ e^- e^- \pi^+$ and $t \to b l^+ l^+ W^-$ decays. Searches for these lepton number violation decays at future facilities can provide complementary constraints on masses and mixings of Majorana neutrinos.

DOI: 10.1103/PhysRevD.84.096011 PACS numbers: 11.30.Fs, 13.20.He, 14.60.Pq, 14.60.St

I. INTRODUCTION

After being established that neutrinos are massive and mixed particles [1–3], one of the most interesting current issues in flavor physics is to elucidate if neutrinos are Dirac or Majorana fermions [4]. If neutrinos turn out to be Majorana particles, important consequences as lepton number-violating (LNV) processes [5,6] and further sources of CP violation become possible [7–10]. Searches for LNV processes (where the lepton number is violated in two units, $\Delta L = 2$) in dedicated low energy experiments as neutrinoless double beta decays, have led to very strong constraints on the effective mass of light Majorana neutrinos [11–15] since the rates for these processes are driven by the effective mass parameter $\langle m_{ee} \rangle$ [16]. On the other hand, very restrictive bounds on $\langle m_{ll'} \rangle$ can be obtained by combining neutrino oscillation data [17], cosmological bounds [18–21] and tritium beta decay [22]. Interestingly, these sub-eV bounds on the scale of effective Majorana masses are at the sensitivity reaches of current experimental projects [23–26].

As it has been extensively discussed by many authors, the existence of very light neutrinos may find a natural explanation by means of heavy neutrinos via the seesaw mechanism [27–33]. Heavy neutrinos naturally appears in some extensions of the standard model and may play an important role in cosmology and various particle physics and astrophysical processes [34,35]. The possibility to observe the effects of heavier neutrinos, accessible in the kinematical range of current experiments, is very exciting as they can induce large rates for $\Delta L = 2$ decays through the mechanism of resonant enhancement [35]. Indeed, the appearance of sterile neutrinos with masses in the range of hundreds of MeV's to a few GeV's is possible in scenarios of dynamical electroweak symmetry breaking as shown for instance in [36–38]. By means of the resonant mechanism, neutrinos with these intermediate mass scales can produce an enhancement in the three-body $\Delta L = 2$ decays of pseudoscalar mesons $M_1^+ \to l^+ l^+ M_2^-$ and the tau lepton $\tau^- \to l^+ M_1^- M_2^-$; these decay processes have been extensively studied by many authors [35,39–43] in the cases where final state hadrons can be pseudoscalar or vector mesons. So far, some experimental uppers bounds have been reported in Refs. [44–47] in the case of heavy meson decays; very recently, by using 36 pb^{-1} of integrated luminosity, the LHCb Collaboration has reported improved upper limits for LNV charged B meson decays $B(B^+ \to K^-(\pi^-)\mu^+\mu^+) < 5.8(5.4) \times 10^{-8}$ at the 95% C.L. [48]. These studies are expected to be extended by the LHCb experiment by including the $B^+ \to D^-_{(s)}\mu^+\mu^+$, $\bar{D}^0\mu^+\mu^+\pi^-$ decay modes [48], which together with similar analyses that can be performed at the SuperB Flavor Factories [49] makes very attractive the studies of LNV B meson decays. Similarly, like-sign dileptons may be produced via the resonance enhancement mechanism in four-body decays of top quarks and W gauge bosons, as it has been investigated for instance in Refs. [50–52].

In the present paper we consider the four-body decays of neutral B mesons, $\bar{B}^0 \to D^+ l^- l^- \pi^+$ with $l = e$, μ, in the favored scenario of resonant neutrino enhancement. The dynamics of this four-body decay involves the transition $B \to D$ form factors and is different from the one driving the three-body decays of mesons and tau leptons which involve the meson decay constants. To our knowledge, these $\Delta L = 2$ decays of neutral B mesons have not been investigated before neither from a theoretical nor from an experimental point of view. In addition, we also consider and update the analogous four-body $t \to b l^+ l^+ W^-$ decays ($l = e$, μ, τ), which was previously studied in [50], since one naively expects it can be largely enhanced due to the resonances in the virtual W boson and heavy neutrino exchanges.

*delepine@fisica.ugto.mx
†glopez@fis.cinvestav.mx
‡nquintero@fis.cinvestav.mx

Physics Letters B 705 (2011) 361–368

Contents lists available at SciVerse ScienceDirect

Physics Letters B

www.elsevier.com/locate/physletb

Supersymmetric contribution to $B \to \rho K$ and $B \to \pi K^*$ decays in SCET

Gaber Faisel [a,b,*], David Delepine [c], M. Shalaby [d]

[a] Department of Physics and Center for Mathematics and Theoretical Physics, National Central University, Chung-li, 32054, Taiwan
[b] Egyptian Center for Theoretical Physics, Modern University for Information and Technology, Cairo, Egypt
[c] Departamento de Física, DCI, Campus León, Universidad de Guanajuato, C.P. 37150, León, Guanajuato, Mexico
[d] Ain Shams University, Faculty of Science, Cairo 11566, Egypt

ARTICLE INFO

Article history:
Received 15 February 2011
Received in revised form 4 October 2011
Accepted 18 October 2011
Available online 20 October 2011
Editor: T. Yanagida

ABSTRACT

We analyze the supersymmetric contributions to the direct CP asymmetries of the decays $B \to \pi K^*$ and $B \to \rho K$ within Soft Collinear Effective Theory. We extend the Standard Model analysis of these asymmetries to include the next leading order QCD corrections. We find that, even with QCD correction, the Standard Model predictions cannot accommodate the direct CP asymmetries in these decay modes. Using Mass Insertion Approximation (MIA), we show that non-minimal flavor SUSY contributions mediated by gluino exchange can enhance the CP asymmetries significantly and thus can accommodate the experimental results.

1. Introduction

In the standard model (SM), Charge conjugation Parity (CP) violation and flavor transition arise from the complex Yukawa couplings in the Cabibbo Kobayashi Maskawa (CKM) matrix. The effect of this phase has been first observed in kaon system and confirmed in B decays. However, the expected CP asymmetries in some decay channels for B meson are in contradiction with the experimental measurements carried by Babar and Belle B-factories and proton antiproton collider as Tevatron, with its experiments CDF and D0. The largest discrepancy has been observed in the decay $B \to K\pi$ where the world averages for the CP asymmetries of $B^0 \to K^\pm\pi^\mp$ and $B^\pm \to K^\pm\pi^0$ are given by [1]:

$$\mathcal{A}_{\rm CP}\big(B^0 \to K^\pm\pi^\mp\big) = -0.098 \pm 0.012, \tag{1}$$

$$\mathcal{A}_{\rm CP}\big(B^\pm \to K^\pm\pi^0\big) = 0.050 \pm 0.025, \tag{2}$$

which implies that

$$\Delta\mathcal{A}_{\rm CP} = \mathcal{A}_{\rm CP}\big(B^\pm \to K^\pm\pi^0\big) - \mathcal{A}_{\rm CP}\big(B^0 \to K^\pm\pi^\mp\big) = 0.14 \pm 0.029. \tag{3}$$

In the SM and using QCD factorization approach, the results of the above two asymmetries read [2]:

$$\mathcal{A}_{\rm CP}\big(B^\pm \to K^\pm\pi^0\big) = \big(7.1^{+1.7+2.0+0.8+9.0}_{-1.8-2.0-0.6-9.7}\big)\%, \tag{4}$$

$$\mathcal{A}_{\rm CP}\big(B^0 \to K^\pm\pi^\mp\big) = \big(4.5^{+1.1+2.2+0.5+8.7}_{-1.1-2.5-0.6-9.5}\big)\%, \tag{5}$$

where the first error corresponds to uncertainties on the CKM parameters and the other three errors correspond to variation of various hadronic parameters. These results imply that $\Delta\mathcal{A}_{\rm CP}^{\rm QCD} = 0.025 \pm 0.015$, which differs from the experimental value by 3.5σ and thus motivate exploring new physics beyond SM.

The decay modes $B \to \pi K^*$ and $B \to \rho K$ are generated at the quark level in the same way as $B \to K\pi$ and hence it is interesting to explore hints of New Physics (NP) in these decays. These decay modes are studied within SM in framework of QCDF [2], PQCD [3,4,6,5] and Soft Collinear Effective Theory (SCET) [7]. A detailed comparison between the results for the branching ratios and CP asymmetries in these different factorizations methods can be found in Ref. [7]. The comparison showed that PQCD results for most $B \to \pi K^*$ and $B \to \rho K$ channels are much larger than SCET results. On the other hand the QCDF results are small and comparable with SCET results but with a relative minus sign. Moreover, in SCET, the direct CP asymmetries of $B^- \to \pi^-\bar{K}^{*0}$ and $B^- \to \rho^-\bar{K}^0$ are zero while the CP asymmetries in other channels are small. Recently, in Ref. [8] fits to $B \to \pi K^*$ and $B \to \rho K$ decays are performed where data can be accommodated within the standard model due principally to the large experimental uncertainties, particularly in the CP-violating asymmetries.

One of the four large experiments operating at the Large Hadron Collider (LHC) is LHCb. The main task of the LHCb is to measure precisely the CP asymmetries in B meson decays. These measurements are so important to test the different mechanisms proposed by many models beyond SM to explain the matter–antimatter asymmetry. This test can be regarded as an indirect search for physics beyond SM.

* Corresponding author at: Department of Physics and Center for Mathematics and Theoretical Physics, National Central University, Chung-li, 32054, Taiwan.
E-mail address: gfaisel@cc.ncu.edu.tw (G. Faisel).

0370-2693/$ – see front matter
doi:10.1016/j.physletb.2011.10.041

PHYSICAL REVIEW D **84,** 033008 (2011)

Dynamical symmetry breaking with a fourth generation

D. Delepine,* M. Napsuciale,† and C. A. Vaquera-Araujo‡

Departamento de Física, Universidad de Guanajuato, Campus León, C.P. 37150, León, Guanajuato, México

(Received 2 April 2010; revised manuscript received 25 July 2011; published 15 August 2011)

Adding a fourth generation to the standard model and assuming it to be valid up to some cutoff Λ, we show that electroweak symmetry is broken by radiative corrections due to the fourth generation. The effects of the fourth generation are isolated using a Lagrangian with a genuine scalar without self-interactions at the classical level. For masses of the fourth generation consistent with electroweak precision data (including the $B \to K\pi$ *CP* asymmetries), we obtain a Higgs mass of the order of a few hundreds GeV and a cutoff Λ around 1–2 TeV. We study the reliability of the perturbative treatment used to obtain these results taking into account the running of the Yukawa couplings of the fourth quark generation with the aid of the renormalization group equations, finding similar allowed values for the Higgs mass but a slightly lower cutoff due to the breaking of the perturbative regime. Such low cutoff means that the effects of new physics needed to describe electroweak interactions at energy above Λ should be measurable at the LHC. We use the minimal supersymmetric extension of the standard model with four generations as an explicit example of models realizing the dynamical electroweak symmetry breaking by radiative corrections and containing new physics. Here, the cutoff is replaced by the masses of the squarks and electroweak symmetry breaking by radiative corrections requires the squark masses to be of the order of 1 TeV.

DOI: 10.1103/PhysRevD.84.033008 PACS numbers: 12.15.Lk, 12.60.Jv, 14.80.Bn

I. INTRODUCTION

Many experimental results on B physics (see [1]) can be seen as hints of physics beyond the standard model (SM). Electroweak precision data also points to new physics scenarios [2]. In the LHC era, new physics related to the observability of the Higgs boson is worthy to study and the elucidation of the Higgs sector properties is a topic of utmost importance.

A simple extension of the standard model (SM) is the introduction of a new generation of quarks and leptons (SM4). Precision data do not exclude the existence of a sequential fourth generation [3–8]. An extensive review and an exhaustive list of references to the work on the subject previous to our century can be found in [9]. Recent highlights on consequences of a fourth generation can be found in [10]. These include mechanisms of dynamical electroweak symmetry breaking by condensates of fourth generation quarks and leptons [11–14], convergence improvement of the three SM gauge couplings due to the Yukawa coupling contributions from the fourth generation [15], the possibility of electroweak baryogenesis through first-order electroweak phase transition with four generations [16–18], *CP* violation based on Jarlskog invariants generalized to four generations [19], and the hierarchy problem [20].

The $B \to K\pi$ *CP* asymmetries puzzles can also be easily solved by a fourth generation [21–23] for a range of extra quark masses within the values allowed by high precision LEP measurements [3–5], namely [24]

$$\begin{aligned} &m_{\ell_4} - m_{\nu_4} \simeq 30\text{–}60\ \text{GeV} \\ &m_{u_4} - m_{d_4} \simeq \left(1 + \frac{1}{5}\ln\frac{m_H}{115\ \text{GeV}}\right) \times 50\ \text{GeV} \\ &|V_{ud_4}|, |V_{u_4 d}| \lesssim 0.04 \\ &|U_{\ell_4}|, |U_{\mu_4}| \lesssim 0.02, \end{aligned} \tag{1}$$

where V (U) is the Cabibbo-Kobayashi-Maskawa (Maki-Nakagawa-Sakata) quark (lepton) mixing matrix which is now a 4×4 unitary matrix. These bounds are subject to direct search limits from LEPII [25] and CDF [26,27]:

$$m_{\nu_4,\ell_4} > 100\,\text{GeV} \quad m_{u_4} > 311\,\text{GeV} \quad m_{d_4} > 338\,\text{GeV}. \tag{2}$$

In Refs. [21–23], in order to solve the *CP* asymmetry puzzles in $B \to K\pi$, one needs the extra quarks to be within the following range [21]:

$$400\ \text{GeV} < m_{u_4} < 600\ \text{GeV}. \tag{3}$$

Such values of new quark masses imply strong Yukawa couplings. So, it is natural to expect that this fourth generation could play a special role in the electroweak symmetry breaking (EWSB). Contrary to other works where it is assumed that Yukawa couplings are strong enough to produce composite scalars at low energy [11–14], we shall assume that the perturbative treatment [28] is still valid. This assumption is justified by the fact that even fourth generation masses in the range of 300–600 GeV imply Yukawa couplings (g_f) around 2–3. In the loop expansion,

*delepine@fisica.ugto.mx
†mauro@fisica.ugto.mx
‡vaquera@fisica.ugto.mx

Printed ISSN 1330–0016
Online ISSN 1333–9133
CD ISSN 1333–8390
CODEN FIZBE7

CLASSICAL AND QUANTUM COSMOLOGY OF THE SÁEZ-BALLESTER THEORY

M. SABIDO, J. SOCORRO and L. ARTURO UREÑA-LÓPEZ

Departamento de Física, DCeI, Universidad de Guanajuato-Campus León, A.P. E-143, C.P. 37150, Guanajuato, México
E-mail addresses: msabido@fisica.ugto.mx, socorro@fisica.ugto.mx, lurena@fisica.ugto.mx

Received 1 June 2010; Revised manuscript received 14 December 2010
Accepted 26 January 2011 Online 7 March 2011

We study the generalization of the Sáez-Ballester theory for a flat FRW cosmology. Classical solutions are obtained by using the Hamilton-Jacobi approach. Contrary to claims in the literature, it is shown that the Sáez-Ballester theory cannot provide a realistic solution to the dark matter problem. Furthermore, the quantization procedure of the theory can be simplified by reinterpreting the theory in the Einstein frame, where the scalar field can be considered as part of the matter content of the theory. Finally, exact solutions are found for the Wheeler-DeWitt equation.

PACS numbers: 04.20.Fy, 04.20.Jb, 04.60.Kz, 98.80.Qc UDC 524.83

Keywords: Sáez-Ballester theory, generalization, flat FRW cosmology, quantization procedure, solutions of Wheeler-DeWitt equation

1. Introduction

The inclusion of scalar fields to homogeneous cosmologies is a typical practice in different scenarios, such as inflation, dark matter, and dark energy [1]. Since the early seventies, the problem of finding the appropriate sources of matter and its corresponding Lagrangian to describe particular scenarios has been studied [2, 3]. An interesting approach was presented by Sáez and Ballester (SB) [4], a scalar-tensor theory of gravity where the metric is coupled to a dimensionless scalar field.

Despite the dimensionless character of the scalar field, an antigravity regime appears, and has been proposed as a possible way to solve the missing-matter problem in non-flat Friedmann-Robertson-Walker (FRW) cosmologies [5, 6, 7, 8]. Also, Armendariz-Picon et al. called this scenario as *K-essence* [9], which is characterized by a scalar field with a non-canonical kinetic energy.

PHYSICAL REVIEW D **84,** 027503 (2011)

Cosmological dark fluid from five-dimensional vacuum

Luz M. Reyes,* José Edgar Madriz-Aguilar,† and L. Arturo Ureña-López‡

Departamento de Física, DCI, Campus León, Universidad de Guanajuato, 37150, León, Guanajuato, Mexico

(Received 10 March 2011; published 26 July 2011)

In the framework of the induced matter theory of gravity, we derive a five-dimensional solution of the field equations that can describe a four-dimensional cosmological scenario where the dark fluid (dark matter plus dark energy) equation of state has a geometrical origin. There is not a natural separation of the dark sector into different components, and so the model may provide a geometrical explanation for the existence of a dark degeneracy in cosmological scenarios.

DOI: 10.1103/PhysRevD.84.027503 PACS numbers: 04.50.−h, 95.35.+d, 95.36.+x

I. INTRODUCTION

The idea of the existence of exotic components in the Universe, namely, dark matter and dark energy, comes basically from three pieces of observational evidence: supernovae of the type Ia, surveys of clusters of galaxies, and observations of anisotropies in the cosmic microwave background radiation [1]. Observations of high redshift of type Ia supernovae suggest that the expansion of the Universe is accelerating [2–4]. Surveys of clusters of galaxies indicate that the energy density of matter is less than the critical density of the Universe [5], whereas observations of the temperature anisotropies of the cosmic microwave background show evidence that our Universe is spatially flat, and so the total energy density parameter is very close to the critical one [6].

In obtaining these observational constraints, it has been considered the model assumption that there are two separated dark components: dark matter, responsible for the formation of cosmological structure, and dark energy, responsible for the accelerated expansion of the Universe. From this arises the so-called standard cosmological model, also known as ΛCDM, where dark matter is a (cold) pressureless fluid and the dark energy is described by a cosmological constant [1,6].

However, the observations through which these two components have been detected are gravitational in nature, and these kinds of measurements are unable to provide information about a unique decomposition of the dark sector into these components [7]. As clearly argued in [8], when we are in a state of total ignorance about the nature of a single one of the dark components, we can also not completely measure the others.

In this case, the separation into dark matter and dark energy can be seen as a convenient parametrization without experimental reality. In models where this split is assumed, it is necessary to impose some additional conditions upon the models in order to make the assumption well-defined. These conditions can be that the dark energy vanishes at high redshift, or that the dark energy constitutes the nonclustering part of the dark energy-momentum tensor. The lack of guidance of gravity observations leads to the so-called dark degeneracy [8].

Theoretically, a great effort has been made to construct models to explain dark energy. In the literature, we can find proposals, among others, like quintessence models, interacting models of dark energy, k-essence models, and proposals coming from modified theories of gravity [9] (see also[10–12] and references therein). Other alternatives are models based in theories with extra dimensions, like the induced matter (IM) theory of gravity [13,14] and brane world (BW) scenarios [15].

In BW scenarios, the four-dimensional (4D) universe is viewed as a hypersurface called the brane, which is embedded in a higher dimensional spacetime called the bulk. In this context, ordinary matter is confined to the brane by a variety of different mechanisms, while gravity can propagate freely through the bulk.

Parallel to BW scenarios we have the IM theory. This theory can be considered as an extension of 4D general relativity to 5D. In this approach, our Universe is described by a 4D hypersurface embedded in a 5D Ricci-flat (${}^{(5)}R_{ab} = 0$) spacetime. The extra dimension is considered as noncompact, and classical sources of matter in 4D are identified with the curvature of the 4D hypersurface. This curvature is a consequence of the embedding [14].

The IM theory is mathematically supported by the Campbell-Magaard theorem, which states that any analytical solution of the n-dimensional Einstein equations can be embedded in a $(n + 1)$-dimensional Ricci-flat manifold [16–18]. Both the BW and the IM theory have different physical motivations; an equivalence to each other has been shown by Ponce de Leon in [19]. In spite of such an equivalence, the requirement in IM theory of starting from a 5D Ricci-flat spacetime makes the task of finding solutions easier than in the BW theories.

The purpose of this paper is to derive a particular solution to the 5D field equations of the IM theory capable of describing not just the dark energy component of the

*luzreyes@fisica.ugto.mx
†jemadriz@fisica.ugto.mx
‡lurena@fisica.ugto.mx

PHYSICAL REVIEW D **84,** 044052 (2011)

Black holes and the absorption rate of cosmological scalar fields

L. Arturo Ureña-López* and Lizbeth M. Fernández†

Departamento de Física, DCI, Campus León, Universidad de Guanajuato, 37150, León, Guanajuato, México

(Received 19 July 2011; published 24 August 2011)

We study the absorption of a massless scalar field by a static black hole. Using the continuity equation that arises from the Klein-Gordon equation, it is possible to define a normalized absorption rate $\Gamma(t)$ for the scalar field as it falls into the black hole. It is found that the absorption mainly depends upon the characteristics wavelengths involved in the physical system: the mean wave number and the width of the wave packet, but that it is insensitive to the scalar field's strength. By taking a limiting procedure, we determine the minimum absorption fraction of the scalar field's mass by the black hole, which is around 50%.

DOI: 10.1103/PhysRevD.84.044052 PACS numbers: 04.40.−b, 04.25.D−, 95.35.+d, 95.36.+x

I. INTRODUCTION

Black holes, a concept that emerged from the simplest exact solution of Einstein's equations, are some of the most fascinating objects in gravitational physics. Equally fascinating is our current belief that most galaxies must host a *supermassive* black hole (SMBH) in their center, with mass values in the range of 10^5 to 10^{10} solar masses, most likely in a state of very low matter accretion nowadays [1,2]. In particular, the measurements of the velocities of stars near the center of the Milky Way have provided strong evidence for the presence of a SBH with a mass of around $4 \times 10^6 M_\odot$ [2].

There are some models that attempt to explain the present existence of galactic SMBH's. Among others, we can mention the collision of two or more black holes to form a larger one, the core collapse of a stellar cluster, and the formation of primordial black holes directly out from the primordial plasma in the first instants of time after the big bang [3].

The key point in the discussion are the features of the precise mechanism under which a black hole can accrete enough matter to become supermassive. In particular, some authors have proposed that primordial black holes (PBH) can go supermassive simply by accreting matter from a cosmological scalar field related to dark energy (quintessence). In a first study, the authors in [4] (see also [5–7]) found that PBH could have effectively accreted enough matter from a quintessence field endowed with an exponential potential.

The calculations for the accretion were in fact based upon the simple and exact results of the accretion of a massless scalar field into a black hole found in [8], see also [7,9,10]. However, the results in [4] were later refuted in [11], where it was shown that the quintessence flux must decrease slower than t^{-2} for PBHs to grow at all. This same result seems to have been confirmed by other authors under more general assumptions [9,10,12].

On the other hand, a related topic is the use of a cosmological scalar field as a model for dark matter in the Universe [13], and the possibility that they can be the dominant matter in galaxy halos [14]. If so, then one has to address the accretion of this dark matter scalar field into the central SBH that seems to be present in most galaxies [15,16].

The aim of this paper is to present some simple results of the interaction of a scalar field with a black hole, with numerical calculations based upon previous works in the literature [17] that may be useful in the understanding of the accretion, in general terms, of cosmological scalar fields into black holes.

We shall make use of the fact that there exists a *continuity equation* of the scalar field as long as the background spacetime is static [17]. This fact will allow us to quantify the absorption rate of a scalar wave packet by a black hole in a more precise manner in terms of absorption flux and decay rates. For simplicity, we will only focus our attention in the case of a massless scalar field.

A brief summary of the paper is as follows. In Sec. II we set the mathematical background for the equations of motion, boundary conditions, and initial conditions for the scalar field's wave packet. Here we also show the existence of a continuity equation arising directly from the equation of motion of the scalar field. In Sec. III, we present the main numerical results, and the description of the fall of the scalar field in terms of a normalized absorption rate. The latter arises naturally from the use of the continuity equation found in Sec. II. Finally, Sec. IV is devoted to conclusions and final comments.

II. MATHEMATICAL BACKGROUND

We first consider a fixed Schwarzschild background with an Eddinton-Finkelstein (EF) gauge, which is defined such that $t + r$ is an ingoing null coordinate. Using the $3 + 1$ decomposition of the metric [17,18], the 3-metric γ_{ij} is

*lurena@fisica.ugto.mx
†lizbeth@fisica.ugto.mx

PHYSICAL REVIEW D **84,** 024015 (2011)

Towards a supersymmetric generalization of the Schwarzschild-(anti)de Sitter space-times

J. C. López-Domínguez,* O. Obregón,† and S. Zacarías‡
Departamento de Física, División de Ciencias e Ingenierías, Campus León, Universidad de Guanajuato, P.O. Box E-143, León, Guanajuato, México
(Received 19 April 2011; published 12 July 2011)

The Wheeler-DeWitt (WDW) equation for the Lambda-Kantowski-Sachs model can also be understood as the WDW-equation corresponding to the Schwarzschild-(anti)deSitter space-times, due to the well-known diffeomorphism between these two metrics. This equation ignores the coordinate patch one chooses and only by imposing coordinate conditions will it be possible to distinguish between black hole or cosmological models. At that point, the foliation parameter t or r will appear in the solution of interest. In this work we supersymmetrize this WDW-equation obtaining an extra term in the potential with two possible signs. We have already, in a similar manner, proposed and analyzed a supersymmetric generalization of a Schwarzschild black hole. The WKB method is then applied, given rise to four classical equations, two for the Schwarzschild-deSitter space-time and another two for the Schwarzschild-anti-deSitter space-time. One can then study the asymptotic cases in which one of two potential terms arising in each Hamiltonian, for each of these space-times, dominates the behavior. One of these limiting (bosonic) cases gives the usual Schwarzschild-(anti)deSitter space-times. We will study here the other four asymptotic regions; they provide six solutions. For the Schwarzschild-deSitter space-time we get two solutions which have singularities at $r = 0$ and r_0^s, and depending on an integration constant C and the sign at the potential due to these SUSY region, they can also present another two singularities in r_h^s and r_c^s. For the Schwarzschild-anti-deSitter space-time the solutions have a singularity at $r = 0$ and depending on the integration constant and the sign of the SUSY potential another singularity can appear at r_+. We find associated masses and, based on the holographic principle, we find also the entropies for the bosonic region, which coincide with the ones obtained by the usual methods. We apply this same procedure to get entropies associated to the supersymmetric asymptotic solutions. Even though we were unable to obtain the complete solution to the model, it is shown that horizons can never be reached because when one would approach the standard horizons (the bosonic region), the relevant term in the potential is the one due to supersymmetry and as mentioned in this asymptotic limit one does not have horizons but instead singularities.

DOI: 10.1103/PhysRevD.84.024015 PACS numbers: 04.70.Bw, 04.60.Ds, 04.60.Kz, 04.65.+e

I. INTRODUCTION

All recently available data from cosmological observations give strong indications that in the framework of inflationary cosmology a nonzero repulsive cosmological constant $\Lambda > 0$, has to be invoked in order to explain the properties of the presently observed Universe [1]. The presence of a cosmological constant alters significantly the asymptotic character of black hole space-times. On the other hand, the anti-deSitter space-time plays a central role in our understanding of the relation between gravity and conformal field theory by means of the well-known and successful AdS-CFT conjecture (for a review, see for example [2]).

Very powerful and sophisticated methods have been developed since the birth of general relativity searching for solutions to its field equations. For a long time it has been known that changing the structure of space-time (i.e. interchanging the coordinates $t \leftrightarrow r$), changes a static solution for a cosmological one and vice versa. The best known case is the Schwarzschild metric that under this particular diffeomorphism transforms into the Kantowski-Sachs metric [3]. This interchange of variables has been recently proposed as a method to generate also new cosmological models from stationary axisymmetric solutions [4]. In string theory, it has been suggested that by interchanging $r \leftrightarrow it$ we can get time-dependent solutions also from static solutions. In this way we may relate Dp-branes solutions to S-brane solutions, i.e. time-dependent backgrounds of the theory [5]. On the other hand, there are proposals to obtain directly S-brane solutions [6]; thus, if cosmological solutions (i.e. S-branes) can be generated from stationary ones (i.e. Dp-branes), this procedure also works the other way around.

For a Schwarzschild black hole, Kuchař [7] has shown how to reconstruct the curvature coordinates T and R (or the Kruskal coordinate U and V) from spherically symmetric initial data. A discussion of the action of space-time diffeomorphism on the quantum geometry is possible by this means. A particular interesting example is the interchange of the curvature coordinates T and R. This choice of coordinates interchanges the static and dynamical

*jlopez@fisica.ugto.mx
†octavio@fisica.ugto.mx
‡szacarias@fisica.ugto.mx

Can noncommutative effects account for the present speed up of the cosmic expansion?

Octavio Obregon* and Israel Quiros†

División de Ciencias e Ingeniería de la Universidad de Guanajuato, A.P. 150, 37150, León, Guanajuato, México

(Received 19 February 2011; revised manuscript received 14 June 2011; published 2 August 2011)

In this paper we investigate to which extent noncommutativity, an intrinsically quantum property, may influence the Friedmann-Robertson-Walker cosmological dynamics at late times/large scales. To our purpose it will be enough to explore the asymptotic properties of the cosmological model in the phase space. Our recipe to build noncommutativity into our model is based in the approach of Ref. [4] and can be summarized in the following steps: i) the Hamiltonian is derived from the Einstein-Hilbert action (plus a self-interacting scalar field action) for a Friedmann-Robertson-Walker space-time with flat spatial sections, ii) canonical quantization recipe is applied, i.e., the mini-superspace variables are promoted to operators, and the WDW equation is written in terms of these variables, iii) noncommutativity in the mini-superspace is achieved through the replacement of the standard product of functions by the Moyal star product in the WDW equation, and, finally, iv) semiclassical cosmological equations are obtained by means of the WKB approximation applied to the (equivalent) modified Hamilton-Jacobi equation. We demonstrate, indeed, that noncommutative effects of the kind considered here can be those responsible for the present speed up of the cosmic expansion.

DOI: 10.1103/PhysRevD.84.044005 PACS numbers: 02.40.Gh, 04.20.Ha, 04.60.Kz, 11.10.Nx

I. INTRODUCTION

Noncommutativity of space-time coordinates, an old idea dated back to 1947 [1], is the simplest expected modification to quantum field theory. Noncommutativity—the central mathematical concept in quantum mechanics—expresses uncertainty in the simultaneous measurement of any pair of conjugate variables, such as position and momentum. In the presence of a strong magnetic field, noncommutativity arises [2], even in a classical context. More recently, noncommutativity has received increased interest in connection with developments in string theory. Attempts to connect M(atrix)-string theory to cosmology on the brane [3] have shown that noncommutativity arises in the former theory.

There are several approaches in the literature to build noncommutativity into field theories. One of the authors and collaborators have explored several of these approaches [4–12]. In some of these formalisms, the assumption of noncommutativity among the space-time coordinates has a consequence that the fields present do not commute themselves. This is the particular case of the Seiberg-Witten map [13] and its generalization by Wess and collaborators [14], in which noncommutative fields are obtained as an (infinite) expansion of the usual commutative fields in the noncommutative parameter. Space-time noncommutativity has as a consequence a different product of functions (the Moyal/star product), which induces noncommutativity among the fields.

In cosmological settings an already well explored way to include the effects of noncommutativity is given in Ref. [4], where deformation of space-time itself is replaced by noncommutativity in mini-superspace instead (see also Refs. [15,16] where similar approaches are applied).[1] The latter proposal is inspired in various related results in the literature, among which we can cite the above mentioned case of the Seiberg-Witten map [6,13,18]. In the case of quantum cosmology, the mini-superspace variables play the role of the coordinates in configuration space.[2] Thus, as stated in [4], it seems reasonable to propose a kind of noncommutativity among these specific gravitational variables. The noncommutative proposal there is formulated in terms of models with a finite number of degrees of freedom, where the Wheeler-DeWitt (WDW) equation resembles a Klein-Gordon equation, this time in terms of the mini-superspace variables. One can then apply the same procedure as in noncommutative quantum mechanics to end up with a noncommutative version of quantum cosmology [21].

In the present paper, we shall investigate the possible effect of noncommutativity in the late-time/large-scale cosmological dynamics. In Ref. [22] the effects of noncommutativity were investigated within a dilatonic cosmological model for an exponential dilaton potential. The existence of such noncommutativity results in a deformed Poisson algebra between the mini-superspace variables and their conjugated momenta. The authors found that noncommutativity modifies the cosmic dynamics at late times. Their result relies, however, on the study

*octavio@fisica.ugto.mx
†iquiros@fisica.ugto.mx

[1]For further consideration of the approach of [4] in the context of extra-dimensional cosmology see, for instance, Ref. [17] and references therein.

[2]See, for instance, Refs. [19,20], for an alternative path integral approach to quantum cosmology.

After-gate attack on a quantum cryptosystem

2011 New J. Phys. 13 013043

(http://iopscience.iop.org/1367-2630/13/1/013043)

New Journal of Physics
The open-access journal for physics

After-gate attack on a quantum cryptosystem

C Wiechers[1,2,3,6], L Lydersen[4,5,6], C Wittmann[1,2,7], D Elser[1,2], J Skaar[4,5], Ch Marquardt[1,2], V Makarov[4] and G Leuchs[1,2]

[1] Max Planck Institute for the Science of Light, Günther-Scharowsky-Straße 1, Bau 24, 91058 Erlangen, Germany
[2] Universität Erlangen-Nürnberg, Staudtstraße 7/B2, 91058 Erlangen, Germany
[3] Departamento de Física, Campus Leon, Universidad de Guanajuato, Loma del Bosque 103, Fracc. Lomas del Campestre, 37150 Leon, Gto, Mexico
[4] Department of Electronics and Telecommunications, Norwegian University of Science and Technology, NO-7491 Trondheim, Norway
[5] University Graduate Center, NO-2027 Kjeller, Norway
E-mail: Christoffer.Wittmann@mpl.mpg.de

New Journal of Physics **13** (2011) 013043 (14pp)
Received 14 September 2010
Published 26 January 2011
Online at http://www.njp.org/
doi:10.1088/1367-2630/13/1/013043

Abstract. We present a method to control the detection events in quantum key distribution systems that use gated single-photon detectors. We employ bright pulses as faked states, timed to arrive at the avalanche photodiodes outside the activation time. The attack can remain unnoticed, since the faked states do not increase the error rate *per se*. This allows for an intercept–resend attack, where an eavesdropper transfers her detection events to the legitimate receiver without causing any errors. As a side effect, afterpulses, originating from accumulated charge carriers in the detectors, increase the error rate. We have experimentally tested detectors of the system id3110 (Clavis2) from ID Quantique. We identify the parameter regime in which the attack is feasible despite the side effect. Furthermore, we outline how simple modifications in the implementation can make the device immune to this attack.

[6] These authors contributed equally to this work.
[7] Author to whom any correspondence should be addressed.

Device Calibration Impacts Security of Quantum Key Distribution

Nitin Jain,[1,2,*] Christoffer Wittmann,[1,2] Lars Lydersen,[3,4] Carlos Wiechers,[1,2,5] Dominique Elser,[1,2]
Christoph Marquardt,[1,2] Vadim Makarov,[3,4] and Gerd Leuchs[1,2]

[1]*Max Planck Institute for the Science of Light, Günther-Scharowsky-Straße 1, Bau 24, 91058 Erlangen, Germany*
[2]*Institut für Optik, Information und Photonik, University of Erlangen-Nuremberg, Staudtstraße 7/B2, 91058 Erlangen, Germany*
[3]*Department of Electronics and Telecommunications, Norwegian University of Science and Technology, NO-7491 Trondheim, Norway*
[4]*University Graduate Center, NO-2027 Kjeller, Norway*
[5]*Departamento de Física, Campus León, Universidad de Guanajuato, Lomas del Bosque 103, Fraccionamiento Lomas del Campestre, 37150, León, Gto, México*

(Received 24 March 2011; published 9 September 2011)

Characterizing the physical channel and calibrating the cryptosystem hardware are prerequisites for establishing a quantum channel for quantum key distribution (QKD). Moreover, an inappropriately implemented calibration routine can open a fatal security loophole. We propose and experimentally demonstrate a method to induce a large temporal detector efficiency mismatch in a commercial QKD system by deceiving a channel length calibration routine. We then devise an optimal and realistic strategy using faked states to break the security of the cryptosystem. A fix for this loophole is also suggested.

DOI: 10.1103/PhysRevLett.107.110501 PACS numbers: 03.67.Dd, 03.67.Ac, 03.67.Hk, 42.50.Ex

Quantum key distribution (QKD) offers unconditionally secure communication as eavesdropping disturbs the transmitted quantum states, which in principle leads to the discovery of the eavesdropper Eve [1]. However, practical QKD implementations may suffer from technological and protocol-operational imperfections that Eve could exploit in order to remain concealed [2,3].

Until now, a variety of eavesdropping strategies have utilized differences between the theoretical model and the practical implementation, arising from (technical) imperfections or deficiencies of the components. Ranging from photon number splitting [4] and Trojan horse [5], to leakage of information in a side channel [6], time shifting [7], and phase remapping [8], several attacks have been proposed and experimentally demonstrated. Recently, proof-of-principle attacks [9–11] based on the concept of faked states [12] have been presented. Eve targets imperfections of avalanche photodiode (APD) based single-photon detectors [13] that allow her to control them remotely.

Another important aspect of QKD security not yet investigated, however, is the calibration of the devices. A QKD protocol requires a classical and a quantum channel; while the former must be authenticated, the latter is merely required to preserve certain properties of the quantum signals [2,14]. The establishment of the quantum channel remains an implicit assumption in security proofs: channel characterization (e.g., channel length) and calibration of the cryptosystem hardware, especially the steps involving two-party communication, have not yet been taken into account. As we show, the calibration of the QKD devices must be carefully implemented, otherwise it is prone to hacks that may strengthen existing (or create new) eavesdropping opportunities for Eve.

In this Letter, we propose and experimentally demonstrate the hacking of a vital calibration sequence during the establishment of the quantum channel in the commercial QKD system model Clavis2 from ID Quantique [15]. Eve induces a parameter mismatch [16] between the detectors that can break the security of the QKD system. Specifically, she causes a temporal separation of the order of 450 ps of the detection efficiencies by deceiving the detection system, shown in Fig. 1. This allows her to control Bob's detection outcomes using time, a parameter already shown to be instrumental in applying a time-shift attack [7]. Alternatively, she could launch a faked-state attack (FSA) [16] for which we calculate the quantum bit error rate (QBER) under realistic conditions. Since FSA is an intercept-resend attack, Eve has full

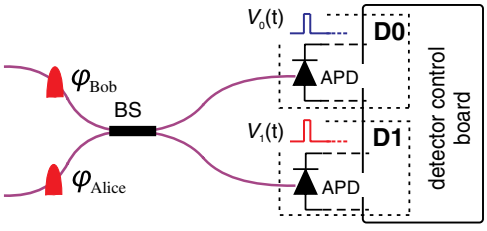

FIG. 1 (color online). Typical detection system in a Mach-Zehnder interferometer based QKD implementation. The bit and basis choices of Alice and Bob (phases φ_{Alice} and φ_{Bob}) determine the interference result at the 50:50 beam splitter (BS), deciding in turn which of the two detectors $D0$ or $D1$ would click. It is thus crucial that $D0$ and $D1$ are indistinguishable to the outside world (i.e., Eve). If gated mode APDs are employed, the detector control board ensures that the activation of $D0$ and $D1$ [via voltage pulses $V_0(t)$ and $V_1(t)$] happens almost simultaneously, to nullify any existing temporal efficiency mismatch.

PHYSICAL REVIEW D **83,** 073001 (2011)

Second order formalism for spin $\frac{1}{2}$ fermions and Compton scattering

E. G. Delgado-Acosta and Mauro Napsuciale
Departamento de Física, Universidad de Guanajuato,
Lomas del Bosque 103, Fraccionamiento Lomas del Campestre, C.P. 37150, León, Guanajuato, México

Simón Rodríguez
Facultad de Ciencias Físico Matemáticas, Universidad Autònoma de Coahuila,
Edificio "D," Unidad Camporredondo, CP 25280, Saltillo, Coahuila, México
(Received 13 January 2011; published 1 April 2011)

We develop a second order formalism for massive spin 1/2 fermions based on the projection over Poincaré invariant subspaces in the $(\frac{1}{2}, 0) \oplus (0, \frac{1}{2})$ representation of the homogeneous Lorentz group. Using the $U(1)_{\rm em}$ gauge principle we obtain a second order description for the electromagnetic interactions of a spin 1/2 fermion with two free parameters, the gyromagnetic factor g and a parameter ξ related to odd-parity Lorentz structures. We calculate Compton scattering in this formalism. In the particular case $g = 2$, $\xi = 0$, and for states with well-defined parity, we recover Dirac results. In general, we find the correct classical limit and a finite value r_c^2 for the forward differential cross section, independent of the photon energy and of the value of the parameters g and ξ. The differential cross section vanishes at high energies for all g, ξ except in the forward direction. The total cross section at high energies vanishes only for $g = 2$, $\xi = 0$. We argue that this formalism is more convenient than Dirac theory in the description of low energy electromagnetic properties of baryons and illustrate the point with the proton case.

DOI: 10.1103/PhysRevD.83.073001 PACS numbers: 12.20.Ds, 13.40.Em, 13.60.Fz, 14.20.Dh

I. INTRODUCTION

States describing a free particle transform in the irreducible representations (irreps) of the Poincaré group. We will denote these states as $|\Gamma\rangle$, where Γ generically denotes the set of good quantum numbers of this group, among which we have the quantum numbers associated with the Casimir operators, the squared four-momentum operator P^2, and the squared Pauli-Lubanski operator W^2. These states can be obtained from the vacuum using the creation and annihilation operators as

$$|\Gamma\rangle = a^\dagger(\Gamma)|0\rangle. \tag{1}$$

The transformation properties of the creation and annihilation operators under the Poincaré group are fixed by this relation. Poincaré invariance of the scattering matrix and cluster decomposition implies the following general form for the fields [1]:

$$\psi_l(x) = \int d\Gamma[\kappa e^{-ip\cdot x} u_l(\Gamma) a(\Gamma) + \lambda e^{ip\cdot x} v_l(\Gamma) a^{c\dagger}(\Gamma)], \tag{2}$$

and $\psi_l(x)$ must transform in some representation of the homogeneous Lorentz group (HLG) which in turn requires (because of the fixed transformation properties of the creation operators) that the coefficients $u_l(\Gamma)$ and $v_l(\Gamma)$ also transform in this representation of the HLG. In this construction, extensively discussed in [1] and which we will adopt here, the coefficients $u_l(\Gamma)$ and $v_l(\Gamma)$ are just the Clebsch-Gordan coefficients to select from the chosen HLG representation the desired Poincaré irrep. The case of particles with well-defined parity in the $(\frac{1}{2}, 0) \oplus (0, \frac{1}{2})$ representation of the HLG can be found in [1] and yields the conventional Dirac formalism where the coefficients $u_l(\Gamma)$ and $v_l(\Gamma)$ are now interpreted as states with well-defined parity. From this point of view, Dirac theory is appropriate for the description of particles with well-defined parity, and it can be shown that the Dirac equation is just the equation for the projection onto well-defined parity states in the $(\frac{1}{2}, 0) \oplus (0, \frac{1}{2})$ representation. Similarly, the conventional Proca equation is just the projection onto a subspace with well-defined parity in the $(\frac{1}{2}, \frac{1}{2})$ representation of the HLG. Unlike the $(\frac{1}{2}, 0) \oplus (0, \frac{1}{2})$ representation which contains only spin 1/2, in the $(\frac{1}{2}, \frac{1}{2})$ case there are two Poincaré sectors, and it can be shown that parity projection and Poincaré projection coincide.

In [2] a formalism was developed for the description of spin 3/2 fields using the projectors over well-defined mass and spin in the spinor-vector representation. These ideas were also applied to the vector representation in [3]. Gauging the formalism to account for electromagnetic interactions, in both cases we obtain a theory containing a free parameter g which can be identified with the gyromagnetic factor. For elementary particles, this parameter is fixed using general arguments. In the spin 3/2 case it is shown in [2] that causality of the interacting theory requires $g_{3/2} = 2$ at tree level. This value for the gyromagnetic factor has been obtained for general fields using unitarity, gauge invariance, and rotational symmetry arguments [4] (see also [5–7]), but to the best of our knowledge has never been related to causality of the interacting theory which historically has been a severe problem for

PHYSICAL REVIEW D **84,** 115010 (2011)

$Z' \to ggg$ decay in left-right symmetric models with three and four fermion families

J. Montaño, M. Napsuciale, and C. A. Vaquera-Araujo

Departamento de Física, Universidad de Guanajuato, Campus León, Lomas del Bosque 103, Fraccionamiento Lomas del Campestre, C.P. 37150, León, Guanajuato, México

(Received 1 December 2010; published 9 December 2011)

We study the $Z' \to \bar{q}q, ggg$ decays in the context of a manifest left-right symmetric gauge theory with three and four generations. The Z' couplings to quarks are fixed essentially by the parameters of the standard model and we obtain $\Gamma(Z' \to q\bar{q}) \approx 14$ GeV for $M_{Z'} \approx 1$ TeV. For the $Z' \to ggg$ decay and three families we obtain a branching ratio $\mathrm{BR}(Z' \to ggg) = \frac{\Gamma(Z' \to ggg)}{\Gamma(Z' \to q\bar{q})} = 1.2 - 2.8 \times 10^{-5}$ for $m_{Z'} =$ 700–1500 GeV. The fourth generation produces an enhancement in the branching ratio for Z' masses close to the $\bar{b}'b'$ threshold and a dip for Z' masses close to the $\bar{t}'t'$ threshold. Using the values of the fourth-generation quark masses allowed by electroweak precision data, we obtain a branching ratio $\mathrm{BR}(Z' \to ggg) = (1 - 6) \times 10^{-5}$ for $m_{Z'} =$ (700–1500) GeV.

DOI: 10.1103/PhysRevD.84.115010 PACS numbers: 12.60.Cn, 13.38.−b, 14.70.Pw, 14.65.Jk

I. INTRODUCTION

Additional Z' gauge bosons are ubiquitous in standard model (SM) extensions. Among them, models based on left-right symmetry groups have been extensively studied [1] and are particularly important from the point of view of LHC phenomenology. The basic assumption of manifest left-right symmetric models is that the fundamental weak interaction Lagrangian is invariant under parity symmetry, which is spontaneously broken at low energy due to a noninvariant vacuum. Models based on the smallest left-right symmetric gauge group $SU(3)_C \otimes SU(2)_L \otimes SU(2)_R \otimes U(1)_{B-L}$ have many additional appealing attributes (for a review see [2]). These include the same quark-lepton symmetry of the weak interaction; the possibility of writing electric charge in terms of purely physical quantum numbers such as weak-isospin, baryon, and lepton number; the natural accommodation of the seesaw mechanism for neutrino masses; understanding of the small CP violation in the quark sector [2]; and the solution to the strong CP problem[3].

In this work we study the $Z' \to \bar{q}q, ggg$ decays in the context of a left-right symmetric model based on the $SU(3)_C \otimes SU(2)_R \otimes SU(2)_L \otimes U(1)_{B-L}$ gauge group with three (LRSM) and four fermion families (LRSM4). The first decay is expected to give an important contribution to the Z' decay width and it is worthy to estimate the size of this channel for the search of Z' bosons in hadron colliders. The $Z' \to ggg$ decay is related to the production mechanism $gg \to gZ'$ and $gg \to \gamma Z'$ which could also be relevant to the searches of the Z' in hadron colliders. In general, the coupling $Vggg$ (with $V = Z, Z'$) is absent in the classical action of any renormalizable extension of the standard model. The process $V \to ggg$ is induced via quark loops and turns out to be a very interesting prediction which allows us to analyze the interplay between strong and weak sectors of a particular model. The $Vggg$ couplings are also important because they are much less suppressed than those coming from purely weak interactions, like $VVVV$.

A detailed analysis of the one-loop couplings $Vggg$ and $Vgg\gamma$, with $V = Z, Z'$, in the context of the minimal 3-3-1 model [4], was performed in [5,6]. It was explicitly shown there that the $Z \to ggg$ decay [7] does not receive sizable contribution from quarks in the loops with masses higher than $m_Z/2$ and therefore neither t nor an additional quark family is expected to contribute significantly to this process. These results remain valid in LRSM provided the mixing angle between neutral gauge bosons is small which is the case [8].

In LRSM the $Z' \to ggg$ decay is induced by quark loops and the necessary $Z'\bar{q}q$ couplings depend only on a mixing angle which is severely constrained by experimental data. As we shall show below, the most important contributions come from the third family of quarks which motivate us to study also the contributions of a fourth family to both $Z' \to \bar{q}q$ and $Z' \to ggg$ decays.

A fourth sequential fermion family is the simplest possible extension to the SM and can be easily adapted to left-right models. It is well-known that the number of families is not fixed by the theory and precision electroweak data do not exclude a fourth one [9–16]. Our results for LRSM suggest that the existence of a fourth generation of quarks could produce an enhancement of the $Z' \to ggg$ branching ratio and it is worthy to quantify this effect. An extensive review and an exhaustive list of references to the work on the possible existence of a fourth generation can be found in [17]. Recent highlights on the consequences of a fourth generation are contained in [18]. These include several appealing features:

(i) A fourth generation could relax the current SM low Higgs mass bounds from electroweak precision observables [11–13].

(ii) Mechanisms of dynamical electroweak symmetry breaking by a fourth generation of quarks and

PHYSICAL REVIEW D **84,** 066010 (2011)

Near-horizon geometry from flux compactification

Oscar Loaiza-Brito* and Liliana Vazquez-Mercado†

Departamento de Física, DCI, Campus León, Universidad de Guanajuato, C.P. 37150, Guanuajuato, México

(Received 22 April 2011; revised manuscript received 18 August 2011; published 28 September 2011)

We study the conditions an arbitrary flux configuration must fulfill in order to construct a 4d space-time of the type $AdS_2 \times S^2$ from a type IIB supergravity flux compactification in which Neveu-Schwarz-Neveu-Schwarz (NS-NS) fluxes are included. We present a solution consisting on a compactification in the presence of 3-form NS-NS andRamond-Ramond (RR) fluxes. The internal manifold is a $SU(3)$ structure six-dimensional manifold, with null curvature and with torsion. By preserving two supersymmetries in the four-dimensional low energy theory, we find a way to obtain the $AdS_2 \times S^2$ geometry as a near-horizon solution by compactification in non-Calabi-Yau manifolds.

DOI: 10.1103/PhysRevD.84.066010 PACS numbers: 11.25.Mj

I. INTRODUCTION

Solutions of $AdS_2 \times S^2$ as near-horizon geometries of extremal black holes have been studied in the past years in the context of $\mathcal{N} = 2$, $d = 4$ ungauged supergravity by performing Calabi-Yau (CY) compactifications in type II superstring theories (see [1] and references therein). A typical example considers type IIB superstring theory compactified on a CY threefold on which D3-branes wrap internal supersymmetric three-cycles. In the low energy four-dimensional (4d) effective theory, this is interpreted as an extremal supersymmetric black hole. The $AdS_2 \times S^2$ geometry emerges once the corresponding near-horizon limit is taken. This is equivalent to consider a compactification of type IIB superstring to a 2-dimensional spacetime in a CY threefold X_6 times S^2 threaded with a 5-form RR flux of the form $F_5 = \omega_2 \wedge F_3$, where ω_2 is the unit volume form on S^2 and F_3 a 3-form in X_6. The 5-form F_5 is the corresponding field strength associated to the aforementioned D3-branes [2].

On the other hand, we have learned in the past decade that CY compactifications in string theory yields the presence of flat potentials in the low energy effective theory, which becomes moduli-dependent once internal fluxes are turned on. The consequent backreaction forces the departure of the nice and smooth geometry on CY manifolds into manifolds with generalized geometry. In this context, string compactifications to Minkowski, anti-de Sitter (AdS) and de Sitter spaces have been extensively studied in the past few years [3–6] (see also [7–9] for recent studies). In particular, the construction of gauged supergravities from type II compactifications on CY manifolds threaded with Ramond-Ramond (RR) and Neveu-Schwarz-Neveu-Schwarz (NS-NS) fluxes has been studied, where the hypermultiplet scalars become charged under the gauge bosons in the vector multiplet.

However, it is known that not all gauged supergravities are obtained from flux compactifications on CY manifolds, since some of them are constructed by compactifications on manifolds with generalized structures (see, for instance, [10] and references therein). In other cases, the gauged supergravity does not have a (known) related flux string compactification, although maximal symmetric solutions have been studied in such scenarios [11] with the subsequent construction of black-hole solutions [12]. Therefore, in the context of gauged supergravities constructed from flux compactifications on manifolds with generalized geometry, supersymmetric black holes is a topic under recent research. In a similar context, within the flux compactification scenario (including NS-NS fluxes), the construction of solutions of the type $AdS_2 \times S^2$ has not been considered in the literature so far. The objective of this work is to start filling this gap.

We study the conditions under which a flux string compactification yields a 4d space-time of the type $AdS_2 \times S^2$, on which arbitrary fluxes are present, including NS-NS fluxes. We find a general constraint that a flux configuration must fulfill in order to be consistent with the desired 4d symmetry. A general solution is difficult to obtain, therefore by constraining the system to have a constant dilaton and in consequence a constant warping factor, we find a simple minimalist solution. It consists on a compactification of type IIB string theory on a $SU(3)$-structure manifold, Ricci-flat and with torsion, in the presence of RR and NS-NS 3-form fluxes. We show that our flux configuration is a solution of the Einstein equations with a null contribution to the scalar curvature in 4d and that it satisfies the corresponding Bianchi identities and integrability conditions. As a result, we provide a novel way to obtain the $AdS_2 \times S^2$ geometry as a near-horizon solution. It is also important to mention that the known solution consisting on 5-form RR fluxes is also a solution in our setup.

Our work is organized as follows. In Sec. II, we study, in the spirit of [13], the allowed flux configurations in supergravity compactifications yielding a Ricci-flat space-time formed by the product $AdS_2 \times S^2$, by computing the

*oloaiza@fisica.ugto.mx
†livazquezm@fisica.ugto.mx

Evolution and stability Φ^4 oscillatons

2012 Class. Quantum Grav. 29 065021

(http://iopscience.iop.org/0264-9381/29/6/065021)

Class. Quantum Grav. **29** (2012) 065021 (25pp) doi:10.1088/0264-9381/29/6/065021

Evolution and stability Φ^4 oscillatons

L Arturo Ureña-López[1], **Susana Valdez-Alvarado**[1] **and Ricardo Becerril**[2]

[1] Departamento de Física, DCI, Campus León, Universidad de Guanajuato, CP 37150, León, Guanajuato, Mexico
[2] Instituto de Física y Matemáticas, Universidad Michoacana de San Nicolás de Hidalgo, Edificio C-3, Cd. Universitaria, CP 58040 Morelia, Michoacán, Mexico

E-mail: lurena@fisica.ugto.mx, svaldez@fisica.ugto.mx and becerril@ifm.umich.mx

Received 18 July 2011, in final form 7 February 2012
Published 2 March 2012
Online at stacks.iop.org/CQG/29/065021

Abstract
We solve numerically the Einstein–Klein–Gordon (EKG) system, assuming spherical symmetry, for a real scalar field endowed with a quartic self-interaction potential, and obtain the so-called oscillatons: oscillating soliton stars. We obtain the equilibrium configurations for $\Phi^4 oscillatons$. Also, we analyze numerically the evolution of the EKG equations to study the stability of such oscillatons. We present the influence of the quartic potential on the behavior of both the stable (*S-oscillatons*) and unstable (*U-oscillatons*) branches, under the influence of small and large radial perturbations.

PACS numbers: 04.40.−b, 04.25.D−, 95.30.Sf, 95.35.+d

(Some figures may appear in colour only in the online journal)

1. Introduction

Oscillatons are non-singular and asymptotically flat solutions of the Einstein–Klein–Gordon (EKG) equations, in which both the metric and scalar field are fully time dependent [1–5]. They can be considered as gravitationally bounded objects made of a real scalar field in the classical regime and were first discovered by Seidel and Suen [1]. Oscillatons should be distinguished from their complex counterparts, the so-called boson stars, for which the spacetime geometry remains static [6–9].

There is a great interest in the study of scalar fields due to the fact that they are viable candidates for dark matter [10–18], and may be the responsible field for the formation and evolution of galaxies. In particular, the properties of galaxies could help to constrain the strength of a possible quartic self-interaction of the scalar field, see [19]. The same kind of self-interaction could also be useful for the use of boson stars as candidates for the ultracompact objects found in the nuclei of active galaxies, see for instance [20, 21].

Unified description of the dynamics of quintessential scalar fields

JCAP03(2012)035

(http://iopscience.iop.org/1475-7516/2012/03/035)

Journal of Cosmology and Astroparticle Physics
An IOP and SISSA journal

Unified description of the dynamics of quintessential scalar fields

L. Arturo Ureña-López

Departamento de Física, DCI, Universidad de Guanajuato,
Campus León, 37150, León, Guanajuato, México

E-mail: lurena@fisica.ugto.mx

Received January 14, 2012
Accepted February 28, 2012
Published March 27, 2012

Abstract. Using the dynamical system approach, we describe the general dynamics of cosmological scalar fields in terms of critical points and heteroclinic lines. It is found that critical points describe the initial and final states of the scalar field dynamics, but that heteroclinic lines give a more complete description of the evolution in between the critical points. In particular, the heteroclinic line that departs from the (saddle) critical point of perfect fluid-domination is the representative path in phase space of quintessence fields that may be viable dark energy candidates. We also discuss the attractor properties of the heteroclinic lines, and their importance for the description of thawing and freezing fields.

Keywords: dark energy theory, cosmology of theories beyond the SM

ArXiv ePrint: 1108.4712

JCAP03(2012)035

doi:10.1088/1475-7516/2012/03/035

PHYSICAL REVIEW D **85,** 044055 (2012)

Unification models with reheating via primordial black holes

J. C. Hidalgo,[1,2,*] L. Arturo Ureña-López,[3,†] and Andrew R. Liddle[4,‡]

[1]*Instituto de Astronomía, UNAM, Ciudad Universitaria, 04510, México D. F., México*
[2]*Depto. de Física, Instituto Nacional de Investigaciones Nucleares, Apdo. Postal 18-1027, 11801, México D. F., México*
[3]*Departamento de Física, DCI, Campus León, Universidad de Guanajuato, 37150, León, Guanajuato, México*
[4]*Astronomy Centre, University of Sussex, Brighton BN1 9QH, United Kingdom*

(Received 31 July 2011; published 23 February 2012)

We study the possibility of reheating the universe through the evaporation of primordial black holes created at the end of inflation. This is shown to allow for the unification of inflation with dark matter or dark energy, or both, under the dynamics of a single scalar field. We determine the necessary conditions to recover the standard big bang by the time of nucleosynthesis after reheating through black holes.

DOI: 10.1103/PhysRevD.85.044055 PACS numbers: 04.70.−s, 98.80.Cq, 98.80.Jk

I. INTRODUCTION

The quest for the unification of inflation, dark matter, and dark energy, in different combinations, by a single field, has been studied in Refs. [1–15]. The main motivation behind all proposals is that we do not yet understand the nature of the components responsible for the three phenomena, but we do know that their special properties are beyond the realm of the ordinary matter described by the standard model of particle physics.

An extreme, most economical, possibility is that all three phenomena can be explained by the existence of one single field. As was first put forward in Ref. [8], the simplest option at hand is a scalar field ϕ with a potential of the form $V(\phi) = V_0 + (1/2)m^2\phi^2$. The energy scale V_0 is to be set at the tiny value of the observed cosmological constant considered in the concordance ΛCDM model, and the mass scale of the field, $m \simeq 10^{-6}m_{\rm pl}$, is determined by the amplitude of primordial perturbations generated during inflation.

A crucial ingredient in unification schemes that include the inflaton field is a proper and smooth transition from an inflationary era to the hot big bang phase we are all familiar with. There needs to be a *reheating* phase in which the inflaton field can transfer most of its energy to other relativistic particles, yet be able to survive the reheating process and attain the right amplitude to later become a subdominant dark matter/dark energy component in the radiation-dominated era.

The viability of some phenomenological models of reheating for unification models was explored in Refs. [2,8]. Some other, more detailed proposals have been explored in the literature, from extra periods of inflation at low energy scales [8], to the more popular gravitational particle production at the end of inflation (e.g., [1,11,16–18]). This reheating mechanism is largely ineffective, however, because the relative proportion of radiation to scalar field $\rho_{\rm rel}/\rho_\phi$ evolves at the same rate as the proportion of gravitational waves to scalar field $\rho_{\rm GW}/\rho_\phi$ [19]. In the case of steep potentials, inflation is followed by a kination era (a possibility first explored in the context of electroweak baryogenesis [20]). If the kinetic energy of the scalar field dominates for some time, the relative density of gravitational waves created during inflation can grow significantly and violate the observational bounds. Specifically, the process of Big Bang Nucleosynthesis (BBN) imposes a condition on the energy density of gravitational waves $\rho_{\rm GW}$, BBN requiring that [21]

$$\rho_{\rm GW}(t_{\rm BBN}) < 0.2\rho_{\rm rel}(t_{\rm BBN}). \tag{1}$$

In fact, the BBN bound in Eq. (1) has been used to constrain and exclude some models of braneworld inflation and other unification models [22].

In this paper, we explore an alternative mechanism to reheat the Universe, exploiting the evaporation of primordial black holes (PBHs) produced at the end of the inflationary phase [23,24], and study its usefulness in unification models. A small initial population of tiny black holes will grow significantly (in relative energy density) in a universe dominated by a stiff fluid. The evaporation of such black holes at the right time would produce the required amount of radiation more effectively than, for instance, the process of quantum particle production in an expanding space-time.

In the PBH reheating scenario, the black hole component effectively reduces the relative density of gravitational waves as

$$\frac{\rho_{\rm GW}}{\rho_{\rm PBH}} \propto \left(\frac{a}{a_{\rm end}}\right)^{-1}. \tag{2}$$

Reheating takes place when the energy density $\rho_{\rm PBH}$ is transformed into relativistic particles. Therefore, even if the densities $\rho_{\rm GW}$ and $\rho_{\rm PBH}$ were equivalent at the end of inflation, we would only require 3 e-folds of kinetic energy domination to meet the nucleosynthesis requirements. PBH reheating therefore solves the problem described

*jhidalgo@astro.unam.mx
†lurena@fisica.ugto.mx
‡a.liddle@sussex.ac.uk

B meson decays into charmless pseudoscalar scalar mesons

D. Delepine, J. L. Lucio M., Carlos A. Ramírez, and J. A. Mendoza S.

Citation: AIP Conf. Proc. **917**, 398 (2007); doi: 10.1063/1.2751983
View online: http://dx.doi.org/10.1063/1.2751983
View Table of Contents: http://proceedings.aip.org/dbt/dbt.jsp?KEY=APCPCS&Volume=917&Issue=1
Published by the American Institute of Physics.

B meson decays into charmless pseudoscalar scalar mesons

D. Delepine*, J. L. Lucio M.*, Carlos A. Ramírez† and J. A. Mendoza S.†

*Instituto de Física, Universidad de Guanajuato
Loma del Bosque # 103, Lomas del Campestre,
37150 León, Guanajuato; México
†Depto. de Física, Universidad Industrial de Santander,
A.A. 678, Bucaramanga, Colombia
Depto. de Fsica-matemáticas, Universidad de Pamplona
Pamplona, Norte de Santander, Colombia.

Abstract. The nonleptonic weak decays of meson B into a scalar and pseudoscalar meson are studied. The scalar mesons under consideration are σ (or $f_0(600)$), $f_0(980)$, $a_0(980)$ and $K_0^*(1430)$. We calculate the Branching ratios in the Naive Factorization approximation. Scalars are assumed to be $q\bar{q}$ bounded sates, but an estimation can be obtained in the case they are four bounded states.

1. INTRODUCTION

There are several reasons to study the $B \to PS$ (P and S are pseudoscalar and scalar mesons) decays, let us mention several ones. Scalars have been an issue for long tine [1] and $B \to PS$ is another window to study their properties [2]. CP asymmetries of these decays provide another way to mesure the CKM angles β and maybe α [3]. Additionally $B \to PS$ decays have to be taken into account in order to analyze the $B \to 3P$ decays in the different channels [4] and perhaps these decays can be used to study mew physics [5].

From the experimental point of view several results have been already obtained [6] and future experiments like LHCB [7] are expected to improve them. It is remarkable how the f_0 properties measured in the $B \to f_0 K$ decay are in total agreement width those obtained at lower energies [6]. Similarly the β angle also agrees with more accurate measurements like $B \to J/\Psi K$ decays. Recently, BABAR has searched for the decays $B \to a_0\pi$ and $B \to a_0 K$ that may allow us to discriminate between 2 and 4 quarks scalars [2], unfortunately the experiment is still not sensible to these decays.

Given the actual experimental an theoretical accuracies we work in the Naive Factorization Approximation (NFA) [8, 9]. This approximation has given a reasonable fit for $B \to PP$ decays, except for these decays dominated by the so called 'color suppressed 'diagrams and for the strong CP phases. Naturally when our knowledge of $B \to PS$ decays improves one has to go use more accurate formalisms

CP917, *Particles and Fields,* edited by H. Castilla Valdez, J. C. D'Olivo, and M. A. Perez

Λ0 Polarization In pp→pfpsΛ0antiΛ0 At 800GeV/c

J. Castorena, J. Félix, M. C. Berisso, D. C. Christian, A. Gara et al.

Citation: AIP Conf. Proc. **917**, 413 (2007); doi: 10.1063/1.2751987
View online: http://dx.doi.org/10.1063/1.2751987
View Table of Contents: http://proceedings.aip.org/dbt/dbt.jsp?KEY=APCPCS&Volume=917&Issue=1
Published by the American Institute of Physics.

Λ^0 Polarization In $pp \rightarrow p_f p_s \Lambda^0_{anti}\text{-}\Lambda^0$ At 800-GeV/c

J. Castorena,[1] J. Félix,[1] M.C. Berisso,[2] D.C. Christian,[3] A. Gara,[4] E.E. Gottschalk,[3] G. Gutiérrez,[3] E.P. Hartouni,[5] B.C. Knapp,[4] M.N. Kreisler,[2] S. Lee,[2] K. Markianos,[2] G. Moreno,[1] M. A. Reyes,[1] M.H.L.S. Wang,[2] A. Wehmann,[3] D. Wesson[2].

[1]*Universidad de Guanajuato, León, Guanajuato, México.*
[2]*University of Massachusetts, Amherst, Massachusetts, USA.*
[3]*Fermilab, Batavia, Illinois, USA.*
[4]*Columbia University, Nevis Laboratory, New York, New York, USA.*
[5]*Lawrence Livermore National Laboratory, Livermore, California, USA.*

Abstract. The preliminary results of a Λ^0 and anti-Λ^0 polarization study as functions of the $M_{(\Lambda\text{-}b\Lambda)}$, X_F and their corresponding P_T are reported in this work.

Keywords: Polarization, E690.
PACS: 13.88.+e

The polarization of Λ^0 or anti-Λ^0 is measured with respect to the normal vector to its corresponding production plane; it is extracted by fitting to a straight line the angular distribution ($\cos\theta$) of the proton decaying from Λ^0 or anti-Λ^0, $\cos\theta$ has the following dependence on the polarization (P): $dN/d\Omega = N_0(1-\alpha P\cos\theta)$.

Λ^0 polarization and anti-Λ^0 polarization depend on $M_{(\Lambda\text{-}b\Lambda)}$ (Λ^0anti-Λ^0 invariant mass), P_T and X_F. Both Λ^0 and anti-Λ^0 polarizations have a similar dependence on P_T; and a symmetric dependence as functions of X_F. The dependence of Λ^0 polarization on $M_{(\Lambda\text{-}b\Lambda)}$ suggests that the origin of the polarization might be related to the production of the Λ^0 anti-Λ^0 system. The preliminary results are shown in Figure 1.

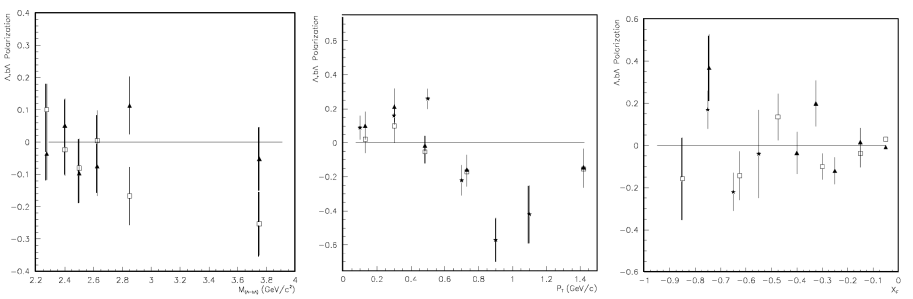

FIGURE 1. Polarization as a function of $M_{(\Lambda\text{-}b\Lambda)}$ (left), X_F (center) and P_T (right). The squares (□) correspond to the results for Lambda, triangles (▲) for anti-Lambda and stars for results reported in [1].

REFERENCES

[1] J. Félix et al, *Phys. Rev. Lett.* 88, 061801 (2002).
[2] Michael H.L.S. Wang, Ph.D. *thesis*, University of Massachusetts, Amherst, 2000.

CP917, *Particles and Fields,* edited by H. Castilla Valdez, J. C. D'Olivo, and M. A. Perez

CP violation in SemiLeptonic τ decays

David Delepine

Citation: AIP Conf. Proc. **917**, 90 (2007); doi: 10.1063/1.2751944
View online: http://dx.doi.org/10.1063/1.2751944
View Table of Contents: http://proceedings.aip.org/dbt/dbt.jsp?KEY=APCPCS&Volume=917&Issue=1
Published by the American Institute of Physics.

CP violation in Semi-Leptonic τ decays

David Delepine

Instituto de Fisica de la Universidad de Guanajuato, Loma del Bosque 103, 37150 Leon, Gto, Mexico

Abstract. We study CP violation in semi-leptonic τ decays and we determine the conditions necessary to be able to define a observable CP asymmetry. We apply these conditions in both models, the standard model for the electroweak interactions and its supersymmetric extensions. In the first case, the leading order contribution to the direct CP asymmetry in $\tau^{\pm} \to K^{\pm}\pi^0\nu_\tau$ decay rates is evaluated. In the second case,we compute the SUSY effective hamiltonian that describes the $|\Delta S| = 1$ semileptonic decays of tau leptons. We show that SUSY contributions may enhance the CP asymmetry of $\tau \to K\pi\nu_\tau$ decays by several orders of magnitude compared to the standard model expectations.

Keywords: CP violation, τ decay, supersymmetry
PACS: 11.30.Er, 11.30.Pb, 12.60.Jv,13.35.Dx

INTRODUCTION

Experimental searches for CP violating asymmetries in tau lepton semileptonic decays have been carried out in the $\tau \to \pi\pi\nu_\tau$ [1] and $\tau \to K_s\pi\nu_\tau$ [2] modes. Motivation for these searches in the context of beyond the Standard Model approaches were provided in refs. [3, 4]. In ref. [2], the missing evidence for a non-zero CP asymmetry was interpreted in terms of a (CP-violating) coupling Λ due to a charged scalar exchange and the limit $-0.172 < Im(\Lambda) < 0.067$ (at 90% c.l.) has been derived. The CP-odd observable studied in [2] depends upon two variables of a particular kinematical distribution of semileptonic tau decays as long as this effect is assumed to have its origin in the interference of scalar and vector form factors In this talk, we shall first determine the general conditions to get observable CP asymmetry. Then we should apply it to Standard Model and its supersymmetric extensions

The general amplitude for $\tau^-(p) \to K^-(k)\pi^0(k')\nu_\tau(p')$is given by

$$\begin{aligned}\mathscr{M} &= \frac{G_F V_{us}}{\sqrt{2}}\left\{\bar{u}(p')\gamma^\mu(1-\gamma_5)u(p)F_V(t)\left[(k-k')_\mu - \frac{\Delta^2}{t}q_\mu\right]\right. \\ &+\bar{u}(p')(1+\gamma_5)u(p)m_\tau\Lambda F_S(t)\frac{\Delta^2}{t} \\ &\left.+F_T\langle K\pi|\bar{s}\sigma_{\mu\upsilon}u|0\rangle\bar{u}(p')\sigma^{\mu\upsilon}(1+\gamma_5)u(p)\right\},\end{aligned}$$

where $q = k + k'$ $(t = q^2)$ is the momentum transfer to the hadronic system, $\Delta^2 \equiv m_K^2 - m_\pi^2$ and $F_{V,S,T}(t)$ are the *effective* form factors describing the hadronic matrix elements (In Standard Model, $F_T = 0, \Lambda = 1$)

CP917, *Particles and Fields,* edited by H. Castilla Valdez, J. C. D'Olivo, and M. A. Perez

Alternative interpretation for the moduli fields of string theories

2007 J. Phys.: Conf. Ser. 91 012014

(http://iopscience.iop.org/1742-6596/91/1/012014)

Journal of Physics: Conference Series **91** (2007) 012014 doi:10.1088/1742-6596/91/1/012014

Alternative interpretation for the moduli fields of string theories

Tonatiuh Matos*[1] , José-Rubén Luévano†[2] , L. Arturo Ureña-López‡[3] and J. Alberto Vázquez*[4]‡

*Departamento de Física, CINVESTAV, A.P. 14-740, 07000 México D.F., México.
†Departamento de Ciencias Básicas, UAM-A, C.P. 02200 México, D.F., México.
‡Instituto de Física, IFUG, A.P. 150, 37150, León, Guanajuato, México.

E-mail: [1]tmatos@fis.cinvestav.mx, [2]jrle@azc.uam.mx, [3]lurena@fisica.ugto.mx,[4]jvazquez@fis.cinvestav.mx

Abstract. In this work we provide a basis for studying the cosmologies derived from superstring theory. Distinct features of these cosmologies are the presence of an axion field, and the interaction of the dilaton field with all the other matter fields. We make a first study of the equations of motion and write them as an autonomous dynamical system. The fixed points of the equations and their corresponding stability are determined in turn. We then discuss the viability of the string fields as dark energy and dark matter.

1. Introduction

Doubtless one of the main problems in physics now is the nature of dark matter and the understanding of the accelerated expansion of the universe. There are a number of observations supporting the existence of dark matter [1] and the accelerated expansion of the universe as well [2]. On the other hand, one of the main problems of superstring theory is that there is no real phenomenology that can support the theory. Usually, superstring theory is supported only by its mathematical and internal consistency, but not by real experiments or observations. One way in which superstring theory can make contact with phenomenology is through cosmology [3]. In the last years, a number of new observations have given rise to a new cosmology and to a new perception of the universe (see for example [4]). The discovery of two kind of substances in the universe, one of them attractive, called dark matter and the other one repulsive, called dark energy, have changed our paradigm on the cosmos. On the other hand, the superstring theory contains a set of fields and particles that have not been seen in nature. In particular, two fields, the *dilaton* and the *axion*, are two very important components of the theory which can not be easily fixed. In fact, one should find a physical interpretation for these fields or give an explanation of why we are not able to see them in nature. Some explanations for the present non-existence of the moduli fields is that there exists a mechanism for eliminating these fields during the evolution of the universe [5]. One of the most popular interpretations for the dilaton

‡ Part of the Instituto Avanzado de Cosmología (IAC) collaboration

Extra-dimensional noncommutative field theory model

J.C. López-Domínguez and O. Obregón
Instituto de Física de la Universidad de Guanajuato,
P.O. Box E-143, 37150 León Gto., México,
e-mail: jlopez@fisica.ugto.mx, octavio@fisica.ugto.mx

C. Ramírez and J.J. Toscano
Facultad de Ciencias Físico Matemáticas, Universidad Autónoma de Puebla,
P.O. Box 1364, 72000 Puebla, México,
e-mail: cramirez@fcfm.buap.mx, jtoscano@fcfm.buap.mx

Recibido el 1 de mayo de 2006; aceptado el 1 de noviembre de 2006

The influence of higher dimensions in noncommutative field theories is considered. For this purpose, we analyze the bosonic sector of a recently proposed 6 dimensional SU(3) orbifold model for the electroweak interactions. The corresponding noncommutative theory is constructed by means of the Seiberg-Witten map in 6D. We find in the reduced bosonic interactions in 4D theory, couplings which are new with respect to other known 4D noncommutative formulations of the Standard Model using the Seiberg-Witten map.

Keywords: non-commutativity; extra dimensions.

Se considera el efecto de la presencia de dimensiones extra en las teorías de campo no conmutativas. Para este propósito, se analiza el sector bosónico del recientemente propuesto modelo de orbifoldio SU(3) para las interacciones electro-débiles. La teoría no conmuntativa correspondiente se contruye utilizando el mapa de Seiberg-Witten en 6D. Encontramos en las interacciones bosónicas reducidas en la teoría de 4D acoplamientos que son nuevos con respecto a otras formulaciones no conmutativas conocidas en 4D del modelo estándar que utilizan el mapa de Seiberg-Witten.

Descriptores: No conmutatividad; dimensiones extra.

PACS: 11.10.Nx; 12.10.-g; 12.60.-i

1. Introduction

A renewed interest in theories in 6D has recently emerged [1]. An anomaly free gauged supergravity in $D = 6$, the Salam-Sezgin model [2], has been considered. This model is compactified on a 2-sphere and in four dimensions gives a $SU(2) \times U(1)$ gauge theory [3]. In particular, it has been argued that these theories with 3-Branes could point out towards solving the cosmological constant problem [4]. Also, in Ref. 5 it is shown that chaotic inflation consistent with constraints coming from the amplitude of the cosmic microwave anisotropies can be naturally realized.

In the search for a unified theory of elementary particles, the incorporation of the Higgs field in the standard model (SM) of electroweak interactions has motivated various proposals in 6D [6]. These are 6D pure gauge theories, in which after dimensional reduction the Higgs field naturally arises. Recently new proposals have been made, considering orbifold compactifications; in Ref. 7, a $U(3) \times U(3)$ model was considered. In these works the mass term of the Higgs potential is generated radiatively, with a finite value without the need of supersymmetry. Further, a $SU(3)$ model was developed in Refs. 8 and 9 with one Higgs doublet and a predicted W-boson mass. In this case the weak angle has a nonrealistic value, although it can be improved by an extended gauge group as in Ref. 7 or by the introduction of an $U(1)$ factor as done in Ref. 8.

Noncommutativity in field theories has been the subject of an important number of works in the last few years. In particular, the Seiberg-Witten construction [10] and its generalization for any gauge group [11] have been studied. This construction allows to express the noncommutative gauge fields in terms of the usual ones and their derivatives, maintaining the same degrees of freedom. It has been extended for noncommutative matter fields, which also can be generated in terms of the commutative matter fields and gauge fields of interest [11]. By this procedure, noncommutative versions of the standard model and consequently the electroweak interaction sector have been give in Ref. 12 (see also Ref. 13). As a consequence, new interactions among the fields of the theory are predicted. In this work, we will investigate the noncommutative generalization of the bosonic sector of Gauge Higgs unification models in 6D based on the $SU(3)$ gauge group compactified on T^2/Z_2 [9]. The noncommutative extension is obtained by means of the Seiberg-Witten map. We calculate, for the bosonic sector, the resulting first order corrections and compare them with the results obtained in other works.

2. The 6-Dimensional Model

Let us consider a Yang-Mills theory in 6-dimensional spacetime with a $SU(3)$ gauge group, the Lagrangian of the theory is

$$\mathcal{L} = -\frac{1}{2}\mathrm{Tr}F_{mn}F^{mn},$$

the field strength tensor is defined by

Noncommutative black holes

2007 J. Phys.: Conf. Ser. 91 012010

(http://iopscience.iop.org/1742-6596/91/1/012010)

Journal of Physics: Conference Series **91** (2007) 012010 doi:10.1088/1742-6596/91/1/012010

Noncommutative Black Holes

J. C. López-Domínguez[1], O. Obregón[1], C. Ramírez[2] and M. Sabido[1].

[1]Instituto de Física de la Universidad de Guanajuato P.O. Box E-143, 37150 León Gto., México.
[2]Facultad de Ciencias Físico Matemáticas, Universidad Autónoma de Puebla, P.O. Box 1364, 72000 Puebla, México.

E-mail: jlopez@fisica.ugto.mx, octavio@fisica.ugto.mx, cramirez@fcfm.buap.mx, msabido@fisica.ugto.mx

Abstract. We study noncommutative black holes, by using a diffeomorphism between the Schwarzschild black hole and the Kantowski-Sachs cosmological model, which is generalized to noncommutative minisuperspace. Through the use of the Feynman-Hibbs procedure we are able to study the thermodynamics of the black hole, in particular, we calculate Hawking's temperature and entropy for the "noncommutative" Schwarzschild black hole.

1. Introduction

In the last years, noncommutativity (NC) has attracted a lot of attention [1, 2]. Although most of the work has been in the context of Yang-Mills theories, noncommutative deformations of gravity have been proposed (see for example [3] and references therein). If we attempt to write down the field equations and solve them, it turns to be technically very difficult, due to the highly non linear character of the theory. In [4], an alternative procedure to incorporate noncommutativity to cosmological models has been proposed, by performing a noncommutative deformation of the minisuperspace. Further, we know that from quantum mechanics we can get the thermodynamical properties of a system. This already has been used in connection with black holes [5]. In [6], the authors use the Feynman-Hibbs path integral procedure [7] to calculate the temperature and entropy of a black hole, in agreement with previous results [8].

In this paper we apply some of these ideas to obtain thermodynamical properties for a quantum black hole and its noncommutative counterpart. We propose a quantum equation for the Schwarzschild black hole, starting from the WDW equation for the Kantowski-Sachs cosmological model. We apply the Feynman-Hibbs method to calculate the thermodynamical properties. We extend this procedure to include noncommutativity by making the same kind of ansatz as in [4], namely, imposing that the minisuperspace variables do not commute; from this we are able to define the WDW equation for the noncommutative Schwarzschild black hole and following a similar procedure as in [6], we find the noncommutative wave function, the temperature and entropy of the *"noncommutative Schwarzschild black hole"*.

This contribution is based on the paper [9] and a parallel talk given in the VII Mexican School on Gravitation and Mathematical Physics.

REVISTA MEXICANA DE FÍSICA S 53 (4) 118–120 AGOSTO 2007

On the WKB approximation of noncommutative quantum cosmology

E. Mena, O. Obregón, and M. Sabido
Instituto de Física de la Universidad de Guanajuato,
P.O. Box E-143, 37150 León Gto., México,
e-mail: emena@fisica.ugto.mx, octavio@fisica.ugto.mx, msabido@fisica.ugto.mx

Recibido el 1 de mayo de 2006; aceptado el 1 de noviembre de 2006

In this work we propose a formalism to introduce the effects of noncommutativity to classical cosmological models. The method is based on noncommutative quantum cosmology and by means of a WKB type approximation the noncommutative classical solutions can be obtained.

Keywords: non-commutativity; quantum cosmology.

En este trabajo se propone un formalismo para introducir los efectos de la no conmutatividad a modelos cosmológicos clásicos. El método esta basado en la cosmología cuántica no conmutativa en la cual por medio de la aproximación WKB se obtienen las soluciones clásicas no conmutativas.

Descriptores: No conmutatividad; cosmología cuántica.

PACS: 02.40.Gh; 04.60.Kz; 98.80.Qc

1. Introduction

During the early days of quantum mechanics and quantum field theory, continuous space-time and Lorentz symmetry was considered inappropriate to describe the small scale structure of the universe. It was also argued that one should introduce a fundamental length scale, limiting the precision of position measurements. The introduction of fundamental length is suggested to cure the ultraviolet divergencies occuring in quantum field theory. H. Snyder was the first to formulate these ideas mathematically [1], introducing noncommutative coordinates brings an uncertainty in the position. The success of the renormalisation made people forget about these ideas for some time. But when the quantization of gravity was considered thoroughly, it became clear that the usual concepts of space-time are inadequate and that space-time has to be quantised or noncommutative, in some way.

Quantum cosmology, is a simplified approach to the study of the very early universe , which means that the gravitational and matter variables have been reduced to a finite number of degrees of freedom (these models were extensively studied by means of Hamiltonian methods in the 1970's, for reviews see [2, 3]); for homogenous cosmological models the metric depends only on time, this permits to integrate the space dependence and obtain a model with a finite dimensional configuration space, *minisuperspace*, whose variables are the 3-metric components. One way to extract useful dynamical information is through a WKB type method. The semiclassical or WKB approximations is usually discussed in text books on nonrelativistic quantum mechanics in the context of stationary states, *i.e.*, determination of the energy eigenvalues and eigenfunctions [4]. This approximation can also be used to obtain approximate and in some cases exact solutions of the dynamical problem, *i.e.*, full Schrödinger equation, so the utility of the semiclassical approximation in obtaining exact solutions of the Schrödinger equation has not yet fully explored. The same seems to be the case for the relativistic quantum mechanics. The importance of the semiclassical approximation in the relativistic case is probably best appreciated in quantum cosmology [5], specifically, in the analysis of the Wheeler-DeWitt equation which is essentially a Klein-Gordon equation on the minisuperspace [6].

In the last few years there have been several attempts to study the possible effects of noncommutativity in the classical cosmological scenario [7, 8]. In Ref. 9 the authors avoid the difficulties of analyzing noncommutative cosmological models, if these would be derived from the full noncommutative theory of gravity. Their proposal introduces the effects of noncommutativity at the quantum level, namely quantum cosmology, by deforming the minisuperspace through a Moyal deformation of the Wheeler-DeWitt equation, similar to noncommutative quantum mechanics [10].

The aim of this work is to apply a WKB type method to noncommutative quantum cosmology, and find the noncommutative classical solutions, avoiding in this way the difficult task to solve this cosmological models in the complicated framework of noncommutative gravity [11]. We know how to introduce noncommutativity at a quantum level, by taking into account the changes that the Moyal product of functions induces on the quantum equation, and from there calculate the effects of noncommutativity at the classical level. This also has the advantage that for some noncommutaive models for which the quantum solutions can not be found, the noncommutative classical solutions arise very easily from this formulation. This procedure is presented through an example,the Kanstowski-Sachs cosmological.

2. The Cosmological Kantowski-Sachs Model

The Kantowski-Sachs Universe is one of the simplest anisotropic cosmological models [12]. The Kanstowski-Sachs line element is

REVISTA MEXICANA DE FÍSICA S **53** (4) 125–128 AGOSTO 2007

Schrödinger's Born-Infeld representation, the non Abelian case

O. Obregón
Instituto de Física de la Universidad de Guanajuato,
P.O. Box E-143, 37150 León Gto., México,
e-mail: octavio@fisica.ugto.mx

Recibido el 1 de mayo de 2006; aceptado el 1 de noviembre de 2006

We propose a non-Abelian Born-Infeld theory based on an Abelian theory by Erwin Schrödinger that, as he showed, is equivalent to Born-Infeld theory. Its construction does not require at any stage the square root structure that characterizes the Dirac-Born-Infeld (DBI) action. Various non-Abelian generalizations are possible. We focus our attention, in this work, in one of them. For it, it is shown that Instantons solutions exist.Our formalism could be of interest in connection with string theory and possible extensions of well known physical results in the usual Born-Infeld Abelian case.

Keywords: Born-Infeld; Non-Abelian.

Se propone una teoría no-Abeliana de Born-Infeld basada en una teoría Abeliana de Erwin Schrödinger que, como él lo ha mostrado, es equivalente a la teoría propuesta por Born e Infeld. Su construcción no requiere en ninguna etapa de la estructura de raíz cuadrada que caracteriza la acción Dirac-Born-Infeld (DBI). Varias generalizaciones no Abelianas son posibles; nos centramos en este trabajo en una de ellas. Para esto, se muestra que las soluciones de Instantones existen. Nuestro formalismo puede ser de interés en conexión con teoría de cuerdas y posibles extensiones de resultados físicos bien conocidos en el caso de Born-Infeld Abeliano usual.

Descriptores: Born-Infeld; no-Abeliano.

PACS: 11.15.-q; 11.90.+t

Seventy years ago Erwin Schrödinger wrote a paper entitled Contributions to Born's New Theory of the Electomagnetic Field [1]. As is known and he himself pointed out the classical (Dirac-Born-Infeld,DBI) Born's theory [2–6] can be constructed by means of the two vectors $\mathbf{B}$ and $\mathbf{E}$, the magnetic induction and the electric field-strength respectively. The partial derivatives of the Lagrangian with respect to the components of $\mathbf{B}$ and $\mathbf{E}$ define a second pair of vectors correspondingly $\mathbf{H}$, the magnetic field and $-\mathbf{D}$, the electric displacement. It was already shown by Born that one can choose four different ways to write a Lagrange function in terms of one of the magnetic vectors with one of the electric vectors. For each of these theories, the Lagrangians have essentially the same structure.

Schrödinger proposed a theory whose structure is entirely different from the above mentioned. He used two complex combinations of $\mathbf{B}$, $\mathbf{E}$, $\mathbf{H}$ and $\mathbf{D}$ as independent variables

$$\mathbf{\Omega} = \mathbf{B} - i\mathbf{D}\ ,\ \mathbf{\Sigma} = \mathbf{E} + i\mathbf{H}, \tag{1}$$

and constructed a Lagrangian in such a way that the complex conjugate of one of these variables is identical with the partial derivative of the Lagrangian with respect to the other one. This he called the condition of conjugateness. The Lagrangian is

$$\mathcal{L} = \frac{\mathbf{\Omega}^2 - \mathbf{\Sigma}^2}{\mathbf{\Omega} \cdot \mathbf{\Sigma}}\ . \tag{2}$$

In this Lagrangian the square root structure typical of the Dirac-Born-Infeld action has disappeared. The Lagrangian results are rational and homogeneous of the zeroth degree.

Schrödinger showed that the classical treatment of the Lagrangian (2) is entirely equivalent to Born's theory (DBI), this will be shown below. He then writes *consequently it cannot provide us with any new insight, which could not, virtually, be derived from Born's original treatment as well.* He recognized that for practical calculations, however, the imaginary vectors structure will be hard to handle with. Quoting, once more Schrödinger: *yet for certain theoretical considerations of a general kind I am inclined to consider the present treatment as the standard form on account of its extremal simplicity, the Lagrangian being simply the ratio of the two invariants, whereas in Maxwell's theory it was equal to one of them.*

In this work we will present a generalization of Schrödinger's Lagrangian (2) to a non-Abelian gauge theory. The complexification of the fields will provide us with a direct clue to find the non-Abelian framework based on the Abelian Schrödinger's representation. As in the standard Yang-Mills theories, this theory admits instantons solutions. This work, however, is also partially motivated by the fact that in the framework of string theory, the possibility to define a non-Abelian generalization of the standard Dirac-Born-Infeld bosonic and/or supersymmetric actions [7] has been extensively explored beginning in 1990 [8]. If this theory could be constructed, it should represent the world-volume U(N) gauge theory that arises when one has N coincident type II Dp branes. The symmetrized trace prescription proposed by Tseytlin [9] seems to be correct up to terms of the order F^4, but if fails at higher orders [10]. Also in the supersymmetric setup certain terms cannot be expressed in terms of symmetrized traces [11]. Lacking a general rule to construct the non-Abelian Born-Infeld theory, our formulation represents different alternatives to be explored in future

Dynamical baryogenesis through complex hybrid inflation

2008 J. Phys.: Conf. Ser. 116 012002

(http://iopscience.iop.org/1742-6596/116/1/012002)

Journal of Physics: Conference Series **116** (2008) 012002 doi:10.1088/1742-6596/116/1/012002

Dynamical baryogenesis through Complex Hybrid Inflation [1]

David Delepine

E-mail: delepine@fisica.ugto.mx
Instituto de Física de la Universidad de Guanajuato, C.P. 37150, León, Guanajuato, México.

Carlos Martínez

E-mail: crmtz@fisica.ugto.mx
Instituto de Física de la Universidad de Guanajuato, C.P. 37150, León, Guanajuato, México.

L. Arturo Ureña–López

E-mail: lurena@fisica.ugto.mx
Instituto de Física de la Universidad de Guanajuato, C.P. 37150, León, Guanajuato, México.

Abstract. We propose a hybrid inflation model with a complex waterfall field which contains an interaction term that breaks the $U(1)$ global symmetry associated to the waterfall field charge. We show that the asymmetric evolution of the real and imaginary parts of the complex field during the phase transition at the end of inflation translates into a charge asymmetry [1].

We know that only 4% of the total material content of the universe is of baryonic nature, the type of matter we seem to understand thanks to the Standard Model of Particle Physics and nucleosynthesis process of the early universe.

However, even in this well understood case one fundamental question remains open: why this baryonic component is almost completely made of matter and not of antimatter? This is usually quoted as the *baryonic asymmetry* problem. Sakharov in Ref.[2] has shown that any quantum field theory could generate a baryonic asymmetry if three conditions are satisfied: no-conservation of the baryonic charge, CP and C violation, and out-of equilibrium condition for the Universe. The electroweak standard model cannot produce the baryonic asymmetry of the Universe as the condition to be out of equilibrium cannot be fulfilled at the electroweak phase transition.

In this paper, we shall present a particular model of hybrid inflation[3, 4] in which a complex scalar field is the responsible for both the symmetry breaking that puts an end to inflation and for the production of a baryonic asymmetry in the early universe.

[1] poster presented at the 2nd school on cosmic rays and astrophysics, Puebla, Mexico, August 30-September 8, 2006

CP violation in neutrino oscillations in Minimal Supersymmetric extension of the Standard Model

David Delepine and Vannia González Macias

Citation: AIP Conf. Proc. **1026**, 132 (2008); doi: 10.1063/1.2965035
View online: http://dx.doi.org/10.1063/1.2965035
View Table of Contents: http://proceedings.aip.org/dbt/dbt.jsp?KEY=APCPCS&Volume=1026&Issue=1
Published by the American Institute of Physics.

CP violation in neutrino oscillations in Minimal Supersymmetric extension of the Standard Model

David Delepine and Vannia González Macias

Instituto de Física de la Universidad de Guanajuato, C.P. 37150, León, Guanajuato, México.

Abstract. In this talk, we estimate the size of lepton flavor and CP violation in neutrino oscillations in the framework of Minimal Supersymmetric extension of the Standard Model (MSSM). We find that we may have significant CP-violating contributions up to an order of magnitude ($\sim 10^{-2}$) smaller than the standard four-Fermi couplings.

Keywords: cp violation, non standard neutrino oscillations, MSSM
PACS: 11.30.Pb, 11.30.Er,14.60.St

INTRODUCTION

In an extension of the Standard Model, it is possible to have non standard neutrino flavor changing interactions. Such interactions may also provide new sources of CP violation accessible in future long-baseline (LBL) neutrino vacuum oscillation experiments. In future experiments the mixing angles and square mass differences are expected to be determined with high precision (for recent reviews see [1] and [2]). Therefore, it might be possible to observe these effects. Our interest is to study new sources of CP violation in the Minimal Supersymmetric Standard Model (MSSM). In the next section, we shall first discuss how to introduce new flavor physics in neutrino oscillations. Then we shall compute analytically and numerically some of the radiative corrections inducing flavor changing current in MSSM. Finally, we shall conclude.

NON-STANDARD PHYSICS IN NEUTRINO OSCILLATIONS

Let us consider a model independent parametrization [3],[4] of these new interaction effects on production processes (at first order) in neutrino oscillation experiments. We will analyse the $\nu_\mu \to \nu_\tau$ oscillation channel, relevant in long-baseline accelerator experiments and neutrino factories. A similar (model-independent) analysis was done for the $\nu_e \to \nu_\mu$ oscillation channel in [3].
Let us assume three interaction eigenstates as a superposition of the mass eigenstates $\nu_\alpha = \sum_{i=1}^{3} U^*_{\alpha i} |\nu_i>$, with $\alpha = e, \mu, \tau$. Where the matrix $U^*_{\alpha i}$ is parametrized with three mixing angles and one CP-violating phase [5].
The new physics interaction is parametrized in the source and in the detector by two sets of effective four-fermion couplings $(G^s_{NP})_{\alpha\beta}$ and $(G^d_{NP})_{\alpha\beta}$, where $\alpha, \beta = e, \mu, \tau$. Here

CP1026, *Particles and Fields, 11th Mexican Workshop on Particles and Fields*
edited by H. Castilla-Valdez, O. Miranda, and E. Santos

Λ0 Polarization in pp→pΛ0K+ at 800 GeV/c

E. Valencia, J. Félix, M. H. L. S. Wang, M. C. Berisso, D. C. Christian et al.

Citation: AIP Conf. Proc. **1026**, 315 (2008); doi: 10.1063/1.2965073
View online: http://dx.doi.org/10.1063/1.2965073
View Table of Contents: http://proceedings.aip.org/dbt/dbt.jsp?KEY=APCPCS&Volume=1026&Issue=1
Published by the American Institute of Physics.

Λ^0 Polarization in $pp \rightarrow p\Lambda^0 K^+$ at 800GeV/c

E. Valencia[a], J. Félix[a], M.H.L.S. Wang[b], M.C. Berisso[b], D.C. Christian[c], A. Gara[d], E. Gottschalk[c], G. Gutiérrez[c], E.P. Hartouni[e], B.C. Knapp[d], M.N. Kreisler[b], S. Lee[b], K. Markianos[b], M.A. Reyes[a], A. Wehmann[c], D. Wesson[b]

[a] *Universidad de Guanajuato, León, Guanajuato, México,*
[b] *University of Massachusetts, Amherst, Mass USA,*
[c] *Fermilab, Batavia, IL USA,*
[d] *Columbia University, Nevis Laboratories, New York, N. Y. USA*
[e] *Livermore National Laboratory, Livermore, CA USA*

Abstract. We determined Λ^0 polarization as function of X_F, P_T, M_X, and E_Λ, with respect to the normal of the following two different production planes: The first one defined by the momentum of the 800 GeV/c proton beam and the moment of Λ^0; the second one, by the momentum of the transferred object and the momentum of Λ^0, from the sample created in the FNAL E690 experiment. We present results, compare and discuss them.

Keywords: Polarization, Production plane, spin
PACS: 13.88.+e, 13.85.Hd, 14.20.Jn

INTRODUCTION

The experiment E690 investigated proton-proton collisions using an 800GeV/c proton beam incident on a liquid Hydrogen target. The E690 detector apparatus consisted of two separate spectrometers; a beam spectrometer and multi-particle spectrometer [1]. The data analysis was done in four steps as follows: Track reconstruction, vertex reconstruction, particle identification, and selection of exclusive events. This experimental study was on a sample of 41899 events obtained with the following cuts: $(\Delta P_T)^2 < 0.001 (\mathrm{GeV/c})^2$ and $-0.02\mathrm{GeV} < \Delta(E-P_L) < 0.015\mathrm{GeV}$, defining exclusive events. The Figure 1 shows the mass distributions.

Important in this study are the following concepts: Invariant mass (M_X), the mass of diffracted object (Λ^0 and K^+); transversal momentum (P_T), the transversal momentum of Λ^0 with respect to the incoming beam proton; Feynman scaling parameter (X_F), the longitudinal momentum of Λ^0 measured in the reaction center of mass with respect to the incoming beam proton divided by its maximum possible value; transferred momentum (P_X), the transferred momentum from the incoming beam proton to the target proton -it is also the sum of Λ^0 momentum and K^+ momentum-; energy of Λ^0 (E_Λ), energy of lambda measured in laboratory coordinate system; production plane defined by the Λ^0 momentum and the beam momentum [2]: $\hat{n} = (\vec{P}_i \times \vec{P}_\Lambda)/|\vec{P}_i \times \vec{P}_\Lambda|$, where i is the incoming beam proton momentum or the

CP1026, *Particles and Fields, 11th Mexican Workshop on Particles and Fields*
edited by H. Castilla-Valdez, O. Miranda, and E. Santos

Mass gap for gravity localized on thick branes

N. Barbosa–Cendejas, A. Herrera–Aguilar, U. Nucamendi, I. Quiros, M. A. Reyes Santos et al.

Citation: AIP Conf. Proc. **1083**, 5 (2008); doi: 10.1063/1.3058580
View online: http://dx.doi.org/10.1063/1.3058580
View Table of Contents: http://proceedings.aip.org/dbt/dbt.jsp?KEY=APCPCS&Volume=1083&Issue=1
Published by the American Institute of Physics.

Mass gap for gravity localized on thick branes

N. Barbosa–Cendejas*, A. Herrera–Aguilar†, U. Nucamendi†, I. Quiros**, M.A. Reyes Santos* and C. Schubert†

*Instituto de Física, Universidad de Guanajuato, Loma del Bosque 103, Frac. Lomas del Campestre, C.P. 37150 León, Guanajuato, México.
†Instituto de Física y Matemáticas, Universidad Michoacana de San Nicolás de Hidalgo. Edificio C–3, Ciudad Universitaria, C.P. 58040 Morelia, Michoacán, México.
**Departamento de Física, Universidad Central de las Villas, C.P. 54830, Santa Clara, Cuba.

Abstract.
We present a scalar thick brane configuration arising in a theory of 5D gravity coupled to a self–interacting scalar field. We start from a classical solution of the field equations and study the physics of linear fluctuations around this background which obey a Schrödinger–like equation. We further focus our attention on a special case in which it is possible to solve this equation analytically for any massive mode. This fact allows us to make a closed analysis of the massive spectrum of Kaluza–Klein (KK) excitations and to compute the corrections to Newton's law in the thin brane limit. There exist two bound states: the massless 4D graviton, which is free of tachyonic instabilities, and a massive KK excitation. There is also a continuous spectrum of massive KK modes. The mass gap existing between the massless and the excited modes is completely defined by the inverse of the brane thickness. This fact eliminates the experimentally dangerous arbitrarily light KK modes. Moreover, in this picture the solution of the mass hierarchy problem is very simple.

Keywords: Brane worlds, Gravity localization, Mass gap.
PACS: 11.25.Mj, 11.27.+d, 11.10.Kk, 04.50.+h

THE MODEL AND ITS FRAMEWORK

The problem of localizing gravity on brane worlds has been addressed by many authors with different approaches [1]–[19]. Some of them have used thin branes [2]–[7], while others have preferred to consider thick configurations [8]–[19].

In this sense, our 4D world could be embedded in a higher dimensional manifold and many natural questions arise like: Why do we not see the extra dimensions? Are they compact or extended? Do they have temporal or spatial nature? What is the topology of the extra dimensional spacetime? How is the spectrum of gravitational fluctuations and/or particles in the higher dimensional world? Are there extra dimensional forces? What is the effect of higher dimensional forces on 4D Newton's law? How can we detect extra dimensional effects or particles? Can extra dimensions help solving standing problems in modern physics?

Quite soon after the appearance of the first papers on gravity localization on brane worlds, the community started proposing high accuracy experiments that could lead to evidence of the existence of extra dimensions. One such experiment started running on early September, 2008, at the Large Hadron Collider (LHC) and many people around the world are wondering about the output of this fascinating event that could lead to revolutionary changes in the human understanding of our universe.

CP1083, *Gravitation and Cosmology, Proceedings of the Third International Meeting* edited by F. S. Guzmán Murillo, A. Herrera-Aguilar, U. Nucamendi, and I. Quiros

A smooth version of the RS model

N. BarbosaCendejas, A. HerreraAguilar, U. Nucamendi, I. Quiros, M. A. Reyes Santos et al.

Citation: AIP Conf. Proc. **1026**, 146 (2008); doi: 10.1063/1.2965037
View online: http://dx.doi.org/10.1063/1.2965037
View Table of Contents: http://proceedings.aip.org/dbt/dbt.jsp?KEY=APCPCS&Volume=1026&Issue=1
Published by the American Institute of Physics.

A smooth version of the RS model

N. Barbosa–Cendejas*, A. Herrera–Aguilar†, U. Nucamendi†, I. Quiros**, M.A. Reyes Santos* and C. Schubert†

*Instituto de Física, Universidad de Guanajuato, Loma del Bosque 103, Frac. Lomas del Campestre, C.P. 37150 León, Guanajuato, México.
†Instituto de Física y Matemáticas, Universidad Michoacana de San Nicolás de Hidalgo. Edificio C–3, Ciudad Universitaria, C.P. 58040 Morelia, Michoacán, México.
**Departamento de Física, Universidad Central de las Villas, C.P. 54830, Santa Clara, Cuba.

Abstract. We study the physical properties of a thick brane solution arising in a 5D theory of gravity coupled to a bulk self–interacting scalar field in a Riemannian manifold. By analyzing the graviton spectrum of this model, we find a particular case in which the 4D graviton is separated from the massive KK gravitons by a mass gap. In this case, the corresponding effective Schrödinger equation can be solved exactly and has a modified Pöschl-Teller potential. Apart from the massless 4D graviton, there is one massive KK bound state, and a continuum spectrum of delocalized KK modes. We discuss on the mass hierarchy problem and, finally, compute the corrections to Newton's law in the thin brane limit for this case.

Keywords: Brane worlds, Gravity localization, Mass gap.
PACS: 11.25.Mj, 11.27.+d, 11.10.Kk, 04.50.+h

INTRODUCTION AND SETUP

Brane world scenarios have been very useful to address some high energy physics problems [1]; moreover, possible experimental evidence of extra dimensions [2]–[7] motivated various modifications and generalizations of the original thin brane models [4]–[7]. Among them there are several types of thick brane configurations: scalar branes [8]–[10], tachyonic branes [11], branes with non–minimally coupled scalar fields [12, 13]; in this context, several physical aspects have been studied like corrections to Newton's law [14], localization of 4D gravity [15]–[20] and matter fields [21], brane stability [22], critical phenomena [23], etc.

The model we shall consider describes gravity coupled to a bulk scalar field and constitutes a generalization of the Randall–Sundrum (RS) model [5, 6] with the advantages that the scalar curvature is nonsingular at the position of the brane, the 5D manifold is not restricted to be an orbifold and there is no need to introduce the thin branes in the action by hand. Moreover, it appears that for a special case there is a mass gap in the graviton KK–spectrum of the linearized metric fluctuations.

Consider a 5D action given by (we take $M_*^3 = 1/8$ for the time being)

$$S_5 = \int d^5x\sqrt{|G|}\left[\frac{1}{4}R_5 - \frac{1}{2}(\nabla\phi)^2 - V(\phi)\right], \tag{1}$$

CP1026, *Particles and Fields, 11th Mexican Workshop on Particles and Fields*
edited by H. Castilla-Valdez, O. Miranda, and E. Santos

Non Commutativity and Λ.

M. Sabido*, O. Obregón* and E. Mena†

*Instituto de Física de la Universidad de Guanajuato,
A.P. E-143, C.P. 37150, León, Guanajuato, México
†Centro Universitario de la Cienega,
Ave. Universidad 1115 Edif. B, C.P. 47820 Ocotlán,
Jalisco, México

Abstract. This paper we study the effects of a noncommutativity minisuperspace on a FRW universe with cosmological constant. A relationship between the non commutative parameter and Λ is obtained.

Keywords: Non Commutativity, Quantum Cosmology, Dark Energy
PACS: 02.40.Gh,95.36.+x,98.80.Qc

INTRODUCTION

The cosmological constant problem has been addressed by means of different approaches for several years and still remains as one of the central issues of not only modern day cosmology but also particle physics [1]. The questions connected to the cosmological constant can be casted as three fundamental problems: why is the cosmological constant so small?, why it is not zero? and why is it comparable to the matter energy-density (cosmic coincidence)?.

In this paper we will focus on the first question, also known as the "old cosmological constant problem". In a more precise manner, why is the effective cosmological constant Λ_{eff} so close to zero. The different contributions to the vacuum energy density, from ordinary particle physics should give a value for $\langle\rho\rangle$ of order M_p^4, which should be canceled by the bare value of Λ. This cancellation has to be better than 10^{-121} if we compare the zero-point energy of a scalar field, using the Planck scale as a cut-off, to the experimental value of $\langle\rho_{obs}\rangle \approx 10^{-47}(GeV)^4$. This incredible degree of fine tuning, suggests that we are missing important physics. Then its likely that the correct way to interpret the tiny value of the cosmological constant by conventional quantum field theory is not the whole story, leading many authors to try different approaches to dark energy.

One interesting possibility lies in the old idea of noncommutative space-time [2]. This idea has seen renewed interest as a consequence of the developments in M-theory and string theory [3, 4]. But still one can ask of the relevance of noncommutativity in the cosmological scenario or its relevance at the early universe. In quantum gravity the measurement of length is limited to distances grater that l_p, because in order to locate a particle we would need an energy greater than M_p. The corresponding gravitational field will have an horizon $R = \frac{2GM_p}{c^2} = 2L_p$. Therefore a minimal size should exist for quanta of space and time configurations. This can be written as an uncertainty relationship

CP1083, *Gravitation and Cosmology, Proceedings of the Third International Meeting*
edited by F. S. Guzmán Murillo, A. Herrera-Aguilar, U. Nucamendi, and I. Quiros

Covariant Noncommutative Field Theory

S. Estrada-Jiménez*, H. García-Compeán†, O. Obregón** and C. Ramírez‡

*Licenciaturas en Física y en Matemáticas,
Facultad de Ingeniería, Universidad Autónoma de Chiapas
Calle 4a Ote. Nte. 1428, Tuxtla Gutiérrez, Chiapas, México
†Departamento de Física, Centro de Investigación y de Estudios Avanzados del IPN
P.O. Box 14-740, 07000 México D.F., México and
Centro de Investigación y de Estudios Avanzados del IPN, Unidad Monterrey
Vía del Conocimiento 201, Parque de Investigación e Innovación Tecnológica (PIIT)
Autopista nueva al Aeropuerto km 9.5, Lote 1, Manzana 29, cp. 66600
Apodaca Nuevo León, México
**Instituto de Física de la Universidad de Guanajuato P.O. Box E-143, 37150 León Gto., México
‡Facultad de Ciencias Físico Matemáticas, Universidad Autónoma de Puebla, P.O. Box 1364,
72000 Puebla, México.

Abstract. The covariant approach to noncommutative field and gauge theories is revisited. In the process the formalism is applied to field theories invariant under diffeomorphisms. Local differentiable forms are defined in this context. The lagrangian and hamiltonian formalism is consistently introduced.

INTRODUCTION

The idea of the noncommutative nature of space-time coordinates is quite old [1]. Many authors have extensively studied it from the mathematical [2], as well as from a physical point of view (for a review, see for instance [3, 4]). One construction of noncommutative theories on a space-time whose coordinates satisfy,

$$[\widehat{x}^{\mu},\widehat{x}^{\nu}] = i\theta^{\mu\nu}, \tag{1}$$

where $\theta^{\mu\nu}$ is a constant tensor, is done by means the Weyl-Wigner-Moyal correspondence [5], which establishes an equivalence between the algebra of operators $\widehat{\mathscr{A}}$ of these noncommutative variables (with the usual product of operators) and the algebra of smooth functions $\mathscr{A}_\theta$ (with the noncommutative Moyal product). This correspondence expresses a Lie algebra isomorphism $[\widehat{f},\widehat{g}] \mapsto \{f,g\}_M$, where $[\widehat{f},\widehat{g}] \equiv \widehat{f}\cdot\widehat{g} - \widehat{g}\cdot\widehat{f}$ is the commutator and $\{f,g\}_M \equiv f\star g - g\star f$ is the Moyal bracket in terms of the Moyal product $\star$ defined by

$$f(x)\star g(x) = \exp\left(\frac{i}{2}\theta^{\mu\nu}\frac{\partial}{\partial x^{\mu}}\frac{\partial}{\partial y^{\nu}}\right) f(x)g(y)\Big|_{x=y}. \tag{2}$$

Noncommutative theories are obtained by the substitution of the usual (commutative) product of functions by the noncomutative one, $f(x)\cdot g(x) \to f(x)\star g(x)$ with some suitable ordering.

CP1026, *Particles and Fields, 11th Mexican Workshop on Particles and Fields*
edited by H. Castilla-Valdez, O. Miranda, and E. Santos

Dynamical Baryogenesis in Complex Hybrid Inflation

David Delepine, Carlos Martínez, and L. Arturo UreñaLópez

Citation: AIP Conf. Proc. **1026**, 158 (2008); doi: 10.1063/1.2965039
View online: http://dx.doi.org/10.1063/1.2965039
View Table of Contents: http://proceedings.aip.org/dbt/dbt.jsp?KEY=APCPCS&Volume=1026&Issue=1
Published by the American Institute of Physics.

Dynamical Baryogenesis in Complex Hybrid Inflation

David Delepine*, Carlos Martínez* and L. Arturo Ureña–López*

*Instituto de Física de la Universidad de Guanajuato, C.P. 37150, León, Guanajuato, México

Abstract. We propose a hybrid inflation model with a complex waterfall field which contains an interaction term that breaks the $U(1)$ global symmetry associated to the waterfall field charge. We show that the asymmetric evolution of the real and imaginary parts of the complex field during the phase transition at the end of inflation translates into a charge asymmetry. The latter strongly depends on the vev of the waterfall field, which is well constrained by diverse cosmological observations.

INTRODUCTION

The model is an hybrid inflationary model where the waterfall field that is responsible to finish inflation is complex and has a barionic charge (global $U(1)$). To generate an asymmetry of the baryonic charge we nedd: Violation of baryonic charge, C and CP violation, and out of equilibrium condition. In our model the violation of the baryonic number is explicit, the violation of C and CP is dynamical and it is due to the asymmetric evolution of the real and imaginary components od the fluctuations of the waterfall field. They have a tachyonic instability at diferent times. This give us a CP phase that is the phase of the fluctuation of the waterfall field. The out of equilibrium condition is given by the inflationary period itself that provided us a direction in the arrow of time[1]. These model could in principle explain how the asymmetry between matter and antimatter is generated.

OBSERVATIONS

In our universe we observe that there are baryons and almost nothing of antibaryons. The process trough wich this asymmetry is generated is called baryogenesis. The asymmetry between baryon and antibaryon can be measured by the quantity

$$B = \frac{\eta_B}{s} \tag{1}$$

where $\eta_B = \eta_b - \eta_{\bar{b}}$ that it is the difference between tha baryonic and antibaryonic density, and s is the entropy density. The astronomical observation give us the numerical constraint [1]

$$6(4) \times 10^{-11} \leq B \leq 1(1.4) \times 10^{-10}. \tag{2}$$

CP1026, *Particles and Fields, 11th Mexican Workshop on Particles and Fields*
edited by H. Castilla-Valdez, O. Miranda, and E. Santos

Hierarchy of scales in B→PS decays

D. Delepine, J. L. Lucio M., J. A. Mendoza S., and Carlos A. Ramírez

Citation: AIP Conf. Proc. **1030**, 328 (2008); doi: 10.1063/1.2973522
View online: http://dx.doi.org/10.1063/1.2973522
View Table of Contents: http://proceedings.aip.org/dbt/dbt.jsp?KEY=APCPCS&Volume=1030&Issue=1
Published by the American Institute of Physics.

Hierarchy of scales in $B \to PS$ decays

D. Delepine*, J. L. Lucio M.*, J. A. Mendoza S.† and Carlos A. Ramírez**

*Instituto de Física, Universidad de Guanajuato
Loma del Bosque # 103, Lomas del Campestre,
37150 León, Guanajuato; México
†Depto. de Física-Matemáticas, Universidad de Pamplona
Pamplona, Norte de Santander, Colombia.
**Escuela de Física, Universidad Industrial de Santander,
A.A. 678, Bucaramanga, Colombia

Abstract. We show that the naive factorization approach can accommodate the existence of the observed hierarchy of branching ratios for the $B \to PS$ decays (P stands for pseudoscalar and S for scalar mesons respectively[1]).

Keywords: Factorization, Scalar Mesons, B-Meson Decays
PACS: 12.39.St, 13.25.Hw

1. INTRODUCTION

The scalar sector below two GeV is poorly understood, nevertheless several features – like the presence of two multiplets and several of their properties – naturally arise in the analysis of a number of authors. Thus the scalars are grouped in a heavy multiplet with masses around 1.5 GeV [2], including the $K_0^*(1430)$, $a_0(1450)$, $f_0(1500)$ for the octet, $f_0(1370)$ which is identified with the singlet and the $f_0(1710)$ which seems to be mainly glueball. The octet is nearly degenerate, like similar pseudoscalar, vector and tensor multiplets, their widths are small (≤ 100 MeV), the octet-singlet mixing is almost ideal and mixing with the glueball is expected. It has been more difficult to establish the other multiplet, the lighter, since even the existence and nature of some of their members is in doubt. The multiplet should include the $a_0(980)$, $f_0(980)$ and the $\kappa = K_0^*(800)$ in the octet; while the singlet could be identified with the $\sigma = f_0(600)$. The mixing is not clear and their widths are very large. Ideally the former multiplet can be identified as the ground state of quark antiquark bound states with angular momenta one while the later with the ground state of four quarks systems with angular momenta zero. In the real world an undetermined mixing between the two multiplets is expected. Alternatively both multiplets could be identified as quark-antiquark states with angular momenta one, the lighter being the ground state while the heavier with the first excited state.

The scalars remain a challenge, both from the experimental perspective as well as from the theory point of view [2]. To start with, there is not enough and conclusive experimental information on the existence and properties of the scalars. The information are poor not because of experimental limitations, in fact energy is easily available, for example many of the decays of particles containing c or b quarks involves the production

CP1030, *SCADRON70 - Workshop on Scalar Mesons and Related Topics*
edited by G. Rupp, E. van Beveren, P. Bicudo, B. Hiller, and F. Kleefeld

A New Model for Baryogenesis through Hybrid Inflation

D. Delepine, C. Martinez Prieto, and L. A. Ureña Lopez

Citation: AIP Conf. Proc. **1115**, 134 (2009); doi: 10.1063/1.3131485
View online: http://dx.doi.org/10.1063/1.3131485
View Table of Contents: http://proceedings.aip.org/dbt/dbt.jsp?KEY=APCPCS&Volume=1115&Issue=1
Published by the American Institute of Physics.

A New Model for Baryogenesis through Hybrid Inflation

D. Delepine, C. Martinez Prieto and L. A. Ureña Lopez.

Instituto de Física, Universidad de Guanajuato
Loma del Bosque # 103, Lomas del Campestre,
37150 León, Guanajuato; México

Abstract. We propose a hybrid inflation model with a complex waterfall field which contains an interaction term that breaks the $U(1)$ global symmetry associated to the waterfall field charge. The asymmetric evolution of the real and imaginary parts of the complex field during the phase transition at the end of inflation translates into a charge asymmetry.

Keywords: Inflation, cosmology, baryogenesis
PACS: 98.80.Cq

INTRODUCTION

We know that only 4% of the total material content of the universe is of baryonic nature, the type of matter we seem to understand thanks to the Standard Model of Particle Physics and nucleosynthesis process of the early universe.

However, even in this well understood case one fundamental question remains open: why this baryonic component is almost completely made of matter and not of antimatter? This is usually quoted as the *baryonic asymmetry* problem. Sakharov in Ref.[1] has shown that any quantum field theory could generate a baryonic asymmetry if three conditions are satisfied: no-conservation of the baryonic charge, CP and C violation, and out-of equilibrium condition for the Universe. The electroweak standard model cannot produce the baryonic asymmetry of the Universe as the condition to be out of equilibrium cannot be fulfilled at the electroweak phase transition.

In this talk, we shall present a particular model of hybrid inflation[2, 7] in which a complex scalar field is the responsible for both the symmetry breaking that puts an end to inflation and for the production of a baryonic asymmetry in the early universe [4]. The Lagrangian of our model is CP conserving for most of inflation, but we shall show that the dynamics of the waterfall field will generate an effective CP asymmetry at the very end of inflation.

THE MODEL

Our model consists of two scalar fields, the inflaton ϕ and another complex one a wearing a charge which we call *baryonic charge*. These fields are both minimally

CP1115, *The Dark Side of the Universe, 4th International Workshop on The Dark Side of the Universe,* edited by S. Khalil

Simulation and Characterization of the MINERvA Dipole Magnets

J. Félix, J. Castorena, A. Higuera, Z. Urrutia, and G. Zavala

Citation: AIP Conf. Proc. **1182**, 108 (2009); doi: 10.1063/1.3293763
View online: http://dx.doi.org/10.1063/1.3293763
View Table of Contents: http://proceedings.aip.org/dbt/dbt.jsp?KEY=APCPCS&Volume=1182&Issue=1
Published by the American Institute of Physics.

Simulation and Characterization of the MINERνA Dipole Magnets

J. Félix*, J. Castorena†, A. Higuera†, Z. Urrutia†, G. Zavala** and The MINERνA Collaboration. FNAL e938‡

*Universidad de Guanajuato, División de Ciencias e Ingenierías, Departamento de Fisica, León GTO, 37150 México. (email: felix@fisica.ugto.mx, felix@fnal.gov)
†Universidad de Guanajuato, División de Ciencias e Ingenierías, Departamento de Fisica, León GTO, 37150 México
**Universidad de Guanajuato, UCEA, Guanajuato GTO, México
‡http://minerva.fnal.gov/

Abstract. -The MINERνA (Main INjector ExpeRiment for ν A) experiment (http://minerva.fnal.gov/) is a neutrino scattering experiment which uses the NuMI beamline at Fermilab. It seeks to measure low energy neutrino interactions both to support neutrino oscillation experiments and to study the strong dynamics of the nucleon and nucleus that affect these interactions. For energy calibration of the main detector, a tertiary test beam line was designed and commissioned. This test beam consisted of target, collimator, two TOF stations and four wire chamber stations. Two dipole trim magnets were used to form a spectrometer. Here we present the simulation and characterization of these dipole magnets.

Keywords: MINERνA, magnets, Test Beam, FERMILAB
PACS: 13.15.+g, 14.60.Lm, 29.00.00

INTRODUCTION

The Fermilab's Meson Test Beam Facility is located in the Meson Detector Building. There, users can set up and dismantle any large equipment, can get the required beam, and can get DAQ and beam monitoring assistance. MINERνA experimenters are setting up the MINERνA Test Beam Line in this area: one Cu target, one iron collimator, two dipole magnets, four Wire Chambers, one time of flight system, and one Test Beam detector, for calibration of the main MINERνA detector. See Figure 1.

The physics that MINERνA experiment is pursuing has more than fifty years of tradition, that started from the detection of electron antineutrino[1, 2, 3, 4, 5], and continue up to these days -MINERνA collaboration (FNAL e938)[6]-.

MINERνA COLLABORATION

MINERνA experiment is a high statistics, high resolution, neutrino-antineutrino nucleon (nucleus) scattering experiment. It uses the neutrino-Main Injector beam line facility at FERMILAB. MINERνA main goal is to measure low energy neutrino interactions to support neutrino oscillation experiments and to study the strong dynamics of the nucleon and nucleus that affects these interactions.

CP1182, *Intersections of Particle and Nuclear Physics, Proceedings of the 10th International Conference,* edited by M. L. Marshak

Commissioning Of The MINERvA Tracking Prototype

J. Castorena, J. Félix, A. Higuera, Z. Urrutia, and G. Zavala

Citation: AIP Conf. Proc. **1182**, 104 (2009); doi: 10.1063/1.3293762
View online: http://dx.doi.org/10.1063/1.3293762
View Table of Contents: http://proceedings.aip.org/dbt/dbt.jsp?KEY=APCPCS&Volume=1182&Issue=1
Published by the American Institute of Physics.

Commissioning Of The MINERνA Tracking Prototype

J. Castorena*, J. Félix*, A. Higuera*, Z. Urrutia*, G. Zavala† and MINERνA Collaboration**

*Universidad De Guanajuato, División De Ciencias E Ingenierías, León, Guanajuato, México
†Universidad De Guanajuato, DCEA, Guanajuato, Guanajuato, México
**Fermilab, Fermi National Accelerator Laboratory, Batavia, IL, USA

Abstract. MINERνA is a neutrino scattering experiment that uses the NuMI beamline at Fermilab. A *Tracking Prototype* was assembled, commissioned and tested at Fermilab before moving it into the NuMI beamline. A description of some of the main commissioning activities is presented here.

Keywords: minerva, e938, numi, neutrino
PACS: 29.25.-t, 29.27.Fh

INTRODUCTION

The FNAL Experiment E-938, MINERνA[1], is a neutrino scattering experiment that has been designed to measure and to study the interaction of a low energy neutrino beam with different nuclear targets. Some of the main goals are: the study of the strong dynamics that rule low energy neutrino interactions with nuclear targets, fully reconstruct exclusive reactions and perform precise measurements of neutrino cross section. In its first phase, it was built a prototype version of the full MINERνA detector; which was assembled, tested, and commissioned on the surface before taking it underground. In this paper it will be described some of the first commissioning activities.

OVERVIEW OF THE MINERνA EXPERIMENT

MINERνA is located at about 105 meters underground in the NuMI[1] beamline at Fermilab. At MINERνA[2] it has been designed a hybrid detector which combines the use of a fully active detector and the use of a series of both electromagnetic and hadronic calorimeters. The fully active region of the MINERνA detector consists of a series of modules containing two scintillator planes each. The scintillator material in every plane is divided in 127 triangular strips. The strips in each plane can be positioned in one of three different orientations: X, U and V views. MINERνA is using the 64-pixel *7600-00-M64 Multi-Anode*[2] PMTs produced by *Hamamatsu Photonics*. FIGURE 1 is an

[1] More information about the NuMI project can be found at http://www-numi.fnal.gov/
[2] The specifications for this PMT can be found at http://sales.hamamatsu.com/en/products/electron-tube-division/detectors/photomultiplier-tubes/part-r7600-00-m64.php

CP1182, *Intersections of Particle and Nuclear Physics,*
Proceedings of the 10th International Conference, edited by M. L. Marshak

MINERvA Test Beam Commissioning

A. Higuera, J. Castorena, Z. Urrutia, J. Félix, and G. Zavala

Citation: AIP Conf. Proc. **1182**, 112 (2009); doi: 10.1063/1.3293764
View online: http://dx.doi.org/10.1063/1.3293764
View Table of Contents: http://proceedings.aip.org/dbt/dbt.jsp?KEY=APCPCS&Volume=1182&Issue=1
Published by the American Institute of Physics.

MINERνA Test Beam Commissioning

A. Higuera [*], J. Castorena[*], Z. Urrutia[*], J. Félix[*], G. Zavala[†] and MINERνA Collaboration[**]

[*]*Universidad de Guanajuato, División De Ciencias e Ingenerías, León Gto., Mex.*
[†]*Universidad de Guanajuato, DCEA, Guanajuato Gto., Mex.*
[**]*Fermi National Accelerator Laboratory, Batavia Il. USA*

Abstract. MINERνA Main INjector ExpeRiment ν - A is a high-statistic neutrino scattering experiment that will run in the NuMI Beam Hall at Fermilab. To calibrate the energy response of the MINERνA detector, a beamline is being designed for the MINERνA Test Beam Detector (TBD). The TBD is a replica of the full MINERνA detector at small scale for calibration studies of the main detector. The beamline design consists of the following parts: a copper target, used to generate tertiaries from an incoming secondary beam; a steel collimator for tertiaries, which also serves as a dump for the incoming beam; a time of fight system (scintillator planes); four wire chambers, for angle measurements and tracking; and two dipole magnets, used as an spectrometer. During last October, the first commissioning run of the MINERνA Test Beam took place in the Meson Test Beam Facility at Fermilab. We commissioned the target and collimator of the new tertiary beamline.

Keywords: MINERνA, Test Beam, First Commissioning,
PACS: 29.25.-t, 29.27.Fh

INTRODUCTION

The MINERνA test beam and detector is being prepared. We will expose a 40 plane mini- MINERνA detector where each plane is 107 x 107 cm square, which is 63 strips wide instead of the full 128 strips. These planes will have the same $UXVX$ sequence and tracking capabilities as the full MINERνA detector [1]. The frame holding the detector will allow the experimenters to insert and remove lead and iron absorbers equivalent to the electron calorimeter (ECAL) and hadron calorimeter (HCAL) portions of the MINERνA detector. With no absorbers, the test detector will be like the fully-active MINERνA inner tracking detector. This will allow us to test all the basic configurations and combinations. In addition to all ECAL and all HCAL configurations, two examples of combinations are: 10 tracker + 20 ECAL + 10 HCAL layers or 20 ECAL + 20 HCAL. The top priority for the test beam effort is to expose the detector to hadrons in a similar momentum range for the three primary processes that MINERνA will study, to obtain a calibration of the calorimetric quantities such as total visible energy deposit and its fluctuations. For quasielastic and resonance interactions, the momentum distribution is dominated by protons and pions at and below 500 MeV/c. At around this momentum, it is already likely that the hadron will undergo an inelastic interaction rather than range out. On the other hand, the spectrum from the low hadron invariant mass interactions has a tail going up to a few GeV while high invariant mass "deep inelastic scattering" events have a much higher momentum spectrum [2].

The MINERvA test beam calibrations will take place in the Meson Test Beam Facility

CP1182, *Intersections of Particle and Nuclear Physics,*
Proceedings of the 10th International Conference, edited by M. L. Marshak

The FNAL e938 Experiment: The Mexican Contribution to the MINERvA Collaboration

J. Félix, J. Castorena, A. Higuera, M. R. Gutierrez, G. Moreno et al.

Citation: AIP Conf. Proc. **1116**, 223 (2009); doi: 10.1063/1.3131559
View online: http://dx.doi.org/10.1063/1.3131559
View Table of Contents: http://proceedings.aip.org/dbt/dbt.jsp?KEY=APCPCS&Volume=1116&Issue=1
Published by the American Institute of Physics.

The FNAL e938 Experiment: The Mexican Contribution to the MINERνA Collaboration

J. Félix*, J. Castorena*, A. Higuera*, M. R. Gutierrez*, G. Moreno*, M. A. Reyes*, Z. Urrutia*, G. Zavala†, J. G. Morfin** and The MINERνA Collaboration. FNAL e938‡

*Universidad de Guanajuato, División de Ciencias e Ingenierías, Departamento de Fisica, León GTO, 37150 México
†Universidad de Guanajuato, UCEA, Guanajuato GTO, México
**Fermi National Accelerator Laboratory, Batavia, Illinois. USA.
‡http://minerva.fnal.gov/

Abstract. The MINERνA (Main INjector ExpeRiment for νA) collaboration (http://minerva.fnal.gov//) is a neutrino scattering experiment which uses the NuMI beamline at Fermilab. It seeks to measure low energy neutrino interactions both to support neutrino oscillation experiments and to study the strong dynamics of the nucleon and nucleus that affect these interactions. It is currently in its final prototyping stage and is preparing for full-scale construction. The first detector module was completed in early 2006 and it is planned to begin taking data in 2009. We present an overview of this experiment, emphasizing the Mexican contribution, and giving the potential physics results that this collaboration can contribute to the physics of neutrino.

Keywords: Test Beam, Tracking Prototype, MINERνA, Cross section
PACS: 13.15.+g, 14.60.Lm, 29.00.00

INTRODUCTION

The detection of electron antineutrino[1], more than fifty years ago, start a new course in high energy physics. For it triggered a vigorous field of research that continues up to these days[2, 3]: Neutrino physics.

Since those days up to today, there are many open problems in neutrino high energy physics: Neutrino oscillations, neutrino mass, neutrino-antineutrino identity, description of neutrino oscillations, neutrino geological problem, nature of neutrinos, precise determination of mixing parameters, CP violation, absolute value of hierarchy mass, relic neutrino, and many others[4].

There are many installed and proposed experiments trying to solve those problems -Underwater Neutrino Telescopes, Reactor Neutrino Oscillation Experiments, Long-Baseline Accelerator Neutrino Oscillation Experiments, Underground Detectors, etc.[5]-. One of those is MINERνA collaboration (FNAL e938)[6].

CP1116, *Particles and Fields,* edited by A. Ayala, C. Calcáneo-Roldan, B. Morales-Ruiz, A. Pérez-Lorenzana, A. Raya, A. Sánchez, and M. E. Tejada-Yeomans

Λ0 Polarization in Exclusive pp Reactions From the FNAL e690 Experiment

J. Félix, M. C. Berisso, D. C. Christian, A. Gara, E. E. Gottschalk et al.

Citation: AIP Conf. Proc. **1116**, 97 (2009); doi: 10.1063/1.3131611
View online: http://dx.doi.org/10.1063/1.3131611
View Table of Contents: http://proceedings.aip.org/dbt/dbt.jsp?KEY=APCPCS&Volume=1116&Issue=1
Published by the American Institute of Physics.

Λ^0 Polarization in Exclusive pp Reactions From the FNAL e690 Experiment

J. Félix[*,†], M. C. Berisso[**,‡], D. C. Christian[†], A. Gara[§,¶], E. E. Gottschalk[†], G. Gutierrez[†], E. P. Hartouni[**,‖], B. C. Knapp[§], M. N. Kreisler[**], S. Lee[**,††], K. Markianos[**,‡‡], G. Moreno[§§], M. A. Reyes[§§], M. H. L. S. Wang[¶¶], A. Wehmann[†] and D. Wesson[**,***]

[*]*Universidad de Guanajuato, División de Ciencias e Ingenierías, Departamento de Física, León GTO. 37150, México*
[†]*Fermilab,Batavia, Illinois 60510, USA.*
[**]*University of Massachusetts, Amherst, Massachusetts 01003, USA.*
[‡]*Present Address: Shasta college, reading, California 96049, USA.*
[§]*Columbia University, Nevis Laboratories, Irvington, New York 10533, USA.*
[¶]*Present Address: IBM, Yorktown Heights, New York 10598, USA.*
[‖]*Present Address: LLNL, Livermore, California 94551, USA.*
[††]*Present Address: Cognex Corp., Natic Massachusetts, 01760 USA.*
[‡‡]*Present Address: University of Washington, Seatle, Washington, 98109, USA.*
[§§]*Universidad de Guanajuato, Instituto de Fisica, México*
[¶¶]*Fermilab, Batavia, Illinois 60510, USA.*
[***]*Present Address: OEO Corporation, Athens, Georgia,30605, USA.*

Abstract.
It is an experimental evidence that all baryons are created polarized from unpolarized $p-nucleus$ collisions. So far, the origin of this polarization remains unexplained in spite of the experimental evidences accumulated in the past thirty years. Up to these days, Λ^0 is the most studied baryon for polarization, for it is copiously produced in $p-nucleus$ collisions at the energies of the principal high energy physics accelerators of the world. This paper is an overview of the experimental evidences accumulated on the polarization of Λ^0 from unpolarized exclusive pp collisions as function of x_F, P_T, and $M(\Lambda^0 K^+)$ in the past fifteen years inside Fermilab e690 experiment, in the particular reactions $pp \to p\Lambda^0 K^0 \pi^+$, $pp \to pp\Lambda^0\overline{\Lambda}^0$, $pp \to p\Lambda^0 K^+$, produced at 800 GeV.

Keywords: Polarization, Λ^0, Production plane, Resonance
PACS: 13.88.+e, 13.85.Hd, 14.20.Jn

INTRODUCTION

Many experiments have reveal that baryons from unpolarized pp inclusive and exclusive collisions, at different energies, are produced polarized[1] -specially Λ^0[2]-; and that this polarization depends on x_F, P_T, and $\Lambda^0 K^+$ invariant mass[3].

Some authors have proposed many theoretical ideas trying to understand Λ^0 polarization[4]. These models lack of predictive power, and the problem of Λ^0 polarization, and in general of baryon polarization, remains as an open problem. Some experiments have been conducted to measure Λ^0 polarization, in exclusive pp collisions, trying to unveil Λ^0 polarization origin studying specific final states where Λ^0 is produced.

CP1116, *Particles and Fields,* edited by A. Ayala, C. Calcáneo-Roldan, B. Morales-Ruiz, A. Pérez-Lorenzana, A. Raya, A. Sánchez, and M. E. Tejada-Yeomans

Electromagnetic multipole moments of spin 3/2 particles in NKR formalism

E. Germán Delgado A. and Mauro Napsuciale

Citation: AIP Conf. Proc. **1116**, 415 (2009); doi: 10.1063/1.3131587
View online: http://dx.doi.org/10.1063/1.3131587
View Table of Contents: http://proceedings.aip.org/dbt/dbt.jsp?KEY=APCPCS&Volume=1116&Issue=1
Published by the American Institute of Physics.

Electromagnetic multipole moments of spin 3/2 particles in NKR formalism

E. Germán Delgado A. and Mauro Napsuciale

Instituto de Física de la Universidad de Guanajuato, C. P. 37150, León, Guanajuato, México.

Abstract. In this work we present results for Compton scattering off spin 3/2 particles in NKR formalism and relate the behavior of the cross section to the electromagnetic multipole moments of the particle included by this formalism. We obtain expressions for such multipole moments using model independent definitions.

Keywords: Compton scattering, electromagnetic properties.
PACS: 13.60.Fz,13.40.Em,13.40.-f

INTRODUCTION

Recently, a new formalism for the description of particles with spin was proposed in [1]. The special case of spin 3/2 shows advantages with respect to the commonly used Rarita-Schwinger (RS) formalism. Unlike the RS method, in the formalism of Ref. [1] (NKR formalism here on) one gets a causal theory in the presence of an electromagnetic field.

In a previous work we calculated Compton Scattering off spin 3/2 particles in the NKR framework, we obtain the correct classical limit and the calculated cross section satisfy the unitarity constraints for center of mass energies up to the mass of the spin 3/2 particle. However, in the high energy limit, we obtain a cross section that violates unitarity. In this work we calculate the electromagnetic moments of a NKR particle.

SPIN 3/2 LAGRANGIAN

The e.o.m. in NKR formalism for spin 3/2 particles is based on the $[(\frac{1}{2},\frac{1}{2})\otimes[(\frac{1}{2},0)\oplus(0,\frac{1}{2})]$ representation, a general construction results in a two parameter expression [1]:

$$[\Gamma_{\alpha\beta\mu\nu}p^\mu p^\nu - m^2 g_{\alpha\beta}]\psi^\beta = 0,$$

where $\Gamma_{\alpha\beta\mu\nu} = \frac{1}{3}\left[(i\sigma_{\alpha\beta}+2g_{\alpha\beta})g_{\mu\nu}+(i\sigma_{\beta\nu}-2g_{\beta\nu})g_{\alpha\nu}-i\sigma_{\alpha\mu}g_{\beta\mu}\right] - ig[M_{\mu\nu}]_{\alpha\beta} - if\gamma^5\varepsilon_{\alpha\beta\mu\nu}$, with $M_{\mu\nu}$ being the generators of the representation. This equation implies the constrictions: $(p^2-m^2)\psi_\alpha = 0, \quad \gamma^\alpha\psi_\alpha = 0, \quad p^\alpha\psi_\alpha = 0$. The propagator can be found as the inverse of the $\Gamma_{\alpha\beta\mu\nu}p^\mu p^\nu - m^2 g_{\alpha\beta}$ operator. Studying the propagation of the spin 3/2 waves in an electromagnetic background , it is shown in [1] that the only values of g leading to causal propagation are $g = 0,2$. The latter value is chosen as appropriate for the description of charged particles and a striking connection between

CP1116, *Particles and Fields,* edited by A. Ayala, C. Calcáneo-Roldan, B. Morales-Ruiz, A. Pérez-Lorenzana, A. Raya, A. Sánchez, and M. E. Tejada-Yeomans

Gauge Transformations as Spacetime Symmetries

René Ángeles and Mauro Napsuciale

Citation: AIP Conf. Proc. **1116**, 399 (2009); doi: 10.1063/1.3131582
View online: http://dx.doi.org/10.1063/1.3131582
View Table of Contents: http://proceedings.aip.org/dbt/dbt.jsp?KEY=APCPCS&Volume=1116&Issue=1
Published by the American Institute of Physics.

Gauge Transformations as Spacetime Symmetries

René Ángeles and Mauro Napsuciale

División de Ciencias e Ingenierías, Universidad de Guanajuato, Lomas del Bosque 103, Fraccionamiento Lomas del Campestre, León Guanajuato, 37150, México

Abstract. Weinberg has shown that massless fields of helicity ± 1 (vector fields) do not transform homogeneously under Unitary Lorentz Transformations (LT). We calculate explicitly the inhomogeneous term. We show that imposing strict invariance of the Lagrangian under LT for an iteracting Dirac field requires the fermion field to transform with a space-time (and photon creation and annihilation operators) dependent phase and dictates the interaction terms as those arising from the conventional gauge principle.

Keywords: gauge symmetries, space-time symmetries
PACS: 11.30.Cp,

A unitary representation of the Poincaré group associates to each Poincaré transformation b^μ, Λ_1 (where b^μ is a space time translation and Λ_1 an homogeneous Lorentz transformation) a unitary operator $U(b,\Lambda_1)$, satisfying the composition rule $U(b,\Lambda_1)U(c,\Lambda_2) = U(b+\Lambda_1 c, \Lambda_2\Lambda_1)$. The transformation properties of free particle states under the Poincaré group is essentially included in the corresponding little group. For massless particles this subgroup is given by the subset of Lorentz Transformations (LT) leaving invariant light-like four vectors, i.e. given k^μ light-like, $\mathscr{R}$ belongs to the little group iff $\mathscr{R}k^\mu = k^\mu$. For the sake of simplicity we take a representative of light-like vector as $k^\mu = (k,0,0,k)$, $k>0$. A massless free particle with helicity σ and momentum $\mathbf{p}$ is described by the state $|\Psi_{p,\sigma}\rangle$ transforming under unitary Lorentz transformation, $U(0,\Lambda) = U(\Lambda)$, as [2]

$$U(\Lambda)|\Psi_{p,\sigma}\rangle = \sqrt{\frac{(\Lambda p)^0}{p^0}} exp(i\sigma\theta(\mathscr{R}(\Lambda,p)))|\Psi_{\Lambda p,\sigma}\rangle, \tag{1}$$

where θ is the Wigner angle [1].

The physical requirement of *locality* forces us to introduce creation and annihilation operators for the particle states, $|\Psi_{p,\sigma}\rangle = a^\dagger(\mathbf{p},\sigma)|0\rangle$. The transformation rule for the creation and annihilation operators of the states $|\Psi_{p,\sigma}\rangle$, is dictated by Eq. (1) as

$$U(\Lambda)a^\dagger(\mathbf{p},\sigma)U^{-1}(\Lambda) = \sqrt{\frac{(\Lambda p)^0}{p^0}} exp(i\sigma\theta(\Lambda,p)), a^\dagger(\mathbf{p}_\Lambda,\sigma). \tag{2}$$

Our physical theories must also be *causal*, thus we must work in configuration space leading us to the integration of creation and annihilation operators over all spatial momenta $\mathbf{p}$. This procedure configures a field which in order to produce a Lorentz covariant S matrix must transform in the irreducible representations (non-necessarily unitary

CP1116, *Particles and Fields,* edited by A. Ayala, C. Calcáneo-Roldan, B. Morales-Ruiz, A. Pérez-Lorenzana, A. Raya, A. Sánchez, and M. E. Tejada-Yeomans

Recent developments in chiral unitary theory of mesons and baryons

E. Oset, D. Gamermann, K. Khemchandani, A. Martinez, L. S. Geng et al.

Citation: AIP Conf. Proc. **1116**, 81 (2009); doi: 10.1063/1.3131609
View online: http://dx.doi.org/10.1063/1.3131609
View Table of Contents: http://proceedings.aip.org/dbt/dbt.jsp?KEY=APCPCS&Volume=1116&Issue=1
Published by the American Institute of Physics.

Recent developments in chiral unitary theory of mesons and baryons

E. Oset*, D. Gamermann*, K. Khemchandani*, A. Martinez*, L.S. Geng* and M. Napsuciale†

*Departamento de Física Teórica and IFIC, Centro Mixto Universidad de Valencia-CSIC, Institutos de Investigación de Paterna Aptd. 22085, 46071 Valencia, Spain.
†Instituto de Fiisica, Universidad de Guanajuato Lomas del Bosque 103, Fraccionamiento Lomas del Campestre 37150, León Guanajuato, México.

Abstract. In this talk I summarize recent findings around the description of axial vector mesons as dynamically generated states from the interaction of pseudoscalar mesons and vector mesons, dedicating some attention to the two $K_1(1270)$ states. Then I review the generation of open and hidden charm scalar and axial states, and how some recent experiment supports the existence of the new hidden charm scalar state predicted. I present recent results showing that the low lying $1/2^+$ baryon resonances for S=−1 can be obtained as bound states or resonances of two mesons and one baryon in coupled channels. Then show the differences with the S=0 case, where the $N^*(1710)$ appears also dynamically generated from the two pion one nucleon system, but the $N^*(1440)$ does not appear, indicating a more complex structure of the Roper resonance. Finally I shall show how the state X(2175), recently discovered at BABAR and BES, appears naturally as a resonance of the $\phi K\bar{K}$ system.

Keywords: Chiral dynamics, Dynamically generated resonances
PACS: 25.80,13.75.Jz,36.10.-k

INTRODUCTION

The combination of nonperturbative unitary techniques in coupled channels with the QCD information contained in the chiral Lagrangians has allowed one to extend the application domain of traditional Chiral Perturbation theory to a much larger range of energies where many low lying meson and baryon resonances appear. For instance, for the interactions between the members of the lightest octet of pseudoscalars, one starts with the chiral Lagrangian of ref. [1, 2] and selects the set of channels that couple to certain quantum numbers. Then, independently of using either the Bethe-Salpeter equation in coupled channels [3], the N/D method [4] or the Inverse Amplitude Method [5], the well known scalar resonances $\sigma(600)$, $f_0(980)$, $a_0(980)$ and $\kappa(800)$ appear as poles in the obtained L=0 meson-meson partial waves. These resonances are not introduced by hand, they appear naturally as a consequence of the meson interaction and they qualify as ordinary bound states or resonances in coupled channels. These are states that we call dynamically generated, by contrast to other states which would rather qualify as $q\bar{q}$ states, such as the ρ [6]. Similarly, in the baryon sector, the interaction of the pseudoscalar mesons with baryons of the octet of the proton generates dynamically $1/2^-$ resonances [7, 8, 9, 10, 11, 12] and the interaction of the pseudoscalar mesons

CP1116, *Particles and Fields,* edited by A. Ayala, C. Calcáneo-Roldan, B. Morales-Ruiz, A. Pérez-Lorenzana, A. Raya, A. Sánchez, and M. E. Tejada-Yeomans

Thermodynamics of the Schwarzschild Black Hole in Noncommutative Space

S. PérezPayán and M. Sabido

Citation: AIP Conf. Proc. **1116**, 451 (2009); doi: 10.1063/1.3131599
View online: http://dx.doi.org/10.1063/1.3131599
View Table of Contents: http://proceedings.aip.org/dbt/dbt.jsp?KEY=APCPCS&Volume=1116&Issue=1
Published by the American Institute of Physics.

Thermodynamics of the Schwarzschild Black Hole in Noncommutative Space

S. Pérez-Payán and M. Sabido

Instituto de Física de la Universidad de Guanajuato P.O. Box E-143, 37150 León Gto., México

Abstract. In this paper we study noncommutative black holes. In particular, we use a deform Schwarzschild solution in noncommutative gauge theory of gravity. By means of euclidean quantum gravity we obtain the entropy, temperatute and the time of evaporation of the noncommutative black hole.

Keywords: Black Holes, Noncommutativity, Thermodynamics
PACS: 02.40.Gh,04.60.-m,04.70.Dy

INTRODUCTION

Recently there has been interest in the properties of black holes in noncommutative space-time(see for example [1], and references there in), where several approaches have been proposed, in particular in [2] the authors obtain a deformed Schwarzschild solution for a noncommutative gauge theory of gravity. The solution is constructed from a deformation of the gravitational fields by gauging the noncommutative de Sitter SO(4,1) group and using the Seibeg-Witten map [3]. The new gauge fields are obtain up to second order in the noncommutative parameters $\Theta^{\mu\nu}$. Finally they calculte the new gravitational gauge potentials by contracting the noncommutative gauge group SO(4,1) to the Poincaré group ISO(3,1).

In this paper we will follow the approach as in [2] to calculate thermodynamical properties. As we will show the temperature, entropy and time of evaporation get corrected by the nature of the noncommutative solution.

Noncommutative Solutions: To calculate the thermodynamical properties of the Schwarzschild black hole in the classical picture, one can use the euclidean quantum gravity approach. In this formalism the path integral procedure is employed to obtain the partition function of the system and then the thermodynamical properties of interest (for details see for example [4]). In this work we proceed in the same manner to calculate the temperature, entropy and time of evaporation for the noncommutative black hole. As mentioned on the introduction, we start with a deformed Schwarzschild solution in noncommutative gauge theory of gravity [2], where the non-zero components of the metric have the following form

$$\hat{g}_{00} = -\left(1-\frac{\alpha}{r}\right) - \frac{\alpha(8\alpha-11\alpha)}{16r^4}\Theta^2, \tag{1}$$

$$\hat{g}_{11} = \left(1-\frac{\alpha}{r}\right)^{-1} + \frac{\alpha(4r-3\alpha)}{16r^2(r-\alpha)^2}\Theta^2, \tag{2}$$

CP1116, *Particles and Fields,* edited by A. Ayala, C. Calcáneo-Roldan, B. Morales-Ruiz, A. Pérez-Lorenzana, A. Raya, A. Sánchez, and M. E. Tejada-Yeomans

Cosmology

L. Arturo Ureña-López

Departamento de Física, DCI, Campus León, Universidad de Guanajuato, C.P. 37150, León, Guanajuato, México.

Abstract. This is a brief account of the short course in Cosmology presented at the Advanced Summer School of Physics 2009 of the Physics Department at CINVESTAV-IPN (Mexico). The purpose of the course was two fold: to draw the attention of Physics students to Cosmology, and to give a concise description of modern Cosmology and of its two main challenges, Dark Matter and Dark Energy.

Keywords: Cosmology, Dark Matter, Dark Energy
PACS: 98.80.-k,95.35.+d,95.36.+x

1. INTRODUCTION

According to John Peacock in his book *Cosmological Physics* [1], Cosmology is *a subject that has the modest aim of understanding the entire Universe and all its contents*. A fortunate definition indeed, as it describes in a few words the out-of-this-world challenge of Cosmology.

It is said that the first article in the history of modern Cosmology was published by Albert Einstein in 1917[2, 3]. This is because a true cosmological model could only arise from Einstein's Theory of General Relativity (TGR), which allows us to deal with a Universe filled everywhere with matter and also probably infinite in extension.

Since the publication of Einstein's paper, a lot of theoretical and observational work has been carried out by many people, and nowadays we have been successful in building up a model of the Universe that is consistent with our accepted physical theories. The model has been dubbed the Standard Cosmological Model, as it has become the standard paradigm in Cosmology.

For the rest of the paper, I shall give a brief description of the main topics and issues in Cosmology, much in the same spirit they were presented during the Cosmology course of the Summer School. The interested reader can find all the details of the calculations in the textbooks of different levels listed at the Bibliography section [4, 5, 6, 7, 8, 2].

2. THEORETICAL COSMOLOGY

To start with, we should first recognize that gravity is the fundamental and leading interaction at cosmological scales, which range from the size of galaxies up to the longest scale corresponding to the farthest object detected by present technology.

It is very illustrative to see Fig. 1 and the full set of figures presented in [9] (see also the webpage `http://www.astro.princeton.edu.mx/universe`, in which the authors describe a comprehensive collection of objects that have been detected so

CP1287, *Advanced Summer School in Physics 2009, Frontiers in Contemporary Physics, 5th Edition—EAV09*
edited by M. García Rocha, G. Torres Vega, R. López Fernández, L. F. Rojas Ochoa, E. De La Cruz Burelo, and A. Pérez Lorenzana

Bose-Einstein condensates from scalar field dark matter

L. Arturo Ureña-López

Departamento de Física, División de Ciencias e Ingenierías, Campus León, Universidad de Guanajuato, C.P. 37150, León, Guanajuato, México

Abstract. We review the properties of astrophysical and cosmological relevance that may arise from the bosonic nature of scalar field dark matter models. The key property is the formation of Bose-Einstein condensates, but we also consider the presence of non-empty excited states that may be relevant for the description of scalar field galaxy halos and the properties of rotation curves.

Keywords: Bose-Einstein condensates, cosmology, dark matter
PACS: 95.35.+d,04.40.-b

INTRODUCTION

According to our modern view of the Universe, dark matter models are necessary, in general, to explain the properties of the so-called cosmological structure[1, 2, 3, 4, 5]. The most succesful proposal is the one that considers that dark matter is composed of weakly interacting massive particles, whose origin could be explained in models beyond the Standard Model of Particle Physics[6, 7]. There is currently little doubt about the capabilities of the model to explain most of the properties observed in galaxies, even though some issues must still be clarified.

A simple alternative proposal is to consider that dark matter is made of a massive scalar field ϕ, whose inherent properties could also explain the behavior of dark matter at all scales[8, 9, 10, 11, 12, 13, 14, 15, 16, 17, 18, 19, 20, 21, 22, 23]; see also[24] for a comprehensive review.

Due to the bosonic nature of scalar fields, scalar field dark matter (SFDM) models, as we shall call them hereafter, must imprint particular features in the behavior of cosmological structure that are, in principle, distinguishable from the ones caused by fermionic dark matter particles.

The most obvious of all inherent properties is the possible formation of Bose-Einstein condensates (BEC) of astrophysical size and relevance. This is an idea that has pervaded SFDM models from the very beginning, and the comparison with the observed rotation curves in galaxies seems promising at first look[8, 9, 10, 11].

However, as noticed already in Ref.[33], it is not usual that BEC exist alone without the presence of particles also populating excited energy states. This may have consequences at astrophysical scales, and then we argue that excited states should be also taken into account in the discussion of SFDM models.

CP1318, *Recent Developments in Gravitation and BEC's Phenomenology*
edited by A. Macías and M. Maceda

What local supersymmetry can do for cosmology?

Celia Escamilla-Rivera, Octavio Obregón and Luis Arturo Ureña-López

Departamento de Física, DCI, Campus León, Universidad de Guanajuato, C.P 37150, León, Gto., México.

Abstract. We study the case of a supersymmetric FRW model in a flat space in the superfield formulation. Some exact solutions of the model are found and we provide a range of possible applications in the evolution of the Universe at early times for two scalar fields potentials.

Keywords: Supergravity, cosmology, scalar fields/superpotentials
PACS: 04.65.+e,04.60.Ds,98.80.-k

INTRODUCTION

One of the cornerstone problems in cosmology is that of the initial conditions of our Universe. In standard Big Bang cosmology, the Universe somehow started a hot expanding phase from a singular state, and later entered a stage of inflation before becoming radiation and matter dominated[1, 2, 3, 4].

The understanding of initial singular state of Universe is beyond the capabilities of our current physical theories, but the inflationary stage that followed can be explored by extending our ideas about gravitational phenomena. Typically, inflationary theories make use of a scalar field, which would be responsible for driving an accelerated expansion of the Universe, solving some caveats of standard Big Bang models, and providing the primordial seeds for structure formation[2, 5, 4].

Scalar fields in cosmological models are of great importance in the study of the early Universe. There have been a number of studies of spatially homogeneous scalar fields cosmological models with a variety of self interaction potentials. One potential that is commonly investigated, and which arises in a number of physical situations, has an exponential dependence on the scalar field[6, 7, 8, 9].

On the other hand, years ago supersymmetric quantum cosmology was first proposed in[10], and later on various formulation were developed (for a review see[11, 12]). One of them, the superfield method, was formulated in[13, 14, 15]. This local supersymmetry procedure has the advantage that, by defining the superfields on superspace, all the component fields in a supermultiplet can be manipulated simultaneously in a manner that automatically preserves supersymmetry. Besides, the fermionic fields, which in a whole supergravity formulation would correspond to a gravitino field, are obtained in a clear manner as the supersymmetric partners of the cosmological bosonic variables.

For the purposes of this paper, we will use the superfield formalism [15, 16], and find the Hamiltonian operator, where the momenta operator are represented, as usual, by differential operators, and the Grassmann variables by matrices [10, 17, 18]. A WKB

CP1256, *Gravitational Physics: Testing Gravity from Submillimeter to Cosmic Scale*
edited by H. A. Morales-Técotl, L. A. Ureña-López, R. Linares-Romero, and H. H. García-Compeán

Attractor dynamics of inflationary monomial potentials

Mayra J. Reyes-Ibarra and L. Arturo Ureña-López

Departamento de Física, DCI, Campus León, Universidad de Guanajuato, CP 37150, León, Gto, México.

Abstract. We study the attractors solutions of the dynamical system of a scalar field endowed with monomial potentials of the form $V(\phi) \sim \phi^{2n}$. The evolution equations of the system are written as a dynamical system, and the critical points represent solutions of physical interest. It is easy to find curves that conect the critical points, some of which behave as attractor inflationary trajectories in phase space.

Keywords: Cosmology, dynamical system, inflation, scalar field
PACS: PACS numbers: 98.80.-k,98.80.Cq,98.80.Jk

INTRODUCTION

Scalar fields play important roles in Cosmology nowadays because their dynamical properties and behavior can help us to understand properties of different models of inflation, dark energy, and also dark matter [1]. Part of the importance of scalar fields resides in the existence of attractor solutions in their dynamics which are almost completely independent of the initial conditions.

There exist several techniques to study the dynamical properties of cosmological scalar field, but one that has proved very useful is that of dynamical systems [2, 3, 4, 5]. The dynamical system techniques can easily reveal the attractor properties of the solutions of the equations of motion.

There are many inflationary models, see [2, 6, 7, 8], where some authors have studied their behavior for different potentials. One of the most studied is a model with an exponential scalar potential [5, 3], because the equations of motion can easily be written as an autonomous dynamical system.

However, sometimes the equations of motion result into a non-autonomous dynamical system, and then the properties of the dynamics are more involved and difficult to study. An example is the dynamical system arising from the inflationary model of a scalar field endowed with a quadratic potential [9]. The dynamics in this model was not only classified in terms of the critical points, but also in terms of trajectories of physical interest.

In this paper, we study the dynamics of inflationary models with monomial potentials using the same kind of variables as in Ref. [9]. As we shall show, when we write the evolution equations as a dynamical system we can find a formal equivalence of all models and also the trajectories that entail useful physical information. The results coincide with those obtained for the quartic potential studied in Ref.[10].

CP1256, *Gravitational Physics: Testing Gravity from Submillimeter to Cosmic Scale*
edited by H. A. Morales-Técotl, L. A. Ureña-López, R. Linares-Romero, and H. H. García-Compeán

Scalar Fields and Black Holes

Lizbeth M. Fernández and L. Arturo Ureña-López

Departamento de Física, DCI, Campus León, Universidad de Guanajuato, C.P. 37150, León, Guanajuato, México

Abstract. In this paper we study the evolution of a scalar field falling into a static black hole, for which we consider Eddington-Finkelstein coordinates. For both the massless and massive cases, we find that dispersion depends upon the mean wave number k_0 of the initial scalar field wave packet. In particular, we find total absorption for large values of k_0 independently of the mass value of the scalar field.

Keywords: Scalar fields, black holes
PACS: 04.40.-b,04.25.D-

INTRODUCTION

It is currently believed that most galaxies host a *supermassive* black hole (SMBH) at their center, with masses in the range of $10^5 - 10^{10}$ solar masses, but currently in a state of very low matter accretion [1, 2, 3]. In particular, the measurements of the velocities of stars near the center of the Milky Way have provided evidence for the presence of a SBH with a mass of around $4 \times 10^6 M_\odot$ [4]. There are some models that attempt to explain the present existence of galactic SBH's. Among others, we can mention the collision of 2 or more black holes to form a larger one, the core-collapse of a stellar cluster, and the formation of primordial black holes directly from external pressure in the first instances of the Big Bang [5].

In any case, the problem still is the precise mechanism under which a black hole can accrete enough matter to become supermassive. Some authors have then proposed that PBHs could have the opportunity to become SBH's simply by accreting some scalar field matter related, for instance, to dark energy. In a first study, the authors in [6, 7] found that PBH could have effectively accreted enough matter from a quintessence field endowed with an exponential potential. The basic calculations were made following the simple results of the flux of a massless scalar field into a black hole [7]. Such a result was later refused by the authors in [8], in which the quintessence flux $\dot{\varphi}^2$ must decrease slower than t^{-2} for PBHs to grow at all.

However, all of those works mentioned above used Schwarzschild-like coordinates to model the spacetime of a black hole, and then an observer at infinity sees that the scalar field from accretion is accumulated outside the Schwarzschild radius and this produces a considerable increasing of the black hole mass [9]. Another drawback is that Schwarzschild coordinates are singular at the event horizon of a black hole, and then it is not possible to reliably follow the evolution of the scalar field accretion; see for instance [10].

The aim of this paper is to present some simple results of the interaction of a scalar

CP1256, *Gravitational Physics: Testing Gravity from Submillimeter to Cosmic Scale*
edited by H. A. Morales-Técotl, L. A. Ureña-López, R. Linares-Romero, and H. H. García-Compeán

Equilibrium Configuration of Φ^4 Oscillatons

Susana Valdez-Alvarado*, Ricardo Becerril† and L. Arturo Ureña-López*

*Departamento de Física, DCI, Campus León, CP 37150, Universidad de Guanajuato,León, Guanajuato, México
†Instituto de Física y Matemáticas, Universidad Michoacana de San Nicolás de Hidalgo. Edificio C-3, Cd. Universitaria, C. P. 58040 Morelia, Michoacán, México

Abstract. We search for equilibrium configurations of the (coupled) Einstein-Klein-Gordon equations for the case of a real scalar field endowed with a quartic self-interaction potential. The resulting solutions are the generalizations of the (massive) oscillating soliton stars, the so-called oscillatons. Among other parameters, we estimate the mass curve of the configurations, and determine their critical mass for different values of the quartic interaction.

Keywords: Scalar fields, oscillatons, self-gravitating systems
PACS: 95.30.Sf, 98.80

INTRODUCTION

Oscillatons (short name for oscillating soliton stars) were first discovered by Seidel and Suen in [1], see also [2], and are non-singular and asymptotically flat solutions of the Einstein-Klein-Gordon (EKG) equations in which the metric and the scalar field are time-dependent.

The time dependence of all field quantities arise because we are working with a real scalar field. This should be distinguished from the case of a complex scalar field, for which the EKG equations provide non-singular solitonic solutions with a static geometry: the components of the complex field oscillate in precisely such a way that the stress-energy tensor is time-independent[3, 4, 5, 6].

The properties of oscillatons have been studied in some extent, and it is now known that in the massive case the equilibrium configurations are stable under any kind of perturbations, see([7]) for spherically symmetric cases, and also[8] for studies without any imposed symmetry.

Oscillatons may have some importance in both Astrophysics and Cosmology, because scalar fields have been proposed as candidates to be dark matter in the Universe [9, 10, 11, 12]. A such, scalar field dark matter would form cosmological structure with properties similar to those of oscillatons. More recently, it has been suggested that multi-state bosonic objects could also provide an alternative explanation for the flat rotation curves in galaxies [13, 14, 15].

The purpose of this work is to study the equilibrium configurations of spherically symmetric oscillatons in which the scalar field is endowed with a quartic scalar field potential. As mentioned before, much work exists for the massive case, but it is known, from boson star studies, that the inclusion of non-linear interactions may change the equilibrium properties of the bosonic configurations.

CP1256, *Gravitational Physics: Testing Gravity from Submillimeter to Cosmic Scale*
edited by H. A. Morales-Técotl, L. A. Ureña-López, R. Linares-Romero, and H. H. García-Compeán

ISBN 978-0-7354-0805-0
90000
9 780735 408050

ISBN 978-0-7354-0805-0
ISSN 0094-243X

Morales-Técotl
Ureña-López
Linares-Romero
García-Compeán

GRAVITATIONAL PHYSICS: TESTING GRAVITY FROM SUBMILLIMETER TO COSMIC SCALE

1256

AIP

GRAVITATIONAL PHYSICS: TESTING GRAVITY FROM SUBMILLIMETER TO COSMIC SCALE

Proceedings of the VIII Mexican School on Gravitation and Mathematical Physics

Playa del Carmen, Quintana Roo, Mexico *6 – 12 December 2009*

EDITORS

Hugo Aurelio Morales-Técotl
Luis Arturo Ureña-López
Román Linares-Romero
Héctor Hugo García-Compeán

AIP
American Institute of Physics

AIP CONFERENCE PROCEEDINGS ■ 1256

GRAVITATIONAL PHYSICS: TESTING GRAVITY FROM SUBMILLIMETER TO COSMIC SCALE

Proceedings of the VIII Mexican School on Gravitation and Mathematical Physics

Playa del Carmen, Quintana Roo, Mexico 6 – 12 December 2009

EDITORS

Hugo Aurelio Morales-Técotl
UAM - Iztapalapa, Mexico

Luis Arturo Ureña-López
University of Guanajuato, Mexico

Román Linares-Romero
UAM - Iztapalapa, Mexico

Héctor Hugo García-Compeán
CINVESTAV, Mexico

All papers have been peer reviewed

SPONSORING ORGANIZATIONS

Mexican National Science and Technology Council - (CONACyT)
Royal Society - (UK)
Mexican Physical Society - (SMF)
Center for Research and Advanced Studies (CINVESTAV)
Iztapalapa Metropolitan Autonomous University - (UAM-I)
University of Guanajuato - (UG)
Mexican National Autonomous University - (UNAM)

AIP
American Institute of Physics

Melville, New York, 2010
AIP CONFERENCE PROCEEDINGS ■ VOLUME 1256

From ten to four dimensions: a brief overview on string compactification

O. LoaizaBrito and L. VazquezMercado

Citation: AIP Conf. Proc. **1287**, 52 (2010); doi: 10.1063/1.3507424
View online: http://dx.doi.org/10.1063/1.3507424
View Table of Contents: http://proceedings.aip.org/dbt/dbt.jsp?KEY=APCPCS&Volume=1287&Issue=1
Published by the American Institute of Physics.

From ten to four dimensions: a brief overview on string compactification

O. Loaiza-Brito and L. Vazquez-Mercado

Departamento de Física, División de Ciencias e Ingeniería, Campus León, Universidad de Guanajuato, C.P. 37150, Guanuajuato, México.

Abstract. We provide a brief introduction on string compactifications for non-experts. The prediction of critical string theory to have a ten-dimensional space-time gives a rich background to answer fundamental questions in theoretical physics. From the Calabi-Yau compactification to recent flux compactification models, we discuss the attempts made to construct a consistent and realistic effective four-dimensional theory.

Keywords: String Theory, String compactification, flux compactification
PACS: 11.25.Mj, 11.25.Wx

INTRODUCTION

Critical string theory predicts the existence of nine spatial dimensions at the perturbative level. This suggests that,by getting rid of extra dimensions, one could reproduce effective four-dimensional (4D) gauge and gravitational theories[1]. Although there is so far no experimental evidence for string theory, still, the model predicts the existence of gravitational and gauge forces in an unified way . In this sense, string theory is a consistent theory of quantum gravity and gauge interactions [1].

This fact has inspired a large part of the *string phenomenology* community to develop novel models and techniques with the purpose to reproduce the (exact) matter content of the (Minimal Supersymmetric) Standard Model (MS)(SM) of particles [2, 3, 4, 5] and to obtain consistent effective 4D theories from string compactifications [6]. All such attempts, faced several and important problems rendering some models inconsistent. However, string theory is not a theory as quantum field theory or general relativity. Unfortunately, it is much less than that, in the sense that we do not know the elementary degrees of freedom of the theory. For this reason, string theory is until now, a collection of data, making the theory to be under development. It is not strange then, that some of the unsolvable problems, at some point become accessible by adding the newest available knowledge. For instance, until recently, it was understood that compactification backgrounds and/or SM-like models from string theory requires the presence of extra degrees of freedom, mainly from fluxes and non-perturbative effects, solving some of the most intriguing problems in previous models and opening up a vast possibility to address some others. Therefore, there is still a long way to cover till we can say by sure,

[1] Plus the inclusion of possible corrections at the scale of the string length. In this note we will not address such corrections.

CP1287, *Advanced Summer School in Physics 2009, Frontiers in Contemporary Physics, 5th Edition—EAV09*
edited by M. García Rocha, G. Torres Vega, R. López Fernández, L. F. Rojas Ochoa, E. De La Cruz Burelo, and A. Pérez Lorenzana

Noncommutative Quantum Scalar Field Cosmology

L. R. Díaz Barrón, J. C. LópezDomínguez, M. Sabido, and C. Yee

Citation: AIP Conf. Proc. **1256**, 188 (2010); doi: 10.1063/1.3473852
View online: http://dx.doi.org/10.1063/1.3473852
View Table of Contents: http://proceedings.aip.org/dbt/dbt.jsp?KEY=APCPCS&Volume=1256&Issue=1
Published by the American Institute of Physics.

Noncommutative Quantum Scalar Field Cosmology.

L. R. Díaz Barrón*, J. C. López-Domínguez*, M. Sabido* and C. Yee†

*Departamento de Física, DCI-Campus León, Universidad de Guanajuato,
A.P. E-143, C.P. 37150, Guanajuato, México.
†Departamento de Matemáticas, Facultad de Ciencias
Universidad Autónoma de Baja California, Ensenada, Baja California, México.

Abstract. In this work we study noncommutative Friedmann-Robertson-Walker (FRW) cosmology coupled to a scalar field endowed with an exponential potential. The quantum scenario is analyzed in the Bohmian formalism of quantum trajectories to investigate the effects of noncommutativity in the evolution of the universe.

Keywords: Noncommutativity, Quantum Cosmology
PACS: 02.40.Gh,98.80.Qc

The purpose of this work is to introduce a noncommutaive deformation on scalar field cosmology with an exponential potential and analyze the evolution at the classical and quantum level. In order to study the time evolution of the system we use Bohm's ontological interpretation of quantum mechanics [1]. The main motivation is the variety of evidence indicating the possibility that noncommutativity could be related to the quantum theory of gravity, then the study of simplified models might give some insight on quantum gravity, for example the effects of noncommutativity might have implications on quantum cosmology [2]. Furthermore, the use of the Bohmian formalism has the advantage that one can adopt it as a tool to get intuition about the nature of quantum phenomena from the detailed description of the underlying dynamics it provides.

QUANTUM GRAVITY AND THE BOHMIAN FORMALISM

The Hamiltonian of general relativity without matter is

$$H = \int dx^3 (NH + N_j H^j), \tag{1}$$

where

$$H = G_{ijkl}\Pi^{ij}\Pi^{kl} - h^{1/2}R^{(3)}, \qquad H^j = 2D_i\Pi^{ij}. \tag{2}$$

The momentum Π_{ij} canonically conjugated to h^{ij} is

$$\Pi_{ij} = -h^{1/2}(K_{ij} - h_{ij}K), \tag{3}$$

where $K_{ij} = -(\partial_t h_{ij} - D_i N_j - D_j N_i)/2N$.

CP1256, *Gravitational Physics: Testing Gravity from Submillimeter to Cosmic Scale*
edited by H. A. Morales-Técotl, L. A. Ureña-López, R. Linares-Romero, and H. H. García-Compeán

Black Hole Evaporation in Hořava and New Massive Gravity

S. PérezPayán and M. Sabido

Citation: AIP Conf. Proc. **1256**, 213 (2010); doi: 10.1063/1.3473856
View online: http://dx.doi.org/10.1063/1.3473856
View Table of Contents: http://proceedings.aip.org/dbt/dbt.jsp?KEY=APCPCS&Volume=1256&Issue=1
Published by the American Institute of Physics.

Black Hole Evaporation in Hořava and New Massive Gravity

S. Pérez-Payán and M. Sabido

Physics Department of the Division of Science and Engineering of the University of Guanajuato, Campus León P.O. Box E-143, 37150 León Gto., México

Abstract.
Recently it has been a lot of interest in the theory proposed by Hořava due to the renormalizability properties of the theory and as a candidate for the UV completion of Einstein gravity. On the other hand, we also investigate three dimensional black holes at a Lifshitz point. In the present work we study thermodynamical properties in this setups. In particular we are able to obtain time of evaporation for black hole solutions for the two formalisim.

Keywords: Hořava Gravity, Black Holes, Thermodynamics
PACS: 02.40.Gh,04.60.-m,04.70.Dy

INTRODUCTION

Recently a new four-dimensional theory of gravity was propesed by Hořava [1], inspired by condesed matter models of dynamical critical systems. This theory has manifest three-dimensional spatial general covariance and time-reparameterisation invariance, but only acquires four-dimensional general covariance in a infra-red large distance limit. It may be describe in a language akin to the ADM 3+1 formulation of general relativity, but in which Einstein gravity is modified so that the full underlying four-dimensional covariance is broken. On the other hand the authors in [2] show that three-dimensional gravity admits Lifshitz metrics with generic values of the dynamical exponent z as exact solutions. In particular they show that at the $z=3$ point they can obtain exact black hole solutions wich are asymptotically Lisfshitz.

HOŘAVA GRAVITY

In the ADM formalism, the four-dimensional metric of general relativity is parameterised as [3]

$$ds_4^2 = -N^2dt^2 + g_{ij}(dx^i - N^i dt)(dx^j - N^j dt), \tag{1}$$

where N is the lapse function, N^i is the shift function and g_{ij} is the 3-metric and all are function of (t,x^i). So the Einstein-Hilbert action for the ADM descomposition is given by

$$S_{EH} = \frac{1}{16\pi G}\int d^4x\sqrt{g}N(K_{ij}K^{ij} - K^2 + R - 2\Lambda), \tag{2}$$

CP1256, *Gravitational Physics: Testing Gravity from Submillimeter to Cosmic Scale*
edited by H. A. Morales-Técotl, L. A. Ureña-López, R. Linares-Romero, and H. H. García-Compeán

Noncommutativity and the Friedmann Equations

M. Sabido, W. Guzmán, and J. Socorro

Citation: AIP Conf. Proc. **1256**, 218 (2010); doi: 10.1063/1.3473857
View online: http://dx.doi.org/10.1063/1.3473857
View Table of Contents: http://proceedings.aip.org/dbt/dbt.jsp?KEY=APCPCS&Volume=1256&Issue=1
Published by the American Institute of Physics.

Noncommutativity and the Friedmann Equations

M. Sabido[1*], W. Guzmán [2†] and J. Socorro.[3*]

[*]*Physics Department of the Division of Science and Engineering of the University of Guanajuato, Campus León P.O. Box E-143, 37150 León Gto., México*
[†]*Instituto de Física, Universidade Federal do Rio de Janeiro, Caixa Postal 68528, 21945-970, Rio de Janeiro, Brazil*

Abstract. In this paper we study noncommutative scalar field cosmology, we find the noncommutative Friedmann equations as well as the noncommutative Klein-Gordon equation, interestingly the noncommutative contributions are only present up to second order in the noncommutitive parameter.

Keywords: Cosmology, Noncommutativity, minisuperspace models.
PACS: 02.40.Gh,04.60.Kz, 98.80.Jk,98.80.Qc

INTRODUCTION

The initial interest in noncommutative field theory [1] slowly but steadily permeated in the realm of gravity, all of these formulations showed that the end result of a noncommutative theory of gravity. Even though working with a full noncommutative theory of gravity looks like a fruitless ordeal, several attempts where made to understand the effects of noncommuativity on different aspects of the universe.

One particularly interesting proposal concerning noncommutative cosmology, was presented in [3], the authors conjectured from the fact that the noncommutative deformations modify the commutative fields, the effects of the full noncummutative theory of gravity should be reflected in the minisuperspace variables. This was achieved by introducing the Moyal product of functions in the Wheeler-DeWitt equation, in the same manner as is done in noncommutative quantum mechanics (NCQM). The authors show that new states of the universe can be created as a consequence of introducing this kind of deformations in the quantum phase space, several works followed with this main idea [4, 5].

Although the noncommutative deformations of the minisuperspace where originally analyzed at the quantum level by introducing the effective noncommutativity on the minisuperspace, classical noncommutative formulations have been proposed, in [4] for example the authors considered classical noncommutative relations in the phase space for the Kantowski-Sach cosmological model, and they establish the classical noncommutative equations of motion. For scalar field cosmology the classical minisuperspace is deformed and a scalar field is used as the matter component of the universe. In [6],

[1] e-mail: msabido@fisica.ugto.mx
[2] e-mail: wguzmanr@if.ufrj.br
[3] e-mail: socorro@fisica.ugto.mx

CP1256, *Gravitational Physics: Testing Gravity from Submillimeter to Cosmic Scale*
edited by H. A. Morales-Técotl, L. A. Ureña-López, R. Linares-Romero, and H. H. García-Compeán

Towards Noncommutative Supersymmetric Quantum Cosmology

M. Sabido, W. Guzmán, and J. Socorro

Citation: AIP Conf. Proc. **1318**, 209 (2010); doi: 10.1063/1.3531633
View online: http://dx.doi.org/10.1063/1.3531633
View Table of Contents: http://proceedings.aip.org/dbt/dbt.jsp?KEY=APCPCS&Volume=1318&Issue=1
Published by the American Institute of Physics.

Towards Noncommutative Supersymmetric Quantum Cosmology

M. Sabido[1*], W. Guzmán [2†] and J. Socorro.[3*]

[*] *Physics Department of the Division of Science and Engineering of the University of Guanajuato, Campus León P.O. Box E-143, 37150 León Gto., México*
[†] *Centro Brasileiro de Pesquisas Físicas, Rua Dr. Xavier Sigaud 150, Urca 22290-180, Rio de Janeiro, RJ, Brazil*

Abstract. In this work a construction of supersymmetric noncommutative cosmology is presented. We start with a "noncommutative" deformation of the minisuperspace variables, and by using the time reparametrization invariance of the noncommutative bosonic model we proceed to construct a super field description of the model.

Keywords: Cosmology, Noncommutativity, minisuperspace models.
PACS: 02.40.Gh,04.65.+e, 98.80.Jk,98.80.Qc

INTRODUCTION

One of the simplest approaches in the study of the very early universe is Quantum Cosmology (QC), which means that the gravitational and matter variables have been reduced to a finite number of degrees of freedom, these models where extensively studied by means of Hamiltonian methods in the 1970's [1]. For homogenous cosmological models the metric depends only on time, this permits to integrate out the space dependence and obtain a model with a finite dimensional configuration space, *minisuperspace*, whose variables are the 3-metric components. This approach is used, because a full quantum theory of gravity does not exist (although several candidates exist String Theory and Loop Quantum Gravity being the more successful), therefore we can canonically quantize these approximate models. From this construction a Klein-Gordon type equation arises, which describes the quantum behavior of the universe.

One of the first attempts to fix the UV behavior of quantum gravity was the use of supersymmetry, the reasoning was that the inclusion of the fermionic degrees of freedom would cancel the divergences of the theory, the resulting theory is Supergravity. In the 80's, to study SUSY quantum cosmology [2] the authors realized that they could construct a Dirac-type equation to the Wheeler-DeWitt equation, this was the beginning on the study of supersymmetric quantum cosmology.

In the last decade there has been a lot of interest in the old idea of noncommutative space-time [3], not to mention an immense amount of work that has been done on this

[1] e-mail: msabido@fisica.ugto.mx
[2] e-mail: wguzman@cbpf.br
[3] e-mail: socorro@fisica.ugto.mx

CP1318, *Recent Developments in Gravitation and BEC's Phenomenology*
edited by A. Macías and M. Maceda

CP asymmetry in Neutrino Oscillations and New Physics1

David Delepine, Vannia González Macias, Shaaban Khalil, and Gabriel López Castro

Citation: AIP Conf. Proc. **1361**, 279 (2011); doi: 10.1063/1.3622714
View online: http://dx.doi.org/10.1063/1.3622714
View Table of Contents: http://proceedings.aip.org/dbt/dbt.jsp?KEY=APCPCS&Volume=1361&Issue=1
Published by the American Institute of Physics.

CP asymmetry in Neutrino Oscillations and New Physics[1]

David Delepine*, Vannia González Macias*, Shaaban Khalil† and Gabriel López Castro**

*Departamento de Fisica, División de Ciencias e Ingenierías de la Universidad de Guanajuato, C.P. 37150, León, Guanajuato, México.
†Centre for Theoretical Physics, The British University in Egypt, El Sherouk City, Postal No, 11837, P.O. Box 43, Egypt
**Departamento de Fisica, Cinvestav, Apartado Postal 14-740, 07000 Mexico D.F., Mexico

Abstract. The CP asymmetry in neutrino oscillations, assuming new physics at production and/or detection processes, is analyzed. We compute this CP asymmetry using the standard quantum field theory within a general new physics scenario that may generate new sources of CP and flavor violation. Well known results for the CP asymmetry are reproduced in the case of V -A operators, and additional contributions from new physics operators are derived.

Keywords: cp violation, new physics, neutrino oscillations, qft approach
PACS: 11.30.Er,12.60.cn, 14.60Pq, 14.60.St

INTRODUCTION

The only evidence for flavor violation in the leptonic sector comes from neutrino oscillations and there is, so far, no confirmation for CP violation in leptonic decays. Hence, measuring any CP asymmetry in neutrino oscillation will open a new window to study CP violation and related problems (such as leptogenesis). We should also expect new sources of CP and lepton flavor violation, if New Physics is probed at the LHC. These new sources, also classified as non-standard interactions (NSI), could give important contributions to the CP asymmetry in neutrino oscillation (see ref.[1, 2, 3, 4]).
A proper procedure to take into account these non-standard interactions is important as neutrino experiments are reaching a high level of accuracy (see refs. [4, 5, 6, 7, 8, 9, 10, 11, 12] for effects of NSI). The following two hypothesis are usually considered: (i) The probability of a process associated to neutrino oscillation can be factorized into three independent parts: the production process, the oscillation probability and the detection cross section. (ii) The CP asymmetry in this process is due to the CP violating phase in the lepton mixing matrix. In a pioneering work, the authors of Ref. [1] have studied CP violating effects due to contributions from new neutrino interactions in the production and/or detection processes in neutrino oscillation experiments. However, only corrections to the V-A SM charged current interactions were considered [1]. In Ref.[2], the (V-A)(V-A) and (V-A)(V+A) operators associated to muon decays, but not to the pion

[1] work presented by David Delepine

XII Mexican Workshop on Particles and Fields
AIP Conf. Proc. 1361, 279-283 (2011); doi: 10.1063/1.3622714

Nuclear reactors Monitoring using neutrinos detectors1

David Delepine, Jose Antonio Hernandez Valencia, and Gerardo Moreno

Citation: AIP Conf. Proc. **1361**, 398 (2011); doi: 10.1063/1.3622738
View online: http://dx.doi.org/10.1063/1.3622738
View Table of Contents: http://proceedings.aip.org/dbt/dbt.jsp?KEY=APCPCS&Volume=1361&Issue=1
Published by the American Institute of Physics.

Nuclear reactors Monitoring using neutrinos detectors. [1]

David Delepine, Jose Antonio Hernandez Valencia and Gerardo Moreno

Departamento de Fisica, División de Ciencias e Ingenierías de la Universidad de Guanajuato, C.P. 37150, León, Guanajuato, México.

Abstract. We study the feasibility to use antineutrinos detectors for monitoring of nuclear reactors. Using a simple model of fission shower with two components, we illustrate how the numbers of antineutrinos detected at a distance L from the reactor depend on the composition of the nuclear combustible and how it could be used for nuclear safeguards policy.

Keywords: neutrino, fission, nuclear reactor
PACS: 25.30.ft, 24.75.+i, 28.41.Te

INTRODUCTION

Since the first anti-neutrino detection done in the 50's using a nuclear reactor as a source of anti-neutrinos[1], it has been proposed to use the technics developed for neutrino detection to nuclear physics and particularly to the nuclear reactor monitoring [2] as a way to improve the nuclear safeguards imposed by the International Agency For Atomic Energy (AIEA). Various previous experiments have demonstrated its feasibility [3, 4]. In the last years, our knowledge on neutrino physics and their technics of detection has impressively improved and these progress are making possible the conception of "mini"-neutrino detectors which could be used for nuclear reactor monitoring [5, 6].

In this work, we shall describe what are the principles on which the nuclear reactor monitoring using neutrino detectors is possible [7]. We shall use a simplified model which will be easy to generalize to a real case.

BASIC PRINCIPLES

The basics principles is to establish a correlation between the observed events number and the composition of the nuclear reactor. To illustrate how to get this correlation, we shall use a simplified model with a fission shower with two components:

$$\begin{aligned} A \rightarrow \quad & B \quad + e^- + \bar{\nu}_e \\ & \hookrightarrow \quad C + e^- + \bar{\nu}_e \end{aligned} \tag{1}$$

[1] work presented by Jose-Antonio Hernandez Valencia

XII Mexican Workshop on Particles and Fields
AIP Conf. Proc. 1361, 398-400 (2011); doi: 10.1063/1.3622738

Difference in 0(B0)→Kπ± and B→Kπ0 CP violation1

D. Delepine, B. Raziel Jaramillo Avila, and C. A. Ramirez

Citation: AIP Conf. Proc. **1361**, 401 (2011); doi: 10.1063/1.3622739
View online: http://dx.doi.org/10.1063/1.3622739
View Table of Contents: http://proceedings.aip.org/dbt/dbt.jsp?KEY=APCPCS&Volume=1361&Issue=1
Published by the American Institute of Physics.

Difference in $\bar{B}^0(B^0) \to K^{\mp}\pi^{\pm}$ and $B^{\mp} \to K^{\mp}\pi^0$ CP violation[1]

D. Delepine*, B. Raziel Jaramillo Avila* and C. A. Ramirez†

*Departamento de Fisica,División de Ciencias e Ingenierías de la Universidad de Guanajuato, C.P. 37150, León, Guanajuato, México.
†Escuela de Física, Universidad Industrial de Santander,A.A. 678, Bucaramanga, Colombia

Abstract. Direct CP asymmetry for $\bar{B}^0(B^0) \to K^{\mp}\pi^{\pm}$ and $B^{\mp} \to K^{\mp}\pi^0$ has been measured[1]. The similarity in the two decays suggest $A^{CP}_{\bar{B}^0 \to K^-\pi^+} \sim A^{CP}_{B^- \to K^-\pi^0}$. However the asymmetries turned out to be very different. In this work we investigate if this could be a result of physics beyond the Standard Model. A numerical model independent approach is proposed.

Keywords: CP violation, *B* decays
PACS: 13.25.Hw

INTRODUCTION

Belle measured direct CP asymmetries for the $\bar{B}^0(B^0) \to K^{\mp}\pi^{\pm}$ and $B^{\mp} \to K^{\mp}\pi^0$ decays[1]. The values found are:

$$A^{CP}_{\bar{B}^0 \to K^-\pi^+} = -0.094 \pm 0.018 \pm 0.008 \qquad A^{CP}_{B^- \to K^-\pi^0} = 0.07 \pm 0.03 \pm 0.01. \tag{1}$$

Due to isospin symmetry of the strong interactions and the similarity in the quark contents of the meson involved, one expect $A^{CP}_{\bar{B}^0 \to K^-\pi^+} \sim A^{CP}_{B^- \to K^-\pi^0}$. The only difference between both processes should be due to color-suppressed contributions or due to weak penguins Feynman diagrams.

AMPLITUDES IN THE FACTORIZATION APPROXIMATION

The operators for $b \to u\bar{u}s$ can be calculated using the Standard Model Feynman rules. Of course, it is an approximation since in a Feynman diagram initial and final states are supposed to be free, however $b, u, \bar{u}, s$ quarks are constituents of meson states and hence not free. The Feynman diagrams contributing to these processes are tree level diagrams, penguin and box diagrams (see fig.1). Dominant contributions come from the tree and strong penguin diagrams. The contributions to this diagrams can be summarized using the effective Hamiltonian:

$$\frac{G_F}{\sqrt{2}}\left[V_{ub}V^*_{us}\big(C_1(\mu)\hat{O}_1 + C_2(\mu)\hat{O}_2\big) + V_{tb}V^*_{ts}\big(\sum_{i=3}^{10} C_i(\mu)\hat{O}_i\big)\right] + \text{h.c.} \tag{2}$$

[1] work presented by Benjamin Raziel Jaramillo Avila

XII Mexican Workshop on Particles and Fields
AIP Conf. Proc. 1361, 401-403 (2011); doi: 10.1063/1.3622739

Pion Charge Asymmetries in e+e−→π+π−γ

A. Gallegos, J. L. Lucio, G. Moreno, and M. Napsuciale

Citation: AIP Conf. Proc. **1361**, 187 (2011); doi: 10.1063/1.3622698
View online: http://dx.doi.org/10.1063/1.3622698
View Table of Contents: http://proceedings.aip.org/dbt/dbt.jsp?KEY=APCPCS&Volume=1361&Issue=1
Published by the American Institute of Physics.

Pion Charge Asymmetries in $e^+e^- \to \pi^+\pi^-\gamma$

A. Gallegos*, J. L. Lucio†, G. Moreno† and M. Napsuciale†

*Departamento de Ciencias Exactas y Tecnología, Centro Universitario de los Lagos, Universidad de Guadalajara, Enrique Díaz de León 1144, Colonia Paseos de la Montaña, 47460, Lagos de Moreno, Jalisco, México

†Departamento de Física, División de Ciencias e Ingenierías, Universidad de Guanajuato, Campus León, Lomas del Bosque 103, Fraccionamiento Lomas del Campestre, 37150, León, Guanajuato, México

Abstract. We consider the forward-backward pion charge asymmetry for the $e^+e^- \to \pi^+\pi^-\gamma$ process. In addition to the Bremsstrahlung and double resonance contributions, we use four different models to describe the final state radiation at the loop level (Kaon Loop Model, Resonance Chiral Perturbation Theory, Unitarized Chiral Perturbation Theory and Linear Sigma Model) and compare our results with experimental data.

Keywords: charge asymmetry, chiral lagrangians
PACS: 13.25.Gv,12.39.Fe,13.40.Fq.

INTRODUCTION

The forward-backward pion charge asymmetries in the process $\phi \to \pi^+\pi^-\gamma$ has been recently measured as a function of the $\pi^+\pi^-$ invariant mass [1]. The asymmetry is sensitive to the mechanisms involved in the final state radiation [2] and it has been proposed as an appropriate observable to test the importance of the different mechanisms at work in this reaction.

The asymmetry requires a non vanishing interference between initial (ISR) and final (FSR) state radiation, the latter being strongly model dependent [3]. The invariant amplitude for the $e^+e^- \to \pi^+\pi^-\gamma$ process can be parameterized in terms of three independent Lorentz structures and thus the model dependence in FSR can be included in three scalar functions f_i [4]. The final state radiation has been calculated in different models. The simplest approximation has been named scalar QED (*sQED*) [3, 5] and it actually includes the ρ contributions to the pion form factor. In that work the contributions of intermediate scalars ($f_0(980)$ and σ) are also considered using a point-like $\phi f_0 \gamma$ interaction, in the so called "no-structure" model. Later on, final state radiation was calculated within Resonance Chiral Perturbation Theory ($R\chi PT$) [6] at tree level [4, 7, 8]. In particular, in [8] sub-leading intermediate vector mesons contributions like $e^+e^- \to \phi \to \rho^-\pi^+ \to \pi^+\pi^-\gamma$, named double resonance contributions, were incorporated.

The aim of this work is to work out the predictions for $e^+e^- \to \pi^+\pi^-\gamma$ at the ϕ resonance at one loop level for four alternative models, namely $R\chi PT$, Unitarized Chiral Perturbation Theory ($U\chi PT$) [9] (containing actually a resumation of loops), Linear Sigma Model (LSM) [10, 11] and the so-called "kaon-loop" model [12]. In each case we add the Bremsstrahlung contributions ($sQED*VMD$) and the double resonance

XII Mexican Workshop on Particles and Fields
AIP Conf. Proc. 1361, 187-191 (2011); doi: 10.1063/1.3622698

Stability of Φ^4 oscillatons

2011 J. Phys.: Conf. Ser. 315 012013

(http://iopscience.iop.org/1742-6596/315/1/012013)

Journal of Physics: Conference Series **315** (2011) 012013 doi:10.1088/1742-6596/315/1/012013

Stability of Φ^4 oscillatons

S Valdez-Alvarado[1], L A Ureña-López[1] and R Becerril-Bárcenas[2]

[1] Departamento de Física, DCI, Campus León, CP 37150, Universidad de Guanajuato,León, Guanajuato, México

[2] Instituto de Física y Matemáticas, Universidad Michoacana de San Nicolás de Hidalgo. Edificio C-3, Cd. Universitaria, C. P. 58040 Morelia, Michoacán, México

E-mail: svaldez@fisica.ugto.mx,lurena@fisica.ugto.mx,becerril@ifm.umich.mx

Abstract. We investigate the stability of oscillatons with a quartic self-interaction. Oscillatons are spherically symmetric solutions of the coupled Einstein-Klein-Gordon for the case of a real scalar field. It is shown that there exist equilibrium configurations which are stables under small and strong (radial) perturbations. Some basic numerical tools are implemented that shall help in the study of arbitrary equilibrium configurations.

1. Introduction

Seidel and Suen were the first that found non-singular and asymptotically flat solutions of the coupled Einstein-Klein-Gordon (EKG) equations, in which both the (real) scalar field and the metric are time-dependent [1, 2]. These solutions are so-called *oscillatons* that is the short name for oscillating soliton stars. Time-dependent of oscillatons arise because we working with real scalar field, and this case is different from its complex counterpart, boson stars, for which the spacetime geometry is static[3].

In an exhaustive analysis presented in[4], it was shown that oscillatons are classified into stable (S-branch) and unstable (U-branch) configurations. S-oscillatons are stable configurations under small radial perturbations, and they typically migrate to other S-profiles if strongly perturbed. On the other hand, U-oscillatons are intrinsically unstable: they migrate to the S-branch if their mass is moderate, but they may collapse into black holes if their mass is large enough.

As we mention in [5], oscillatons may have some importance in both Astrophysics and Cosmology, because scalar fields have been proposed as candidates to be dark matter in the Universe [6, 7, 8, 9]. Scalar field dark matter would form cosmological structure with properties similar to those of oscillatons.More recently, it has been suggested that multistate bosonic objects could also provide an alternative explanation for the flat rotation curves in galaxies [10, 11, 12, 13].

In this work, we study the evolution of oscillatons with a quartic self-interaction in the scalar field potential, and analyze the stability in some selected cases following closely the numerical tools presented in Ref.[4].

Preface: VIII Workshop of the Gravitation and Mathematical Physics Division of the Mexican Physical Society

Luis Arturo UreñaLópez, Hugo Aurelio MoralesTécotl, Román LinaresRomero, Elí SantosRodríguez, and Sendic EstradaJiménez

Citation: AIP Conf. Proc. **1396**, 1 (2011); doi: 10.1063/1.3647522
View online: http://dx.doi.org/10.1063/1.3647522
View Table of Contents: http://proceedings.aip.org/dbt/dbt.jsp?KEY=APCPCS&Volume=1396&Issue=1
Published by the American Institute of Physics.

Cosmological constraints for a two braneworld system with single equation of state

Juan L. Pérez, Rubén Cordero, and L. Arturo UreñaLópez

Citation: AIP Conf. Proc. **1396**, 208 (2011); doi: 10.1063/1.3647549
View online: http://dx.doi.org/10.1063/1.3647549
View Table of Contents: http://proceedings.aip.org/dbt/dbt.jsp?KEY=APCPCS&Volume=1396&Issue=1
Published by the American Institute of Physics.

Cosmological constraints for a two brane-world system with single equation of state

Juan L. Pérez*, Rubén Cordero† and L. Arturo Ureña-López*

*Departamento de Física, DCI, Campus León, Universidad de Guanajuato, C.P. 37150, León, Guanajuato, México
†Departamento de Física, Escuela Superior de Física y Matemáticas del IPN Unidad Adolfo López Mateos, Edificio 9, 07738, México D.F., México

Abstract. We present the study of two 3-brane system embedded in a 5-dimensional space-time in which the fifth dimension is compactified on a S^1/Z_2 orbifold. Assuming isotropic, homogeneous, and static branes, it can be shown that the dynamics of one brane is dominated by the other one when the metric coefficients have a particular form. We study the resulting cosmologies when one brane is dominated by a given single-fluid component.

Keywords: Braneworlds, cosmology
PACS: 04.50.-h, 98.80.-k, 11.10.Kk, 98.80.Jk

INTRODUCTION

In the last years, there has been a great expectation about braneworld scenario as an alternative proposal to explain some unsolved problems in particle physics and cosmology, including the hierarchy and the dark matter-energy problems. It is in this context that diverse braneworld models have emerged in an attempt to put a final point to these problems.

Superstring and M-theory suggest that we may live in a world that has more than three spatial dimensions [1]. Because only three of these dimensions are presently observable, one has to explain why the others are hidden from detection. One such explanation is the so-called Kaluza-Klein (KK) compactification (see [2] and [3] for a review), according to which the extra dimensions are very small, probably with a size of the order of the Planck length. As a consequence, modes that have momentum in the directions of the extra dimensions are excited at currently inaccessible energies.

In 1998, N. Arkani-Hamed, S. Dimopoulus and G. R. Dvali (ADD) [4] pointed out that the extra dimensions are not necessarily small, and may even be in the scale of millimeters. This model assumes that the Standard Model fields are confined to a three dimensional surface (a 3-brane) embedded in a larger dimensional background spacetime (bulk) where the gravitational field is free to propagate. Additional fields may live only on the brane or in the bulk, provided that their current undetectability is consistent with experimental bounds [5].

An alternative approach was proposed by L. Randall and R. Sundrum (RS) [6], which will be hereafter referred to as RS1 model (see [7] for a general treatment of two 3-branes in a RS setup). The bulk in this model is 5-dimensional, with the extra dimension being compactified on an S_1/Z_2 orbifold i.e. the extra dimension y is periodic, and its

VIII Workshop of the Gravitation and Mathematical Physics Division of the Mexican Physical Society
AIP Conf. Proc. 1396, 208-212 (2011); doi: 10.1063/1.3647549

Preheating studies in a chaotic inflationary model

E. TorresLomas and L. Arturo UreñaLópez

Citation: AIP Conf. Proc. **1396**, 213 (2011); doi: 10.1063/1.3647550
View online: http://dx.doi.org/10.1063/1.3647550
View Table of Contents: http://proceedings.aip.org/dbt/dbt.jsp?KEY=APCPCS&Volume=1396&Issue=1
Published by the American Institute of Physics.

Preheating studies in a chaotic inflationary model

E. Torres-Lomas and L. Arturo Ureña-López

Departamento de Física, DCI, Campus León, CP 37150, Universidad de Guanajuato,León, Guanajuato, México

Abstract. Inflationary cosmological models must include a process able to produce an evolution towards a phase of radiation domination so that Hot Big Bang is retrieved satisfactory. At the end of inflation, the universe enters to the stage known as (p)reheating during which cosmological reheating temperature should be increased in an explosive way. We study the process of preheating in a model that includes two scalar fields, one of which is the inflaton field, and four-leg interaction term in the Lagrangian.

Keywords: Scalar fields, reheating, preheating.
PACS: 95.30Cq, 95.30.Tg, 98.80.

INTRODUCTION

During the period of inflation all energy is contained in a classical scalar field ϕ (inflaton) with negligible kinetic energy. Eventually, the inflaton field decays and transfers all its energy to relativistic particles causing that the universe evolves to a state of domination of radiation; this process should produce a hot Friedmann universe. This stage is known as *reheating*, and during its development (almost) all elementary particles are created and subsequently populate the universe. It is then important to analyze the processes that take place and the potential consequences on the late-time cosmological evolution.

The basic idea for cosmological reheating was proposed by A. D. Linde in[1, 2, 3, 4]. Particle production occurs due to oscillations of the scalar field ϕ around the minimum of the self-interaction potential, immediately after the inflationary era ends. The particles interact with each other, and eventually reach a thermal equilibrium state with a *reheating* temperature T_r. This process is considered complete once the inflaton has given all its energy to relativistic particles. Reheating can be analyzed by perturbative methods[4], but in many inflationary models the production of particles is carried out by non-perturbative processes in the so-called parametric excitation regime[5, 6, 7, 8]. This process is known as *preheating* and occurs immediately after inflation has ended and before perturbative contributions come into play.

The preheating stage occurs in a very short time period in which relativistic particles are produced copiously, and is followed by turbulent interactions between different oscillation modes of the scalar fields. We present the analytical study for preheating in a model with two scalar fields, one of which is the inflaton field with quadratic self-interaction potential, and the second scalar field is an auxiliary one with negligible bare mass. An interaction term of four-legs is included in the theory which induces resonant parametric solutions for the field equations.

VIII Workshop of the Gravitation and Mathematical Physics Division of the Mexican Physical Society
AIP Conf. Proc. 1396, 213-217 (2011); doi: 10.1063/1.3647550

VIII WORKSHOP OF THE GRAVITATION AND MATHEMATICAL PHYSICS DIVISION OF THE MEXICAN PHYSICAL SOCIETY

Tuxtla Gutiérrez, Chiapas, Mexico 22 – 26 November 2010

EDITORS

Luis Arturo Ureña-López
Hugo Aurelio Morales-Técotl
Román Linares-Romero
Elí Santos-Rodríguez
Sendic Estrada-Jiménez

AIP
American Institute of Physics

AIP | CONFERENCE PROCEEDINGS ■ 1396

Ureña-López
Morales-Técotl
Linares-Romero

Santos-Rodríguez
Estrada-Jiménez

VIII WORKSHOP OF THE GRAVITATION AND MATHEMATICAL PHYSICS DIVISION OF THE MEXICAN PHYSICAL SOCIETY

1396

AIP

ISBN 978-0-7354-0969-9
ISSN 0094-243X

VIII WORKSHOP OF THE GRAVITATION AND MATHEMATICAL PHYSICS DIVISION OF THE MEXICAN PHYSICAL SOCIETY

Tuxtla Gutiérrez, Chiapas, Mexico 22 – 26 November 2010

EDITORS

Luis Arturo Ureña-López
University of Guanajuato (UG), Guanajuato, Mexico

Hugo Aurelio Morales-Técotl
Román Linares-Romero
Iztapalapa Metropolitan Autonomous University (UAM-I), Mexico City, Mexico

Elí Santos-Rodríguez
Sendic Estrada-Jiménez
Chiapas Autonomous University (CEFyMAP-UNACH), Chiapas, Mexico

All papers have been peer reviewed.

SPONSORING ORGANIZATIONS
Mexican National Science and Technology Council (CONACyT)
Mexican Physical Society (SMF)
Center for Research and Advanced Studies (CINVESTAV)
Iztapalapa Metropolitan Autonomous University (UAM-I)
University of Guanajuato (UG)
Mexican National Autonomous University (UNAM)
Autonomous University of Chiapas (UNaCh)

AIP
American Institute of Physics

Melville, New York, 2011
AIP | CONFERENCE PROCEEDINGS ■ 1396

A quantum cosmological model in HořavaLifshitz gravity

O. Obregón and J. A. Preciado

Citation: AIP Conf. Proc. **1396**, 151 (2011); doi: 10.1063/1.3647539
View online: http://dx.doi.org/10.1063/1.3647539
View Table of Contents: http://proceedings.aip.org/dbt/dbt.jsp?KEY=APCPCS&Volume=1396&Issue=1
Published by the American Institute of Physics.

A quantum cosmological model in Hořava-Lifshitz gravity

O. Obregón and J. A. Preciado

Departamento de Física, División de Ciencias e Ingenierías, Campus León, Universidad de Guanajuato, A.P. E-143, C.P. 37150, León, Guanajuato, México.

Abstract. A Wheeler-DeWitt equation for the Kantowski-Sachs model is derived within the framework of the minimal quantum gravity theory proposed by Hořava. We study the solution to this equation in the ultraviolet limit for the specific case where the λ parameter of the theory takes its relativistic value $\lambda = 1$. It is observed that the minisuperspace variables switch their role compared with their usual infrared (General Relativity) behavior.

Keywords: Horava gravity, quantum cosmology, minisuperspace models
PACS: 04.60.-m; 04.50.Kd; 98.80.Qc; 04.60.Kz

1. INTRODUCTION

Recently Petr Hořava proposed an interesting approach to quantum gravity [1, 2]. The central idea of his theory is to combine gravity with the concept of anisotropic scaling between space and time, motivated by the recent developments in the study of condensed matter systems. Based on this principle, higher-derivative correction terms may be added to the standard Einstein-Hilbert action such as different powers of the spatial curvature. This improves the ultraviolet (UV) behavior of the graviton propagator and makes the theory power counting renormalizable, but at the cost of giving up to Lorentz invariance as a fundamental symmetry. Instead of that, it is expected to emerge as an accidental symmetry in the infrared (IR) regime where general covariance must be restored.

In the minimal version of the theory the nature of the modifications is governed by the gravitational analog of the "detailed balance" principle, frequently used in the study of the dynamics of nonequilibrium systems, and the so called "projectability condition" which restricts the lapse function to be a function of time only. However, it is possible to construct a generalization by relaxing any or both of these conditions. This has lead to the projectable and non-projectable versions of the theory [3, 4].

It has been claimed that Hořava's proposal and its extensions suffer from several issues related to a badly behaved scalar mode [5, 6]. However, it has many desirable features and seems worth exploring it. Many aspects of the theory have been discussed in the literature, particularly, cosmological and black hole solutions have been obtained [7, 8]. Many issues of cosmology arising from it have also been analyzed (see for example [9]). However, no model that provides information about the quantum properties of this theory seems to have been considered up to now.

For this purpose in this work we consider the Kantowski-Sachs (KS) universe which is one of the simplest anisotropic models. A Wheeler-DeWitt (WDW) equation for this model is derived in the context of the minimal theory proposed by Hořava. We study the

VIII Workshop of the Gravitation and Mathematical Physics Division of the Mexican Physical Society
AIP Conf. Proc. 1396, 151-155 (2011); doi: 10.1063/1.3647539

Low energy theorems for gauge boson scattering in leftright symmetric models

C. A. VaqueraAraujo and M. Napsuciale

Citation: AIP Conf. Proc. 1361, 238 (2011); doi: 10.1063/1.3622707
View online: http://dx.doi.org/10.1063/1.3622707
View Table of Contents: http://proceedings.aip.org/dbt/dbt.jsp?KEY=APCPCS&Volume=1361&Issue=1
Published by the American Institute of Physics.

Low energy theorems for gauge boson scattering in left-right symmetric models

C. A. Vaquera-Araujo and M. Napsuciale

Departamento de Física, Universidad de Guanajuato, Campus Leon, C.P. 37150, León, Guanajuato, México.

Abstract. In this work, low energy theorems for gauge boson longitudinal modes of the $SU(2)_L \times SU(2)_R \times U(1)_{B-L}$ electroweak gauge theory are derived. These theorems are valid for energies in the domain of applicability of the Equivalence Theorem, and hold for all left-right symmetric models assuming that there are no extra contributions from light scalars to the scattering amplitudes.

Keywords: Left-right, gauge boson scattering, electroweak chiral lagrangian
PACS: 12.39.Fe, 12.60.Cn, 12.15.Ji

INTRODUCTION

The standard model (SM) of weak interactions is extremely successful. Nevertheless the actual electroweak symmetry breaking (EWSB) mechanism is still unknown. Perhaps the most important goal of the Large Hadron Collider (LHC) is to elucidate this phenomenon, and an essential part of the prescription is the analysis of gauge boson scattering reactions $VV \to VV$ [1]. If we do observe those reactions, it means that the quanta of the symmetry breaking sector are of strong magnitude; otherwise, EWSB is accomplished by weakly coupled quanta below $\mathcal{O}(1)$ TeV, the typical scale where the amplitude of this class of processes would saturate tree-unitarity. If the Higgs mechanism turns to be realized, a Higgs boson is enough to restore unitarity, and that is a very desirable feature of the theory, but unsatisfactorily theories with fundamental scalars are probably trivial. Beyond SM, a huge class of new physics models exist in which the population of fundamental scalars increases dramatically, and therefore they inherit many problems of the SM related with the symmetry breaking sector. This is the case for many models based on left-right (L-R) symmetry.

L-R symmetric extensions of the SM which implement the gauge group

$$SU(2)_L \times SU(2)_R \times U(1)_{B-L} \tag{1}$$

have several attractive features (for a review see [2]). These include the same quark-lepton symmetry with respect to the $SU(2)$ group, the understanding of space-time inversion symmetry violation as a consequence of the vacuum structure of the theory and the natural existence of right handed neutrinos. Plenty of L-R symmetric models have been proposed with different contents of Higgs multiplets, but there also exist the possibility of strong dynamics taking place in this kind of models. In this work we find LETs for the scattering of longitudinally polarized gauge bosons in a general L-R

XII Mexican Workshop on Particles and Fields
AIP Conf. Proc. 1361, 238-242 (2011); doi: 10.1063/1.3622707

DPyCSMF Medal Award in Honor of José Luis Lucio Martínez

M. Napsuciale

Citation: AIP Conf. Proc. **1361**, 4 (2011); doi: 10.1063/1.3622681
View online: http://dx.doi.org/10.1063/1.3622681
View Table of Contents: http://proceedings.aip.org/dbt/dbt.jsp?KEY=APCPCS&Volume=1361&Issue=1
Published by the American Institute of Physics.

DPyC-SMF Medal Award in Honor of José Luis Lucio Martínez

M. Napsuciale

Departamento de Física, División de Ciencias e Ingenierías, Universidad de Guanajuato, Campus León, Lomas del Bosque 103, Fraccionamiento Lomas del Campestre, 37150, León, Guanajuato, México

Abstract. The DPyC Medal award 2009 has been granted to José Luis Lucio for his contributions to the field of particle physics and to the development of the Mexican high energy physics community. In this contribution I briefly discuss these topics.

INTRODUCTION

The 2009 edition of the medal award of Division of Particles and Fields-Mexican Physical Society has been granted to José Luis Lucio Martínez and it is my pleasure to attend the organizing committee invitation to account for his contributions to the field of particle physics and to the development of the Mexican community working in this field. I will dwell first on the second topic and then go through the different problems in particle physics on which José Luis did work .

CONTRIBUTIONS TO THE DEVELOPMENT OF PARTICLE PHYSICS IN MEXICO

José Luis emigrated from his born place, San Luis Potosí, during his third year (out of five) of the bachelor program, to México City where he got his Master degree at Cinvestav in 1977 working in elementary particle physics. Since then he has worked in this discipline getting his PhD in 1980 at the Catholic University of Louvain (UCL), Belgium, after which he got back to México to work at Cinvestav. I meet José Luis for the first time in 1986 at the Physics Department of Cinvestav where I went to start the Master program in physics. There was a small group at this place doing particle physics (Arnulfo Zepeda, Augusto García, Miguel Angel Perez, José Luis Lucio, Alfonso Rosado and Rodrigo González) and a nice academic atmosphere, where the close relationship between professors and students of the Physics Department stimulated intense discussions on the different topics on which the members of the Department were working. These discussions were specially interesting during the Department celebrations when a student presented his/her thesis defense and it was in these meetings where I learn most of what I will write here about the particle physics community before 1986.

The Mexican School of Particle and Fields (MSPF) was created in 1984 by José Luis Lucio, Matías Moreno and Arnulfo Zepeda. José Luis gave continuity to this conference

XII Mexican Workshop on Particles and Fields
AIP Conf. Proc. 1361, 4-7 (2011); doi: 10.1063/1.3622681

Spinor fields in 4+1 dimensions and the Dirac equation

Selim GómezÁvila and Mauro Napsuciale Mendivil

Citation: AIP Conf. Proc. **1361**, 288 (2011); doi: 10.1063/1.3622716
View online: http://dx.doi.org/10.1063/1.3622716
View Table of Contents: http://proceedings.aip.org/dbt/dbt.jsp?KEY=APCPCS&Volume=1361&Issue=1
Published by the American Institute of Physics.

Spinor fields in $4+1$ dimensions and the Dirac equation

Selim Gómez-Ávila[*,†] and Mauro Napsuciale Mendivil[*,**]

[*]*Departamento de Física, Universidad de Guanajuato*
[†]*selimibn@fisica.ugto.mx*
[**]*mauro@fisica.ugto.mx*

Abstract. We discuss the local properties of free spinor fields in $4+1$ dimensions. The Poincaré group has in this case three algebraic invariants $(\mathscr{C}_2,\mathscr{C}_3,\mathscr{C}_4)$, which correspond to extra dimensional mass, spin, and a new quantum number related to the little algebra $\mathfrak{so}(4)$. We construct the eigenspaces for these invariant operators in the spinor representation. In the fermion case the eigenvalue equation $(\mathscr{C}_3 \pm 3m)\psi = 0$ for the cubic Casimir turns out to be equal to the Dirac equation.

Keywords: Extra dimensions, field theory
PACS: 11.10.Kk, 11.30.Cp

GOOD QUANTUM NUMBERS

In order to use the induced representation method to construct a quantum field theory in extra dimensions [1] we need to adequately characterize the spacetime quantum numbers of $D+1$ spacetime. This is a first step necessary for the consistency of extra dimensional models; it means both finding the abstract independent algebraic invariants of the $\mathfrak{iso}(1,D)$ and $\mathfrak{so}(1,D)$ spacetime algebras and contructing representations where they can be explicitely realized. In particular we are interested in the most immediate case of the $4+1$ spacetime. There are many systematic studies of the global properties of contracted spacetimes (see for an example [2], or the review [3] and references therein), but the local structure can also provide interesting information; this will be the focus of this work.

First we discuss the extra dimensional Poincaré algebra and its invariants. Then we proceed with the construction of irreducible representations of the $\mathfrak{so}(1,4)$ algebra through the standard Cartan-Weyl decomposition (see for example [4] for a detailed discussion).

THE $\mathfrak{iso}(1,D)$ AND $\mathfrak{so}(1,D)$ ALGEBRAS

The Poincaré algebra is the semidirect product $\mathfrak{t}_D \ltimes \mathfrak{so}(1,D)$, with Lie brackets given by

$$\begin{aligned}[M_{\mu\nu},P_\rho] &= -i(\eta_{\mu\rho}P_\nu - \eta_{\nu\rho}P_\mu) \qquad [P_\mu,P_\nu] = 0 \\ [M_{\mu\nu},M_{\rho\sigma}] &= -i(\eta_{\mu\rho}M_{\nu\sigma} - \eta_{\mu\sigma}M_{\nu\rho} - \eta_{\nu\rho}M_{\mu\sigma} + \eta_{\nu\sigma}M_{\mu\rho}).\end{aligned} \tag{1}$$

The generalization of the Poincaré algebra to an arbitrary number of dimensions is direct. Since P^2 is an invariant for every D, the idea of *mass* makes sense across dimen-

XII Mexican Workshop on Particles and Fields
AIP Conf. Proc. 1361, 288-292 (2011); doi: 10.1063/1.3622716

Hard photon production by inverse Compton scattering

A. Castilla, M. Napsuciale, and J. M. López Romero

Citation: AIP Conf. Proc. **1361**, 375 (2011); doi: 10.1063/1.3622731
View online: http://dx.doi.org/10.1063/1.3622731
View Table of Contents: http://proceedings.aip.org/dbt/dbt.jsp?KEY=APCPCS&Volume=1361&Issue=1
Published by the American Institute of Physics.

Hard photon production by inverse Compton scattering

A. Castilla*, M. Napsuciale* and J. M. López Romero†

*Departamento de Física, Universidad de Guanajuato
†Departamento de Tiempo y Frecuencia, Centro Nacional de Metrología

Abstract. The controlled production of hard photons (X and γ-rays) is of relevance in many medical, industrial and science applications. In this work an alternative method for producing both X and γ-rays via *Inverse Compton Scattering* with both electron and proton beams is discussed. We present results for the cross section for this process with non static electron and protons. The results are evaluated for a particular energy interval, and an experimental design is proposed.

Keywords: Compton scattering, inverse, hard photon, X rays, γ rays
PACS: 12.39.Fe

INTRODUCTION

The *Inverse Compton Scattering* (*ICS*) is basically a momentum transference process using photon collisions with non-static electrons, to increase the energy of incoming light. Kinematics calculations are made to estimate the scattered photon frequency ω' as a function of the incoming photon frequency ω and the electron source energy, using visible range incoming photons (500nm), then an analysis of Feynman Diagrams is discussed to get differential cross sections and establish if this method is experimentally viable to get hard photons (X and γ-rays) using visible light and electron sources at the corresponding energy. A specific case for red photons (670nm) going into blue (470nm) by *ICS* is analyzed and a demonstrative experimental design is discussed.

A second alternative using $\gamma\, p$ collisions is calculated and found impractical compared with the *ICS* case.

CALCULATIONS

For *ICS* using both electron or proton sources, there are two contribution of tree Feynman diagrams, one on s-channel and the second on u-channel.

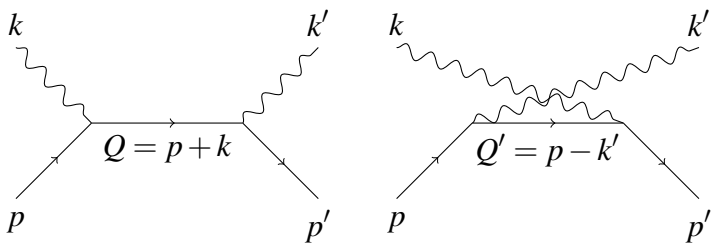

XII Mexican Workshop on Particles and Fields
AIP Conf. Proc. 1361, 375-377 (2011); doi: 10.1063/1.3622731

Topological effects on string vacua

Oscar LoaizaBrito

Citation: AIP Conf. Proc. **1361**, 334 (2011); doi: 10.1063/1.3622724
View online: http://dx.doi.org/10.1063/1.3622724
View Table of Contents: http://proceedings.aip.org/dbt/dbt.jsp?KEY=APCPCS&Volume=1361&Issue=1
Published by the American Institute of Physics.

Topological effects on string vacua

Oscar Loaiza-Brito

Departamento de Física, División de Ciencias e Ingenierías, Campus León, Universidad de Guanajuato, P.O. Box E-143, León, Guanajuato, México

Abstract. We review some topological effects on the construction of string flux-vacua. Specifically we study the effects of brane-flux transitions on the stability of D-branes on a generalized tori compactificaction, the transition that a black hole suffers in a background threaded with fluxes and the connections among some Minkowsky vacua solutions.

Keywords: String theory, string compactificaction, fluxes
PACS: 11.25.-w

INTRODUCTION

During the last decade, flux string compactifications have become an important setup on the construction of realistic string vacua [1]. The main reason for that lies on the possibility to construct a superpotential depending on the compactificaction moduli which in turn yields their stabilization. However, the presence of such fluxes impose some stringent constraints on the models involving wrapping D-branes on internal cycles. An important consequence is the realization of a topological transition between a brane configuration into one involving fluxes.

Wrapping a D-brane on a submanifold supporting NS-NS flux flux makes the D-brane, Freed-Witten (FW) anomalous [2]. This anomaly in the corresponding string worldsheet, can be understood in the following way. Consider a $D(p+2)$-brane wrapping a submanifold $\mathscr{W}_{p+3}$. If there exists a NS-NS 3-form H_3 with its three legs on the worldvolume of the D-brane (a non-vanishing pullback of H_3 on $\mathscr{W}_{p+3}$), a monopole charge is induced through the action term $\int_{\mathscr{W}} A_p \wedge H_3$, where A_p is the dual gauge potential on $\mathscr{W}_{p+3}$. The corresponding equations of motion are not fulfilled unless the source for the magnetic charge is added. This is accomplished by considering an extra D-brane ending at the worldvolume of the FW-anomalous brane. Altogether, the system is well defined and consistent.

Hence, in the presence of NS-NS flux, D-branes cannot wrap any submanifold. A consistent brane configuration should involve a net of submanifolds on which branes of different dimensions are wrapped. Specifically, if a $D(p+2)$-brane wraps a submanifold $\mathscr{W}_{p+3}$ on which the pullback of H_3 is different from zero, an extra Dp-brane wrapping a $(p-1)$-submanifold of $\mathscr{W}_{p+3}$ and extending on one coordinate on the transversal space to $\mathscr{W}_{p+3}$ is required. Being the submanifolds adequate to define spinors and their coupling with gauge fields, this configuration guarantees the absence of inconsistencies.

There are however, D-branes which in spite of being FW anomaly-free, are nevertheless unstable. This is physically interpreted as a topological transformation between D-branes and fluxes through the appearance of instantonic branes [3]. Formally, the tran-

XII Mexican Workshop on Particles and Fields
AIP Conf. Proc. 1361, 334-338 (2011); doi: 10.1063/1.3622724

Evaporation Time of Hořava Gravity Black Holes

S. PérezPayán and M. Sabido

Citation: AIP Conf. Proc. **1361**, 410 (2011); doi: 10.1063/1.3622742
View online: http://dx.doi.org/10.1063/1.3622742
View Table of Contents: http://proceedings.aip.org/dbt/dbt.jsp?KEY=APCPCS&Volume=1361&Issue=1
Published by the American Institute of Physics.

Evaporation Time of Hořava Gravity Black Holes

S. Pérez-Payán and M. Sabido

Physics Department of the Division of Science and Engineering of the University of Guanajuato, Campus León P.O. Box E-143, 37150 León Gto., México

Abstract.
Recently it has been a lot of interest in the theory proposed by Hořava because is a remormalizable theory of gravity and may be a candidate for the UV completion of Einstein gravity. In the present work we study thermodynamical properties of black hole type solutions in this setup. In particular we are able to obtain times of evaporation for black hole solution in this formalism.

Keywords: Hořava Gravity, Black Holes, Thermodynamics
PACS: 02.40.Gh,04.60.-m,04.70.Dy

INTRODUCTION

Recently a new four-dimensional renormalizable theory of gravity was proposed by Hořava [1], inspired by condensed matter models of dynamical critical systems. This theory has manifest three-dimensional spatial general covariance and time-reparameterization invariance, but only acquires four-dimensional general covariance in a infra-red large distance limit. It may be describe in a language akin to the ADM 3+1 formulation of general relativity, but in which Einstein gravity is modified so that the full underlying four-dimensional covariance is broken.

THE HOŘAVA THEORY

In the ADM formalism, the four-dimensional metric of general relativity is parameterized as [2]

$$ds_4^2 = -N^2 dt^2 + g_{ij}(dx^i - N^i dt)(dx^j - N^j dt), \tag{1}$$

where N is the lapse function, N^i is the shift function and g_{ij} is the 3-metric and all are function of (t, x^i). So the Einstein-Hilbert action for the ADM decomposition is given by

$$S_{EH} = \frac{1}{16\pi G}\int d^4x\sqrt{g}N(K_{ij}K^{ij} - K^2 + R - 2\Lambda), \tag{2}$$

where G is the Newton constant and K_{ij} is defined by $K_{ij} = 1/2N(\dot{g}_{ij} - \nabla_i N_j - \nabla_j N_i)$, and a dot represents a derivative with respect to t. The action of the theory proposed by

XII Mexican Workshop on Particles and Fields
AIP Conf. Proc. 1361, 410-412 (2011); doi: 10.1063/1.3622742